HYPOXIA AND CARDIORESPIRATORY CONTROL

EDITED BY: Yasumasa Okada, Jose Lopez-Barneo, Nephtali Marina, Mieczyslaw Pokorski, Richard James Wilson and Julian Paton

PUBLISHED IN: Frontiers in Physiology, Frontiers in Neuroscience and Frontiers in Neurology

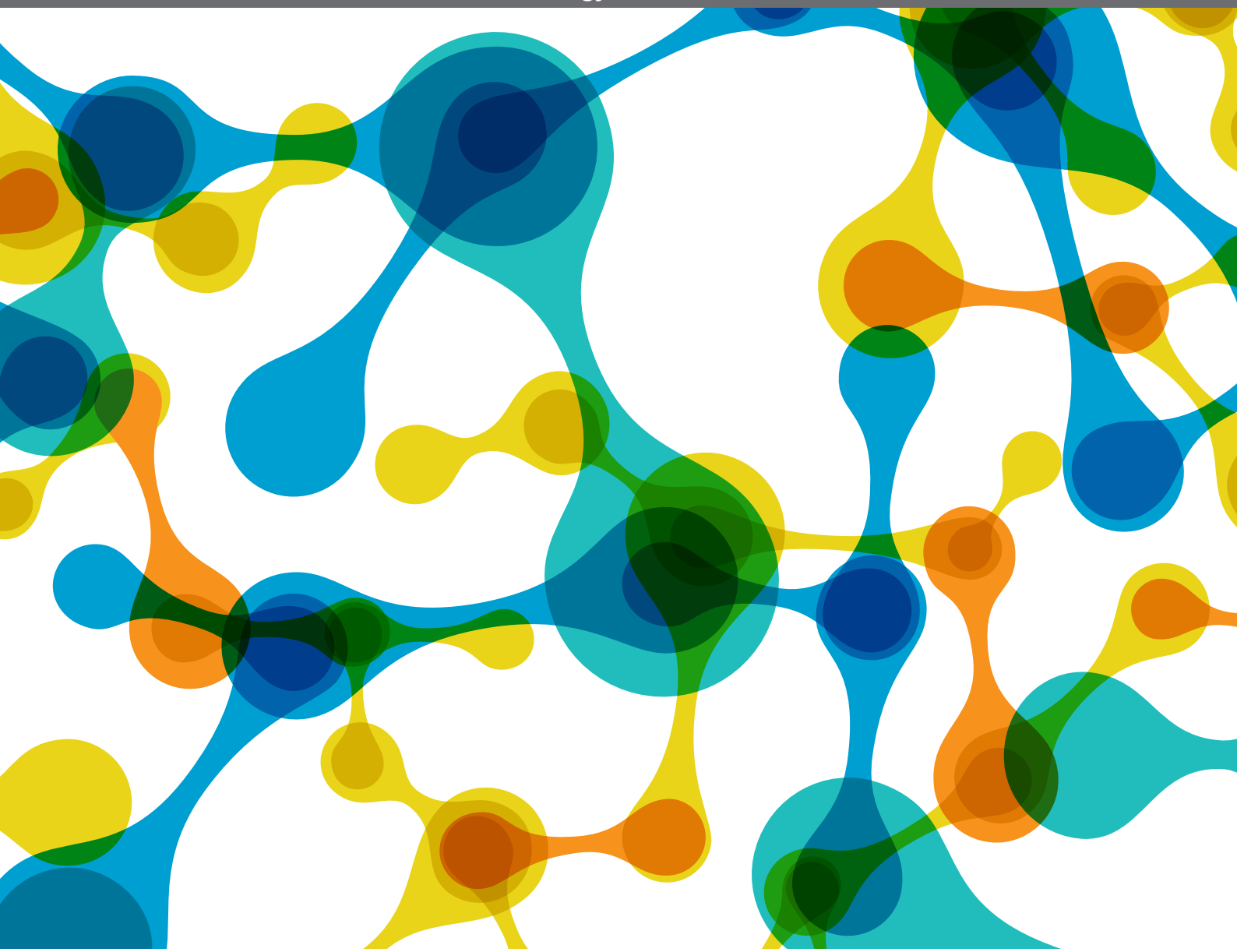

frontiers Research Topics

ISSN 1664-8714
ISBN 978-2-88974-313-1
DOI 10.3389/978-2-88974-313-1

About Frontiers

Frontiers is more than just an open-access publisher of scholarly articles: it is a pioneering approach to the world of academia, radically improving the way scholarly research is managed. The grand vision of Frontiers is a world where all people have an equal opportunity to seek, share and generate knowledge. Frontiers provides immediate and permanent online open access to all its publications, but this alone is not enough to realize our grand goals.

Frontiers Journal Series

The Frontiers Journal Series is a multi-tier and interdisciplinary set of open-access, online journals, promising a paradigm shift from the current review, selection and dissemination processes in academic publishing. All Frontiers journals are driven by researchers for researchers; therefore, they constitute a service to the scholarly community. At the same time, the Frontiers Journal Series operates on a revolutionary invention, the tiered publishing system, initially addressing specific communities of scholars, and gradually climbing up to broader public understanding, thus serving the interests of the lay society, too.

Dedication to Quality

Each Frontiers article is a landmark of the highest quality, thanks to genuinely collaborative interactions between authors and review editors, who include some of the world's best academicians. Research must be certified by peers before entering a stream of knowledge that may eventually reach the public - and shape society; therefore, Frontiers only applies the most rigorous and unbiased reviews.
Frontiers revolutionizes research publishing by freely delivering the most outstanding research, evaluated with no bias from both the academic and social point of view. By applying the most advanced information technologies, Frontiers is catapulting scholarly publishing into a new generation.

What are Frontiers Research Topics?

Frontiers Research Topics are very popular trademarks of the Frontiers Journals Series: they are collections of at least ten articles, all centered on a particular subject. With their unique mix of varied contributions from Original Research to Review Articles, Frontiers Research Topics unify the most influential researchers, the latest key findings and historical advances in a hot research area! Find out more on how to host your own Frontiers Research Topic or contribute to one as an author by contacting the Frontiers Editorial Office: frontiersin.org/about/contact

HYPOXIA AND CARDIORESPIRATORY CONTROL

Topic Editors:
Yasumasa Okada, Murayama Medical Center (NHO), Japan
Jose Lopez-Barneo, Sevilla University, Spain
Nephtali Marina, University College London, United Kingdom
Mieczyslaw Pokorski, Opole University, Poland
Richard James Wilson, University of Calgary, Canada
Julian Paton, University of Auckland, New Zealand

Citation: Okada, Y., Lopez-Barneo, J., Marina, N., Pokorski, M., Wilson, R. J., Paton, J., eds. (2022). Hypoxia and Cardiorespiratory Control. Lausanne: Frontiers Media SA. doi: 10.3389/978-2-88974-313-1

Table of Contents

frontiers in Physiology

EDITORIAL
published: 22 December 2021
doi: 10.3389/fphys.2021.820815

Editorial: Hypoxia and Cardiorespiratory Control

Yasumasa Okada[1], Julian F. R. Paton[2], José López-Barneo[3,4,5], Richard J. A. Wilson[6], Nephtali Marina[7] and Mieczyslaw Pokorski[8,9]*

[1] Clinical Research Center, Murayama Medical Center, Tokyo, Japan, [2] Manaaki Manawa—The Centre for Heart Research, Department of Physiology, Faculty of Health and Medical Sciences, University of Auckland, Auckland, New Zealand, [3] Instituto de Biomedicina de Sevilla (IBiS), Hospital Universitario Virgen del Rocío, Consejo Superior de Investigaciones Científicas (CSIC), Universidad de Sevilla, Seville, Spain, [4] Departamento de Fisiología Médica y Biofísica, Facultad de Medicina, Universidad de Sevilla, Seville, Spain, [5] Centro de Investigación Biomédica en Red sobre Enfermedades Neurodegenerativas (CIBERNED), Madrid, Spain, [6] Department of Physiology and Pharmacology, Hotchkiss Brain Institute and Alberta Children's Hospital Research Institute, University of Calgary, Calgary, AB, Canada, [7] Division of Medicine, University College London, London, United Kingdom, [8] Institute of Health Sciences, Opole University, Opole, Poland, [9] Faculty of Health Sciences, The Jan Dlugosz University, Czestochowa, Poland

Keywords: intermittent hypoxia, sleep apnea, pulmonary hypertension, sympathetic excitation, astrocyte, TRPA1, carotid body, plasticity

Editorial on the Research Topic

Hypoxia and Cardiorespiratory Control

INTRODUCTION

To maintain adequate oxygen levels in the body, which is essential for a healthy life, the respiratory and cardiovascular systems play vitally important roles. When the oxygen content is insufficient, i.e., when hypoxia is loaded, respiratory and cardiovascular systems respond to restore, compensate, or adapt to hypoxia, e.g., by increasing ventilation and blood flow to maintain oxygen transport to vital organs. Traditionally, it has been thought that hypoxia is detected solely by carotid and aortic bodies, i.e., by peripheral chemoreceptors, and information from the peripheral chemoreceptors is transmitted to respiratory and cardiovascular centers in the brainstem whose respiratory and cardiovascular neural outputs are regulated. However, recent progress in neurophysiology has clarified that there are hypoxia-sensors not only in the periphery but also in the central nervous system. Hypoxia also affects the vascular system causing atherosclerosis and pulmonary hypertension and impairs blood glucose regulation that also facilitates atherosclerosis. The effects of hypoxia on vital organs and tissues vary depending on the modality of hypoxia exposure, i.e., acute, chronically sustained, or intermittent hypoxia. Although these issues have been vigorously investigated, the underlying mechanisms are yet to be unraveled. Likewise, long-range consequences for organ and tissue functions affected by hypoxia have not been fully elucidated. In the article collection of this Research Topic, a series of studies report the latest and most notable pathophysiological findings that are categorized into four areas: respiratory control, glucose metabolism, pulmonary hypertension, and sympathetic nervous system activation. The articles attempt to clarify many of the unsolved issues summarized below.

RESPIRATORY CONTROL

When the body is exposed to hypoxia, ventilation is augmented to increase oxygen uptake from the lungs, although ventilation decreases when the level of loaded hypoxia is too severe. To respond to hypoxia, the body must sense the oxygen content. Carotid body chemosensory or glomus cells

OPEN ACCESS

Edited and reviewed by:
John T. Fisher, Queen's University School of Medicine, Canada

****Correspondence:***
Yasumasa Okada
yasumasaokada@1979.jukuin.keio.ac.jp

Specialty section:
This article was submitted to Respiratory Physiology, a section of the journal Frontiers in Physiology

Received: *23 November 2021*
Accepted: *06 December 2021*
Published: *22 December 2021*

Citation:
Okada Y, Paton JFR, López-Barneo J, Wilson RJA, Marina N and Pokorski M (2021) Editorial: Hypoxia and Cardiorespiratory Control. Front. Physiol. 12:820815. doi: 10.3389/fphys.2021.820815

play a major role in the monitoring of arterial oxygen levels. However, the exact mechanisms of chemosensing and the nature of the sensor have remained elusive. Ortega-Saenz et al. have reviewed the latest experimental findings concerning the role of specialized mitochondria in acute O_2 sensing by carotid body glomus cells. They have found that activation of glomus cells by hypoxia depends on the generation of mitochondrial signals (NADH and reactive oxygen species) which modulate membrane ion channels to induce depolarization, Ca^{2+} influx, and transmitter release. Hypoxia is also sensed, to an extent, in tissues other than the carotid body, because peripheral chemodenervated animals augment ventilation in response to hypoxic stimulus (Miller and Tenney, 1975). Chen et al. have reported that a non-selective cation channel, transient receptor potential ankyrin 1 (TRPA1), mediates the physiological responses to mild hypoxia (13–15% O_2), including avoidance behavior in the hypoxic environment and the wake-up response to hypoxic gas inhalation. They suggested that TRPA1 channels in the sensory nerves innervating the airways detect the hypoxic environment. Recently, it has been reported that medullary astrocytes play a role in central hypoxic sensing (Angelova et al., 2015) with the astrocytic TRPA1 channels as the hypoxia-sensing molecule (Uchiyama et al., 2020). Onimaru et al. have found that some astrocytes in the solitary tract nucleus (NTS) of the dorsal medulla are hypoxia and hypercapnia dual-sensitive. Thus, astrocytes in the NTS may play an essential role in the prevention of hypercapnic hypoxia, which is seen in patients with chronic obstructive pulmonary disease (COPD). Acute hypoxia increases ventilation, and after cessation of hypoxic loading, ventilation decreases but remains above the pre-exposure baseline level for a limited time (Dahan et al., 1995). This post-hypoxic persistent respiratory augmentation (PHRA), i.e., short-term potentiation of breathing, is essential for stabilizing the respiratory output, but the underlying mechanisms have not been well-understood (Eldridge, 1996). Fukushi et al. have investigated this issue and demonstrated that the astrocytes do mediate the PHRA but by mechanisms other than TRPA1 channels that are engaged in hypoxia sensing. These mechanisms are open to conjecture for the time being. Perim et al. have also investigated the issue of respiratory neural plasticity. Moderate acute intermittent hypoxia (mAIH) elicits a progressive increase in the phrenic motor output lasting hours post-mAIH, a form of respiratory motor plasticity known as the phrenic long-term facilitation (pLTF). The authors have demonstrated that elevated $PaCO_2$ undermines mAIH-induced pLTF in anesthetized rats, which opposes the known effects of $PaCO_2$ on ventilatory long-term facilitation in wakeful humans (Harris et al., 2006). This finding indicates that anesthesia profoundly affects respiratory neural plasticity. It has been postulated that the renin-angiotensin system in the respiratory controller promotes hypoxia-induced chemoreflex sensitization, e.g., by increasing the carotid body sensitivity, and induces central sleep apnea (Fung, 2014). Brown et al. have demonstrated that the severity of hypoxia-induced central sleep apnea is associated with the loop gain, which was assessed by the dynamic ventilatory drive response consequent to a reduction in ventilation due to apnea. However, losartan, an angiotensin-II type-1 receptor (AT1R) antagonist, did not modulate the chemoreflex sensitivity in healthy men before or after nocturnal hypoxia, which sensitizes hypoxia-induced chemoreflex. The contribution of AT1R to the chemoreflex sensitivity in pathological conditions, e.g., heart failure, obstructive sleep apnea, and chronically hypoxic diseases, requires further investigation.

GLUCOSE METABOLISM AND INTERMITTENT HYPOXIA/SLEEP APNEA

Sleep-disordered breathing and intermittent hypoxia often accompany insulin resistance and type 2 diabetes (Koren et al., 2016). Gabryelska et al. have reviewed the role of oxygen-sensitive α-subunit of hypoxia-inducible factor 1 (HIF-1α), a key regulator of oxygen metabolism, as a mediator of insulin resistance and type 2 diabetes in obstructive sleep apnea patients and proposed a concept that stabilization of HIF-1α helps control insulin resistance and diabetes. Concerning the experiments to induce hyperglycemia by loading intermittent hypoxia in animals, Nedoboy et al. have reported that the use of pentobarbital anesthesia is unsuitable because the anesthetic suppresses the intermittent hypoxia-induced blood glucose elevation.

PULMONARY HYPERTENSION

Hypoxia induces constriction of pulmonary arteries and causes pulmonary hypertension. Fan et al. have investigated the underlying mechanisms of pulmonary hypertension in intermittent hypoxia in rats. They reported that the insulin-induced pulmonary vasodilation and the balance of insulin-induced signaling mediated by upregulated Tribbles homolog 3 (TRIB3), a key mediator of insulin signaling, are impaired in the endothelium, resulting in the development of hypoxic pulmonary hypertension. Umeda et al. have also investigated the mechanisms of chronic intermittent hypoxia-associated atherosclerosis and pulmonary hypertension by evaluating the intima-media thickness (IMT) in the aorta and pulmonary artery in mice. They demonstrated that intermittent hypoxia mimicking obstructive sleep apnea induces IMT thickening that is reversed during the normoxic recovery in both aorta and pulmonary artery. Pulmonary embolism causes hypoxia and may lead to death when the embolus is massive. However, the pathophysiological mechanisms of pulmonary circulation disturbance caused by pulmonary embolism have not been fully elucidated. Wang et al. have investigated the role of inflammatory responses and their relationship to the pulmonary blood flow in the rabbit model of acute pulmonary embolism. The authors suggested that the activation of inflammatory mediators in the tissue around the pulmonary vessels with and without embolus is crucially responsible for pulmonary vascular constriction and pulmonary blood flow attenuation in the model animal.

SYMPATHETIC ACTIVATION

Hypoxia causes excitation of the sympathetic nervous system (Marina et al., 2015; Pijacka et al., 2018). The sympathetic activity

is precisely controlled *via* baroreflex. However, the effects of natural hypoxia on the baroreflex function have not been well-understood. Beltrán et al. have investigated this issue in rats placed at a high altitude of 3,270 m above sea level and reported that high altitude produces autonomic and baroreceptor control impairment characterized by parasympathetic withdrawal. High altitude environment in the Himalayas was utilized as a model of hypobaric hypoxia by Verratti et al. The authors compared the delivery of oxygen to muscles in response to resistance exercise between Italian trekkers and native Nepalese porters. The porters had a greater muscle oxygen delivery than Italians, and this ability of porters was attributed to the long-range adaptive memory secondary to frequent exposures to hypoxia. Saha et al. have analyzed the effects of acute hypoxia and hypercapnia on the enhancement of respiratory-sympathetic nerve coupling (respSNA) in the rat model of chronic kidney disease (CKD). The authors demonstrated that female rats with CKD exhibit a heightened respSNA coupling at baseline that is augmented by mild hypoxia but not by hypercapnia. They suggested that this mechanism contributes to driving hypertension in CKD. Postural orthostatic tachycardia syndrome (POTS) is a heterogeneous disease that predominantly affects children and adolescents. POTS patients are markedly sensitized to hypoxia when upright (Taneja et al., 2011). There is a significant difference between children and adults in the diagnosis and treatment of POTS patients. Zhang et al. have classified the clinical forms of POTS into the hypovolemic, neuropathic, and hyperadrenergic POTS, and reviewed the updated individualized treatment strategies for POTS in children. The results may become valuable guidelines in the treatment of POTS.

CONCLUSION

Hopefully, the articles published in this Research Topic help readers understand how hypoxia affects the respiratory and cardiovascular systems and how these systems respond to the hypoxic stimulus. A savvy judgment of hypoxia action and adaptation is fundamental for the development of basic research and its translation into improved clinical outcomes in many a disorder, notably hypoxic brain injuries or hypoxic pulmonary pathologies. The understanding of how hypoxia is detected and acts is also essential for psychosomatic and anti-aging rehabilitation strategies to improve the health span. This Research Topic, undoubtedly, reveals the necessity to further investigate the molecular mechanisms of hypoxia-associated cardiorespiratory alterations in health and disease.

AUTHOR CONTRIBUTIONS

YO wrote the draft of the manuscript. JP, JL-B, RW, NM, and MP edited the manuscript. All authors contributed to the article and approved the submitted version.

REFERENCES

Angelova, P. R., Kasymov, V., Christie, I., Sheikhbahaei, S., Turovsky, E., Marina, N., et al. (2015). Functional oxygen sensitivity of astrocytes. *J. Neurosci.* 35, 10460–10473. doi: 10.1523/JNEUROSCI.0045-15.2015

Dahan, A., Berkenbosch, A., DeGoede, J., van den Elsen, M., Olievier, I., and van Kleef, J. (1995). Influence of hypoxic duration and post-hypoxic inspired O_2 concentration on short term potentiation of breathing in humans. *J. Physiol.* 488, 803–813. doi: 10.1113/jphysiol.1995.sp021012

Eldridge, F. L. (1996). "The North Carolina respiratory model," in *Bioengineering Approaches to Pulmonary Physiology and Medicine*, ed M. C. K. Khoo (Boston, MA: Springer), 1–23.

Fung, M. L. (2014). The role of local renin-angiotensin system in arterial chemoreceptors in sleep-breathing disorders. *Front. Physiol.* 5:336. doi: 10.3389/fphys.2014.00336

Harris, D. P., Balasubramaniam, A., Badr, M. S., and Mateika, J. H. (2006). Long-term facilitation of ventilation and genioglossus muscle activity is evident in the presence of elevated levels of carbon dioxide in awake humans. *Am. J. Physiol. Regul. Integr. Comp. Physiol.* 291, R1111–R1119. doi: 10.1152/ajpregu.00896.2005

Koren, D., Dumin, M., and Gozal, D. (2016). Role of sleep quality in the metabolic syndrome. *Diabetes Metab. Syndr. Obes.* 9, 281–310. doi: 10.2147/DMSO.S95120

Marina, N., Ang, R., Machhada, A., Kasymov, V., Karagiannis, A., Hosford, P. S., et al. (2015). Brainstem hypoxia contributes to the development of hypertension in the spontaneously hypertensive rat. *Hypertension* 65, 775–783. doi: 10.1161/HYPERTENSIONAHA.114.04683

Miller, M. J., and Tenney, S. M. (1975). Hypoxia-induced tachypnea in carotid-deafferented cats. *Respir. Physiol.* 23, 31–39. doi: 10.1016/0034-5687(75)90069-9

Pijacka, W., Katayama, P. L., Salgado, H. C., Lincevicius, G. S., Campos, R. R., McBryde, F. D., et al. (2018). Variable role of carotid bodies in cardiovascular responses to exercise, hypoxia and hypercapnia in spontaneously hypertensive rats. *J. Physiol.* 596, 3201–3216. doi: 10.1113/JP275487

Taneja, I., Medow, M. S., Clarke, D. A., Ocon, A. J., and Stewart, J. M. (2011). Baroreceptor unloading in postural tachycardia syndrome augments peripheral chemoreceptor sensitivity and decreases central chemoreceptor sensitivity. *Am. J. Physiol Heart Circ. Physiol.* 301, H173–H179. doi: 10.1152/ajpheart.01211.2010

Uchiyama, M., Nakao, A., Kurita, Y., Fukushi, I., Takeda, K., Numata, T., et al. (2020). O_2-dependent protein internalization underlies astrocytic sensing of acute hypoxia by restricting multimodal TRPA1 channel responses. *Curr. Biol.* 30, 3378–3396.e7. doi: 10.1016/j.cub.2020.06.047

Conflict of Interest: The authors declare that the research was conducted in the absence of any commercial or financial relationships that could be construed as a potential conflict of interest.

frontiers in Neuroscience

ORIGINAL RESEARCH
published: 28 April 2020
doi: 10.3389/fnins.2020.00382

Angiotensin II-Type I Receptor Antagonism Does Not Influence the Chemoreceptor Reflex or Hypoxia-Induced Central Sleep Apnea in Men

*Courtney V. Brown[1], Lindsey M. Boulet[1], Tyler D. Vermeulen[1], Scott A. Sands[2], Richard J. A. Wilson[3], Najib T. Ayas[4,5], John S. Floras[6] and Glen E. Foster[1]**

[1] Centre for Heart, Lung, and Vascular Health, School of Health and Exercise Science, University of British Columbia – Okanagan, Kelowna, BC, Canada, [2] Division of Sleep and Circadian Disorders, Brigham and Women's Hospital and Harvard Medical School, Boston, MA, United States, [3] Department of Physiology and Pharmacology, Hotchkiss Brain Institute, Cumming School of Medicine, University of Calgary, Calgary, AB, Canada, [4] Sleep Disorders Program, University of British Columbia, Vancouver, BC, Canada, [5] Respiratory and Critical Care Divisions, University of British Columbia, Vancouver, BC, Canada, [6] University Health Network and Sinai Health System Division of Cardiology, Department of Medicine, University of Toronto, Toronto, ON, Canada

OPEN ACCESS

Edited by:
Bernhard Schaller, University of Zurich, Switzerland

Reviewed by:
Vincent Joseph, Laval University, Canada
Noah J. Marcus, Des Moines University, United States

***Correspondence:**
Glen E. Foster
glen.foster@ubc.ca

Specialty section:
This article was submitted to Autonomic Neuroscience, a section of the journal Frontiers in Neuroscience

Received: *27 January 2020*
Accepted: *27 March 2020*
Published: *28 April 2020*

Citation:
Brown CV, Boulet LM, Vermeulen TD, Sands SA, Wilson RJA, Ayas NT, Floras JS and Foster GE (2020) Angiotensin II-Type I Receptor Antagonism Does Not Influence the Chemoreceptor Reflex or Hypoxia-Induced Central Sleep Apnea in Men. Front. Neurosci. 14:382. doi: 10.3389/fnins.2020.00382

Components of the renin-angiotensin system (RAS) situated within the carotid body or central nervous system may promote hypoxia-induced chemoreceptor reflex sensitization or central sleep apnea (CSA). We determined if losartan, an angiotensin-II type-I receptor (AT_1R) antagonist, would attenuate chemoreceptor reflex sensitivity before or after 8 h of nocturnal hypoxia, and consequently CSA severity. In a double-blind, randomized, placebo-controlled, crossover protocol, 14 men (age: 25 ± 2 years; BMI: 24.6 ± 1.1 kg/m^2; means ± SEM) ingested 3 doses of either losartan (50 mg) or placebo every 8 h. Chemoreceptor reflex sensitivity was assessed during hypoxic and hyperoxic hypercapnic ventilatory response (HCVR) tests and during six-20s hypoxic apneas before and after 8 h of sleep in normobaric hypoxia (F_IO_2 = 0.135). Loop gain was assessed from a ventilatory control model fitted to the ventilatory pattern of CSA recorded during polysomnography. Prior to nocturnal hypoxia, losartan had no effect on either the hyperoxic (losartan: 3.6 ± 1.1, placebo: 4.0 ± 0.6 l/min/mmHg; P = 0.9) or hypoxic HCVR (losartan: 5.3 ± 1.4, placebo: 5.7 ± 0.68 l/min/mmHg; P = 1.0). Likewise, losartan did not influence either the hyperoxic (losartan: 4.2 ± 1.3, placebo: 3.8 ± 1.1 l/min/mmHg; P = 0.5) or hypoxic HCVR (losartan: 6.6 ± 1.8, placebo: 6.3 ± 1.5 l/min/mmHg; P = 0.9) after nocturnal hypoxia. Cardiorespiratory responses to apnea and participants' apnea hypopnea indexes during placebo and losartan were similar (73 ± 15 vs. 75 ± 14 events/h; P = 0.9). Loop gain, which correlated with CSA severity (r = 0.94, P < 0.001), was similar between treatments. In summary, in young healthy men, hypoxia-induced CSA severity is strongly associated with loop gain, but the AT_1R does not modulate chemoreceptor reflex sensitivity before or after 8 h of nocturnal hypoxia.

Keywords: chemoreceptor reflex, angiotensin receptor, hypoxia, sleep apnea, human

INTRODUCTION

Angiotensin-II (ANG-II) is a physiologically active hormone of the renin-angiotensin system (RAS) and has target receptors in various tissues, including the carotid bodies and central nervous system (Allen, 1998; Li et al., 2006). Animal models have demonstrated that ANG-II primarily exerts its effect on the carotid body through the ANG-II type-I receptor (AT_1R) (Allen, 1998). AT_1Rs are found on chemosensitive glomus cells of mouse carotid bodies and are upregulated following ANG-II infusion (Allen, 1998). Administration of ANG-II consequently elevates peripheral chemoreceptor activity and augments the chemoreceptor response to hypoxia in animal models of heart failure (Allen, 1998; Li et al., 2006). In isolated rat carotid bodies, blockade of the AT_1R with losartan, severely reduces the afferent response to hypoxic-hypercapnic challenges (Roy et al., 2018), suggesting the AT_1R is critical for peripheral chemoreceptor sensitivity.

Exposure to sustained hypoxia also sensitizes the chemoreceptor reflex response in both animals and humans (Aaron and Powell, 1993; Richard et al., 2014). In rats exposed to chronic hypoxia, there is increased expression of angiotensinogen and AT_1Rs in carotid body glomus cells, and activation by ANG-II is associated with increased excitatory response which is attenuated by AT_1R blockade (Leung et al., 2000; Lam and Leung, 2003). In rats, administering an AT_1R blocker attenuates the long-lasting activity in the carotid sinus nerve (CSN) following acute hypoxic-hypercapnic bouts, demonstrating a critical role for the AT_1R in the chemoreceptor reflex response to intermittent hypercapnic hypoxia (Roy et al., 2018). While AT_1R antagonists (i.e., losartan) effectively mitigate the lasting effects of intermittent hypoxia on muscle sympathetic nerve activity (MSNA) and blood pressure in humans (Foster et al., 2010; Jouett et al., 2017), it remains to be determined if AT_1R blockade attenuates chemosensitivity (either peripheral or central) before or after hypoxia in humans.

Heightened chemosensitivity during hypoxia is understood to contribute to the development of periodic breathing with sojourn to high altitude. Mechanistically, the presence of arterial hypoxia acutely increases the ventilatory responsiveness to hypoxia and to hypercapnia (e.g., manifests as a reduced gap between eupneic partial pressure of carbon dioxide (PCO_2) and the apneic threshold). This heightened peripheral chemoreceptor sensitivity, via an increase in the overall loop gain of the ventilatory control system, leads to reduced stability and overt patterns of cyclic apnea and hyperventilation particularly during sleep. Loop gain – a term that describes the overall stability of the ventilatory control system – combines the unique contributions of chemoreceptor sensitivity (controller gain) as well as how effectively ventilation increases arterial partial pressure of oxygen and reduces the arterial PCO_2 (plant gain) (White, 2005). While high loop gain is considered the leading mechanism of central sleep apnea (CSA) in patients with heart failure or at altitude, it is also the leading cause of obstructive sleep apnea (OSA) (White, 2005; Edwards et al., 2012). Although acetazolamide has been shown to lower both plant and loop gain, and improves sleep apnea severity (OSA and CSA), no study has pharmacologically lowered loop gain via chemosensitivity and consequently improved sleep apnea (Edwards et al., 2012).

Here we tested whether AT_1R blockade consequently reduces chemoreceptor sensitivity, loop gain, and the severity of CSA in human subjects. Specifically, we assessed the influence of AT_1R blockade on chemosensitivity before and after 8 h of nocturnal hypoxia, and on the severity of hypoxia induced CSA as a human model of high-loop gain, chemoreflex-dependent sleep apnea. We hypothesized that losartan administration would attenuate the hypercapnic ventilatory response (HCVR) and the cardiorespiratory response to apnea before and after nocturnal hypoxia. Additionally, we hypothesized that losartan would reduce the severity of hypoxia induced CSA by reducing loop gain during 8 h of nocturnal hypoxia.

MATERIALS AND METHODS

Ethical Approval

This study was approved by the University of British Columbia Clinical Research Ethics Board (H17-02920), was registered as a clinical trial (ClinicalTrials.gov; NCT03335904) and conformed to the latest revision of the Declaration of Helsinki. Prior to enrollment in the study all participants provided written informed consent.

Participants

Male participants ($n = 14$) recruited from the University of British Columbia – Okanagan campus were screened to ensure they were normotensive (systolic blood pressure (SBP) < 140 mmHg, diastolic blood pressure (DBP) < 90 mmHg), had normal pulmonary function ($>80\%$ of predicted), and were free of sleep disordered breathing (apnea hypopnea index (AHI) < 5 events/hour) based on a home sleep study. Females were excluded from participation because they reportedly develop less severe CSA compared with males at high altitude (Lombardi et al., 2013) and in heart failure (Sin et al., 1999). Additionally, resting ventilation and blood pressure regulation are sensitive to menstrual cycle phase (Behan et al., 2003; Hart and Charkoudian, 2014). Participants were excluded if they have smoked within the past year and have a history of impaired renal function, cardiovascular disease, or respiratory disease. Participants were also excluded if they were taking any medication, prescribed or over the counter, or were obese ($BMI > 30\ Kg/m^2$).

Protocol

Participants were asked to abstain from strenuous physical activity, alcohol or caffeine during the 12 h preceding each experimental session. Using a double-blind, placebo controlled, randomized, crossover design participants took either 50 mg of losartan, or a placebo pill three times over the course of 24 h (see section Pharmacological Intervention). Each experimental visit was separated by a 1 week washout period. Losartan was selected to target the AT_1R as it has a high affinity for the AT_1R and has been shown to be void of any agonist activity

(Ohtawa et al., 1993). The experimental protocol consisted of (1) a hyperoxic hypercapnic ventilatory response (HCVR) test, (2) a hypoxic HCVR test and (3) a hypoxic apnea response (HAR) test measured before and after a night of sleep in a normobaric hypoxia chamber (8850 SUMMIT+; Altitude Tech, Kingston, ON, Canada). In addition, venous blood samples were collected before and after a night of hypoxic sleep and assayed for plasma renin activity (PRA) and aldosterone to confirm effective dosing of losartan. Cardiovascular and respiratory variables were recorded continuously throughout the HCVR and HAR tests. Following the evening pre-tests, participants were instrumented with a sleep system (see section Monitoring Sleep in Normobaric Hypoxia) prior to entering the hypoxic chamber. The fraction of inspired O_2 within the normobaric chamber was set to 0.135 which has been shown to sufficiently induce CSA in young, healthy men (Lombardi et al., 2013). Eight hours after entering the chamber, participants were wakened, exited the hypoxic chamber and took the third and final dose of their assigned intervention. They then completed the Lake Louise Acute Mountain Sickness (AMS) Scoring System and the ESQ-Cerebral Symptoms Questionnaire (Roach et al., 1993; Beidleman et al., 2007). The chemoreceptor reflex sensitivity tests were repeated 1 h after the last drug or placebo dose.

Pharmacological Intervention

Participants were randomly assigned to orally ingest either losartan tablets (50 mg), or placebo pills (microcrystalline cellulose, identical in appearance and packaged in identical blister packages) at 8 h intervals. The first of the three doses was taken ∼10 h before the experimental visit. The second dose was given 2 h before the evening chemoreceptor reflex tests while the third dose was given 1 h prior to morning testing. This timing was selected as plasma concentrations of both losartan and E-3174, its active metabolite, peak after a single dose and are not significantly different than concentrations after 7 days of losartan use (Ohtawa et al., 1993). Additionally, we elected the dosing protocol to ensure plasma concentrations of losartan and E-3147 remained sufficiently high throughout the entire protocol. Peak plasma concentration of losartan occurs an hour after ingestion while E-3147 reaches peak concentrations 2 h after ingestion and as such ventilatory response tests were performed within this time frame (Ohtawa et al., 1993).

Chemoreceptor Reflex Test Instrumentation

All respiratory and cardiovascular parameters were acquired using an analog-to-digital converter (Powerlab/16SP ML 880; AD Instruments, Colorado Springs, CO, United States) interfaced with a personal computer. Commercially available software was used to analyze ventilatory and cardiovascular variables (LabChart V7.1, AD Instruments). During both sets of ventilatory tests, subjects breathed through a mouthpiece while wearing a nose clip, and a two-way non-rebreathing valve. Respired gas pressures were sampled at the mouth and analyzed for the partial pressure of end tidal oxygen and carbon dioxide ($P_{ET}O_2$ and $P_{ET}CO_2$ respectively) (ML206; AD Instruments). Expired gases were passed through a 4.7 L mixing chamber (MLA246; AD Instruments), as well as an oxygen (O_2) and carbon dioxide (CO_2) gas analyzer connected in series (S-3A and CD-3A, AEI Technologies, Pittsburgh, PA, United States) to measure the fraction of inspired O_2 and fraction of inspired CO_2 to calculate resting metabolic parameters including O_2 and CO_2 consumption as well as respiratory exchange rate. These parameters were necessary to determine the isometabolic hyperbola. Respiratory flow was also measured near the mouth using a pneumotachograph (HR 800L, Hans Rudolph, Shawnee, KS, United States) and a differential pressure amplifier (PA1 1110, Hans Rudolph). Heart rate (HR) was determined from a standard lead II electrocardiogram (ML132, AD Instruments). Beat-by-beat blood pressure was measured from a cuff placed on the right middle finger using pulse photoplethysmography (Finometer PRO; Finapress Medical Systems, Amsterdam, the Netherlands). A return to flow calibration was completed and the Finometer was referenced to manual blood pressures taken with an automated sphygmomanometer (Carescape V100; GE Medical Systems, Milwaukee, WI, United States) on the contralateral arm three times during baseline of each testing protocol.

Hypercapnic Ventilatory Response (HCVR)

Two HCVR tests were administered to assess ventilatory and cardiovascular responses to CO_2, first on the background of hyperoxia and secondly on the background of hypoxia, with the latter maximizing peripheral chemoreflex activity. Each protocol was separated by 10 min. Performing the HCVR test in hyperoxia minimizes the peripheral chemoreceptor contribution to the chemoreflex response, while a background of hypoxia maximizes the peripheral chemoreceptor input (Duffin, 2007). Prior to starting the HCVR tests, participants rested supine for 10 min while breathing through a mouthpiece with their nose-clamped to collect baseline values of all variables. Throughout the test, participants listened to relaxing music with no prominent rhythm. Dynamic end-tidal forcing (see section Dynamic End-Tidal Forcing) was used to clamp $P_{ET}O_2$ and $P_{ET}CO_2$ values throughout the HCVR tests (Tymko et al., 2016). In short, $P_{ET}O_2$ was clamped at 350 mmHg for the hyperoxic HCVR test and at 50 mmHg for the hypoxic HCVR. $P_{ET}CO_2$ was clamped for 3 min each at 0, +2, +4, and +6 mmHg respective to each subject's baseline value.

Dynamic End-Tidal Forcing

Control of $P_{ET}O_2$ and $P_{ET}CO_2$ was accomplished through an end-tidal forcing system which uses independent gas solenoid valves for O_2, CO_2, and nitrogen (N_2) to deliver a precise quantity of each gas into an inspiratory reservoir where it is humidified (Tymko et al., 2015, 2016). Breath-by-breath measures of $P_{ET}O_2$, $P_{ET}CO_2$, tidal volume, breathing frequency and minute ventilation were done online using specifically designed software (Labview 13.0, National Instruments, Austin, TX, United States). The forcing system uses $P_{ET}O_2$, $P_{ET}CO_2$, inspired and expired tidal volumes feedback and alters the

inspired gas to bring end-tidal gas levels to the target value. Feed-forward control of the inspirate is based on estimates of metabolic O_2 consumption and CO_2 production and utilizes the alveolar gas equation to determine the required fraction of inspired O_2 and fraction of inspired CO_2. Feedback control is accomplished using a proportional and integral error reduction control system.

Calculating Chemoreflex Sensitivity

For both hyperoxic and hypoxic HCVR tests minute ventilation was plotted against $P_{ET}CO_2$ for all participants. Individual data were regressed using a linear mixed effects model (see section Statistical Analyses) from which individual coefficients (i.e., slopes and intercepts) were calculated from random effects. Reported group means were determined from the global model coefficients representing the group's response to condition and drug.

Hypoxic Apnea Response (HAR)

Following the HCVR protocols, participants remained instrumented and performed the hypoxic apnea response (HAR) protocol. A 5 min baseline was collected prior to performing six hypoxic apneas during which all respiratory and cardiovascular variables were recorded. Each apneic cycle was repeated 6 times and consisted of (1) 2–3 breaths through a three-way valve connected to a reservoir containing 100% N_2, (2) a 20 s end-expiratory breath-hold, and (3) 40 s of room air breathing. A nadir arterial oxyhemoglobin saturation (SpO_2) between 85 and 90% was targeted during each apnea, and the number of N_2 breaths prior to each apnea was adjusted to achieve this range. Following the hypoxic apnea cycles, all variables were recorded throughout a 5 min recovery period. The HAR test was performed to assess if ventilatory and cardiovascular responses to apnea were influenced by losartan.

Monitoring Sleep in Normobaric Hypoxia

Sleep disordered breathing was measured using a continuous, overnight, cardiopulmonary monitoring system (Somte PSG, Compumedics, VIC, Australia). The device consists of an oximeter to record SpO_2, an electrocardiogram to record HR, a pressure transducer to record nasal airflow, chest and abdomen bands to measure respiratory effort, as well as a body position sensor. Additionally, monitoring of FP1-A2 and FP2-A1 by electroencephalography was combined with electrooculography of the left and right eye to assess sleep vs. wakefulness. Total sleep time was produced once wakefulness and sleep had been scored. The data were manually scored by the same investigator (Profusion 4, Compumedics, VIC, Australia) for the calculation of the AHI, the oxygen desaturation index (ODI) and the peak and nadir oxyhemoglobin saturation according to the criteria established by the American Academy of Sleep Medicine (Berry et al., 2012). In short, apneas ($\geq$90% reduction in peak nasal pressure) and hypopneas ($\geq$30% reduction in peak nasal pressure) were required to be at least 10 s in duration. Additionally, hypopneas had to be associated with a $\geq$4% desaturation. Arousals and sleep staging were not scored.

Dynamic Loop Gain During Sleep

Loop gain is the dynamic ventilatory drive response that occurs consequent to a reduction in ventilation. We modified an established method to estimate loop gain during sleep (Terrill et al., 2015). The method involved (1) extracting scored respiratory events, and (2) generating a ventilation signal (tidal volume $\times$ respiratory rate, uncalibrated) based on the overnight airflow signal (nasal pressure, linearized). For each window of data (3 min, modified from the usual 7 min to fit the faster cycling of hypoxia-induced CSA), ventilation data were used to model (i.e., explain) future values of ventilatory drive, where ventilatory drive was considered to be equal to ventilation between events (during central apneas ventilatory drive was considered to be subthreshold; i.e., late in the apnea, chemical drive increases and passes zero at the point of central apnea cessation). Using this approach, the average dynamic loop gain was calculated (for each participant, on each experimental night) by taking the median of the values from each 3 min window.

Venous Blood Sample Collection and Processing

Venous blood samples taken for the measurement of PRA and aldosterone were drawn once in the evening following the ventilatory response tests and once in the morning at least 2 h following administration of the prescribed drug. With oral administration of losartan, PRA levels increase (Goldberg et al., 1993) which we utilized to confirm functional blockade of the AT_1R. Venous blood samples were collected in two 6.0 mL EDTA coated vacutainers. Collected samples were centrifuged at 4°C and separated into 2.0 mL aliquots. The separated plasma was stored in flat top microcentrifuge tubes and stored at −80°C until later analyzed. PRA and aldosterone were assayed by radioimmunoassay techniques and the PRA assessed by measuring the amounts of ANG-I generated per hour.

Statistical Analyses

Drug treatment was assigned using an online randomization tool[1]. All statistical analyses were performed in R statistical language (R Foundation for Statistical Computing, Vienna, Austria), lme4 (Bates et al., 2015), lmerTest (Kuznetsova et al., 2017), and emmeans (Lenth, 2019) statistical packages. Mixed effect linear modeling was used to interrogate all defined relationships and the correlation between loop gain and CSA severity, but not AMS responses. Across all models, participant was considered as a random effect, allowing for variable intercepts for each participant. When a significant F-test was achieved, pairwise comparisons were made with a Tukey's *post hoc* analysis to determine differences between the least square means. Statistical significance was set at a level of $P < 0.05$. A Mann–Whitney *U*-test was run on the AMS scores to detect differences in responses based on drug. With the exception of AMS scores and ESQ-Cerebral Symptoms Questionnaire (presented as medians and interquartile range [IQR]) data are presented as means ± SEM.

[1] www.random.org

RESULTS

Participants

Due to technical and logistical limitations, three HCVR tests were excluded from analysis. An additional subject had less than 2 h of recorded sleep on their experimental night. While taking losartan, two participants developed symptoms of AMS, including nausea and vomiting, causing them to withdraw from further study. Both recovered within a few hours. Despite this, the Lake Louise AMS Score (losartan: 2.5 [3.2] (median [IQR], placebo: 3.5 [3.0]; $P = 0.3$) and ESQ-Cerebral Symptoms Questionnaire (losartan: 3.5 [13.0], placebo: 5.5 [10.2]; $P = 0.3$) did not differ between treatments. **Figure 1** illustrates the flow of participants through the chemosensitivity tests and the sample sizes used for statistical analysis.

All participants showed normal pulmonary function [forced vital capacity (FVC) = 105 ± 3% predicted, forced expiratory volume in 1 s (FEV_1) = 97 ± 3% predicted, FEV_1/FVC = 93 ± 1% predicted], had a body mass index of 24.6 ± 1.1 kg/m^2, and were 25 ± 2 years. Participants did not suffer from undiagnosed sleep disordered breathing (AHI = 2.0 ± 0.5, ODI = 0.9 ± 0.3 events/hour), were not taking any additional medications and were normotensive (SBP = 119 ± 2, DBP = 67 ± 2 mmHg).

Influence of AT_1R Blockade on Hypoxia-Induced CSA and Loop Gain

Sleep time did not differ between losartan and placebo (losartan: 363 ± 26; placebo: 324 ± 16 min, $P = 0.2$). Additionally, we observed similar ODI (losartan: 78 ± 12; placebo: 81 ± 14 events/hour, $P = 0.7$), AHI (losartan: 75 ± 14; placebo: 73 ± 15 events/hour, $P = 0.9$), average oxyhemoglobin desaturation (losartan: 9.5 ± 0.9; placebo: 8.9 ± 1.0%, $P = 0.3$), and nadir SpO_2 (losartan: 61.3 ± 1.2; placebo: 60.5 ± 1.7%, $P = 0.7$) between losartan and placebo. Loop gain was similar between treatments (losartan: 0.88 ± 0.05, placebo: 0.88 ± 0.06 arbitrary units; $P = 0.2$). There was a strong correlation present between loop gain and AHI ($r = 0.93$, $P < 0.001$; see **Figure 2**) while loop gain was moderately correlated with ODI ($r = 0.63$, $P = 0.02$).

Influence of AT_1R Blockade on Resting Cardiorespiratory Parameters Before and After Normobaric Hypoxia

As anticipated, $P_{ET}O_2$ was higher following sleep in the hypoxic chamber (90.7 ± 1.1 and 97.3 ± 1.1 mmHg, $P < 0.001$) while $P_{ET}CO_2$ fell (40.4 ± 0.6 and 36.3 ± 0.6 mmHg, $P < 0.001$). Alveolar ventilation was elevated in the post-test compared with the pre-test (5.4 ± 0.3 and 6.4 ± 0.3 l/min, $P < 0.05$) but was not influenced by drug (losartan: 5.9 ± 0.3, placebo: 6.1 ± 0.6; $P = 0.8$). Both $P_{ET}O_2$ (losartan: 93.4 ± 1.0, placebo: 94.6 ± 1.0 mmHg, $P = 0.03$) and $P_{ET}CO_2$ (losartan: 38.0 ± 0.5, placebo: 38.7 ± 0.5 mmHg, $P = 0.05$) were similar between drug treatments.

Although we observed a drug by condition interaction for SBP ($P = 0.02$), *post hoc* analysis did not reveal any pairwise differences. Losartan did not influence DBP (losartan: 63 ± 1, placebo: 65 ± 1 mmHg), mean arterial pressure (MAP) (losartan:

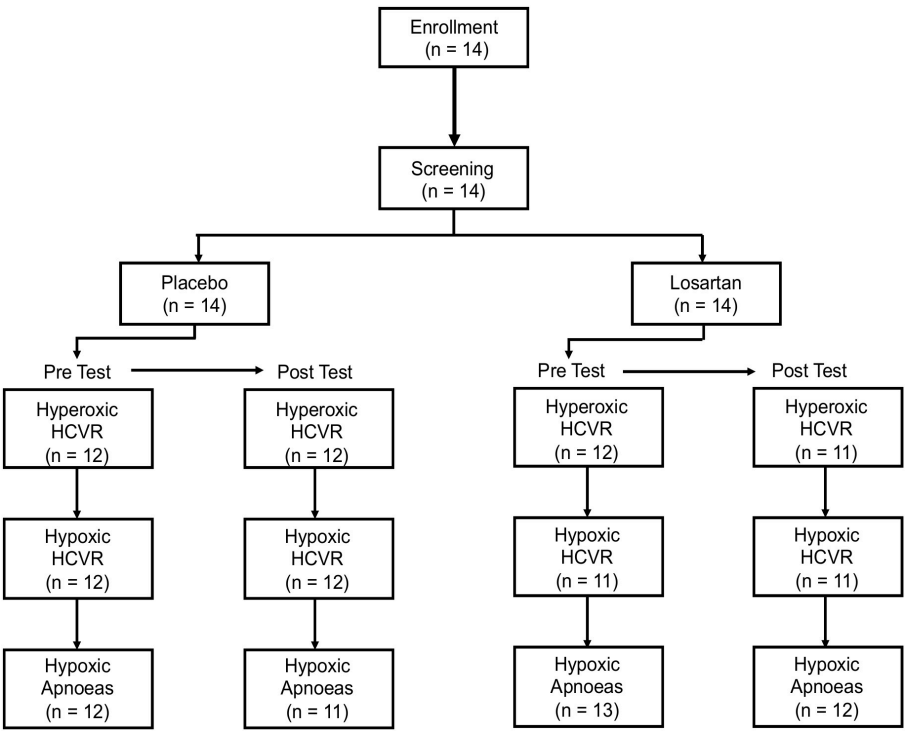

FIGURE 1 | Participant flow chart.

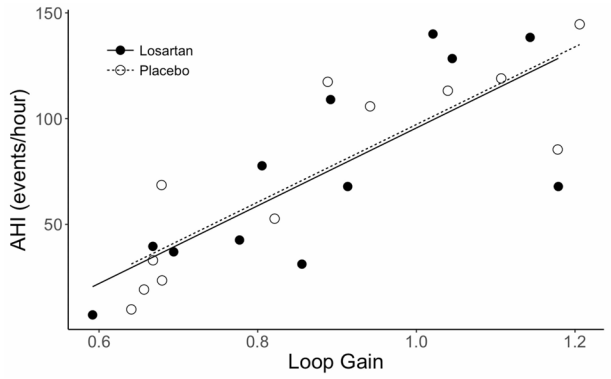

FIGURE 2 | Correlation between AHI and loop gain during sleep in normobaric hypoxia. AHI, apnea hypopnea index. Lines fit to data are based on a mixed effects linear model which accounts for correlation between subjects. The correlation coefficient (*r*) is 0.93, $P < 0.001$.

81 ± 1, placebo: 83 ± 2 mmHg), or HR (losartan: 63 ± 2, placebo: 63 ± 2 bpm; $P > 0.05$ for all comparisons). Similarly, DBP (63 ± 2, post: 65 ± 2 mmHg), MAP (pre: 81 ± 2, post: 83 ± 2 mmHg), and HR (pre: 62 ± 2, post: 63 ± 2) did not differ between the pre- and post-tests ($P > 0.1$ for all conditions).

Influence of AT_1R Blockade and Normobaric Hypoxia on the HCVR Test

Figure 3 shows mean data, isometabolic hyperbola, and mixed effect linear models illustrating the hyperoxic and hypoxic HCVR before and after 8 h of nocturnal hypoxia for losartan and placebo. As expected, the HCVR was significantly greater in hypoxia (5.3 ± 1.1 l/min/mmHg) compared with hyperoxia (3.6 ± 0.6 l/min/mmHg; $P = 0.02$). There was no significant difference to the HCVR following 8 h of sleep in normobaric hypoxia (5.0 ± 0.5 and 6.2 ± 0.5 l/min/mmHg, $P = 0.7$). Detailed results for these tests are presented in the following two sections.

Hyperoxic HCVR Test

The hyperoxic HCVR (**Figure 3A**) was similar in both losartan and placebo conditions during the pre- (3.9 ± 1.1 and 3.5 ± 0.5 l/min, respectively; $P = 0.9$) and post-tests (3.4 ± 0.5 and 3.6 ± 1.2, respectively; $P = 0.5$), and did not differ following poikilocapnic normobaric hypoxia ($P = 0.8$). **Table 1** summarizes cardiorespiratory parameters throughout the hyperoxic HCVR. There was no significant main effect of condition (pre vs. post), or a condition-by-drug-by-$P_{ET}CO_2$ stage interaction across all cardiorespiratory variables. $P_{ET}O_2$ and $P_{ET}CO_2$ were significantly increased from baseline across all stages of the test. A main effect for stage was observed for minute ventilation, which was significantly greater than baseline at all $P_{ET}CO_2$ stages (see **Table 1**). MAP was not affected by drug or condition and increased with each $P_{ET}CO_2$ level (**Table 1**). The HR response was similar between losartan and placebo and increased with $P_{ET}CO_2$ level.

Hypoxic HCVR Test

The hypoxic HCVR (**Figure 3B**) was similar in both losartan and placebo conditions during the pre- (losartan: 5.6 ± 1.5, placebo: 5.4 ± 0.6 l/min; $P = 1.0$) and post-tests (losartan: 5.6 ± 1.5, placebo: 6.4 ± 1.2 l/min/mmHg; $P = 0.9$), and did not differ following poikilocapnic normobaric hypoxia ($P = 0.7$). **Table 2** summarizes the cardiorespiratory parameters throughout the hypoxic HCVR test. There was no significant main effect of condition (pre vs. post), or a condition-by-drug-by-$P_{ET}CO_2$ stage interaction across all cardiorespiratory variables. $P_{ET}O_2$ was slightly lower on losartan (59.7 ± 0.3 and 60.6 ± 0.3 mmHg; $P = 0.03$) and was reduced from baseline across all levels of $P_{ET}CO_2$ by study design. $P_{ET}CO_2$ was increased across each stage of the test, but was slightly lower overall on losartan compared with placebo (41.0 ± 0.8 and 42.2 ± 0.8 mmHg; $P = 0.001$). A main effect for stage was observed for minute ventilation, which was significantly greater than baseline at all $P_{ET}CO_2$ stages (**Table 2**). Neither MAP nor HR were affected by drug or condition, but both increased with each $P_{ET}CO_2$ level (**Table 2**).

Influence of AT_1R Blockade and Normobaric Hypoxia on Hypoxic Apnea Response

Ventilatory Response

During the HAR tests SpO_2 fell to 87 ± 1% and was similar across conditions ($P = 0.10$) and drug ($P = 0.07$). **Figure 4** shows the mean breath-by-breath change in ventilatory variables, ensemble averaged across all 6 hypoxic apneas. All ventilatory parameters were significantly elevated from baseline during the first breath following apnea cessation with the exception of breathing frequency which was significantly higher following exposure to normobaric hypoxia (20.9 ± 1.5 and 18.7 ± 1.4 bpm; $P = 0.03$). Losartan attenuated breathing frequency following normobaric hypoxia during the post-test (11.3 ± 1.2 and 12.4 ± 1.2 bpm; $P = 0.03$) but not during the pre-test (12.0 ± 1.1 and 11.9 ± 1.2 bpm; $P = 0.5$). Tidal volume and breathing frequency were similar between conditions.

Cardiovascular Response

Figure 5 displays the change in HR and MAP averaged over six apneas. All parameters increased over the duration of the end expiratory breath hold. The 20 s apnea elicited a similar increase in both HR and MAP between both losartan and placebo conditions. Both drug and condition did not have a significant impact on changes in SBP, DBP, or MAP with respect to percent desaturation as summarized in **Table 3**. There was a trend toward a heightened HR response following sleep in the hypoxic chamber ($P = 0.06$).

Influence of AT_1R Blockade on Markers of the RAS

Angiotensin-I was significantly higher following losartan compared with placebo (8.92 ± 1.32 and 2.94 ± 1.30 ng/mL, $P < 0.001$). Angiotensin-I was also greater following normobaric hypoxia compared with baseline (7.61 ± 1.32 and 4.25 ± 1.30 ng/mL, $P = 0.02$). PRA was elevated by losartan compared with

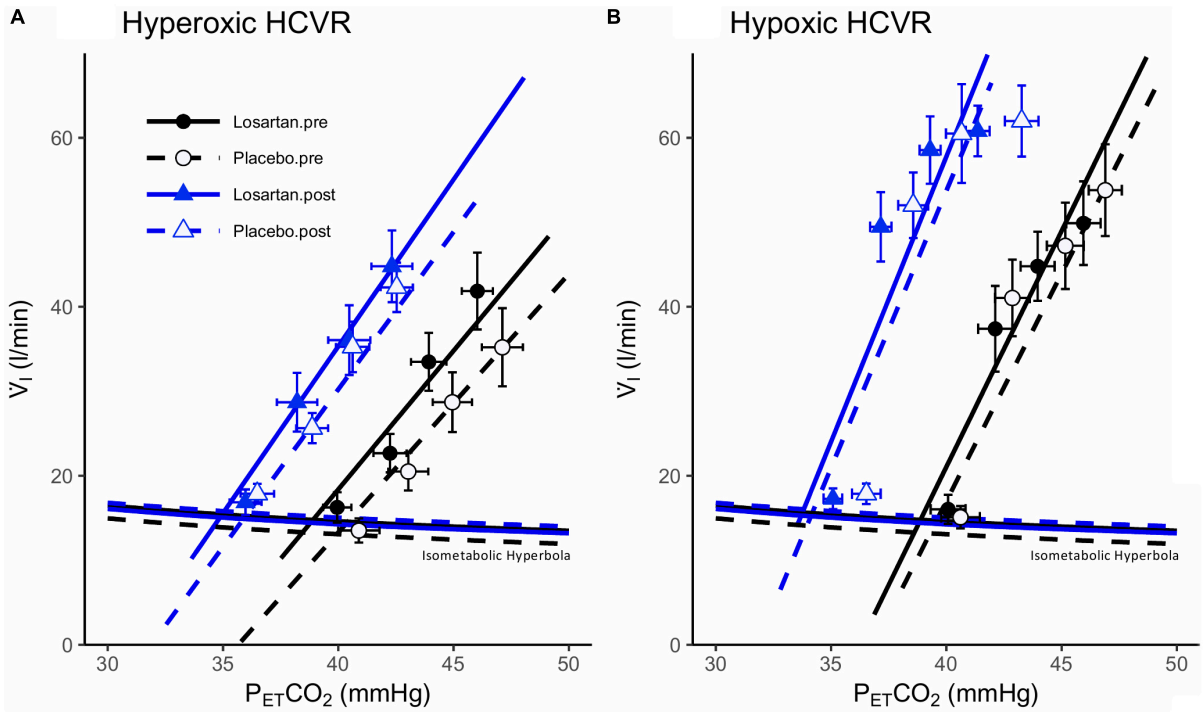

FIGURE 3 | Hypercapnic ventilatory responses during **(A)** hyperoxia and **(B)** hypoxia. Data points are means ± SEM. Lines fit to data using a mixed effects linear model. $\dot{V}_I$, minute ventilation; $P_{ET}CO_2$, end-tidal carbon dioxide.

TABLE 1 | Cardiorespiratory parameters measured during the hyperoxic HCVR test.

	Drug	Baseline $P_{ET}CO_2$		+2 mmHg $P_{ET}CO_2$		+4 mmHg $P_{ET}CO_2$		+6 mmHg $P_{ET}CO_2$	
		Pre	Post	Pre	Post	Pre	Post	Pre	Post
$\dot{V}_I$	Losartan	16 ± 2	17 ± 2	23 ± 2	29 ± 4	34 ± 3	36 ± 4	42 ± 5	45 ± 4
(l/min)	Placebo	14 ± 1	18 ± 1	20 ± 2	26 ± 2	29 ± 3	35 ± 3	35 ± 4	42 ± 3
LSM		18 ± 2		27 ± 2*		37 ± 2*†		45 ± 2*†‡	
				Drug: P = 0.8		***Stage: P < 0.001***		*Drug*Stage: P = 1.0*	
$P_{ET}O_2$	Losartan	91 ± 1	96 ± 2	343 ± 7	353 ± 13	337 ± 3	348 ± 15	339 ± 3	347 ± 16
(mmHg)	Placebo	91 ± 1	99 ± 1	339 ± 4	339 ± 7	346 ± 3	346 ± 2	347 ± 3	345 ± 3
LSM		94 ± 3		343 ± 3*		344 ± 3*		344 ± 3*	
				Drug: P = 0.6		***Stage P < 0.001***		*Drug*Stage: P = 0.3*	
$P_{ET}CO_2$	Losartan	40 ± 1	36 ± 1	42 ± 1	38 ± 1	44 ± 1	41 ± 1	46 ± 1	42 ± 1
(mmHg)	Placebo	41 ± 1	37 ± 1	43 ± 1	39 ± 1	45 ± 1	41 ± 1	47 ± 1	43 ± 1
LSM		38 ± 1		41 ± 1*		43 ± 1*†		45 ± 1*†‡	
				Drug: P = 0.09		***Stage: P < 0.001***		*Drug*Stage: P = 1.0*	
MAP	Losartan	80 ± 1	81 ± 2	84 ± 2	84 ± 2	87 ± 2	86 ± 2	91 ± 2	89 ± 2
(mmHg)	Placebo	83 ± 2	84 ± 2	86 ± 3	87 ± 2	87 ± 3	88 ± 2	90 ± 3	92 ± 3
LSM		82 ± 1		85 ± 1*		87 ± 1*		91 ± 1*†‡	
				Drug: P = 0.6		***Stage: P < 0.001***		*Drug*Stage: P = 0.9*	
HR	Losartan	62 ± 2	64 ± 3	61 ± 2	63 ± 3	64 ± 2	64 ± 3	68 ± 2	70 ± 3
(bpm)	Placebo	63 ± 2	63 ± 2	61 ± 2	60 ± 2	63 ± 2	63 ± 2	66 ± 2	65 ± 2
LSM		63 ± 1		61 ± 1		64 ± 1†		67 ± 1*†‡	
				Drug: P = 0.4		***Stage: P < 0.001***		*Drug*Stage: P = 0.4*	

*All values are mean ± SEM. *Indicates a significant difference from baseline ($p < 0.05$); †significant difference from +2 mmHg ($p < 0.05$); ‡significant difference from +4 mmHg ($p < 0.05$). LSM, least square marginal means for stage; $\dot{V}_I$, minute ventilation; $P_{ET}O_2$, end-tidal oxygen; $P_{ET}CO_2$, end-tidal carbon dioxide; MAP, mean arterial pressure; HR, heart rate. Bolded values indicate significant main effects.*

TABLE 2 | Ventilatory parameters measured during the hypoxic HCVR test.

	Drug	Baseline $P_{ET}CO_2$		+2 mmHg $P_{ET}CO_2$		+4 mmHg $P_{ET}CO_2$		+6 mmHg $P_{ET}CO_2$	
		Pre	Post	Pre	Post	Pre	Post	Pre	Post
$\dot{V}_I$	Losartan	16 ± 2	17 ± 1	37 ± 5	50 ± 4	45 ± 4	59 ± 4	50 ± 5	61 ± 3
(l/min)	Placebo	15 ± 1	18 ± 1	41 ± 5	52 ± 4	47 ± 5	60 ± 5	54 ± 5	62 ± 4
LSM		18 ± 2		47 ± 2*		55 ± 2*†		59 ± 3*†‡	
				Drug: P = 0.3		***Stage: P < 0.001***		*Drug*Stage: P = 0.6*	
$P_{ET}O_2$	Losartan	92 ± 2	96 ± 1	49 ± 1	50 ± 0	49 ± 0	50 ± 0	49 ± 1	49 ± 0
(mmHg)	Placebo	92 ± 2	98 ± 1	50 ± 1	51 ± 1	50 ± 1	50 ± 1	50 ± 1	50 ± 1
LSM		92 ± 1		50 ± 1*		50 ± 0*		49 ± 1*	
				Drug: P = 0.03		***Stage: P < 0.001***		*Drug*Stage: P = 1.0*	
$P_{ET}CO_2$	Losartan	40 ± 1	35 ± 0	42 ± 1	37 ± 1	44 ± 1	39 ± 1	46 ± 1	41 ± 1
(mmHg)	Placebo	41 ± 1	37 ± 1	43 ± 1	39 ± 1	45 ± 1	41 ± 1	47 ± 1	43 ± 1
LSM		39 ± 1		41 ± 1*		43 ± 1*†		45 ± 1*†	
				Drug: P = 0.03		***Stage: P < 0.001***		*Drug*Stage: P = 0.6*	
MAP	Losartan	82 ± 2	86 ± 3	87 ± 3	94 ± 3	90 ± 3	96 ± 3	91 ± 3	99 ± 4
(mmHg)	Placebo	87 ± 3	88 ± 2	94 ± 3	98 ± 2	98 ± 3	99 ± 3	102 ± 4	101 ± 3
LSM		86 ± 1		94 ± 2*		97 ± 2*		99 ± 2*†	
				Drug: P = 0.3		***Stage: P< 0.001***		*Drug*Stage: P = 0.9*	
HR	Losartan	63 ± 2	60 ± 2	77 ± 2	77 ± 2	80 ± 2	82 ± 2	82 ± 2	82 ± 2
(bpm)	Placebo	63 ± 2	60 ± 3	79 ± 2	82 ± 2	82 ± 2	82 ± 2	86 ± 2	88 ± 2
LSM		61 ± 1		78 ± 2*		81 ± 2*		83 ± 2*†	
				Drug: P = 0.7		***Stage: P < 0.001***		*Drug*Stage: P = 0.2*	

*All values are mean ± SEM. *Indicates a significant difference from baseline ($p < 0.05$); †Significant difference from +2 mmHg ($p < 0.05$); ‡significant difference from +4 mmHg ($p < 0.05$). LSM, least mean squares; $\dot{V}_I$, minute ventilation; $P_{ET}O_2$, end-tidal oxygen; $P_{ET}CO_2$, end-tidal carbon dioxide; MAP, mean arterial pressure; HR, heart rate. Bolded values indicate significant main effects.*

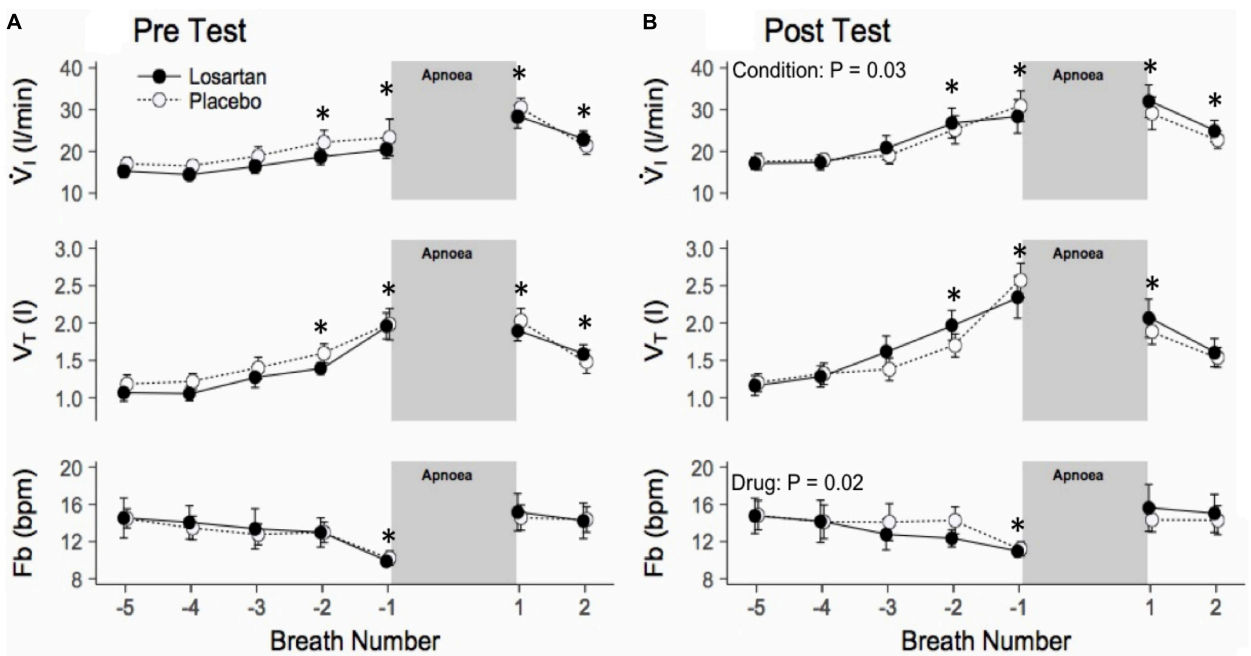

FIGURE 4 | Ensemble averaged breath-by-breath trace of hypoxic apnea response test before **(A)** and after **(B)** normobaric hypoxia. Breath-by-breath trace beginning 5 breaths prior to apnea start. Ventilation is increased prior to the apnea, as participants were asked to take large breaths during nitrogen administration. Values are mean ± SEM. *$P < 0.05$ compared with respective baseline. $\dot{V}_I$, minute ventilation; V_T, tidal volume; Fb, breathing frequency.

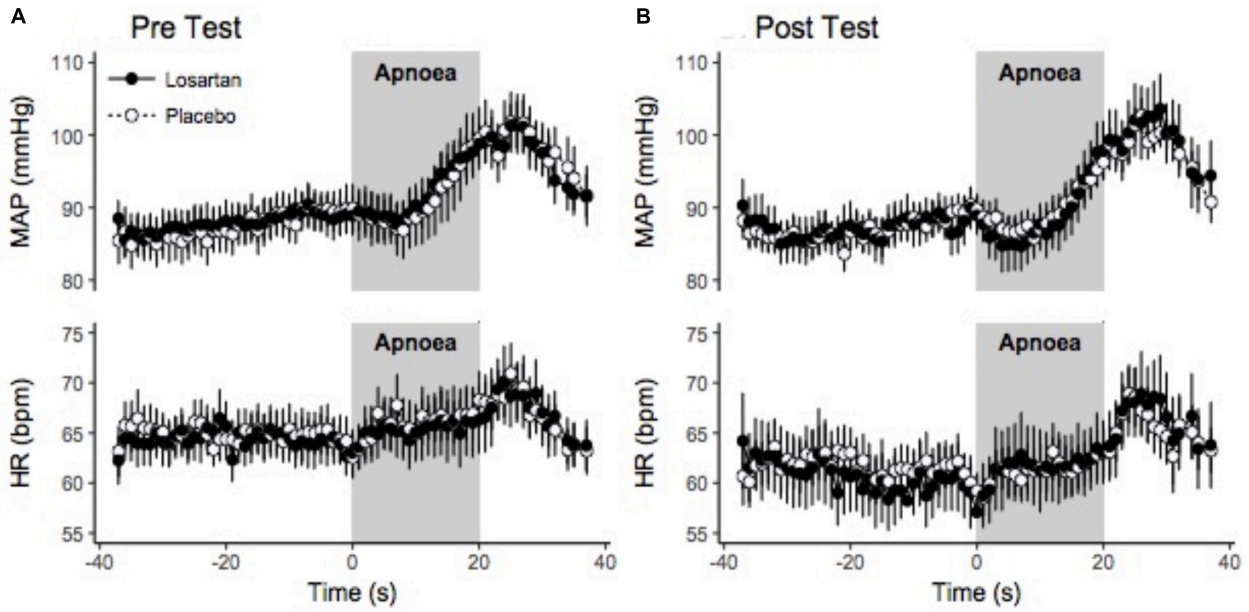

FIGURE 5 | Beat-by-beat ensemble averaged trace of hypoxic apnea response test before **(A)** and after **(B)** normobaric hypoxia. Beat-by-beat trace beginning 30 s prior to apnea start. Values were signal averaged between participants and across the 6 apneas. Values shown are the mean ± SEM. HR, heart rate; MAP, mean arterial pressure.

TABLE 3 | Effect of AT1R blockade on cardiovascular sensitivity to hypoxic apnea before (Pre) and after (Post) 8 h of nocturnal hypoxia.

	Drug	Pre	Post	Drug	Condition	Interaction
$\Delta SBP/\Delta SpO_2$	Losartan	3.1 ± 0.6	3.6 ± 0.7	$P = 0.22$	$P = 0.90$	$P = 0.28$
(mmHg/%desaturation)	Placebo	3.1 ± 0.6	2.4 ± 0.6			
$\Delta DBP/\Delta SpO_2$	Losartan	2.3 ± 0.4	2.9 ± 0.5	$P = 0.60$	$P = 0.30$	$P = 0.23$
(mmHg/%desaturation)	Placebo	2.5 ± 0.4	2.2 ± 0.5			
$\Delta MAP/\Delta SpO_2$	Losartan	2.5 ± 0.5	3.1 ± 0.7	$P = 0.43$	$P = 0.98$	$P = 0.24$
(mmHg/%desaturation)	Placebo	2.7 ± 0.5	2.1 ± 0.4			
$\Delta HR/\Delta SpO_2$	Losartan	1.6 ± 0.3	2.5 ± 0.4	$P = 0.42$	$P = 0.06$	$P = 0.14$
(bpm/%desaturation)	Placebo	1.8 ± 0.3	1.9 ± 0.3			

All values are mean ± SEM. ΔSpO_2, % of oxyhemoglobin desaturation; ΔSBP, change in systolic blood pressure; ΔDBP, change in diastolic blood pressure; ΔMAP, change in mean arterial pressure; ΔHR, change in heart rate.

placebo (0.83 ± 0.12 and 0.27 ± 0.12 ng/l/s, $P < 0.001$) and following the sleep in the hypoxic chamber (0.70 ± 0.12 and 0.39 ± 0.12 ng/l/s, respectively, $P = 0.01$). Although aldosterone was higher following normobaric hypoxia compared with baseline (135.8 ± 14.6 and 78.1 ± 14.3 pmol/l, respectively; $P < 0.01$), it was reduced by losartan compared with placebo (76.3 ± 14.6 and 137.5 ± 14.3 pmol/l, $P < 0.01$).

DISCUSSION

The purpose of this study was to determine if AT_1R blockade would attenuate (1) the chemoreceptor reflex to CO_2 and voluntary hypoxic apnea before or after 8 h of nocturnal hypoxia, and (2) the severity of hypoxia-induced CSA through reductions in loop gain. We observed similar ventilatory response to hypercapnia and cardiorespiratory responses to voluntary hypoxic apneas between losartan and placebo before and after nocturnal hypoxia. Additionally, the severity of hypoxia-induced CSA and loop gain was unaffected by AT_1R blockade. Our data suggests that in healthy, young males the chemoreceptor reflex and the severity of hypoxia-induced CSA occurs through a pathway independent of the AT_1R and local RAS. Upregulation of the AT_1R through pathology (e.g., heart failure) or chronic hypoxia may be required before functional changes in the chemoreceptor reflex are observed following AT_1R blockade.

Influence of AT_1R Blockade on the Hypercapnic and Voluntary Hypoxic Apnea Chemoreceptor Reflex Before and Following Nocturnal Hypoxia

The AT_1R is highly expressed in animal carotid body glomus cells and brain regions involved in cardiorespiratory control

including the nucleus tractus solitarius, subfornical organ, median preoptic nucleus, paraventricular nucleus, and rostral ventrolateral medulla (Dampney et al., 2002; Gao et al., 2005; Saxena et al., 2015; Wang et al., 2016; Shell et al., 2019). Activation of AT_1R by ANG-II in these regions are implicated in the long-term facilitation of the carotid body and the sympathetic nervous system following exposure to intermittent hypoxia (Roy et al., 2018). Additionally, carotid body sensitivity is severely attenuated by losartan in the isolated carotid body preparation (Roy et al., 2018). However, we found the chemoreceptor reflex to hypercapnia and hypoxic hypercapnia to be similar between placebo and losartan which may reflect minimal AT_1R expression and involvement in chemoreflex modulation in the healthy human. Indeed, our results corroborate those of Foster et al. (2010) who observed no effect of losartan on ventilatory and MAP responses to hypoxia and those of Solaiman et al. (2014) who found no effect of ANG-II infusion in potentiating the ventilatory response to hypoxia or hypercapnia in healthy humans.

Hypoxia activates the carotid body leading to greater ventilatory drive and chemoreceptor reflex sensitivity (Allen, 1998; Marcus et al., 2010). The mechanisms responsible for hypoxic mediated plasticity of the chemoreceptor reflex are not well understood. In rats, carotid body AT_1R expression was doubled following 4 weeks of chronic hypoxia (10% O_2) and the carotid body's sensitivity to ANG-II was enhanced but could be blocked by losartan (Leung et al., 2000). These data support a role of the AT_1R in mediating carotid body neuroplasticity in response to hypoxia. In addition, carotid body angiotensin converting enzyme activity is doubled following 7 days of hypoxia supporting the presence of a local RAS (Lam et al., 2004). In contrast, we exposed healthy humans to 8 h of continuous hypoxia during sleep which led to minimal chemoreceptor reflex alteration as evidenced by the insignificant change in the hypoxic and hyperoxic HCVR. We observed evidence of augmented chemoreflex drive following 8 h of hypoxia including greater alveolar ventilation, $P_{ET}O_2$, and reduced $P_{ET}CO_2$. However, hyperoxic and hypoxic chemoreceptor reflex sensitivity were similar following 8 h of hypoxia and losartan did not modulate chemoreflex sensitivity indicating that AT_1Rs may not contribute to changes in chemoreflex sensitivity, in healthy young males, following a single night of hypoxia.

Losartan is able to effectively attenuate the increase in sympathetic nerve activity and oxidative stress following both sustained and intermittent hypoxia (Leung et al., 2000; Marcus et al., 2010; Pialoux et al., 2011; Jouett et al., 2017). In rats exposed to 28 days of chronic intermittent hypoxia, the lumbar sympathetic nerve activity response to 20 s apneas was attenuated by losartan (Marcus et al., 2010). The exaggerated lumbar sympathetic and MAP responses to breath hold following chronic intermittent hypoxia were attenuated by losartan, an effect likely mediated by blunted upregulation of AT_1R expression on the carotid body (Marcus et al., 2010). In contrast, losartan does not influence the ventilatory response to step changes in normocapnic hypoxia in patients with OSA (Morgan et al., 2018). In agreement with our findings, this indicates an alternative mechanism involved in chemoreceptor sensitization that is independent of the AT_1R. For example, heart failure models suggest a reduction in carotid body blood flow is necessary to reduce neural nitric oxide synthase expression while elevating carotid body AT_1R expression and ANG-II concentration (Li and Schultz, 2006). Until upregulation of the AT_1R occurs in animal models of congestive heart failure, losartan has no effect on chemosensitivity (Li et al., 2006). Once AT_1Rs are upregulated, losartan is able to abolish the ventilatory and renal sympathetic responses to graded levels of hypoxia (Ding et al., 2011). Therefore, the AT_1R may determine hypoxic chemoreceptor sensitivity in pathological states such as heart failure rather than in healthy humans acclimating to acute hypoxia.

There is limited data regarding chemosensitive signaling mechanisms within the human carotid body. In a previous human study, ANG-II infusion did not potentiate the ventilatory response to hypoxia or hypercapnia further suggesting that the AT_1R may not play a role in chemosensitivity in healthy subjects (Solaiman et al., 2014). Supporting this, existing data suggests some similarities as well as species differences with respect to carotid body oxygen sensing and reactive oxygen species (ROS) generation. Similar to animal models, the human carotid body releases acetylcholine and ATP in response to hypoxia and expresses haemoxygenase-2, NADPH oxidase (NOX-2), AMP activated protein kinase (AMPK), and oxygen sensitive K^+ channels (Fagerlund et al., 2010; Mkrtchian et al., 2012; Kåhlin et al., 2014). However, there are also important differences from mice such as the presence of hydrogen sulfide (H_2S) synthesizing enzyme cystathione-γ-lyase and absence of TASK-3 channels in human carotid bodies (Mkrtchian et al., 2012). Despite these known species differences, there remains no evidence within the literature for the local expression of AT_1Rs or the components of a RAS in the human carotid body.

Influence of AT_1R Blockade on Loop Gain and the Severity of Hypoxia Induced CSA

Elevated loop gain contributes to OSA severity and a high controller gain (mostly measured during wakefulness) is associated with CSA in healthy humans at high altitude, in idiopathic CSA (Ainslie et al., 2013; Terrill et al., 2015), and in patients with heart failure (Solin et al., 2000; Javaheri, 2006). Notably, loop gain during sleep, measured using dynamic application of hypoxic-hypercapnia is remarkably similar to values during wakefulness (Messineo et al., 2018). Thus, individuals with high chemoreflex sensitivity likely suffer from worse CSA severity (Messineo et al., 2018). Our findings support this idea, demonstrating a strong relationship between dynamic loop gain measured during sleep and hypoxia-induced CSA severity (r = 0.93). Likewise, interventions that reduce loop gain (acetazolamide, supplemental oxygen) are associated with attenuated central and obstructive sleep apnea severity (Javaheri, 2006; Edwards et al., 2012). In animals, losartan attenuates

chemosensitivity, a key contributor to loop gain, which we postulated would reduce CSA severity (Marcus et al., 2010; Ding et al., 2011; Roy et al., 2018). However, we did not observe differences between placebo and losartan for any indices of CSA severity. Similarly, Lombardi et al. (2013) did not find an effect of telmisartan, another AT_1R antagonist, on the severity of high-altitude CSA during sojourn to 5400 m. This effect is most likely explained by the lack of drug effect on chemosensitivity.

LIMITATIONS AND CONCLUSION

Limitations

The AT_1R block may have had a limited effect at baseline due to relatively low RAS activity in our participants. Jones et al. (2007) found that baseline PRA levels are correlated with changes in PRA 24 h following administration of an AT_1R blockade in healthy volunteers. Participants with the lowest resting PRA levels experienced the smallest increases in PRA following oral administration of the drugs, indicating that AT_1R blockade has a smaller effect in those that do not have an already upregulated RAS (Jones et al., 2007). However, we found no relationship between changes in PRA and the HCVR. It may be that an upregulated RAS is first necessary for an AT_1R blockade to have a potent effect on chemosensitivity and sympathetic activity (Li et al., 2006).

A larger dose or dosing period of losartan may have led to different results. At baseline, participants had already received two 50 mg doses of losartan, 10 and 2 h prior to experimentation. We observed significant increases in PRA suggesting functional AT_1R blockade, although this response was variable amongst participants. Previously, Foster et al. (2010) found that 4 days of losartan (100 mg) blocked the hypertensive response induced by 6 h of intermittent hypoxia. Another human study investigating long-term facilitation of sympathetic nerve activity induced by intermittent hypoxia found that a single 100 mg dose of losartan 1 h prior to experimentation was sufficient to abolish this response. This effect is also believed to be a function of AT_1R activation within the carotid body. Considering these two extremes, the dosing protocol used in this study should have been adequate to detect any significant physiological outcomes.

We may not have seen a potentiation in chemosensitivity following nocturnal hypoxia because of the time of day the chemoreceptor reflex was measured. Chemoreceptor reflex sensitivity is affected by circadian rhythms independent of changes in metabolic rate (Stephenson et al., 2000). Although basal ventilation remains constant, the chemoreceptor reflex response to hypercapnia is heightened at night and attenuated during the day. This may explain why we did not see a greater difference in the chemoreflex response following exposure to nocturnal hypoxia. Since all participants performed both placebo and treatment arms of this study, diurnal variations in chemoreceptor sensitivity would not have influenced the effect of losartan on ventilatory response to hypercapnia or apnea.

Conclusion

The current study examined whether AT_1R blockade attenuates chemoreceptor reflex sensitivity, loop gain, and CSA severity in healthy, young males using a model of nocturnal hypoxia. We found that losartan did not influence chemoreceptor reflex sensitivity, loop gain, or the severity of CSA. Interestingly, we observed a strong relationship between dynamic loop gain measured during sleep and the severity of hypoxia-induced CSA, consistent with the view that the manifest pattern was indeed chemoreflex driven as intended. Overall, our data show that activation of the AT_1R does not contribute to the chemoreceptor response to hypercapnia including its central and peripheral contributions, before or after a single night of sustained hypoxia in healthy males. It remains feasible that the AT_1R may contribute to chemoreceptor reflex sensitivity in pathological states such as heart failure, obstructive sleep apnea, or following chronic hypoxia.

DATA AVAILABILITY STATEMENT

The datasets generated for this study are available on request to the corresponding author.

ETHICS STATEMENT

This study involving human participants was reviewed and approved by Clinical Research Ethics Board, University of British Columbia. The participants provided their written informed consent to participate in this study.

AUTHOR CONTRIBUTIONS

CB, RW, SS, and GF: study design. CB, LB, TV, and GF: data collection. CB, LB, SS, and GF: data analysis. All authors: Interpretation, drafting and approval of the manuscript.

FUNDING

This work was supported by the Natural Sciences and Engineering Research Council of Canada (NSERC) Discovery Grant (GF), Heart and Stroke Foundation of Canada Grant-in-aid (GF, NA, and JF), Canada Foundation for Innovation (GF), Canadian Institute of Health Research (RW). GF was a Michael Smith Foundation for Health Research Scholar. LB was funded by a Canada Graduate Scholarship - Doctoral from NSERC. SS was supported by the American Heart Association (15SDG25890059).

ACKNOWLEDGMENTS

Analytical assistance by Amanda Vallance is gratefully acknowledged.

REFERENCES

Aaron, E. A., and Powell, F. L. (1993). Effect of chronic hypoxia on hypoxic ventilatory response in awake rats. *J. Appl. Physiol.* 74, 1635–1640. doi: 10.1152/jappl.1993.74.4.1635

Ainslie, P. N., Lucas, S. J. E., and Burgess, K. R. (2013). Breathing and sleep at high altitude. *Respir. Physiol. Neurobiol.* 188, 233–256. doi: 10.1016/j.resp.2013.05.020

Allen, A. M. (1998). Angiotensin AT1 receptor-mediated excitation of rat carotid body chemoreceptor afferent activity. *J. Physiol.* 510, 773–781. doi: 10.1111/j.1469-7793.1998.773bj.x

Bates, D., Mächler, M., Bolker, B. M., and Walker, S. C. (2015). Fitting linear mixed-effects models using lme4. *J. Stat. Softw.* 67, 1–48. doi: 10.18637/jss.v067.i01

Behan, M., Zabka, A. G., Thomas, C. F., and Mitchell, G. S. (2003). Sex steroid hormones and the neural control of breathing. *Respir. Physiol. Neurobiol.* 136, 249–263.

Beidleman, B. A., Muza, S. R., Fulco, C. S., Rock, P. B., and Cymerman, A. (2007). Validation of a shortened electronic version of the environmental symptoms questionnaire. *High Alt. Med. Biol.* 8, 192–199. doi: 10.1089/ham.2007.1016

Berry, R. B., Budhiraja, R., Gottlieb, D. J., Gozal, D., Iber, C., Kapur, V. K., et al. (2012). Rules for scoring respiratory events in sleep: update of the 2007 AASM manual for the scoring of sleep and associated events. *J. Clin. Sleep Med.* 8, 597–619. doi: 10.5664/jcsm.2172

Dampney, R. A. L., Fontes, M. A. P., Hirooka, Y., Horiuchi, J., Potts, P. D., and Tagawa, T. (2002). Role of angiotensin II receptors in the regulation of vasomotor neurons in the ventrolateral medulla. *Clin. Exp. Pharmacol. Physiol.* 29, 467–472. doi: 10.1046/j.1440-1681.2002.03658.x

Ding, Y., Li, Y. L., and Schultz, H. D. (2011). Role of blood flow in carotid body chemoreflex function in heart failure. *J. Physiol.* 589, 245–258. doi: 10.1113/jphysiol.2010.200584

Duffin, J. (2007). Measuring the ventilatory response to hypoxia. *J. Physiol.* 584, 285–293. doi: 10.1113/jphysiol.2007.138883

Edwards, B. A., Sands, S. A., Eckert, D. J., White, D. P., Butler, J. P., Owens, R. L., et al. (2012). Acetazolamide improves loop gain but not the other physiological traits causing obstructive sleep apnoea. *J. Physiol.* 590, 1199–1211. doi: 10.1113/jphysiol.2011.223925

Fagerlund, M. J., Kåhlin, J., Ebberyd, A., Schulte, G., Mkrtchian, S., and Eriksson, L. I. (2010). The human carotid body: expression of oxygen sensing and signaling genes of relevance for anesthesia. *Anesthesiology* 113, 1270–1279. doi: 10.1097/ALN.0b013e318fac061

Foster, G. E., Hanly, P. J., Ahmed, S. B., Beaudin, A. E., Pialoux, V., and Poulin, M. J. (2010). Intermittent hypoxia increases arterial blood pressure in humans through a renin-angiotensin system-dependent mechanism. *Hypertension* 56, 369–377. doi: 10.1161/HYPERTENSIONAHA.110.152108

Gao, L., Wang, W., Li, Y.-L., Schultz, H. D., Liu, D., Cornish, K. G., et al. (2005). Sympathoexcitation by central ANG II: roles for AT 1 receptor upregulation and NAD(P)H oxidase in RVLM. *Am. J. Physiol. Heart Circ. Physiol.* 288, H2271–H2279. doi: 10.1152/ajpheart.00949.2004

Goldberg, M. R., Tanaka, W., Barchowsky, A., Bradstreet, T. E., McCrea, J., Lo, M. W., et al. (1993). Effects of losartan on blood pressure, plasma renin activity, and angiotensin II in volunteers. *Hypertension* 21, 704–713. doi: 10.1161/01.HYP.21.5.704

Hart, E. C. J., and Charkoudian, N. (2014). Sympathetic neural regulation of blood pressure: influences of sex and aging. *Physiology* 29, 8–15. doi: 10.1152/physiol.00031.2013

Javaheri, S. (2006). Acetazolamide improves central sleep apnea in heart failure: a double-blind, prospective study. *Am. J. Respir. Crit. Care Med.* 173, 234–237. doi: 10.1164/rccm.200507-1035OC

Jones, M. R., Sealey, J. E., and Laragh, J. H. (2007). Effects of angiotensin receptor blockers on ambulatory plasma renin activity in healthy, normal subjects during unrestricted sodium intake. *Am. J. Hypertens.* 20, 907–916. doi: 10.1016/j.amjhyper.2007.04.009

Jouett, N. P., Moralez, G., Raven, P. B., and Smith, M. L. (2017). Losartan reduces the immediate and sustained increases in muscle sympathetic nerve activity after hyperacute intermittent hypoxia. *J. Appl. Physiol.* 122, 884–892. doi: 10.1152/japplphysiol.00683.2016

Kåhlin, J., Mkrtchian, S., Ebberyd, A., Hammarstedt-Nordenvall, L., Nordlander, B., Yoshitake, T., et al. (2014). The human carotid body releases acetylcholine, ATP and cytokines during hypoxia. *Exp. Physiol.* 99, 1089–1098. doi: 10.1113/expphysiol.2014.078873

Kuznetsova, A., Brockhoff, P. B., and Christensen, R. H. B. (2017). lmerTest package: tests in linear mixed effects models. *J. Stat. Softw.* 82, 1–26. doi: 10.18637/jss.v082.i13

Lam, S. Y., Fung, M. L., and Leung, P. S. (2004). Regulation of the angiotensin-converting enzyme activity by a time-course hypoxia in the carotid body. *J. Appl. Physiol.* 96, 809–813. doi: 10.1152/japplphysiol.00684.2003

Lam, S. Y., and Leung, P. S. (2003). Chronic hypoxia activates a local angiotensin-generating system in rat carotid body. *Mol. Cell. Endocrinol.* 203, 147–153. doi: 10.1016/S0303-7207(03)00087-X

Lenth, R. (2019). *emmeans: Estimated Marginal Means, aka Least-Squares Means, R package version 1.4.3.01*. Available online at: https://CRAN.R-project.org/package=emmeans

Leung, P. S., Lam, S. Y., and Fung, M. L. (2000). Chronic hypoxia upregulates the expression and function of AT(1) receptor in rat carotid body. *J. Endocrinol.* 167, 517–524.

Li, Y., Xia, X., Zheng, H., Gao, L., Li, Y., and Liu, D. (2006). Angiotensin II enhances carotid body chemoreflex control of sympathetic outflow in chronic heart failure rabbits. *Cardiovasc. Res.* 71, 129–138. doi: 10.1016/j.cardiores.2006.03.017

Li, Y.-L., and Schultz, H. D. (2006). Enhanced sensitivity of Kv channels to hypoxia in the rabbit carotid body in heart failure: role of angiotensin II. *J. Physiol.* 575, 215–227. doi: 10.1113/jphysiol.2006.110700

Lombardi, C., Meriggi, P., Agostoni, P., Faini, A., Bilo, G., Revera, M., et al. (2013). High-altitude hypoxia and periodic breathing during sleep: gender-related differences. *J. Sleep Res.* 22, 322–330. doi: 10.1111/jsr.12012

Marcus, N. J., Li, Y.-L., Bird, C. E., Schultz, H. D., and Morgan, B. J. (2010). Chronic intermittent hypoxia augments chemoreflex control of sympathetic activity: role of the angiotensin II type 1 receptor. *Respir. Physiol. Neurobiol.* 171, 36–45. doi: 10.1016/j.resp.2010.02.003

Messineo, L., Taranto-Montemurro, L., Azarbarzin, A., Oliveira Marques, M. D., Calianese, N., White, D. P., et al. (2018). Breath-holding as a means to estimate the loop gain contribution to obstructive sleep apnoea. *J. Physiol.* 596, 4043–4056. doi: 10.1113/JP276206

Mkrtchian, S., Kåhlin, J., Ebberyd, A., Gonzalez, C., Sanchez, D., Balbir, A., et al. (2012). The human carotid body transcriptome with focus on oxygen sensing and inflammation – a comparative analysis. *J. Physiol.* 590, 3807–3819. doi: 10.1113/jphysiol.2012.231084

Morgan, B. J., Teodorescu, M., Pegelow, D. F., Jackson, E. R., Schneider, D. L., Plante, D. T., et al. (2018). Effects of losartan and allopurinol on cardiorespiratory regulation in obstructive sleep apnoea. *Exp. Physiol.* 103, 941–955. doi: 10.1113/EP087006

Ohtawa, M., Takayama, F., Saitoh, K., Yoshinaga, T., and Nakashima, M. (1993). Pharmacokinetics and biochemical efficacy after single and multiple oral administration of losartan, an orally active nonpeptide Angiotensin-II receptor antagonist, in humans. *Br. J. Clin. Pharmacol.* 35, 290–297. doi: 10.111/j.1365-2125.1993.tb05696.x

Pialoux, V., Foster, G. E., Ahmed, S. B., Beaudin, A. E., Hanly, P. J., and Poulin, M. J. (2011). Losartan abolishes oxidative stress induced by intermittent hypoxia in humans. *J. Physiol.* 589, 5529–5537. doi: 10.1113/jphysiol.2011.218156

Richard, N. A., Sahota, I. S., Widmer, N., Ferguson, S., Sheel, A. W., and Koehle, M. S. (2014). Acute mountain sickness, chemosensitivity, and cardiorespiratory responses in humans exposed to hypobaric and normobaric hypoxia. *J. Appl. Physiol.* 116, 945–952. doi: 10.1152/japplphysiol.00319.2013

Roach, R. C., Bartsch, P., Oelz, O., and Hackett, P. H. (1993). "The Lake Louise Acute Mountain Sickness Scoring System," in *Hypoxia and Molecular Medicine.*, eds J. R. Sutton, C. S. Houson, and G. COates (Burlington, VT: Queen City Press), 272–274.

Roy, A., Farnham, M. M. J., Derakhshan, F., Pilowsky, P. M., and Wilson, R. J. A. (2018). Acute intermittent hypoxia with concurrent hypercapnia evokes P2X and TRPV1 receptor dependent sensory long-term facilitation in naïve carotid bodies. *J. Physiol.* 596, 3149–3169. doi: 10.1113/JP275001

Saxena, A., Little, J. T., Nedungadi, T. P., and Cunningham, J. T. (2015). Angiotensin II type 1a receptors in subfornical organ contribute towards chronic intermittent hypoxia-associated sustained increase in mean arterial

pressure. *Am. J. Physiol. Heart Circ. Physiol.* 308, H435–H446. doi: 10.1152/ajpheart.00747.2014

Shell, B., Farmer, G. E., Nedungadi, T. P., Wang, L. A., and Marciante, A. B. (2019). Angiotensin type 1a receptors in the median preoptic nucleus support intermittent hypoxia-induced hypertension. *Am. J. Physiol. Integr. Comp. Physiol.* 316, R651–R665.

Sin, D. D., Fitzgerald, F., Parker, J. D., Newton, G., Floras, J. S., and Bradley, T. D. (1999). Risk factors for central and obstructive sleep apnea in 450 men and women with congestive heart failure. *Am. J. Respir. Crit. Care Med.* 160, 1101–1106. doi: 10.1164/ajrccm.160.4.9903020

Solaiman, A. Z., Feehan, R. P., Chabitnoy, A. M., Leuenberger, U. A., and Monahan, K. D. (2014). Ventilatory responses to chemoreflex stimulation are not enhanced by angiotensin II in healthy humans. *Auton. Neurosci.* 183, 72–79. doi: 10.1016/j.autneu.2014.01.010

Solin, P., Roebuck, T., Johns, D. P., Walters, H. E., and Naughton, M. T. (2000). Peripheral and central ventilatory responses in central sleep apnea with and without congestive heart failure. *Am. J. Respir. Crit. Care Med.* 162, 2194–2200. doi: 10.1164/ajrccm.162.6.2002024

Stephenson, R., Mohan, R. M., Duffin, J., Jarsky, T. I. M. M., Mohan, R. M., Duffin, J., et al. (2000). Circadian rhythms in the chemoreflex control of breathing. *Am. J. Physiol. Regul. Integr. Comp. Physiol.* 278, 282–286. doi: 10.1152/ajpregu.2000.278.1R282

Terrill, P. I., Edwards, B. A., Nemati, S., Butler, J. P., Owens, R. L., Eckert, D. J., et al. (2015). Quantifying the ventilatory control contribution to sleep apnoea using polysomnography. *Eur. Respir. J.* 45, 408–418. doi: 10.1183/09031936.00062914

Tymko, M. M., Ainslie, P. N., MacLeod, D. B., Willie, C. K., and Foster, G. E. (2015). End tidal-to-arterial CO_2 and O_2 gas gradients at low- and high-altitude during dynamic end-tidal forcing. *Am. J. Physiol. Regul. Integr. Comp. Physiol.* 308, R895–R906. doi: 10.1152/ajpregu.00425.2014

Tymko, M. M., Hoiland, R. L., Kuca, T., Boulet, L. M., Tremblay, J. C., Pinske, B. K., et al. (2016). Measuring the human ventilatory and cerebral blood flow response to CO_2: a technical consideration for the end-tidal-to-arterial gas gradient. *J. Appl. Physiol.* 120, 282–296. doi: 10.1152/japplphysiol.00787.2015

Wang, H. W., Huang, B. S., White, R. A., Chen, A., Ahmad, M., and Leenen, F. H. H. (2016). Mineralocorticoid and angiotensin II type 1 receptors in the subfornical organ mediate angiotensin II – induced hypothalamic reactive oxygen species and hypertension. *Neuroscience* 329, 112–121. doi: 10.1016/j.neuroscience.2016.04.050

White, D. P. (2005). Pathogenesis of obstructive and central sleep apnea. *Am. J. Respir. Crit. Care Med.* 172, 1363–1370. doi: 10.1164/rccm.200412-1631SO

Conflict of Interest: SS has worked as a consultant for Nox Medical, Merck, and Apnimed; he also received grant support from Apnimed and Prosomnus.

The remaining authors declare that the research was conducted in the absence of any commercial or financial relationships that could be construed as a potential conflict of interest.

frontiers in Neurology

REVIEW
published: 11 June 2020
doi: 10.3389/fneur.2020.00525

Update of Individualized Treatment Strategies for Postural Orthostatic Tachycardia Syndrome in Children

Qingyou Zhang[1,2], *Bowen Xu*[1] *and Junbao Du*[1,3]*

[1] *Department of Pediatrics, Peking University First Hospital, Beijing, China,* [2] *Research Unit of Clinical Diagnosis and Treatment of Pediatric Syncope and Cardiovascular Diseases, Chinese Academy of Medical Sciences, Beijing, China,* [3] *Key Laboratory of Molecular Cardiovascular Sciences, The Ministry of Education, Beijing, China*

Postural orthostatic tachycardia syndrome (POTS) is a heterogeneous disease that predominantly affects children and adolescents. There is a great difference between children and adults in the diagnosis and treatment of POTS patients. POTS in children and adolescents is marked by chronic symptoms of orthostatic intolerance with a heart rate (HR) rise of ≥40 bpm, or heart rate exceeding 130 bpm for 6–12-years-old children and exceeding 125 bpm for those 13–18 years old without orthostatic hypotension, which is different from adult patients. The three major clinical forms of POTS include hypovolemic POTS, neuropathic POTS, and hyperadrenergic POTS; these are distinguished by their major mechanisms. The different subtypes of POTS in children and adolescents each have their own clinical characteristics and biomarkers. Based on these, we propose individualized treatment strategies. Individualized management strategies based on different subtypes of POTS would largely improve the curative effects of drugs for children with POTS. However, a further clinical investigation is still required to better understand the pathophysiology and treatment options.

Keywords: autonomic dysfunction, orthostatic intolerance, postural orthostatic tachycardia syndrome, treatment, children

OPEN ACCESS

Edited by:
Nephtali Marina, University College London, United Kingdom

Reviewed by:
Antonio Roberto Zamunér, Catholic University of Maule, Chile
Moacir Fernandes Godoy, Faculty of Medicine of São José do Rio Preto, Brazil

***Correspondence:**
Junbao Du
junbaodu1@126.com

Specialty section:
This article was submitted to Autonomic Neuroscience, a section of the journal Frontiers in Neurology

Received: *08 January 2020*
Accepted: *13 May 2020*
Published: *11 June 2020*

Citation:
Zhang Q, Xu B and Du J (2020) Update of Individualized Treatment Strategies for Postural Orthostatic Tachycardia Syndrome in Children. Front. Neurol. 11:525. doi: 10.3389/fneur.2020.00525

Postural orthostatic tachycardia syndrome (POTS) is a form of chronic orthostatic intolerance (1). POTS is more common in children than in adults, and most POTS patients develop their symptoms in childhood or adolescence (2, 3). It is increasingly recognized in children (4, 5). However, because of the varying symptoms of POTS in children and adolescents, including cardiovascular, neurologic and gastrointestinal symptoms, it is often misdiagnosed. In recent years, more and more attention has been paid to the diagnosis and treatment of this syndrome (6–9). This review details the characteristics of POTS in pediatric patients.

POTS is a syndrome, not a disease, and features hemodynamic abnormalities of upright position and other symptoms. It results in inability to attend school, take part in physical activities and even the normal activities of daily life. As a result, POTS patients face significant social and economic consequences (9–12), and early diagnosis is crucial to the launch of effective therapy. However, the clinical features of POTS in children and adolescents have not yet been fully summarized (13). Therefore, we reviewed the literature related to pediatric POTS, which provides a broad understanding of the characteristics of this syndrome.

CLINICAL CHARACTERISTIC OF POTS IN PEDIATRIC PATIENTS

POTS is a common disorder of chronic orthostatic intolerance in children. The disorder is characterized by dizziness, palpations, fatigue, headache, chest tightness, abdominal pain, nausea, and even syncope on standing. Although its symptoms are primarily associated with the upright position, some patients report their persistence when they are sitting or lying down. The definition of POTS is that the symptoms of orthostatic intolerance persist at least 6 months, and are accompanied with an increase in heart rate (HR) exceeding 30 bpm (or a rate that exceeds 120 bpm) within 10 min of standing or achieving upright tilt without orthostatic hypotension (>20 mmHg drop in systolic blood pressure) (1–6, 8). However, children and adolescents display different pictures related to their particular types of growth and development. In our previous study, the HR and blood pressure of 1,449 school children (6–18 years old) in China were recorded during active standing. During tests, the HR and BP had significantly changing profiles in children and adolescents, and our group proposed that the diagnosis of POTS in the pediatric population be made when the HR rises by ≥40 beats per minute, or the fastest heart rate of children aged 6–12 exceeded 130 beats per minute, and exceeded 125 beats per minute for adolescents aged 13–18, within 10 min of standing, accompanied by symptoms of orthostatic intolerance (13–15).

POTS predominantly affects females, with the ratio of females to males in adult studies being 4:1 (4, 12, 16). Researchers speculate that menstruation, which features periodic variations in levels of estrogen and progesterone, is related to the incidence of POTS (17). However, in our cohort, the male: female gender ratio was only 1:1.1, since we expected that the impact of menstruation in children would be small (5). POTS can occur throughout adolescence, and the children with POTS were mainly aged between 7 and 14 years in this study, a figure consistent with previous reports from our center (4, 5).

The symptoms of POTS in children and adolescents vary. Common symptoms of our patients include dizziness (84.00%), fatigue (72.00%), orthostatic faint (62.67%), shortness of breath (55.33%), pallor (51.33%), blurred vision (50.00%), hyperhidrosis (43.33%), gastrointestinal difficulties (40.67%), and fatigue (37.33%) (5). Some authors have reported that 30% of their patients have a variety of symptoms (18). Female patients often experience a worsening of symptoms during menstruation.

The numerous co-morbidities of POTS in children have attracted the attention of many researchers. These include chronic fatigue syndrome, sleep disorders, migraines, irritable bowel syndrome or functional dyspepsia, cyclic-vomiting syndrome, fibromyalgia, and Ehlers-Danlos syndrome (6, 18). However, the relationship between these disorders and POTS is still unclear. Many investigators suggest that POTS share the similar mechanisms for the co-morbid disorders. However, some authors have found that no difference can be found in the incidence of those co-morbid conditions in children and adolescents with POTS and those without POTS. They are syndromes which may occur together with POTS, but POTS itself is not a cause of the co-morbidities (19).

Psychiatric disorders including anxiety and depression are associated with POTS in child and adolescent family members of patients, and child patients with POTS often encounter tragic experiences after contracting the illness, with no regular attendance at school and social activities, underachievement, and frequent visits to doctors. They often receive a variety of diagnoses, take multiple drugs, and sometimes even receive surgery.

POTS SUBTYPES IN CHILDREN AND ADOLESCENTS

Based on the mechanisms of potential pathophysiology of POTS, 3 main clinical subtypes of the syndrome have been established: hypovolemic POTS, neuropathic POTS, and hyperadrenergic POTS (20–22). These phenotypes may overlap.

Hypovolemic POTS

Central hypovolemia leads to a decrease in venous return, resulting in an increase of heart rate as compensation. Low blood volumes have been observed in many children and adolescents with POTS (23, 24). In patients with hypovolemia, the abnormal activation of the renin-angiotensin-aldosterone system has been found in children (24–26). Hypovolemia could be observed in nearly 30% of POTS patients, as Thieben et al. estimated (16). In our experience, over fifty percent of children and adolescents with POTS have low blood volume (5). Hypovolemic POTS patients have symptoms, such as obvious weakness and decreased tolerance for exercise. Increasing central blood volume with intravenous fluids or salt supplements can significantly improve these patients' symptoms (23, 27). El-Sayed and Hainsworth found that 24-h urinary sodium was a valuable marker of hypovolemic status (23). According to our research, a 24-h sodium excretion of <124 mmol is a good indicator of the effectiveness of replenishment of blood with salt supplementation in children and adolescents with POTS (27).

Neuropathic POTS

Partial autonomic neuropathy is the characteristics of this subtype of POTS. The main mechanism of this type of POTS is patchy denervation of the sympathetic fibers to the blood vessels in the extremities (28). We found that the incidence of Valsalva maneuver (Valsalva ratio, VR) of <1.5 was 84.72% in our cohort patients with POTS (5). In another study, loss of sweating function of the extremities was found in over 50% of patients with POTS (16). The denervation of the sympathetic fibers to the blood vessels in the extremities might affect their contractile function and cause the pooling of blood in the extremities. When patients stand up, their abnormal vessel tone and pooling in the lower extremities lead to a decrease of returned-blood volume, causing a decrease of cardiac output, and a heart-rate increase in compensation. We also found that some patients with POTS had augmented flow-mediated vasodilation (FMD) of the brachial artery, indicating that an increase of the vasodilation response of the peripheral may lead to the poor blood circulation of the lower extremities when standing, resulting in a decrease of returned-blood volume and symptoms of POTS (29). Severe

venous pooling in the lower extremities is characterized by cyanosis of the feet upon standing in this subtype of POTS children. Many patients report having a history of fever before the onset of disease, likely viral infection, or having a history of surgery, infection or trauma. Therefore, some researchers propose immune pathogenesis of neuropathic POTS (30). We found that 24.39% of patients were positive for antibodies of acetylcholine receptor (AChR-ab). The symptoms of those POTS children were significantly severe and syncope and fatigue were common (31). Other autoimmune antibodies in POTS, such as alpha 1 and/or beta adrenergic-receptor autoimmune antibodies, and angiotensin II Type 1-receptor autoimmune antibodies, were also observed (32, 33). At present, it is considered that neuropathic POTS is a mild autoimmune disorder.

Hyperadrenergic POTS

The definition of hyperadrenergic POTS is a syndrome with an increase of above 10 mmHg in systolic BP within 10 min of standing or tilting, and an upright-position plasma norepinephrin of ≥600 pg/mL (34, 35). In our cohort, 51.28% of children with POTS were hyperadrenergic. These patients manifested with hypertension upon standing, and may complain of lightheadedness, faintness, palpitations, shortness of breath, syncope, tremulousness, headache, fatigue and nausea and vomiting. The most common symptoms of hyperadrenergic POTS in children are dizziness, headache and tremulousness, compared with other types of POTS patients (35). Hyperadrenergic POTS can be caused by norepinephrine transporter deficiency (36), pheochromocytoma, mast-cell-activation disorders (37), and baroreflex failure resulting from trauma to or irradiation of the neck. However, most of the children had not suffered either of these.

TREATMENT APPROACHES (TABLE 1)

Accurate diagnosis is the basis for controlling this disease that excludes true cardiac disorders. The majority of patients with POTS show substantial improvement after proper diagnosis leads to a comprehensive therapeutic regimen being put in place. There are many ways to treat the disease, including drugs and physical therapy.

NON-PHARMACOLOGICAL TREATMENTS

Lowered water intake and shorter sleeping time were identified as POTS risk factors in children and adolescents (45). Health education is an important part of treatment of POTS patients. The basic treatment of the disease is to increase water and salt intake. Most children with POTS need have salt intake of up to 5–6 g. Urine osmolality of <300 mmol/L or 24-h urinary sodium excretion of more than 200 mmol are the goals (46). Good sleep may also be an important consideration, since we found that those getting <8 h of sleep per day were at 5.9 times greater risk of getting POTS than those with sleeping longer than 8 h (45).

Some investigators have found that a regular, short-term progressive physical-exercise program leads to improved symptoms in POTS patients (47). Such a regimen consists of rowing on a machine, swimming, recumbent and upright biking, and treadmill walking. However, one major challenge of successful physical therapy is patient compliance with regular and consistent with the program (6, 48).

Children and adolescents with POTS should be treated using a multidisciplinary approach that includes alternative nutritional, psychological, and drug therapies. Like other researchers, we have found that children with POTS have poor nutrition,

TABLE 1 | The main clinical studies included in the review.

Study group	Methods	No. of patients	Drug	Biomarkers	Outcomes
Lu et al. (38)	Case-control study	35	ORS	MCHC	MCHC >347.5 g/L predicts the effect of ORS for treating POTS
Li et al. (39)	Case-control study	54	ORS	BMI	BMI < 18 kg/m^2 predicts the effect of ORS for treating POTS
Lin et al. (40)	Case-control study	34	Metoprolol	CNP	CNP >32.55 pg/m predicts the effect of metoprolol for treating POTS
Zhang et al. (41)	Case-control study	27	Metoprolol	Orthostatic plasma norepinephrine	Orthostatic plasma norepinephrine level of >3.59 pg/ml predicts the effect of metoprolol for treating POTS
Zhao et al. (42)	Case-control study	33	Midodrine	Copeptin	A plasma copeptin level >10.482 pmol/L predicts the effect of midodrine for treating POTS
Yang et al. (43)	Case-control study	28	Midodrine	Erythrocytic hydrogen sulfide	Erythrocytic hydrogen sulfide production rate >27.1 nmol/min/10^8 erythrocytes predicts the effect of midodrine for treating POTS
Liao et al. (29)	Case-control study	108	Midodrine	FMD	FMD >9.85% predicts the effect of midodrine for treating POTS
Zhang et al. (44)	Case-control study	57	Midodrine	MR-proADM	The plasma concentration of MR-proADM >61.5 pg/ml predicts the effect of midodrine for treating POTS
Zhang et al. (27)	Case-control study	30	Midodrine	24-h urinary sodium excretion	The 24-h urinary sodium excretion <124 mmol predicts the effect of midodrine for treating POTS

POTS, postural orthostatic tachycardia syndrome; ORS, oral rehydration solution; MCHC, mean corpuscular hemoglobin concentration; BMI, body mass index; CNP, C-type natriuretic peptide; FMD, flow-mediated vasodilation; MR-proADM, midregional fragment of pro-adrenomedullin.

including low iron storage (5, 49), vitamin B12 deficiency (50), vitamin B1 deficiency (51), hypovitaminosis D (52), and elevated plasma homocysteine levels (53). Correcting these would be very beneficial to the recovery of patients.

PHARMACOLOGICAL TREATMENTS

There is currently no pharmacologic therapy approved by the FDA for children with POTS. All the medications used to treat POTS in children are "off-label", and most of the studies assessing POTS treatments are not evidence-based. There is lack of drug for POTS in multi-center randomized-control trials (RCT), and longitudinal long-term follow-up data of any medication for POTS are in need (6–9, 54). Wells et al. reported in a systemic review article that only 3 RCTs including 103 patients were studied for medications treatment of POTS in a single center (55). Our center reported that midodrine hydrochloride is effective in the treatment of children with POTS through a small non-blinded randomized controlled study (38). Drug therapy includes fludrocortisones for increasing central blood volume, the peripheral selective alpha-1-adrenergic agonist midodrine to constrict peripheral veins and reduce stagnant venous blood, β-adrenergic blockers, including non-selective propranolol, and cardioselective metoprolol, to decrease standing excessive tachycardia, and the acetylcholinesterase inhibitor pyridostigmine to increase acetylcholine on the autonomic ganglia, thereby enhancing ganglionic neurotransmission, increasing the release of norepinephrine by post-ganglionic sympathetic nerves and potentiating vagal effects upon standing (1, 4, 6, 8). However, the fact that "what works for one patient does not always work for another" was clearly displayed by this POTS patient, as Boris said (9). Wells et al. also pointed out that due to heterogeneity in the pathophysiology underlying POTS, biomarkers may play an incremental role in refining therapy (55). Based on our studies, POTS is a group of heterogeneous ailments caused by multiple sources of pathogenesis. If we could target drugs based on the pathogeneses of individual patients, the curative effects of drugs on children with POTS would be greatly enhanced. Each of the three major subtypes represents a different mechanism, and on this basis we have proposed an individualized-treatment strategy.

TREATMENT OF HYPOVOLEMIC POTS: SALT SUPPLEMENTS, ORAL REHYDRATION AND FLUDROCORTISONE

Hypovolemia can be seen in many POTS patients, and increasing fluids intake is an effective treatment of POTS symptoms. A low concentration of urinary sodium is an indirect marker of hypovolemia (23, 27). Our previous work showed that, compared with the healthy control group, the concentration of 24-h urinary sodium was significantly lower in the POTS patients, and the symptom severity of children with POTS inversely correlated at a significant level with their 24-h urinary-sodium concentrations. Twenty-four hours sodium concentrations of <124 mmol/24 h indicated the effectiveness of salt supplements for treating POTS patients (sensitivity 76.9%; specificity 93%) (27).

Recent studies have found that using oral-rehydration solution (ORS) can conveniently, safely and effectively relieve the symptoms of children with POTS (56). Lu et al. found that among these children, those responding to ORS had a lower baseline mean-corpuscular volume (MCV) and higher mean-corpuscular hemoglobin concentration (MCHC) than non-responders, and that MCHC values are good predictors of ORS therapy for children and adolescents with POTS (39).

Stewart et al. found that, compared with POTS patients with normal blood volumes, the body-mass index (BMI) of POTS patients with hypovolemia was significantly lower. This finding suggests that BMI is related to blood volume (57). Our team found that BMI value lower than 18 kg/m^2 indicated the effectiveness of ORS treatment for POTS children and adolescents (sensitivity 92%; specificity 82.8%). Compared with 24-h sodium concentrations, BMI is a simple and easily measured indicator (58).

Fludrocortisone is a synthetic mineralocorticoid that promotes the reabsorption of sodium and water in the kidneys. Therefore, it can increase plasma volume in patients with POTS (59–61). Theoretically, it can ameliorate the symptoms of hypovolemic POTS. However, compared with a placebo, fludrocortisone was found to be ineffective at relieving the symptoms of patients with neurally-mediated hypotension and chronic-fatigue syndrome in a placebo-controlled randomized trial (62). In another double-blind, placebo-controlled randomized trial, fludrocortisone also did not ameliorate the frequency of syncope in the treatment of vasovagal syncope patients (63). The reason that the drug has not been shown to be effective is non-selective use of it. Fludrocotisone should be used for hypovoleomic patients only. Also, attention should be paid to hypokalemia in the application of flurocortisoneone, since flurocortisone can promote the excretion of potassium. Fludrocortisone increases potassium excretion (59, 60). Fludrocortisone is now in the Heart Rhythm Society (HRS) Expert Consensus Class 2B recommendation for POTS patients (8).

TREATMENT OF NEUROPATHIC POTS: MIDODRINE AND PYRIDOSTIGMINE

In neuropathic POTS, impaired peripheral vasoconstriction caused by adrenergic denervation can lead to peripheral venous pooling (64). Midodrine, an alpha1-adrenergic agonist, can effectively constrict peripheral vessels, and increase venous return. In a small non-blinded RCT, we found that midodrine could improve the symptoms of POTS in children and reduce standing heart rate (38). In order to select the drugs accurately, we seek biomarkers that reflect the presence of peripheral vasoconstriction dysfunction in POTS patients. FMD is an ultrasound technique used to assess blood-vessel elasticity (43). We found that, compared with the control children, baseline FMD increase was significantly greater in children with POTS, and the sensitivity and specificity of FMD at 9.85% as a

cutoff value for predicting the short-term efficacy of midodrine-hydrochloride (1 month) treatment for POTS were 71.6 and 77.8%, respectively (29).

Hydrogen sulfide (H_2S) is an important gaseous intracellular signal transducer. It is involved in the regulation of the cardiovascular system; it plays an important role in the pathogenesis of a variety of heart diseases, and is a novel gasotransmitter in the cardiovascular system (65). Our previous study demonstrated that erythrocytic H_2S could indicate the effectiveness of midodrine hydrochloride for treating POTS patients. The sensitivity and specificity of erythrocytic H_2S production of 27 nmol/min/10^8 erythrocytes as a cutoff value for predicting the effectiveness of midodrine hydrochloride for children with POTS were 78.9 and 77.8%, respectively (44).

Adrenomedullin (ADM) is a potent vasodilator and has peripheral vasorelaxing effects. It is also associated with peripheral vasoconstriction and relaxation. But ADM has a short half-life, and easily adheres non-specifically to cellular surfaces, making its quantification impossible. Therefore, a midregional fragment of pro-adrenomedullin (MR-proADM), which produced quantities equivalent to those of ADM, is more stable than ADM (42). Zhang et al. found that the responders to midodrine hydrochloride in children with POTS had higher plasma levels of MR-proADM. MR-proADM >61.5 pg/ml predicts the efficacy of midodrine-hydrochloride therapy for treating POTS (sensitivity 100% and specificity 71.6%) (66).

Arginine vasopressin (AVP) plays an important role in circulatory and water homoeostasis. Copeptin and arginine vasopressin (AVP) are derived from a common precursor molecule and have equimolar secretion, and copeptin is more stable in plasma than AVP. Our group found that copeptin was also a good biomarker predicting the effectiveness of midodrine hydrochloride in treating children with POTS (67). Midodrine is now in an HRS Class 2B recommendation for the treatment of POTS (8).

Neuropathic POTS is regarded as a restricted autoimmune autonomic ganglionopathy (AAG), associated with auto-antibodies in the ganglionic acetylcholine receptor (30, 31). Along with others, we found that this type of POTS in children and adolescents was associated with positive acetylcholine receptor antibodies (AChR-ab) (16, 31). Pyridostigmine, a peripheral acetylcholinesterase inhibitor, could be used to treat patients with POTS. Its therapeutic mechanism involves increasing synaptic acetylcholine in the autonomic ganglia and functional enhancement of nerve conduction of parasympathetic nervous systems. It has also been shown that pyridostigmine can increase the baroreceptor sensitivity of POTS patients and thereby ameliorate their symptoms (68). In a randomized crossover study, Raj et al. found that pyridostigmine significantly attenuated tachycardia and ameliorated the symptoms of POTS, and in another long-term retrospective study they also found that pyridostigmine could improve the standing heart rate and ameliorated the symptoms of POTS (41, 68). Filler et al. reported that a 16-years-old girl with severe POTS was treated with pyridostigmine, and that after 9 months there were persistent positive effects without additional blood-pressure abnormalities (40). We propose that if a child with POTS is seropositive for AChR-ab, pyridostigmine should be used appropriately. It is in an HRS Class 2B recommendation for the treatment of POTS (8).

TREATMENT OF HYPERADRENERGIC POTS: β-BLOCKERS

The characteristics of hyperadrenergic POTS is an elevated upright plasma norepinephrine levels. This subtype of patients with orthostatic hypertension has posed a great challenge to the traditional treatment of POTS (34, 35). Salt supplements and peripheral vasoconstrictor-midodrine should be used with caution in treating these patients. In the treatment of this type of POTS, β-blockers for blocking β-adrenoceptors are preferred, which could prevent the effect of having excessive catecholamines in the plasma. We found that the severity of symptoms and increments of the heart rate when standing was positively correlated with the plasma norepinephrine levels of patients in upright positions, and compared with non-responders to metoprolol, the upright plasma norepinephrine levels in responders to metoprolol were significantly high. The sensitivity and specificity of an orthostatic plasma-norepinephrine level of 3.59 mmol/ml as a cutoff value for predicting the effectiveness of metoprolol for children with POTS were 76.9 and 91.7%, respectively (69). However, plasma-norepinephrine levels were not stable in circulation, and were affected by many factors, including exercise and emotions. Thus, we should seek a stable, easily detected and inexpensive biomarker of hyperadrenergic POTS. C-type natriuretic peptide (CNP) is a regulatory peptide that can affect catecholamine release. Lin et al. reported that, compared with non-responders to metoprolol therapy of POTS in children and adolescents, plasma CNP in responders was significantly high before treatment, and baseline plasma CNP of >32.6 pg/ml predicted the efficacy of metoprolol therapy for treating POTS in children (sensitivity 100% and specificity 71.6%). Thus, plasma CNP is a useful clinical predictor of the therapeutic response to metoprolol in POTS patients (70).

Propranolol, a non-selective β-blocker, can pass the blood-brain barrier. Thus, it is considered to work better than other β-blockers in the treatment of POTS (71). Some studies have found that low doses of propranolol are superior to higher doses in the treatment of POTS adult patients. Low dosages of oral propranolol ameliorates the upright tachycardia and enhances the capacity for exercise of POTS patients (72). Propranolol is also used as a migraine prophylaxis medication (73), making it sometimes useful for treating patients with POTS co-morbid migraine. Propranolol is in an HRS Class 2B recommendation for treatment of POTS (8).

In summary, we have categorized the pathophysiology of POTS into 3 major subtypes that may overlap: hypovolemic, neuropathic and hyperadrenergic. It is important to note that strategies that work for some patients may not be applicable to all. Thus, in clinical practice, it is very important to search for biomarkers of the pathogenesis of POTS in children as a guide to select the drugs best suited to any given individuals. With this goal in mind, we have proposed

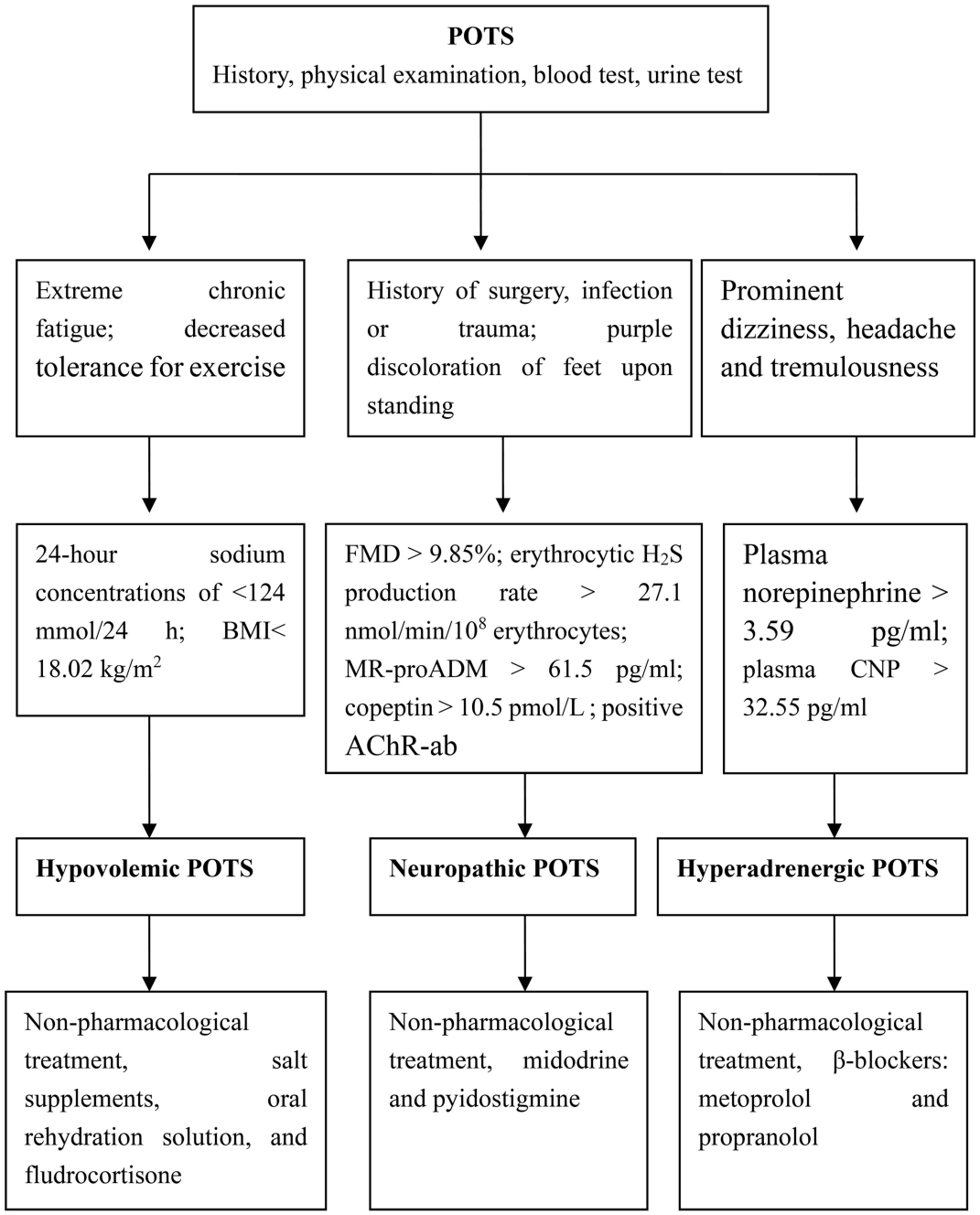

FIGURE 1 | Individualized treatment strategies for children based on POT subtypes. POTS, postural orthostatic tachycardia syndrome; BMI, body-mass index; FMD, flow-mediated vasodilation; MR-proADM, mid-regional fragment of pro-adrenomedullin; AChR-ab, antibodies of acetylcholine receptor; CNP, C-type natriuretic peptide.

a subtype pathophysiology-based personalized-treatment strategy (**Figure 1**).

CONCLUSION

POTS is a common and heterogeneous disorder in children and adolescents that significantly reduces quality of life. Its common categories are hypovolemic, hyperadrenergic and neuropathic. Management always involves cross-disciplinary care that includes lifestyle changes, nutritional adjustments, exercise and drugs. Different sub-types of POTS have different clinical characteristics, and involve different physiological and biochemical changes. Some biomarkers reflect the pathogenesis of POTS in children and guide the choice of

drugs for individualized treatment. However, a further clinical investigation of its pathophysiology and the options for treating it is still required.

AUTHOR CONTRIBUTIONS

QZ had primary responsibility for the design and execution of the study, data collection, preliminary data analysis, and writing the manuscript. BX participated in data collection, preliminary data analysis, and the writing of the manuscript. JD supervised the design and execution of the study, performed the final data analyses, and contributed to the writing of the manuscript.

FUNDING

This work was supported by National Natural Science Foundation of China (81921001), CAMS Innovation Fund for Medical Sciences (2019-I2M-5-047), Peking University Clinical Scientist Program (BJMU2019LCKXJ001), and the Fundamental Research Funds for the Central Universities.

REFERENCES

1. Stewart JM. Orthostatic intolerance in pediatrics. *J Pediatr.* (2002) 140:404–11. doi: 10.1067/mpd.2002.122727
2. Tanaka H, Fujita Y, Takenaka Y, Kajiwara S, Masutani S, Ishizaki Y, et al. Japanese clinical guidelines for juvenile orthostatic dysregulation version 1. *Pediatr Int.* (2009) 51:169–79. doi: 10.1111/j.1442-200X.2008.02783.x
3. Zhang Q, Du J, Wang C, Du Z, Wang L, Tang C. The diagnostic protocol in children and adolescents with syncope-a multi-center prospective study. *Acta Pediatr.* (2009) 98:879–84. doi: 10.1111/j.1651-2227.2008.01195.x
4. Medow MS. Postural tachycardia syndrome from a pediatrics perspective. *J Pediatr.* (2011) 158:4–6. doi: 10.1016/j.jpeds.2010.08.038
5. Li J, Zhang Q, Hao H, Jin H, Du J. Clinical features and management of postural tachycardia syndrome in children: a single-center experience. *Chin Med J (Engl).* (2014) 127:3684–9. doi: 10.3760/cma.j.issn.0366-6999.20140244
6. Bryarly M, Phillips LT, Fu Q, Vernino S, Levine BD. Postural Orthostatic Tachycardia syndrome: JACC focus seminar. *J Am Coll Cardiol.* (2019) 73:1207–28. doi: 10.1016/j.jacc.2018.11.059
7. Wang C, Li Y, Liao Y, et al. Chinese Pediatric Cardiology Society (CPCS) guideline for diagnosis and treatment of syncope in children and adolescents. *Sci Bull.* (2018) 63:1558–64. doi: 10.1016/j.scib.2018.09.019
8. Sheldon RS, Grubb BP II, Olshansky B, Shen WK, Calkins H, Brignole M, et al. 2015 Heart Rhythm Society expert consensus statement on the diagnosis and treatment of postural tachycardia syndrome, inappropriate sinus tachycardia, and vasovagal syncope. *Heart Rhythm.* (2015) 12:e41–63. doi: 10.1016/j.hrthm.2015.03.029
9. Boris JR. Postural orthostatic tachycardia syndrome in children and adolescents. *Auton Neurosci.* (2018) 215:97–101. doi: 10.1016/j.autneu.2018.05.004
10. Kizilbash SJ, Ahrens SP, Bruce BK, Chelimsky G, Driscoll SW, Harbeck-Weber C, et al. Adolescent fatigue, POTS, and recovery: a guide for clinicians. *Curr Probl Pediatr Adolesc Health Care.* (2014) 44:108–33. doi: 10.1016/j.cppeds.2013.12.014
11. Bruce BK, Harrison TE, Bee SM, Luedtke CA, Porter CJ, Fischer PR, et al. Improvement in functioning and psychological distress in adolescents with postural orthostatic tachycardia syndrome following interdisciplinary treatment. *Clin Pediatr (Phila).* (2016) 55:1300–4. doi: 10.1177/0009922816638663
12. Shaw BH, Stiles LE, Bourne K, Green EA, Shibao CA, Okamoto LE, et al. The face of postural tachycardia syndrome-insights from a large cross-sectional online community-based suvery. *J Intern Med.* (2019) 286:438–48. doi: 10.1111/joim.12895
13. Stewart JM. A new guideline for diagnosis and treatment of syncope in children and adolescents that stimulates further thought and discussion. *Sci Bull.* (2018) 63:1527–8. doi: 10.1016/j.scib.2018.09.020
14. Zhao J, Han Z, Zhang X, Du S, Liu AD, Holmberg L, et al. A cross-sectional study on upright heart rate and BP changing characteristics: basic data for establishing diagnosis of postural orthostatic tachycardia syndrome and orthostatic hypertension. *BMJ Open.* (2015) 5:e007356. doi: 10.1136/bmjopen-2014-007356
15. Tao C, Liu X, Zhang C, Chen Y. Comments on 2018 CPCS guideline for diagnosis and treatment of syncope in children and adolescents. *Sci Bull.* (2019) 64:291–2. doi: 10.1016/j.scib.2019.01.008
16. Thieben MJ, Sandroni P, Sletten DM, Benrud-Larson LM, Fealey RD, Vernino S, et al. Postural orthostatic tachycardia syndrome: the mayo clinic experience. *Mayo Clin Proc.* (2007) 82:308–13. doi: 10.4065/82.3.308
17. Fu Q, VanGundy TB, Shibata S, Auchus RJ, Williams GH, Levine BD. Menstrual cycle affects renal-adrenal and hemodynamic responses during prolonged standing in the postural orthostatic tachycardia syndrome. *Hypertension.* (2010) 56:82–90. doi: 10.1161/HYPERTENSIONAHA.110.151787
18. Boris JR, Bernadzikowski T. Demographics of a large paediatric postural orthostatic tachycardia syndrome program. *Cardiol Young.* (2018) 28:668–74. doi: 10.1017/S1047951117002888
19. Chelimsky G, Kovacic K, Nugent M, Mueller A, Simpson P, Chelimsky TC. Comorbid conditions do not differ in children and young adults with functional disorders with or without postural tachycardia syndrome. *J Pediatr.* (2015) 167:120–4. doi: 10.1016/j.jpeds.2015.03.039
20. Jarjour IT. Postural tachycardia syndrome in children and adolescents. *Semin Pediatr Neurol.* (2013) 20:18–26. doi: 10.1016/j.spen.2013.01.001
21. Benarroch EE. Postural tachycardia syndrome: a heterogeneous and multifactorial disorder. *Mayo Clin Proc.* (2012)87:1214–25. doi: 10.1016/j.mayocp.2012.08.013
22. Mar PL, Raj SR. Postural orthostatic tachycardia syndrome: mechanisms and new therapies. *Annu Rev Med.* (2019) 7:235–48. doi: 10.1146/annurev-med-041818-011630
23. El-Sayed H, Hainsworth R. Salt supplement increases plasma volume and orthostatic tolerance in patients with unexplained syncope. *Heart.* (1996) 75:134–40. doi: 10.1136/hrt.75.2.134
24. Li J, Liao Y, Du J, Zhang Q. Relationship between 24-hour urinary sodium and renin-angiotensin-aldosterone system in children with postural tachycardia syndrome. *Zhonghua Yi Xue Za Zhi.* (2015) 95:2928–32. doi: 10.3760/cma.j.issn.0376-2491.2015.36.009
25. Raj SR, Biaggioni I, Yamhure PC, Black BK, Paranjape SY, Byrne DW, et al. Renin-aldosterone paradox and perturbed blood volume regulation underlying postural tachycardia syndrome. *Circulation.* (2005) 111:1574–82. doi: 10.1161/01.CIR.0000160356.97313.5D
26. Mustafa HI, Garland EM, Biaggioni I, Black BK, Dupont WD, Robertson D, et al. Abnormalities of angiotensin regulation in postural tachycardia syndrome. *Heart Rhythm.* (2011) 8:422–8. doi: 10.1016/j.hrthm.2010.11.009
27. Zhang Q, Liao Y, Tang C, Du J, Jin H. Twenty-four-hour urinary sodium excretion and postural orthostatic tachycardia syndrome. *J Pediatr.* (2012) 161:281–4. doi: 10.1016/j.jpeds.2012.01.054
28. Gibbons CH, Bonyhay I, Benson A, Wang N, Freeman R.Structural and functional small fiber abnormalities in the neuropathic postural tachycardia syndrome. *PLoS ONE.* (2013) 8:e84716. doi: 10.1371/journal.pone.0084716
29. Liao Y, Yang J, Zhang F, Chen S, Liu X, Zhang Q, et al. Flow-mediated vasodilation as a predictor of therapeutic response to midodrine hydrochloride in children with postural orthostatic tachycardia syndrome. *Am J Cardiol.* (2013) 112:816–20. doi: 10.1016/j.amjcard.2013.05.008
30. Steven V, Lauren ES. Autoimmunity in postural orthostatic tachycardia syndrome: current understanding. *Auton Neurosci.* (2018) 215:78–82. doi: 10.1016/j.autneu.2018.04.005
31. Li J, Zhang Q, Liao Y, Zhang C, Hao H, Du J. The value of acetylcholine receptor antibody in children with postural tachycardia syndrome. *Pediatr Cardiol.* (2015) 36:165–70. doi: 10.1007/s00246-014-0981-8

32. Fedorowski A, Li H, Yu X, Koelsch KA, Harris VM, Liles C, et al. Antiadrenergic autoimmunity in postural tachycardia syndrome. *Europace.* (2017) 19:1211–9. doi: 10.1093/europace/euw154
33. Yu X, Li H, Murphy TA, Nuss Z, Liles C, Aston CE, et al. Angiotensin II Type 1 receptor autoantibodies in postural tachycardia syndrome. *J Am Heart Assoc.* (2018) 7:e008351. doi: 10.1161/JAHA.117.008351
34. Kanjwal K, Saeed B, Karabin B, Kanjwal Y, Grubb BP. Clinical presentation andmanagement of patients with hyperadrenergic postural orthostatic tachycardia syndrome. A single center experience. *Cardiol J.* (2011) 18:527–31. doi: 10.5603/CJ.2011.0008
35. Zhang Q, Chen X, Li J, Du J. Clinical features of hyperadrenergic postural tachycardia syndrome in children. *Pediatr Int.* (2014) 56:813–6. doi: 10.1111/ped.12392
36. Shannon JR, Flattem NL, Jordan J, Jacob G, Black BK, Biaggioni I, et al. Orthostatic intolerance and tachycardia associated with norepinephrine-transporter deficiency. *N Engl J Med.* (2000) 342:541–9. doi: 10.1056/NEJM200002243420803
37. Shibao C, Arzubiaga C, Roberts LJ II, Raj S, Black B, Harris P, et al. Hyperadrenergic postural tachycardia syndrome in mast cell activation disorders. *Hypertension.* (2005) 45:385–90. doi: 10.1161/01.HYP.0000158259.68614.40
38. Chen L, Wang L, Sun J, Qin J, Tang C, Jin H, et al. Midodrine hydrochloride is effective in the treatment of children with postural orthostatic tachycardia syndrome. *Circ J.* (2011) 75:927–31. doi: 10.1253/circj.CJ-10-0514
39. Lu W, Yan H, Wu S, Xu W, Jin H, Du J. Hemocytometric Measures predict the efficacy of oral rehydration for children with postural tachycardia syndrome. *J Pediatr.* (2017) 187:220–4. doi: 10.1016/j.jpeds.2017.04.034
40. Filler G, Gow RM, Nadarajah R, Jacob P, Johnson G, Zhang YL, et al. Pharmacokinetics of pyridostigmine in a child with postural tachycardia syndrome. *Pediatrics.* (2006) 118:e1563–8. doi: 10.1542/peds.2006-0904
41. Kanjwal K, Karabin B, Sheikh M, Elmer L, Kanjwal Y, Saeed B, et al. Pyridostigmine in the treatment of postural orthostatic tachycardia: a single-center experience. *Pacing Clin Electrophysiol.* (2011) 34:750–5. doi: 10.1111/j.1540-8159.2011.03047.x
42. Al-omari MA, Khaleghi M, Mosley TH Jr, Morgenthaler NG, Struck J, Bergmann A, et al. Mid-regional pro-adrenomedullin is associated with pulse pressure, left ventricular mass, and albuminuria in African Americans with hypertension. *Am J Hypertens.* (2009) 22:860–6. doi: 10.1038/ajh.2009.82
43. Liao Y, Chen S, Liu X, Zhang Q, Ai Y, Wang Y, et al. Flow-mediated vasodilation and endothelium function in children with postural orthostatic tachycardia syndrome. *Am J Cardiol.* (2010) 106:378–82. doi: 10.1016/j.amjcard.2010.03.034
44. Yang J, Zhao J, Du S, Liu D, Fu C, Li X, et al. Postural orthostatic tachycardia syndrome with increased erythrocytic hydrogen sulfide and response to midodrine hydrochloride. *J Pediatr.* (2013) 163:1169–73. doi: 10.1016/j.jpeds.2013.04.039
45. Lin J, Han Z, Li X, Ochs T, Zhao J, Zhang X, et al. Risk factors for postural tachycardia syndrome in children and adolescents. *PLoS ONE.* (2014) 9:e113625. doi: 10.1371/journal.pone.0113625
46. Stewart JM, Boris JR, Chelimsky G, Fischer PR, Fortunato JE, Grubb BP, et al. Pediatric disorders of orthostatic intolerance. *Pediatrics.* (2018) 141:e20171673. doi: 10.1542/peds.2017-1673
47. George SA, Bivens TB, Howden EJ, Saleem Y, Galbreath MM, Hendrickson D, et al. The International POTS Registry: evaluating the efficacy of an exercise training intervention in a community setting. *Heart Rhythm.* (2016)13:943–50. doi: 10.1016/j.hrthm.2015.12.012
48. Sousa A, Lebreiro A, Freitas J, Maciel MJ. Long-term follow-up of patients with postural tachycardia syndrome. *Clin Auton Res.* (2012) 22:151–3. doi: 10.1007/s10286-011-0155-1
49. Jarjour IT, Jarjour LK. Low iron storage and mild anemia in postural tachycardia syndrome in adolescents. *Clin Auton Res.* (2013) 23:175–9. doi: 10.1007/s10286-013-0198-6
50. Öner T, Guven B, Tavli V, Mese T, Yilmazer MM, Demirpence S. Postural orthostatic tachycardia syndrome (POTS) and vitamin B12 deficiency in adolescents. *Pediatrics.* (2014) 133:e138–42. doi: 10.1542/peds.2012-3427
51. Blitshteyn S. Vitamin B1 deficiency in patients with postural tachycardia syndrome (POTS). *Neurol Res.* (2017) 39:685–8. doi: 10.1080/01616412.2017.1331895
52. Antiel RM, Caudill JS, Burkhardt BE, Brands CK, Fischer PR. Iron insufficiency and hypovitaminosis D in adolescents with chronic fatigue and orthostatic intolerance. *South Med J.* (2011) 104:609–11. doi: 10.1097/SMJ.0b013e3182246809
53. Li Y, He B, Li H, Zhang Q, Tang C, Du J, Jin H. Plasma homocysteine level in children with postural tachycardia syndrome. *Front Pediatr.* (2018) 6:375. doi: 10.3389/fped.2018.00375
54. Xu WR, Wang TY. Diagnosis and treatment of syncope in pediatric patients: a new guideline. *Sci Bull.* (2019) 64:357. doi: 10.1016/j.scib.2019.01.024
55. Wells R, Elliott AD, Mahajan R, Page A, Lodice V, Sanders P, et al. Efficacy of therapies for postural tachycardia syndrome: a systematic review and meta-analysis. *Mayo Clin Proc.* (2018)93:1043–53. doi: 10.1016/j.mayocp.2018.01.025
56. Medow MS, Guber K, Chokshi S, Terilli C, Visintainer P, Stewart JM. The benefits of oral rehydration on orthostatic intolerance in children with postural tachycardia syndrome. *J Pediatr.* (2019) 214:96–102. doi: 10.1016/j.jpeds.2019.07.041
57. Stewart JM, Taneja I, Medow MS. Reduced body mass index is associated with increased angiotensin II in young women with postural tachycardia syndrome. *Clin Sci (Lond).* (2007) 113:449–57. doi: 10.1042/CS20070104
58. Li H, Wang Y, Liu P, Chen Y, Feng X, Tang C, et al. Body mass index (BMI) is associated with the therapeutic response to oral rehydration solution in children with postural tachycardia syndrome. *Pediatr Cardiol.* (2016) 37:1313–8. doi: 10.1007/s00246-016-1436-1
59. Miller AJ, Raj SR. Pharmacotherapy for postural tachycardia syndrome. *Auton Neurosci.* (2018) 215:28–36. doi: 10.1016/j.autneu.2018.04.008
60. Zadourian A, Doherty TA, Swiatkiewicz I, Taub PR. Postural orthostatic tachycardia syndrome: prevalence, pathophysiology, and management. *Drugs.* (2018) 78:983–94. doi: 10.1007/s40265-018-0931-5
61. Freitas J, Santos R, Azevedo E, Costa O, Carvalho M, de Freitas AF. Clinical improvement in patients with orthostatic intolerance after treatment with bisoprolol and fludrocortisone. *Clin Auton Res.* (2000) 10:293–9. doi: 10.1007/BF02281112
62. Rowe PC, Calkins H, DeBusk K, McKenzie R, Anand R, Sharma G, et al. Fludrocortisone acetate to treat neurally mediated hypotension in chronic fatigue syndrome: a randomized controlled trial. *JAMA.* (2001) 285:52–9. doi: 10.1001/jama.285.1.52
63. Sheldon R, Raj SR, Rose MS, Morillo CA, Krahn AD, Medina E, et al. Fludrocortisone for the prevention of vasovagal syncope: a randomized, placebo-controlled trial. *J Am Coll Cardiol.* (2016) 68:1–9. doi: 10.1016/j.jacc.2016.04.030
64. Streeten DH. Pathogenesis of hyperadrenergic orthostatic hypotension. Evidence of disordered veous innervation exclusively in the lower limbs. *J Clin Invest.* (1990) 86:1582–8. doi: 10.1172/JCI114878
65. Tang C, Li X, Du J. Hydrogen sulfide as a new endogenous gaseous transmitter in the cardiovascular system. *Curr Vasc Pharmacol.* (2006) 4:17–22. doi: 10.2174/157016106775203144
66. Zhang F, Li X, Ochs T, Chen L, Liao Y, Tang C, et al. Midregional pro-adrenomedullin as a predictor for therapeutic response to midodrine hydrochloride in children with postural orthostatic tachycardia syndrome. *J Am Coll Cardiol.* (2012) 60:315–20. doi: 10.1016/j.jacc.2012.04.025
67. Zhao J, Tang C, Jin H, Du J. Plasma copeptin and therapeutic effectiveness of midodrine hydrochloride on postural tachycardia syndrome in children. *J Pediatr.* (2014) 165:290–4. doi: 10.1016/j.jpeds.2014.04.032
68. Raj SR, Black BK, Biaggioni I, Harris PA, Robertson D. Acetylcholinesterase inhibition improves tachycardia in postural tachycardia syndrome. *Circulation.* (2005) 111:2734–40. doi: 10.1161/CIRCULATIONAHA.104.497594
69. Zhang Q, Chen X, Li J, Du J. Orthostatic plasma norepinephrine level as a predictor for therapeutic response to metoprolol in children with postural tachycardia syndrome. *J Transl Med.* (2014) 12:249. doi: 10.1186/s12967-014-0249-3
70. Lin J, Han Z, Li H, Chen SY, Li X, Liu P, et al. Plasma C-type natriuretic peptide as a predictor for therapeutic response to metoprolol in children with postural tachycardia syndrome. *PLoS ONE.* (2015) 10:e0121913. doi: 10.1371/journal.pone.0121913

71. Low PA, Sandroni P, Joyner M, Shen WK. Postural tachycardia syndrome (POTS). *J Cardiovasc Electrophysiol.* (2009) 20:352–8. doi: 10.1111/j.1540-8167.2008.01407.x
72. Raj SR, Black BK, Biaggioni I, Paranjape SY, Ramirez M, Dupont WD, et al. Propranolol decreases tachycardia and improves symptoms in the postural tachycardia syndrome: less is more. *Circulation.* (2009) 120:725–34. doi: 10.1161/CIRCULATIONAHA.108.846501
73. Pringsheim T, Davenport W, Mackie G, Worthington I, Aubé M, Christie SN, et al. Canadian Headache Society guideline for migraine prophylaxis: supplement 2. *Can J Neurol Sci.* (2012) 39:S1–59. doi: 10.1017/S0317167100015109

Conflict of Interest: The authors declare that the research was conducted in the absence of any commercial or financial relationships that could be construed as a potential conflict of interest.

frontiers in Physiology

ORIGINAL RESEARCH
published: 21 August 2020
doi: 10.3389/fphys.2020.01049

Baroreflex Modulation During Acute High-Altitude Exposure in Rats

Ana Rosa Beltrán[1,2†], Alexis Arce-Álvarez[3†], Rodrigo Ramirez-Campillo[4,5], Manuel Vásquez-Muñoz[5], Magdalena von Igel[5], Marco A. Ramírez[2], Rodrigo Del Rio[6,7,8] and David C. Andrade[5,6,9]*

[1] Departamento de Educación, Facultad de Educación, Universidad de Antofagasta, Antofagasta, Chile, [2] Laboratorio de Fisiología Celular, Departamento Biomédico, Facultad de Ciencias de la Salud, Universidad de Antofagasta, Antofagasta, Chile, [3] Escuela de Kinesiología, Facultad de Salud, Universidad Católica Silva Henríquez, Santiago, Chile, [4] Laboratory of Human Performance, Quality of Life and Wellness Research Group, Department of Physical Activity Sciences, Universidad de Los Lagos, Osorno, Chile, [5] Centro de Investigación en Fisiología del Ejercicio, Facultad de Ciencias, Universidad Mayor, Santiago, Chile, [6] Laboratory of Cardiorespiratory Control, Department of Physiology, Pontificia Universidad Católica de Chile, Santiago, Chile, [7] Centro de Envejecimiento y Regeneración (CARE), Pontificia Universidad Católica de Chile, Santiago, Chile, [8] Centro de Excelencia en Biomedicina de Magallanes (CEBIMA), Universidad de Magallanes, Punta Arenas, Chile, [9] Pedagogía en Educación Física, Deportes y Recreación, Universidad Mayor, Santiago, Chile

OPEN ACCESS

Edited by:
Julian Paton, University of Bristol, United Kingdom

Reviewed by:
Marli Cardoso Martins-Pinge, State University of Londrina, Brazil
Luciana A. Campos, Abu Dhabi University, United Arab Emirates

***Correspondence:**
David C. Andrade
david.andrade@umayor.cl

† These authors have contributed equally to this work

Specialty section:
This article was submitted to Integrative Physiology, a section of the journal Frontiers in Physiology

Received: *02 March 2020*
Accepted: *30 July 2020*
Published: *21 August 2020*

Citation:
Beltrán AR, Arce-Álvarez A, Ramirez-Campillo R, Vásquez-Muñoz M, von Igel M, Ramírez MA, Del Rio R and Andrade DC (2020) Baroreflex Modulation During Acute High-Altitude Exposure in Rats. Front. Physiol. 11:1049. doi: 10.3389/fphys.2020.01049

Baroreflex (BR) control is critically dependent of sympathetic and parasympathetic modulation. It has been documented that during acute hypobaric hypoxia there is a BR control impairment, however, the effect of a natural hypoxic environment on BR function is limited and controversial. Therefore, the aim of this study was to determine the effect of acute High-Altitude exposure on sympathetic/parasympathetic modulation of BR control in normal rats. Male Sprague Dawley rats were randomly allocated into Sea-Level (n = 7) and High-Altitude (n = 5) (3,270 m above sea level) groups. The BR control was studied using phenylephrine (Phe) and sodium nitroprusside (SNP) through sigmoidal analysis. The autonomic control of the heart was estimated using heart rate variability (HRV) analysis in frequency domain. Additionally, to determine the maximum sympathetic and parasympathetic activation of BR, spectral non-stationary method analysis, during Phe (0.05 μg/mL) and SNP administration (0.10 μg/mL) were used. Compared to Sea-Level condition, the High-Altitude group displayed parasympathetic withdrawal (high frequency, 0.6–2.4 Hz) and sympathoexcitation (low frequency, 0.04–0.6 Hz). Regarding to BR modulation, rats showed a significant decrease ($p < 0.05$) of curvature and parasympathetic bradycardic responses to Phe, without significant differences in sympathetic tachycardic responses to SNP after High-Altitude exposure. In addition, the non-stationary analysis of HRV showed a reduction of parasympathetic activation (Phe) in the High-Altitude group. Our results suggest that acute exposure to High-Altitude produces an autonomic and BR control impairment, characterized by parasympathetic withdrawal after 24 h of high-altitude exposure.

Keywords: baroreflex, autonomic nervous system, sympathetic nervous system, parasympathetic nervous system, baroreceptors

INTRODUCTION

The cardiac baroreflex (BR) function governs short-term fluctuations of blood pressure and, therefore, plays an important role in the regulation of several homeostatic functions (Stauss, 2002). The main baroreceptors are allocated in the aortic arc and the carotid sinus area (Stauss, 2002). The increase of blood pressure (BP) triggers a BR-dependent increase of parasympathetic drive, while a decrease of BP produces a massive sympathoexcitation (Cowley and Guyton, 1975). It has been demonstrated that modification of this reflex arc is implicated in several physiological and pathophysiological conditions, such as microgravity, aging processes, hypertension, heart failure, High-Altitude exposure, among others (Ferguson et al., 1992; Wang et al., 2004; Hainsworth et al., 2007; Monahan, 2007; Eckberg et al., 2010; Del Rio et al., 2013, 2016; Fernandez et al., 2015; Andrade et al., 2017, 2019).

Among the aforementioned conditions, High-Altitude is amongst the most inhospitable environments on earth and it has been demonstrated that exposure to hypobaric hypoxia is strongly related to impairment of autonomic control (Lanfranchi et al., 2005; Hainsworth et al., 2007). Although it has been observed that BR control is compromised during hypobaric hypoxia, the evidence is limited and controversial; nevertheless, the major differences related to autonomic modulation could be related to the atmospheric pressure (Sagawa et al., 1997; Hainsworth et al., 2007). Human studies, using the neck chamber method, showed that hypobaric hypoxia had no effect on the BR set point, but reduce the BR gain (Sagawa et al., 1997). Contrarily, it has been shown that during normobaric hypoxia, the BR gain was not modified (Bourdillon et al., 2017). In addition, Obrezchikova et al. (2000) showed that the exposure to chronic hypobaric hypoxia (hypoxic chamber) inhibits vagal bradycardia BR in rats. Despite the fact, that these evidences strongly suggest that BR control is affected during hypoxic environment, it does not necessarily have to be reproducible during natural conditions (i.e., High-Altitude environment). Indeed, most studies address the contribution of sympathetic modulation of the BR function during hypobaric hypoxia simulating High-Altitude ambient (Hainsworth et al., 2007; Simpson et al., 2019), but none of these focused on the estimation of the parasympathetic contribution on BR modulation. Considering that there are few evidences underpinning the acute effect of high-altitude exposure on BR control, we proposed to determine the effect of acute high-altitude environment (3,270 m above sea level) on sympathetic/parasympathetic modulation of BR control in normal rats.

TABLE 1 | Effect of high-altitude exposure on baseline physiological parameters.

	Sea Level (n = 7)	High Altitude (n = 5)	p-value
Body Weight (g)	386.57 ± 7.67	355.01 ± 11.47	0.45
SBP (mmHg)	140.68 ± 2.35	145.28 ± 5.56	0.61
DBP (mmHg)	104.17 ± 3.57	107.22 ± 4.79	0.41
MABP (mmHg)	116.34 ± 3.02	119.91 ± 5.01	0.53
PP (mmHg)	36.51 ± 2.38	38.06 ± 1.51	0.63
HR (bpm)	353.64 ± 11.18	371.94 ± 16.91	0.37

Values are mean ± standard error of the mean (SEM). SBP, systolic blood pressure; DBP, diastolic blood pressure; MABP, mean arterial blood pressure; PP, pulse pressure; HR, heart rate. Unpaired t-test.

MATERIALS AND METHODS

Ethical Approval and Animals

Twelve male Sprague-Dawley rats were used in these experiments. All surgical procedures and protocols used, were in accordance with guidelines of the American Physiological Society and the National Institutes of Health Guide for the Care and Use of Laboratory Animals and were approved by the University of Antofagasta Scientific Research Ethical Committee (CEIC-210/2019).

Experimental Procedure

Male Sprague-Dawley rats (n = 12) were housed in individual cages with a 12/12-h light/dark schedule and were allowed free access to food and water. The rats were randomly allocated into Sea-Level group (n = 7) and to High-Altitude group (n = 5). Sea-level rats were subjected to catheterization surgery according to the method of Li et al. (1999) and basal BP recording was preformed (1-hour). Afterward, BR experiment was performed as follows: 8 boluses of phenylephrine to increase BP were injected (*i.v.*) and after 30 min of recovery, 8 boluses of sodium nitroprusside to decrease BP were injected (*i.v.*). The second series of rats (High-Altitude group) ascended at 3,270 m above sea level (Caspana, Antofagasta, Chile) in a costume made mobile laboratory and after 24 h, the catheterization surgery was performed. Similar to the first animal series (Sea-Level group), 8 h after (Masson et al., 2014) the surgical procedure, basal recordings of BP (1-hour) and the BR experiment were performed. At Sea-Level the relative humidity was between 66 and 68% and the temperature between 19 and 21°C, while at 3,270 m (High-Altitude), the relative humidity was between 21 and 25% and the temperature was 19°C (Chilean Meteorological Service).

Arterial Blood Pressure in Freely Moving Rats

Arterial BP measurement was performed in conscious freely moving rats. The carotid artery and jugular vein cannulations (PE-50 polyethylene tubing, Clay Adams, Parsippany, NJ, United States), were performed to measure BP and for drugs administration. The rats were anesthetized (*i.p.*) using ketamine (80 mg/kg; Fort Dodge Animal Health, United States) plus xylazine (12 mg/kg; Alcon, United States) (Li et al., 1999; Feng et al., 2015). A midline incision in the neck was performed to isolate a lateral branch of the carotid artery. A small incision was made and a 3 Fr polyurethane catheter was guided into the artery and was tunneled subcutaneously to the back of the neck and connected to a vascular access port. Eight hours before BP measurement, the rats were anesthetized (i.p.) using ketamine (80 mg/kg; Fort Dodge Animal Health, United States)

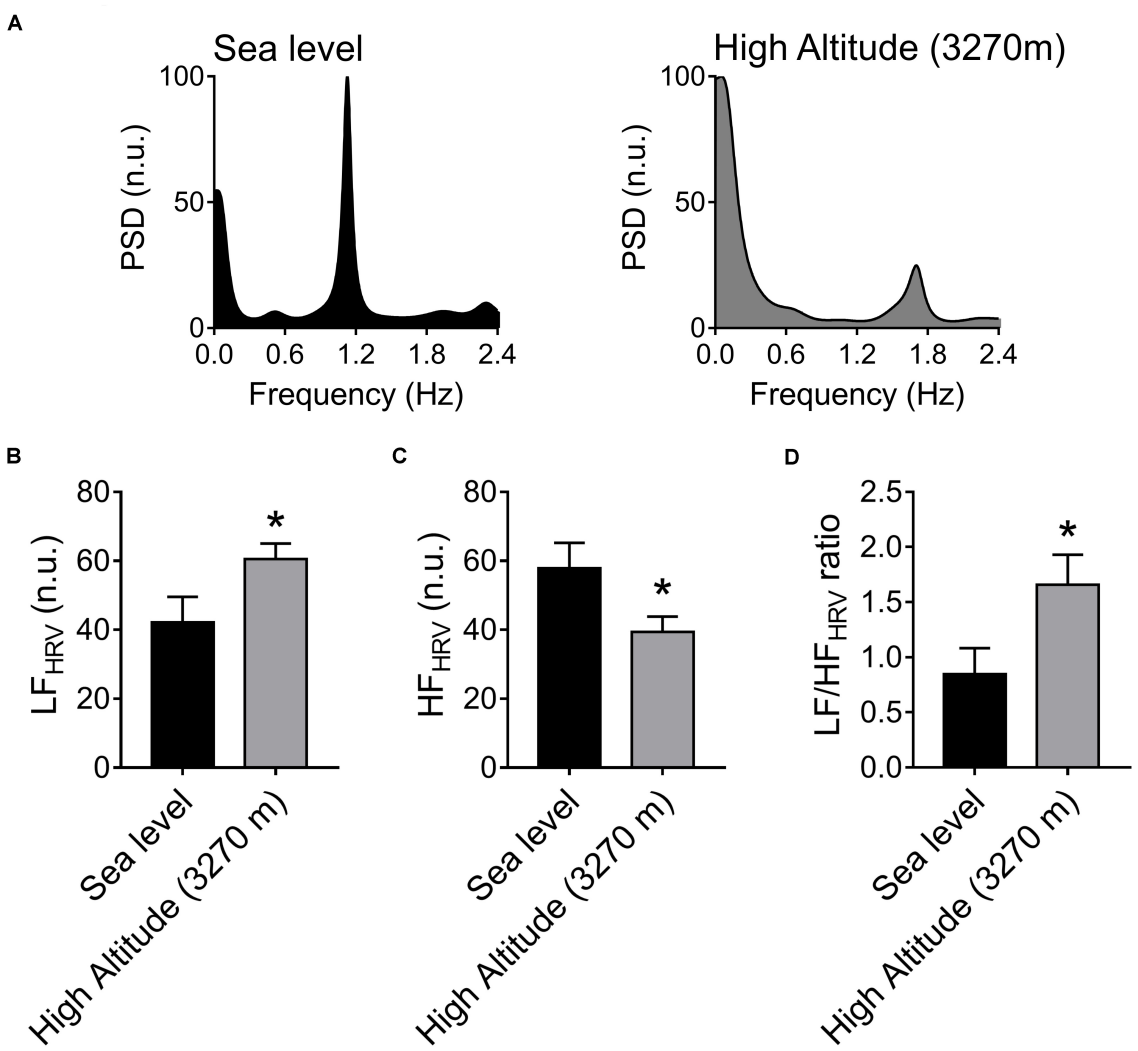

FIGURE 1 | Effect of High-Altitude (3,270 m above sea level) on heart rate variability (HRV) alterations. **(A)** Representative heart rate variability (HRV) spectrums from one Sea-Level rat and one High-Altitude rat. During hypoxic natural environment HRV spectrum was altered in High-Altitude rats. **(B–D)** Summary of the effects of High-Altitude on **(B)** low frequency (LF) component of the HRV, **(C)** high frequency (HF) component of HRV and **(D)** LF/HF ratio. During High-Altitude exposure the animals displayed an increase of LF (**B**, sympathoexcitation) component, decrease of HF (**C**, parasympathetic withdrawal) component, and consequently an increase of LF/HF ratio of HRV **(D)**. Values are mean ± SEM. Data was analyzed by unpaired *T*-test. $^*p < 0.05$ vs. Sea-Level. Sea-Level $n = 7$; High-Altitude, $n = 5$.

plus xylazine (12 mg/kg; Alcon, United States) for catheterization of the common carotid artery and jugular vein (Li et al., 1999; Feng et al., 2015). The BP was continuously recorded in a BIOPAC system (DA100C, BIOPAC system, United States) at a sampling rate of 1 KHz. From recordings we were able to estimate systolic blood pressure (SBP), diastolic blood pressure (DBP), pulse pressure (PP = SBP–DBP) and mean arterial blood pressure (MABP = 1/3 of SBP + 2/3 of DBP). In addition, the heart rate (HR) was derived from dP/dt signal obtained from the BP recordings (Del Rio et al., 2016; Andrade et al., 2017).

Baroreflex Control

The BR was evaluated by repeated bolus injections (0.1 ml) of graded doses of sodium nitroprusside (0.4, 0.8, 1.6, 3.2, 6.4, 12.8, and 25.6 μg/kg; Sigma-Aldrich, United States) and phenylephrine (0.2, 0.4, 0.8, 1.6, 3.2, 6.4, and 12.8 μg/kg; Sigma-Aldrich, United States). These drugs were used to induce a decrease or increase in BP, respectively. Sodium nitroprusside and phenylephrine injections were given in a random order and subsequent injections were not given until the recorded parameters had returned to pre-injection levels. The cardiac BR function was analyzed using a logistic regression over the entire pressure range (Negrão et al., 1993; Michelini et al., 2003). Data was fit to the equation: $HR = A/[1 + \exp\{B(MAP-C)\}] + D$, where A is HR range; B is the slope coefficient; C is the pressure at the midpoint of the range (midpoint BP); and D is the minimum HR. The peak slope (maximum gain) was determined by the first derivative of the baroreflex curve and was calculated with the equation: Gain = A(1) × A(2) × [1/4], where A(1) is the range and A(2) is the average slope. The mean values for

TABLE 2 | Effect of high-altitude exposure on heart rate variability parameters at rest.

	Sea Level (n = 7)	High Altitude (n = 5)	p-value
RMSSD	2.17 ± 0.31	1.84 ± 0.19	0.43
SDNN	3.06 ± 0.31	2.27 ± 0.26	0.09
VLF (ms^2)	1.36 ± 0.16	0.52 ± 0.11	0.01
LF (ms^2)	3.39 ± 0.50	3.24 ± 0.74	0.20
HF (ms^2)	3.93 ± 1.51	2.01 ± 0.47	0.28
Total power	6.24 ± 1.79	5.76 ± 1.20	0.08
SD1	1.53 ± 0.21	1.31 ± 0.14	0.43
SD2	4.02 ± 0.40	2.91 ± 0.35	0.07
SD2/SD1 ratio	2.79 ± 0.30	2.24 ± 0.19	0.19

Values are mean ± standard error of the mean (SEM). RMSSD: Root-mean-square of the successive differences between adjacent normal R-R intervals; SDNN, Standard deviation of the normal-to-normal intervals; VLF, very low frequency component of HRV; LF, low frequency component of HRV; HF, high frequency component of HRV; SD1, short-term standard deviation from Poincare plots; SD2, long-term standard deviation from Poincare plots; SD2/SD1 ratio, of standard deviations of Poincare plots, Unpaired t-test.

each curve parameter were used to derive composite curves for each group of rats.

Dose-Responses Analysis to BR Stimulation

To determine whether the effects of High-Altitude in BR control could be associated to differences in BP stimulus, we constructed a dose-response curve for SNP and Phe. We used 8 doses of SNP (concentration: 0.0512 μg/μL; at 0.1; 0.2; 0.4; 0.8; 1.6; 3.2; 6.4; and 12.8 μL/kg) and 8 doses of Phe (concentration: 0.1024 μg/μL; at 0.2; 0.4; 0.8; 1.6; 3.2; 6.4; 12.8; 25.6 μL/kg). The curve was constructed using the logarithm of different doses. The responses were estimated using the delta of MABP (ΔMABP) from previous baseline measurements.

Autonomic Control

Heart rate variability (HRV) was used as an indirect measurement of autonomic balance of the heart (Del Rio et al., 2016; Andrade et al., 2017). The first derivative of the BP (Dp/dt) signal was used to calculate the HR. Autoregressive algorithm, after Hann windowing with 50% overlap, was used to obtain power spectral density of HRV. Cut-off frequencies were defined as low frequency (LF_{HRV}): 0.04–0.6 Hz and high frequency (HF_{HRV}) 0.6–2.4 Hz (Andrade et al., 2017). Additionally, we used LF/HF_{HRV} ratio as an indicator of autonomic balance of the heart. LF_{HRV} and HF_{HRV} were expressed as normalized units (n.u.). Analysis was performed within a 10 min window. This analysis was performed in LabChart 7.3.8 HRV module software (ADInstruments, Bella Vista, NSW, Australia). In addition, to estimate the autonomic contribution on BR function, spectral non-stationary analysis was used (2-s resolution). The HF_{HRV} component (0.6–2.4 Hz) was used as an indicator of parasympathetic modulation. This analysis was performed with Kubios HRV Premium Software V 3.1 (Kubios, Finlandia).

Statistical Analysis

Data were expressed as mean ± standard error of the mean. All data were subjected to Shapiro-Wilk normality test. The unpaired t-test at two tails was employed to compare the differences between groups. $p < 0.05$ was considered statistically significant. Statistical analyses were performed by GraphPad Prism 8.0 (GraphPad software Inc., San Diego, CA, United States).

RESULTS

Effect of High-Altitude Exposure on Baseline Physiological Variables

Baseline physiological variables for both groups are shown in **Table 1**. At baseline, there were no significant differences between Sea-Level and High-Altitude exposure on body weight DBP, SBP, MABP, PP, and HR (**Table 1**).

Effect of High-Altitude Exposure on Cardiac Autonomic Control at Rest

The autonomic control of the heart was estimated by HRV disturbances (**Figure 1**). After acute High-Altitude exposure rats displayed an increase of sympathetic drive and decrease of parasympathetic modulation of the heart (**Figure 1**). Indeed, the LF_{HRV} component was significantly increased ($p < 0.05$) from Sea-Level (42.12 ± 7.44 n.u.) to High-Altitude (60.55 ± 4.47 n.u.) (**Figures 1A,B**), while the HF_{HRV} component was significantly reduced ($p < 0.05$) from Sea-Level (39.37 ± 4.44 n.u.) to High-Altitude (57.82 ± 7.43 n.u.) (**Figures 1A,C**). Consequently, the LF/HF_{HRV} ratio was significantly increased ($p < 0.05$) at High-Altitude compared to Sea-Level (1.66 ± 0.27 vs. 0.85 ± 0.23, respectively, **Figures 1A,D**). In addition, our data did not reveal significant differences between Sea-Level and High-Altitude on RMSSD, SDNN, LF, and HF non-normalized units, total power, SD1, SD2, and SD2/SD1 ratio (**Table 2**).

Effect of High-Altitude Exposure on Cardiac Baroreflex Control

The BR parameters after High-Altitude exposure are shown in **Figure 2** and **Table 2**. A representative recording of BP and HR after Phe and SNP administration at Sea-level and High-Altitude. After acute High-Altitude exposure and after Phe administration the bradycardic responses was significantly decreased ($p < 0.05$) (**Figure 2A**). Indeed, the sigmoidal curve of BR analysis, showed a blunted BR vagal bradycardia (**Figure 2B**). Moreover, the curvature (0.04 ± 0.01 vs. 0.07 ± 0.01 mmHg/beats/min, **Figure 2C**) and maximal bradycardia (50.70 ± 0.28 vs. 58.01 ± 0.81 beats/min, **Figure 2D**) were significantly reduced ($p < 0.05$) after acute High-Altitude exposure compared to Sea-Level. However, maximum tachycardic response to SNP, range, slope, midpoint of BP, lower plateau and upper plateau of BR analysis, were not significantly different between Sea-Level and High-Altitude groups (**Figures 2A,E** and **Table 3**).

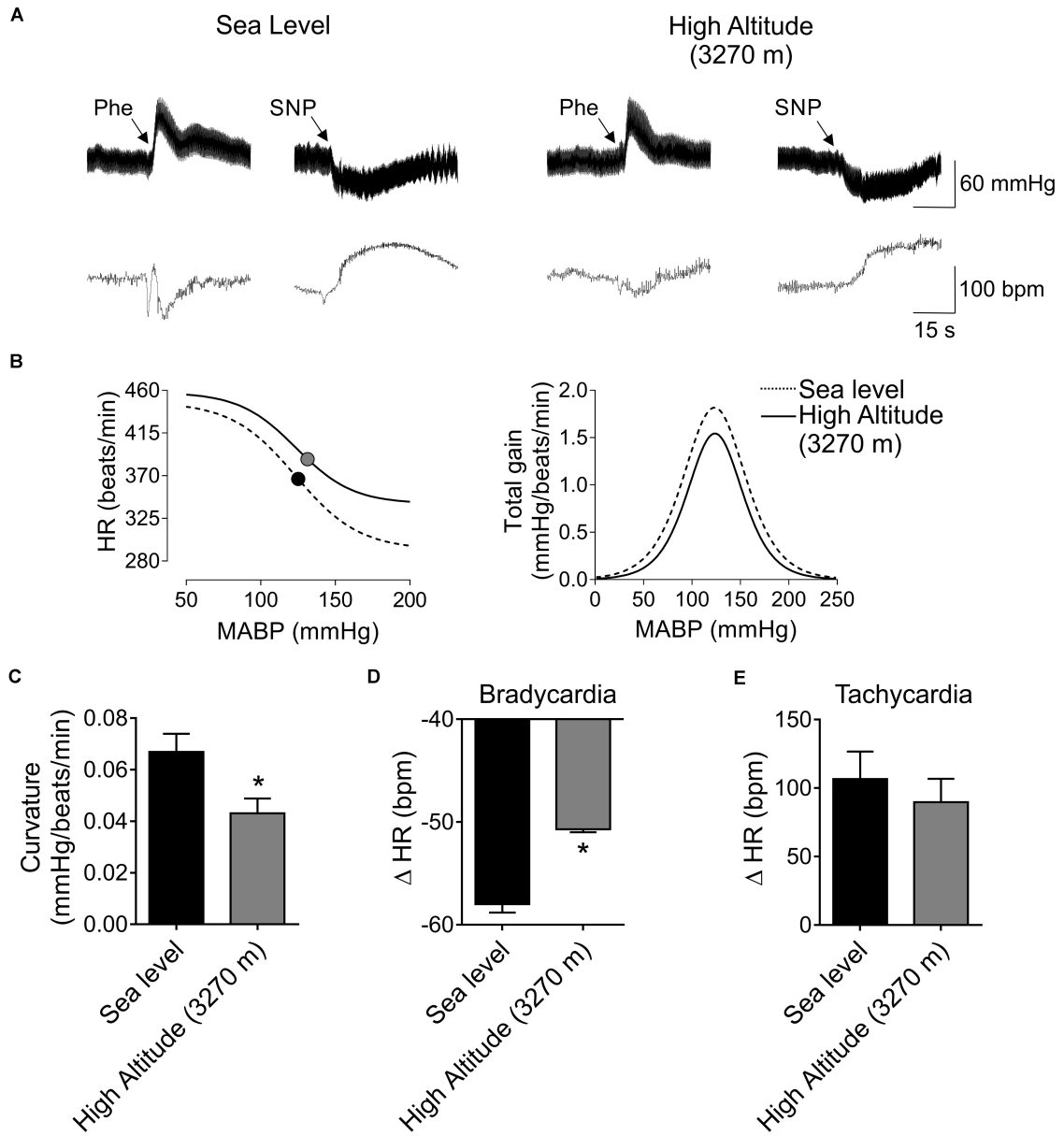

FIGURE 2 | Effect of High-Altitude (3,270 m above sea level) on baroreflex (BR) control in freely moving rats. **(A)** Representative traces of blood pressure (BP) and heart rate (HR), during phenylephrine (Phe) and sodium nitroprusside (SNP) bolus, in one Sea-Level rat and one High-Altitude rat. Note that, during Phe there is a decrease of HR responses. **(B)** Summary curve of BR responses during Sea-Level and High-Altitude exposure. Note that maximum vagal bradycardia response was decreased during hypoxic natural environment. However, the maximum tachycardic responses was indistinguishable between Sea-Level and High-Altitude conditions. Total gain was not different between experimental groups. **(C–E)** summary data of curvature **(C)**, maximum bradycardia **(D)** and tachycardia responses **(E)**. Note that curvature and maximum bradycardic responses of BR function, were significant different between Sea-Level compared to High-Altitude exposure. Values are mean ± SEM. Data was analyzed by unpaired *T*-test. *$p < 0.05$ vs. Sea-Level. Sea-Level $n = 7$; High-Altitude, $n = 5$.

Effect of High-Altitude Exposure on Parasympathetic Modulation of R-R Interval Time Series

Whereas there are very few evidences showing changes in parasympathetic and/or sympathetic outflow during natural High-Altitude environment. Considering current results showing a decrease of maximum vagal bradycardia induced by Phe, we determine if a diminished maximum parasympathetic activation occurs during acute High-Altitude exposure (**Figure 3**). The Phe administration (0.05 μg/mL) induces an increase of parasympathetic drive to the heart (0.6–2.4 Hz) (Sea level: 58.25 ± 2.30 vs. 65.89 ± 6.37 n.u., basal vs. Phe peak activation, respectively, $p < 0.05$) (**Figures 3A,C**),

TABLE 3 | Effect of high-altitude exposure on baroreflex control.

	Sea Level (n = 7)	High Altitude (n = 5)	p-value
Range (beats/min)	112.81 ± 11.93	122.80 ± 34.09	0.75
Slope (beats/mmHg)	1.88 ± 0.17	1.56 ± 0.11	0.20
Midpoint BP (mmHg)	135.81 ± 4.69	123.30 ± 5.43	0.12
Lower plateau (beats/min)	298.31 ± 13.74	338.90 ± 19.48	0.11
Upper plateau (beats/min)	411.10 ± 17.18	461.71 ± 21.16	0.09

Values are mean ± standard error of the mean (SEM). Unpaired t-test.

however, the vagal activation after High-Altitude exposure was reduced (High-Altitude: 48.69 ± 6.61 vs. 57.21 ± 9.15 n.u., basal vs. Phe peak activation, respectively, $p < 0.05$) (**Figures 3A,C**). LF and LF/HF ratio, were not different between groups during phenylephrine administration. In addition, in both conditions RMSSD, SDNN, SD1 and SD2 were significantly different ($p < 0.05$) between resting condition compared to SNP administration (**Table 4**). Regarding to Phe administration, Sea-Level group showed a significant decreased of non-normalized HF component of HRV (**Table 4**). VLF, LF, SD2/SD1 were no different between groups (**Table 4**).

The Effects of High-Altitude Exposure on Baroreflex Control and Parasympathetic Modulation Are Not Dependent of Blood Pressure Stimulation

To determine if differences observed during High-Altitude exposure are dependent of BP changes, we determine the dose-responses of BP at different concentration of Phe and SNP (**Figure 4**). Phenylephrine bolus administration produces a sigmoidal response in BP (**Figure 4A**). There are no significant differences in Log EC50 between groups (0.25 ± 0.07 vs. 0.25 ± 0.12 μg/kg, Sea-Level vs. High-Altitude group, **Figure 4A**) and R^2 (0.99 ± 0.98 Sea-Level vs. High-Altitude group, **Figure 4A**). Similarly, the effect of sodium

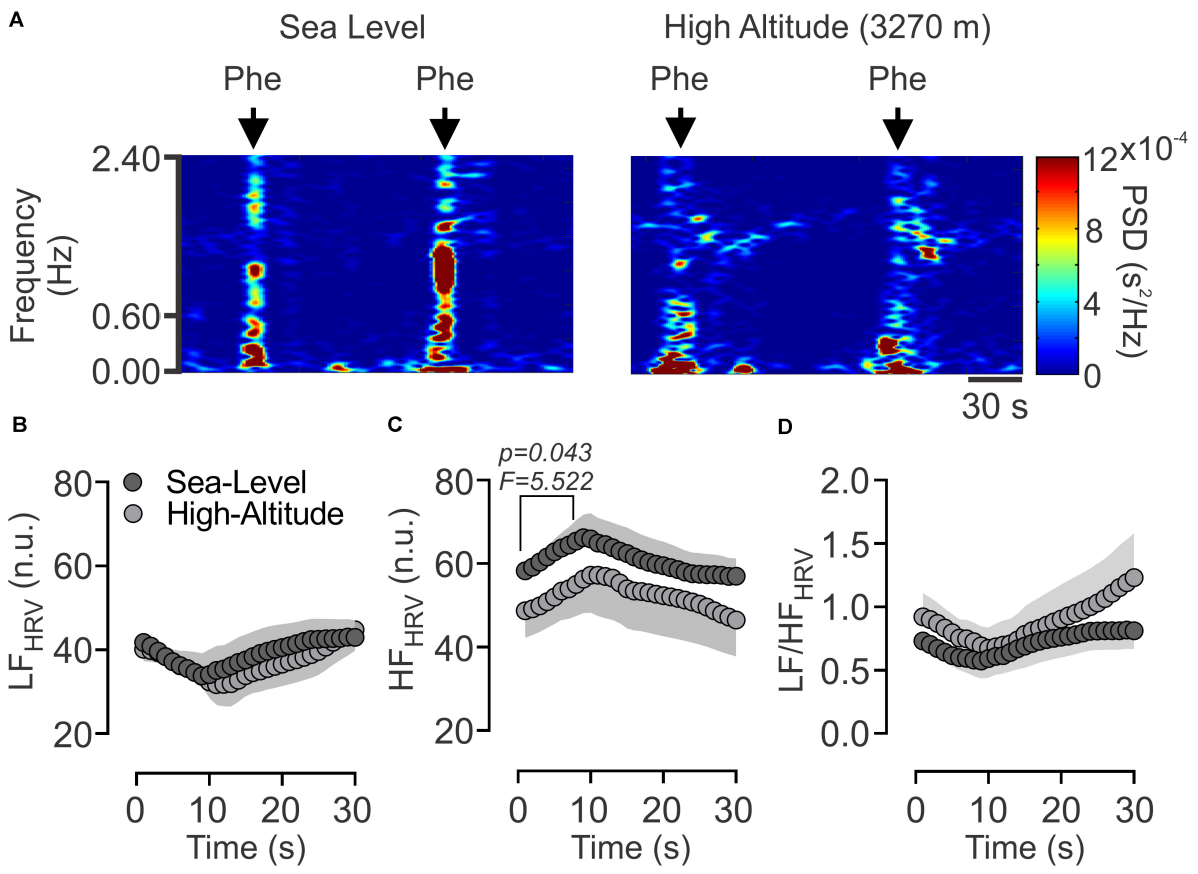

FIGURE 3 | Effect of High-Altitude (3,270 m above sea level) on heart rate variability (HRV) alteration in time-varying domain, following phenylephrine (Phe) administration in freely moving rats. **(A)** Representative time-varying domain spectrum (2-s resolution) of heart rate variability (HRV) during phenylephrine administration (0.05 μg/mL) in one rat per group. Note that High-Altitude rat showed a reduced response to Phe between 0.60 and 2.4 Hz [high frequency (HF) component of HRV] related to parasympathetic control. **(B–D)** Summary of the effects of High-Altitude on **(B)** low frequency (LF) component of the HRV, **(C)** HF component of HRV and **(D)** LF/HF ratio during administration period of Phe. Note that between 2 at 8-s following Phe administration, the power spectral density of HF component of HRV **(C)**, was significantly reduced during High-Altitude exposure. Values are mean ± SEM. Two-ways ANOVA followed by Fisher *post hoc* test. Sea-Level n = 7; High-Altitude, n = 5.

TABLE 4 | Effect of high-altitude exposure on heart rate variability parameters at sea level and high-altitude during phenylephrine (Phe) and sodium nitroprusside (SNP).

	Sea Level (n = 7)			High-Altitude (n = 5)		
	Rest	**SNP**	**Phe**	**Rest**	**SNP**	**Phe**
RMSSD	3.11 ± 0.94	5.73 ± 0.53*	2.00 ± 0.31	1.91 ± 0.32	5.40 ± 0.88*	1.45 ± 0.29
SDNN	3.60 ± 0.97	8.86 ± 1.91*	3.35 ± 0.37	1.90 ± 0.31	7.32 ± 0.97*	2.49 ± 0.43
VLF (ms^2)	8.62 ± 3.32	24.59 ± 9.80	10.69 ± 4.31	4.21 ± 2.10	939.36 ± 705.90	5.34 ± 1.98
LF (ms^2)	21.36 ± 5.86	65.33 ± 43.34	6.31 ± 1.34	11.23 ± 2.35	27.60 ± 10.47	5.77 ± 3.26
HF (ms^2)	16.28 ± 4.29	14.38 ± 3.41	4.14 ± 1.30*	16.99 ± 4.79	14.65 ± 5.69	2.42 ± 0.76
SD1	2.21 ± 0.66	4.06 ± 0.37*	1.42 ± 0.22	1.35 ± 0.22	3.83 ± 0.62*	1.02 ± 0.20
SD2	4.52 ± 1.20	11.60 ± 2.77*	4.45 ± 0.52	2.28 ± 0.42	9.39 ± 1.42*	3.33 ± 0.58
SD2/SD1	2.22 ± 0.25	2.84 ± 0.62	3.53 ± 0.69	1.77 ± 0.40	2.70 ± 0.58	3.45 ± 0.35

*Values are mean ± standard error of the mean (SEM). RMSSD, Root-mean-square of the successive differences between adjacent normal R-R intervals; SDNN, Standard deviation of the normal-to-normal intervals; VLF, very low frequency component of HRV; LF, low frequency component of HRV; HF, high frequency component of HRV; SD1, short-term standard deviation from Poincare plots; SD2, long-term standard deviation from Poincare plots; SD2/SD1 ratio, of standard deviations of Poincare plots, *p-value < 0.05 vs. Rest. Two-way ANOVA.*

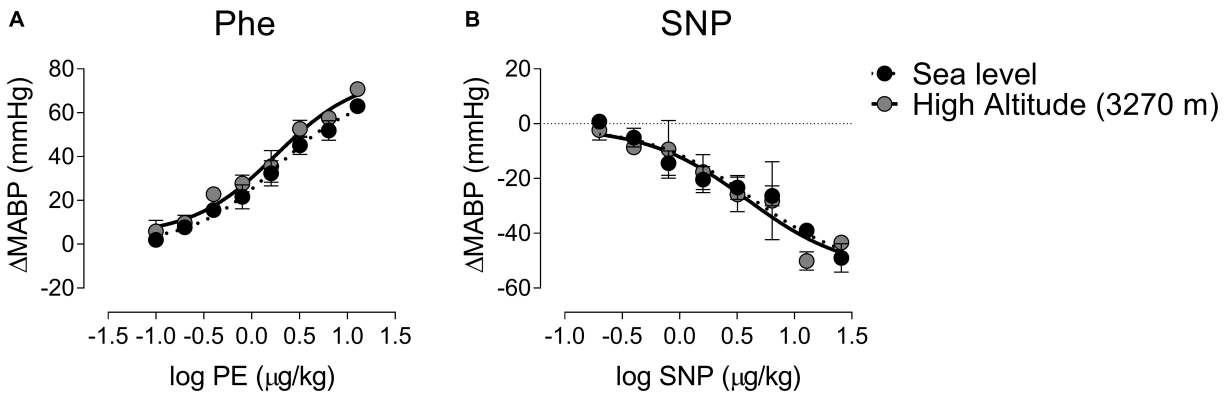

FIGURE 4 | Dose-response curve of phenylephrine (Phe) and sodium nitroprusside (SNP) during Sea-Level and High-altitude (3,270 m above sea level) exposure. During Sea-Level and High-Altitude exposure were not found significant differences on mean arterial blood pressure (MABP) responses between Sea-Level and High-Altitude exposure, following Phe **(A)** and SNP **(B)** administration. Values are mean ± SEM. Two-ways ANOVA followed by Fisher *post hoc* test. Sea-Level n = 7; High-Altitude, n = 5.

nitroprusside administration on BP was not significantly different between environments (Log EC50 = 0.63 ± 0.24 vs. 0.58 ± 0.24 μg/kg, Sea-Level vs. High-Altitude group; and R^2 = 0.93 ± 0.94 Sea-Level vs. High-Altitude group, **Figure 4B**).

DISCUSSION

The major findings of the present study were: (i) after acute High-Altitude exposure there is a cardiac autonomic control impairment; (ii) exposure to High-Altitude produces a deterioration of cardiac BR control (vagal bradycardic responses and curvature) in normal rats; and (iii) there is a reduced activation of parasympathetic drive during acute High-Altitude exposure in normal rats. The present results suggest that acute exposure to high-altitude produces an autonomic control impairment and a deterioration of BR function, mainly characterized by parasympathetic withdrawal after 24 h of high-altitude exposure.

Baroreflex Control and High-Altitude Environment

Estimations of the World Health Organization (World Health Organization [WHO], 1996) indicate that ∼140 million people in the World are living at high-altitude (≥2,500 m). It has been showed that during hypoxia there is a BR control impairment, however, some differences may be associated to atmospheric pressure. In fact, during hypobaric-hypoxia there is a reduce of BR gain, without modification of BR set point (Sagawa et al., 1997; Yazdani et al., 2016); but contrarily, normobaric-hypoxia did not modify BR gain (Sagawa et al., 1997). In addition, Obrezchikova et al. (2000), showed that exposure to hypobaric hypoxia (hypoxic chamber) inhibits BR vagal bradycardia in rats. Contrarily to these evidences, our data showed that during High-Altitude exposure (acute exposure), there are no modifications of BR gain either BR set point, which could be related to different levels of High-Altitude simulation (Sagawa et al., 1997; Obrezchikova et al., 2000; Yazdani et al., 2016), some interaction between environmental factors as well as related to some methodological differences (natural

environments vs. simulated high-altitude; catheterization vs. indirect BP measurements; drugs administration vs. neck collar, among others). Also, our results strongly suggest that BR control could be affected by atmospheric pressure, therefore, showing that BR control impairment is not exclusively related to oxygen reduction. However, it has been very well demonstrated that hypoxia produces an increase of chemoreflex drive, which could be associated to a reduction of BR control (Del Rio et al., 2014). Therefore, it is possible that our results may be related to a chemoreflex potentiation and consequently a reduction of BR sensitivity (Del Rio et al., 2014). Along with this, previously we found that in a pre-clinical model of hypertension induced by chronic intermittent hypoxia, the BR control impairment was restored after peripheral chemoreceptor ablation (Del Rio et al., 2016). This suggest that at the central level, chemoreceptor neurons could modulate BR function. Indeed, it has been proposed that at the level of the nucleus of tracts solitaries (NTS), chemo and baroreceptor neurons interact with each other (Miura and Reis, 1972; Somers et al., 1991), which may partially explain BR impairment at high-altitude exposure. Nevertheless, our experiments cannot reveal if a chemoreflex-baroreflex interaction during High-Altitude exposure exists. However, despite that our data showed a robust effect of High-Altitude on parasympathetic modulation of BR function, we did not discard the possible role of atmospheric pressure on baroreflex control. Then, it is necessary to determine the possible contribution of the reduction of atmospheric pressure and the role of hypoxia, but in a natural environment.

High-Altitude Exposure and Autonomic Control Impairment

It has been proposed that acute hypoxia is a potent activator of sympathetic drive in a time dependent manner (Rostrup, 1998; Hainsworth et al., 2007). Moreover, after acute hypoxic exposure there is an autonomic control impairment, increasing muscle sympathetic nerve activity and HRV disturbances (Cornolo et al., 2004). Indeed, using HRV analysis, healthy patients display an increase of LF/HF ratio and only the HF (n.u.) component of HRV was severely decreased after 24 h of hypoxic environment (Cornolo et al., 2004). Accordingly, Obrezchikova et al. (2000) also showed that during hypoxic challenges (hypobaric hypoxic chamber), the parasympathetic modulation is decreased in conscious freely moving rats. Similarly, it has been shown that chronic exposure to High-Altitude, causes increases in HR due to parasympathetic withdrawal (Dhar et al., 2014; Siebenmann et al., 2017). Something interesting to note, is that the parasympathetic withdrawal could persist after one month of high-altitude exposure (Farinelli et al., 1994; Dhar et al., 2014). Our results are in line with those obtained by the aforementioned studies. Indeed, our animals displayed an increase of LF, decrease HF and, consequently, increase of LF/HF ratio after 24 h of high-altitude exposure. Interestingly, it has been shown that plasma norepinephrine was decreased 2 days after high-altitude exposure and the increase was only observed at the third day (Rostrup, 1998). Thus, considering that after 2 days of high-altitude exposure the norepinephrine is decreased (Rostrup, 1998), it is possible that the HRV disturbances in our data may be related to parasympathetic modulation rather than sympathetic activation. Indeed, using non-stationary analysis, after 24 h of high-altitude exposure, it showed that the parasympathetic activation (phenylephrine) is decreased compared to the sea level condition. Therefore, the autonomic disturbances may be mainly related to parasympathetic withdrawal than to sympathoexcitation during high-altitude exposure.

In addition, despite that in our experiments we did not evaluate norepinephrine release, our results showed that BR maximum tachycardic response was not different between sea level and high-altitude exposure, suggesting that the sympathetic drive during high-altitude could not be related to BR control, if not to an interaction between peripheral chemoreflex activation and baroreflex control impairment, triggering parasympathetic withdrawal (Del Rio et al., 2016). Nevertheless, we did not evaluate chemoreflex response in our experiments, which might be related to autonomic control impairment observed in our data (Hayashida et al., 1996; Schultz et al., 2007). Thus, further research is needed to elucidate the possible relationship between baroreflex and chemoreflex and their role on cardiac autonomic function, but in a natural environment, which is characterized by differences in atmospheric pressure, humidity and in several territories with different temperatures.

In addition, from a practical perspective, our work could be applied to people exposed to "live low – work high" conditions. In several countries, (i.e., Peru, Chile, among others) the growth domestic product is critically dependent of bigger mining whose operations are mostly at high-altitude. Additionally, Chile is a country with an important number of astronomers (e.g., ALMA project) exposed to the aforementioned "live low – work high" conditions. Further, in several sports, competitions are celebrated at high-altitude (e.g., Olympic Games, Mexico 1968). Therefore, our results could transfer to people which are subjected to high-altitude exposure with a focus on improving baroreflex control and parasympathetic modulation of the heart, which could improve the functional capacity at high-altitude.

Limitations

Regarding some potential limitations of our study, we did not use the same animals at Sea-Level and at High-Altitude conditions, which could mask some physiological responses to High-Altitude exposure. However, our results showed that after acute High-Altitude exposure our animals displayed several characteristics of hypobaric hypoxic exposure. In addition, our experiments were limited to 24 h post-High-Altitude condition. Thus, it is not possible to infer the long-term effects of High-Altitude exposure on cardiac BR control from our study. Moreover, we did not determine the contribution of ventilatory chemoreflex control, which could be related to BR control impairment after 24 h of High-Altitude exposure (Halliwill et al., 2003). In addition, we performed our physiological experiments 8 h after surgical catheterization, which could affect BR control (Tohyama et al., 2018), however, all animals were subjected to the same procedure, therefore, they should be comparable. Other potential limitation of our study, was the different relative air humidity during the two experimental conditions. Nevertheless, it is important to mention that the experiments were carried out in typical environmental

condition to which it is subjected when a person is exposed to High-Altitude (Bruce-Low et al., 2006; Abellán-Aynés et al., 2019). Finally, we did not use pharmacological approaches to characterize sympathetic and parasympathetic contributions to cardiac BR control after high-altitude exposure.

CONCLUSION

Cardiac autonomic dysfunction and BR control impairment occur after 24 h (i.e., acute) of High-Altitude exposure. In addition, the parasympathetic activation was decreased after high-altitude exposure. Therefore, the short-term exposure to high-altitude produces an autonomic control impairment and BR dysfunction, which could be more related to parasympathetic modulation of the heart rather than sympathetic drive.

DATA AVAILABILITY STATEMENT

The datasets generated for this study are available on request to the corresponding author.

ETHICS STATEMENT

The animal study was reviewed and approved by University of Antofagasta Scientific Research Ethical Committee (CEIC-210/2019).

AUTHOR CONTRIBUTIONS

AB, AA-Á, MV-M, RR-C, MI, MR, RD and DA designed the work and contributed to analysis, interpreted the the data, and drafted the work. AB and DA performed the data collection and analysis and contributed to the concept of the project and experimental design. All authors approved the final version of the manuscript.

FUNDING

This work was supported by Semillero de Investigación, Universidad de Antofagasta (5313). AA-Á was supported by Proyecto Interinstitucional, Dirección de Postgrado, Universidad Católica Silva Henríquez. DA was supported by Proyecto Puente, Vicerrectoría de Investigación, Universidad Mayor, Chile (I-2019050). RR-C was supported by Proyecto de Investigación API4, Dirección de Investigación, Universidad de Los Lagos. RD was supported by Fondecyt grant 1180172 and the Basal Center of Excellence in Aging and Regeneration (AFB 170005) and the special grant "Lithium in Health and Disease" from the Sociedad Química y Minera de Chile (SQM).

ACKNOWLEDGMENTS

We thank Mr. Hernán Ubillo for his help in managing the animal facility.

REFERENCES

Abellán-Aynés, A., López-Plaza, D., Alacid, F., Naranjo-Orellana, J., and Manonelles, P. (2019). Recovery of heart rate variability after exercise under hot conditions: the effect of relative humidity. *Wilderness Environ. Med.* 30, 260–267. doi: 10.1016/j.wem.2019.04.009

Andrade, D. C., Arce-Alvarez, A., Toledo, C., Díaz, H. S., Lucero, C., Schultz, H. D., et al. (2017). Exercise training improves cardiac autonomic control, cardiac function, and arrhythmogenesis in rats with preserved-ejection fraction heart failure. *J. Appl. Physiol.* 123, 567–577. doi: 10.1152/japplphysiol.00189.2017

Andrade, D. C., Toledo, C., Díaz, H. S., Lucero, C., Arce-Álvarez, A., Oliveira, L. M., et al. (2019). Ablation of brainstem C1 neurons improves cardiac function in volume overload heart failure. *Clin. Sci.* 133, 393–405. doi: 10.1042/cs20180589

Bourdillon, N., Saugy, J., Schmitt, L., Rupp, T., Yazdani, S., Vesin, J. M., et al. (2017). Acute and chronic changes in baroreflex sensitivity in hypobaric vs. normobaric hypoxia. *Eur. J. Appl. Physiol.* 117, 2401–2407. doi: 10.1007/s00421-017-3726-6

Bruce-Low, S., Cotterrell, D., and Jones, E. (2006). Heart Rate Variability During High Ambient Heat Exposure. *Aviat. Space Environ. Med.* 77, 915–920.

Cornolo, J., Mollard, P., Brugniaux, J. V., Robach, P., and Richalet, J. P. (2004). Autonomic control of the cardiovascular system during acclimatization to high altitude: effects of sildenafil. *J. Appl. Physiol.* 97, 935–940. doi: 10.1152/japplphysiol.00239.2004

Cowley, A. W. Jr., and Guyton, A. C. (1975). Baroreceptor reflex effects on transient and steady-state hemodynamics of salt-loading hypertension in dogs. *Circ. Res.* 36, 536–546. doi: 10.1161/01.res.36.4.536

Del Rio, R., Andrade, D. C., Lucero, C., Arias, P., and Iturriaga, R. (2016). Carotid Body Ablation Abrogates Hypertension and Autonomic Alterations Induced by Intermittent Hypoxia in Rats. *Hypertension* 68, 436–445. doi: 10.1161/hypertensionaha.116.07255

Del Rio, R., Marcus, N. J., and Schultz, H. D. (2013). Carotid chemoreceptor ablation improves survival in heart failure: rescuing autonomic control of cardiorespiratory function. *J. Am. Coll. Cardiol.* 62, 2422–2430. doi: 10.1016/j.jacc.2013.07.079

Del Rio, R., Moya, E., and Iturriaga, R. (2014). Carotid body potentiation during chronic intermittent hypoxia: Implication for hypertension. *Front. Physiol.* 5:434. doi: 10.3389/fphys.2014.00434

Dhar, P., Sharma, V. K., Hota, K. B., Das, S. K., Hota, S. K., Srivastava, R. B., et al. (2014). Autonomic cardiovascular responses in acclimatized lowlanders on prolonged stay at high altitude: a longitudinal follow up study. *PLoS One* 9:e84274. doi: 10.1371/journal.pone.0084274

Eckberg, D. L., Halliwill, J. R., Beightol, L. A., Brown, T. E., Taylor, J. A., and Goble, R. (2010). Human vagal baroreflex mechanisms in space. *J. Physiol.* 588(Pt 7), 1129–1138. doi: 10.1113/jphysiol.2009.186650

Farinelli, C. C., Kayser, B., Binzoni, T., Cerretelli, P., and Girardier, L. (1994). Autonomic nervous control of heart rate at altitude (5050 m). *Eur. J. Appl. Physiol. Occupat. Physiol.* 69, 502–507. doi: 10.1007/bf00239867

Feng, J., Fitz, Y., Li, Y., Fernandez, M., Cortes Puch, I., Wang, D., et al. (2015). Catheterization of the carotid artery and jugular vein to perform hemodynamic measures, infusions and blood sampling in a conscious rat model. *J. Vis. Exp.*

Ferguson, D. W., Berg, W. J., Roach, P. J., Oren, R. M., and Mark, A. L. (1992). Effects of heart failure on baroreflex control of sympathetic neural activity. *Am. J. Cardiol.* 69, 523–531. doi: 10.1016/0002-9149(92)90998-e

Fernandez, G., Lee, J. A., Liu, L. C., and Gassler, J. P. (2015). The Baroreflex in Hypertension. *Curr. Hyperten. Rep.* 17:19.

Hainsworth, R., Drinkhill, M. J., and Rivera-Chira, M. (2007). The autonomic nervous system at high altitude. *Clin. Autonomic Res.* 17, 13–19. doi: 10.1007/s10286-006-0395-7

Halliwill, J. R., Morgan, B. J., and Charkoudian, N. (2003). Peripheral chemoreflex and baroreflex interactions in cardiovascular regulation in humans. *J. Physiol.* 552(Pt 1), 295–302. doi: 10.1113/jphysiol.2003.050708

Hayashida, Y., Hirakawa, H., Nakamura, T., and Maeda, M. (1996). Chemoreceptors in autonomic responses to hypoxia in conscious rats. *Adv. Exp. Med. Biol.* 410, 439–442. doi: 10.1007/978-1-4615-5891-0_67

Lanfranchi, P. A., Colombo, R., Cremona, G., Baderna, P., Spagnolatti, L., Mazzuero, G., et al. (2005). Autonomic cardiovascular regulation in subjects with acute mountain sickness. *Am. J. Physiol. Heart Circ. Physiol.* 289, H2364–H2372.

Lanfranchi, P. A., and Somers, V. K. (2002). Arterial baroreflex function and cardiovascular variability: interactions and implications. *Am. J. Physiol. Regul. Integr. Compar. Physiol.* 283, R815–R826.

Li, P., Sur, S. H., Mistlberger, R. E., and Morris, M. (1999). Circadian blood pressure and heart rate rhythms in mice. *Am. J. Physiol. Regul. Integr. Compar. Physiol.* 276, R500–R504.

Masson, G. S., Costa, T. S., Yshii, L., Fernandes, D. C., Soares, P. P., Laurindo, F. R., et al. (2014). Time-dependent effects of training on cardiovascular control in spontaneously hypertensive rats: role for brain oxidative stress and inflammation and baroreflex sensitivity. *PLoS One* 9:e94927. doi: 10.1371/journal.pone.0094927

Michelini, L. C., Marcelo, M. C., Amico, J., and Morris, M. (2003). Oxytocinergic regulation of cardiovascular function: studies in oxytocin-deficient mice. *Am. J. Physiol. Regul. Integr. Compar. Physiol.* 284, H2269–H2276.

Miura, M., and Reis, D. J. (1972). The role of the solitary and paramedian reticular nuclei in mediating cardiovascular reflex responses from carotid baro- and chemoreceptors. *J. Physiol.* 223, 525–548.

Monahan, K. D. (2007). Effect of aging on baroreflex function in humans. *Am. J. Physiol. Regul. Integr. Compar. Physiol.* 293, R3–R12.

Negrão, C. E., Irigoyen, M. C., Moreira, E. D., Brum, P. C., Freire, P. M., and Krieger, E. M. (1993). Effect of exercise training on RSNA, baroreflex control, and blood pressure responsiveness. *Am. J. Physiol. Regul. Integr. Compar. Physiol.* 265(2 Pt 2), R365–R370.

Obrezchikova, M. N., Tarasova, O. S., Borovik, A. S., and Koshelev, V. B. (2000). Adaptation to periodic high-altitude hypoxia inhibits baroreflex vagal bradycardia in rats. *Bull. Exp. Biol. Med.* 129, 327–329. doi: 10.1007/bf02439257

Rostrup, M. (1998). Catecholamines, hypoxia and high altitude. *Acta Physiol. Scand.* 162, 389–399. doi: 10.1046/j.1365-201x.1998.00335.x

Sagawa, S., Torii, R., Nagaya, K., Wada, F., Endo, Y., and Shiraki, K. (1997). Carotid baroreflex control of heart rate during acute exposure to simulated altitudes of 3,800 m and 4,300 m. *Am. J. Physiol. Regul. Integr. Compar. Physiol.* 273, R1219–R1223.

Schultz, H. D., Li, Y. L., and Ding, Y. (2007). Arterial chemoreceptors and sympathetic nerve activity: implications for hypertension and heart failure. *Hypertension* 50, 6–13. doi: 10.1161/hypertensionaha.106.076083

Siebenmann, C., Rasmussen, P., Hug, M., Keiser, S., Flück, D., Fisher, J. P., et al. (2017). Parasympathetic withdrawal increases heart rate after 2 weeks at 3454 m altitude. *J. Physiol.* 595, 1619–1626. doi: 10.1113/jp273726

Simpson, L. L., Busch, S. A., Oliver, S. J., Ainslie, P. N., Stembridge, M., Steinback, C. D., et al. (2019). Baroreflex control of sympathetic vasomotor activity and resting arterial pressure at high altitude: insight from Lowlanders and Sherpa. *J. Physiol.* 597, 2379–2390. doi: 10.1113/jp277663

Somers, V. K., Mark, A. L., and Abboud, F. M. (1991). Interaction of baroreceptor and chemoreceptor reflex control of sympathetic nerve activity in normal humans. *J. Clin. Invest.* 87, 1953–1957. doi: 10.1172/JCI115221

Stauss, H. M. (2002). Baroreceptor reflex function. *Am. J. Physiol. Regul. Integr. Compar. Physiol.* 283, R284–R286.

Tohyama, T., Saku, K., Kawada, T., Kishi, T., Yoshida, K., Nishikawa, T., et al. (2018). Impact of lipopolysaccharide-induced acute inflammation on baroreflex-controlled sympathetic arterial pressure regulation. *PLoS One* 13:e0190830. doi: 10.1371/journal.pone.0190830

Wang, W., Zhu, G. Q., Gao, L., Tan, W., and Qian, Z. M. (2004). Baroreceptor reflex in heart failure. *Acta Physiol. Sin.* 56, 269–281.

World Health Organization [WHO], (1996). *World Health Statistics Annual 1995*. Geneva: World Health Organization.

Yazdani, S., Bourdillon, N., Subudhi, A., Lovering, A., Roach, R., Kayser, B., et al. (2016). "AltitudeOmics: effect of exercise on baroreflex sensitivity at sea level and altitude," in *Proceedings of the Computing in Cardiology*, (Vancouver, BC: IEEE), 529–532.

Conflict of Interest: The authors declare that the research was conducted in the absence of any commercial or financial relationships that could be construed as a potential conflict of interest.

frontiers in Physiology

ORIGINAL RESEARCH
published: 02 September 2020
doi: 10.3389/fphys.2020.01051

Association Between Inflammatory Mediators and Pulmonary Blood Flow in a Rabbit Model of Acute Pulmonary Embolism Combined With Shock

*Yuting Wang†, Delong Yu†, Yijun Yu, Xiaoyan Liu, Liqun Hu and Ye Gu**

Department of Cardiology, Wuhan Fourth Hospital, Puai Hospital Affiliated to Tongji Medical College, Huazhong University of Science and Technology, Wuhan, China

OPEN ACCESS

Edited by:
Mieczyslaw Pokorski, Public Higher Medical Professional School in Opole, Poland

Reviewed by:
Andrew T. Lovering, University of Oregon, United States
Camillo Di Giulio, University of Studies G. d'Annunzio Chieti and Pescara, Italy

***Correspondence:**
Ye Gu
yegu2003cn@163.com

†These authors have contributed equally to this work and share first authorship

Specialty section:
This article was submitted to Respiratory Physiology, a section of the journal Frontiers in Physiology

Received: *23 April 2020*
Accepted: *30 July 2020*
Published: *02 September 2020*

Citation:
Wang Y, Yu D, Yu Y, Liu X, Hu L and Gu Y (2020) Association Between Inflammatory Mediators and Pulmonary Blood Flow in a Rabbit Model of Acute Pulmonary Embolism Combined With Shock. Front. Physiol. 11:1051. doi: 10.3389/fphys.2020.01051

Background: The pro-inflammatory cytokines were detected in pulmonary embolism (PE) and non-pulmonary embolism (non-PE) tissues to explore the role of inflammation responses and their relationship with the pulmonary blood flow in a rabbit model of acute pulmonary embolism combined with shock.

Methods and Results: Nineteen rabbits were randomly divided into sham operation group (S group, n = 8) and massive PE (MPE group, n = 11). The MPE model was established by injecting the autologous blood clots into the main pulmonary artery of rabbit. Pulmonary angiography showed that the pulmonary circulation time was significantly prolonged in the MPE group, and pulmonary blood flow was attenuated at 120 min post PE. Hematoxylin–eosin (HE) staining revealed enhanced inflammatory cell infiltration around the pulmonary vessels in PE and non-PE tissues, and obvious edema on the perivascular region. Meanwhile, the expressions of inducible nitric oxide synthase (iNOS) and arginase 1 (Arg-1) in pulmonary vascular and alveolar tissues were significantly upregulated and the iNOS/Arg-1 ratio was significantly higher in the MPE group than in the S group. Moreover, the levels of tumor necrosis factor-alpha (TNF-α) and interleukin-1 beta (IL-1β) were also significantly increased in PE and non-PE tissues, and interleukin-6 (IL-6) level was significantly increased in non-PE tissues in the MPE group as compared to the S group. Thromboxane A2 (TXA_2) and alpha smooth muscle actin (α-SMA) levels were significantly higher in both PE and non-PE tissues in the MPE group than in the S group.

Conclusion: Activation of inflammation mediators in PE and non-PE tissues might be one of the crucial factors responsible for pulmonary vasculature constriction and pulmonary blood flow attenuation in this MPE model.

Keywords: acute pulmonary embolism, pro-inflammatory cytokines, TNF-α, IL-1β, IL-6, pulmonary vasoconstriction, pulmonary blood flow attenuation

INTRODUCTION

Blockade of pulmonary vasculature by the blood clots in the case of acute pulmonary embolism (APE) can lead to pulmonary hypertension and cardiopulmonary injury (Zhao et al., 2015; Wang et al., 2019). Loss of blood flow to the distal pulmonary vasculature and reduced blood filling to the left ventricle post APE might also result in systemic circulatory failure (shock) and death. Several studies have explored means to reduce the high mortality in the acute phase of massive PE (MPE) and improve its long-term prognosis, however, the achieved benefits were limited (Kinoshita et al., 2000; Neto-Neves et al., 2011; Chun et al., 2012). Our previous studies (Yu et al., 2018; Wang et al., 2019) found that reduced pulmonary artery blood flow in case of APE was jointly induced by pulmonary artery spasm in PE tissues and pulmonary vasculature spasm in non-PE regions. Nonetheless, the detailed mechanism regarding pulmonary vasospasm of PE and non-PE tissues in MPE is not fully understood. A previous study indicated that hypoxia-induced sympathetic system activation served as one of the determinants of pulmonary vasculature spasm and blood flow attenuation in the whole lung during MPE combined with shock (Chun et al., 2012). In the setting of PE, hypoxia is also an important driving factor to enhance inflammatory response, and hypoxia-induced generation of reactive oxygen free radicals is a known stimulator of inflammation (He et al., 2016; Chen et al., 2020). Hence, hypoxia might play a crucial role in PE-induced inflammatory response. In addition, PE-induced pulmonary vascular spasm could also result in hypoxia and lead to a vicious circle of hypoxia-inflammation cascade in both PE and non-PE tissues in this model. Thus far, the association between inflammatory response and pulmonary blood flow failure in MPE remains elusive. This study therefore explored the expressions of inflammatory mediators in PE and non-PE tissues and its relationship with the pulmonary blood flow change in a rabbit model of MPE combined with shock.

MATERIALS AND METHODS

Animals

All animal treatment complied with the Guide for the Care and Use of Laboratory Animals published by the US National Institute of Health (NIH Publication No. 85-23, revised 1996), and the study protocol was approved by the Animal Care Committee at Huazhong University of Science and Technology. Healthy adult New Zealand rabbits, weighing 2.5–3.0 kg, were purchased from the Experimental Animal Center of Tongji Medical College, Huazhong University of Science and Technology. The rabbits were housed under standard conditions with free access to food and drinking water for 1 week before the experiments. Nineteen rabbits were used: 8 rabbits underwent sham operation (S group, puncture and catheterization, followed by bolus injection of saline), and 11 rabbits were used to establish the MPE model (puncture and catheterization, followed by bolus injection of autologous blood clots until shock status was reached).

Abbreviations: α-SMA, alpha smooth muscle actin; APE, acute pulmonary embolism; Arg-1, arginase 1; cAMP, cyclic adenosine monophosphate; ELISA, enzyme-linked immunosorbent assay; HE, hematoxylin–eosin; IL-1β, interleukin-1 beta; IL-6, interleukin-6; iNOS, inducible nitric oxide synthase; MAP, mean arterial pressure; MPAP, mean pulmonary arterial pressure; MPE, massive pulmonary embolism; NE, norepinephrine; non-PE, non-pulmonary embolism; PE, pulmonary embolism; PGI_2, prostaglandin I2; PKA, protein kinase A; TH, tyrosine hydroxylase; TNF-α, tumor necrosis factor-alpha; TXA_2, thromboxane A2.

Anesthesia and Custody

All surgical procedures were performed under sodium pentobarbital anesthesia, in that 3% sodium pentobarbital (20 mg/kg) was injected through the rabbit ear vein. After anesthetic induction, the rabbit was fixed on the operating table in the supine position and heart rate and blood pressure were monitored by the cardiogram monitor (LEAD-7000).

Paracentesis, Catheterization, and the Establishment of MPE Model Combined With Shock

First, skin in the right groin area was prepared and disinfected. After isolating the femoral artery and femoral vein, they were punctured using the Seldinger puncturing method. A 4F Cordis catheter (Cordis Corporation, Florida, United States) was placed in the main trunk of the pulmonary artery through the femoral vein under radiographic guidance. The 5F sheath tube (Radiofocus TERUMO) was inserted into the femoral artery. Second, the MPE model was established as previously described (Yu et al., 2018; Wang et al., 2019). The autologous blood clots [3 mm (± 0.5) × 10 mm] were prepared and placed at the tail end of the 4F catheter and then slowly injected into the main pulmonary artery of the rabbit with 5 mL saline. Autologous blood clots were delivered to the main pulmonary artery in a two-stage manner. In the first stage, a single clot was injected at 60-s intervals four times. Then, the tail end of the 4F Cordis catheter was connected to the pressure transducer for real-time continuous monitoring of the mean arterial pressure (MAP) and mean pulmonary artery pressure (MPAP) by LEAD-7000 monitor (Sichuan Jinjiang Electronic Technology Co., China). The model was considered successful when both following criteria were reached for 2 min: (a) The MAP reduced to < 60 mmHg, and (b) the MPAP increased to up to 2 times the baseline level. MAP and MPAP were dynamically monitored during this period. Third, if MAP and MPAP did not reach the defined levels after the four times of clot injections after the first stage (within 15 min after the first clot injection), more clots were injected at 60-s intervals at the second stage. All rabbits reached the shock status with a maximal of 3 additional clot injections in this experiment. MAP and MPAP were dynamically monitored before PE, during the PE procedure, at the moment of shock status post bolus injection of autologous blood clots, and at 120 min after initiation of MPE. MPE with shock was achieved in all rabbits within 15 min after the clot injection.

Pulmonary Artery Angiography

Pulmonary arterial blood flow imaging was obtained by pulmonary artery angiography (Allura Xper FD20 Philips).

Pulmonary embolism, pulmonary blood flow imaging characteristics, and pulmonary circulation times were compared between the two groups. The pulmonary circulation time was determined by calculating the time taken for the contrast medium to reach from the initiation site of the pulmonary artery trunk to the left atrium through the pulmonary artery trunk and branches, pulmonary capillary, and pulmonary vein. The pulmonary circulation time was calculated for all of the survived rabbits at 120 min, which was the designed study end point [S group ($n = 8$), MPE group ($n = 6$)].

Histological Detection

At the end of the experiment, the rabbits were sacrificed under deep anesthesia (Yu et al., 2018). Based on a previous report (Dias-Junior et al., 2006), 120 min post MPE was chosen for measurement of inflammation. Tissues from four rabbits in the S group and five in the MPE group were randomly selected for pathological detection by hematoxylin–eosin (HE) and immunohistochemistry staining. Similarly, tissues from four and five rabbits in the S and MPE groups, respectively, were used for PCR and enzyme-linked immunosorbent assay (ELISA)-based experiments. Lung tissues were excised and underwent fixation with paraformaldehyde. PE and non-PE tissues were cut into sections for pathological examination after paraffin embedding, respectively. The HE stain was used to analyze the pathology of PE and non-PE tissues. Immunohistochemistry staining was also performed on lung tissue sections with the following antibodies: inducible nitric oxide synthase (iNOS) (1:100, abcam, Cambridge, MA, United States), arginase 1 (Arg-1) (1:100, abcam), and alpha smooth muscle actin (α-SMA) (1:100, abcam). The pathological changes were quantified using commercial software (Image-Pro Plus, Media Cybernetics, Inc., Rockville, Maryland, United States) and evaluated by assessing the percentage of the positive area. In addition, the levels of thromboxane A2 (TXA_2) and prostaglandin I2 (PGI_2) in PE and non-PE tissues were evaluated by ELISA.

Determination of the mRNA Expression of Pro-inflammatory Cytokines in PE and Non-PE Tissues by Real-Time Polymerase Chain Reaction

Total RNA was extracted from PE and non-PE lung tissues using RNA Tissue Mini Kit (Takara, Dalian, Liaoning, China) according to the manufacturer's instructions. Reverse transcription and cDNA synthesis were performed using PrimeScript RT Master Mix Perfect Real Time (Takara, Dalian, Liaoning, China). Real-time polymerase chain reaction was performed to detect the expression of various cytokines such as tumor necrosis factor-alpha (TNF-α), interleukin-1 beta (IL-1β), and interleukin-6 (IL-6) by QuantiFast SYBR Green PCR Kit (Qiagen, Dusseldorf, Germany) and Bio-Rad CFX96 (Bio-Rad, Hercules, CA, United States) according to the manufacturer's instructions. PCR primers are shown in **Table 1**. Relative gene expression was calculated using the $2^{-\Delta\Delta CT}$ method.

TABLE 1 | PCR primers sequences.

Forward/reverse	Sequence (5′–3′)
β-Actin	S: 5′-CCCAGATCATGTTCGAGACGT-3′
	F: 5′-TAGCCCTCGTAGATGGGCAC-3′
IL-1β	S: 5′-TCCTGCGTGATGAAAGACGAT-3′
	F: 5′-GGAAGACGGGCATGTACTCTGT-3′
IL-6	S: 5′-CTACCGCTTTCCCCACTTCA-3′
	F 5′-GGCAGGTCTCATTATTCACCG-3′
TNF-α	S: 5′-AGTAGCAAACCCGCAAGTGG-3′
	F: 5′-CCTTGTTCGGGTAGGAGACG-3′

IL-1β, interleukin-1 beta; IL-6, interleukin-6; TNF-α, tumor necrosis factor-alpha.

Statistical Analysis

All statistical data were expressed as mean ± SD. All data were normally distributed as assessed by the Shapiro–Wilk test. Student's *t*-test was employed to evaluate the differences between the two groups. $P < 0.05$ was considered to indicate statistical significance. All statistical analyses were performed with IBM SPSS 19.0 software (IBM, NY, United States).

RESULTS

All eight rabbits in the S group and six out of eleven rabbits in the MPE group survived at the end of the study. Five rabbits in the MPE group died at 7, 8, 21, 32, and 36 min after reaching the shock status, most likely because of irreversible shock.

Pulmonary Angiography Assessment Results

Pulmonary angiography was performed at 120 min post pulmonary occlusion to explore the features of pulmonary circulation. The perfusion of lung field was obviously decreased, and the pulmonary blood flow to the left and right lower lobes was attenuated in the MPE group. The pulmonary circulation time was significantly prolonged in the MPE group compared to the S group (**Figure 1**, $P < 0.05$).

HE Pathology Results

The morphological change of lung tissue is presented in **Figure 2**. Obvious interstitial edema (red lines) and enhanced inflammatory cell infiltration in the pulmonary vessels (green arrows) were seen in the pulmonary vasculature of both PE and non-PE tissues in the MPE group.

iNOS and Arg-1 Expression in PE and Non-PE Tissues

The expressions of iNOS and Arg-1 in pulmonary vascular and alveolar cells in PE and non-PE tissues were significantly higher in the MPE group than in the S group ($P < 0.05$, **Figure 3**). Meanwhile, the ratio of iNOS and Arg-1 in the PE and non-PE tissues was significantly higher in the MPE group than in the S group.

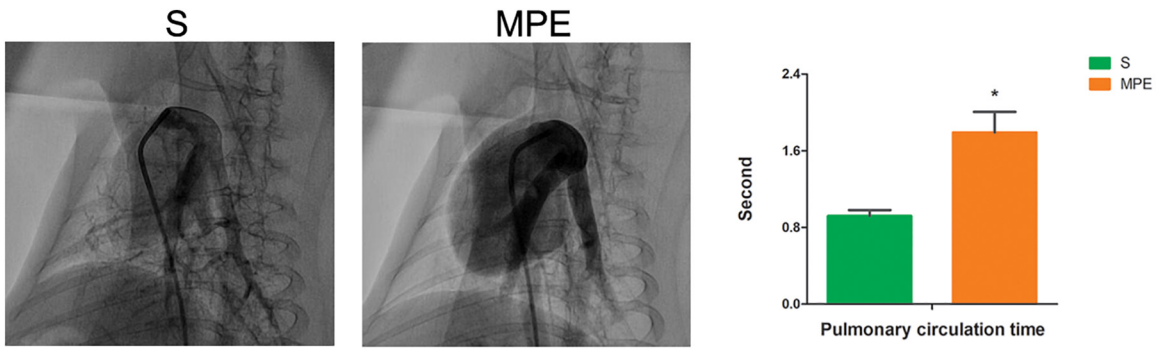

FIGURE 1 | Pulmonary angiography results in S and MPE groups. The pulmonary circulation time was significantly prolonged in the MPE group (n = 6) compared with that of the S group (n = 8). *P < 0.05 vs. S group. S, sham operation group; MPE, massive pulmonary embolism group.

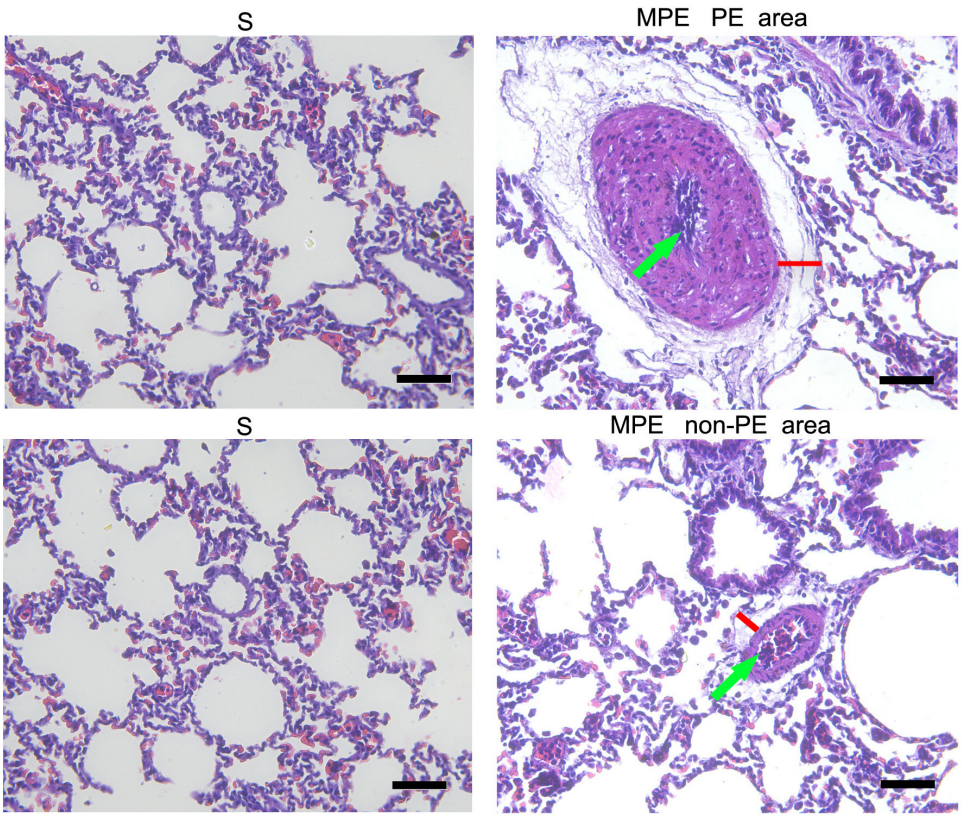

FIGURE 2 | Histological features of PE and non-PE tissues with hematoxylin and eosin (HE). The interstitial edema (red lines) and the inflammatory cell infiltration (green arrows). PE, pulmonary embolism tissue; non-PE, non-pulmonary embolism tissue. S, sham operation group (n = 4); MPE, massive pulmonary embolism group (n = 5). Scale bars: 50 μm.

mRNA Expression of TNF-α, IL-1β, and IL-6 in PE and Non-PE Tissues

As shown in **Figure 4**, mRNA expressions of TNF-α and IL-1β in PE tissues were significantly higher in the MPE group than in the S group (P < 0.05, **Figure 4A**). mRNA expression of IL-6 also tended to be higher in PE tissue in the MPE group. mRNA expressions of TNF-α, IL-1β, and IL-6 were also significantly upregulated in non-PE tissues in the MPE group than in the S group (all P < 0.05, **Figure 4B**).

TXA2 and PGI2 Levels in PE and Non-PE Tissues

The TXA_2 level was higher in both PE and non-PE tissues, while the PGI_2 level tended to be lower in PE and non-PE tissues in the MPE group than in the S group (**Figures 5A,B**).

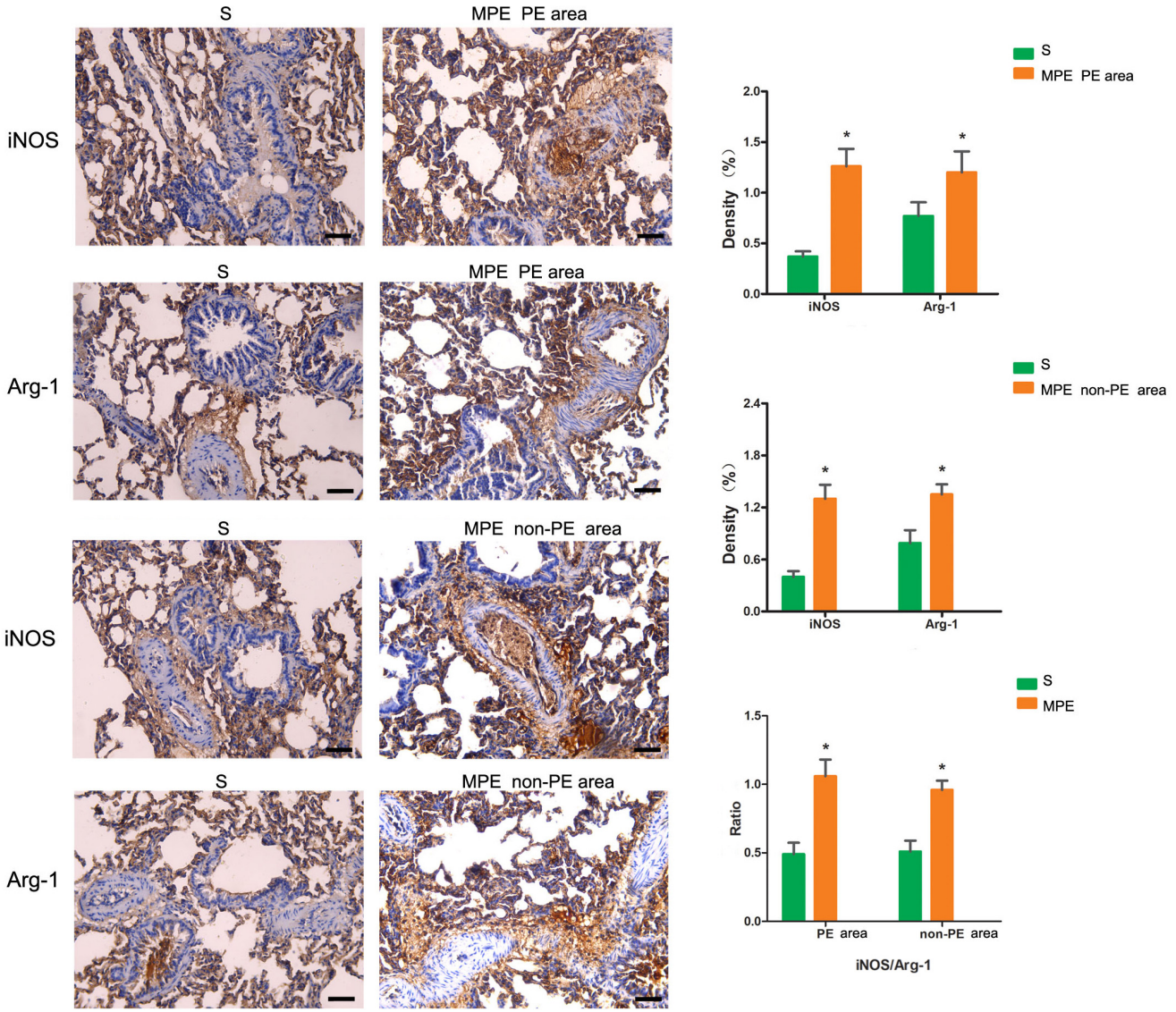

FIGURE 3 | iNOS and Arg-1 immunohistochemical staining features of PE and non-PE tissues. Bar graphs showed the significant increase of iNOS, Arg-1, and iNOS/Arg-1 ratio in the MPE group (n = 5) compared with the S group (n = 4). Data are expressed as mean ± SD by bar graphs, *P < 0.05 vs. S group. PE, pulmonary embolism tissue; non-PE, non-pulmonary embolism tissue. S, sham operation group; MPE, massive pulmonary embolism group. Scale bars: 50 μm.

Expression of α-SMA in PE and Non-PE Tissues

As shown in **Figure 6**, the α-SMA expression in PE and non-PE tissues was significantly higher in the MPE group than in the S group ($P < 0.05$).

DISCUSSION

Our results showed that APE induced significant inflammatory responses in this rabbit MPE model, as expressed by enhanced inflammatory cell infiltration in the pulmonary vessels in both PE and non-PE tissues; obvious edema in the interstitial cell vasculature; and increased expression of TXA_2, TNF-α, IL-1β, and IL-6 in both PE and non-PE tissues. We believe these results might indicate a crucial role of inflammatory responses in the pathogenesis of MPE. The pathophysiological mechanisms of the high mortality caused by acute MPE combined with shock are multiple, whereas the key factor leading to shock was the acute pulmonary blood flow failure. Pulmonary artery spasm and blood flow attenuation could jointly result in the reduction of blood filling to the left ventricle. Our previous studies have shown that pulmonary artery spasm in both PE and non-PE tissues contributed to acute pulmonary failure in this MPE model (Yu et al., 2018; Wang et al., 2019). The present study further highlighted the potential role of increased inflammatory

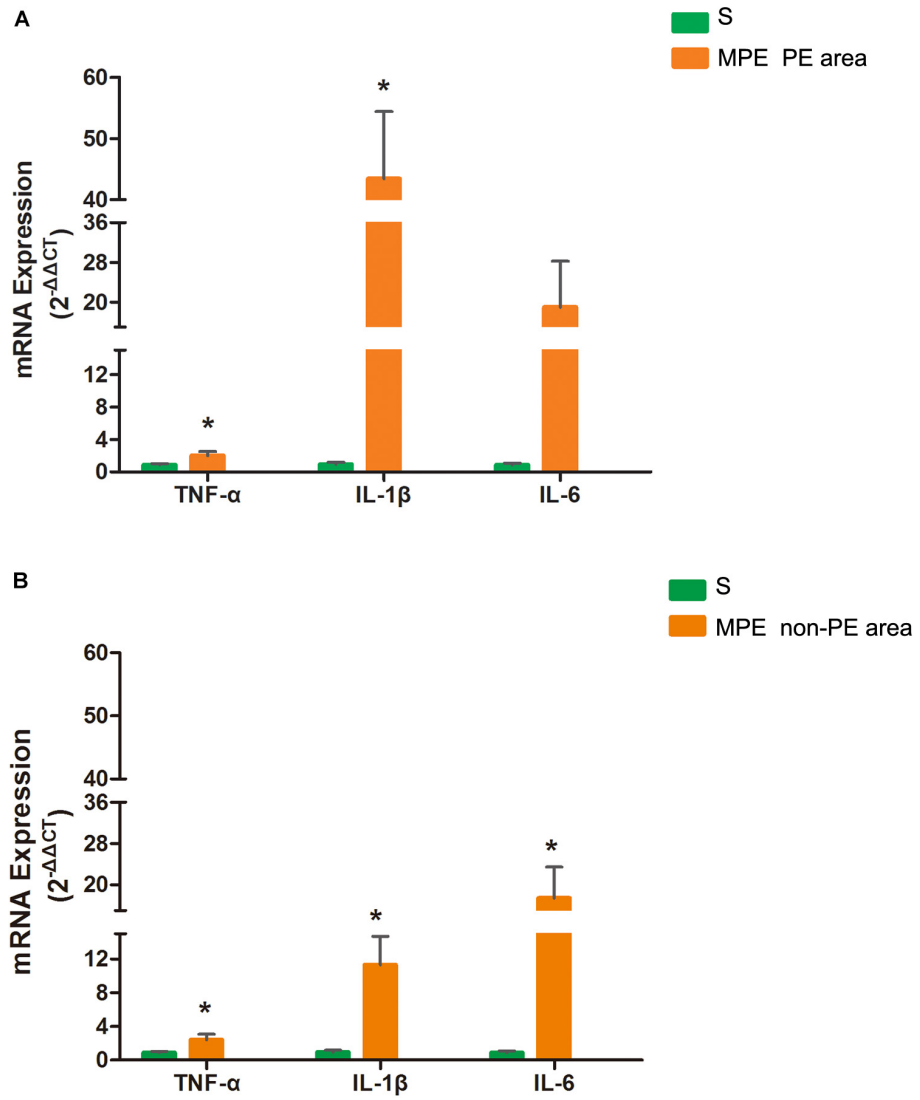

FIGURE 4 | mRNA expressions of TNF-α, IL-1, and IL-6 in PE **(A)** and non-PE **(B)** tissues by RT-PCR. Bar graphs indicated that TNF-α, IL-1β, mRNA expressions of the MPE group (n = 5) in PE and non-PE tissues were significantly increased. IL-6 mRNA levels in non-PE tissues were significantly increased than in the S group (n = 4), which was tended to be higher in PE tissues. Data are expressed as mean ± SD by bar graphs. *P < 0.05 vs. S group. PE, pulmonary embolism tissue; non-PE, non-pulmonary embolism tissue. S, sham operation group; MPE, massive pulmonary embolism group.

responses in both PE and non-PE tissues on enhancing the vicious progression of pulmonary hypertension in the disease course of MPE.

The Enhanced Inflammation Response and Possible Mechanisms in Case of MPE

In this MPE combined shock rabbit model, we saw that the pulmonary vessels were filled with numerous neutrophils in both PE and non-PE tissues. Furthermore, there were significant edematous changes in vascular interstitial tissue (**Figure 2**). We also observed an increased expression of iNOS and Arg-1 in pulmonary vascular and alveolar cells in PE and non-PE tissues in the MPE group. It is known that iNOS is released from the vascular endothelium in response to hypoxia (Hua et al., 2018). Cheng et al. reported that the pulmonary macrophages of animal lung tissues could also secrete iNOS (Cheng et al., 2018) under pathological stimulation such as acute lung injury and inflammatory disease. The increased iNOS expression in lung tissues further indicates the enhanced inflammation status in this model. The ratio of iNOS and Arg-1 was increased in PE and non-PE tissues in the MPE group (**Figure 3**), indicating a hyperactive inflammation status and which might contribute to the increased expression of proinflammatory cytokines such as TNF-α, IL-1β, and IL-6 in PE and non-PE tissues of the MPE group (**Figure 4**). Increased inflammatory response and overexpression of inflammatory mediators may be regulated by

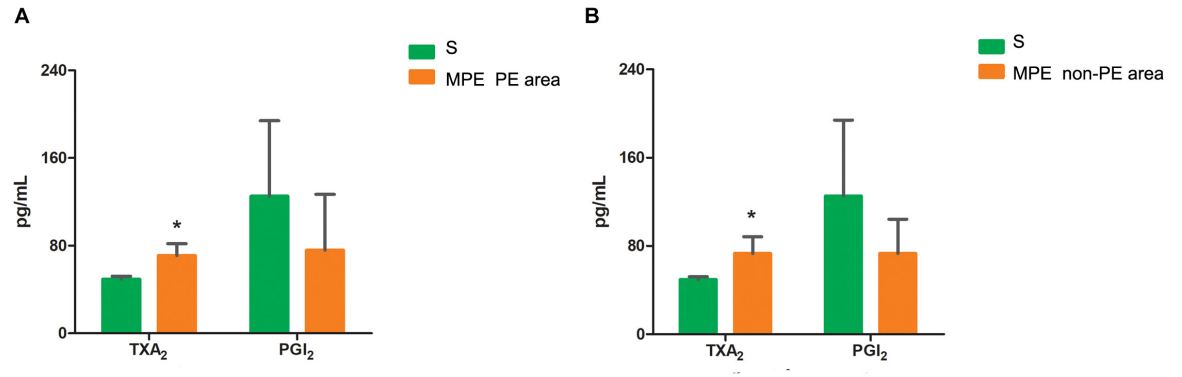

FIGURE 5 | Levels of TXA_2 and PGI_2 in PE **(A)** and non-PE **(B)** tissues by ELISA. The vasoconstrictor factor TXA_2 was increased and the vasodilator factor PGI_2 of MPE group (n = 5) tended to be lower in PE and non-PE tissues. Data are expressed as mean ± SD by bar graphs, $^*P < 0.05$ vs. S group (n = 4). PE, pulmonary embolism tissue; non-PE, non-pulmonary embolism tissue. S, sham operation group; MPE, massive pulmonary embolism group.

many aspects: (1) In a previous study (Olschewski et al., 2018), the authors showed that under the stress of hypoxia, inflammatory cells such as neutrophils and macrophages could adhere and aggregate on the pulmonary artery blood vessel walls to infiltrate lung tissue. (2) The pulmonary blood flow was reduced in the setting of MPE, which could cause ischemia and hypoxia of lung tissues. Our previous study demonstrated that MAP, PaO_2, and pH derived from blood gas analysis were significantly decreased in MPE rabbits, indicating the hypoxia status of respiratory failure in MPE rabbits associated with shock (Wang et al., 2019). Hypoxia induced generation of oxygen free radicals which are known stimulators of inflammation (He et al., 2016; Chen et al., 2020). Therefore, hypoxia might serve as a crucial factor in PE-induced inflammatory response. In addition, PE-induced pulmonary vascular spasm could also result in hypoxia and lead to a vicious circle of hypoxia-inflammation cascade in both PE and non-PE tissues in this model. (3) In our previous study, we found that the sympathetic activity of lung tissue was hyperactivated, and tyrosine hydroxylase (TH) increase could catalyze norepinephrine (NE) on vascular α-receptors; these factors could exacerbate vasospasm and simultaneously stimulate the inflammatory reaction. The above findings are in line with previous reports in that the levels of inflammatory mediators were increased in MPE and were characterized by aggregation of neutrophils and macrophages in pulmonary vasculature and reduced pulmonary blood flow (Pongratz and Straub, 2014; Barrios-Payán et al., 2016). Therefore, during the acute phase of MPE, thromboembolic vasculature, tissue ischemia, hypoxia, and the sympathetic nervous system might all mediate enhanced lung tissue inflammatory responses in this rabbit model of MPE.

Expression of the Inflammatory Response in PE and Non-PE Tissues

The present study not only determined the inflammation of PE tissues but also evaluated the inflammation reaction in the non-PE tissues in this model. A large number of inflammatory cells infiltrated the PE tissues (**Figure 2**), the levels of iNOS and Arg-1 were obviously increased (**Figure 3**), and the mRNA expressions of pro-inflammatory cytokines including TNF-α, IL-1β, and IL-6 were all upregulated in PE tissues (**Figure 4**). Interestingly, non-PE tissues were also infiltrated with a large number of inflammatory cells along with obvious edema in the vascular tissues of the non-PE region. The expressions of iNOS and Arg-1 in the pulmonary vascular and alveolar tissue were significantly increased in the MPE group compared to the S group, and the ratio of iNOS/Arg-1 was significantly higher in non-PE tissues. Furthermore, the expressions of the pro-inflammatory cytokines TNF-α, IL-1β, and IL-6 were all significantly upregulated in the non-PE tissues of the MPE group compared to the S group (**Figure 4B**). Although the pulmonary vasculature was not blocked in the non-PE area, the pulmonary blood flow was still reduced. These phenomena might be explained as follows: (1) Under the condition of ischemia and hypoxia, a large number of neutrophils and macrophages infiltrate into the non-PE tissues and led to pulmonary vascular lesions and vascular interstitial edema, which might contribute to the pulmonary blood flow attenuation in this region. (2) The excessive activation of sympathetic activity as shown in our previous study (Wang et al., 2019) might also be an important driving force responsible for the induction of inflammatory response in non-PE areas.

The Relationship Between Inflammation and Blood Flow Attenuation in the Whole Pulmonary Tissues

Vascular endothelial cells and smooth muscle cells play important roles in the pulmonary circulation and pulmonary blood flow. Strielkov et al. reported that hypoxia could stimulate the membrane potential on the surface of pulmonary vascular endothelial cells during the process of hypoxic pulmonary vasoconstriction, thereby contributing to the Ca^{2+} influx and pulmonary vasoconstriction (Strielkov et al., 2017). Besides hypoxia, excessive inflammation was also seen in both PE and non-PE areas post MPE, indicating a central role of inflammation in the setting of MPE besides other known factors (Trow and Taichman, 2009; Clapp and Gurung, 2015; Strielkov et al., 2017). We found that the TXA_2 levels were obviously increased

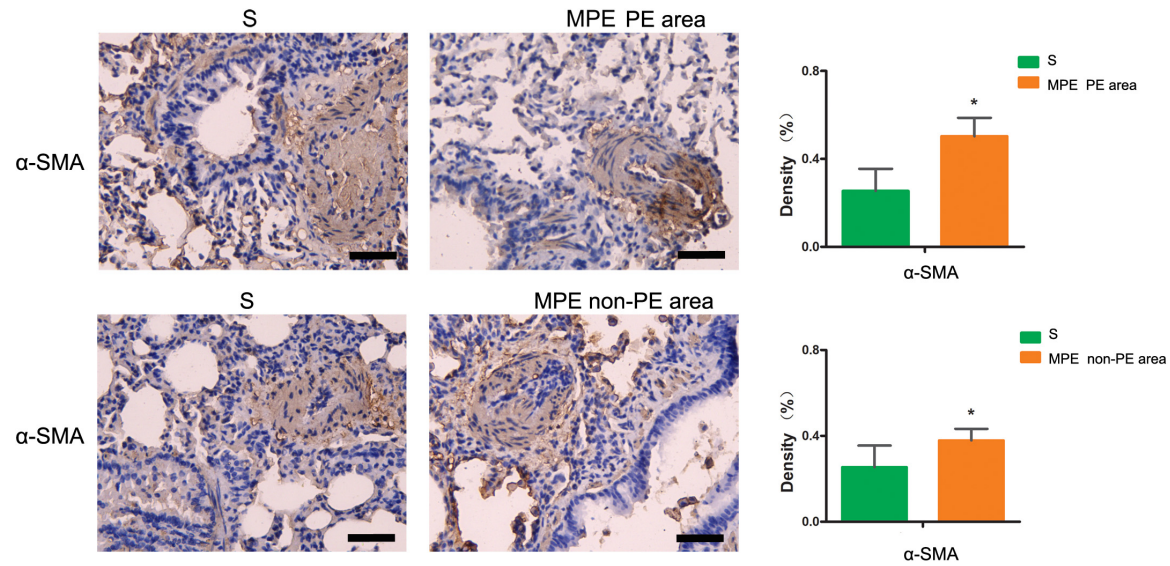

FIGURE 6 | α-SMA immunohistochemical staining features of PE and non-PE tissues. The α-SMA expression in PE and non-PE tissues in the MPE group (n = 5) was significantly higher than in the S group (n = 4). Data are expressed as mean ± SD by bar graphs, $^*P < 0.05$ vs. S group. PE, pulmonary embolism tissue; non-PE, non-pulmonary embolism tissue. S, sham operation group; MPE, massive pulmonary embolism group. Scale bars: 50 μm.

and PGI_2 contents tended to be lower in both PE and non-PE areas (**Figure 5**). This finding is in line with a previous report by Foudi et al. who demonstrated that inflammatory cytokines could reduce PGI_2 through modulating protein kinase A (PKA)/cyclic adenosine monophosphate (cAMP) pathways, and the imbalances of TXA_2/PGI_2 were linked with enhanced platelet aggregation, leading to vascular dysfunction in case of hypoxia (Foudi et al., 2017). Pulmonary artery smooth muscle could specifically express contraction protein α-SMA under the normal physiological condition, which played an important role in the regulation of pulmonary artery pressure (Liu et al., 2017; Li et al., 2019). Hence, we measured the expression of α-SMA in lung tissues in this model. As expected, the α-SMA expression in PE and non-PE tissues was significantly increased in the MPE group compared to the S group (**Figure 6**). Hypoxia, inflammatory cell infiltration in the pulmonary artery wall, vascular dysfunction, and enhanced expression of pulmonary vascular α-SMA in both PE and non-PE areas could have jointly contributed to pulmonary artery contraction and pulmonary blood flow reduction in both PE and non-PE tissues.

Study Limitation

Our study has some limitations. First, in the setting of MPE, pulmonary artery embolization induced inflammatory response, hypoxia, pulmonary vasospasm, and blood flow attenuation; these multifaced disease features occurred in both PE and non-PE tissues. Although we evaluated inflammatory cytokines in the PE and non-PE areas in this study, we could not differentiate the exact impact of PE or hypoxia on the observed inflammatory responses in our study. Future studies are warranted to clarify this issue in the presence or absence of strategies specifically targeting the hypoxia, e.g., by supplying oxygen via a respirator to the incubated rabbit to evaluate the impact of hypoxia in this MPE model. Second, iNOS could be released from both vascular endothelium in response to hypoxia (Hua et al., 2018) and pulmonary macrophages under pathological state stimulation such as acute lung injury and inflammatory disease (Cheng et al., 2018). The present study design could not differentiate and confirm the origin of iNOS. Future studies are warranted to demonstrate the origin of iNOS by labeling pulmonary macrophages with multiple immunofluorescence tags. Thus, increased iNOS in this model could only reflect the inflammation status in our study. Third, inflammatory proteins were not measured for both mRNA and protein quantification due to experimental design deficiency. Therefore, it remains unknown whether the mRNA and protein changes were proportional; our results should thus be interpreted with caution.

CONCLUSION

Excessive inflammatory response was evidenced in both PE and non-PE tissues in this rabbit model of MPE combined with shock. Inflammation might thus be one of the important factors to aggravate the pulmonary blood flow attenuation and pulmonary failure in this rabbit model of MPE combined with shock. Future studies are warranted to observe the effects of targeted intervention on inflammation in this model.

DATA AVAILABILITY STATEMENT

The raw data supporting the conclusions of this article will be made available by the authors, without undue reservation, to any qualified researcher.

ETHICS STATEMENT

The animal study was reviewed and approved by the Animal Care Committee at Huazhong University of Science and Technology.

AUTHOR CONTRIBUTIONS

YG conceived and designed the study. YW, DY, and YY carried out the molecular data analyses and drafted the manuscript. YW, DY, and XL developed and supervised the animal model. LH drafted and edited the manuscript. All of the authors read and approved the final manuscript.

FUNDING

This study was supported by the grants from the National Natural Science Foundation of China (Grant No. 81900051) and the Wuhan health research fund (Grant No. WX19Z29).

REFERENCES

Barrios-Payán, J., Revuelta, A., Mata-Espinosa, D., Marquina-Castillo, B., Villanueva, E. B., Gutiérrez, M. E. H., et al. (2016). The contribution of the sympathetic nervous system to the immunopathology of experimental pulmonary tuberculosis. *J. Neuroimmunol.* 298, 98–105. doi: 10.1016/j.jneuroim.2016.07.012

Chen, M., Ding, Z., Zhang, F., Shen, H., Zhu, L., Yang, H., et al. (2020). A20 attenuates hypoxia-induced pulmonary arterial hypertension by inhibiting NF-κB activation and pulmonary artery smooth muscle cell proliferation. *Exp. Cell Res.* 390:111982. doi: 10.1016/j.yexcr.2020.111982

Cheng, D.-L., Fang, H.-X., Liang, Y., Zhao, Y., and Shi, C.-S. (2018). MicroRNA-34a promotes iNOS secretion from pulmonary macrophages in septic suckling rats through activating STAT3 pathway. *Biomed. Pharmacother.* 105, 1276–1282. doi: 10.1016/j.biopha.2018.06.063

Chun, C., Wang, Y., Xueding, C., Qi, Z., Xiaoying, H., Honglei, X., et al. (2012). Resveratrol downregulates acute pulmonary thromboembolism-induced pulmonary artery hypertension via p38 mitogen-activated protein kinase and monocyte chemoattractant protein-1 signaling in rats. *Life Sci.* 90, 721–727. doi: 10.1016/j.lfs.2012.03.008

Clapp, L. H., and Gurung, R. (2015). The mechanistic basis of prostacyclin and its stable analogues in pulmonary arterial hypertension: role of membrane versus nuclear receptors. *Prostaglandins Other Lipid Mediat.* 120, 56–71. doi: 10.1016/j.prostaglandins.2015.04.007

Dias-Junior, C. A., Gladwin, M. T., and Tanus-Santos, J. E. (2006). Low-dose intravenous nitrite improves hemodynamics in a canine model of acute pulmonary thromboembolism. *Free Radic Biol. Med.* 41, 1764–1770. doi: 10.1016/j.freeradbiomed.2006.08.022

Foudi, N., Ozen, G., Amgoud, Y., Louedec, L., Choqueux, C., Badi, A., et al. (2017). Decreased vasorelaxation induced by iloprost during acute inflammation in human internal mammary artery. *Eur. J. Pharmacol.* 804, 31–37. doi: 10.1016/j.ejphar.2017.03.060

He, Y. Y., Liu, C. L., Li, X., Li, R. J., Wang, L. L., and He, K. L. (2016). Salubrinal attenuates right ventricular hypertrophy and dysfunction in hypoxic pulmonary hypertension of rats. *Vascul. Pharmacol.* 87, 190–198. doi: 10.1016/j.vph.2016.09.009

Hua, C., Zhao, J., Wang, H., Chen, F., Meng, H., Chen, L., et al. (2018). Apple polyphenol relieves hypoxia-induced pulmonary arterial hypertension via pulmonary endothelium protection and smooth muscle relaxation: in vivo and in vitro studies. *Biomed. Pharmacother.* 107, 937–944. doi: 10.1016/j.biopha.2018.08.080

Kinoshita, M., Ono, S., and Mochizuki, H. (2000). Neutrophils mediate acute lung injury in rabbits: role of neutrophil elastase. *Eur. Surg. Res.* 32, 337–346. doi: 10.1159/000052215

Li, T., Luo, X. J., Wang, E. L., Li, N. S., Zhang, X. J., Song, F. L., et al. (2019). Magnesium lithospermate B prevents phenotypic transformation of pulmonary arteries in rats with hypoxic pulmonary hypertension through suppression of NADPH oxidase. *Eur. J. Pharmacol.* 847, 32–41. doi: 10.1016/j.ejphar.2019.01.020

Liu, H. X., Hou, L. F., Chen, T., Qu, W., Liu, S., Yan, H. Y., et al. (2017). Prenatal caffeine ingestion increases susceptibility to pulmonary inflammation in adult female rat offspring. *Reprod. Toxicol.* 74, 212–218. doi: 10.1016/j.reprotox.2017.10.006

Neto-Neves, E. M., Dias-Junior, C. A., Uzuelli, J. A., Pereira, R. P., Spiller, F., Czaikoski, P. G., et al. (2011). Sildenafil improves the beneficial hemodynamic effects exerted by atorvastatin during acute pulmonary thromboembolism. *Eur. J. Pharmacol.* 670, 554–560. doi: 10.1016/j.ejphar.2011.09.018

Olschewski, A., Berghausen, E. M., Eichstaedt, C. A., Fleischmann, B. K., Grunig, E., Grunig, G., et al. (2018). Pathobiology, pathology and genetics of pulmonary hypertension: update from the cologne consensus conference 2018. *Int. J. Cardiol.* 272S, 4–10. doi: 10.1016/j.ijcard.2018.09.070

Pongratz, G., and Straub, R. (2014). The sympathetic nervous response in inflammation. *Arthritis Res. Ther.* 16:504.

Strielkov, I., Pak, O., Sommer, N., and Weissmann, N. (2017). Recent advances in oxygen sensing and signal transduction in hypoxic pulmonary vasoconstriction. *J. Appl. Physiol. (1985)* 123, 1647–1656. doi: 10.1152/japplphysiol.00103.2017

Trow, T. K., and Taichman, D. B. (2009). Endothelin receptor blockade in the management of pulmonary arterial hypertension: selective and dual antagonism. *Respir. Med.* 103, 951–962. doi: 10.1016/j.rmed.2009.02.016

Wang, Y., Yu, D., Yu, Y., Zou, W., Zeng, X., Hu, L., et al. (2019). Potential role of sympathetic activity on the pathogenesis of massive pulmonary embolism with circulatory shock in rabbits. *Respir. Res.* 20:97. doi: 10.1186/s12931-019-1069-z

Yu, D., Wang, Y., Yu, Y., Zhong, Y., Huang, L., Zhang, M., et al. (2018). Acute beneficial effects of sodium nitroprusside in a rabbit model of massive pulmonary embolism associated with circulatory shock. *Am. J. Pathol.* 188, 1768–1778. doi: 10.1016/j.ajpath.2018.04.014

Zhao, L. B., Jia, Z. Y., Lu, G. D., Zhu, Y. S., Jing, L., and Shi, H. B. (2015). Establishment of a canine model of acute pulmonary embolism with definite right ventricular dysfunction through introduced autologous blood clots. *Thromb. Res.* 135, 727–732. doi: 10.1016/j.thromres.2015.01.016

Conflict of Interest: The authors declare that the research was conducted in the absence of any commercial or financial relationships that could be construed as a potential conflict of interest.

frontiers in Physiology

MINI REVIEW
published: 09 September 2020
doi: 10.3389/fphys.2020.01035

HIF-1α as a Mediator of Insulin Resistance, T2DM, and Its Complications: Potential Links With Obstructive Sleep Apnea

Agata Gabryelska, Filip Franciszek Karuga, Bartosz Szmyd and Piotr Białasiewicz*

Department of Sleep Medicine and Metabolic Disorders, Medical University of Łódź, Łódź, Poland

Obstructive sleep apnea syndrome (OSA) is described as an independent risk factor for the onset and progression of type 2 diabetes (T2DM), as well as for insulin resistance (IR). The mechanisms underlying these processes remain unclear. One of the proposed molecular mechanism is based on the oxygen-sensitive α-subunit of hypoxia-inducible factor 1 (HIF-1α)—a key regulator of oxygen metabolism. The concept that stabilization of HIF-1α may influence T2DM and IR is supported by cell and animal models. Cell culture studies revealed that both glucose uptake and glycolysis are regulated by HIF-1α. Furthermore, animal models indicated that increased fasting glucose may be caused by a single night with intermittent hypoxia. Moreover, in these models, hypoxia time was correlated with IR. Mice models revealed that inhibition of HIF-1α protein may downregulate fasting blood glucose and plasma insulin level. Administration of superoxide dismutase mimetic resulted in inhibition of HIF-1α protein, catecholamines, and chronic intermittent hypoxia-induced hypertension in a mice model. The hypothesis that hypoxia is an independent risk factor for IR is strengthened by experimentally confirmed improvement of insulin sensitivity among OSA patients treated with the continuous positive airway pressure. Furthermore, recent studies suggest that HIF-1α protein concentration is increased in individuals with OSA. In this literature review, we summarize the current knowledge about HIF-1α in OSA in relation to the possible pathways in which they contribute to metabolic disorders.

Keywords: insulin resistance, T2DM2, OSA, hypoxia, HIF-1α

OPEN ACCESS

Edited by:
Yasumasa Okada, Murayama Medical Center (NHO), Japan

Reviewed by:
Sotirios G. Zarogiannis, University of Thessaly, Greece
Vincent Joseph, Laval University, Canada

****Correspondence:***
Agata Gabryelska
agata.gabryelska@gmail.com

Specialty section:
This article was submitted to Respiratory Physiology, a section of the journal Frontiers in Physiology

Received: *04 March 2020*
Accepted: *28 July 2020*
Published: *09 September 2020*

Citation:
Gabryelska A, Karuga FF, Szmyd B and Białasiewicz P (2020) HIF-1α as a Mediator of Insulin Resistance, T2DM, and Its Complications: Potential Links With Obstructive Sleep Apnea. Front. Physiol. 11:1035. doi: 10.3389/fphys.2020.01035

Abbreviations: AHI, apnea–hypopnea index; CPAP, continuous positive air pressure; DFO, deferoxamine; DFU, diabetic foot ulcers; DPP-4, dipeptidyl peptidase-4; GLP-1, glucagon-like peptide-1; GLUT-1, glucose transporter type 1; GLUT-2, glucose transporter type 2; GLUT-4, glucose transporter type 4; HDF, human dermal fibroblasts; HIF, hypoxia-inducible factors; HIF-1α, α-subunit of hypoxia-inducible factor 1; HIF-2α, α-subunit of hypoxia-inducible factor 2; IL-1, interleukin-1; IR, insulin resistance; M-DDO, modified diallyl disulfide oxide; OSA, obstructive sleep apnea syndrome; PDH, pyruvate dehydrogenase complex; PFD, pirfenidone; PI3K, phosphatidylinositol 3-kinase; PSG, polysomnography; SGLT2, sodium-glucose cotransporter 2; T2DM, type 2 diabetes; TAC, tricarboxylic acid cycle; VEGF, vascular endothelial growth factor.

INTRODUCTION

Obstructive sleep apnea (OSA) constitutes a rapidly growing health problem in the modern world (Gabryelska and Białasiewicz, 2020). Recent data suggest that the moderate and severe form of this disorder affect between 6 and 17% adults in the general population (Senaratna et al., 2017), while some research suggest that its prevalence is up to 23% among women and 49% among men (Heinzer et al., 2016). This trend may be an effect of increasing frequency of overweight/obesity, which is one of the strongest modifiable OSA risk factors. Interestingly, this dependency is bidirectional: BMI increment leads not only to higher OSA frequency but also to more severe course of this disease, whereas frequent sleep disruptions result in weight gain accompanied by poorer metabolic outcome (Farr and Mantzoros, 2017).

Numerous studies revealed connection between OSA and abnormal glucose metabolism [insulin resistance (IR), onset and progression of type 2 diabetes (T2DM)] (Morgenstern et al., 2014; Anothaisintawee et al., 2016). Additionally, Bulcun et al. (2012) observed that progression from snoring and/or mild OSA to severe OSA led to increased frequency of abnormal glucose metabolism. Thus, they suggested regular examination of possible glucose metabolism derangements among OSA patients, especially those with severe OSA (Bulcun et al., 2012). Moreover, they noted that subjective daytime sleepiness indices were independent risk factors of IR and T2DM (Bulcun et al., 2012). It is assumed that IR and T2DM in this group are related to recurrent tissue hypoxia (Drager et al., 2013). This hypothesis is supported by the observation that relatively mild, but intermittent desaturations were independent risk factors for metabolic dysfunction (Stamatakis et al., 2008; Drager et al., 2013). OSA is linked not only with IR/T2DM frequency but also with their severity, namely, OSA severity positively correlated with deterioration of T2DM outcomes (Farr and Mantzoros, 2017). Moreover, one of the most common OSA complications/comorbidities is a metabolic syndrome. Interestingly, a meta-analysis revealed that OSA predicted risk of metabolic syndrome, independently of obesity (Mesarwi et al., 2015; Qian et al., 2016); Coughlin et al. (2004) observed that metabolic syndrome was over nine times more likely to be present among OSA patients.

Although the relationship between OSA and metabolic disorders is intensively analyzed nowadays and OSA is described as an independent risk factor for onset and progression of T2DM and IR, the mechanisms underlying these processes remain not fully elucidated. Better understanding of this link may lead to a more efficient diagnostic process, as well as facilitate personalized treatment strategy (Mihaicuta et al., 2017; Carberry et al., 2018). Possibly underlying mechanisms include hypoxia, sleep fragmentation, inflammation, and oxidative stress, hormonal changes or increased sympathetic tone (Mesarwi et al., 2015; Farr and Mantzoros, 2017). In this minireview, we aim to analyze the link between metabolic complications of OSA and hypoxia in the context of hypoxia-inducible factors (HIFs). The importance of this choice is highlighted by publications supporting the central role of hypoxia in OSA-related comorbidities and possible severity biomarkers among OSA patients (Vavougios et al., 2014, 2016; Natsios et al., 2016).

THE MOLECULAR BIOLOGY OF HYPOXIA-INDUCIBLE FACTOR

Hypoxia-inducible factor is a heterodimer composed of two units: α-subunit, which is oxygen-regulated, and constitutively expressed β-subunit (Semenza et al., 1997), belonging to helix-loop-helix Per/Arnt/Sim transcription factor family. To date, three analogs of HIF α-subunits are known (HIF-1α, HIF-2α—established regulatory factors; HIF-3α—uncertain role). The first one, HIF-1α, is the best-examined HIF α-subunit. Although its transcriptional level remains stable, HIF-1α protein is highly unstable under normoxia conditions (Wang et al., 1995), which entails the presence of oxygen-dependent degradation domain. Its low half-life time under normoxia condition, hydroxylation, and acetylation of oxygen-dependent degradation domains lead to its association with pVHL E3 ligase complex resulting in its degradation in the ubiquitin-proteasome pathway (Ke and Costa, 2006; Badawi and Shi, 2017). Upon post-translational stabilization under hypoxia conditions, active dimeric protein complex is transported to nucleus, wherein it binds hypoxia-response elements located in gene promoters, affecting expression of over 100 genes (Semenza, 2001; Masoud and Li, 2015; Wen et al., 2019; Gabryelska et al., 2020a). As hypoxia occurs in tissues with high proliferation rate (Czarnecka et al., 2019), HIF-1α is widely described in carcinogenesis pertaining to upregulation of genes involved in angiogenesis as well as proliferation.

On the other hand, under hypoxia, HIF is responsible for reprogramming of metabolic pathways (Rankin et al., 2009). HIF-1α is crucial for many physiological and pathological processes by controlling expression of genes involved in glucose metabolism, erythropoiesis/iron metabolism, vascular resistance, and circadian rhythm. The impact of HIF-1α on glucose metabolisms is described in relation to glucose uptake, glycolysis, as well as regulation of the tricarboxylic acid cycle (TAC). Genes mediating these processes, which are affected by HIF, were collected in **Table 1**. Considering effects of intermittent hypoxia present in OSA patients, one of the proposed molecular mechanisms of IR and T2DM is based on HIF-1 molecule.

IMPACT OF HIF-1α ON IR AND T2DM IN CELL CULTURE MODELS

Cell culture studies indicate that HIF-1α regulates both glucose uptake and glycolytic enzyme activity, significantly enhancing the process of glycolysis (Nagao et al., 2019). HIF-1α also plays a role in the downregulation of TAC (Kim et al., 2006). Overexpression of HIF-1α in cells under hypoxic conditions makes them secrete more lactate (Sato et al., 2014). In three cell types, HT1080 (fibrosarcoma), HepG2 (hepatoma), and HeLa (cervical carcinoma), the induction of glucose transporter 1 (GLUT-1) mRNA was measured after exposure to an atmosphere of 1% (hypoxia) and 21% (normoxia) oxygen for 16 h. Cells under

TABLE 1 | HIF-1 regulated genes involved in glucose metabolism.

Gene	Abbreviation	Source
Aldolase-A	*ALDA*	Semenza et al., 1996
Aldolase-C	*ALDC*	Semenza et al., 1996
Carbonic anhydrase-9	–	Wykoff et al., 2000
Eldolase-1	*ENO1*	Semenza et al., 1996
Glucose transporter 1	*GLUT1*	Chen et al., 2001
Glucose transporter 3	*GLUT3*	Chen et al., 2001
Glucose transporter 4	*GLUT4*	Sakagami et al., 2014.
Glyceraldehyde phosphate dehydrogenase	*GAPDH*	Graven et al., 1999
Hexokinase 1	*HK1*	Soni and Padwad, 2017
Hexokinase 2	*HK2*	Soni and Padwad, 2017
Lactate dehydrogenase A	*LDHA*	Semenza et al., 1996
Pyruvate dehydrogenase kinase 1	*PDK1*	Kim et al., 2006
Pyruvate kinase M	*PKM*	Semenza et al., 1994
Phosphofructokinase L	*PFKL*	Semenza et al., 1994
Phosphoglycerate kinase 1	*PGK1*	Semenza et al., 1994
6-phosphofructo-2-kinase/fructose-2,6-bisphosphate-3	*PFKFB3*	Minchenko et al., 2002
Ras-Related Protein Rab-20	*RAB20*	Hackenbeck et al., 2011
Thioredoxin interacting protein	*TXNIP*	Li et al., 2015

hypoxia transcribed three- to fivefold more *GLUT-1* mRNA (Ebert et al., 1995). Influence of HIF-1α on activity of glycolytic enzymes was confirmed in the following cell lines: HepG2, HeLa, and L cells (mouse fibroblast). It was found that the action of HIF-1α is mediated by two enzymes: phosphoglycerate kinase-1 and lactate dehydrogenase A; HIF-1α binds to genes encoding these glycolytic enzymes modulating their expression (Firth et al., 1994; Weidemann and Johnson, 2008). Further studies allowed for new glycolytic enzymes influenced by HIF-1α to be determined, namely, hexokinase 1, hexokinase 2 (Soni and Padwad, 2017), enolase 1, aldolase A, and phosphofructokinase L (Iyer et al., 1998).

The effect of HIF-1α on GLUT-4 is similar to that on GLUT-1 the glucose uptake is increased. Knockdown of HIF-1α causes severe reduction in insulin-stimulated glucose uptake in cultured skeletal muscle cells due to impaired mobilization of GLUT4 to the plasma membrane (Sakagami et al., 2014).

The substrate for TAC is acetyl-CoA, which is produced from the end product of glycolysis, pyruvate. This process is called pyruvate decarboxylation and is mediated by the pyruvate dehydrogenase (PDH) complex, whose first component enzyme is PDH E1α. Pyruvate dehydrogenase kinase 1 can suppress PDH E1α activity through its phosphorylation and in this manner inhibit pyruvate decarboxylation (Nagao et al., 2019). Kim et al. found that HIF-1 suppressed TAC, activating the gene encoding pyruvate dehydrogenase kinase 1 (Kim et al., 2006; Semenza, 2007).

Surprisingly, HIF-1α is stabilized not only in a hypoxemic environment but also in normoxemia by interleukin-1 (IL-1) and insulin (Stiehl et al., 2002; Sakagami et al., 2014). Expression of HIF-1α protein in cultured skeletal muscle cells, even under normoxemia, was increased by stimulation with insulin for half an hour and remained elevated for at least the next 2 h (Sakagami et al., 2014). In some cell lines, hypoxia activates the phosphatidylinositol 3-kinase (PI3K)/Akt pathway (Chen et al., 2001), which also involved insulin signaling. The PI3K/Akt signaling pathway in HepG2 cells seems to be essential in HIF-1α response to hypoxia, insulin, and IL-1 due to its role in HIF-1α accumulation and stabilization (Stiehl et al., 2002).

Results from the Sato et al. (2014) research on mouse insulinoma cells (MIN6) provides information that hypoxia is responsible for transition of glucose metabolism from an oxidative to a glycolytic pathway, which consequently leads to decreased production of ATP in those cells. Investigating insulin secretion by MIN6 cells, insulin level in these cells was similar under either normoxic or hypoxic conditions. However, high glucose stimulation of MIN6 cells caused threefold higher insulin production under normoxia than under hypoxia. Furthermore, insulin secretion of MIN6 cells slightly decreased in normoxia compared to hypoxia in response to low glucose stimulation. The same study provides the data suggesting that hypoxia can lead to the downregulation of selected genes, which play important roles in β-cell function: *Foxa2, Mafa, Ins1, Neurod1, Pdx1, Wfs1, Slc2a2, Kcnj11,* and *Ndufa5* in both mouse islets and MIN6 cells; however, majority of the hypoxia-induced gene downregulations in cells were not related to HIF-1α suppression, suggesting a HIF-1α-autonomous mechanism (Sato et al., 2014).

Some studies showed that cells cultured in high glucose concentration medium present with decreased levels of HIF-1α. This led to a consensus that hyperglycemia was responsible for decreased HIF-1α protein levels (Xiao et al., 2013; Cerychova and Pavlinkova, 2018). Investigation of the effect of certain glucose concentrations on HIF-1α expression in human dermal fibroblasts (HDF) at normoxia and hypoxia showed that HIF-1α expression depends on glucose concentration only in hypoxia. At normoxia, no HIF-1α protein could be detected by Western blot analysis of HDF cell extracts and exposure to high glucose concentrations had no influence on HIF-1α expression. In the cells under hypoxic conditions, expression was decreasing gradually with the growing glucose concentrations of 5.5, 11, 25, and 30 mmol/l. Thus, the process of hypoxia-regulated stabilization of HIF-1α interferes with exposure of HDFs to high glucose concentrations (Catrina et al., 2004).

Although many studies support the thesis that hypoxia accompanied by HIF-1α overexpression is harmful to metabolism, there are also reports that suggest the beneficial influence of HIF-1α stabilization on glucose and lipid metabolism (Mackenzie et al., 2012; Jun et al., 2013; Mesarwi et al., 2015; Thomas et al., 2017). The study of Görgens et al. (2017) on human skeletal muscle cells reports that hypoxia in combination with muscle activity improved glucose metabolism and insulin activity via the HIF-1α and its influence on RAB20 and TXNIP transcription. Rab20 is a member of the Rab family of proteins, regulating intracellular trafficking and vesicle formation (Hackenbeck et al., 2011). Deletion of RAB20 impairs insulin-stimulated glucose uptake by blocking the translocation of GLUT4 to the cell surface. TXNIP encodes a thioredoxin-binding protein that is a member of the alpha arrestin protein family, which, among other functions, also regulates cellular metabolism (Shalev, 2014). TXNIP has been found to enhance insulin secretion

and glucagon-like peptide 1 (GLP-1) signaling via regulation of a microRNA (Alhawiti et al., 2017; Thielen and Shalev, 2018). Under conditions applied in the study of Görgens et al. (2017) simulating physical exertion and hypoxia, RAB20 upregulation and TXNIP downregulation mediated by HIF-1α were detected in the investigated tissues, which may explain the beneficial influence in this case. These results suggest that HIF-1α stabilization in the combined setting of muscle contraction and hypoxia can counteract the development of IR (Görgens et al., 2017).

IMPACT OF HIF-1α ON IR AND T2DM IN ANIMAL MODELS

Glucagon-like peptide 1 is a hormone belonging to the incretin group, which enhances glucose-stimulated insulin secretion in β-cells (Carlessi et al., 2017) and suppresses glucagon secretion (Seino et al., 2010). Dipeptidyl peptidase-4 (DPP-4) is a multi-purpose protein, and one of its functions is the degradation of GLP-1, which leads to a decrease in endogenous GLP-1 levels (Deacon, 2019). Levels of active GLP-1 in T2DM are decreased (Vilsbøll et al., 2001; Holst et al., 2011). It was shown on a mice model that obesity reduces the level of active GLP-1 in peripheral circulation with increased level of DPP4, which leads to impaired glucose tolerance. Hepatocyte-specific HIF-1α knockout in mice blocked these changes induced by obesity (Lee et al., 2019).

Similar findings were disclosed in adipose tissue. To assess the influence of HIF-1α on the progression of obesity-induced diabetes in adipocytes, HIF-1α mRNA expression and GLP-1 levels were measured in epididymal adipose tissues of mice with and without HIF-1α knockout. The findings suggested that the knockout of HIF-1α in adipocytes increases glucose tolerance by enhancing insulin secretion through the increased GLP-1 levels (Kihira et al., 2014). The other known action of GLP-1 is induction of the expansion of β-cell mass responsible for insulin secretion, which results in the augmentation of glucose-stimulated insulin secretion (MacDonald et al., 2002). It was reported that deletion of HIF-1α in adipose tissue also ameliorates IR, which implies that HIF-1α could provide a novel potential therapeutic target for T2DM (Jiang et al., 2011).

The hypoxia and HIF-1α stabilization are also involved in the promotion of tissue inflammation, which further contributes to IR and T2DM development. With the onset of obesity, the adipose tissue becomes hypoxic (Ota et al., 2019). Various mechanisms thereof were suggested. The oxygen demand is increased due to uncoupled respiration in adipocytes (Lee et al., 2014). The capillary density is decreased and the perfusion of adipose tissue is reduced in obese patients, which makes oxygen delivery difficult and leads to hypoxia (Pasarica et al., 2009; Fujisaka et al., 2013). Furthermore, in obesity the oxygen diffusion in adipose tissue is less effective due to increased diameter of the cell (Lee et al., 2014). In response to tissue hypoxia, HIF-1α stabilization occurs. HIF-1α and NF-κB are involved in enhancing the inflammatory pathways in adipocytes, which leads to IR in the adipose tissue and other metabolic disturbances (Ota et al., 2019). Hypoxia-induced adipose tissue inflammation is characterized by the infiltration of classically activated macrophages M1. Macrophage phenotype is affected by HIF-1α-dependent and HIF-1α-independent pathways (Fujisaka et al., 2013). Interestingly, in the study performed on mice exposed to high-fat diet and the chronic intermittent hypoxia during sleep, it was reported that resveratrol administration may be beneficial in normalizing inflammatory process mediated by HIF-1α, leading to restoration of insulin responsiveness (Carreras et al., 2015).

Sacramento et al. (2016) exposed rats during sleep to hypoxic cycles for 28 or 35 days while the control group slept in normoxic conditions. After exposure to hypoxia, IR and fasting insulinemia increased along with chronic intermittent hypoxia duration, being significantly higher after exposure of 35 days. Additionally, chronic intermittent hypoxia decreased phosphorylation and expression of insulin receptor in adipose tissue and skeletal muscles, but not in the liver. Conversely, expression of GLUT-2 in the liver of animals exposed to chronic intermittent hypoxia was increased. Thirty-five days of chronic intermittent hypoxia also caused changes in the HIF-1α levels. HIF-1α upregulation was found in the liver cells, while it was downregulated in skeletal muscles (Sacramento et al., 2016). In another study, mice with partial deletion of HIF-1α were exposed to hypoxia for 8 h daily for the period of 2 weeks. Regardless of the partial HIF-1α deletion, the IR was increased in mice exposed to hypoxia in majority of tissues, suggesting the limited role of HIF-1α in hypoxia-induced IR (Thomas et al., 2017). Unexpectedly, in the same study, hypoxia induced improvement of glucose tolerance. This might be caused by muscle-specific stimulation of the AMPK-AS160/TBC1D1 signaling, which plays an important role in the regulation of glucose uptake (Thomas et al., 2017).

Sodium-glucose cotransporter 2 (SGLT2) inhibitors are a new group of medications used for treating T2DM; their action is based on reduction of glucose reabsorption, targeting the proximal tubules of nephrons. Bessho et al. (2019) treated male diabetic mice with SGLT2 inhibitor for 8–16 weeks. The results showed reduced cortical tubular HIF-1α expression followed by decreased tubular injury in mice. This implies SGLT2 inhibitors' effect on diabetic mice (Bessho et al., 2019).

HIF-1α IN OSA PATIENTS; IR, T2DM, AND ITS COMPLICATIONS

HIF-1α in OSA Patients

To date, only few studies evaluated HIF-1α expression in OSA patients. Increased level of HIF-1α level in serum was observed in OSA patients compared to controls, regardless of measurement method (ELISA/western blot) (Lu et al., 2016; Gabryelska et al., 2019). Lack of difference between evening and morning concentrations suggests its chronic increasement caused by intermittent nocturnal hypoxia among OSA patients (Gabryelska et al., 2020c). Furthermore, one-night of CPAP

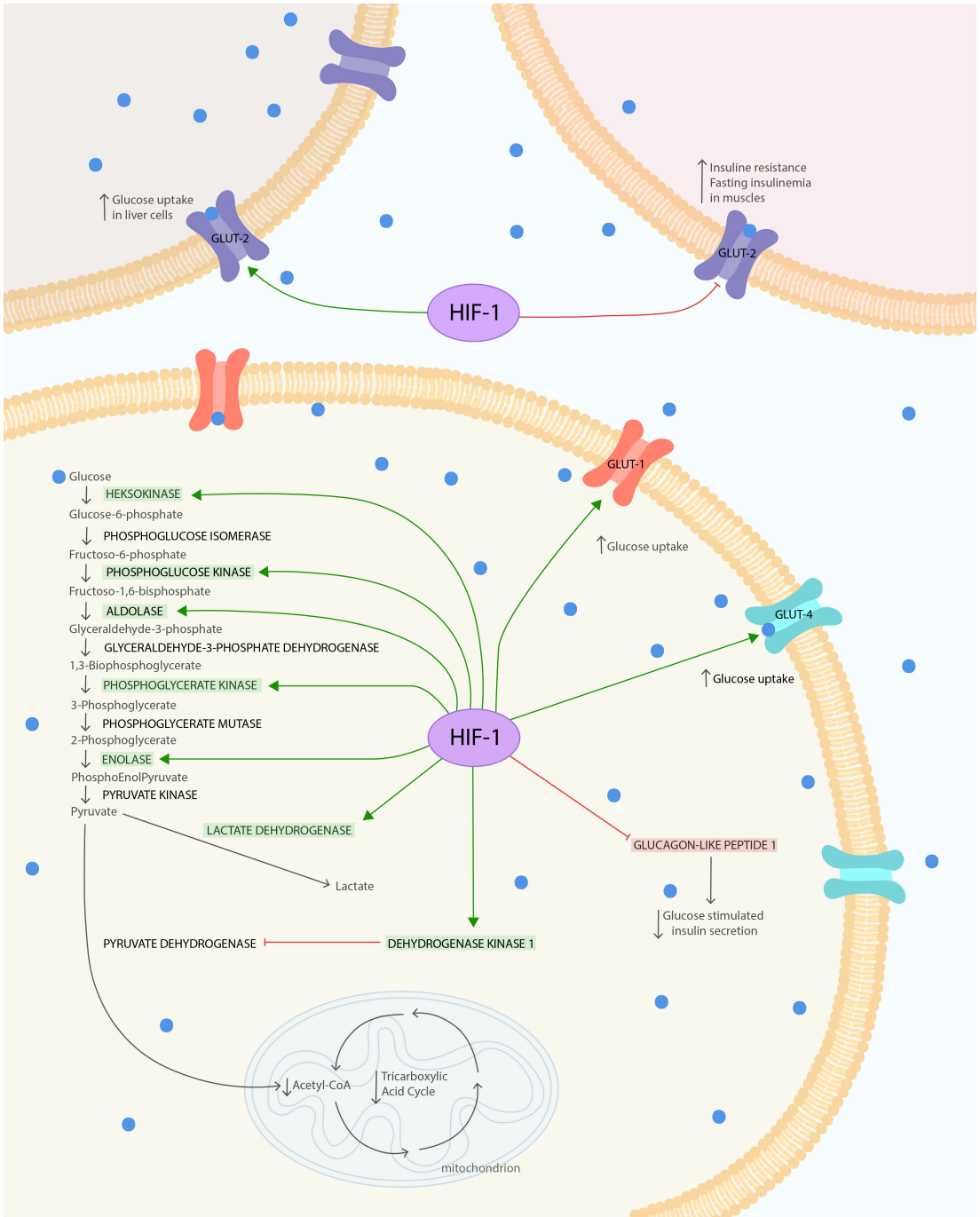

FIGURE 1 | HIF-1α influence on glucose metabolism and insulin resistance. The HIF is composed of both oxygen-regulated α-subunit and constitutively expressed β-subunit. HIF-1α protein is highly unstable under normoxia condition. Hypoxia leads to stabilization of HIF-1α. HIF-1α under hypoxic conditions causes several changes in glucose metabolism. It increases glucose uptake via glucose transporters GLUT-1 and GLUT-4 to cells. In the cell, glucose is used in glycolysis, which is also enhanced due to the modulated expression of glycolytic enzymes: phosphoglycerate kinase-1, hexokinase 1, hexokinase 2, aldolase A, enolase 1, and phosphofructokinase L. The final product of glycolysis—pyruvate—is mostly converted to lactate instead of acetyl-CoA, due to the increased lactate dehydrogenase A activity and pyruvate decarboxylation inhibition. Pyruvate dehydrogenase kinase 1 (PDK1) action leads to suppression of dehydrogenase complex (PDH) through its phosphorylation and thereby inhibits pyruvate decarboxylation. Secondary to the decreased levels of acetyl-CoA and the action of PDK1, the TAC is downregulated. At the same time, the increased expression of HIF-1α reduces GLUT-2 phosphorylation and its expression in skeletal muscles. This leads to increased IR and fasting insulinemia after exposure to chronic hypoxia. To compensate for this metabolic imbalance, the expression of GLUT-2 in liver is increased. The glucose tolerance can also be impaired by upregulation of HIF-1α, leading to GLP-1 downregulation, which causes reduction in glucose-stimulated insulin secretion via pancreatic β-cells. The **Figure 1** was prepared in Adobe Illustrator (Adobe Inc., San Jose, CA, United States).

therapy seems to be not sufficient to affect the increased level of the protein (Gabryelska et al., 2020b). On the other hand, Lu et al. (2016) observed decreased level of HIF-1α following 2 months of CPAP treatment compared to baseline results. In another study, Kaczmarek et al. (2013) examined skin biopsies from OSA patient (AHI $\geq$ 10) and found significant differences in *HIF-1*α mRNA expression level between groups with minimal oxygen saturation during PSG above or below 75%. Possibly showing that oxygen blood saturation might be the curtail factor for *HIF-1*α mRNA expression (aside from AHI as groups were matched regarding this variable), especially in tissues such as skin, which is more prone to hypoxia (Kaczmarek et al., 2013).

Effects of HIF-1α on IR, TD2M, and Its Complications in Humans

The level of serum HIF-1α was found to be significantly increased in patients suffering from T2DM compared to the control group (Shao et al., 2016). Furthermore, the presence of the non-synonymous single-nucleotide polymorphism (rs11549465) in HIF-1α gene in the Japanese and Hungarian populations reduced the risk of developing diabetes (Geza et al., 2009). Additionally, some reports suggested that HIF-1α is involved in development of T2DM complications. Diabetic foot ulcers (DFU) are among very frequent complications of diabetes mellitus, especially when disease is not well controlled (Yazdanpanah et al., 2015). DFU develops as a consequence of a combination of factors: peripheral neuropathy, peripheral vascular disease, and trauma (Boulton and Whitehouse, 2000). It has been shown that biopsy samples obtained from the margin of chronic DFU express decreased HIF-1α levels compared to samples from the margin of chronic venous ulcers (Catrina et al., 2004; Catrina and Zheng, 2016). Faint HIF-1α staining in DFU, similar to the staining pattern characteristic of exposure to the normoxic conditions, was found. In contrast, positive HIF-1α staining, like in cells under hypoxic conditions, was identified in both the nuclei and cytoplasm in majority of fibroblasts and a few endothelial cells in venous ulcers. It may suggest an important involvement of hyperglycemia in control of HIF1-α protein levels in tissues under hypoxia (Catrina et al., 2004). Unfortunately, wounds in DFU heal poorly. The reason for that phenomenon can be compromised blood vessel formation in response to ischemia and hyperglycemia (Thangarajah et al., 2010). This impairment in vascularization can result from hyperglycemia-induced inhibition of HIF-1α, which is transcription factor regulating the expression of vascular endothelial growth factor (VEGF). Deferoxamine (DFO) is a drug that may reverse the effect of HIF1-α inhibition (Thangarajah et al., 2010). DFO is an iron ion chelator-antioxidant. The main indication for DFO treatment is diseases with iron overload such as hemosiderosis (Di Nicola et al., 2015). However, DFO can also upregulate HIF-1α via triggering the ERK signaling pathway (Guo et al., 2016). HIF-1α upregulation accelerates the recovery process of humanized diabetic wounds in animal models. It suggests that HIF1-α can be the target of therapy in this very common T2DM complication (Thangarajah et al., 2010). There is a clinical trial pending, which investigates the effect of local DFO (0.66 mg/ml) treatment on the wound healing process in patients with DFU. The main endpoint of this trial will be to reduce more than 50% the wound area after 12 weeks of DFO treatment (ClinicalTrials.gov: NCT03137966). The other drug increasing HIF1-α expression in DFU being tested in clinical trials is pirfenidone (PFD) applied with modified diallyl disulfide oxide (M-DDO). PFD indication is treatment of idiopathic pulmonary fibrosis due to its antifibrogenic action. M-DDO is an antimicrobial and antiseptic agent. However, their combined administration can influence the gene expression and increase HIF1-α action (ClinicalTrials.gov: NCT02632877) (Gasca-Lozano et al., 2017).

Another common complication of T2DM is diabetic retinopathy. Abnormal retinal blood vessel growth and diabetic macular edema are two crucial problems causing vision loss in diabetic patients (Crawford et al., 2009). Increased levels of HIF-1α in hypoxia are significantly related to retinal angiogenesis responsible for abnormal retinal blood vessels growth. Suppression of HIF-1α reduced VEGF expression and can prevent unwanted angiogenesis. This phenomenon suggests that HIF-1α may be a target in pharmacological treatment for diabetic retinopathy (Cheng et al., 2017; Zhang et al., 2018).

CONCLUSION

Available literature shows that HIF-1α is involved in regulation of metabolic processes and mediates development of IR and diabetes mellites. However, vast majority of the studies are based on cellular and animal models of hypoxia. As few available studies show that HIF-1α in OSA patients is upregulated, it is probable that HIF-1α might be involved in development of metabolic comorbidities in this group. Nevertheless, further studies are needed to support this plausible pathomechanism. Taking under consideration the fact that animal studies suggest HIF-1α as a possible therapeutic target in impaired glucose metabolism, this might be a promising research direction in OSA patients.

AUTHOR CONTRIBUTIONS

AG created the concept of the manuscript. AG, FK, and BS conducted the literature research and wrote the manuscript. PB revised the manuscript.

FUNDING

The study was supported by the Polish Ministry of Science and Higher Education (no. 0067/DIA/2018/47 to AG).

REFERENCES

Alhawiti, N. M., Al Mahri, S., Aziz, M. A., Malik, S. S., and Mohammad, S. (2017). TXNIP in metabolic regulation: physiological role and therapeutic outlook. *Curr. Drug Targets* 18, 1095–1103. doi: 10.2174/1389450118666170130145514

Anothaisintawee, T., Reutrakul, S., Van Cauter, E., and Thakkinstian, A. (2016). Sleep disturbances compared to traditional risk factors for diabetes development: systematic review and meta-analysis. *Sleep Med. Rev.* 30, 11–24. doi: 10.1016/j.smrv.2015.10.002

Badawi, Y., and Shi, H. (2017). Relative contribution of prolyl hydroxylase-dependent and -independent degradation of HIF-1alpha by proteasomal pathways in cerebral ischemia. *Front. Neurosci.* 11:239. doi: 10.3389/fnins.2017.00239

Bessho, R., Takiyama, Y., Takiyama, T., Kitsunai, H., Takeda, Y., Sakagami, H., et al. (2019). Hypoxia-inducible factor-1α is the therapeutic target of the SGLT2 inhibitor for diabetic nephropathy. *Sci. Rep.* 9:14754. doi: 10.1038/s41598-019-51343-1

Boulton, A. J., and Whitehouse, R. W. (2000). *The Diabetic Foot*. Available online at: http://www.ncbi.nlm.nih.gov/pubmed/28121117 (accessed January 12, 2020).

Bulcun, E., Ekici, M., and Ekici, A. (2012). Disorders of glucose metabolism and insulin resistance in patients with obstructive sleep apnoea syndrome. *Int. J. Clin. Pract.* 66, 91–97. doi: 10.1111/j.1742-1241.2011.02795.x

Carberry, J. C., Amatoury, J., and Eckert, D. J. (2018). Personalized management approach for OSA. *Chest* 153, 744–755. doi: 10.1016/j.chest.2017.06.011

Carlessi, R., Chen, Y., Rowlands, J., Cruzat, V. F., Keane, K. N., Egan, L., et al. (2017). GLP-1 receptor signalling promotes β-cell glucose metabolism via mTOR-dependent HIF-1α activation. *Sci. Rep.* 7:2661. doi: 10.1038/s41598-017-02838-2

Carreras, A., Zhang, S. X. L., Almendros, I., Wang, Y., Peris, E., Qiao, Z., et al. (2015). Resveratrol attenuates intermittent hypoxia-induced macrophage migration to visceral white adipose tissue and insulin resistance in male mice. *Endocrinology* 156, 437–443. doi: 10.1210/en.2014-1706

Catrina, S.-B., Okamoto, K., Pereira, T., Brismar, K., and Poellinger, L. (2004). Hyperglycemia regulates hypoxia-inducible factor-1alpha protein stability and function. *Diabetes* 53, 3226–3232. doi: 10.2337/diabetes.53.12.3226

Catrina, S. B., and Zheng, X. (2016). Disturbed hypoxic responses as a pathogenic mechanism of diabetic foot ulcers. *Diabetes Metab. Res. Rev.* 32, 179–185. doi: 10.1002/dmrr.2742

Cerychova, R., and Pavlinkova, G. (2018). HIF-1, metabolism, and diabetes in the embryonic and adult heart. *Front. Endocrinol.* 9:460. doi: 10.3389/fendo.2018.00460

Chen, E. Y., Mazure, N. M., Cooper, J. A., and Giaccia, A. J. (2001). Hypoxia activates a platelet-derived growth factor receptor/phosphatidylinositol 3-kinase/Akt pathway that results in glycogen synthase kinase-3 inactivation. *Cancer Res.* 61, 2429–2433.

Cheng, L., Yu, H., Yan, N., Lai, K., and Xiang, M. (2017). Hypoxia-inducible factor-1α target genes contribute to retinal neuroprotection. *Front. Cell. Neurosci.* 11:20. doi: 10.3389/fncel.2017.00020

Coughlin, S., Mawdsley, L., Mugarza, J. A., Calverley, P. M. A., and Wilding, J. P. H. (2004). Obstructive sleep apnoea is independently associated with an increased prevalence of metabolic syndrome. *Eur. Heart J.* 25, 735–741. doi: 10.1016/j.ehj.2004.02.021

Crawford, T., Alfaro, D. III, Kerrison, J., and Jablon, E. (2009). Diabetic retinopathy and angiogenesis. *Curr. Diabetes Rev.* 5, 8–13. doi: 10.2174/157339909787314149

Czarnecka, K. H., Szmyd, B., Barańska, M., Kaszkowiak, M., Kordiak, J., Antczak, A., et al. (2019). A strong decrease in TIMP3 expression mediated by the presence of miR-17 and 20a enables extracellular matrix remodeling in the NSCLC lesion surroundings. *Front. Oncol.* 9:1372. doi: 10.3389/fonc.2019.01372

Deacon, C. F. (2019). Physiology and pharmacology of DPP-4 in glucose homeostasis and the treatment of Type 2 diabetes. *Front. Endocrinol.* 10:80. doi: 10.3389/fendo.2019.00080

Di Nicola, M., Barteselli, G., Dell'Arti, L., Ratiglia, R., and Viola, F. (2015). Functional and structural abnormalities in deferoxamine retinopathy: a review of the literature. *Biomed. Res. Int.* 2015:249617. doi: 10.1155/2015/249617

Drager, L. F., Togeiro, S. M., Polotsky, V. Y., and Lorenzi-Filho, G. (2013). Obstructive sleep apnea: a cardiometabolic risk in obesity and the metabolic syndrome. *J. Am. Coll. Cardiol.* 62, 569–576. doi: 10.1016/j.jacc.2013.05.045

Ebert, B. L., Firth, J. D., and Ratcliffe, P. J. (1995). Hypoxia and mitochondrial inhibitors regulate expression of glucose transporter-1 via distinct cis-acting sequences. *J. Biol. Chem.* 270, 29083–29089. doi: 10.1074/jbc.270.49.29083

Farr, O. M., and Mantzoros, C. S. (2017). Sleep apnea in relation to metabolism: an urgent need to study underlying mechanisms and to develop novel treatments for this unmet clinical need. *Metabolism* 69, 207–210. doi: 10.1016/j.metabol.2017.01.028

Firth, J. D., Ebert, B. L., Pugh, C. W., and Ratcliffe, P. J. (1994). Oxygen-regulated control elements in the phosphoglycerate kinase 1 and lactate dehydrogenase A genes: similarities with the erythropoietin 3' enhancer. *Proc. Natl. Acad. Sci. U.S.A.* 91, 6496–6500. doi: 10.1073/pnas.91.14.6496

Fujisaka, S., Usui, I., Ikutani, M., Aminuddin, A., Takikawa, A., Tsuneyama, K., et al. (2013). Adipose tissue hypoxia induces inflammatory M1 polarity of macrophages in an HIF-1α-dependent and HIF-1α-independent manner in obese mice. *Diabetologia* 56, 1403–1412. doi: 10.1007/s00125-013-2885-1

Gabryelska, A., and Białasiewicz, P. (2020). Association between excessive daytime sleepiness, REM phenotype and severity of obstructive sleep apnea. *Sci. Rep.* 10:34. doi: 10.1038/s41598-019-56478-9

Gabryelska, A., Sochal, M., Turkiewicz, S., and Białasiewicz, P. (2020a). Relationship between HIF-1 and circadian clock proteins in obstructive sleep apnea patients—preliminary study. *J. Clin. Med.* 9:1599. doi: 10.3390/JCM9051599

Gabryelska, A., Stawski, R., Sochal, M., Szmyd, B., and Białasiewicz, P. (2020b). Influence of one-night CPAP therapy on the changes of HIF-1α protein in OSA patients: a pilot study. *J. Sleep Res.* [Epub ahead of print]. doi: 10.1111/jsr.12995

Gabryelska, A., Szmyd, B., Panek, M., Szemraj, J., Kuna, P., and Białasiewicz, P. (2019). Serum Hypoxia-Inducible Factor-1α protein level as a diagnostic marker of obstructive sleep apnea. *Polish Arch. Intern. Med.* 130, 158–160. doi: 10.20452/pamw.15104

Gabryelska, A., Szmyd, B., Szemraj, J., Stawski, R., Sochal, M., and Białasiewicz, P. (2020c). Patients with obstructive sleep apnea present with chronic up-regulation of serum HIF-1α protein. *J. Clin. Sleep Med.* [Epub ahead of print]. doi: 10.5664/jcsm.8682

Gasca-Lozano, L. E., Lucano-Landeros, S., Ruiz-Mercado, H., Salazar-Montes, A., Sandoval-Rodríguez, A., Garcia-Bañuelos, J., et al. (2017). Pirfenidone accelerates wound healing in chronic diabetic foot ulcers: a randomized, double-blind controlled trial. *J. Diabetes Res.* 2017:3159798. doi: 10.1155/2017/3159798

Geza, N., Reka, K. N., Kereszturi, E., Somogyi, A., Szekely, A., Nemeth, N., et al. (2009). Association of hypoxia inducible factor-1 alpha gene polymorphism with both type 1 and type 2 diabetes in a Caucasian (Hungarian) sample. *BMC Med. Genet.* 10:79. doi: 10.1186/1471-2350-10-79

Görgens, S. W., Benninghoff, T., Eckardt, K., Springer, C., Chadt, A., Melior, A., et al. (2017). Hypoxia in combination with muscle contraction improves insulin action and glucose metabolism in human skeletal muscle via the HIF-1α pathway. *Diabetes* 66, 2800–2807. doi: 10.2337/db16-1488

Graven, K. K., Yu, Q., Pan, D., Roncarati, J. S., and Farber, H. W. (1999). Identification of an oxygen responsive enhancer element in the glyceraldehyde-3-phosphate dehydrogenase gene. *Biochim. Biophys. Acta - Gene Struct. Expr.* 1447, 208–218. doi: 10.1016/S0167-4781(99)00118-9

Guo, C., Hao, L. J., Yang, Z. H., Chai, R., Zhang, S., Gu, Y., et al. (2016). Deferoxamine-mediated up-regulation of HIF-1α prevents dopaminergic neuronal death via the activation of MAPK family proteins in MPTP-treated mice. *Exp. Neurol.* 280, 13–23. doi: 10.1016/j.expneurol.2016.03.016

Hackenbeck, T., Huber, R., Schietke, R., Knaup, K. X., Monti, J., Wu, X., et al. (2011). The GTPase RAB20 is a HIF target with mitochondrial localization mediating apoptosis in hypoxia. *Biochim. Biophys. Acta - Mol. Cell Res.* 1813, 1–13. doi: 10.1016/j.bbamcr.2010.10.019

Heinzer, R., Marti-Soler, H., and Haba-Rubio, J. (2016). Prevalence of sleep apnoea syndrome in the middle to old age general population. *Lancet Respir. Med.* 4, e5–e6. doi: 10.1016/s2213-2600(16)00006-0

Holst, J. J., Knop, F. K., Vilsbøll, T., Krarup, T., and Madsbad, S. (2011). Loss of incretin effect is a specific, important, and early characteristic of type 2 diabetes. *Diabetes Care* 34, S251–S257. doi: 10.2337/dc11-s227

Iyer, N. V., Kotch, L. E., Agani, F., Leung, S. W., Laughner, E., Wenger, R. H., et al. (1998). Cellular and developmental control of O2 homeostasis by hypoxia-inducible factor 1α. *Genes Dev.* 12, 149–162. doi: 10.1101/gad.12.2.149

Jiang, C., Qu, A., Matsubara, T., Chanturiya, T., Jou, W., Gavrilova, O., et al. (2011). Disruption of hypoxia-inducible factor 1 in adipocytes improves insulin sensitivity and decreases adiposity in high-fat diet–fed mice. *Diabetes* 60, 2484–2495. doi: 10.2337/DB11-0174

Jun, J. C., Shin, M. K., Yao, Q., Devera, R., Fonti-Bevans, S., and Polotsky, V. Y. (2013). Thermoneutrality modifies the impact of hypoxia on lipid metabolism. *Am. J. Physiol. Endocrinol. Metab.* 304, E424–E435. doi: 10.1152/ajpendo.00515.2012

Kaczmarek, E., Bakker, J. P., Clarke, D. N., Csizmadia, E., Kocher, O., Veves, A., et al. (2013). Molecular biomarkers of vascular dysfunction in obstructive sleep apnea. *PLoS One* 8:e70559. doi: 10.1371/journal.pone.0070559

Ke, Q., and Costa, M. (2006). Hypoxia-inducible factor-1 (HIF-1). *Mol. Pharmacol.* 70, 1469–1480. doi: 10.1124/mol.106.027029

Kihira, Y., Miyake, M., Hirata, M., Hoshina, Y., Kato, K., Shirakawa, H., et al. (2014). Deletion of hypoxia-inducible factor-1α in adipocytes enhances glucagon-like peptide-1 secretion and reduces adipose tissue inflammation. *PLoS One* 9:e93856. doi: 10.1371/journal.pone.0093856

Kim, J. W., Tchernyshyov, I., Semenza, G. L., and Dang, C. V. (2006). HIF-1-mediated expression of pyruvate dehydrogenase kinase: a metabolic switch required for cellular adaptation to hypoxia. *Cell Metab.* 3, 177–185. doi: 10.1016/j.cmet.2006.02.002

Lee, Y. S., Kim, J. W., Osborne, O., Oh, D. Y., Sasik, R., Schenk, S., et al. (2014). Increased adipocyte O2 consumption triggers HIF-1α, causing inflammation and insulin resistance in obesity. *Cell* 157, 1339–1352. doi: 10.1016/j.cell.2014.05.012

Lee, Y. S., Riopel, M., Cabrales, P., and Bandyopadhyay, G. K. (2019). Hepatocyte-specific HIF-1 ablation improves obesity-induced glucose intolerance by reducing first-pass GLP-1 degradation. *Sci. Adv.* 5:eaaw4176. doi: 10.1126/sciadv.aaw4176

Li, Y., Miao, L. Y., Xiao, Y. L., Huang, M., Yu, M., Meng, K., et al. (2015). Hypoxia induced high expression of thioredoxin interacting protein (TXNIP) in non-small cell lung cancer and its prognostic effect. *Asian Pacific J. Cancer Prev.* 16, 2953–2958. doi: 10.7314/APJCP.2015.16.7.2953

Lu, D., Li, N., Yao, X., and Zhou, L. (2016). Potential inflammatory markers in obstructive sleep apnea-hypopnea syndrome. *Bosn. J. Basic Med. Sci.* 17, 47–53. doi: 10.17305/bjbms.2016.1579

MacDonald, P. E., El-Kholy, W., Riedel, M. J., Salapatek, A. M. F., Light, P. E., and Wheeler, M. B. (2002). The multiple actions of GLP-1 on the process of glucose-stimulated insulin secretion. *Diabetes* 51(Suppl. 3), S434–S442. doi: 10.2337/diabetes.51.2007.s434

Mackenzie, R., Maxwell, N., Castle, P., Elliott, B., Brickley, G., and Watt, P. (2012). Intermittent exercise with and without hypoxia improves insulin sensitivity in individuals with type 2 diabetes. *J. Clin. Endocrinol. Metab.* 97, E546–E555. doi: 10.1210/jc.2011-2829

Masoud, G. N., and Li, W. (2015). HIF-1α pathway: role, regulation and intervention for cancer therapy. *Acta Pharm. Sin. B* 5, 378–389. doi: 10.1016/j.apsb.2015.05.007

Mesarwi, O. A., Sharma, E. V., Jun, J. C., and Polotsky, V. Y. (2015). Metabolic dysfunction in obstructive sleep apnea: a critical examination of underlying mechanisms. *Sleep Biol. Rhythms* 13, 2–17. doi: 10.1111/sbr.12078

Mihaicuta, S., Udrescu, M., Topirceanu, A., and Udrescu, L. (2017). Network science meets respiratory medicine for OSAS phenotyping and severity prediction. *PeerJ* 5:e3289. doi: 10.7717/peerj.3289

Minchenko, A., Leshchinsky, I., Opentanova, I., Sang, N., Srinivas, V., Armstead, V., et al. (2002). Hypoxia-inducible factor-1-mediated expression of the 6-phosphofructo-2-kinase/fructose-2,6-bisphosphatase-3 (PFKFB3) gene: Its possible role in the warburg effect. *J. Biol. Chem.* 277, 6183–6187. doi: 10.1074/jbc.M110978200

Morgenstern, M., Wang, J., Beatty, N., Batemarco, T., Sica, A. L., and Greenberg, H. (2014). Obstructive sleep apnea: an unexpected cause of insulin resistance and diabetes. *Endocrinol. Metab. Clin. North Am.* 43, 187–204. doi: 10.1016/j.ecl.2013.09.002

Nagao, A., Kobayashi, M., Koyasu, S., Chow, C. C. T., and Harada, H. (2019). HIF-1-dependent reprogramming of glucose metabolic pathway of cancer cells and its therapeutic significance. *Int. J. Mol. Sci.* 20:238. doi: 10.3390/ijms20020238

Natsios, G., Pastaka, C., Vavougios, G., Zarogiannis, S. G., Tsolaki, V., Dimoulis, A., et al. (2016). Age, body mass index, and daytime and nocturnal hypoxia as predictors of hypertension in patients with obstructive sleep apnea. *J. Clin. Hypertens.* 18, 146–152. doi: 10.1111/jch.12645

Ota, H., Fujita, Y., Yamauchi, M., Muro, S., Kimura, H., and Takasawa, S. (2019). Relationship between intermittent hypoxia and type 2 diabetes in sleep apnea syndrome. *Int. J. Mol. Sci.* 20:4756. doi: 10.3390/ijms20194756

Pasarica, M., Sereda, O. R., Redman, L. M., Albarado, D. C., Hymel, D. T., Roan, L. E., et al. (2009). Reduced adipose tissue oxygenation in human obesity evidence for rarefaction, macrophage chemotaxis, and inflammation without an angiogenic response. *Diabetes* 58, 718–725. doi: 10.2337/db08-1098

Qian, Y., Xu, H., Wang, Y., Yi, H., Guan, J., and Yin, S. (2016). Obstructive sleep apnea predicts risk of metabolic syndrome independently of obesity: a meta-analysis. *Arch. Med. Sci.* 12, 1077–1087. doi: 10.5114/aoms.2016.61914

Rankin, E. B., Rha, J., Selak, M. A., Unger, T. L., Keith, B., Liu, Q., et al. (2009). Hypoxia-inducible factor 2 regulates hepatic lipid metabolism. *Mol. Cell. Biol.* 29, 4527–4538. doi: 10.1128/MCB.00200-09

Sacramento, J. F., Ribeiro, M. J., Rodrigues, T., Guarino, M. P., Diogo, L. N., Seiça, R., et al. (2016). Insulin resistance is associated with tissue-specific regulation of HIF-1α and HIF-2α during mild chronic intermittent hypoxia. *Respir. Physiol. Neurobiol.* 228, 30–38. doi: 10.1016/j.resp.2016.03.007

Sakagami, H., Makino, Y., Mizumoto, K., Isoe, T., Takeda, Y., Watanabe, J., et al. (2014). Loss of HIF-1α impairs GLUT4 translocation and glucose uptake by the skeletal muscle cells. *Am. J. Physiol. Metab.* 306, E1065–E1076. doi: 10.1152/ajpendo.00597.2012

Sato, Y., Inoue, M., Yoshizawa, T., and Yamagata, K. (2014). Moderate hypoxia induces β-cell dysfunction with HIF-1-independent gene expression changes. *PLoS One* 9:e114868. doi: 10.1371/journal.pone.0114868

Seino, Y., Fukushima, M., and Yabe, D. (2010). GIP and GLP-1, the two incretin hormones: similarities and differences. *J. Diabetes Investig.* 1, 8–23. doi: 10.1111/j.2040-1124.2010.00022.x

Semenza, G. L. (2001). HIF-1 and mechanisms of hypoxia sensing. *Curr. Opin. Cell Biol.* 13, 167–171. doi: 10.1016/S0955-0674(00)00194-0

Semenza, G. L. (2007). Oxygen-dependent regulation of mitochondrial respiration by hypoxia-inducible factor 1. *Biochem. J.* 405, 1–9. doi: 10.1042/BJ20070389

Semenza, G. L., Agani, F., Booth, G., Forsythe, J., Iyer, N., Jiang, B.-H., et al. (1997). Structural and functional analysis of hypoxia-inducible factor 1. *Kidney Int.* 51, 553–555. doi: 10.1038/ki.1997.77

Semenza, G. L., Jiang, B. H., Leung, S. W., Passantino, R., Concordat, J. P., Maire, P., et al. (1996). Hypoxia response elements in the aldolase A, enolase 1, and lactate dehydrogenase a gene promoters contain essential binding sites for hypoxia-inducible factor 1. *J. Biol. Chem.* 271, 32529–32537. doi: 10.1074/jbc.271.51.32529

Semenza, G. L., Roth, P. H., Fang, H. M., and Wang, G. L. (1994). Transcriptional regulation of genes encoding glycolytic enzymes by hypoxia-inducible factor 1. *J. Biol. Chem.* 269, 23757–23763. doi: 10.3410/f.13410988.14782101

Senaratna, C. V., Perret, J. L., Lodge, C. J., Lowe, A. J., Campbell, B. E., Matheson, M. C., et al. (2017). Prevalence of obstructive sleep apnea in the general population: a systematic review. *Sleep Med. Rev.* 34, 70–81. doi: 10.1016/j.smrv.2016.07.002

Shalev, A. (2014). Minireview: Thioredoxin-interacting protein: Regulation and function in the pancreatic β-cell. *Mol. Endocrinol.* 28, 1211–1220. doi: 10.1210/me.2014-1095

Shao, Y., Lv, C., Yuan, Q., and Wang, Q. (2016). Levels of Serum 25(OH)VD3, HIF-1α, VEGF, vWf, and IGF-1 and their correlation in type 2 diabetes patients with different urine albumin creatinine ratio. *J. Diabetes Res.* 2016:1925424. doi: 10.1155/2016/1925424

Soni, S., and Padwad, Y. S. (2017). HIF-1 in cancer therapy: two decade long story of a transcription factor. *Acta Oncol.* 56, 503–515. doi: 10.1080/0284186X.2017.1301680

Stamatakis, K., Sanders, M. H., Caffo, B., Resnick, H. E., Gottlieb, D. J., Mehra, R., et al. (2008). Fasting glycemia in sleep disordered breathing: lowering the threshold on oxyhemoglobin desaturation. *Sleep* 31, 1018–1024. doi: 10.1016/s8756-3452(08)79156-4

Stiehl, D. P., Jelkmann, W., Wenger, R. H., and Hellwig-Bürgel, T. (2002). Normoxic induction of the hypoxia-inducible factor 1α by insulin and interleukin-1β involves the phosphatidylinositol 3-kinase pathway. *FEBS Lett.* 512, 157–162. doi: 10.1016/S0014-5793(02)02247-0

Thangarajah, H., Vial, I. N., Grogan, R. H., Yao, D., Shi, Y., Januszyk, M., et al. (2010). HIF-1α dysfunction in diabetes. *Cell Cycle* 9, 75–79. doi: 10.4161/cc.9.1.10371

Thielen, L., and Shalev, A. (2018). Diabetes pathogenic mechanisms and potential new therapies based upon a novel target called TXNIP. *Curr. Opin. Endocrinol. Diabetes. Obes.* 25, 75–80. doi: 10.1097/MED.0000000000000391

Thomas, A., Belaidi, E., Moulin, S., Horman, S., Van Der Zon, G. C., Viollet, B., et al. (2017). Chronic intermittent hypoxia impairs insulin sensitivity but improves whole-body glucose tolerance by activating skeletal muscle AMPK. *Diabetes* 66, 2942–2951. doi: 10.2337/db17-0186

Vavougios, G., Pastaka, C., Tsilioni, I., Natsios, G., Seitanidis, G., Florou, E., et al. (2014). The DJ-1 protein as a candidate biomarker in obstructive sleep apnea syndrome. *Sleep Breath.* 18, 897–900. doi: 10.1007/s11325-014-0952-6

Vavougios, G. D., Natsios, G., Pastaka, C., Zarogiannis, S. G., and Gourgoulianis, K. I. (2016). Phenotypes of comorbidity in OSAS patients: combining categorical principal component analysis with cluster analysis. *J. Sleep Res.* 25, 31–38. doi: 10.1111/jsr.12344

Vilsbøll, T., Krarup, T., Deacon, C. F., Madsbad, S., and Holst, J. J. (2001). Reduced postprandial concentrations of intact biologically active glucagon-like peptide 1 in type 2 diabetic patients. *Diabetes* 50, 609–613. doi: 10.2337/diabetes.50.3.609

Wang, G. L., Jiang, B. H., Rue, E. A., and Semenza, G. L. (1995). Hypoxia-inducible factor 1 is a basic-helix-loop-helix-PAS heterodimer regulated by cellular O2 tension. *Proc. Natl. Acad. Sci. U.S.A.* 92, 5510–5514. doi: 10.1073/pnas.92.12.5510

Weidemann, A., and Johnson, R. S. (2008). Biology of HIF-1α. *Cell Death Differ.* 15, 621–627. doi: 10.1038/cdd.2008.12

Wen, Y., Zhou, X., Lu, M., He, M., Tian, Y., Liu, L., et al. (2019). Bclaf1 promotes angiogenesis by regulating HIF-1α transcription in hepatocellular carcinoma. *Oncogene* 38, 1845–1859. doi: 10.1038/s41388-018-0552-1

Wykoff, C. C., Beasley, N. J., Watson, P. H., Turner, K. J., Pastorek, J., Sibtain, A., et al. (2000). Hypoxia-inducible expression of tumor-associated carbonic anhydrases. *Cancer Res.* 60, 7075–7083.

Xiao, H., Gu, Z., Wang, G., and Zhao, T. (2013). The possible mechanisms underlying the impairment of hif-1α pathway signaling in hyperglycemia and the beneficial effects of certain therapies. *Int. J. Med. Sci.* 10, 1412–1421. doi: 10.7150/ijms.5630

Yazdanpanah, L., Nasiri, M., and Adarvishi, S. (2015). Literature review on the management of diabetic foot ulcer. *World J. Diabetes* 6, 37–53. doi: 10.4239/wjd.v6.i1.37

Zhang, D., Lv, F. L., and Wang, G. H. (2018). Effects of HIF-1α on diabetic retinopathy angiogenesis and VEGF expression. *Eur. Rev. Med. Pharmacol. Sci.* 22, 5071–5076. doi: 10.26355/eurrev_201808_15699

Conflict of Interest: The authors declare that the research was conducted in the absence of any commercial or financial relationships that could be construed as a potential conflict of interest.

frontiers in Physiology

ORIGINAL RESEARCH
published: 22 October 2020
doi: 10.3389/fphys.2020.576209

Transient Receptor Potential Ankyrin 1 Mediates Hypoxic Responses in Mice

*Sichong Chen[1,2†], Nobuaki Takahashi[3,4†], Changping Chen[1,5], Jordan L. Pauli[1], Chiharu Kuroki[1,6], Jun Kaminosono[1], Hideki Kashiwadani[1], Yuichi Kanmura[6], Yasuo Mori[3], Shaowu Ou[5], Liying Hao[2] and Tomoyuki Kuwaki[1]**

[1]Department of Physiology, Graduate School of Medical and Dental Sciences, Kagoshima University, Kagoshima, Japan, [2]Department of Pharmaceutical Toxicology, School of Pharmacy, China Medical University, Shenyang, China, [3]Department of Synthetic Chemistry and Biological Chemistry, Graduate School of Engineering, Kyoto University, Kyoto, Japan, [4]The Hakubi Center for Advanced Research, Kyoto University, Kyoto, Japan, [5]Department of Neurosurgery, First Affiliated Hospital of China Medical University, Shenyang, China, [6]Department of Anesthesiology and Critical Care Medicine, Graduate School of Medical and Dental Sciences, Kagoshima University, Kagoshima, Japan

Transient receptor potential ankyrin 1 (TRPA1) is a non-selective cation channel that is broadly expressed in sensory pathways, such as the trigeminal and vagus nerves. It is capable of detecting various irritants in inspired gasses and is activated during hypoxia. In this study, the role of TRPA1 in hypoxia-induced behavioral, respiratory, and cardiovascular responses was examined through four lines of experiments using TRPA1 knockout (KO) mice and wild type (WT) littermates. First, KO mice showed significantly attenuated avoidance behavior in response to a low (15%) oxygen environment. Second, the wake-up response to a hypoxic ramp (from 21 to 10% O_2 in 40 s) was measured using EEG electrodes. WT mice woke up within 30 s when oxygen was at 13–14%, but KO mice did not wake up until oxygen levels reached 10%. Histological analysis confirmed that mild (13% O_2) hypoxia resulted in an attenuation of trigeminal neuronal activation in KO mice. Third, the ventilatory response to hypoxia was measured with whole body plethysmography. KO mice showed attenuated responses to mild hypoxia (15% O_2) but not severe hypoxia (10% O_2). Similar responses were observed in WT mice treated with the TRPA1 blocker, AP-18. These data clearly show that TRPA1 is necessary for multiple mild hypoxia (13–15% O_2)-induced physiological responses. We propose that TRPA1 channels in the sensory pathways innervating the airway can detect hypoxic environments and prevent systemic and/or cellular hypoxia from occurring.

Keywords: transient receptor potential ankyrin-1, avoidance behavior, hypoxic arousal, respiratory chemoreflex, trigeminal afferent nerve

OPEN ACCESS

Edited by:
Mieczyslaw Pokorski, Opole University, Poland

Reviewed by:
Vincent Joseph, Laval University, Canada
Ching Jung Lai, Tzu Chi University, Taiwan

****Correspondence:***
Tomoyuki Kuwaki
kuwaki@m3.kufm.kagoshima-u.ac.jp

[†]These authors have contributed equally to this work

Specialty section:
This article was submitted to Respiratory Physiology, a section of the journal Frontiers in Physiology

Received: *25 June 2020*
Accepted: *23 September 2020*
Published: *22 October 2020*

Citation:
Chen S, Takahashi N, Chen C, Pauli JL, Kuroki C, Kaminosono J, Kashiwadani H, Kanmura Y, Mori Y, Ou S, Hao L and Kuwaki T (2020) Transient Receptor Potential Ankyrin 1 Mediates Hypoxic Responses in Mice. Front. Physiol. 11:576209. doi: 10.3389/fphys.2020.576209

INTRODUCTION

A supply of oxygen is essential for aerobic animals, and maintaining it is a matter of life and death. There are several levels of regulatory systems that monitor oxygen supply. For example, the carotid body is a small organ that responds to decreases in partial pressure of oxygen in arterial blood, or hypoxemia, by increasing respiration (Prabhakar and Semenza, 2015), and hypoxia inducible factors (HIFs) are transcription factors that respond to decreases in available oxygen in

the cellular environment (Choudhry and Harris, 2018). These are examples of feedback control systems, which trigger responses after a change has been detected in their monitored target (in this case, oxygen partial pressure in arterial blood and oxygen concentration in tissue fluid around the cells). A feedforward control system, however, detects an environmental change and triggers responses before an actual effect is able to take place in the monitored target (Mateika and Duffln, 1995). A proper oxygen supply is critically important so it stands to reason that a feedforward control system should participate in its regulation.

Transient receptor potential ankyrin 1 (TRPA1) is a non-selective cation channel that is likely to be involved in regulation of a feedforward system that monitors oxygen supply. TRPA1 is expressed in sensory nerves including those that innervate the respiratory tract, such as the trigeminal and vagus nerves (Takahashi et al., 2011; Yonemitsu et al., 2013). TRPA1 detects irritants such as pungent chemicals found in onion, garlic, wasabi, tobacco smoke, and predator odor in inspired gasses, and induces escape behavior or respiratory arrest (Yonemitsu et al., 2013; Akahoshi et al., 2016; Inui et al., 2016; Wang et al., 2018). We have previously reported that nasal TRPA1 is important for detection of airborne irritant by showing lack of escaping behavior from formalin vapor by nasal but not subcutaneous application AP18, one of the blockers of TRPA1 (Yonemitsu et al., 2013). Allyl isothiocyanate, a component of mustard and wasabi, activated trigeminal ganglion neurons in wild type (WT) mice but not in TRPA1-KO mice (Inui et al., 2016). These reports indicated importance of trigeminal TRPA1 for irritant detection.

TRPA1 also detects oxygen concentration, and its sensitivity is the highest in the TRP family molecules *in vitro* (Takahashi et al., 2011). TRPA1 is activated by hyperoxia through direct modification of cysteine residues by oxygen (Takahashi et al., 2011). Under normoxia, TRPA1 is inhibited through prolyl hydroxylation by prolyl hydroxylase domain (PHD) enzymes (Takahashi et al., 2011) that are related to the hypoxia-inducible factor HIF-1. TRPA1 is activated by hypoxia through inactivation of PHD and de-hydroxylation of prolyl residues (Takahashi et al., 2011). Of note, TRPA1 is most inactive at normal atmospheric oxygen partial pressure (~150 mmHg) and almost maximally activated at oxygen partial pressure less than 80 mmHg and more than 300 mmHg (Takahashi et al., 2011). These molecular characteristics support our hypothesis but *in vivo* evidence for participation of TRPA1 in sensing oxygen in the inhaled gas is still sparse (Pokorski et al., 2014). In order to obtain more comprehensive evidence for participation of TRPA1 in oxygen sensing and possible physiological role of TRPA1 *in vivo*, we examined hypoxia-induced behavioral, respiratory, and anatomical changes in TRPA1-KO mice and in wild type (WT) mice.

MATERIALS AND METHODS

Ethics Approval

All experiments were conducted at Kagoshima University in accordance with the guiding principles for the care and use of animals in the field of physiological sciences published by the Physiological Society of Japan (2015) and were approved by the Experimental Animal Research Committee of Kagoshima University (MD13007 and MD17105). All efforts were made to minimize the number, and reduce the pain of animals.

Animals

TRPA1 knockout (KO) mice were purchased from Jackson Laboratory and genotyped as previously described (Kwan et al., 2006). Mice were maintained as heterozygotes in our facility and crossed to obtain null mutants and wild type (WT) littermates (male, 12–24 weeks old). TRPA1 KO mice were backcrossed with C57BL/6 mice (CLEA, Japan) for more than 10 generations and were thought of as congenic to C57BL/6. In this study, 48 KO mice and 73 WT mice were used.

Immunohistochemistry

Distribution of TRPA1 in the Nasal Cavity

Wild type mice were deeply anesthetized with urethane (2.0 g/kg) and transcardially perfused with 0.01 mol/L phosphate-buffered saline (PBS) followed by a fixative solution containing 4% paraformaldehyde in PBS. The head was dissected and immersed in the same fixative solution for 24 h at 4°C. After removal of the skin and mandibula, the head block was immersed in 0.5 M EDTA in PBS for decalcification for 1 week. After cryoprotection with 30% sucrose in PBS, a coronal block (thickness~5 mm) was made and immersed in O.C.T. compound (Sakura Finetek, Tokyo, Japan). Before freezing, a negative pressure was applied to the specimen for better penetration of the compound into the narrow and complex structure of the nasal meatus (Dunston et al., 2013). Serial coronal sections of 16 μm thicknesses were cut using a freezing microtome and mounted onto a slide glass (Platinum pro, Matsunami, Osaka, Japan). The sections were immunohistochemically stained for TRPA1 (1/1,000, raised in rabbit, ACC-037, Alomone labs) using a slide rack immunostaining system (Shandon Sequenza, Thermo Fisher Scientific) and visualized with a CF488-conjugated donkey anti-rabbit IgG antibody (1/500, #20015, Biotium). Specificity of the anti-TRPA1 antibody was examined by pre-mixing with an excess amount of antigen peptide (weight ratio 1:1, which corresponds molar ratio of ~1:100, Alomone) for 60 min. The sections were examined with a fluorescence microscope (BZ-8000, Keyence, Osaka, Japan) according to the position in the nasal cavity (**Figure 1A**).

Activation of Trigeminal Ganglion Neurons

To examine possible activation of the trigeminal nerve by hypoxia, we used immunohistochemical detection of the phosphorylated form of extracellular signal-regulated kinase (p-ERK) in trigeminal ganglion neurons. P-ERK is a cellular activation marker that has a more rapid and narrow time window than that of other activation markers including c-Fos (Antoine et al., 2014). We have previously shown that allyl isothiocyanate, one of the activators of TRPA1, activates trigeminal neurons in WT but not in TRPA1-KO mice (Inui et al., 2016). For this purpose, mice exposed to hypoxia

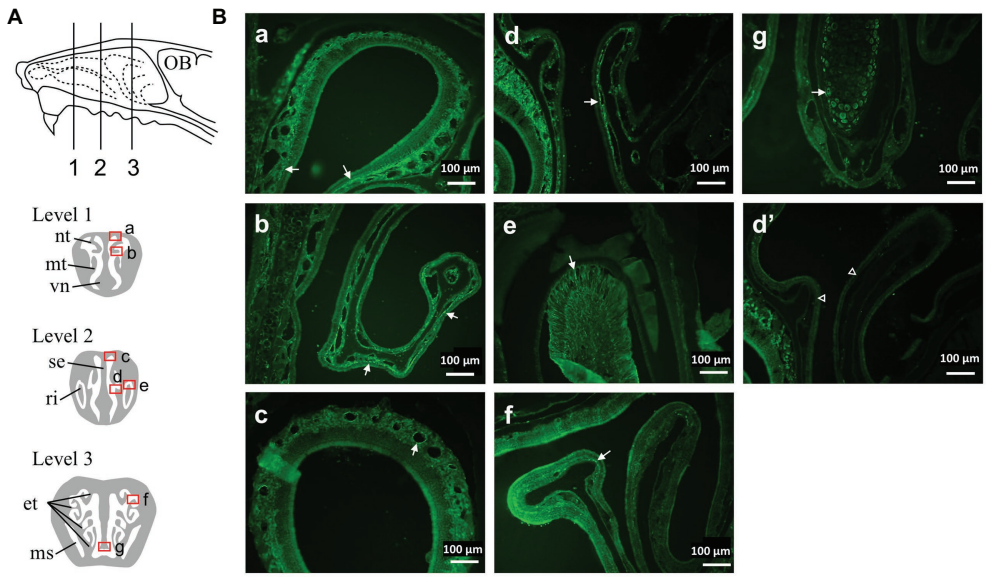

FIGURE 1 | Distribution of Transient receptor potential ankyrin 1 (TRPA1) immunoreactivity in the nasal cavity of mouse. **(A)** Schematic representation of the lateral view of the mouse nasal area showing three levels of the coronal sections examined. **(B)** Photomicrographs taken from the areas indicated by squares **(a–g)** in **(A)** of a representative mouse. Arrows indicate TRPA1-positive structures (see text). **(d')** was taken from a similar region to **(d)** and treated with a mixture of anti-TRPA1 antibody and an excess amount of antigen peptide. Similar results were obtained in three animals. et, ethmoturbinate; ms, maxillary sinus; mt, maxilloturbinate; nt, nasoturbinate; OB, olfactory bulb; ri, root of incisor tooth; se, septum; vn, vomeronasal organ.

(13% or 10% O_2) for 3 min were immediately anesthetized with urethane (1.8 g/kg) and transcardially perfused as described in the above section. The trigeminal ganglia were dissected and post-fixed for 24 h at 4°C. After cryoprotection with 30% sucrose in PBS, 16 μm thick serial longitudinal frozen sections were cut, and every fourth section (10 slices/animal) was immunohistochemically stained for p-ERK (1/400, raised in rabbit, #4370S, Cell Signaling Technology) and a neuronal marker, NeuN (1/400, raised in guinea pig, #266004, Synaptic Systems). P-ERK was visualized with a biotinylated donkey anti-rabbit IgG antibody (1/250, #711-065-152, Jackson Immunoresearch) and streptavidin-conjugated Alexa Fluor 488 (1/200, S11223, Invitrogen). NeuN was visualized with a CF568-conjugated anti guinea pig IgG antibody (1/200, raised in donkey, #20377, Biotium). The number of labeled cells was counted in a manner blinded to the treatment.

Behavioral Tests

All behavioral experiments were performed in a quiet, air-conditioned (25 ± 1°C) room from 10:00 to 16:00, during the mouse's inactive cycle. The mouse was acclimatized to the measuring chamber at least three times prior to the experimental day.

Hypoxia Avoidance Test

We used a home-made oxygen gradient chamber (**Figure 2A**). Two plastic boxes (1.2 L) with a roof door were connected *via* a tube that allowed the animal to freely move back and forth. Room air (21% O_2) and hypoxic gas (15 or 10% O_2) were introduced (0.8 L/min) to the opposite chambers from the side, and the gas mixture was removed from the chamber through a hole in the connecting tube in the center. In a preliminary experiment without animals in the chamber, we confirmed that the oxygen concentration near the inlet of the room air, the inlet of the 15% O_2, and the center of the connecting tube was 21, 15, and 17%, respectively, 10 min after the chamber roof was closed. Oxygen concentration was monitored with an O_2 sensor (JKO-25LJII, JIKCO, Japan). After a period of time allowing for an equilibrium in the oxygen gradient in the chamber to be established (>15 min), the roof of the room air-inlet side was briefly opened, and a mouse was placed in the chamber. Animal behavior was observed for 10 min.

Simultaneous Measurement of EEG and Ventilation by Whole Body Plethysmography

Following previously published methods (Nakamura et al., 2003; Deng et al., 2007; Terada et al., 2007; Iwakawa et al., 2019), electroencephalography (EEG) and electromyography (EMG) were recorded during ventilation measurement by whole body plethysmography in freely moving mice (see also **Figure 3A**). EEG and nuchal EMG electrodes were implanted at least 2 weeks prior to the experiment. An animal's vigilance state was manually judged by EEG and EMG recordings. Plethysmographic signals were recorded as changes of the pressure in the recording chamber and transformed into tidal volume according to a previously reported method (Onodera et al., 1997; Nakamura et al., 2003). Chamber was

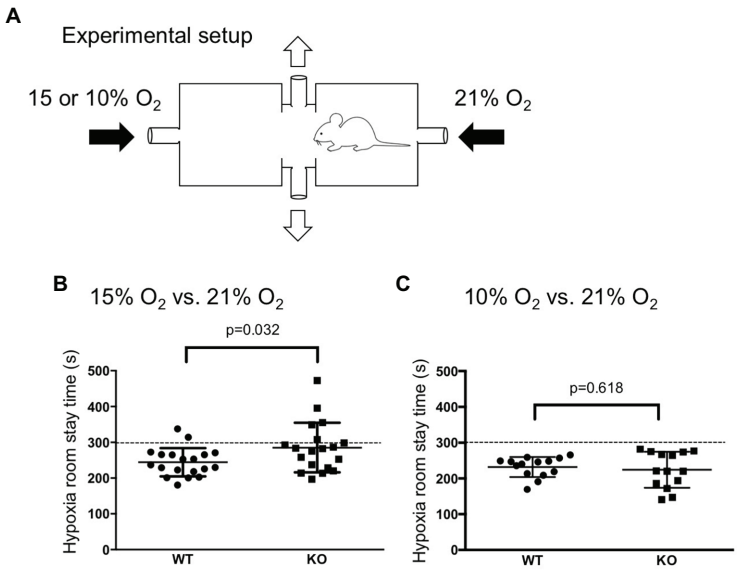

FIGURE 2 | Hypoxia avoidance test. **(A)** Illustration of an apparatus to create an oxygen concentration gradient in which a mouse can move back and forth (see method section for detail). **(B,C)** WT mice (n = 19) avoided both mild (15% O_2, **B**) and severe (10% O_2, **C**) hypoxia whereas knockout (KO) mice (n = 19) avoided only severe hypoxia. The dotted lines at 300 s indicates chance level during the observation period of 10 min. Horizontal lines indicate mean and SEM. The difference between the two genotypes was assessed using the Student's t-test, and value of p is shown.

continuously flushed with room air or mixed gas of room air and N_2. O_2 concentration was continuously monitored with an O_2 sensor at the outlet of the chamber.

Hypoxia-Induced Wakeup Test

Mice were placed in a plethysmography chamber (700 ml) that was continuously flushed with room air (500 ml/min). When animals fell asleep (slow wave sleep) for more than 1 min, the inlet gas was switched to a hypoxic gas mixture (10% O_2 balance with N_2) at a rate of 500 ml/min (**Figure 3B**). When the O_2 concentration in the chamber reached 10%, the condition was continued for 3 min before being switched back to the room air. For the control, the process remained exactly the same with the exception that room air was introduced into the chamber and not hypoxic gas. Each animal was given four trials of hypoxia and four trials of control with an interval of >10 min in a random order. The average value of the four trials was treated as the value for each animal.

Measurement of Hypoxic Chemoreflex Using Whole Body Plethysmography

Whole body plethysmographic chamber was continuously flushed with a gas mixture (10–100% O_2) at a rate of 500 ml/min, and change of pressure in the chamber was continuously monitored in a similar manner to those in hypoxia-induced arousal test described above (**Figure 3A**) except for EEG/EMG recording. After a baseline measurement for 5 min, 100, 15, and 10% O_2 was introduced into the chamber in this order. Finally, hypercapnic chemoreflex was measured in 5% CO_2–21% O_2-residual N_2. Each test gas continued for 3 min, and the intervals between each exposure was at least 20 min until when respiratory parameters (frequency and tidal volume) returned to the value within ±10% of the baseline value. In the test period of 3 min, values during the last 20-s were averaged and used for further analysis.

Aerosol Administration of a TRPA1 Blocker, AP-18, During Body Plethysmography

AP-18 (ab144587, Abcam, Cambridge, England) was dissolved in 20% ethanol in saline. AP-18 was aerosolized with an ultrasonic nebulizer (NE-U17, Omron, Kyoto, Japan), mixed with air, and subsequently distributed into the whole-body plethysmography chamber. At the time of measurement, the supply of air and monitoring of O_2 were paused for 3 min by closing the inlet and outlet stopcocks of the chamber to avoid fluctuation of the basal gas flow from vibration of the nebulizer because accurate recording of respiration by the flow-through type whole body plethysmography depends on constant air flow (Onodera et al., 1997).

Isolation of Carotid Body and RNA Measurement by RT-PCR

Carotid body was excised under dissecting microscope from decapitated mice. Dorsal root ganglia (DRG) were also sampled as the control. Total RNA was extracted using ISOGENE (Nippon Gene, Tokyo, Japan) following the manufacturer's instructions. The concentration and purity of RNA were determined spectrophotometrically. Two hundred nanograms of total RNA were reverse-transcribed into first-strand cDNA

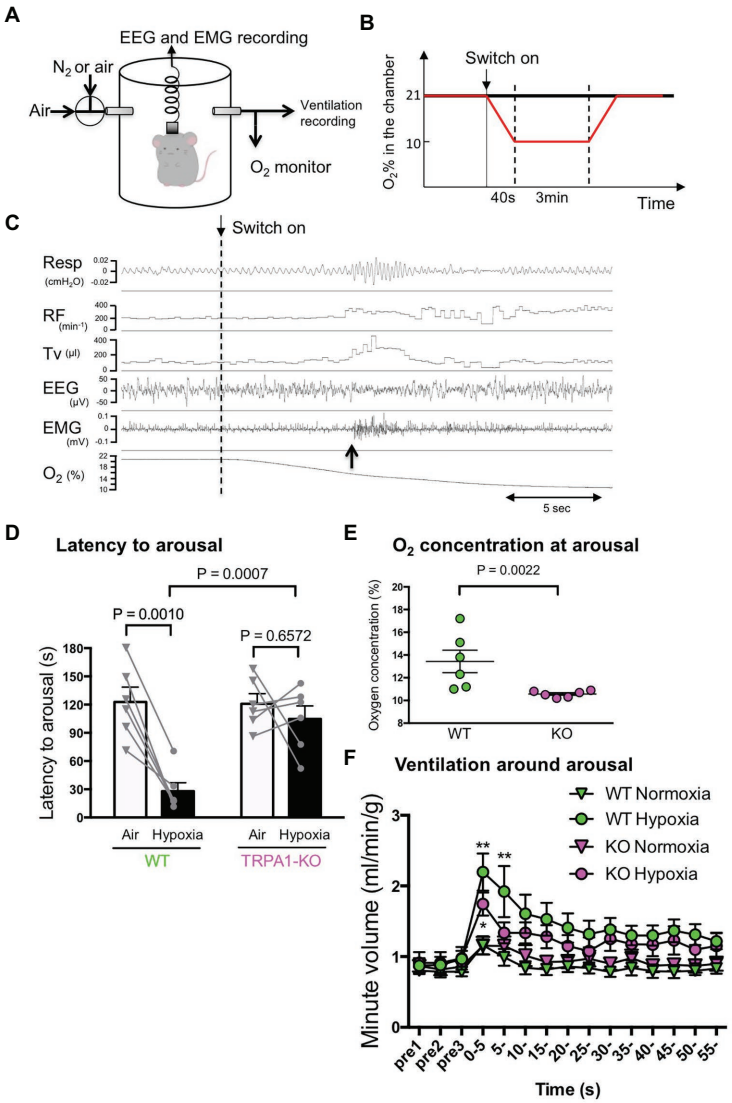

FIGURE 3 | Hypoxia-induced wakeup test. **(A)** Simultaneous measurement of EEG, EMG, and ventilation by whole body plethysmography. Continuous measurement was obtained using flow-through type body plethysmography. **(B)** Experimental schedule used to apply hypoxia to mice. **(C)** Typical recording from a WT mouse showing ventilatory parameters (RF, respiratory frequency; TV, tidal volume), electrophysiological measures, and O_2 concentration in the chamber. The dashed vertical line shows the timing when the inflow was changed from room air to hypoxic (10% O_2) gas. The upward arrow shows the timing when the mouse woke up as judged by EEG and EMG. Note that the increase in ventilation was not associated with the start of hypoxia but with the timing of arousal. **(D)** Latency to arousal from the time of inflow change. The bar indicates mean and SEM, $n = 6$ for both WT and KO mice. Two-way ANOVA revealed a significant difference between genotypes ($F1,10 = 9.851$, $p = 0.0105$) and between gas conditions ($F1, 10 = 17.24$, $p = 0.0020$). Values of p from Sidak's multiple comparison test are shown. **(E)** O_2 concentration in the chamber at arousal. A nonparametric Mann-Whitney U-test was used to compare WT and KO mice because data in KO mice were not normally distributed. **(F)** Minute ventilation was calculated by RF × TV, normalized with body weight and averaged every 5 s with arousal timing set to be time zero. Two-way ANOVA revealed there was a significant difference among times ($F14, 280 = 16.20$, $p < 0.0001$) but not among genotypes × gas conditions ($F3, 20 = 2.786$, $p = 0.0673$).

by use of the RNA LA PCR kit at the final volume of 20 μl. PCR was conducted with a GeneAmp PCR system 9700 (Applied Biosystems) using LA Taq polymerase with GC buffer (Takara Bio, Kusatsu, Japan) for 32 cycles under the following conditions: initial denaturation was 3 min at 95°C, then 30 s at 95°C, following by a 30-s annealing step at 55°C and 30-s elongation at 72°C, and a final elongation of 7 min at 72°C. We used primer sets for TRPA1 (forward: ACAAGAAGTACCAAACATTGACACA and reverse: TTAA CTGCGTTTAAGACAAAATTC), tyrosine hydroxylase (TH; forward: GGACATTGGACTTGCATCTCTGGG and reverse: GCTTGGGTCAGGGTGTGCAG), and beta-action (forward: GATGACGATATCGCTGCGCTG and reverse: GTACGACCA GAGGCATACAGG). Tyrosine hydroxylase was used as a marker of glomus cells in the carotid body (Mills et al., 1978), and beta-actin was used as an internal standard.

Statistical Analyses

All data are expressed as means ± SEM. Statistical analyses were carried out using Prism Software v.6 (GraphPad). We evaluated statistical significance with the Student's *t*-test or nonparametric Mann-Whitney's U test (when the data distribution was different between two groups) for comparisons between two mean values. We carried out multiple comparisons among more than three groups with ANOVA followed by Tukey's or Sidak's *post hoc* tests. Respiratory parameters were also assessed by ANOVA with repeated measures design. A value of $p < 0.05$ was considered significant.

RESULTS

Expression of TRPA1 in the Nasal Cavity

Although many studies have reported on the existence of TRPA1 in the trigeminal ganglion neurons (Kim et al., 2010; Takahashi et al., 2011; Yonemitsu et al., 2013; Inui et al., 2016), distribution in the nasal cavity has not been fully explored (Nakashimo et al., 2010). Therefore, we set out to examine the distribution of TRPA1 in the nasal cavity. TRPA1-like immunoreactivity was found in several structures in the various rostro-caudal levels of the nasal cavity (**Figure 1**). These include nerve fiber-like structures running under epithelial cell layer (**Figures 1Ba**,**Bb**,**Bd**,**Bf**), perivasculature (**Figure 1Bc**), root of the incisor (**Figure 1Be**), and cells in the septum (**Figure 1Bg**). Of these, the nerve fiber-like structures were strongly positive in the rostral levels (**Figures 1Ba**,**Bb**,**Bd**) under the respiratory epithelium and relatively sparse in the caudal level (**Figure 1Bf**), where olfactory epithelium is dominant (Harkema et al., 2006). This distribution was similar to that of trigeminal nerve fibers (Lee et al., 1995). Specificity of the antibody was confirmed by elimination of the positive signal after preincubation of the antibody with an excess amount of antigen peptide (**Figure 1Bd'**).

TRPA1-KO Mice Did Not Avoid Mild Hypoxia

We examined whether the mice are able to discriminate between differences in oxygen concentration and avoid a hypoxic atmosphere by using a home-made apparatus (**Figure 2A**). When there was no oxygen concentration gradient during the acclimatization period, both WT mice and TRPA1-KO mice showed no bias to either chamber and spent equal time in both chambers (data not shown). When an oxygen concentration gradient did exist, WT mice, but not TPRA1-KO mice, avoided the 15% O_2 room (**Figure 2B**). When the oxygen concentration gradient was steeper, both WT mice and TPRA1-KO mice avoided the 10% O_2 room (**Figure 2C**). This result indicated that the mice can discriminate between the differences in oxygen concentration and avoid hypoxic environments. TRPA1 seems to contribute to detecting mild hypoxia but another mechanism must be involved in the detection of severe hypoxia.

Hypoxia-Induced Arousal Was Delayed in TRPA1-KO

Hypoxic environments can induce arousal in animals, allowing the body to respond in order to avoid a potentially life-threatening situation (Phillipson et al., 1978). The possible contribution of TRPA1 in hypoxia-induced arousal was examined using a previously established method of simultaneous measurement of EEG, EMG, and ventilation in freely behaving mice (**Figure 3A**). When mice fell asleep for over 1 min, either hypoxic gas or normal room air was introduced into the recording chamber (**Figure 3B**), and the wake up time was judged from EEG and EMG recordings (upward arrow in **Figure 3C**). When hypoxic gas was introduced into the chamber, the latency to wake up in WT mice was significantly shortened (28.0 ± 9.0 s, $n = 6$) from the latency in normoxia (122.7 ± 15.7 s, $p = 0.0010$, Sidak's multiple comparison test; **Figure 3D**). Whereas in TRPA1-KO mice, latency to wake up did not change under hypoxia (from 120.8 ± 10.9 s to 104.7 ± 13.9 s, $p = 0.6572$). When a hypoxic challenge was given to the animals, the O_2 concentration in the chamber reached 10% in 40 s in our experimental setting. Therefore, a latency of >40 s means that the animal did not wake up until O_2 concentration reached 10%. The O_2 concentration at arousal in TRPA1-KO mice (10.6 ± 0.1%) was significantly lower than in WT mice (13.4 ± 1.0%, $p = 0.0022$, Mann-Whitney U test; **Figure 3E**). Hypoxia-induced arousal was associated with a brief increase in ventilation in both WT and KO mice (**Figure 3F**). Within the first 5 s after arousal, minute ventilation in KO mice (1.744 ± 0.163 ml/min/g, $n = 6$) seemed to be lower than in WT mice (2.196 ± 0.263 ml/min/g, $n = 6$) but the difference did not reach statistical significance ($p = 0.3623$, Sidak's multiple comparison test). Thus, TRPA1 seems to contribute to mild hypoxia-induced arousal but has less of an effect, if any, on sever hypoxia-associated respiratory augmentation.

Mild Hypoxia Failed to Activate Trigeminal Ganglion Neurons in TRPA1-KO

In order to examine if trigeminal ganglion neurons play a role in mild hypoxia-induced arousal, we counted the number of cells activated in the region under various levels of oxygen concentrations (**Figure 4**). For mild hypoxia, we selected 13% O_2 (**Figure 4A**) because the previous experiment showed that half (three out of six) of the WT mice woke up at 13% or higher O_2 but none of the KO mice did (**Figure 3E**). P-ERK-like immunoreactivity was observed in both neurons (**Figure 4B**, arrows) and satellite glial cells (**Figure 4B**, open triangles) in the trigeminal ganglion. To analyze neuronal activation, we counted the number of cells that were positive for NeuN (**Figure 4B**, closed triangle) and the cells that were positive for both p-ERK and NeuN (**Figure 4B**, star). Sampling bias seemed minimal because the number of NeuN-positive cells (~1,000/animal) was not different among the groups (effect of genotype, $F1, 24 = 0.02695$, $p = 0.8710$; effect of O_2 concentration, $F2, 24 = 0.002347$, $p = 0.9977$, two-way ANOVA, $n = 5$ in each group). As expected, exposure to 13 and 10% hypoxia

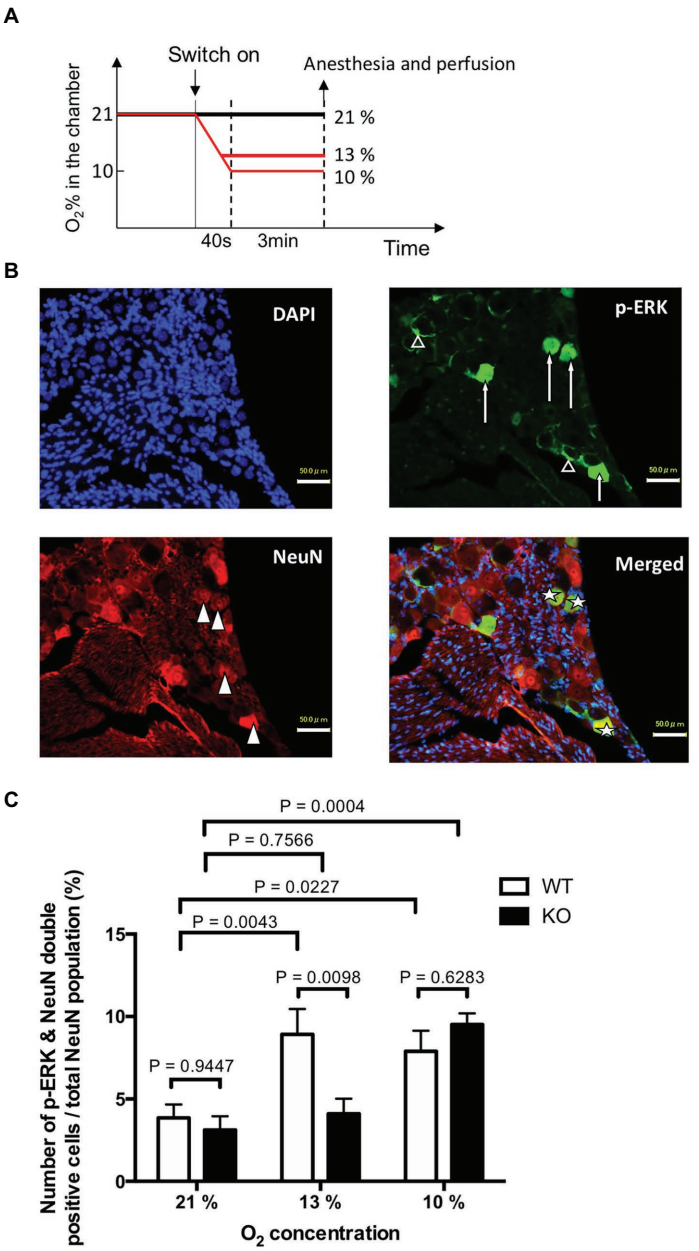

FIGURE 4 | Hypoxia induced activation of trigeminal ganglion neurons. **(A)** Experimental design. TRPA1-KO mice and WT mice were exposed to mild (13% O_2) or severe (10% O_2) hypoxia for 3 min, quickly euthanized, and then the trigeminal ganglion was sampled. Room air (21% O_2) was used as the control. **(B)** Typical example from WT mice that experienced 13% hypoxia. Note that p-ERK was positive in both neurons (arrows) and satellite cells (open triangles). **(C)** Ratio of p-ERK and NeuN double positive cells out of the total NeuN positive population. Each column represents mean and SEM in five animals. Two-way ANOVA revealed that there was a significant difference among O_2 concentrations ($F2, 24 = 12.67$, $p = 0.0002$) and interaction between O_2 concentration and genotype ($F2, 24 = 4.882$, $p = 0.0166$). Values of p in the figure were calculated by Sidak's multiple comparison test.

for 3 min in WT mice significantly increased the number of cells that were both p-ERK and NeuN positive (**Figure 4C**). In KO mice, 10% ($p = 0.0004$, Sidak's multiple comparison test) but not 13% ($p = 0.7566$) hypoxia activated the trigeminal neurons. Thus, TRPA1 seems to contribute to mild hypoxia-induced activation of trigeminal neurons.

Genetic Ablation and Pharmacological Inhibition of TRPA1 Reduced Mild Hypoxia-Induced Respiratory Chemoreflex

We next examined whether a normal respiratory chemoreflex was intact in TRPA1-KO mice. Hyperoxia (100% O_2), mild hypoxia (15% O_2), severe hypoxia (10% O_2), and hypercapnia

(5% CO_2), separated by intervals with normal room air (21% O_2), were applied in this order (**Figures 5A,B**). A similar experimental setting to that shown in **Figure 3A** was used without EEG and EMG measurement. In WT mice, hyperoxia reduced respiratory frequency and hypoxia and hypercapnia increased it as expected. Tidal volume did not change under hyperoxia but did increase under hypoxia and hypercapnia. As a result, minute volume significantly decreased under hyperoxia and significantly increased under hypoxia and hypercapnia. Baseline values during room air exposure did not differ between KO and WT under any of the respiratory parameters. As for chemoreflex, a qualitatively similar response was observed in KO mice but there was a quantitative difference between KO and WT mice. Namely, respiratory frequency during hyperoxia was significantly higher in KO (141 ± 3 min^{-1}) than in WT (121 ± 6 min^{-1}, n = 8 each, p = 0.043, Sidak's multiple comparison test) and was significantly lower during mild hypoxia (163 ± 4 min^{-1} in KO vs. 183 ± 5 min^{-1} in WT). There was no statistical difference in tidal volume between KO and WT in any condition. As a result, minute ventilation during mild hypoxia was significantly lower in KO (1.15 ± 0.10 ml/min/g) than in WT (1.47 ± 0.06 ml/min/g, n = 8 each, p = 0.041, Sidak's multiple comparison test). There was no difference between WT and KO mice with respect to their responses to severe hypoxia and hypercapnia.

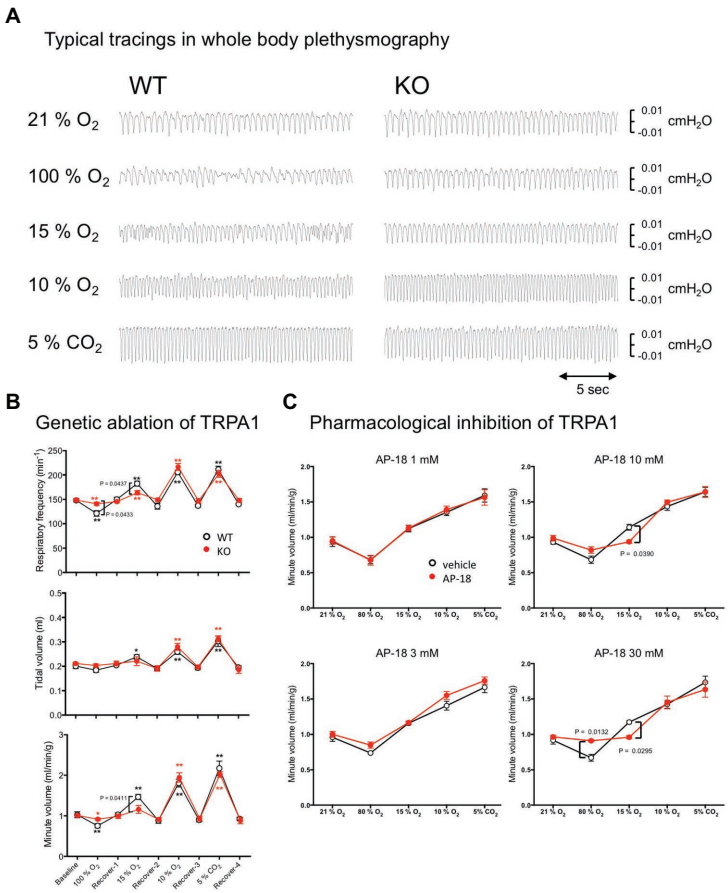

FIGURE 5 | Effect of genetic and pharmacological inhibition of TRPA1 on respiratory chemoreflex. **(A)** Representative tracing of pressure signals in whole body plethysmography. Respiration of WT and KO mice was measured using flow-through type whole body plethysmography. Every gas condition was maintained for 3 min, and the data were collected during the last 20-s period. Each stimulus was separated by intervals of 20 min or more of normal room air. Plethysmographic signal that is a pressure difference between the measuring chamber and the reference chamber, and O_2 concentration in the measuring chamber were continuously monitored. Data for baseline and recovery periods were obtained during the last 3 min before the next stimulation. **(B)** Group data obtained in whole body plethysmography. Data are shown as mean ± SEM. n = 8 for WT and n = 8 for KO mice. Two-way ANOVA revealed that there was a significant difference among gas conditions (F8, 112 = 101.7, $p < 0.0001$) and interaction between gas condition and genotype (F8, 112 = 2.415, p = 0.0191). $^{*}p < 0.05$, $^{**}p < 0.01$ as compared to preceding control values (one-way ANOVA followed by Sidak's multiple comparisons test). Values of p in the figure were calculated by Sidak's multiple comparison test to compare between WT and KO mice. **(C)** Using four sets of WT animals (n = 5/group), the possible effect of the TRPA1-blocker, AP-18, on respiratory chemoreflex was examined. Every animal was exposed to an aerosol made from vehicle (20% ethanol in saline) and an assigned concentration of AP-18 solution. Data are shown as mean ± SEM. Two-way ANOVA revealed that there was a significant interaction among drugs × gas conditions for 10 mM (F4, 16 = 3.668, p = 0.0265) and 30 mM (F4, 16 = 6.386, p = 0.0029) but not for 1 mM (F4, 16 = 0.1507, p = 0.9600) and 3 mM (F4, 16 = 0.7821, p = 0.5532). Values of p in the figure were calculated by Sidak's multiple comparison test.

We also examined whether abnormalities observed in KO mice can be reproduced by acute pharmacological blockade of TRPA1 in WT mice (**Figure 5C**). An aerosol of the TRPA1-selective blocker AP-18 was given to mice to attempt an administration that remained localized to the airway. A whole body plethysmographic apparatus similar to the above-mentioned experiment was used with the exception that the gas flow into the recording chamber was stopped for the 3 min of the recording period because the nebulizer responsible for aerosolizing the drug can cause fluctuations in the basal gas flow and result in inaccurate measurements of plethysmographic signals. When compared to the vehicle, 1 and 3 mM of AP-18 did not affect hyperoxic, hypoxic, and hypercapnic responses. When 10 mM of AP-18 was used, the chemoreflex increase in ventilation under mild hypoxia was significantly inhibited (0.94 ± 0.02 ml/min/g for 10 mM AP-18 vs. 1.14 ± 0.04 ml/min/g for vehicle, $n = 5$, $p = 0.0390$, Sidak's multiple comparisons test). With 30 mM AP-18, hyperoxic depression (0.91 ± 0.01 ml/min/g for 30 mM AP-18 vs. 0.67 ± 0.05 ml/min/g for vehicle, $n = 5$, $p = 0.0132$) and mild hypoxia-induced excitation (0.96 ± 0.02 ml/min/g for 30 mM AP-18 vs. 1.17 ± 0.02 ml/min/g for vehicle, $p = 0.0295$) were significantly attenuated.

Both genetic and pharmacological blockade of TRPA1 indicate its probable contribution to mild hypoxia-induced respiratory excitation and, to a lesser extent, hyperoxia-induced respiratory depression.

RNA Expression of TRPA1 in the Carotid Body

To evaluate possible expression of TRPA1, the carotid body and DRG in WT mice ($n = 2$) were analyzed using RT-PCR (**Figure 6**). Abundant RNA for TRPA1 was detected in the dorsal root ganglion as expected (Takahashi et al., 2011). Although carotid body expressed RNA for tyrosine hydroxylase, a marker of the hypoxia-sensing glomus cell in the carotid body (Mills et al., 1978), TRPA1 RNA was not detected in our protocol.

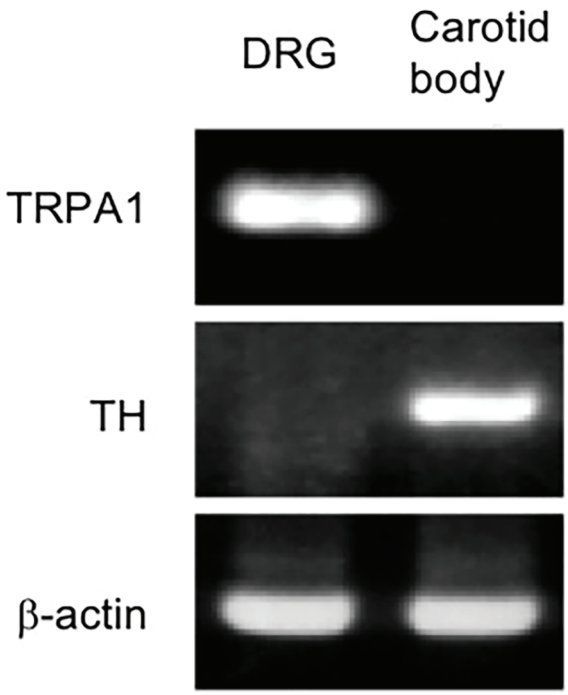

FIGURE 6 | RNA expression of TRPA1 was undetectable in the mouse carotid body. RNAs are subjected to RT-PCR from the mouse carotid body and that from dorsal root ganglia (DRG) as a positive control of TRPA1 expression. Identification of carotid body is confirmed by the detection of tyrosine hydroxylase (TH) RNA, a specific marker for carotid body in the carotid artery region. A similar result was obtained in two mice.

DISCUSSION

We report here that TRPA1-like immunoreactivity in the nasal cavity is in line with trigeminal distribution of TRPA1. In addition, using TRPA1-KO mice, we show three lines of evidence that TRPA1 is indispensable for multiple mild hypoxia-induced physiological responses. First, KO mice showed a significantly attenuated avoidance behavior in response to a low (15%) oxygen environment. Second, the wakeup response to a hypoxic ramp (from 21 to 10% O_2 in 40 s) was measured using EEG electrodes implanted in the mice. While WT mice awoke at 13–14% O_2 within 30 s, KO mice did not wake up until O_2 reached 10%. Histological analysis confirmed a decrease in the amount of trigeminal neuronal activation caused by mild hypoxia in KO mice. Third, KO mice showed attenuated chemoreflex ventilatory responses to mild hypoxia (15% O_2) but not severe hypoxia (10% O_2). Similar responses were observed in WT mice treated with an aerosol of the TRPA1 blocker, AP-18 (10–30 mM). These data clearly show that TRPA1 is indispensable for multiple mild hypoxia-induced physiologic responses. We propose that TRPA1 expressed in the sensory nerves along the airway plays a protective role against hypoxia, which presumably occurs before systemic and/or cellular hypoxia takes place.

Although our results indicate a role for TRPA1 in hypoxia-induced physiological responses, it was restricted to mild hypoxia (15% O_2). Severe hypoxia (10% O_2) evoked similar responses in TRPA1-KO mice to those in WT mice (**Figures 2–5**). This may be due to the existence of the canonical sensor for oxygen, the carotid body, in TRPA1-KO mice. Although the carotid body can also be activated by mild hypoxia, the relationship between O_2 concentration and carotid body activation is not linear but rather hyperbolic (Peng et al., 2010). As a result, sensitivity (activation/change in O_2) is not as high during mild hypoxia as it is during severe hypoxia. In the case of TRPA1, however, sensitivity to hypoxia was relatively linearly related to the change in O_2 *in vitro* (Takahashi et al., 2011). Hypoxemia must be occurring before the carotid body is recruited, and because cardiac output of mice is reported to be ~20 ml/min (Kreissl et al., 2006) and blood volume around 3 ml (Riches et al., 1973), there would be a delay of approximately 9 s for blood PO_2 to reach a new equilibrium with inhaled PO_2. These factors may explain why only mild hypoxia induced differences

between TRPA1-KO and WT mice, especially in the delayed arousal in TRPA1-KO mice (**Figure 3**).

In support for above interpretation about mild vs. server hypoxia induced responses, we found negligible expression level of mRNA for TRPA1 in the carotid body of the WT mice based on RT-PCR (**Figure 6**). Thus, function of the carotid body in TRPA1-KO mice is expected to be normal. Our observation is in line with the report showing upregulation of TRPC5 in the carotid body as compared to the superior cervical ganglion neurons, which are practically O_2-insensitive, using microarray analysis (Gao et al., 2017). Nevertheless, further analyses, such as quantitative PCR and western blotting, would be necessary for precise understanding of TRPA1 expression in the carotid bodies.

In studying trigeminal activation during hypoxia (**Figure 4C**), we expected a lower activation in TRPA1-KO mice in both mild and severe hypoxia because the carotid body may not be involved in this effect. We do not know the precise explanation for severe hypoxia-induced activation of trigeminal ganglion neurons in TRPA1-KO mice at present. One possibility may be HIF mediated cellular activation in the trigeminal ganglion neurons. We showed that hypoxia induced both trigeminal neuronal activation and arousal from sleep. Although there is no evidence for causative relationship between trigeminal activation and arousal, involvement of TRPA1 in both phenomena is evident from the data of TRPA1-KO mice.

We used a conventional knockout model of TRPA1. This animal is supposed to be deficient in TRPA1 throughout the body. Thus, we cannot distinguish any possible roles of TRPA1 in trigeminal nerve and vagus nerve, which are located along the upper and lower air ways, respectively. In addition, we cannot eliminate the possibility of developmental changes in TRPA1-containing cells in KO mice. Therefore, a time-dependent and/or tissue-dependent knockout model (Zappia et al., 2016) and carotid body denervation (Hemelrijk et al., 2019) may be useful in future studies.

The abnormalities in TRPA1-KO mice's physiological and behavioral responses to mild hypoxia (13–15% O_2), along with location of TRPA1 in the trigeminal nerve in the nasal cavity, indicate not only a high sensitivity of TRPA1 to hypoxia *in vivo* but also its participation in a feedforward control of oxygen availability. With TRPA1, a normal animal can behaviorally avoid hypoxic environments and increase ventilation before hypoxemia takes place. As a result of these findings, we propose that TRPA1 plays a role as a frontline alarm for environmental hypoxia.

DATA AVAILABILITY STATEMENT

All datasets presented in this study are included in the article/ supplementary material.

ETHICS STATEMENT

The animal study was reviewed and approved by Experimental Animal Research Committee of Kagoshima University.

AUTHOR CONTRIBUTIONS

SC, NT, and TK designed the study. SC, JP, NT, and TK wrote the manuscript. All authors conducted the study, analyzed the data, and approved the final version of the manuscript.

FUNDING

This work was supported by JSPS KAKENHI Grants (25670121 and 17H05536 to TK) and Smoking Research Foundation (to TK and HK). SC and CC are awardees of scholarships for foreign students from JASSO.

ACKNOWLEDGMENTS

We thank all the members of the Department of Physiology for their valuable discussion and support and Ms. Miki Sakoda for her excellent technical assistance. We also thank all the staff members of the Institute of Laboratory Animal Sciences at Kagoshima University for keeping the animals in good condition. We also acknowledge the Joint Research Laboratory, Kagoshima University Graduate School of Medical and Dental Sciences, for the use of their facilities.

REFERENCES

Akahoshi, R., Katayama, Y., Yamaguchi, R., Yonemitsu, T., Pauli, J. L., Kashiwadani, H., et al. (2016). "TRPA1 is indispensable to escaping from predator" in *SfN Annual Meeting*. Abstract 724.06. San Diego, USA.

Antoine, B., Serge, L., and Jocelyne, C. (2014). Comparative dynamics of MAPK/ERK signalling components and immediate early genes in the hippocampus and amygdala following contextual fear conditioning and retrieval. *Brain Struct. Funct.* 219, 415–430. doi: 10.1007/s00429-013-0505-y

Choudhry, H., and Harris, A. L. (2018). Advances in hypoxia-inducible factor biology. *Cell Metab.* 27, 281–298. doi: 10.1016/j.cmet.2017.10.005

Deng, B. -S., Nakamura, A., Zhang, W., Yanagisawa, M., Fukuda, Y., and Kuwaki, T. (2007). Contribution of orexin in hypercapnic chemoreflex: evidence from genetic and pharmacological disruption and supplementation studies in mice. *J. Appl. Physiol.* 103, 1772–1779. doi: 10.1152/japplphysiol.00075.2007

Dunston, D., Ashby, S., Krosnowski, K., Ogura, T., and Lin, W. (2013). An effective manual deboning method to prepare intact mouse nasal tissue with preserved anatomical organization. *J. Vis. Exp.* 78:50538. doi: 10.3791/50538

Gao, L., Bonilla-Henao, V., García-Flores, P., Arias-Mayenco, I., Ortega-Sáenz, P., and López-Barneo, J. (2017). Gene expression analyses reveal metabolic specifications in acute O_2-sensing chemoreceptor cell. *J. Physiol.* 595, 6091–6099. doi: 10.1113/JP274684

Harkema, J. R., Carey, S. A., and Wagner, J. G. (2006). The nose revisited: a brief review of the comparative structure, function, and toxicologic pathology of the nasal epithelium. *Toxicol. Pathol.* 34, 252–269. doi: 10.1080/01926230600713475

Hemelrijk, S. D., Vangulik, T. M., and Heger, M. (2019). Carotid chemoreceptor denervation does not impair hypoxiainduced thermal downregulation but vitiates recovery from a hypothermic and hypometabolic state in mice. *Sci. Rep.* 9:5132. doi: 10.1038/s41598-019-41546-x

Inui, K., Chen, C., Pauli, J. L., Kuroki, C., Tashiro, S., Kanmura, Y., et al. (2016). Nasal TRPA1 mediates irritant-induced bradypnea in mice. *Phys. Rep.* 4:e13098. doi: 10.14814/phy2.13098

Iwakawa, S., Kanmura, Y., and Kuwaki, T. (2019). Orexin receptor blockade-induced sleep preserves the ability to wake in the presence of threat in mice. *Front. Behav. Neurosci.* 12:327. doi: 10.3389/fnbeh.2018.00327

Kim, Y. S., Son, J. Y., Kim, T. H., Paik, S. K., Dai, Y., Noguchi, K., et al. (2010). Expression of transient receptor potential ankyrin 1 (TRPA1) in the rat trigeminal sensory afferents and spinal dorsal hor. *J. Comp. Neurol.* 518, 687–698. doi: 10.1002/cne.22238

Kreissl, M. C., Wu, H. -M., Stout, D. B., Ladno, W., Schindler, T. H., Zhang, X., et al. (2006). Noninvasive measurement of cardiovascular function in mice with high-temporal-resolution small-animal PET. *J. Nucl. Med.* 47, 974–980.

Kwan, K. Y., Allchorne, A. J., Vollrath, M. A., Christensen, A. P., Zhang, D. -S., Woolf, C. J., et al. (2006). TRPA1 contributes to cold, mechanical, and chemical nociception but is not essential for hair-cell transduction. *Neuron* 50, 277–289. doi: 10.1016/j.neuron.2006.03.042

Lee, S. H., Iwanaga, T., Hoshi, O., Adachi, I., and Fujita, T. (1995). Regional differences of CGRP-immunoreactive nerve fibers in nasal epithelium of the rat. *Arch. Histol. Cytol.* 58, 117–126. doi: 10.1679/aohc.58.117

Mateika, J. H., and Duffln, J. (1995). A review of the control of breathing during exercise. *Eur. J. Appl. Physiol.* 71, 1–27. doi: 10.1007/BF00511228

Mills, E., Smith, P. G., Slotkin, T. A., and Breese, G. (1978). Role of carotid body catecholamines in chemoreceptor function. *Neuroscience* 3, 1137–1146. doi: 10.1016/0306-4522(78)90134-3

Nakamura, A., Fukuda, Y., and Kuwaki, T. (2003). Sleep apnea and effect of chemostimulation on breathing instability in mice. *J. Appl. Physiol.* 94, 525–532. doi: 10.1152/japplphysiol.00226.2002

Nakashimo, Y., Takumida, M., Fukuiri, T., Anniko, M., and Hirakawa, K. (2010). Expression of transient receptor potential channel vanilloid (TRPV) 1–4, melastin (TRPM) 5 and 8, and ankyrin (TRPA1) in the normal and methimazole-treated mouse olfactory epithelium. *Acta Oto-Laryngo.* 130, 1278–1286. doi: 10.3109/00016489.2010.489573

Onodera, M., Kuwaki, T., Kumada, M., and Masuda, Y. (1997). Determination of ventilatory volume in mice by whole body plethysmography. *Jpn. J. Physiol.* 47, 317–326. doi: 10.2170/jjphysiol.47.317

Peng, Y. -J., Nanduri, J., Raghuraman, G., Souvannakitti, D., Gadalla, M. M., Kumar, G. K., et al. (2010). H_2S mediates O_2 sensing in the carotid body. *Proc. Natl. Acad. Sci. U. S. A.* 107, 10719–10724. doi: 10.1073/pnas.1005866107

Phillipson, E. A., Sullivan, C. E., Read, D. J., Murphy, E., and Kozar, L. F. (1978). Ventilatory and waking responses to hypoxia in sleeping dogs. *J. Appl. Physiol. Respir. Environ. Exerc. Physiol.* 44, 512–520. doi: 10.1152/jappl.1978.44.4.512

Pokorski, M., Takeda, K., Sato, Y., and Okada, Y. (2014). The hypoxic ventilatory response and TRPA1 antagonism in conscious mice. *Acta Physiol.* 210, 928–938. doi: 10.1111/apha.12202

Prabhakar, N. R., and Semenza, G. L. (2015). Oxygen sensing and homeostasis. *Physiology* 30, 340–348. doi: 10.1152/physiol.00022.2015

Riches, A. C., Sharp, J. G., Thomas, D. B., and Smith, S. V. (1973). Blood volume determination in the mouse. *J. Physiol.* 228, 279–284. doi: 10.1113/jphysiol.1973.sp010086

Takahashi, N., Kuwaki, T., Kiyonaka, S., Numata, T., Kozai, D., Mizuno, Y., et al. (2011). TRPA1 underlies a sensing mechanism for O_2. *Nat. Chem. Biol.* 7, 701–711. doi: 10.1038/NChemBio.640

Terada, J., Nakamura, A., Zhang, W., Yanagisawa, M., Kuriyama, T., Fukuda, Y., et al. (2007). Ventilatory long-term facilitation in mice can be observed during both sleep and wake periods and depends on orexin. *J. Appl. Physiol.* 104, 499–507. doi: 10.1152/japplphysiol.00919.2007

Wang, Y., Cao, L., Lee, C. -Y., Matsuo, T., Wu, K., Asher, G., et al. (2018). Large-scale forward genetics screening identifies Trpa1 as a chemosensor for predator odor-evoked innate fear behaviors. *Nat. Commun.* 9:2041. doi: 10.1038/s41467-018-04324-3

Yonemitsu, T., Kuroki, C., Takahashi, N., Mori, Y., Kanmura, Y., Kashiwadani, H., et al. (2013). TRPA1 detects environmental chemicals and induces avoidance behavior and arousal from sleep. *Sci. Rep.* 3:3100. doi: 10.1038/srep03100

Zappia, K. J., Garrison, S. R., Palygin, O., Weyer, A. D., Barabas, M., Lawlor, M. W., et al. (2016). Mechanosensory and ATP release deficits following keratin14-Cre-mediated TRPA1 deletion despite absence of TRPA1 in murine keratinocytes. *PLoS One* 11:e0151602. doi: 10.1371/journal.pone.0151602

Conflict of Interest: The authors declare that the research was conducted in the absence of any commercial or financial relationships that could be construed as a potential conflict of interest.

frontiers in Physiology

ORIGINAL RESEARCH
published: 22 October 2020
doi: 10.3389/fphys.2020.583735

Effects of Normoxic Recovery on Intima-Media Thickness of Aorta and Pulmonary Artery Following Intermittent Hypoxia in Mice

Akira Umeda[1], Kazuya Miyagawa[2], Atsumi Mochida[2], Hiroshi Takeda[2], Kotaro Takeda[3], Yasumasa Okada[4] and David Gozal[5]*

[1] Department of Respiratory Medicine, International University of Health and Welfare Shioya Hospital, Yaita, Japan, [2] Department of Pharmacology, School of Pharmacy, International University of Health and Welfare, Otawara, Japan, [3] Faculty of Rehabilitation, School of Healthcare, Fujita Health University, Toyoake, Japan, [4] Department of Internal Medicine, National Hospital Organization Murayama Medical Center, Musashimurayama, Japan, [5] Department of Child Health and the Child Health Research Institute, MU Women's and Children's Hospital, University of Missouri, Columbia, MO, United States

Obstructive sleep apnea (OSA) patients are at risk for increased blood pressure and carotid intima-media thickness (IMT), with pulmonary hypertension and right-sided heart failure potentially developing as well. Chronic intermittent hypoxia (IH) has been used as an OSA model in animals, but its effects on vascular beds have not been evaluated using objective unbiased tools. Previously published and current experimental data in mice exposed to IH were evaluated for IMT in aorta and pulmonary artery (PA) after IH with or without normoxic recovery using software for meta-analysis, Review Manager 5. Because IMT data reports on PA were extremely scarce, atherosclerotic area percentage from lumen data was also evaluated. IH significantly increased IMT parameters in both aorta and PA as illustrated by Forest plots ($P < 0.01$), which also confirmed that IMT values after normoxic recovery were within the normal range in both vascular beds. One-sided scarce lower areas in Funnel Plots were seen for both aorta and PA indicating the likelihood of significant publication bias. Forest and Funnel plots, which provide unbiased assessments of published and current data, suggest that IH exposures may induce IMT thickening that may be reversed by normoxic recovery in both aorta and PA. In light of the potential likelihood of publication bias, future studies are needed to confirm or refute the findings. In conclusion, OSA may induce IMT thickening (e.g., aorta and/or PA), but the treatment (e.g., nasal continuous positive airway pressure) will likely lead to improvements in such findings.

Keywords: intermittent hypoxia, aorta, pulmonary artery, mouse, sleep apnea syndrome, intima-media thickness

OPEN ACCESS

Edited by:
Antonio Colantuoni, University of Naples Federico II, Italy

Reviewed by:
Roy Sutliff, Emory University, United States
Dominga Lapi, University of Naples Federico II, Italy

****Correspondence:***
Akira Umeda
umeda@iuhw.ac.jp;
aumeda@hf.catv.ne.jp

Specialty section:
This article was submitted to Vascular Physiology, a section of the journal Frontiers in Physiology

Received: *15 July 2020*
Accepted: *05 October 2020*
Published: *22 October 2020*

Citation:
Umeda A, Miyagawa K, Mochida A, Takeda H, Takeda K, Okada Y and Gozal D (2020) Effects of Normoxic Recovery on Intima-Media Thickness of Aorta and Pulmonary Artery Following Intermittent Hypoxia in Mice. Front. Physiol. 11:583735. doi: 10.3389/fphys.2020.583735

INTRODUCTION

Obstructive sleep apnea (OSA) and elevated systemic blood pressure tend to co-exist (Davies et al., 2000) and are associated with insulin resistance, dyslipidemia, atherosclerosis and increased risk of ischemic cardiovascular diseases. However, the causal contributions of chronic intermittent hypoxia (IH), one of the hallmarks phenotypic features of OSA, to these cardiovascular and

metabolic abnormalities is unclear. Inferential evidence derived from OSA interventional studies indicates that nasal continuous positive airway pressure (CPAP) can improve baroreceptor responsiveness and reduce waking blood pressure (Coughlin et al., 2007). Systemic blood pressure in mice is elevated by chronic IH (Campen et al., 2005; Schulz et al., 2014), with possible mechanisms of OSA-related hypertension including sympathetic overactivity, and up-regulation of the endothelin and renin-angiotensin systems (Narkiewicz and Somers, 1997; Phillips et al., 1999; Møller et al., 2003). In the context of atherosclerosis and vascular dysfunction, increased carotid intima-media thickness (IMT) has been reported in OSA patients (Drager et al., 2005). Subsequent studies revealed independent associations between hypoxic stress and IMT in OSA (Minoguchi et al., 2005) that can be reversed by nasal CPAP (Bradley and Floras, 2009).

Similarly, IH exposures mimicking OSA induce pulmonary hypertension in mice (Fagan et al., 2001; Campen et al., 2005; Haslip et al., 2015), and work by Fagan et al. (2001) in mice showed that IH induced pulmonary vascular remodeling that paralleled the effects seen during chronic sustained hypoxia. Severe OSA patients have been reported to develop chronic pulmonary hypertension and right-sided heart failure in 12–20% (Bradley et al., 1985; Weitzenblum et al., 1988). Medial thickness of the pulmonary artery (PA) is increased by hypoxia in mice (Hales et al., 1983; Wanstall et al., 2002; Matsui et al., 2004; Ambalavanan et al., 2005; Yu et al., 2008; Mizuno et al., 2011)

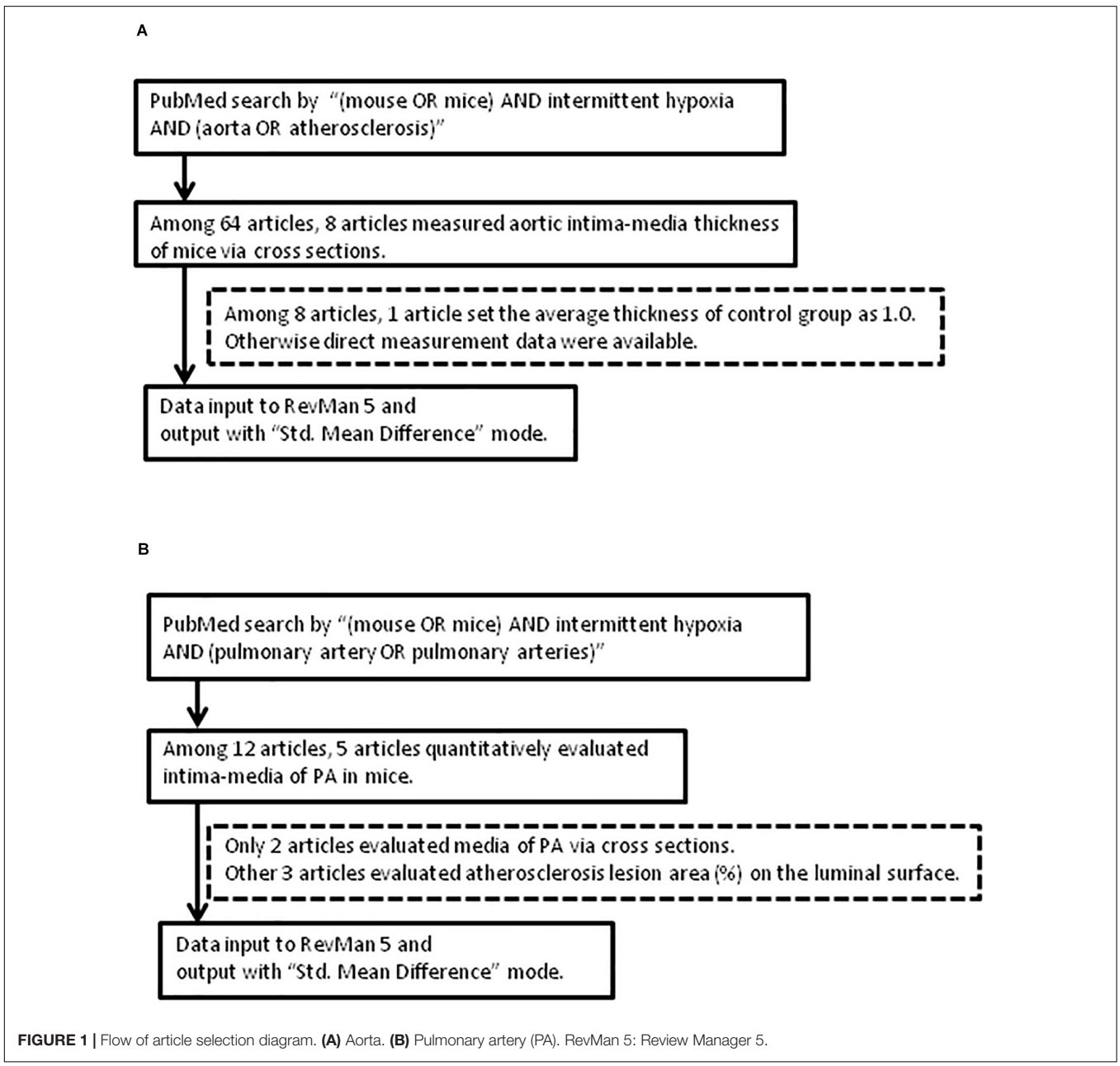

FIGURE 1 | Flow of article selection diagram. **(A)** Aorta. **(B)** Pulmonary artery (PA). RevMan 5: Review Manager 5.

and in rats (Meyrick and Reid, 1980; Hu et al., 1989; Jeffery and Wanstall, 1999). IH combined with episodic hypercapnia accelerates atherosclerosis of PA in ApoE knockout mice and Ldlr knockout mice (Xue et al., 2017; Imamura et al., 2019), as illustrated by increases in the atherosclerotic area percentage of the PA lumen.

Recently, we conducted experiments in C57BL/7J male mice and found that chronic IH did not decrease O_2 consumption or energy expenditure, but increased the size of visceral adipocytes during normoxic recovery, the latter aimed at exploring the effect of efficacious treatment of OSA (Umeda et al., 2020; Readers are encouraged to download this paper and its supplementary files). Here, we took advantage of existing fixed aorta and PA from these experiments, and evaluated the effects of 8-week IH exposures followed by normoxic recovery on the IMT of aorta and PA. To enable unbiased comparisons of our experimental data with the data originating from published studies, we used the freely available software Review Manager 5 (RevMan 5).

MATERIALS AND METHODS

Animals and Exposures to IH

C57BL/6J male mice (4–5 week old) were assigned to one of 3 exposure profiles with body weight matching, as

TABLE 1 | Profiles of similar experiments compared on aorta.

First author (year)	Mice	Sex	Starting age	*N*	IH duration (normoxic recovery duration)	IH condition
Dematteis et al., 2008	WT (C57BL/6J)	Male	8 week	4–5/group	14 day (-)	8 h/d, F_IO_2-4-21%, 30 s cycle
Arnaud et al., 2011	WT (C57BL/6J)	Male	8 week	7/group	14 day (-)	8 h/d, F_IO_2-5-21%, 60 s cycle
Zhou et al., 2014	WT (129S1)	?	Adult	6/group	8 week (-)	12 h/d, F_IO_2-8-21%, 30 cycles/h
Poulain et al., 2015	WT (C57BL/6J)	Male	17 week	10/group	4 week (-)	8 h/d, F_IO2-5-21%, 1 min cycle,
Gras et al., 2016	WT (C57BL/6J)	?	7–9 week	5–6/group	14 day (-)	8 h/d, F_IO_2-5-21%, 1 min cycle
Castro-Grattoni et al., 2016	WT (C57BL/6J)	Male	6 week	10/group	6 week (-)	6 h/d, F_IO_2-5-21%, 1 min cycle
	WT (C57BL/6J)	Male	6 week	10/group	6 week (6 week)	
Lan et al., 2017	WT (C57BL/6J)	Female	5–8 week	6/group	28 day (-)	8 h/d, F_IO_2-5-21%, 40 cycle/h
Arnaud et al., 2018	WT (C57BL/6J)?	?	?	9–13/group	14 day (-)	8 h/d, F_IO_2-5-21%, 1 min cycle
Suarez-Giron et al., 2018	WT (C57BL/6J)	Male	6 week	10/group	6 week (-)	6 h/d, F_IO_2-5-21%, 60 s cycle
Umeda et al., 2020	WT (C57BL/6J)	Male	4–5 week	7/group	8 week (5 week)	12 h/d, F_IO_2-6-7% and normoxia, 180 s cycle

All the reports measured intima-media thickness of aorta via cross sections. Zhou et al. (2014) set the average thickness of control group as 1.0. Otherwise direct measurements in microns were reported.
WT, wild-type mice.

TABLE 2 | Profiles of similar experiments compared on pulmonary artery.

First author (year)	Mice	Sex	Starting age	*N*	Chow	IH duration (Normoxic recovery duration)	IH condition
Douglas et al., 2013	Ldlr	Male	2–3 month	CO 4, IH 4	HFD	8 week (-)	10 h/d. 4 min F_IO_2-8%, F_ICO_2-8%/4 min normoxia F_IO_2-21%, F_ICO_2-0.1%, Ramp intervals of 1–2 min.
	Ldlr	Male	2–3 month	4/group?	Regular	8 week (-)	
Xue et al., 2017	ApoE	Male	10 week	CO 4, IH 8	HFD	8 week (-)	10 h/d, 4 min F_IO_2-8%, F_ICO_2-8%/4 min normoxia F_IO_2-21%, F_ICO_2-0.1%, Ramp intervals of 1–2 min.
	Ldlr	Male	10 week	CO 7, IH 8	HFD	8 week (-)	
Imamura et al., 2019	Ldlr	Male	?	CO 7, IH 6	HFD	8 week (-)	10 h/d, F_IO_2-8-21%, F_ICO_2 (0.5–8) 4 min alternating (1–2 min Ramp intervals)
Fu et al., 2020	WT (C57BL/6J)	Male	6 week	5/group	Regular	6 week (-)	9 h/d, F_IO_2-5-21%, 1 min cycle.
Song et al., 2020	WT (C57BL/6J)	Male	8 week	6/group	Regular (?)	4 week (-)	8 h/d, F_IO_2-4-21%, 1 min cycle.
Umeda et al., 2020	WT (C57BL/6J)	Male	4–5 week	7/group	Regular	8 week (5 week)	12 h/d, F_IO_2-6-7% and normoxia, 180 s cycle

Only Fu et al. (2020) and Song et al. (2020), and we evaluated intima-media thickness of pulmonary arteries via cross sections. Other three articles evaluated atherosclerosis lesion area (%) on the luminal surface. ApoE, ApoE knockout mice; CO, control; HFD, high fat diet; IH, intermittent hypoxia; Ldlr, Ldlr knockout mice; WT, wild-type mice.

previously described (Umeda et al., 2020): (a) 12 h/day of mild IH (IHM) consisting of alternating F_IO_2-10-11% and normoxia (F_IO_2-21%) with a 640 s total cycle duration (n = 7); (b) 12 h/day of severe IH (IHS) consisting of alternating F_IO_2-6-7% and normoxia, and a 180 s cycle duration) (n = 7); (c) sham IH [Control (CO)] with normoxic air every day, with all exposures lasting for 8 weeks (n = 7). After completion of exposures, all mice were kept under normoxic conditions for 5 weeks (IUHW animal experiment ethic committee approval number: 18020). An approximate 12-h dark/light cycle was maintained (approximately 18:00–6:00/6:00–18:00, according to natural light). Mice had free access to regular chow and water for the duration of the experiments.

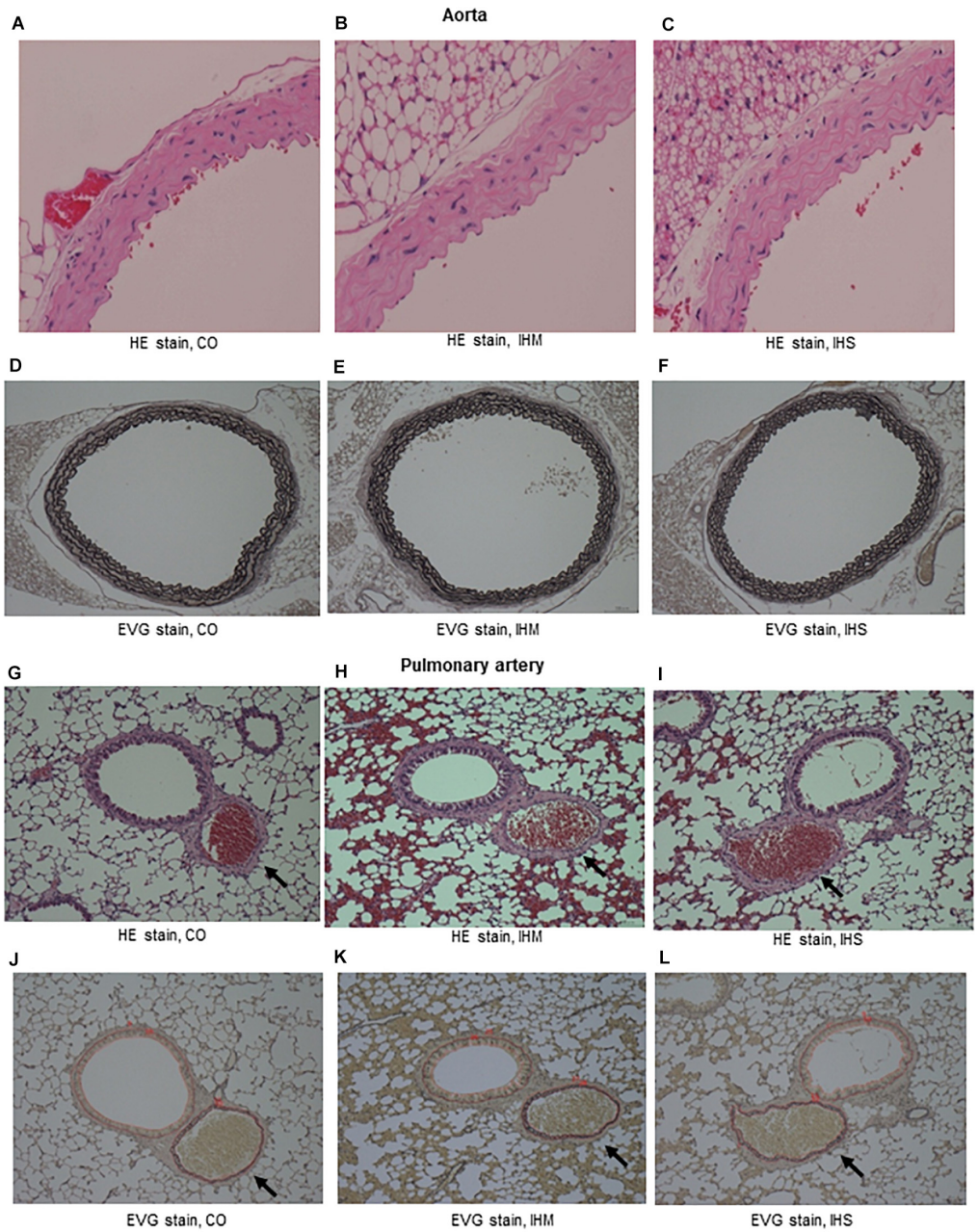

FIGURE 2 | Microphotographs of cross-sectional specimens. **(A–C)** Aorta, Hematoxylin and eosin (HE) stain, initial magnification: x40. **(D–F)** Aorta, Elastica van Gieson stain (EVG) stain, initial magnification: x10. **(G–I)** Pulmonary artery (PA, arrows), HE stain, initial magnification: x10. **(J–L)** PA (arrows), EVG stain, initial magnification: x10. Intima-media thickness of PA is under measure using WinROOF software. Thickness of bronchial epithelium is also measured (data not shown). CO, control; IHM, mild intermittent hypoxia; IHS, severe intermittent hypoxia. Neither IHS nor IHM induced significant changes in intima-media thickness of aorta or PA in the normoxic recovery phase. Persistent disruptions of the elastic laminae were not clearly seen for aorta or PA.

Histological Analysis

After euthanasia by decapitation at the end of the 5-week normoxic recovery period, organs underwent fixation with 4% paraformaldehyde. The descending aorta and lung were cross-sectioned using paraffin at a thickness of 3 micrometer, and digital photographs were acquired using light microscopy (MCD-350, Olympus, Tokyo, Japan). Hematoxylin and eosin stain and Elastica van Gieson stain were performed. The IMT data of aorta and PA were analyzed by WinROOF software (Mitani Corporation, Tokyo, Japan), by measuring the area of intima-medial layer on the cross sections of descending aorta or PA. The PA with diameter size of approximately 200 μm was selected. Wanstall et al. (2002) reported that the morphological changes of PA medial thickness by hypoxia in mice were more definitively identified when vessels examined had outer diameters of 151–420 μm when compared to pulmonary vessels with diameters ranging from 50 to 150 μm.

Collection of Published Data

PubMed database was used for the identification and collection of similar experiments with the search commands of "(mouse OR mice) AND intermittent hypoxia AND (aorta OR atherosclerosis)" for aorta, and "(mouse OR mice) AND intermittent hypoxia AND (pulmonary artery OR pulmonary arteries)" for PA. All published articles were then reviewed and relevant studies were retained for analyses (**Figure 1**).

Data Analysis

Data are expressed as mean ± standard error of the mean (SEM), unless otherwise indicated. Comparisons among groups were conducted with ANOVA procedures followed by Fisher's *post hoc* tests. Excel Statistics software, 2010 version (Social Survey Research Information, Co., Ltd., Tokyo, Japan) was used. For comparisons with previous similar experimental data, the free software RevMan 5 (Cochrane) was used. RevMan is the software developed for Cochrane review authors to perform analyses toward a Cochrane systematic review of a healthcare intervention, and this software (currently version 5.3) is available as free software[1]. We undertook the evaluation of experimental data from our own studies and those of previous publications using this software, and uncovered its usefulness for the unbiased overview of relevant experimental data. For all statistical analyses, P-value < 0.05 was considered to denote a statistically significant difference.

RESULTS

Identification and Collection of Similar Experimental Data

The approach and selection of relevant studies are shown in **Figure 1**, and ultimately eight articles were found with data on IMT measures of cross-sectional specimens of aorta in mice (**Figure 1A** and **Table 1**). In one of these eight articles, the average control IMT was set as an arbitrary value of 1.0. All other articles showed data of IMT measures as micrometers. All the experiments were performed on wild-type mice on aorta (**Table 1**). However, we found only two articles which evaluated IMT of PA via cross sectional specimens (**Figure 1B** and **Table 2**). Because the number of articles on PA IMT measures was very small, we also selected three additional articles which evaluated the atherosclerosis lesion area (%) on the luminal surface of PA. Douglas et al. (2013); Xue et al. (2017), and Imamura et al. (2019) used transgenic mice on PA (**Table 2**).

Histological Analysis

When compared to matched controls, we found no evidence that either IHS or IHM induced significant changes in

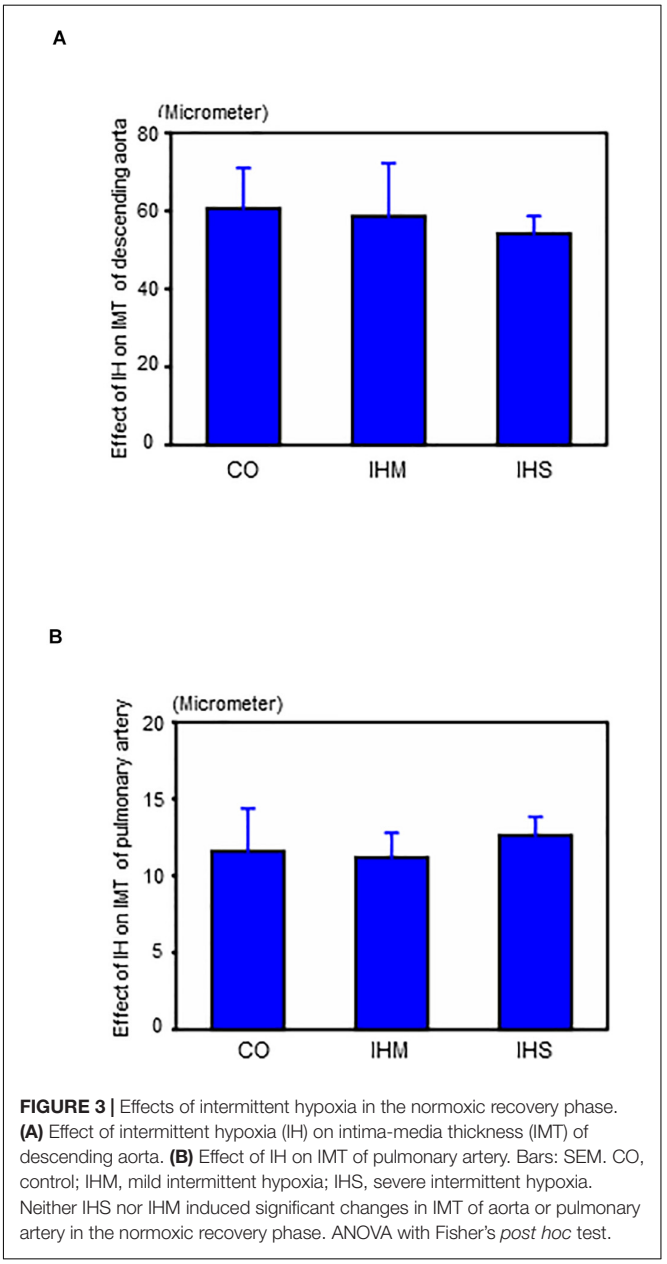

FIGURE 3 | Effects of intermittent hypoxia in the normoxic recovery phase. **(A)** Effect of intermittent hypoxia (IH) on intima-media thickness (IMT) of descending aorta. **(B)** Effect of IH on IMT of pulmonary artery. Bars: SEM. CO, control; IHM, mild intermittent hypoxia; IHS, severe intermittent hypoxia. Neither IHS nor IHM induced significant changes in IMT of aorta or pulmonary artery in the normoxic recovery phase. ANOVA with Fisher's *post hoc* test.

[1]https://training.cochrane.org/online-learning/core-software-cochrane-reviews/revman/revman-5-download

IMT of aorta or PA after completing the 5-week normoxic recovery phase (**Figures 2**, **3**). Persistent disruptions of the elastic laminae were not apparent in either the aorta or PA (**Figure 2**), suggesting that if such lesions were induced by IH, they had recovered at the end of the normoxic period.

Evaluation With Review Managing Software

Data from previous studies and current data are included in **Figure 4** (Forest Plot) and **Figure 5** (Funnel Plot). Most of previous studies focused on the aorta showed statistically significant increases in the IMT values following chronic IH (**Figure 4A**). The study by Castro-Grattoni et al. (2016) is the only one that examined IMT changes immediately upon completion of the 6-week exposure to IH and following a normoxic recovery phase of equivalent duration. Both that study and our current experimental data reveal that normoxic recovery is accompanied by reversal and normalization of IH-induced IMT increases in aorta (**Figure 4A** and **Table 1**).

Previous studies focused on PA showed statistically significant increases induced by chronic IH on PA IMT or atherosclerosis lesion area (%) data on the luminal surface of PA (**Figure 4B**). We could not find any previous studies examining the normoxic recovery phase for PA (**Table 2**). From our experimental results, IMT values in the normoxic recovery phase were smaller than those obtained just after IH for both aorta and PA, and such recovery values were similar to control conditions.

Of note, in the Funnel Plot, fewer data in the left lower area than in the right lower area were apparent for both aorta and PA (**Figures 5A,B**).

DISCUSSION

The current study adds incremental inferential data that suggests that following chronic IH exposures mimicking OSA of relative

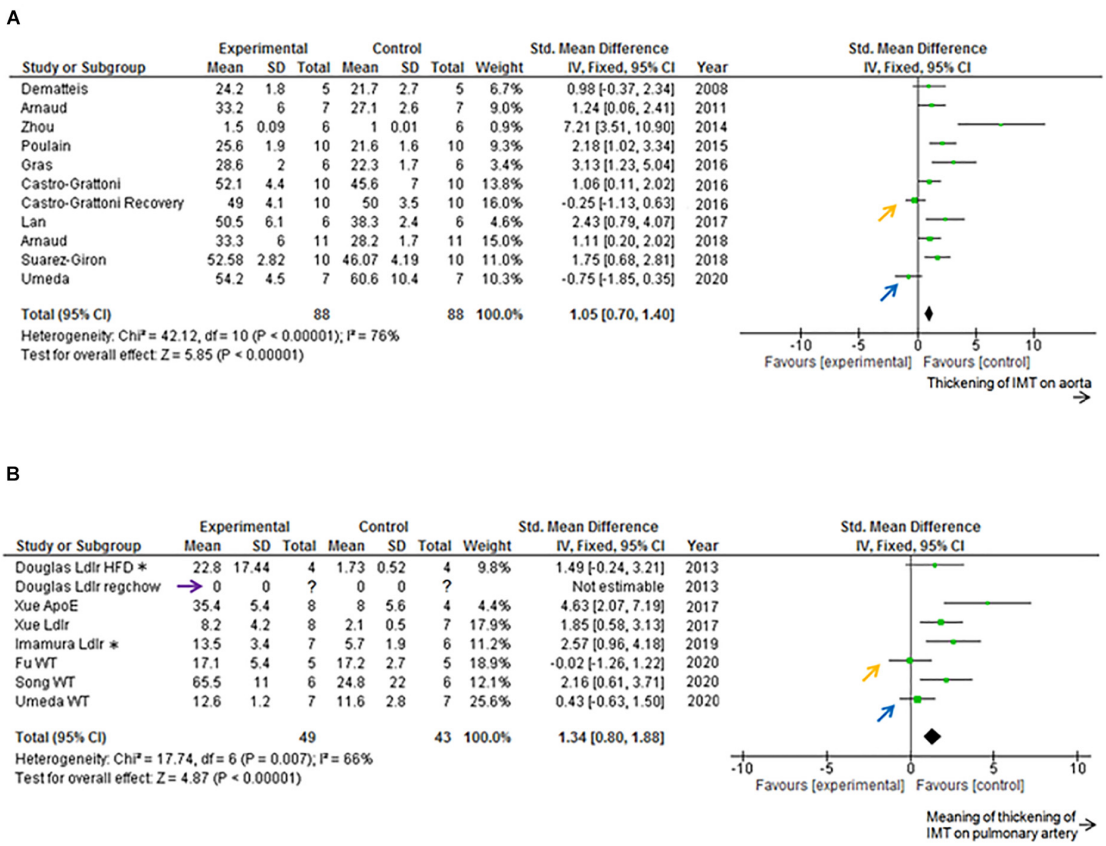

FIGURE 4 | Forest plot. **(A)** Effect of intermittent hypoxia (IH) on intima-media thickness (IMT) of descending aorta. IH significantly increased aortic IMT ($P < 0.01$). Castro-Grattoni et al. (2016) examined both the effects of IH and those after 6 weeks of normoxic recovery (orange arrow). Current data are those after 5 weeks of normoxic recovery (blue arrow). Only 4–5 per condition were used by Dematteis et al. (2008) and Gras et al. (2016) used 5–6 mice per condition, and Arnaud et al. (2018) employed 9–13 mice per condition. All the experiments were performed on wild-type mice. **(B)** Effect of IH on IMT of pulmonary artery (PA). IH significantly increased IMT-associated parameters of PA ($P < 0.01$). Douglas et al. (2013) used both regular chow and high fat diet, and reported that regular chow did not cause atherosclerotic lesions of PA (purple arrow). Xue et al. (2017) and Imamura et al. (2019) used high fat diets. Douglas et al. (2013); Xue et al. (2017), and Imamura et al. (2019) used transgenic mice. Fu et al. (2020) reported that IH did not increase IMT of PA (orange arrow). Current data after normoxic recovery phase (blue arrow). ApoE, ApoE knockout mice; CI, confidence interval; HFD, high fat diet; IV, inverse variance-weighted method; Ldlr, Ldlr knockout mice; regchow, regular chow; SD, standard deviation; WT, wild-type mice. *Data of 8 week, 10 h/d exposure to Ldlr knockout mice.

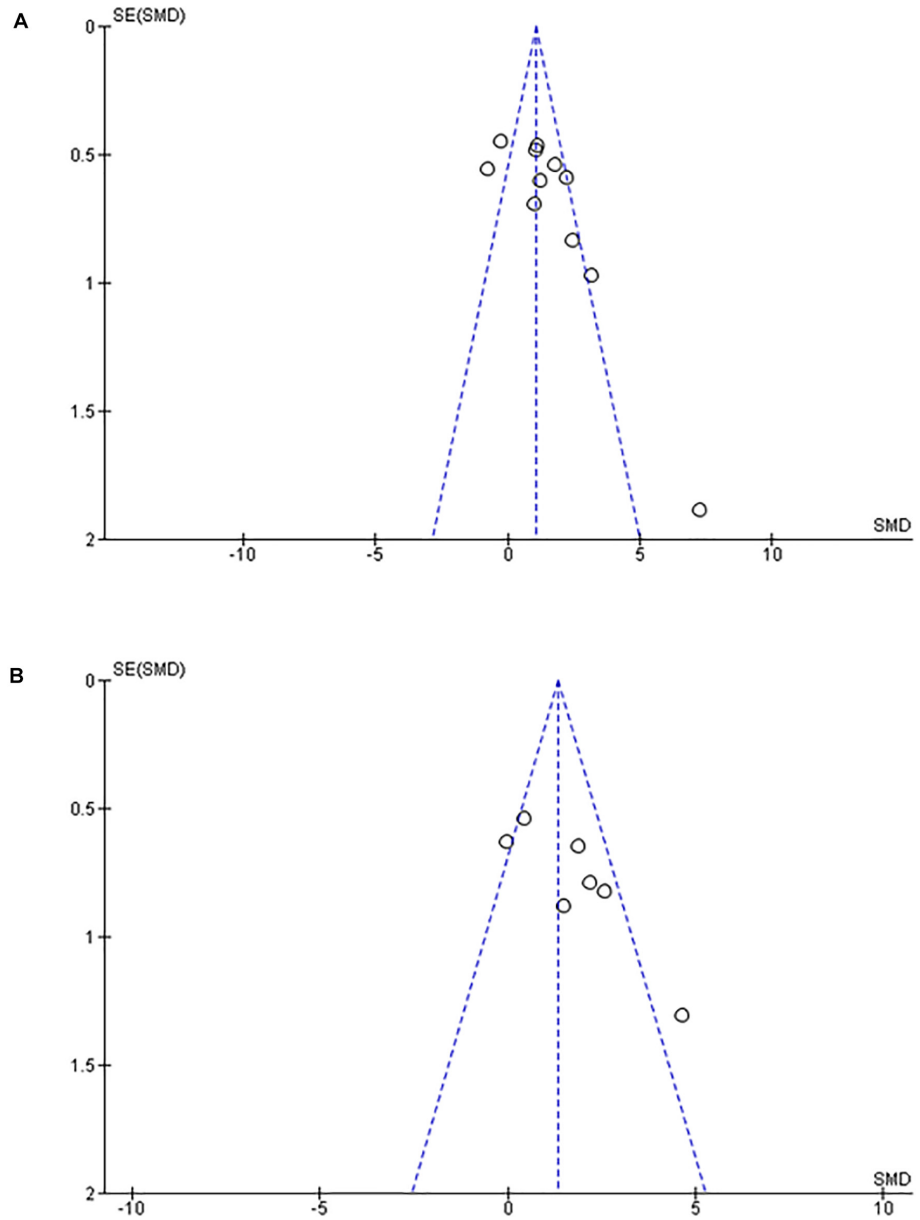

FIGURE 5 | Funnel plot. **(A)** Effect of intermittent hypoxia on intima-media thickness of aorta. **(B)** Effect of intermittent hypoxia on intima-media thickness of pulmonary artery. Scarceness of plots in left lower area emerged for both aorta **(A)** and pulmonary artery **(B)**. SE, standard error; SMD, standardized mean difference.

short duration (6–8 weeks), normoxic recovery is associated with normalization of the IMT in both aorta and PA. Review of previous publications reporting findings on IH exposures in mice, and the effects on IMT enabled us to proceed with unbiased comparisons of their findings with those of our experimental data. More importantly, the unbiased review revealed that evidence related to recovery of the effects of IH on either the aorta or PA is markedly scarce, and therefore deserves to be expanded in future studies. Notably, the Funnel plot graphs for both aorta and PA revealed a potential "publication bias," and therefore further reinforce the need for incremental studies that should possibly include longer exposure durations as well as longer recovery periods (Cortese et al., 2017; Trzepizur et al., 2018). Indeed, one-sided scarce plots in the lower area in Funnel plot graphs are suggestive of publication biases. Thus, use of the RevMan software was particularly helpful for interpretation of our new experimental data with previously published findings in an unbiased fashion. Indeed, considering the scarcity of articles investigating the effects of IH on PA IMT, it is likely that IMT thickening may occur on aorta, but it is less likely to occur on PA. However, Xue et al. (2017) reported that PA atherosclerosis occurred in both ApoE knockout mice and Ldlr knockout mice, while aortic atherosclerosis occurred only in ApoE knockout mice. Based on the current results and the potential publication

biases inherent to the available datasets, we conclude that the evidence indicating that IH induces IMT thickening of either the aorta or PA is less than definitive and requires extensive future exploration to either confirm or refute such assumptions.

Prior to our current experimental data, we found only two articles exploring normoxic recovery after IH exposures (Castro-Grattoni et al., 2016; Cortese et al., 2017), and only one of these articles evaluated IMT in the mouse aorta (Castro-Grattoni et al., 2016). These investigators showed that after 6 week-exposures to IH there was a complete recovery from IH-induced IMT thickening of the aorta by exposures to normoxia for additional 6 weeks. However, when the IH exposures were lengthened to 12 weeks, i.e., potentially more relevant durations as related to OSA (most patients with OSA are usually diagnosed many months or years after symptom onset), persistent disruption of the elastic laminae and ongoing pro-inflammatory signaling of aorta vascular wall macrophages was detected, suggesting that the reversibility of IH-induced vascular changes may progressively be attenuated as the duration of IH is increasingly prolonged (Cortese et al., 2017). This issue if obviously of great importance in light of the recent negative multicenter trials, whereby patients with OSA treated with CPAP did not derive specific cardiovascular benefits from the therapy (McEvoy et al., 2016; Labarca et al., 2020; Sánchez-de-la-Torre et al., 2020). Other murine studies have also shown either incomplete or time-dependent functional recovery following IH-induced deficits. For example, 12-week IH exposures induced significant insulin resistance and white adipose tissue inflammation in mice that were only partially reversed after a 6-week normoxic recovery (Gileles-Hillel et al., 2017). Furthermore, Gozal et al. (2017) showed that as the duration of IH increased, the probability of cognitive function recovery was reduced. Thus, on the one hand there appear to be exposure duration, mouse strain, and hypoxia severity dependencies that may dictate the potential emergence of specific vascular phenotypes, and on the other, the reversibility of such putative changes may be dependent of the same antecedent determinants of the vascular changes.

Meyrick and Reid. (1980) demonstrated that sustained hypoxia of 380 torr for 10 days caused thickening of PA media in rats and 70 days of normoxic recovery reduced the medial thickness to within normal range. However, we could not find any articles on the time course of chronic IH-induced IMT thickening of PA and its reversibility during a normoxic recovery phase in mice. Therefore, our findings suggest for the first time the possibility that such changes, if indeed induced by IH, are reversible under normoxia. Inferential clinical evidence would suggest that treatment with CPAP is accompanied by improved pulmonary hemodynamics in patients with severe OSA (Laks, 1995; Sajkov et al., 2002; Lattimore et al., 2008). However, critical review of the evidence casts significant doubt as to whether OSA indeed directly induced pulmonary vascular changes that manifest as pulmonary hypertension, or whether the latter is the result of left heart dysfunction (Ismail et al., 2015; Kholdani et al., 2015; Wong et al., 2017).

We took advantage of existing specimens from our previous experiments, in which energy expenditure and body weight changes were evaluated during the normoxic recovery phase in mice (Umeda et al., 2020). Specimens were fixed after the exposure experiments were completed. Therefore, limitations of the current study are that histopathological specimens immediately after cessation of IH were not available. Such specimens would better illustrate the IMT changes induced by IH, and therefore lend further reinforcement to the reversal upon return to normoxia.

In summary, our original assumptions that chronic IH would lead to sustained aortic atherosclerosis and PA thickening were not confirmed, since following normoxic recovery after chronic IH of different severities the IMT values were within normative control ranges. Careful review of the extant literature reveals a high likelihood of publication bias on this particular issue, and therefore well-designed studies examining both the effects of IH on aorta and PA IMT and the effect of normoxic recovery as a correlate of OSA treatment are urgently needed. OSA may induce IMT thickening (e.g., aorta and/or PA), but adherent treatment (e.g., nasal CPAP) will improve it.

DATA AVAILABILITY STATEMENT

All datasets generated for this study are included in the article/supplementary material.

ETHICS STATEMENT

The animal study was reviewed and approved by the institution animal experiment ethical committee approved the protocol (International University of Health and Welfare animal experiment ethic committee approval number: 18020).

AUTHOR CONTRIBUTIONS

AU, YO, and DG: study design. AU, KM, AM, and HT: animal experiments and data collection. KT: making of IH system. AU: data analysis. All authors: interpretation, drafting, and approving of the manuscript.

FUNDING

This work was partly supported by the International University of Health and Welfare. And also partly supported by Chiyoda Health Development Agency. DG was supported in part by US National Institutes of Health grants HL130984, AG061824, and HL140548.

ACKNOWLEDGMENTS

We greatly appreciate the assistance of Dr. Morio Takumi (President, Nara Byori, Nara-City, Japan) for processing the specimens and measuring IMT of aorta and PA in double blinded manner.

REFERENCES

Ambalavanan, N., Bulger, A., Murphy-Ullrich, J., Oparil, S., and Chen, Y. F. (2005). Endothelin-A receptor blockade prevents and partially reverses neonatal hypoxic pulmonary vascular remodeling. *Pediatr. Res.* 57(5 Pt 1), 631–636. doi: 10.1203/01.PDR.0000159512.55862.69

Arnaud, C., Beguin, P. C., Lantuejoul, S., Pepin, J. L., Guillermet, C., Pelli, G., et al. (2011). The inflammatory preatherosclerotic remodeling induced by intermittent hypoxia is attenuated by RANTES/CCL5 inhibition. *Am. J. Respir. Crit. Care Med.* 184, 724–731. doi: 10.1164/rccm.201012-2033OC

Arnaud, C., Belaïdi-Corsat, E., and Godin-Ribuot, D. (2018). Concerning "Comments and Question on "Selective Inhibition of Endothelial NF-kB Signaling Attenuates Chronic Intermittent Hypoxia-Induced Atherosclerosis in Mice". *Atherosclerosis* 277, 227–228. doi: 10.1016/j.atherosclerosis.2018.06.862

Bradley, T. D., and Floras, J. S. (2009). Obstructive sleep apnoea and its cardiovascular consequences. *Lancet* 373, 82–93. doi: 10.1016/S0140-6736(08)61622-0

Bradley, T. D., Rutherford, R., Grossman, R. F., Lue, F., Zamel, N., Moldofsky, H., et al. (1985). Role of daytime hypoxemia in the pathogenesis of right heart failure in the obstructive sleep apnea syndrome. *Am. Rev. Respir. Dis.* 131, 835–839. doi: 10.1164/arrd.1985.131.6.835

Campen, M. J., Shimoda, L. A., and O'Donnell, C. P. (2005). Acute and chronic cardiovascular effects of intermittent hypoxia in C57BL/6J mice. *J. Appl. Physiol. (1985)* 99, 2028–2035. doi: 10.1152/japplphysiol.00411.2005

Castro-Grattoni, A. L., Alvarez-Buvé, R., Torres, M., Farré, R., Montserrat, J. M., Dalmases, M., et al. (2016). Intermittent hypoxia-induced cardiovascular remodeling is reversed by normoxia in a mouse model of sleep apnea. *Chest* 149, 1400–1408. doi: 10.1016/j.chest.2015.11.010

Cortese, R., Gileles-Hillel, A., Khalyfa, A., Almendros, I., Akbarpour, M., Khalyfa, A. A., et al. (2017). Aorta macrophage inflammatory and epigenetic changes in a murine model of obstructive sleep apnea: potential role of CD36. *Sci. Rep.* 7:43648. doi: 10.1038/srep43648

Coughlin, S. R., Mawdsley, L., Mugarza, J. A., Wilding, J. P., and Calverley, P. M. (2007). Cardiovascular and metabolic effects of CPAP in obese males with OSA. *Eur. Respir. J.* 29, 720–727. doi: 10.1183/09031936.00043306

Davies, C. W., Crosby, J. H., Mullins, R. L., Barbour, C., Davies, R. J., and Stradling, J. R. (2000). Case-control study of 24 hour ambulatory blood pressure in patients with obstructive sleep apnoea and normal matched control subjects. *Thorax* 55, 736–740. doi: 10.1136/thorax.55.9.736

Dematteis, M., Julien, C., Guillermet, C., Sturm, N., Lantuejoul, S., Mallaret, M., et al. (2008). Intermittent hypoxia induces early functional cardiovascular remodeling in mice. *Am. J. Respir. Crit. Care Med.* 177, 227–235. doi: 10.1164/rccm.200702-238OC

Douglas, R. M., Bowden, K., Pattison, J., Peterson, A. B., Juliano, J., Dalton, N. D., et al. (2013). Intermittent hypoxia and hypercapnia induce pulmonary artery atherosclerosis and ventricular dysfunction in low density lipoprotein receptor deficient mice. *J. Appl. Physiol. (1985)* 115, 1694–1704. doi: 10.1152/japplphysiol.00442.2013

Drager, L. F., Bortolotto, L. A., Lorenzi, M. C., Figueiredo, A. C., Krieger, E. M., and Lorenzi-Filho, G. (2005). Early signs of atherosclerosis in obstructive sleep apnea. *Am. J. Respir. Crit. Care Med.* 172, 613–618. doi: 10.1164/rccm.200503-340OC

Fagan, K. A., Morrissey, B., Fouty, B. W., Sato, K., Harral, J. W., Morris, K. G. Jr., et al. (2001). Selected contribution: pulmonary hypertension in mice following intermittent hypoxia. *J. Appl. Physiol. (1985)* 90, 2502–2507. doi: 10.1152/jappl.2001.90.6.2502

Fu, C., Hao, S., Liu, Z., Xie, L., Wu, X., Wu, X., et al. (2020). SOD2 ameliorates pulmonary hypertension in a murine model of sleep apnea via suppressing expression of NLRP3 in CD11b + cells. *Respir. Res.* 21:9. doi: 10.1186/s12931-019-1270-0

Gileles-Hillel, A., Almendros, I., Khalyfa, A., Nigdelioglu, R., Qiao, Z., Hamanaka, R. B., et al. (2017). Prolonged exposures to intermittent hypoxia promote visceral white adipose tissue inflammation in a murine model of severe sleep apnea: effect of normoxic recovery. *Sleep* 40:zsw074. doi: 10.1093/sleep/zsw074

Gozal, D., Khalyfa, A., Qiao, Z., Almendros, I., and Farré, R. (2017). Temporal trajectories of novel object recognition performance in mice exposed to intermittent hypoxia. *Eur. Respir. J.* 50, 1701456. doi: 10.1183/13993003.01456-2017

Gras, E., Belaidi, E., Briançon-Marjollet, A., Pépin, J. L., Arnaud, C., and Godin-Ribuot, D. (2016). Endothelin-1 mediates intermittent hypoxia-induced inflammatory vascular remodeling through HIF-1 activation. *J. Appl. Physiol. (1985)* 120, 437–443. doi: 10.1152/japplphysiol.00641.2015

Hales, C. A., Kradin, R. L., Brandstetter, R. D., and Zhu, Y. J. (1983). Impairment of hypoxic pulmonary artery remodeling by heparin in mice. *Am. Rev. Respir. Dis.* 128, 747–751. doi: 10.1164/arrd.1983.128.4.747

Haslip, M., Dostanic, I., Huang, Y., Zhang, Y., Russell, K. S., Jurczak, M. J., et al. (2015). Endothelial uncoupling protein 2 regulates mitophagy and pulmonary hypertension during intermittent hypoxia. *Arterioscler. Thromb Vasc. Biol.* 35, 1166–1178. doi: 10.1161/ATVBAHA.114.304865

Hu, L. M., Geggel, R., Davies, P., and Reid, L. (1989). The effect of heparin on the haemodynamic and structural response in the rat to acute and chronic hypoxia. *Br. J. Exp. Pathol.* 70, 113–124.

Imamura, T., Xue, J., Poulsen, O., Zhou, D., Karin, M., and Haddad, G. G. (2019). Intermittent hypoxia and hypercapnia induces inhibitor of nuclear factor-κB Kinase subunit β-dependent atherosclerosis in pulmonary arteries. *Am. J. Physiol. Regul. Integr. Comp. Physiol.* 317, R763–R769. doi: 10.1152/ajpregu.00056.2019

Ismail, K., Roberts, K., Manning, P., Manley, C., and Hill, N. S. (2015). OSA and pulmonary hypertension: time for a new look. *Chest* 147, 847–861. doi: 10.1378/chest.14-0614

Jeffery, T. K., and Wanstall, J. C. (1999). Perindopril, an angiotensin converting enzyme inhibitor, in pulmonary hypertensive rats: comparative effects on pulmonary vascular structure and function. *Br. J. Pharmacol.* 128, 1407–1418. doi: 10.1038/sj.bjp.0702923

Kholdani, C., Fares, W. H., and Mohsenin, V. (2015). Pulmonary hypertension in obstructive sleep apnea: is it clinically significant? A critical analysis of the association and pathophysiology. *Pulm Circ.* 5, 220–227. doi: 10.1086/679995

Labarca, G., Dreyse, J., Drake, L., Jorquera, J., and Barbe, F. (2020). Efficacy of continuous positive airway pressure (CPAP) in the prevention of cardiovascular events in patients with obstructive sleep apnea: systematic review and meta-analysis. *Sleep Med. Rev.* 52:101312. doi: 10.1016/j.smrv.2020.101312

Laks, L. (1995). Pulmonary artery pressure in sleep apnoea and snoring. *J. Sleep Res.* 4, 182–184. doi: 10.1111/j.1365-2869.1995.tb00211.x

Lan, X. F., Zhang, X. J., Lin, Y. N., Wang, Q., Xu, H. J., Zhou, L. N., et al. (2017). Estradiol regulates Txnip and prevents intermittent hypoxia-induced vascular injury. *Sci. Rep.* 7:10318. doi: 10.1038/s41598-017-10442-7

Lattimore, J. D., Wilcox, I., Adams, M. R., Kilian, J. G., and Celermajer, D. S. (2008). Treatment of obstructive sleep apnoea leads to enhanced pulmonary vascular nitric oxide release. *Int. J. Cardiol.* 126, 229–233. doi: 10.1016/j.ijcard.2007.04.001

Matsui, H., Shimosawa, T., Itakura, K., Guanqun, X., Ando, K., and Fujita, T. (2004). Adrenomedullin can protect against pulmonary vascular remodeling induced by hypoxia. *Circulation* 109, 2246–2251. doi: 10.1161/01.CIR.0000127950.13380.FD

McEvoy, R. D., Antic, N. A., Heeley, E., Luo, Y., Ou, Q., Zhang, X., et al. (2016). CPAP for prevention of cardiovascular events in obstructive sleep apnea. *N. Engl. J. Med.* 375, 919–931. doi: 10.1056/NEJMoa1606599

Meyrick, B., and Reid, L. (1980). Hypoxia-induced structural changes in the media and adventitia of the rat hilar pulmonary artery and their regression. *Am. J. Pathol.* 100, 151–178.

Minoguchi, K., Yokoe, T., Tazaki, T., Minoguchi, H., Tanaka, A., Oda, N., et al. (2005). Increased carotid intima-media thickness and serum inflammatory markers in obstructive sleep apnea. *Am. J. Respir. Crit. Care Med.* 172, 625–630. doi: 10.1164/rccm.200412-1652OC

Mizuno, S., Bogaard, H. J., Kraskauskas, D., Alhussaini, A., Gomez-Arroyo, J., Voelkel, N. F., et al. (2011). p53 gene deficiency promotes hypoxia-induced pulmonary hypertension and vascular remodeling in mice. *Am. J. Physiol. Lung Cell. Mol. Physiol.* 300, L753–L761. doi: 10.1152/ajplung.00286.2010

Møller, D. S., Lind, P., Strunge, B., and Pedersen, E. B. (2003). abnormal vasoactive hormones and 24-hour blood pressure in obstructive sleep apnea. *Am. J. Hypertens.* 16, 274–280. doi: 10.1016/s0895-7061(02)03267-3

Narkiewicz, K., and Somers, V. K. (1997). The sympathetic nervous system and obstructive sleep apnea: implications for hypertension. *J. Hypertens.* 15(12 Pt 2), 1613–1619. doi: 10.1097/00004872-199715120-00062

Phillips, B. G., Narkiewicz, K., Pesek, C. A., Haynes, W. G., Dyken, M. E., and Somers, V. K. (1999). Effects of obstructive sleep apnea on endothelin-1 and blood pressure. *J. Hypertens.* 17, 61–66. doi: 10.1097/00004872-199917010-00010

Poulain, L., Richard, V., Lévy, P., Dematteis, M., and Arnaud, C. (2015). Toll-like receptor-4 mediated inflammation is involved in the cardiometabolic alterations induced by intermittent hypoxia. *Mediators Inflamm.* 2015:620258. doi: 10.1155/2015/620258

Sajkov, D., Wang, T., Saunders, N. A., Bune, A. J., and Mcevoy, R. D. (2002). Continuous positive airway pressure treatment improves pulmonary hemodynamics in patients with obstructive sleep apnea. *Am. J. Respir. Crit. Care Med.* 165, 152–158. doi: 10.1164/ajrccm.165.2.2010092

Sánchez-de-la-Torre, M., Sánchez-de-la-Torre, A., Bertran, S., Abad, J., Duran-Cantolla, J., Cabriada, V., et al. (2020). Effect of obstructive sleep apnoea and its treatment with continuous positive airway pressure on the prevalence of cardiovascular events in patients with acute coronary syndrome (ISAACC study): a randomised controlled trial. *Lancet Respir. Med.* 8, 359–367. doi: 10.1016/S2213-2600(19)30271-1

Schulz, R., Murzabekova, G., Egemnazarov, B., Kraut, S., Eisele, H.-J., Dumitrascu, R., et al. (2014). Arterial hypertension in a murine model of sleep apnea: role of NADPH oxidase 2. *J. Hypertens.* 32, 300–305. doi: 10.1097/HJH.0000000000000016

Song, J. Q., Jiang, L. Y., Fu, C. P., Wu, X., Liu, Z. L., Xie, L., et al. (2020). Heterozygous SOD2 deletion deteriorated chronic intermittent hypoxia-induced lung inflammation and vascular remodeling through mtROS-NLRP3 signaling pathway. *Acta Pharmacol. Sin.* 41, 1197–1207. doi: 10.1038/s41401-020-0453-z

Suarez-Giron, M. C., Castro-Grattoni, A., Torres, M., Farré, R., Barbé, F., Sánchez-de-la-Torre, M., et al. (2018). Acetylsalicylic acid prevents intermittent hypoxia-induced vascular remodeling in a murine model of sleep apnea. *Front. Physiol.* 9:600. doi: 10.3389/fphys.2018.00600

Trzepizur, W., Cortese, R., and Gozal, D. (2018). Murine models of sleep apnea: functional implications of altered macrophage polarity and epigenetic modifications in adipose and vascular tissues. *Metabolism* 84, 44–55. doi: 10.1016/j.metabol.2017.11.008

Umeda, A., Miyagawa, K., Mochida, A., Takeda, H., Takeda, K., Okada, Y., et al. (2020). Intermittent hypoxia, energy expenditure, and visceral adipocyte recovery. *Respir. Physiol. Neurobiol.* 273:103332. doi: 10.1016/j.resp.2019.103332

Wanstall, J. C., Gambino, A., Jeffery, T. K., Cahill, M. M., Bellomo, D., Hayward, N. K., et al. (2002). Vascular endothelial growth factor-B-deficient mice show impaired development of hypoxic pulmonary hypertension. *Cardiovasc. Res.* 55, 361–368. doi: 10.1016/s0008-6363(02)00440-6

Weitzenblum, E., Krieger, J., Apprill, M., Vallée, E., Ehrhart, M., Ratomaharo, J., et al. (1988). Daytime pulmonary hypertension in patients with obstructive sleep apnea syndrome. *Am. Rev. Respir. Dis.* 138, 345–349. doi: 10.1164/ajrccm/138.2.345

Wong, H. S., Williams, A. J., and Mok, Y. (2017). The relationship between pulmonary hypertension and obstructive sleep apnea. *Curr. Opin. Pulm Med.* 23, 517–521. doi: 10.1097/MCP.0000000000000421

Xue, J., Zhou, D., Poulsen, O., Imamura, T., Hsiao, Y.-H., Smith, T. H., et al. (2017). Intermittent hypoxia and hypercapnia accelerate atherosclerosis, partially via trimethylamine-oxide. *Am. J. Respir. Cell Mol. Biol.* 57, 581–588. doi: 10.1165/rcmb.2017-0086OC

Yu, L., Quinn, D. A., Garg, H. G., and Hales, C. A. (2008). Deficiency of the NHE1 gene prevents hypoxia-induced pulmonary hypertension and vascular remodeling. *Am. J. Respir. Crit. Care Med.* 177, 1276–1284. doi: 10.1164/rccm.200710-1522OC

Zhou, S., Wang, Y., Tan, Y., Cai, X., Cai, L., Cai, J., et al. (2014). Deletion of metallothionein exacerbates intermittent hypoxia-induced oxidative and inflammatory injury in aorta. *Oxid. Med. Cell Longev.* 2014:141053. doi: 10.1155/2014/141053

Conflict of Interest: The authors declare that the research was conducted in the absence of any commercial or financial relationships that could be construed as a potential conflict of interest.

frontiers in Physiology

ORIGINAL RESEARCH
published: 30 October 2020
doi: 10.3389/fphys.2020.542146

Tribbles Homolog 3-Mediated Vascular Insulin Resistance Contributes to Hypoxic Pulmonary Hypertension in Intermittent Hypoxia Rat Model

Fang Fan[1†], Jinxiao He[1†], Hui Su[2†], Haifeng Zhang[3], Hao Wang[1], Qianqian Dong[4], Minghua Zeng[1], Wenjuan Xing[5,6] and Xin Sun[1*]*

[1]Department of Pediatrics, Xijing Hospital, Fourth Military Medical University, Xi'an, China, [2]Department of Geratology, Xijing Hospital, Fourth Military Medical University, Xi'an, China, [3]Teaching Experiment Center, Fourth Military Medical University, Xi'an, China, [4]Department of Natural Medicine, School of Pharmacy, Fourth Military Medical University, Xi'an, China, [5]School of Aerospace Medicine, Fourth Military Medical University, Xi'an, China, [6]State Key Laboratory of Space Medicine Fundamentals and Application, China Astronaut Research and Training Center, Beijing, China

This study aimed to investigate the role of vascular insulin resistance (VIR) and Tribbles homolog 3 (TRIB3) in the pathogenesis of hypoxia-induced pulmonary hypertension (HPH). Rats were subjected to low air pressure and low oxygen intermittently for 4 weeks to induce HPH. The mean right ventricular pressure (mRVP), mean pulmonary arterial pressure (mPAP), and right ventricular index (RVI) were significantly increased in HPH rats. Pulmonary arteries from HPH rats showed VIR with reduced vasodilating effect of insulin. The protein levels of peroxisome proliferator-activated receptor gamma (PPARγ), phosphoinositide 3-kinase (PI3K), phosphorylations of Akt, and endothelial nitric oxide (NO) synthase (eNOS) were decreased, and TRIB3 and phosphorylated extracellular signal-regulated protein kinases (ERK1/2) were increased in pulmonary arteries of HPH rats. Early treatment of pioglitazone (PIO) partially reversed the development of HPH, improved insulin-induced vasodilation, and alleviated the imbalance of the insulin signaling. The overexpression of TRIB3 in rat pulmonary arterial endothelial cells (PAECs) reduced the levels of PPARγ, PI3K, phosphorylated Akt (p-Akt), and phosphorylated eNOS (p-eNOS) and increased p-ERK1/2 and the synthesis of endothelin-1 (ET-1), which were further intensified under hypoxic conditions. Moreover, TRIB3 knockdown caused significant improvement in Akt and eNOS phosphorylations and, otherwise, a reduction of ERK1/2 activation in PAECs after hypoxia. In conclusion, impaired insulin-induced pulmonary vasodilation and the imbalance of insulin-induced signaling mediated by TRIB3 upregulation in the endothelium contribute to the development of HPH. Early PIO treatment improves vascular insulin sensitivity that may help to limit the progression of hypoxic pulmonary hypertension.

Keywords: hypoxic pulmonary hypertension, proliferator-activated receptor gamma, pulmonary arterial endothelium, vascular insulin resistance, Tribbles homolog 3

OPEN ACCESS

Edited by:
Richard James Wilson, University of Calgary, Canada

Reviewed by:
Etto Christoph Eringa, VU University Medical Center, Netherlands
Sharath C. Kandhi, New York Medical College, United States
Melissa Mary Jean Farnham, Heart Research Institute, Australia

****Correspondence:***
Xin Sun
sunxin6@fmmu.edu.cn
Wenjuan Xing
xwjfmmu@126.com

†These authors have contributed equally to this work

Specialty section:
This article was submitted to Vascular Physiology, a section of the journal Frontiers in Physiology

Received: *11 March 2020*
Accepted: *29 September 2020*
Published: *30 October 2020*

Citation:
Fan F, He J, Su H, Zhang H, Wang H, Dong Q, Zeng M, Xing W and Sun X (2020) Tribbles Homolog 3-Mediated Vascular Insulin Resistance Contributes to Hypoxic Pulmonary Hypertension in Intermittent Hypoxia Rat Model. Front. Physiol. 11:542146. doi: 10.3389/fphys.2020.542146

INTRODUCTION

Pulmonary hypertension (PH) is a progressive disease featuring vascular remodeling of small pulmonary arteries, elevated pulmonary arterial resistance, and right ventricle hypertrophy (Latus et al., 2015). The mortality and morbidity of PH are remarkable. The etiology of PH is very complicated; it can be idiopathic, heritable, drug/toxin-induced, or associated with HIV infection, congenital heart diseases, lung diseases, and high-altitude habitancy. The development of pulmonary circulation disorders in hypoxia-induced pulmonary hypertension (HPH) is a response unique to the hypoxic environment. This pathological condition triggers the hypoxic vasoconstriction of pulmonary arteries to redistribute the blood flow from hypoxic alveoli to ample alveoli so as to fully oxygenate the blood (Serne et al., 1999; Kekalainen et al., 2000). In the long term, this compensatory strategy can intensify the constriction of pulmonary vessels and eventually cause endothelial dysfunction, remodeling, and stenosis of vessels. Therefore, acute and chronic hypoxia is one of the most effective and reproducible method to induce PH.

Insulin is a key regulator of blood glucose in the body. The condition of insulin resistance is a precursor to developing type 2 diabetes and many cardiovascular disorders. Insulin also has a vasoactive effect on the vascular endothelium in parallel with the metabolic effect on tissues (Munir and Quon, 2013; Xing et al., 2013a,b). It stimulates the production and release of nitric oxide (NO) from the vascular endothelial cells through protein kinase B (also known as Akt) mediated phosphorylation of endothelial NO synthase (eNOS) in a phosphoinositide 3-kinases (PI3K) dependent manner (Yu et al., 2011). Simultaneously, insulin triggers the activation of the mitogen-activated protein kinase (MAPK) pathway to promote the secretion of endothelin-1 (ET-1). The overall response of insulin on the healthy vascular endothelium depends on a balance of the two pathways and presents a vasodilated effect (Muniyappa et al., 2007). Abated vasodilatory effects and augmented vasoconstrictor actions of insulin are referred to as vascular insulin resistance (VIR). The molecular basis of VIR is selectively impaired in insulin-induced PI3K-dependent and intact or even enhanced MAPK-dependent signaling pathways (Muniyappa et al., 2020). The underproduction of NO and the imbalance of NO/ET-1 production are the signposts of endothelial dysfunction. VIR and endothelial dysfunction are vicious cycles in the development of diabetes, cardiovascular disease, and hypertension. However, whether VIR participated in the development of pulmonary circulation disorders and HPH remains largely elusive.

Tribbles homolog 3 (TRIB3) is a pseudokinase of the Tribbles family (Du et al., 2003). It is involved in various cellular functions, including endoplasmic reticulum stress, cell proliferation, and differentiation. TRIB3 is coupled to insulin resistance in oxidative stress, antioxidant stress, inflammation, adiponectin actions, peroxisome proliferator-activated receptor (PPAR) actions, SIRT1 actions, and insulin signal transduction (Koh et al., 2013; Zhang et al., 2016). Overexpression of TRIB3 downregulates insulin-induced Akt phosphorylation, and subsequent downstream insulin signaling and suppression of TRIB3 enhances insulin-stimulated signaling. Several studies demonstrated the key role of TRIB3 in regulating insulin's metabolic function. High-fat diet induced the high TRIB3 expression, which consequently affects insulin-induced glucose uptake and oxidation in muscle and fat tissues in rats (Liu et al., 2012a). TRIB3 proteins are upregulated in diabetic rats and distorted phosphorylation of Akt, and MAPK in diabetic rats is restored by the suppression of TRIB3 (Ti et al., 2011). Hypoxia was reported that induced TRIB3 expression (Wennemers et al., 2011). However, whether TRIB3 is responsible for VIR in HPH is still unknown.

Life style like exercise and intervention such as PPAR gamma (PPARγ) agonist pioglitazone (PIO) have been shown to improve cardiovascular insulin sensitivity and benefit cardiovascular function (Zhang et al., 2008). Most recently, PIO has been reported to reverse pulmonary arterial hypertension, another type of PH, and reverse vascular remodeling *via* fatty acid oxidation (Legchenko et al., 2018), inhibiting transforming growth factor-β (TGFβ1) signaling (Calvier et al., 2019) and 5-HT receptor signaling (Liu et al., 2012b). In addition, systemic insulin resistance (i.e., elevated fasting blood glucose and insulin levels) is associated with the development of pulmonary arterial hypertension (Hansmann et al., 2007) and treatment with PIO abnormal pulmonary artery muscularization. Whether PIO limited VIR in the development of hypoxia-induced pulmonary arterial disorders and HPH is still unknown. This study aimed to investigate the alterations and the mechanisms of the vascular insulin sensitivity of pulmonary arteries in an HPH rat model and the potential role of PIO in HPH.

MATERIALS AND METHODS

Animals

The 6-week male Sprague-Dawley rats (body weight: 200–220 g) were purchased from the Experimental Animal Center of the Fourth Military Medical University (Xi'an, Shaanxi province, China). They were fed with normal diet and water *ad libitum*. The experimental protocol was approved by the ethics committee of the Animal Experimentation of the Fourth Military Medical University and conducted according to the Guidelines of the Animal Experimentation of the Fourth Military Medical University.

Design of the Experiment

The rats were randomly assigned to four groups with seven rats in each group: normal control, HPH, HPH + PIO (E), and HPH + PIO (L). The rats in the last three groups were subjected to low air pressure (50 kPa) and low oxygen (10%) intermittently in an auto-modulating plastic cabin for 8 h and normoxia for 16 h every day, for a total of 4 weeks (Li et al., 2020). Anhydrous calcium chloride and soda lime were used in the plastic box to absorb water and CO_2. PIO pellets were dissolved in physiological saline to form a solution (1.5 mg/ml). Besides, HPH + PIO (E) group rats received early (E) PIO solution [10 mg/(kg d)] once daily for 7 days a week through

intragastric administration in the 2nd week of the experiment. HPH + PIO (L) group rats received late (L) treatment of PIO in the same way in the last week of the experiment. HPH group rats were given saline as control. The normal control group was maintained in the same room under normal conditions (at atmospheric pressure and oxygen concentration).

Hemodynamic Measurement and Right Ventricular Hypertrophy

The mean pulmonary arterial pressure (mPAP) and mean right ventricular pressure (mRVP) were measured by jugular vein catheterization and followed the methodology in the previous study (Michelakis et al., 2002).

In addition, the right ventricular index (RVI) was calculated as an indicator of right ventricular hypertrophy. RVI represents the weight of the RV relative to LV + septum.

Morphometric Analysis

The same full section in the mid-portion of the lung parallel to the hilum was taken from all rats and embedded in paraffin. Transverse 10-μm left lung sections were stained using Verhoeff-van Gieson staining and H&E staining. The external diameter (ED), medial wall thickness (MT), medial cross-sectional area (MA), and total arterial cross-sectional area (TAA) of the peripheral pulmonary artery were measured in micrographs. Then, the MT (%) and MA (%) were calculated as follows: MT% = (MT/ED) × 100% and MA% = (MA/TAA) × 100%. The two ratios indicated the level of pathological thickening and remodeling of pulmonary arteries. Further, 7–10 pulmonary arteries were picked from random views of every lung, and the averages of morphometric parameters were used for conducting the statistical analysis.

Isometric Tension Measurement

The pulmonary arteries were isolated from rats and cut into 3-mm rings. Vascular responses to insulin in arteries were studied by exposing pulmonary arterial segments to insulin (10^{-10} ~ 10^{-6} mol/L; Sigma-Aldrich, MO, United States), sodium nitroprusside (SNP) (10^{-10}~10^{-6} mol/L; Sigma-Aldrich, MO, United States), or PE (10^{-10}~10^{-5} mol/L; Sigma-Aldrich, MO, United States). PE (10^{-7} mol/L) was used before testing relaxation to insulin and SNP. The resulting changes in isometric tension were recorded using an RM6240 multichannel physiological recording and processing system (Chengdu Instrument Factory, China).

Primary Culture of Rat Pulmonary Microvascular Endothelial Cells

Rat primary pulmonary microvascular endothelial cells were cultured and maintained as previously described with modifications. The rats were anesthetized by the intraperitoneal injection of 0.3–0.5 ml/100 g chloral hydrate. The thoracic and abdominal regions were sterilized by applying 1% povidone-iodine on the skin. The abdominal cavity was opened, and the abdominal aorta was cut off to drain the blood. Subsequently, the thoracic cavity was opened, and the lungs were immediately removed and rinsed in phosphate-buffered saline (PBS) at pH equal to 7.4 thoroughly. About 1 mm of the fringe of the lung was cut off and cut into pieces of 0.5 × 0.5 × 0.5 mm^3 in fetal bovine serum (FBS). Small pieces of lung tissue were placed evenly at the bottom of the cell culture flask. The flask was placed upside down for incubation at 37°C (210 ml/L O_2) with minimal cell culture medium (M200; Sigma-Aldrich; 15% FBS and 20 g/L LSGS) at the bottom. The flask was reverted back after 4 h. The medium was replaced after 24 h to wash off erythrocytes. Small pieces of lung tissues were removed after 2 days of incubation. Light microscopic images showed the cobblestone morphology of cultured cells typical for endothelial cells. Factor VIII was positive in immunofluorescence staining. The cells were split after >80% confluence at the ratio of 1:2 and used for experiments between passages 2 and 4. A rabbit anti-human factor VIII antibody was purchased from Santa Cruz Biotechnology (TX, United States). Fluorescein isothiocyanate (FITC)-conjugated goat anti-rabbit immunoglobulin G was purchased from Abcam (Cambridge, United Kingdom).

In vitro Experiment Design

Experimental design No. 1: healthy pulmonary arterial endothelial cells (PAECs) at passages 2–4 were plated in a 60-mm cell culture dish (Corning) in 10% FBS M200 medium. After the cells grew to 60% confluence, a fresh medium with 10^{-7} mmol/L insulin was replaced. The dishes were then divided into normoxia and hypoxia groups and placed in a normoxia incubator (37°C, 210 ml/L O_2) and a hypoxia incubator (37°C, 100 ml/L O_2), respectively. The cells and culture media were collected after 6, 24, 48, and 96 h of incubation.

Experimental design No. 2: healthy PAECs at passages 2–4 were plated in a 60-mm cell culture dish (Corning) in 10% FBS M200 medium. For exposure to hypoxia, PAECs were placed in a hypoxia incubator (Thermo Fisher, Boston, MA, United States) filled with a mixture of 10% O2 and 5% CO2 at 37°C. The normoxic control group was filled with a mixture of 21% O2 and 5% CO2 at 37°C. Cells were treated with 10^{-7} mmol/L insulin. The cells were harvested after 48 h of incubation. The proteins were extracted for the immunoblotting test.

Small Interfering RNA Transfection

For gene silencing assay, small interfering RNA (siRNA) for TRIB3 messenger RNA (mRNA) was designed and purchased from GenePharma (ShangHai, China). The target sequence used for TRIB3 siRNA knockdown was 5'-GAAGAAACCGUUGGA GUUTT-3'. PAECs were transfected with TRIB3 siRNA or scramble control by Lipofectamine™ RNAiMAX (Invitrogen) following the manufacturer's instructions. Cells were harvested for western blot analyses 48 h later.

Quantification of NO and ET-1 Expression

The NO concentration in the cell culture media was quantified using a commercial NO assay kit (nitrate reductase method) from Nanjing Jiancheng Bioengineering Institute (Jiangsu Province, China).

Total RNA was isolated from cells using TRIzol reagent according to the manufacturer's protocol (TaKaRa, Japan). Total RNA (0.5 μg) was converted into first-strand complementary DNA in a 20-μl reaction mixture using a One-step Reverse Transcriptase kit (TaKaRa). ET-1 expression was determined by real-time quantitative PCR (forward: 5'-CAAACCGATGTCCTCGTA-3' and reverse: 5'-ACCAAACACATTTCCCTATT-3'). The quantitative expression of the genes was normalized against glyceraldehyde 3-phosphate dehydrogenase (GAPDH; forward: 5'-GATTTGGCCGTATCGG AC-3' and reverse: 5'-GAAGACGCCAGTAGACTC-3'). The reactions were carried out using SYBR Green as a fluorescence dye on a real-time PCR thermal cycler (CFX96 Real-Time PCR cycler; Bio-Rad Laboratories, CA, United States). The $2^{-\triangle\triangle}$CT method was used for relative expression analysis. The experiment was repeated three times.

Western Blot Analysis

To analyze the insulin-induced signaling pathway, mice were given hypodermic injections of 5 mU/g body weight insulin (Novo Nordisk, Plainsboro, NJ, United States) and sacrificed 30 min later to collected vascular tissues. Tissues or cells were lysed with western radio immunoprecipitation assay (RIPA) lysis buffer (Beyotime Institute of Biotechnology, China) supplemented with Complete Mini Protease Inhibitor mixture (Roche Applied Science, Penzberg, Germany) and 1% phosphatase inhibitor mixture (Roche Applied Science). The protein concentration was determined using a bicinchoninic acid (BCA) Protein Quantification Kit (Beyotime Institute of Biotechnology, China). Each lysate containing an equal amount of total protein was loaded and separated using the sodium dodecyl sulfate-polyacrylamide gel electrophoresis method, transferred to polyvinylidene fluoride (Invitrogen, CA, United States) membrane, and probed with specific antibodies. After incubation with horseradish peroxidase-conjugated secondary antibodies (Boster Biological Technology, CA, United States), the blots were visualized with enhanced chemiluminescence detection reagents (Millipore, MA, United States), followed by autoradiography using a Kodak developing system. The intensity of images was quantified using Quantity One 4.0. Western blot analysis was performed using antibodies against Akt (60 kDa, 1:1000), phosphorylated Akt (p-Akt; 60 kDa, 1:1000), extracellular signal-regulated protein kinases 1 and 2 (ERK1/2, 42 and 44 kDa, 1:1000), p-ERK1/2 (42 and 44 kDa, 1:1000), and PI3K (110 kDa, 1:1000) obtained from Cell Signaling Technology (MA, United States); phosphorylated eNOS (p-eNOS; 130 kDa, 1:1000) and eNOS (130 kDa, 1:1000) from BD Biosciences (CA, United States); and TRIB3 (45 kDa, 1:200) and PPARγ (55 kDa, 1:500) from Santa Cruz Biotechnology.

Overexpression of TRIB3 With Lentivirus

Primary PAECs at the second passage were plated into six-well plates. They were infected with the lentivirus harboring *TRIB3* (GeneChem, Shanghai, China) gene according to the manufacturer's protocol. PAECs (80%) were positively infected with lentivirus (green fluorescence) after 3 days of incubation. The cell culture medium was replaced with fresh M200 medium (Gibco, Invitrogen, CA, United States) with 10% FBS (Hyclone, South Logan, UT, United States) and insulin (10^{-7} mmol/L).

Statistical Analysis

All values are presented as means ± SEM of n independent experiments. Statistical significance was determined by Student's t-test (analysis of two groups) or ANOVA (analysis of four groups), and *post hoc* comparisons, adjusted for multiple comparisons by Bonferroni's correction, were performed if ANOVAs revealed significances. Repetitive measure ANOVA was used in analyzing vascular tension at different points. In all statistical comparisons, probabilities of 0.05 or less were considered to be statistically significant.

RESULTS

Chronic Hypoxia Induced Pulmonary Hypertension and Impaired Insulin-Induced Vasodilation in Pulmonary Arteries

Chronic hypoxia was induced by exposing animals in HPH group to both hypobaric pressure and oxygen-poor air for 4 weeks. The pathological features of pulmonary vascular function and hypertrophy mimic the ones observed in human PH. The main parameters to define PH were tested in all the studied groups. The mPAP, mRVP, and RVI all significantly increased in rats in the HPH group compared with the control group ($p < 0.01$). Vascular remodeling is an important pathological feature of PH, which leads to increased pulmonary vascular resistance. The histological structure and thickness of pulmonary arteries from the control group were normal. Remodeling of the arteries in the HPH group was manifested by a significant alteration in the ratio of MT to ED (MT%) and the ratio of MA to TAA (MA%; **Table 1**). The media thickened, and the arterial lumen was narrowed in the HPH group compared with the control group (**Figures 1D,E**). We also detected RV mRNA levels of brain natriuretic peptide (BNP) and β-myosin heavy chain (β-MHC). Chronic hypoxia caused increased BNP and β-MHC levels (**Figures 1F,G**), indicating right ventricular hypertrophy.

Insulin has a vasodilated effect on arterial rings *in vitro*. VIR is manifested by the reduced vasodilating response to insulin (Wang et al., 2011). Insulin induced a dose-dependent vasodilation in pulmonary arteries from rats of all groups.

TABLE 1 | Comparing MT and MA% between different study groups ($n = 6$, $\bar{x} \pm s$).

Group	MT%	MA%
Control	11.0 ± 1.4	25.6 ± 2.6
HPH	24.7 ± 2.2*	54.0 ± 2.3*
HPH + PIO (E)	13.7 ± 2.1*#	30.5 ± 1.8*#
HPH + PIO (L)	23.0 ± 2.8*	52.9 ± 2.2*

*$p < 0.01$ vs. control group.
#$p < 0.05$ vs. HPH group.
The external diameter (ED), medial wall thickness (MT), medial cross-sectional area (MA), and total arterial cross-sectional area (TAA) of peripheral pulmonary artery were measured. Then, MT and MA% were calculated as follows: MT% = (MT/ED) × 100%; MA% = (MA/TAA) × 100%.

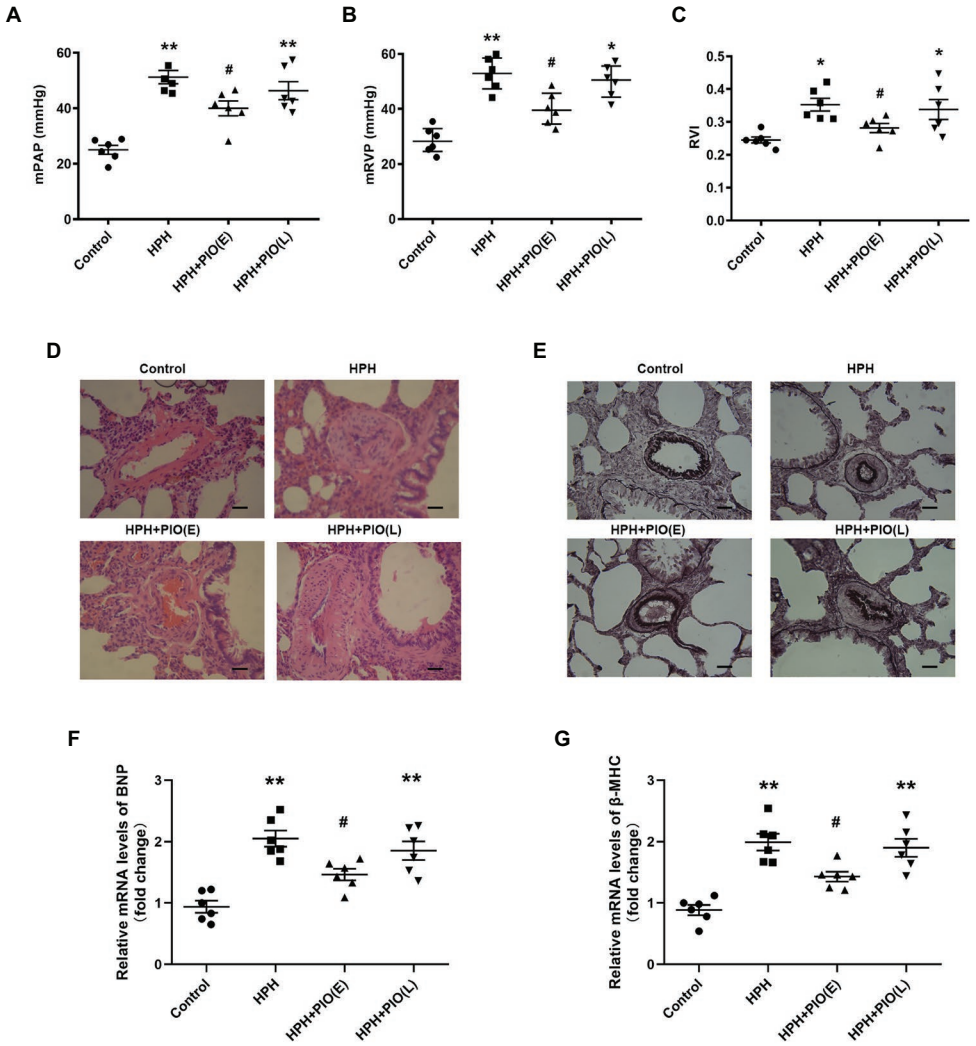

FIGURE 1 | Early treatment with peroxisome proliferator-activated receptor gamma (PPARγ) agonist pioglitazone (PIO) partly reversed the hypoxia-induced pulmonary hypertension (HPH). **(A)** Mean pulmonary artery pressure (mPAP) of different study groups; **(B)** Mean right ventricular pressure (mRVP) of different study groups; **(C)** Right ventricle index (RVI) of different study group. **(D)** Representative microphotographs of pulmonary arteries in rats obtained from four study groups (H&E staining), scale bar = 25 μm; **(E)** Representative microphotographs of pulmonary arteries in rats obtained from four study groups (Verhoeff-van Gieson staining), scale bar = 25 μm. **(F)** and **(G)** messenger RNA (mRNA) levels of brain natriuretic peptide (BNP) and β-myosin heavy chain (β-MHC) in right ventricular of hearts. Data were presented as means ± SEM. $n = 6$–8. $^{*}p < 0.05$, $^{**}p < 0.01$ vs. control group; $^{\#}p < 0.05$ vs. HPH group.

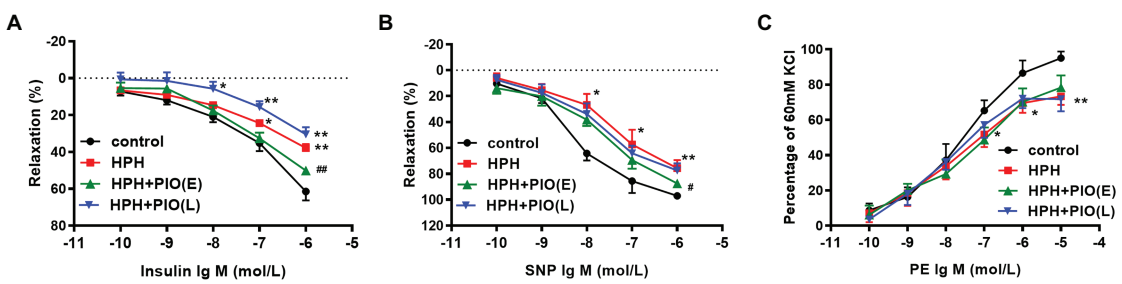

FIGURE 2 | Early treatment of PIO partly reversed the system insulin resistance and the pulmonary arterial insulin resistance. **(A)** Response of the pulmonary artery of each study group to insulin. **(B)** Response of the pulmonary artery of each study group to SNP. **(C)** Response of the pulmonary artery of each study group to PE. Arterial segments of 2–5 from each rat were used. Data were presented as means ± SEM. $n = 6$. $^{*}p < 0.05$, $^{**}p < 0.01$ vs. control group; $^{\#}p < 0.05$, $^{\#\#}p < 0.01$ vs. HPH group.

The insulin-induced relaxation was significantly attenuated in the pulmonary arteries from HPH rats compared with the control group (**Figures 2A–C**), indicating VIR occurred in the pulmonary arteries in HPH rat models.

Early Treatment of PIO Partly Alleviated Vascular Insulin Resistance and Pulmonary Hypertension

Considering PIO is a potent insulin-sensitizing agent, we next treated the HPH rats with PIO. After exposure to chronic hypoxia for 4 weeks, treatment with PIO at early stage of HPH significantly reduced mPAP and RVI (**Figure 1**; $p < 0.05$). However, treatment with PIO at late stage did not improve the HPH as no significant differences were found in these parameters between the HPH + PIO (L) and HPH groups. Consistently, the histopathological alterations were alleviated after early treatment of PIO in the HPH + PIO (E) group. Early treatment with PIO attenuated hypoxia-induced increases in both BNP and β-MHC levels (**Figures 1F,G**). However, PIO treatment in the late stage failed to reverse the

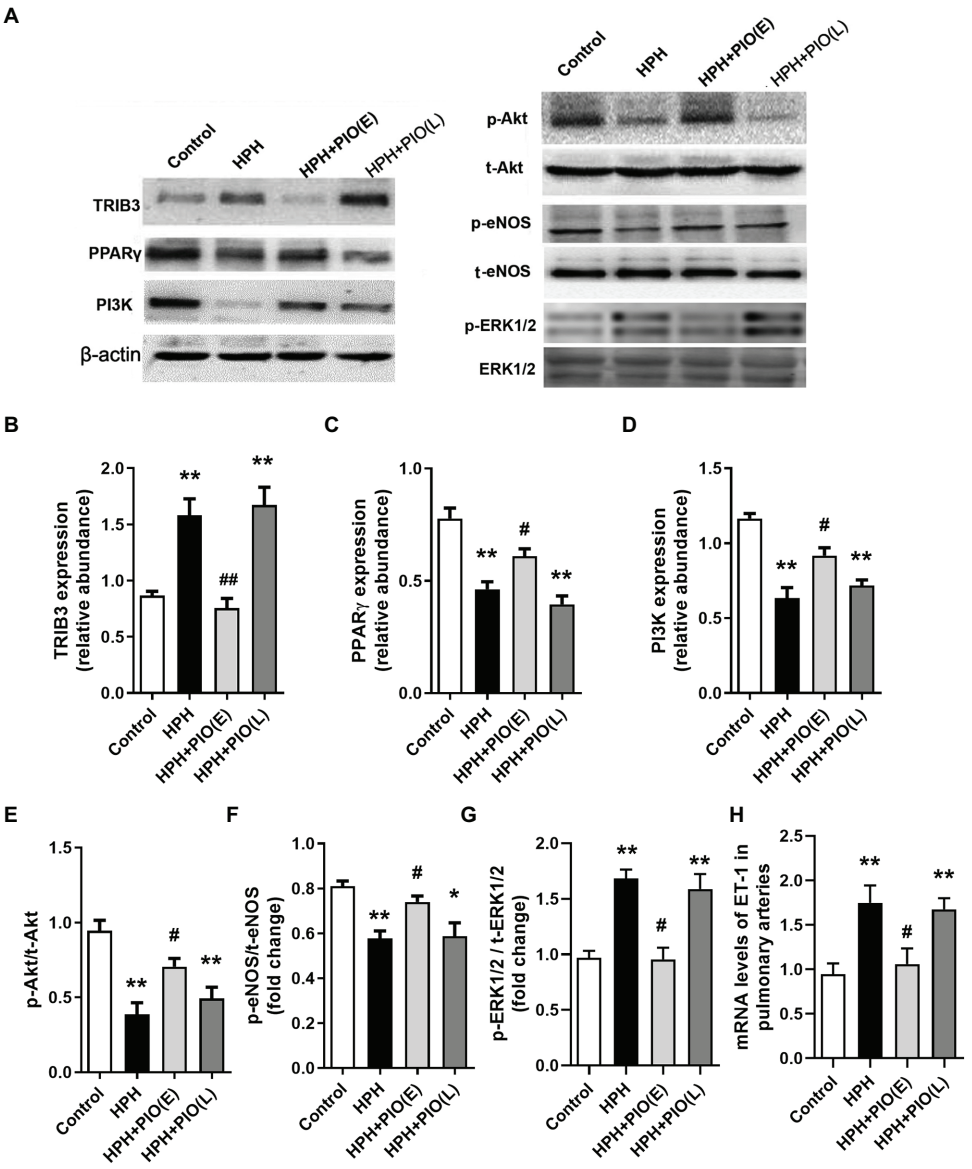

FIGURE 3 | Changes in the protein levels of tribbles homolog 3 (TRIB3), PPARγ, and insulin signaling pathways in the pulmonary arteries of HPH rats. **(A)** Representative western blots showing the expressions of TRIB3, PPARγ, phosphoinositide 3-kinase (PI3K), Akt, and endothelial NO synthase (eNOS), and phosphorylations of Akt and eNOS. **(B)** Western blotting analyzing the protein TRIB3 expression. **(C)** Western blotting analyzing the protein PPARγ expression. **(D)** Western blotting analyzing the protein PI3K expression. **(E)** Western blotting analyzing ratio of phosphorylated Akt (p-Akt) to total Akt. **(F)** Western blotting analyzing ratio of phosphorylated eNOS (p-eNOS) to total eNOS. **(G)** Western blotting analyzing ratio of phosphorylated ERK1/2 (p-ERK1/2) to total ERK1/2. **(H)** mRNA levels of ET-1. Data were presented as means ± SEM. $n = 4$. $^{*}p < 0.05$, $^{**}p < 0.01$ vs. control group; $^{\#}p < 0.05$, $^{\#\#}p < 0.01$ vs. HPH group.

histopathological alterations in the pulmonary arteries of rats in the HPH + PIO (L) group.

We next checked the insulin's effect on pulmonary arterial rings *in vitro*. Early treatment with PIO improved insulin-induced pulmonary arterial relaxation in the HPH rats. While the insulin-induced relaxation of pulmonary arterial rings from rats in the HPH + PIO (L) group was not significantly different from that in the HPH group. In addition, responses to SNP and PE were also impaired in HPH pulmonary arteries. Early treatment with PIO partially improved SNP induced vasodilation but not PE induced vasoconstriction. These data suggested that PIO treatment in the early stage partly alleviate VIR and pulmonary hypertension.

Dysregulation of TRIB3, PPARγ, and Insulin Signaling in the Pulmonary Arteries of Rats With HPH

Tribbles homolog 3 expression significantly increased, while PPARγ expression decreased remarkably in the pulmonary arteries from HPH rat models compared with the control group. Early PIO treatment partly reversed the protein levels of both TRIB3 and PPARγ; however, no effect was noted when PIO was given in the late stage of the HPH. The levels of PI3K, p-Akt, and p-eNOS significantly reduced in the pulmonary arteries of rats with HPH compared with those in the control group. Early PIO treatment reversed the reduction of p-Akt, PI3K, and p-eNOS compared with those in the HPH group; however, late treatment failed to act in the same way (**Figure 3**).

NO Production Decreased and ET-1 Production Increased in Hypoxic Primary Pulmonary Artery Endothelial Cells

In the presence of insulin in the cell culture medium, the NO production by PAECs under the normoxic condition was similar for four time points. After 6 h, hypoxia induced higher NO production than that under the normoxic condition. After 24 h, the concentrations of NO under the hypoxic condition declined dramatically over time and were lower than those under the normoxic condition at each time point (**Figure 4A**). No significant difference in the mRNA levels of ET-1 was observed between different time intervals under the normoxic condition. ET-1 mRNA levels significantly increased under the hypoxic condition than under the normoxic condition with the same time interval; it progressively increased over time under the hypoxic condition (**Figure 4B**).

Dysregulation of Proteins in PAECs in the Insulin Signaling Pathway at Different Time Intervals Under the Normoxic or Hypoxic Condition

Pulmonary arterial endothelial cells were cultured in the medium with 10^{-7} mmol/L of insulin. Among groups with different time intervals under the normoxic condition, the protein levels of TRIB3, PPARγ, PI3K, p-Akt, p-ERK1, and p-eNOS were comparable. In the acute phase of hypoxia (6 or 8 h), the protein level of TRIB3 increased significantly compared with that at the same time interval under the normoxic condition and further increased over time under the hypoxic condition. The protein levels of p-Akt, PI3K, and p-eNOS showed similar trends, which significantly increased after 6 h compared with the same time interval under the normoxic condition, and decreased over time under the hypoxic condition (**Figures 5C–F**). In the acute phase of hypoxia, the protein level of PPARγ was comparable with that under the normoxic condition. It decreased after 24 h under the hypoxic condition compared with the same time point under the normoxic condition, and further decreased over time (**Figure 5B**). The protein level of p-ERK1/2 increased at every time point under the hypoxic condition compared with the normoxic condition; it dramatically increased over time under the hypoxic condition (**Figure 5**).

PPARγ and PI3K/Akt/eNOS in PAECs Were Reduced With TRIB3 Overexpression Under Normoxic and Hypoxic Conditions

Pulmonary arterial endothelial cells were cultured in a medium with 10^{-7} mmol/L of insulin under hypoxic or normoxic condition, with the overexpression of TRIB3 or control vehicle. TRIB3 level was increased and PPARγ levels was decreased in PAECs under hypoxia condition. Hypoxia caused reduced PPARγ and the protein levels of PI3K, p-Akt, and p-eNOS. Importantly, overexpression of TRIB3 further decreased the protein levels of PPARγ, PI3K, p-Akt, and p-eNOS. The p-ERK1/2 levels increased in the TRIB3 + hypoxia, TRIB3 + normoxia, and control + hypoxia groups compared with the control + normoxia group, with the highest level detected in the TRIB3 + hypoxia group (**Figure 6**).

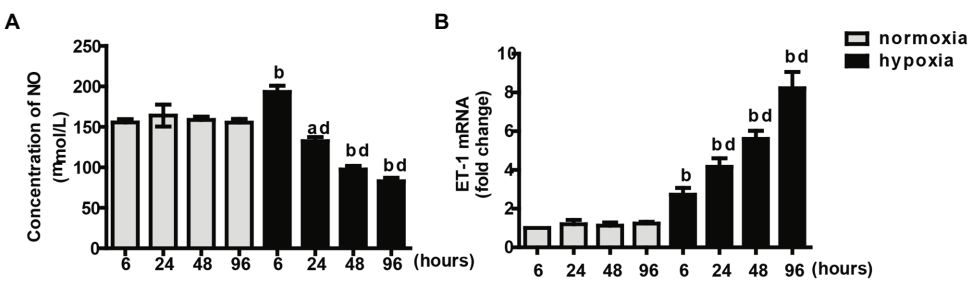

FIGURE 4 | Measurements of NO concentration **(A)** and endothelin-1 (ET-1) mRNA **(B)** at different time intervals under normoxia or hypoxia condition. Values are presented as mean ± SEM, $n = 7$. $^{a}p < 0.05$, $^{b}p < 0.01$ vs. the same time point under normoxia condition; $^{d}p < 0.01$ vs. 6 h under hypoxia condition.

TRIB3 Knockdown Improved Akt and eNOS Phosphorylations and Reduced ERK1/2 Activation in PAECs After Hypoxia

To determine whether TRIB3 is responsible for the impaired insulin signaling, PAECs were cultured in a medium with 10^{-7} mmol/L of insulin under hypoxic condition and measured the activation of insulin signaling with TRIB3 knockdown by siRNA. The results showed that TRIB3 was significantly reduced by siRNA in PAECs. The effect of knockdown of TRIB3 with siTRIB3 or scrambled siRNA on insulin signaling pathway in hypoxia treated PAECs was detected by western blot. p-Akt and p-eNOS were significantly enhanced in the PAECs after knockdown of TRIB3, while activation of ERK1/2 was markedly decreased after siTRIB3 treatment (**Figure 7**).

DISCUSSION

The present study has novel findings that VIR mediated by TRIB3 played an important role in the development of HPH.

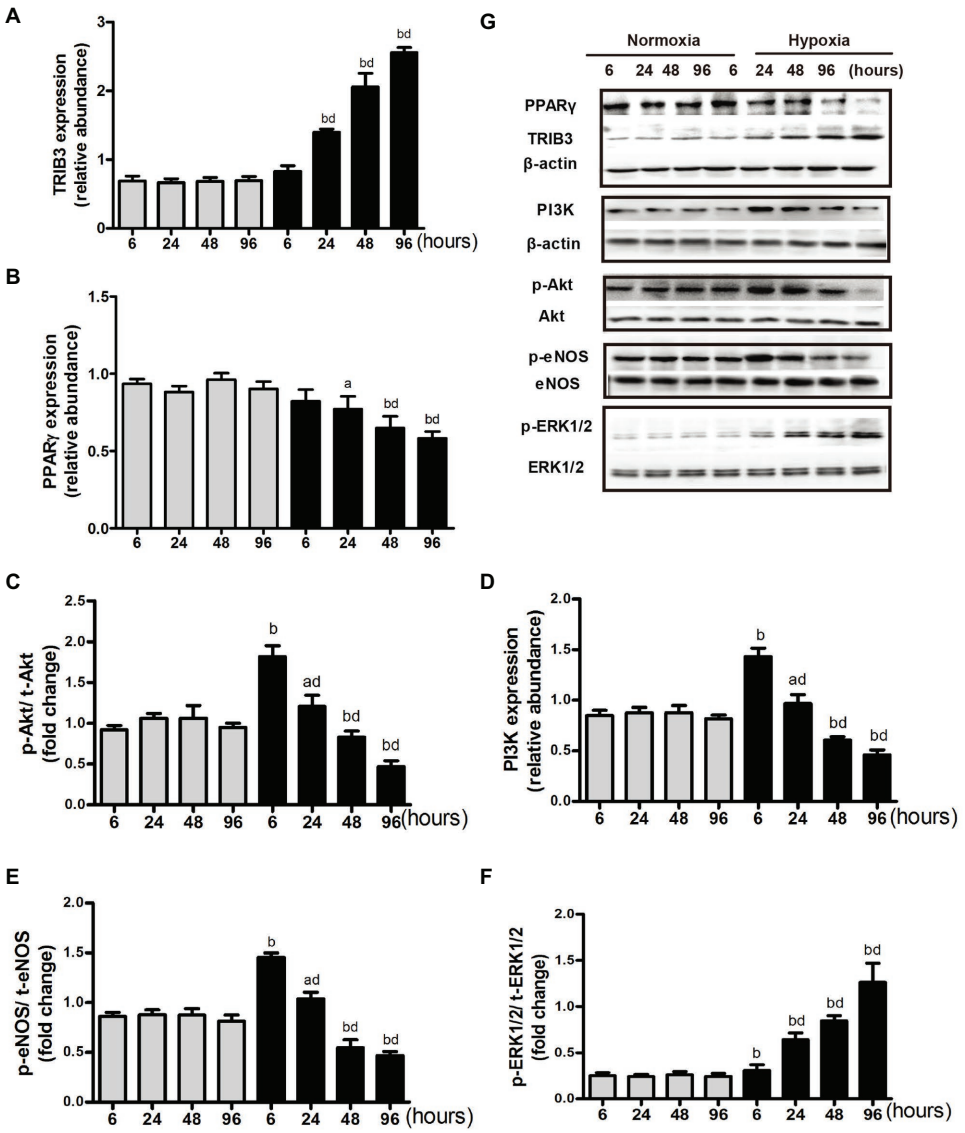

FIGURE 5 | Expression of proteins in insulin signaling pathway under normoxia or hypoxia condition. **(A)** Western blotting analyzing the protein TRIB3 expression. **(B)** Western blotting analyzing the protein PPARγ expression. **(C)** Western blotting analyzing ratio of phosphorylated Akt to total Akt. **(D)** Western blotting analyzing the protein PI3K expression. **(E)** Western blotting analyzing ratio of phosphorylated eNOS to total eNOS. **(F)** Western blotting analyzing ratio of phosphorylated ERK1/2 (p-ERK1/2) to total ERK1/2. **(G)** Representative western blots showing the expressions of TRIB3, PPARγ, PI3K, Akt, eNOS, and ERK1/2, and phosphorylations of Akt, eNOS, and ERK1/2. $^{a}p < 0.05$, $^{b}p < 0.01$ vs. the same time point under normoxia condition; Values are presented as mean ± SEM, $n = 7$. $^{d}p < 0.01$ vs. 6 h under hypoxia condition.

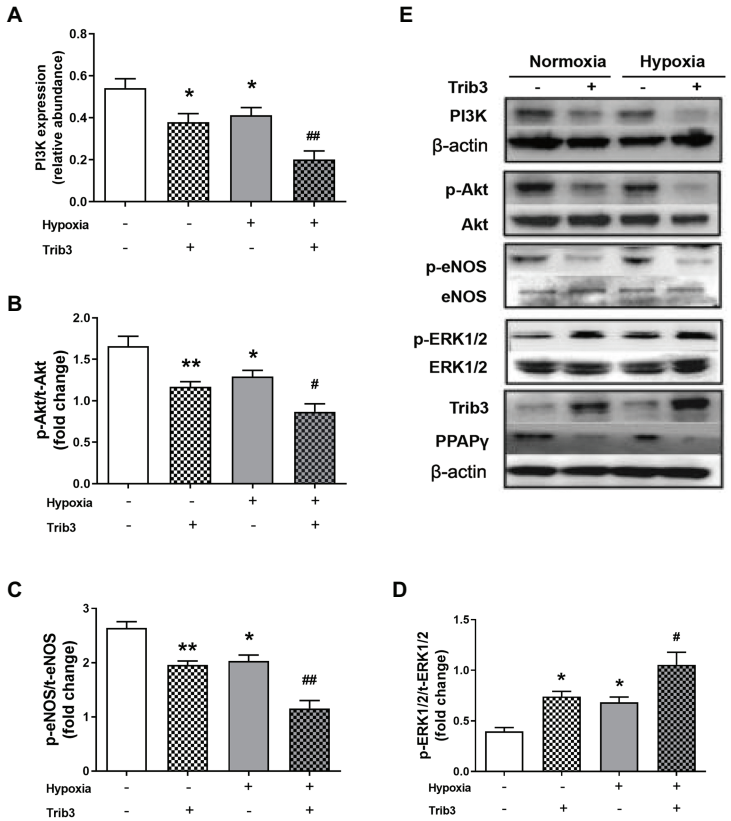

FIGURE 6 | The effect of over-expression of TRIB3 with lentivirus on the protein levels of insulin signaling pathway in PAECs. **(A)** Western blotting analyzing the protein PI3K expression. **(B)** Western blotting analyzing ratio of p-Akt to total Akt. **(C)** Western blotting analyzing ratio of p-eNOS to total eNOS. **(D)** Western blotting analyzing ratio of phosphorylated extracellular signal-regulated protein kinases 1 and 2 (ERK1/2) to total ERK1/2. **(E)** Representative western blots showing the expressions of PI3K, Akt, eNOS, and ERK1/2 and phosphorylations of Akt, eNOS, and ERK1/2. Values are presented as mean ± SEM, $n = 6$. $^{*}p < 0.05$, $^{**}p < 0.01$ vs. normoxia control group; $^{\#}p < 0.05$, $^{\#\#}p < 0.01$ vs. hypoxia control group.

And improvement of the vascular insulin sensitivity at early stage by PIO alleviated HPH.

Insulin's actions on vascular are of great importance as it enhances the compliance of arteries, relaxes arterioles to increase tissue blood flow, and expands perfusion. The present study reveals that VIR is closely associated with the development of HPH. The disturbance of the balance between ET-1 and NO weakened the vasodilating activity and increased the vasoconstrictive activity of the vessels. Disturbance of endothelium may further lead to vessel injury, remodeling, thrombogenesis, and occlusion. We also observed increased systemic blood glucose and insulin levels in HPH rats. Research has shown that hypoxia acutely or chronically influences the control of blood glucose and related hormones. In our study, the increase of glucose is likely due to the intermittent nature of the hypoxia challenge. This is a limitation of the study.

The present study showed an association between hypoxia-induced TRIB3 expression and VIR in pulmonary arteries. TRIB3 levels were increased in pulmonary arteries from HPH rats, accompanied with reduced PPARγ, and imbalance between insulin-induced Akt/eNOS/NO and ERK1/2/ET-1 signaling. Overexpression of TRIB3 in PAECs caused impaired Akt and eNOS activation. These findings were consistent with previous observations that pathological overexpression of TRIB3 blocked insulin-induced Akt phosphorylation, negatively regulated insulin action, and contributed to hyperglycemia and insulin resistance in liver and skeletal muscle (Du et al., 2003; Liu et al., 2010). Therefore, upregulated TRIB3 decreased the level of p-Akt and distorted subsequent signaling pathways. On the other hand, overexpression of TRIB3 in PAECs enhanced insulin-stimulated ERK1/2 phosphorylation. TRIB3 is a known regulator of MAPK–ERK pathway in cancer and cardiomyopathy models (Tang et al., 2008; Izrailit et al., 2013) by directly interacted with ERK or increased posttranslational phosphorylation. Moreover, TRIB3 knockdown caused significant improvement in Akt and eNOS phosphorylations and otherwise a reduction of ERK1/2 activation in PAECs after hypoxia, suggesting that TRIB3 mediates hypoxia-induced VIR and endothelial dysfunction.

Most recent study found that PPARγ activation by PIO prevents pulmonary arterial hypertension, the pathogenesis of which is different from that HPH. The present study for the first time identified PIO treatment at the early stage benefits hypoxia-induced pulmonary arterial dysfunction and HPH, which is at least partially relies on the improvement of vascular

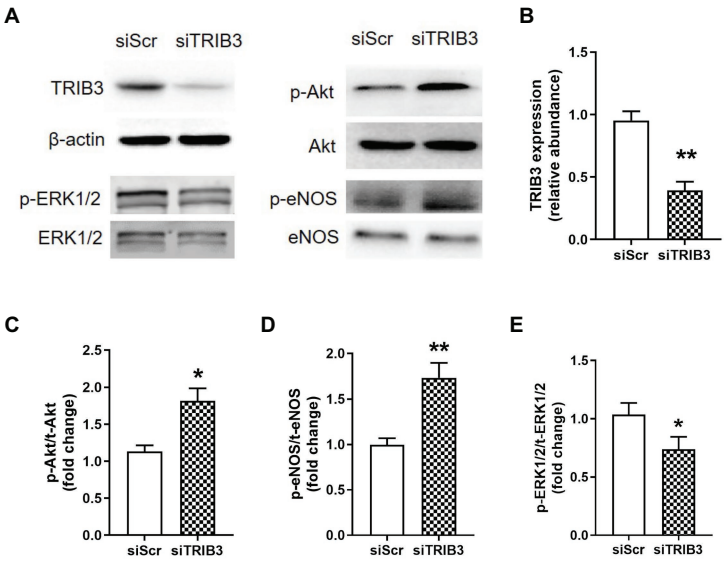

FIGURE 7 | The effect of knockdown of TRIB3 with siTRIB3 or scrambled siRNA on the protein levels of insulin signaling pathway in PAECs after hypoxia. **(A)** Representative western blots showing the expressions of TRIB3, Akt, eNOS, and ERK1/2 and phosphorylations of Akt, eNOS, and ERK1/2. **(B)** Western blotting analyzing the protein TRIB3 expression. **(C)** Western blotting analyzing ratio of p-Akt to total Akt. **(D)** Western blotting analyzing ratio of p-eNOS to total eNOS. **(E)** Western blotting analyzing ratio of phosphorylated ERK1/2 to total ERK1/2. Values are presented as mean ± SEM, $n = 4$. $^{*}p < 0.05$, $^{**}p < 0.01$ vs. siScr control group.

insulin sensitivity and vasodilation. TRIB3 has been identified acting as a potent negative regulator of PPARγ (Takahashi et al., 2008), indicating that the increase of TRIB3 level may be responsible for the limit effects of late PIO treatment.

The present study provided new insights into the development of therapeutics for HPH. Hypoxia-induced TRIB3 upregulation is a potential molecular basis of HPH. TRIB3 suppresses PPARγ and regulates insulin signaling pathway, resulting in the reduction of vascular NO production and raise of ET-1 secretion. Nevertheless, whether other subtypes of PH can benefit from improving insulin sensitivity or TRIB3 reduction need further study. TRIB3 is also a positive regulator of canonical TGF-β signaling to regulate fibroblast activation and tissue fibrosis (Tomcik et al., 2016). PPARγ, which could be regulated by TRIB3, was reported that inhibited TGF-β signaling and acted as a link between pro-proliferative TGF-β and anti-proliferative bone morphogenetic protein 2 (BMP2) signalings in vascular smooth muscle cells and inhibited pulmonary arterial hypertension (Calvier et al., 2017). Additionally, TRIB3 deficiency ameliorates metabolic disturbance inflammation, fibrosis, and myocardial hypertrophy in rats with dilated cardiomyopathy (Ti et al., 2011) indicating the potential benefits of TRIB3 regarding its anti-fibrotic and metabolic modulating effects.

In summary, this study indicated that VIR plays an important role in the development of HPH. The impaired insulin-induced pulmonary vasodilation and the imbalance of insulin-induced signalings are mediated by TRIB3 upregulation in the endothelium of HPH. PIO treatment beginning at the early stage improves vascular insulin sensitivity that may help to limit the progression of hypoxic pulmonary hypertension, which could provide a new perspective in managing patients with HPH, focusing on improving the pulmonary vascular IR in the early stage.

DATA AVAILABILITY STATEMENT

All datasets generated for this study are included in the article/supplementary material.

ETHICS STATEMENT

The animal study was reviewed and approved by the ethics committee of the Animal Experimentation of the Fourth Military Medical University.

AUTHOR CONTRIBUTIONS

FF, JH, and HS carried out the studies, collected data, and drafted the manuscript. HW, QD, and MZ collected data and performed the statistical analysis. HZ, WX, and XS designed the study and revised the manuscript. All authors contributed to the article and approved the submitted version.

FUNDING

This study was supported by the National Natural Science Foundation of China (grant nos. 81700342, 81701487, 81870280, 81670449, 31371151, and 31271219) and the Shaanxi Science and Technology Research and Development Program Project (grant nos. 2013KW30-2, 2014KW20-01, 2017KW-045, and 2019JQ-330), Young Talent Fund of University Association for Science and Technology in Shaanxi, China (No. 20180302), Medicine Improvement Program Project of Fourth Military Medical University (No. 2018HKTS08), and Young Talent Fund in school of Aerospace Medicine (No. 2019HBRC06).

REFERENCES

Calvier, L., Boucher, P., Herz, J., and Hansmann, G. (2019). LRP1 deficiency in vascular SMC leads to pulmonary arterial hypertension that is reversed by PPARgamma activation. *Circ. Res.* 124, 1778–1785. doi: 10.1161/CIRCRESAHA.119.315088

Calvier, L., Chouvarine, P., Legchenko, E., Hoffmann, N., Geldner, J., Borchert, P., et al. (2017). PPARgamma links BMP2 and TGFbeta1 pathways in vascular smooth muscle cells, regulating cell proliferation and glucose metabolism. *Cell Metab.* 25, 1118.e7–1134.e7. doi: 10.1016/j.cmet.2017.03.011

Du, K., Herzig, S., Kulkarni, R. N., and Montminy, M. (2003). TRB3: a tribbles homolog that inhibits Akt/PKB activation by insulin in liver. *Science* 300, 1574–1577. doi: 10.1126/science.1079817

Hansmann, G., Wagner, R. A., Schellong, S., Perez, V. A., Urashima, T., Wang, L., et al. (2007). Pulmonary arterial hypertension is linked to insulin resistance and reversed by peroxisome proliferator-activated receptor-gamma activation. *Circulation* 115, 1275–1284. doi: 10.1161/CIRCULATIONAHA.106.663120

Izrailit, J., Berman, H. K., Datti, A., Wrana, J. L., and Reedijk, M. (2013). High throughput kinase inhibitor screens reveal TRB3 and MAPK-ERK/TGFbeta pathways as fundamental notch regulators in breast cancer. *Proc. Natl. Acad. Sci. U. S. A.* 110, 1714–1719. doi: 10.1073/pnas.1214014110

Kekalainen, P., Sarlund, H., and Laakso, M. (2000). Long-term association of cardiovascular risk factors with impaired insulin secretion and insulin resistance. *Metabolism* 49, 1247–1254. doi: 10.1053/meta.2000.9514

Koh, H. J., Toyoda, T., Didesch, M. M., Lee, M. Y., Sleeman, M. W., Kulkarni, R. N., et al. (2013). Tribbles 3 mediates endoplasmic reticulum stress-induced insulin resistance in skeletal muscle. *Nat. Commun.* 4:1871. doi: 10.1038/ncomms2851

Latus, H., Delhaas, T., Schranz, D., and Apitz, C. (2015). Treatment of pulmonary arterial hypertension in children. *Nat. Rev. Cardiol.* 12, 244–254. doi: 10.1038/nrcardio.2015.6

Legchenko, E., Chouvarine, P., Borchert, P., Fernandez-Gonzalez, A., Snay, E., Meier, M., et al. (2018). PPARgamma agonist pioglitazone reverses pulmonary hypertension and prevents right heart failure via fatty acid oxidation. *Sci. Transl. Med.* 10:eaao0303. doi: 10.1126/scitranslmed.aao0303

Li, J., Jia, M., Liu, M., Cao, Z., Wang, X., Feng, N., et al. (2020). The effect of activated kappa-opioid receptor (kappa-OR) on the role of calcium sensing receptor (CaSR) in preventing hypoxic pulmonary hypertension development. *Biomed. Pharmacother.* 125:109931. doi: 10.1016/j.biopha.2020.109931

Liu, Y., Tian, X. Y., Mao, G., Fang, X., Fung, M. L., Shyy, J. Y., et al. (2012b). Peroxisome proliferator-activated receptor-gamma ameliorates pulmonary arterial hypertension by inhibiting 5-hydroxytryptamine 2B receptor. *Hypertension* 60, 1471–1478. doi: 10.1161/HYPERTENSIONAHA.112.198887

Liu, J., Wu, X., Franklin, J. L., Messina, J. L., Hill, H. S., Moellering, D. R., et al. (2010). Mammalian Tribbles homolog 3 impairs insulin action in skeletal muscle: role in glucose-induced insulin resistance. *Am. J. Physiol. Endocrinol. Metab.* 298, E565–E576. doi: 10.1152/ajpendo.00467.2009

Liu, J., Zhang, W., Chuang, G. C., Hill, H. S., Tian, L., Fu, Y., et al. (2012a). Role of TRIB3 in regulation of insulin sensitivity and nutrient metabolism during short-term fasting and nutrient excess. *Am. J. Physiol. Endocrinol. Metab.* 303, E908–E916. doi: 10.1152/ajpendo.00663.2011

Michelakis, E. D., Mcmurtry, M. S., Wu, X. C., Dyck, J. R., Moudgil, R., Hopkins, T. A., et al. (2002). Dichloroacetate, a metabolic modulator, prevents and reverses chronic hypoxic pulmonary hypertension in rats: role of increased expression and activity of voltage-gated potassium channels. *Circulation* 105, 244–250. doi: 10.1161/hc0202.101974

Munir, K. M., and Quon, M. J. (2013). Distinct mechanisms for globular adiponectin that integrate vascular and metabolic actions of insulin to help maintain coordinated cardiovascular and glucose homeostasis. *Circ. Res.* 112, 1205–1207. doi: 10.1161/CIRCRESAHA.113.301316

Muniyappa, R., Chen, H., Montagnani, M., Sherman, A., and Quon, M. J. (2020). Endothelial dysfunction due to selective insulin resistance in vascular endothelium: insights from mechanistic modeling. *Am. J. Physiol. Endocrinol. Metab.* 319, E629–E646. doi: 10.1152/ajpendo.00247.2020

Muniyappa, R., Montagnani, M., Koh, K. K., and Quon, M. J. (2007). Cardiovascular actions of insulin. *Endocr. Rev.* 28, 463–491. doi: 10.1210/er.2007-0006

Serne, E. H., Stehouwer, C. D., Ter Maaten, J. C., Ter Wee, P. M., Rauwerda, J. A., Donker, A. J., et al. (1999). Microvascular function relates to insulin sensitivity and blood pressure in normal subjects. *Circulation* 99, 896–902. doi: 10.1161/01.cir.99.7.896

Takahashi, Y., Ohoka, N., Hayashi, H., and Sato, R. (2008). TRB3 suppresses adipocyte differentiation by negatively regulating PPARgamma transcriptional activity. *J. Lipid Res.* 49, 880–892. doi: 10.1194/jlr.M700545-JLR200

Tang, M., Zhong, M., Shang, Y., Lin, H., Deng, J., Jiang, H., et al. (2008). Differential regulation of collagen types I and III expression in cardiac fibroblasts by AGEs through TRB3/MAPK signaling pathway. *Cell. Mol. Life Sci.* 65, 2924–2932. doi: 10.1007/s00018-008-8255-3

Ti, Y., Xie, G. L., Wang, Z. H., Bi, X. L., Ding, W. Y., Wang, J., et al. (2011). TRB3 gene silencing alleviates diabetic cardiomyopathy in a type 2 diabetic rat model. *Diabetes* 60, 2963–2974. doi: 10.2337/db11-0549

Tomcik, M., Palumbo-Zerr, K., Zerr, P., Sumova, B., Avouac, J., Dees, C., et al. (2016). Tribbles homologue 3 stimulates canonical TGF-beta signalling to regulate fibroblast activation and tissue fibrosis. *Ann. Rheum. Dis.* 75, 609–616. doi: 10.1136/annrheumdis-2014-206234

Wang, Y., Cheng, K. K., Lam, K. S., Wu, D., Wang, Y., Huang, Y., et al. (2011). APPL1 counteracts obesity-induced vascular insulin resistance and endothelial dysfunction by modulating the endothelial production of nitric oxide and endothelin-1 in mice. *Diabetes* 60, 3044–3054. doi: 10.2337/db11-0666

Wennemers, M., Bussink, J., Scheijen, B., Nagtegaal, I. D., Van Laarhoven, H. W., Raleigh, J. A., et al. (2011). Tribbles homolog 3 denotes a poor prognosis in breast cancer and is involved in hypoxia response. *Breast Cancer Res.* 13:R82. doi: 10.1186/bcr2934

Xing, W., Li, Y., Zhang, H., Mi, C., Hou, Z., Quon, M. J., et al. (2013a). Improvement of vascular insulin sensitivity by downregulation of GRK2 mediates exercise-induced alleviation of hypertension in spontaneously hypertensive rats. *Am. J. Physiol. Heart Circ. Physiol.* 305, H1111–H1119. doi: 10.1152/ajpheart.00290.2013

Xing, W., Yan, W., Liu, P., Ji, L., Li, Y., Sun, L., et al. (2013b). A novel mechanism for vascular insulin resistance in normotensive young SHRs: hypoadiponectinemia and resultant APPL1 downregulation. *Hypertension* 61, 1028–1035. doi: 10.1161/HYPERTENSIONAHA.111.00728

Yu, Q., Gao, F., and Ma, X. L. (2011). Insulin says NO to cardiovascular disease. *Cardiovasc. Res.* 89, 516–524. doi: 10.1093/cvr/cvq349

Zhang, H., Li, J., Li, R., Zhang, Q., Ma, H., Ji, Q., et al. (2008). Reduced cardiotropic response to insulin in spontaneously hypertensive rats: role of peroxisome proliferator-activated receptor-gamma-initiated signaling. *J. Hypertens.* 26, 560–569. doi: 10.1097/HJH.0b013e3282f343e1

Zhang, W., Wu, M., Kim, T., Jariwala, R. H., Garvey, W. J., Luo, N., et al. (2016). Skeletal muscle TRIB3 mediates glucose toxicity in diabetes and high-fat diet-induced insulin resistance. *Diabetes* 65, 2380–2391. doi: 10.2337/db16-0154

Conflict of Interest: The authors declare that the research was conducted in the absence of any commercial or financial relationships that could be construed as a potential conflict of interest.

frontiers in Physiology

ORIGINAL RESEARCH
published: 10 November 2020
doi: 10.3389/fphys.2020.607616

Muscle Oxygen Delivery in the Forearm and in the *Vastus Lateralis* Muscles in Response to Resistance Exercise: A Comparison Between Nepalese Porters and Italian Trekkers

Vittore Verratti[1], Danilo Bondi[2], Gabriele Mulliri[3], Giovanna Ghiani[3], Antonio Crisafulli[3], Tiziana Pietrangelo[2], Maria Erika Marinozzi[4] and Paolo Cerretelli[5]*

[1]Department of Psychological, Health and Territorial Sciences, University "G. d'Annunzio" of Chieti-Pescara, Chieti, Italy, [2]Department of Neuroscience, Imaging and Clinical Sciences, University "G. d'Annunzio" of Chieti-Pescara, Chieti, Italy, [3]Department of Medical Sciences and Public Health, University of Cagliari, Cagliari, Italy, [4]Faculty of Veterinary Medicine, University of Teramo, Teramo, Italy, [5]Institute of Bioimaging and Molecular Physiology, National Research Council of Italy, Segrate, Italy

OPEN ACCESS

Edited by:
Mieczyslaw Pokorski, Opole University, Poland

Reviewed by:
Aleksandra Zebrowska, Academy of Physical Education, Poland
Dariusz Jastrzębski, Medical University of Silesia, Poland

***Correspondence:**
Antonio Crisafulli
crisaful@unica.it;
antonio.crisafulli67@gmail.com

Specialty section:
This article was submitted to Integrative Physiology, a section of the journal Frontiers in Physiology

Received: *17 September 2020*
Accepted: *19 October 2020*
Published: *10 November 2020*

Citation:
Verratti V, Bondi D, Mulliri G, Ghiani G, Crisafulli A, Pietrangelo T, Marinozzi ME and Cerretelli P (2020) Muscle Oxygen Delivery in the Forearm and in the Vastus Lateralis Muscles in Response to Resistance Exercise: A Comparison Between Nepalese Porters and Italian Trekkers. Front. Physiol. 11:607616. doi: 10.3389/fphys.2020.607616

Altitude ascending represents an intriguing experimental model reproducing physiological and pathophysiological conditions sharing hypoxemia as the denominator. The aim of the present study was to investigate fractional oxygen extraction and blood dynamics in response to hypobaric hypoxia and to acute resistance exercises, taking into account several factors including different ethnic origin and muscle groups. As part of the "Kanchenjunga Exploration & Physiology" project, six Italian trekkers and six Nepalese porters took part in a high altitude trek in the Himalayas. The measurements were carried out at low (1,450 m) and high altitude (HA; 4,780 m). Near-infrared spectroscopy (NIRS)-derived parameters, i.e., Tot-Hb and tissue saturation index (TSI), were gathered at rest and after bouts of 3-min resistive exercise, both in the quadriceps and in the forearm muscles. TSI decreased with altitude, particularly in forearm muscles (from 66.9 to 57.3%), whereas the decrement was less in the quadriceps (from 62.5 to 57.2%); Nepalese porters were characterized by greater values in thigh TSI than Italian trekkers. Tot-Hb was increased after exercise. At altitude, such increase appeared to be higher in the quadriceps. This effect might be a consequence of the long-term adaptive memory due to the frequent exposures to altitude. Although speculative, we suggest a long-term adaptation of the Nepalese porters due to improved oxygenation of muscles frequently undergoing hypoxic exercise. Muscle structure, individual factors, and altitude exposure time should be taken into account to move on the knowledge of oxygen delivery and utilization at altitude.

Keywords: resistance exercise, hemodynamic response, Himalayas, near-infrared spectroscopy, hypobaric hypoxia

INTRODUCTION

Traveling at high altitude (HA) is nowadays very popular, but it requires medical advice in respect to altitude tolerance and acclimatization (Schommer and Bärtsch, 2011). In addition, altitude training has been widely investigated for its effects of environmental stressor on body homeostasis (Tam et al., 2016; Grocott et al., 2019). Common traveling conditions with Caucasian tourists along with local porters may have practical implications. For example, it may help in unraveling differences between native lowlanders and highlanders in response to hypobaric hypoxia (Magliulo et al., 2020), thereby shedding light on the physiological adaptation to living permanently or working occasionally at altitude. Moreover, high altitude hypoxia represents an intriguing experimental model to reproduce physiological and pathophysiological conditions commonly present at low altitude (LA), sharing hypoxemia as the common denominator (Di Giulio et al., 2003; Verratti et al., 2009; Sarkar et al., 2017): a classic example of long-life scientific interest is periodic breathing (Douglas, 1910). With regard to exercise physiology, most of the plans for altitude training were based on oxygen delivery and supply adaptations, with a faster response of O_2 muscular uptake (Doria et al., 2011), an enhanced vascular endothelial growth factor (Vogt et al., 2001), along with a detrimental effect on muscle tissue over the period of typical Himalayan expeditions (Vogt and Hoppeler, 2010).

Oxygen delivery depends on cardiac output, arterial saturation and partial pressure of oxygen, and hemoglobin concentration. Oxygen supply is determined by oxygen delivery and carrying capacity, macro- and micro-vascular architecture, and blood flow dynamics. Direct oxygen consumption measurement and arteriovenous oxygen difference reflect the whole-body and local oxygen utilization. Studying local oxygen dynamics in field studies requires to use portable devices, along with feasible and non-invasive methods. Concerning the topic of field measurement, peripheral oxygenation and blood flow can be measured with the non-invasive technology of near-infrared spectroscopy (NIRS), based on the assumption of light-absorbing chromophores in skeletal muscle tissue, i.e., mainly hemoglobin (Hb) and myoglobin (Mb); thus, NIRS reflects the presence of heme in small vessels (<1 mm diameter; Barstow, 2019). Moreover, NIRS can be applied to different muscle groups, thereby allowing to discern regional adaptations, both in Lab settings (Volianitis et al., 2003) and during sport-specific exercise (Hesford et al., 2013), but no study has addressed the differences among muscle groups in hypobaric hypoxic field conditions.

Taking into account the limitations of the method, NIRS can provide valuable insight into the regional blood flow, skeletal muscle O_2 consumption, fractional O_2 extraction, and oxidative metabolic thresholds, during exercise and other conditions (Grassi and Quaresima, 2016). In this regard, many studies have addressed the topic of hypoxia, in terms of training (Fryer et al., 2019), acute (Peltonen et al., 2009), or chronic (Cheung et al., 2014) exposure. However, to the best of our knowledge, few studies if any, have investigated oxygen delivery and utilization in response to hypoxia comparing altitude (e.g., porters) to non-altitude workers.

Despite evidence of physiological differences among ethnic groups (Wu and Kayser, 2006), little is known about the differences in response to hypoxic conditioning. In this regard, Feeback et al. (2017) investigated arterial saturation and cerebral oxygenation in response to exercise hypoxia comparing African-American and Caucasian males, highlighting a differential response between the two ethnic groups. Simonson et al. (2015) highlighted the advantage of Tibetans in exerting higher exercise capacity at altitude to be supported by enhanced muscle O2 transport capacity. Thus, considering the adaptations in terms of chronic exposure and predisposition to altitude tolerance, it can be speculated that altitude populations or altitude workers may be different in blood flow and oxygen delivery and utilization in respect to lowlanders or non-altitude workers. We, therefore, hypothesized that Nepalese porters showed different adaptations as compared to Italian trekkers, due to a lesser impairment in oxygen delivery, supply and utilization, and in hemodynamic response to a middle-term altitude hypoxia exposure. We also hypothesized these adaptive differences to be present both at rest and in response to a resistance exercise at altitude. Thus, with the present study, we aimed to investigate the physiological adaptations in Nepalese porters vs. Italian trekkers during an altitude trek, considering different muscle groups, in response to strength exercise vs. rest.

MATERIALS AND METHODS

Design and Participants

The research project "Kanchenjunga Exploration & Physiology" was a subset of "Environmentally-modulated metabolic adaptation to hypoxia in altitude natives and sea-level dwellers: from integrative to molecular (proteomics, epigenetics, and ROS) level" approved by the Ethical Review Board of the Nepal Health Research Council (NHRC). All study procedures were performed in accordance with the ethical standards of the 1964 Helsinki declaration and its later amendments or comparable ethical standards. Written informed consent was obtained from all participants.

The experimental subjects completed a combined circuit of 300 km length (south and north base camps), covering a daily walk average of 6 h, for a total of 110 h, along a demanding route with ascent and descent tracts, covering a total of over 16,000 m of vertical displacement in the Himalayan mountain range of eastern Nepal, at the border with Sikkim (India). The project investigated adaptive physiological responses to trekking throughout low (500–2,000 m), moderate (2,000–3,000 m), and high (3,000–5,500 m) altitudes (Schommer and Bärtsch, 2011), by two experimental groups composed, respectively by six healthy Caucasian lowlanders and six healthy Nepalese porters (see **Table 1**, for anthropometric characteristics). The Caucasian trekkers' abode normally was at sea level and some of them reported previous high altitude experiences, although no one in the last 3 years. The Nepalese trekkers habitually live at LA and reported frequent exposure to high altitude, with a working experience of 2–5 similar expeditions

per year in the last 3 years. The expedition was continuously supervised by an expert medical doctor; neither participants suffered from Acute Mountain Sickness during the trek, nor they reported any cardiovascular or respiratory disease. The average sleep duration was approximately 6–7 h for all participants. The Caucasian participants only took one acetazolamide pill of 250 mg daily, at 6 PM. during the 2 days between the acclimatization day and the stay at the highest altitude point of the expedition.

From Kathmandu, the subjects were transferred to Biratnagar by plane to initiate the active phase of the expedition. From Biratnagar, participants reached Basantapur, a village at 2,300 m altitude, by an off-road vehicle. They then trekked to Lhonak at 4,780 in 12 days and on the 13th day reached the North Camp of Kanchenjunga. The control measurement at LA was carried out at Kathmandu (1,450 m), while those at HA were performed at Lhonak (4,780 m; see **Figure 1**). Considering the two groups planned the identical distance, and the groups trekked almost together, we analyzed the data of the wearable system of one Nepalese porter only to inform about the exercise load during the trek. Even though distance and difference in altitude were identical for the two groups, the workload was changing, reflecting the typical situation of modern altitude traveling: in fact, Caucasians carried light loads (up to 10 kg), whereas Nepalese carried heavier loads (up to 30 kg), along the whole route.

TABLE 1 | Descriptive characteristics of participants and oxygen saturation measured in the same days of NIRS testing; Blood pressure (BP) is expressed as SystolicBP/DiastolicBP; group values are expressed as mean ± SD.

	Ethnicity	Sex	Age (years)	BMI (Kg/m^2)	Basal BP (mmHg)	SpO_2-LA (%)	SpO_2-HA (%)
It1	Italian	Female	36	25.07	117/76	99	84
It2	Italian	Male	63	28.91	133/83	97	84
It3	Italian	Male	59	21.91	139/87	98	80
It4	Italian	Male	25	24.31	126/68	99	85
It5	Italian	Male	32	24.14	124/67	98	89
It6	Italian	Male	48	30.54	136/82	97	92
Italian Group			44 ± 15	25.81 ± 3.25	129 ± 8/77 ± 8	98 ± 1	86 ± 4
Ne1	Nepalese	Male	26	26.49	128/87	96	85
Ne2	Nepalese	Male	18	17.51	112/62	99	90
Ne3	Nepalese	Male	39	22.99	143/92	96	88
Ne4	Nepalese	Male	40	28.83	131/89	96	85
Ne5	Nepalese	Male	30	29.41	127/93	95	82
Ne6	Nepalese	Male	29	20.94	130/93	96	82
Nepalese group			30 ± 8	24.36 ± 4.70	129 ± 10/86 ± 12	96 ± 1	85 ± 3

BMI, body mass index; BP, blood pressure; SpO2, oxygen saturation; LA, low altitude; and HA, high altitude.

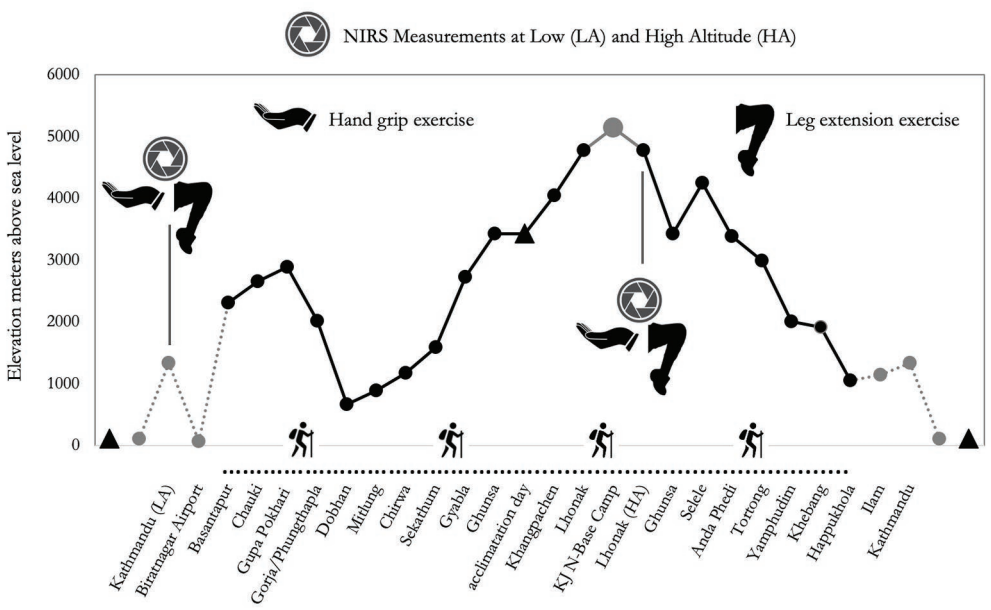

FIGURE 1 | Altimetric plan of the "Kanchenjunga Exploration & Physiology" project. Measurements refer to near-infrared spectroscopy (NIRS) assessment, both on forearm (handgrip task) and anterior thigh (leg extension task).

Measurements

Trekking load was assessed with the wearable device Zephyr™ BioHarness 3 (Medtronic, United States), basing on accelerometry. Raw data were then analyzed by the software Omni Sense 5.0 (Medtronic, United States). Vector magnitude units (VMUs) were calculated as $\sqrt{x^2+y^2+z^2}$ where x, y, and z are the averages of the three axial acceleration magnitudes over the previous 1 s, sampled at 100 Hz. Axial accelerometer output was band-pass filtered, to remove non-human artifacts and gravity. Results are reported as gravity units, ranging from 0 to 16.

Measures by NIRS were performed in the quadriceps and forearm muscles. These were chosen mainly to include two different muscle groups, one directly involved in the walking effort, whereas the other was not. In addition, we chose *vastus lateralis* and anterior forearm muscles considering all the following tips: to limit the problem of adipose tissue contamination to NIRS signal, the lower thickness of those body parts in our participants (Barstow, 2019); because of the low presence of dark hair; because of the high simplicity to repeat the test; because largely used in NIRS assessments in previous studies (Jones et al., 2016); and because easy to set in respect to the bandages and logistics. To be specific, the NIRS probe was placed: (1) on the skin of the dominant forearm, over the middle part of the anterior compartment, and (2) on the skin of the dominant thigh, over the lower third of the *vastus lateralis* muscle. Both for forearm and thigh, an elastic dark bandage and an additional non-elastic dark bandage were applied over the probes.

After the positioning of the probes and the explanation of the exercise, without any warm-up, NIRS-derived parameters were collected for 3 min at rest; subsequently, during 3 min of exercise consisting in 18 concentric and eccentric contractions (5 s + 5 s) by the forearm muscles; and finally, 3 min of further recording was applied during recovery. Hereinafter, the 9 min of the protocol will be defined as stages. Then, after the re-positioning of the probe, the same procedure was repeated for the quadriceps. An operator paced the time. For forearm exercise, participants were required to grip and release a soft ball. For the quadriceps exercise, participants were required to extend and release the knee joint against an elastic training band, held by the same operator. Before testing, participants were allowed to attempt both kinds of exercise. This allowed them to get used to the instrumentation and to adapt their strength to the subsequent strain. For both forearm and thigh, the participants were asked to provide a progressive maximal effort and active release. To be specific, they were required to increase progressively the effort in 5 s to reach the maximal effort with a concentric contraction, and immediately release with an eccentric contraction during the following 5 s, back to resting condition, and so forth for 18 reps. The operator checked the real-time reactivity of parameters by the software, and continuously supported the participants for maintaining the exercise intensity and the pace. All tests were conducted in the late afternoon, after some hours of rest from daily trek. To ensure the exact re-positioning in different measurements, probes were placed onto the middle point of the forearm, and the one-third of the distance from the upper margin of the patella to the anterior superior iliac spine.

Near-infrared spectroscopy was used to assess the concentration changes of oxy-, deoxy- and total-hemoglobin (Tot-Hb), as measures of local vascular and metabolic response to muscle action, with a spatially resolved spectrometer specifically set to measure oxygenation in muscle tissue (PortaMon device and Oxysoft software, Artinis Medical Systems, Netherlands). PortaMon is a compact and lightweight device (75 g), containing three pairs of LEDs (at distances of 30, 35, and 40 mm from the silicon photodiode sensor) that uses the spatially resolved spectroscopy and the modified Beer-Lambert law (due to scattering and absorption in the tissue) to calculate the absolute concentration of chromophores. Multidistance continuous wave technique, with two different wavelengths (850 and 760 nm), and a sample rate of 10 Hz was used. Operating temperature requirements (10–35°C) were met. The usefulness of this device in measuring at rest and during exercise has already been reported (McManus et al., 2018). From the measures of oxy-Hb (O_2Hb) and deoxy-Hb (HHb), we calculated to-Hb (O_2Hb + HHb), diff-Hb (O_2Hb − HHb), and tissue saturation index (TSI) as the percentage of oxygenated hemoglobin detected: TSI = (O_2Hb) ÷ (O_2Hb + HHb) × 100. Tot-Hb and TSI are indexes directly linked to local blood flow and oxygen consumption. To be noted that, throughout the text, we used Hb instead of (Hb + Mb); indeed, as suggested, it can be assumed that signal in mainly related to Hb, rather than Mb (Barstow, 2019). NIRS probe was posed parallel to the muscle, with a soft elastic bandage and two anelastic dark bandages to cover from ambient light. We calculated the minute-by-minute average of each parameter.

Peripheral oxygen saturation (SpO_2) was measured in the same days of NIRS testing, using a pulse oximeter (APN-100, Contec Medical Systems Co. Ltd., China); values were considered allowing several seconds to detect a pulse and waiting for a stable value. The device measured in a range of 70–100% with an accuracy of 2%. The positioning of the rubber finger probe was done carefully, after cleaning and drying fingers (WHO, 2011), and the tests were performed in duplicate.

Statistics

The statistical analysis and plots were carried out using R-based open source software Jamovi Version 1.2.5.0 (retrieved from https://www.jamovi.org) using GAMLj and Flexplot modules. Assumption check consisted of the Shapiro-Wilk test for normality of distributions, the Levene's test for homogeneity of residual variances, and the Kolmogorov-Smirnov test for normality of residuals. Considering the results of the assumption check, the TSI values were undergone to $\log_{10}$ transformation while Tot-Hb values to square root transformation (even though with this transformation some missing points occurred, due to original negative values), then General Linear Mixed Model (GLMM) with Restricted Maximum Likelihood (REML) estimation method was used (Armstrong, 2017). Stage (1st, 2nd, 3rd, 7th, 8th, and 9th min), altitude (LA vs. HA), ethnicity (Nepalese vs. Italians), and muscle (quadriceps vs. forearm) were set as fixed factors and participants as a random factor. Two-way interactions

were considered. Fit measures [Akaike Information Criterion (AIC) and Bayesian Information Criterion (BIC)] were reported, as well as marginal R^2 (proportion of variance explained by the fixed factors only), and conditional R^2 (proportion of variance explained by the fixed and random factors) and Likelihood Ratio Test (LRT) for the random effect. The effect size of fixed factors was calculated and reported as Cohen's f^2 (Selya et al., 2012).

TABLE 2 | General Linear Mixed Model (GLMM) statistics of NIRS parameters; stage, ethnicity, muscle and altitude: fixed factors; participants: random factor.

	TSI	Tot-Hb
AIC	−1,082	603
BIC	−572	786
R^2 marginal	0.435	0.414
R^2 conditional	0.468	0.575
Random LRT	$p = 0.022$	$p < 0.001$
Stage	$p = 0.898$	$p < 0.001$
Ethnicity	$p = 0.396$	$p = 0.485$
Muscle	$p < 0.001$	$p = 0.588$
Altitude	$p < 0.001$	$p = 0.710$
Stage × ethnicity	$p = 0.997$	$p = 0.896$
Stage × muscle	$p = 0.753$	$p = 0.927$
Muscle × ethnicity	$p < 0.001$	$p = 0.234$
Stage × altitude	$p = 0.992$	$p = 0.850$
Altitude × ethnicity	$p = 0.117$	$p = 0.918$
Muscle × altitude	$p < 0.001$	$p = 0.008$

The lesser are fit measures [Akaike Information Criterion (AIC) and Bayesian Information Criterion (BIC)], the better is the model. Stage (1st, 2nd, 3rd, 7th, 8th, and 9th min), altitude (LA vs. HA), ethnicity (Nepalese vs. Italians), and muscle (quadriceps vs. forearm) were set as fixed factors and participants as a random factor. Two-way interactions were considered and reported. TSI, tissue saturation index; Tot-Hb, total hemoglobin; AIC, akaike information criterion; BIC, bayesian information criterion; LRT, likelihood ratio test.

RESULTS

The trek was conducted with average gravity units of 0.18 in the 1st day of monitoring (3rd day of trek, at moderate altitude, and 16.2 km of distance covered), and 0.15 in the 2nd day (16th day of trek, at high altitude, and 7.8 km of distance covered). To be noted that 0.2 corresponds to a normal walk. The results we obtained averaged also the resting phase during the daily trek, and the total workload consisted also of the carrying. Two Nepalese carried 10–20 kg daily, the others four Nepalese 25–30 kg daily. The Italians carried 2–10 kg daily.

As expected, oxygen saturation decreased with altitude in all participants, ranging from 80 to 92% at high altitude; all participants showed values in the normal physiological range at LA (see **Table 1**). Model fit measures suggested that TSI had a better fit of the current analyses compared to Tot-Hb. In both cases, individuality significantly affected the analyses, especially for Tot-Hb (see LRT values on **Table 2**).

Regarding TSI, significant differences were found in respect to muscle (higher values in forearm: $p < 0.001$, $f^2 = 0.158$), altitude (higher values at LA: $p < 0.001$, $f^2 = 0.695$), ethnicity × muscle (Nepalese had higher values in thigh: $p < 0.001$, $f^2 = 0.156$), and muscle × altitude (higher decrease in forearm with altitude: $p < 0.001$, $f^2 = 0.833$), and a tendency for ethnicity × altitude (lesser decrease in Italians with altitude: $p = 0.117$, $f^2 = 0.776$; see **Table 2**; **Figure 2**). Mean parameters before and after exercise are reported in **Table 3**.

Regarding tot-Hb, significant differences were found in respect to stage (increment after exercise: $p < 0.001$, $f^2 = 0.913$) and muscle × altitude (higher increase in thigh with altitude: $p = 0.008$, $f^2 = 0.052$; see **Table 2**; **Figure 3**). Considering the behavior of this parameter, we additionally ran the analysis setting the

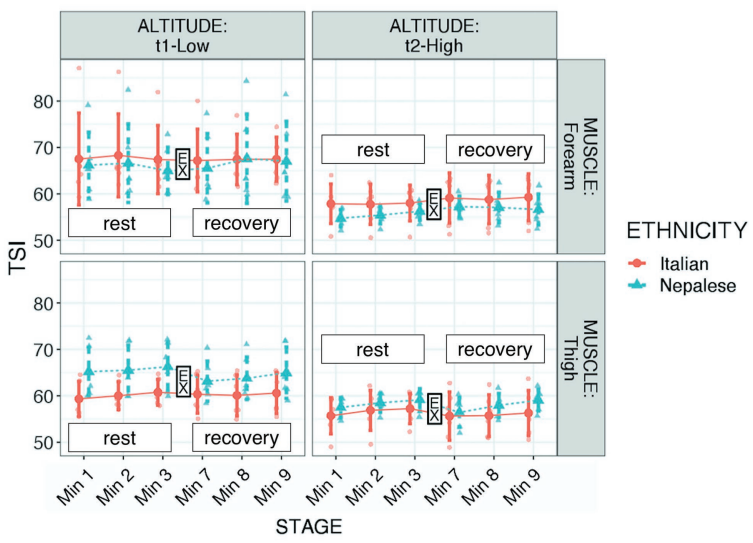

FIGURE 2 | Tissue saturation index (TSI) of participants during "Kanchenjunga Exploration & Physiology" project. Measurements were done with a NIRS device on forearm **(upper panels)** and anterior thigh **(lower panels)**, 3 min before (rest) and 3 min after (recovery) a 3-min-lasting exercise. EX represents the 3-min time spot of resistance exercise, constituted by 18 submaximal contractions. Both groups (Italians and Nepalese) were measured at low (1,450 m, **left panels**) and high (4,750 m, **right panels**) altitude. Data represent single values with mean ± SD, averaged by 1-min recording.

average at the 3rd-min-before exercise and the 3rd-min-after exercise, instead of six stages. Those values underwent the same assumption check and consequently a square root transformation was applied. The robust evidence was the strong increment after exercise ($p < 0.001$, $f^2 = 1.045$). Although only descriptive, as shown in **Figure 3**, it seemed that Nepalese could achieve a more consistent blood flow increase in the exercised muscle.

DISCUSSION

From an epistemological point of view, the MEDLINE database revealed a systematic increase in the adaptive responses of humans to high altitude since the second half of the 19th century (Donaldson, 1888). This interest had been cultivated with a certain constancy in the following years, but only since the '50s occurred an exponential growth in quantity and quality of the related articles (Margaria, 1951; Swan, 1953; Cerretelli and Margaria, 1961). This phenomenon was strictly connected to the desire of generations of climbers, who followed dreams of glory and aimed to conquer the 14 mountains above 8,000 m (Messner, 1999). This opened an intriguing door for those scholars interested in studying extreme adaptations (West, 1990; Grocott et al., 2009). In recent years, a 3-fold alliance has been appearing, linking climbers and scientists with local workers (porters and guides), who offered skills and knowledge to realize expeditions with mountaineering and scientific purposes.

TABLE 3 | Tissue saturation index (TSI) values, obtained from NIRS measurement, before and after the exercise, clustered by ethnic group, muscle group, and altitude.

	Altitude	Forearm muscle		*Vastus lateralis*	
		Before Ex	After Ex	Before Ex	After Ex
Italians	Low	67.8 ± 8.7	67.4 ± 5.6	60.0 ± 3.2	60.4 ± 4.3
trekkers	High	57.9 ± 4.0	59.1 ± 5.2	56.6 ± 3.7	55.9 ± 4.8
Nepalese	Low	65.9 ± 6.5	66.7 ± 8.5	65.7 ± 5.3	64.0 ± 4.7
porters	High	55.5 ± 1.8	57.0 ± 2.9	58.4 ± 2.1	57.8 ± 2.7

Data are percent values and are reported as mean ± SD. Ex: Exercise; TSI = (O_2Hb) ÷ (O_2Hb + HHb) × 100.

The altitude increase generates a simultaneous and roughly linear reduction in atmospheric pressure and inspired oxygen pressure (Peacock, 1998). Respiration, oxygen transport, and alveolar-arterial oxygen-tension gradient regulate the oxygen supply to the new metabolic needs that the high altitude presents cardiac output and hemoglobin concentration. Oxygen delivery and supply are the crucial topic in hypobaric hypoxic adaptations (West, 1990; O'Brien et al., 2018).

With the present study, we investigated fractional oxygen extraction and reactive hyperemia during an altitude expedition, through the NIRS method. We aimed to compare two common groups of altitude travelers (Nepalese vs. Caucasian) and two diverse muscle groups (forearm and anterior thigh) at low and high altitudes, before and in response to a submaximal exercise. The originality of the work consisted in the possibility to include NIRS equipment within the luggage during a high altitude trek, allowing of conducting field-based measurements in two diverse ethnic groups.

First, the decrease of peripheral oxygen saturation revealed through the pulse oximeter in both groups, proved the known adaptations of altitude sojourn in our model. In addition, the duration of exercise (3 min with 18 submaximal repetitions) allowed observing a marked and sustained hemodynamic response. With this regard, the NIRS method optimally fitted our model, unveiling valuable insights into the regional blood

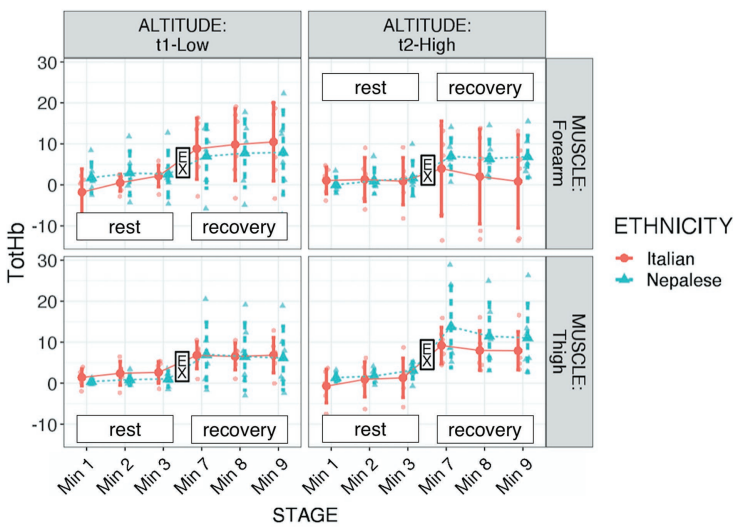

FIGURE 3 | Total hemoglobin (tot-HB) of participants during "Kanchenjunga Exploration & Physiology" project. Measurements were done with a NIRS device on forearm **(upper panels)** and anterior thigh **(lower panels)**, 3 min before (rest) and 3 min after (recovery) a 3-min-lasting exercise. Exercise (EX) represents the 3-min time spot of resistance exercise, constituted by 18 submaximal contractions. Both groups (Italians and Nepalese) were measured at low (1,450 m, **left panels**) and high (4,750 m, **right panels**) altitude. Data represent single values with mean ± SD, averaged by 1-min recording.

dynamics and muscle oxygenation. Between the two parameters, we evaluated (TSI and Tot-Hb), TSI fitted better the current analysis; both were significantly affected by individuality, Tot-Hb to a greater extent.

As expected, at altitude, TSI decreased. This reduction was particularly evident in the forearm muscle. The reason for this difference in muscle groups may have two reasons: (1) both muscle groups reached low values of saturation, thus starting from higher values, the forearm muscle may have been reached that critical threshold. On average, TSI moved from 66.9 to 57.3% in the forearm and from 62.5 to 57.2% in the thigh. Although speculative, we may indeed interpret 57% as a critical threshold, at least in our findings and (2) a different interpretation lies on middle-term adaptation: as discussed below, the exercise carried on a greater extent by lower limb muscles may have inhibited tissue desaturation in the thigh. We also found a difference between the ethnic groups: the Nepalese porters had greater values in thigh TSI than the Italian trekkers. This result may lie on long-term adaptive memory of porters, due to the frequent exposure to altitude load-carrying trek. Hence, the greater workload of lower limbs may lead the selective adaptation of these muscle groups (Tam et al., 2016) in altitude porters. Therefore, frequent exercise protocols at altitude may produce increases in local tissue oxygenation.

It seemed that Italians had a lesser reduction with altitude; this result may have been related to the lighter load carried by this group. Martin et al. (2009) showed that tissue oxygen saturation in the *vastus lateralis* decreases during maximal oxygen consumption to increase again during the recovery phase. The same authors revealed how the response pattern to different stages of the exercise protocol was similar at moderate and high altitude in respect to sea level, although rest values were lower at all stages in altitude. Furthermore, the exposure to extremely high altitudes had a protective effect during exercise, reducing the degree of de-saturation. In respect to the maximal aerobic exercise, in our model, tissue saturation was not influenced by the resistive exercise, opening the way to a prospective new study determining differences in response to hypoxic exercise in terms of exercise typology. Thus, high altitude may represent a stressor to the oxygen system, capable of entailing beneficial effects in oxygen delivery and utilization (Tam et al., 2016), in addition to muscular structural and functional changes (Doria et al., 2011). Prospectively, the specific definition of exercise loads should drive the plan of exercise protocols at altitude for stressing the local tissue oxygenation response. There were no changes in TSI after the submaximal exercise; this result agrees with the recent findings of Yoshiko et al. (2020), who reported a significant deoxygenation during hypoxic exercise, but not in the recovery.

Hemodynamic response to submaximal resistive exercise showed an increase in blood flow, as estimated by the Tot-Hb parameter. At altitude, it seemed that this increase was particularly high in the thigh rather than in the forearm muscle. In addition, even though our model did not allow the three-way statistical analysis, from **Figure 3** it can be observed a difference between ethnic groups: Nepalese porters may have required a higher blood flow increment after exercise in altitude, both in the forearm and in the thigh muscle. The marked hemodynamic response to submaximal dynamic exercise, as found in the present study, might be further characterized in terms of hemodynamic reserves (Bassareo and Crisafulli, 2020): hypoxia has a role in muscle metaboreflex (Mulliri et al., 2019), and the dynamics of diverse muscle groups can be stressed to achieve further insight. This response might be the result of systemic advantage, achieved by heritable factors or due to long-term adaptation, representing a likely basis for a further adaptation in exercised muscles. Therefore, the adequate definition of blood flow response to isometric vs. dynamic exercise under hypoxic conditions is required to define the training methods.

Concerning ethnicity, it has been suggested that the physiological advantages of Andeans may be related to a greater efficiency in oxygen transfer and utilization, supported by a likely genetic adaptation, non-selective to oxygen-sensitive genes (Julian and Moore, 2019). On the Himalayan side, genetic and epigenetic bases of Sherpas were extensively studied in Xtreme Everest 2 project (Martin et al., 2013) whose major conclusion, among others, was that Peroxisome Proliferator Activated Receptor Alpha (PPARA) gene may entail the metabolic basis to permit a superior survival and performance at high altitude (Horscroft et al., 2017). Beyond ethnicity, Puthon et al. (2016) described how elite climbers can elicit advantages with respect to trained non-climber controls: these authors suggested that these advantages were the consequence of a lower hypoxic and hypercapnic ventilatory response rather than to an enhanced peripheral saturation. Wang et al. (2010) showed that 4-week hypoxic exercise training enhanced oxygen perfusion and utilization in exercising skeletal muscles. Thus, we may speculate about a likely long-term adaptation of the Nepalese porters to improved oxygenation in those muscles involved in hypoxic exercise (herein altitude trekking). At least in part, this adaptation may lie on the better capability to increase the regional blood flow. One plausible pathway possibly involved lies on the nitric oxide (NO) system, known to be a major contributor of the compensatory vasodilation in response to hypoxia (Joyner and Casey, 2014). Here, we suggest ethnic differences may lie in some non-NO synthase pathways (Lepore, 2000), excluding nutritional factors (Luiking et al., 2010). Extending pieces of evidence on genetic advantages of altitude populations, further studies may investigate possible genetic advantages of acute or middle-term response to hypobaric hypoxia. Such an investigation may address the intriguing world of potentially heritable epigenetic factors.

Individuality had a significant effect on both NIRS parameters, more marked for Tot-Hb. Thus, further studies on a larger sample size and more accurate control of individual factors (e.g., age, sex, metabolic diseases, frequency of altitude exposure, time since last exposure, recent injuries, cardiovascular measures, and muscle structure) should extend our results. Indeed, differences in age and carried loads between the two groups could have affected the results we obtained. Differences in intrinsic characteristics of the forearm and the thigh muscles may also have played a role: Yoshiko et al. (2020) recently reported some differences in the diverse muscles of *quadriceps* comparing deoxygenation during submaximal exercise in normoxic and hypoxic trials. Thus, it should be of interest to

study the diverse behavior of muscles basing of morpho-functional characterization. Ethnic differences in the muscle structural and functional characteristics may affect the response to hypoxia and should deserve further investigation: despite evidence of muscular inborn characteristics of Himalayan population (Kayser et al., 1996), the high heterogeneity of Caucasian ethnic group does not allow to speculate about likely ethnic difference in muscle composition for affecting the current results.

Limitations

Like other methods, NIRS investigates a small and relatively superficial portion of the muscle, thus those portions cannot be assumed as representative for the whole muscle. Several confounding variables, i.e., age difference, unequal sex distribution within the two groups, and the difference in the load carried, some participants having elevated blood pressure. The anthropometric and training status of participants may also have affected the results. The exercise protocol during the NIRS measurements were not quantitatively measured, due to the logistical difficulty to provide a real-time monitoring of dynamometer data in field conditions. The small sample size makes difficult to derive firm conclusions. Workload, medicine intake, diet, and sleep were not standardized between groups. However, these conditions were due given the nature of this work, i.e., an outdoor field-based study conducted in a harsh environment.

Perspectives

The pieces of evidence of the present work further support investigations on this topic, designing outdoor field studies with the accurate external and internal workload, metabolic performance characterization, and follow-up assessment. Some additional measures of very thin vessels and some clustering based on likely different pattern of hemodynamic response during exercise (Dech et al., 2020) may add new levels of comprehension. Further studies may extend these results verifying whether the common principle of climbers "Climb High and sleep low" based on induced hypoxia (pre)conditioning for a safe rapid ascent to extreme altitudes (Burtscher and Koch, 2016) may lead the optimal response to exercise in terms of muscle oxygen saturation.

Intriguing perspectives lie on cross adaptation: the use of one stimulus (herein altitude hypoxia) to model the responses to a similar stimulus in other circumstances (e.g., clinics; Lee et al., 2019). Moreover, considering the differences we found between muscle groups, it remains to be investigated whether hypoxia modulates tissue cross-talk. Exercised muscles provide a means for systemic cross-talk, both from a molecular (Whitham et al., 2018) and a functional (Pietrangelo et al., 2019) basis. Thus, it should be of interest to verify the adaptation of muscle-related cross-talk in response to hypobaric hypoxia.

In conclusion, individual factors should be taken into account if oxygen delivery and utilization are addressed. Muscular morpho-functional characteristics may unveil further determinants of specific responses to hypoxia. The combined use of both saturation and blood flow indexes deserves further investigation to clarify the role of ethnicity, muscle group, and hypoxic condition in response to altitude physical exercise.

DATA AVAILABILITY STATEMENT

The raw data supporting the conclusions of this article will be made available by the authors, without undue reservation.

ETHICS STATEMENT

The studies involving human participants were reviewed and approved by Ethical Review Board of the Nepal Health Research Council. The patients/participants provided their written informed consent to participate in this study.

AUTHOR CONTRIBUTIONS

VV, DB, GM, AC, and TP: conceptualization. VV, DB, GM, GG, AC, and TP: methodology. VV, DB, GM, GG, and AC: formal analysis. DB and MM: investigation. VV and AC: resources. DB and GM: data curation. VV, DB, AC, and TP: writing – original draft preparation. VV, DB, GM, GG, AC, TP, MM, and PC: writing – review and editing. DB: visualization. VV, AC, and PC: supervision. VV: project administration and funding acquisition. All authors contributed to the article and approved the submitted version.

FUNDING

The work was funded by the Department of Psychological, Health and Territorial Sciences, University "G. d'Annunzio" of Chieti-Pescara, Italy.

ACKNOWLEDGMENTS

We thank ADITECH srl (Ancona, Italy), Mission Nepal Holidays Pvt. Ltd. (Kathmandu, Nepal), and all the Italian trekkers and Nepalese porters involved in this project.

REFERENCES

Armstrong, R. A. (2017). Recommendations for analysis of repeated-measures designs: testing and correcting for sphericity and use of MANOVA and mixed model analysis. *Ophthalmic Physiol. Opt.* 37, 585–593. doi: 10.1111/opo.12399

Barstow, T. J. (2019). Understanding near infrared spectroscopy and its application to skeletal muscle research. *J. Appl. Physiol.* 126, 1360–1376. doi: 10.1152/japplphysiol.00166.2018

Bassareo, P. P., and Crisafulli, A. (2020). Gender differences in hemodynamic regulation and cardiovascular adaptations to dynamic exercise. *Curr. Cardiol. Rev.* 16, 65–72. doi: 10.2174/1573403X15666190321141856

Burtscher, M., and Koch, R. (2016). Effects of pre-acclimatization applying the "climb high and sleep low" maxim: an example of rapid but safe ascent to extreme altitude. *J. Hum. Perf. Extrem. Environ.* 12:2. doi: 10.7771/2327-2937.1081

Cerretelli, P., and Margaria, R. (1961). Maximum oxygen consumption altitude. *Int. Z. Angew. Physiol.* 18, 460–464. doi: 10.1007/bf00699458

Cheung, S. S., Mutanen, N. E., Karinen, H. M., Koponen, A. S., Kyröläinen, H., Tikkanen, H. O., et al. (2014). Ventilatory chemosensitivity, cerebral and muscle oxygenation, and total hemoglobin mass before and after a 72-day mt. Everest expedition. *High Alt. Med. Biol.* 15, 331–340. doi: 10.1089/ham.2013.1153

Dech, S., Bittmann, F., and Schaefer, L. (2020). Behavior of oxygen saturation and blood filling in the venous capillary system of the biceps brachii muscle during a fatiguing isometric action. *Eur. J. Transl. Myol.* 30:8800. doi: 10.4081/ejtm.2019.8800

Di Giulio, C., Bianchi, G., Cacchio, M., Macrì, M. A., Ferrero, G., Rapino, C., et al. (2003). Carotid body HIF-1alpha, VEGF and NOS expression during aging and hypoxia. *Adv. Exp. Med. Biol.* 536, 603–610. doi: 10.1007/978-1-4419-9280-2_76

Donaldson, F. (1888). Further remarks on the circulatory changes at high altitude. *Trans. Am. Climatol. Assoc. Meet.* 5, 96–99.

Doria, C., Toniolo, L., Verratti, V., Cancellara, P., Pietrangelo, T., Marconi, V., et al. (2011). Improved VO2 uptake kinetics and shift in muscle fiber type in high-altitude trekkers. *J. Appl. Physiol.* 111, 1597–1605. doi: 10.1152/japplphysiol.01439.2010

Douglas, C. G. (1910). Periodic breathing at high altitudes. *J. Physiol.* 40, 454–471. doi: 10.1113/jphysiol.1910.sp001382

Feeback, M. R., Seo, Y., Dancy, M., and Glickman, E. L. (2017). The effect of psychomotor performance, cerebral and arterial blood saturation between African-American and Caucasian males before, during and after normobaric hypoxic exercise. *Int. J. Exerc. Sci.* 10, 655–665.

Fryer, S., Stone, K., Dickson, T., Wilhelmsen, A., Cowen, D., Faulkner, J., et al. (2019). The effects of 4 weeks normobaric hypoxia training on microvascular responses in the forearm flexor. *J. Sports Sci.* 37, 1235–1241. doi: 10.1080/02640414.2018.1554177

Grassi, B., and Quaresima, V. (2016). Near-infrared spectroscopy and skeletal muscle oxidative function in vivo in health and disease: a review from an exercise physiology perspective. *J. Biomed. Opt.* 21:091313. doi: 10.1117/1.JBO.21.9.091313

Grocott, M. P. W., Levett, D. Z. H., and Ward, S. A. (2019). Exercise physiology: exercise performance at altitude. *Curr. Opin. Physiol.* 10, 210–218. doi: 10.1016/j.cophys.2019.06.008

Grocott, M. P. W., Martin, D. S., Levett, D. Z. H., McMorrow, R., Windsor, J., and Montgomery, H. E. (2009). Arterial blood gases and oxygen content in climbers on Mount Everest. *N. Engl. J. Med.* 360, 140–149. doi: 10.1056/NEJMoa0801581

Hesford, C. M., Laing, S., and Cooper, C. E. (2013). Using portable NIRS to compare arm and leg muscle oxygenation during roller skiing in biathletes: a case study. *Adv. Exp. Med. Biol.* 789, 179–184. doi: 10.1007/978-1-4614-7411-1_25

Horscroft, J. A., Kotwica, A. O., Laner, V., West, J. A., Hennis, P. J., Levett, D. Z. H., et al. (2017). Metabolic basis to Sherpa altitude adaptation. *Proc. Natl. Acad. Sci. U. S. A.* 114, 6382–6387. doi: 10.1073/pnas.1700527114

Jones, S., Chiesa, S. T., Chaturvedi, N., and Hughes, A. D. (2016). Recent developments in near-infrared spectroscopy (NIRS) for the assessment of local skeletal muscle microvascular function and capacity to utilise oxygen. *Artery Res.* 16, 25–33. doi: 10.1016/j.artres.2016.09.001

Joyner, M. J., and Casey, D. P. (2014). Muscle blood flow, hypoxia, and hypoperfusion. *J. Appl. Physiol.* 116, 852–857. doi: 10.1152/japplphysiol.00620.2013

Julian, C. G., and Moore, L. G. (2019). Human genetic adaptation to high altitude: evidence from the Andes. *Genes* 10:150. doi: 10.3390/genes10020150

Kayser, B., Hoppeler, H., Desplanches, D., Marconi, C., Broers, B., and Cerretelli, P. (1996). Muscle ultrastructure and biochemistry of lowland Tibetans. *J. Appl. Physiol.* 81, 419–425. doi: 10.1152/jappl.1996.81.1.419

Lee, B. J., Gibson, O. R., Thake, C. D., Tipton, M., Hawley, J. A., and Cotter, J. D. (2019). Editorial: cross adaptation and cross tolerance in human health and disease. *Front. Physiol.* 9:1827. doi: 10.3389/fphys.2018.01827

Lepore, D. A. (2000). Nitric oxide synthase-independent generation of nitric oxide in muscle ischemia–reperfusion injury. *Nitric Oxide* 4, 541–545. doi: 10.1006/niox.2000.0308

Luiking, Y. C., Engelen, M. P. K. J., and Deutz, N. E. P. (2010). Regulation of nitric oxide production in health and disease. *Curr. Opin. Clin. Nutr. Metab. Care* 13, 97–104. doi: 10.1097/MCO.0b013e328332f99d

Magliulo, L., Bondi, D., Pietrangelo, T., Fulle, S., Piccinelli, R., Jandova, T., et al. (2020). Serum ferritin and vitamin D evaluation in response to high altitude comparing Italians trekkers vs Nepalese porters. *Eur. J. Sport Sci.* 1–21. doi: 10.1080/17461391.2020.1792559

Margaria, R. (1951). Respiration at low barometric pressure. *Minerva Med.* 42, 1235–1242.

Martin, D. S., Gilbert-Kawai, E., Levett, D. Z., Mitchell, K., Kumar, B. C. R., Mythen, M. G., et al. (2013). Xtreme Everest 2: unlocking the secrets of the Sherpa phenotype? *Extrem. Physiol. Med.* 2:30. doi: 10.1186/2046-7648-2-30

Martin, D. S., Levett, D. Z. H., Mythen, M. Grocott, M. P. W., and Caudwell Xtreme Everest Research Group (2009). Changes in skeletal muscle oxygenation during exercise measured by near-infrared spectroscopy on ascent to altitude. *Crit. Care* 13:S7. doi: 10.1186/cc8005

McManus, C. J., Collison, J., and Cooper, C. E. (2018). Performance comparison of the MOXY and PortaMon near-infrared spectroscopy muscle oximeters at rest and during exercise. *J. Biomed. Opt.* 23, 1–14. doi: 10.1117/1.JBO.23.1.015007

Messner, R. (1999). *All 14 eight-thousanders*. Seattle, USA: Mountaineers Books.

Mulliri, G., Sainas, G., Magnani, S., Roberto, S., Ghiani, G., Mannoni, M., et al. (2019). Effects of exercise in normobaric hypoxia on hemodynamics during muscle metaboreflex activation in normoxia. *Eur. J. Appl. Physiol.* 119, 1137–1148. doi: 10.1007/s00421-019-04103-y

O'Brien, K. A., Pollock, R. D., Stroud, M., Lambert, R. J., Kumar, A., Atkinson, R. A., et al. (2018). Human physiological and metabolic responses to an attempted winter crossing of Antarctica: the effects of prolonged hypobaric hypoxia. *Phys. Rep.* 6:e13613. doi: 10.14814/phy2.13613

Peacock, A. J. (1998). ABC of oxygen: oxygen at high altitude. *BMJ* 317, 1063–1066. doi: 10.1136/bmj.317.7165.1063

Peltonen, J. E., Paterson, D. H., Shoemaker, J. K., Delorey, D. S., Dumanoir, G. R., Petrella, R. J., et al. (2009). Cerebral and muscle deoxygenation, hypoxic ventilatory chemosensitivity and cerebrovascular responsiveness during incremental exercise. *Respir. Physiol. Neurobiol.* 169, 24–35. doi: 10.1016/j.resp.2009.08.013

Pietrangelo, T., Bondi, D., Kinel, E., and Verratti, V. (2019). The bottom-up rise strength transfer in elderly after endurance and resistance training: the BURST. *Front. Physiol.* 9:1944. doi: 10.3389/fphys.2018.01944

Puthon, L., Bouzat, P., Rupp, T., Robach, P., Favre-Juvin, A., and Verges, S. (2016). Physiological characteristics of elite high-altitude climbers. *Scand. J. Med. Sci. Sports* 26, 1052–1059. doi: 10.1111/sms.12547

Sarkar, M., Niranjan, N., and Banyal, P. (2017). Mechanisms of hypoxemia. *Lung India* 34, 47–60. doi: 10.1016/s1078-5337(05)70087-3

Schommer, K., and Bärtsch, P. (2011). Basic medical advice for travelers to high altitudes. *Dtsch. Arztebl. Int.* 108:839. doi: 10.3238/arztebl.2011.0839

Selya, A. S., Rose, J. S., Dierker, L. C., Hedeker, D., and Mermelstein, R. J. (2012). A practical guide to calculating cohen's f(2), a measure of local effect size, from PROC MIXED. *Front. Psychol.* 3:111. doi: 10.3389/fpsyg.2012.00111

Simonson, T. S., Wei, G., Wagner, H. E., Wuren, T., Qin, G., Yan, M., et al. (2015). Low haemoglobin concentration in Tibetan males is associated with greater high-altitude exercise capacity. *J. Physiol.* 593, 3207–3218. doi: 10.1113/JP270518

Swan, C. (1953). Climbing Everest: some notes on the medical team. *Br. Med. J.* 1, 1329–1330.

Tam, E., Bruseghini, P., Calabria, E., Dal Sacco, L., Doria, C., Grassi, B., et al. (2016). Gokyo Khumbu/Ama Dablam trek 2012: effects of physical training and high-altitude exposure on oxidative metabolism, muscle composition, and metabolic cost of walking in women. *Eur. J. Appl. Physiol.* 116, 129–144. doi: 10.1007/s00421-015-3256-z

Verratti, V., Giulio, C. D., Bianchi, G., Cacchio, M., Petruccelli, G., Artese, L., et al. (2009). "Neuroglobin in aging carotid bodies" in *Arterial chemoreceptors: Advances in experimental medicine and biology*. eds. C. Gonzalez, C. A. Nurse and C. Peers (Dordrecht: Springer Netherlands), 191–195.

Vogt, M., and Hoppeler, H. (2010). Is hypoxia training good for muscles and exercise performance? *Prog. Cardiovasc. Dis.* 52, 525–533. doi: 10.1016/j.pcad.2010.02.013

Vogt, M., Puntschart, A., Geiser, J., Zuleger, C., Billeter, R., and Hoppeler, H. (2001). Molecular adaptations in human skeletal muscle to endurance training under simulated hypoxic conditions. *J. Appl. Physiol.* 91, 173–182. doi: 10.1152/jappl.2001.91.1.173

Volianitis, S., Krustrup, P., Dawson, E., and Secher, N. H. (2003). Arm blood flow and oxygenation on the transition from arm to combined arm and leg exercise in humans. *J. Physiol.* 547, 641–648. doi: 10.1113/jphysiol.2002.034496

Wang, J. -S., Wu, M. -H., Mao, T. -Y., Fu, T., and Hsu, C. -C. (2010). Effects of normoxic and hypoxic exercise regimens on cardiac, muscular, and cerebral hemodynamics suppressed by severe hypoxia in humans. *J. Appl. Physiol.* 109, 219–229. doi: 10.1152/japplphysiol.00138.2010

West, J. B. (1990). Tolerance to severe hypoxia: lessons from Mt. Everest. *Acta Anaesthesiol. Scand.* 34, 18–23. doi: 10.1111/j.1399-6576.1990.tb03216.x

Whitham, M., Parker, B. L., Friedrichsen, M., Hingst, J. R., Hjorth, M., Hughes, W. E., et al. (2018). Extracellular vesicles provide a means for tissue crosstalk during exercise. *Cell Metab.* 27, 237.e4–251.e4. doi: 10.1016/j.cmet.2017.12.001

WHO (2011). Pulse oximetry training manual. Available at: https://www.who.int/patientsafety/safesurgery/pulse_oximetry/who_ps_pulse_oxymetry_training_manual_en.pdf?ua=1 (Accessed September 10, 2019).

Wu, T., and Kayser, B. (2006). High altitude adaptation in Tibetans. *High Alt. Med. Biol.* 7, 193–208. doi: 10.1089/ham.2006.7.193

Yoshiko, A., Katayama, K., Ishida, K., Ando, R., Koike, T., Oshida, Y., et al. (2020). Muscle deoxygenation and neuromuscular activation in synergistic muscles during intermittent exercise under hypoxic conditions. *Sci. Rep.* 10:295. doi: 10.1038/s41598-019-57099-y

Conflict of Interest: The authors declare that the research was conducted in the absence of any commercial or financial relationships that could be construed as a potential conflict of interest.

frontiers in Physiology

REVIEW
published: 23 November 2020
doi: 10.3389/fphys.2020.614893

Molecular Mechanisms of Acute Oxygen Sensing by Arterial Chemoreceptor Cells. Role of Hif2α

Patricia Ortega-Sáenz[1,2,3], Alejandro Moreno-Domínguez[1,2], Lin Gao[1,2,3] and José López-Barneo[1,2,3]**

[1]*Instituto de Biomedicina de Sevilla (IBiS), Hospital Universitario Virgen del Rocío/CSIC/Universidad de Sevilla, Seville, Spain,* [2]*Departamento de Fisiología Médica y Biofísica, Facultad de Medicina, Universidad de Sevilla, Seville, Spain,* [3]*Centro de Investigación Biomédica en Red sobre Enfermedades Neurodegenerativas (CIBERNED), Madrid, Spain*

Carotid body glomus cells are multimodal arterial chemoreceptors able to sense and integrate changes in several physical and chemical parameters in the blood. These cells are also essential for O_2 homeostasis. Glomus cells are prototypical peripheral O_2 sensors necessary to detect hypoxemia and to elicit rapid compensatory responses (hyperventilation and sympathetic activation). The mechanisms underlying acute O_2 sensing by glomus cells have been elusive. Using a combination of mouse genetics and single-cell optical and electrophysiological techniques, it has recently been shown that activation of glomus cells by hypoxia relies on the generation of mitochondrial signals (NADH and reactive oxygen species), which modulate membrane ion channels to induce depolarization, Ca^{2+} influx, and transmitter release. The special sensitivity of glomus cell mitochondria to changes in O_2 tension is due to Hif2α-dependent expression of several atypical mitochondrial subunits, which are responsible for an accelerated oxidative metabolism and the strict dependence of mitochondrial complex IV activity on O_2 availability. A mitochondrial-to-membrane signaling model of acute O_2 sensing has been proposed, which explains existing data and provides a solid foundation for future experimental tests. This model has also unraveled new molecular targets for pharmacological modulation of carotid body activity potentially relevant in the treatment of highly prevalent medical conditions.

Keywords: carotid body, glomus cells, acute O_2 sensing, electron transport chain, mitochondrial signaling, ion channels, mechanism of disease, paraganglioma

OPEN ACCESS

Edited by:
Gregory D. Funk,
University of Alberta, Canada

Reviewed by:
Colin A. Nurse,
McMaster University, Canada
Christopher Wyatt,
Wright State University,
United States

****Correspondence:***
Patricia Ortega-Sáenz
gortega1@us.es
José López-Barneo
lbarneo@us.es

Specialty section:
This article was submitted to Respiratory Physiology, a section of the journal Frontiers in Physiology

Received: *07 October 2020*
Accepted: *03 November 2020*
Published: *23 November 2020*

Citation:
Ortega-Sáenz P, Moreno-Domínguez A, Gao L and López-Barneo J (2020) Molecular Mechanisms of Acute Oxygen Sensing by Arterial Chemoreceptor Cells. Role of Hif2α. Front. Physiol. 11:614893. doi: 10.3389/fphys.2020.614893

INTRODUCTION

Oxygen (O_2) is essential for survival of mammalian cells due to its role in numerous biochemical reactions, in particular, in mitochondrial ATP synthesis by oxidative phosphorylation. O_2 deficiency (hypoxia), even if transient, can produce irreversible cellular damage. Chronic and acute adaptive responses to hypoxia have evolved to favor O_2 homeostasis. Sustained (chronic) hypoxia, lasting hours or days, induces a powerful and generalized transcriptional response characterized by the expression of a broad cohort of genes that, among other changes, favors

glycolysis, to obtain non-aerobically ATP, as well as angiogenesis and increased red blood cell number to enhance the O_2-carrying capacity of the blood and its distribution to the tissues. Modulation of O_2-sensitive genes depends on a family of prolyl hydroxylases (PHD), which use O_2 as a substrate to hydroxylate and regulate the activity of hypoxia inducible transcription factors (HIFs; see for a recent comment Lopez-Barneo and Simon, 2020). To date, the PHD-HIF signaling pathway has been reported to modulate over 2,000 transcripts, many of them critically involved in numerous pathophysiological processes such as embryogenesis, stem cell fate and differentiation, tissue regeneration, inflammation and cancer, among others (Ratcliffe, 2013; Semenza, 2014; Colgan et al., 2020).

Exposure to hypoxia, as it occurs in high altitude or in patients with altered gas exchange in the lungs, also induces acute adaptive responses (hyperventilation and sympathetic activation) that in few seconds increase O_2 uptake and its distribution to tissues. These life-saving cardiorespiratory reflexes are mediated by specialized cells in the homeostatic acute O_2-sensing system (Weir et al., 2005). The prototypical acute O_2-sensing organ is the carotid body (CB), a small arterial chemoreceptor located in the carotid bifurcation, which contains chemosensory and neurosecretory glomus cells (**Figure 1A**). Glomus cells release transmitters during exposure to hypoxia and other stimuli to activate afferent fibers of the glossopharyngeal nerve terminating at the brainstem respiratory and autonomic centers. Although it is over 30 years that the basic cellular physiology of the CB was described (see for a recent review Ortega-Saenz and Lopez-Barneo, 2020), the molecular mechanism underlying acute O_2-sensing by glomus cells has remained elusive. Among the several attractive hypotheses postulated are the involvement of a specific NADPH oxidase, activation of AMP kinase during hypoxia, the reversible fast regulation of ion channels by gasotransmitters such as carbon monoxide and hydrogen sulfide, or the expression of an atypical olfactory receptor (Olfr78; see for recent reviews Lopez-Barneo et al., 2016; Rakoczy and Wyatt, 2018). Although all these processes can influence glomus cell function, none of them seem to be essential for acute O_2 sensing because the various mouse models generated after ablation of the genes coding the relevant enzymes or receptors showed CB with practically normal responsiveness to hypoxia (He et al., 2002; Ortega-Saenz et al., 2006; Mahmoud et al., 2016; Wang et al., 2017; Torres-Torrelo et al., 2018). It has recently been reported that Olfr78-deficient CB cells have decreased responsiveness to mild hypoxia (Peng et al., 2020). Olfr78 is one of the most

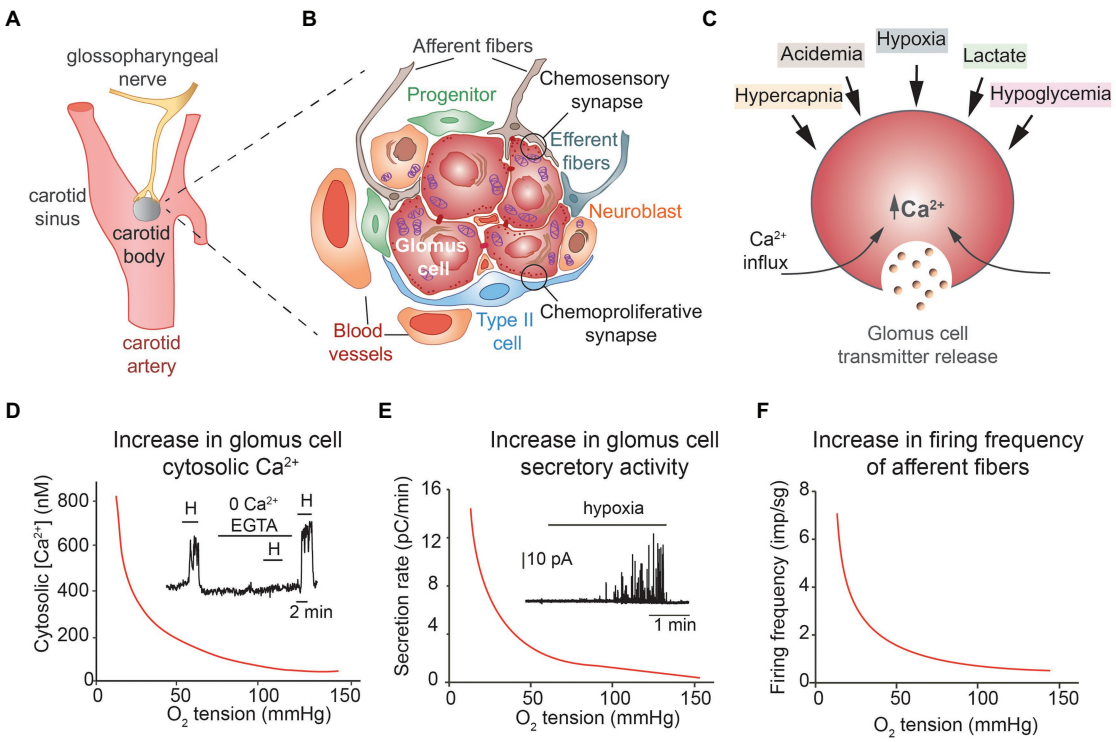

FIGURE 1 | Structural and functional properties of carotid arterial chemoreceptors. **(A)** Location and innervation of the carotid body (CB). **(B)** Schematic representation of a CB glomerulus with indication of the various structural components and cell types. **(C)** Schematic representation of CB glomus cell activation by several stimuli. **(D,E)** Hyperbolic relationships between cytosolic Ca^{2+} (inset in **D**) and catecholamine release (inset in **E**) in single glomus cells as a function of oxygen tension in the external solution. Hypoxia-induced increase in cytosolic Ca^{2+} depends on extracellular Ca^{2+} influx **(D)**. **(F)** Relationship between firing frequency in afferent fibers of the sinus nerve as a function of blood oxygen tension. **(A–C)** Modified from Ortega-Saenz and Lopez-Barneo (2020). **(D,E)** Modified from Montoro et al. (1996) and Ortega-Saenz et al. (2006). **(F)** Modified from Lopez-Barneo (1996).

abundant mRNA species expressed in CB glomus cells (Zhou et al., 2016; Gao et al., 2017), as other highly expressed G-protein-coupled receptors, which may influence the input/output properties of chemoreceptor cells (Nurse, 2014; Ortega-Saenz and Lopez-Barneo, 2020). In recent years new experimental data have provided strong support for a "mitochondrial-to-membrane signaling (MMS) model" of acute O_2 sensing, which combines the "membrane" and "metabolic" hypotheses. Here, after a succinct presentation of the general properties of CB glomus cells, we focus on the description of the MMS model of acute O_2 sensing. We also discuss the potential medical implications of recent advances in CB research.

PROPERTIES OF POLYMODAL CAROTID BODY CHEMORECEPTOR CELLS

The CB is organized in clusters of cells called glomeruli. Each glomerulus contains neuron-like and tyrosine hydroxylase (TH)-positive glomus (or type I) cells, which appear grouped (normally 4–8 units) in the center, enveloped by processes of glia-like, glial fibrillary acidic protein (GFAP)-positive, type II or sustentacular cells (**Figure 1B**). Glomus cells have large nuclei, abundant mitochondria, and numerous secretory vesicles, containing dopamine, ATP, acetylcholine, and several other neurotransmitters and neuropeptides. These cells establish chemical synapses with afferent fibers ("chemosensory synapses"; **Figure 1B**) originating in the petrosal ganglion. It is well-established that the main transmitter in the chemosensory synapse is ATP, which binds to postsynaptic P2X receptors, although acetylcholine may also have a stimulatory effect (Zhang et al., 2000; Rong et al., 2003; Shirahata et al., 2007). Dopamine has an auto or paracrine role inhibiting Ca^{2+} channels in glomus cells (Benot and Lopez-Barneo, 1990) and, in addition, it can also inhibit postsynaptic HCH cationic channels in petrosal afferent neuros *via* D2 receptors (Zhang et al., 2018). Although mature O_2-sensitive glomus cells seem to be post-mitotic, the CB also contains a population of immature TH-positive cells, normally localized in the periphery of the glomerulus, with fewer secretory vesicles and smaller sensitivity to hypoxia than mature glomus cells (Sobrino et al., 2018). In hypoxic conditions, these TH-positive "neuroblasts" proliferate and differentiate into mature glomus cells and in this way contribute to adult CB growth, a plastic CB response that increases the stimulatory input to the respiratory center and thereby facilitates chronic adaptation to hypoxic environments. Glomus cells also establish numerous chemical synapses with type II cells (Platero-Luengo et al., 2014). Indeed, transmitters released from glomus cells can induce ATP release from type II cells to potentiate the chemosensory synapse (Xu et al., 2003; Zhang et al., 2012). GFAP-positive type II cells, or a subpopulation of them, are quiescent multipotent stem cells that upon exposure to hypoxia are activated to proliferate and differentiate into new glomus cells, endothelial cells, and smooth muscle (Pardal et al., 2007; Navarro-Guerrero et al., 2016; Annese et al., 2017). Glomus cells and type II cells form "chemoproliferative synapses" (**Figure 1B**), such that neurotransmitters and neuromodulators (endothelin-1 among others) released from glomus cells (Chen et al., 2002) induce type II cells to exit the quiescent state and to start proliferating and differentiating (Platero-Luengo et al., 2014). Therefore, the adult CB is a sophisticated germinal niche that contains differentiated cells with complex sensory functions, as well as immature neuroblasts and progenitors with strong neurogenic and angiogenic potential that support the structural plasticity of the organ.

Chemosensory glomus cells are small (~10–15 μm in diameter) and electrically compact elements able to generate action potentials repetitively due to the expression of voltage-gated Na^+, Ca^{2+}, and K^+ channels. They also express a broad spectrum of other ion channels types, notably background K^+ channels, in particular, TASK1 and TASK 3 channels, and cationic TRP channels (Zhou et al., 2016; Gao et al., 2017). It is established that hypoxia produces glomus cell depolarization due to the inhibition of background and voltage-gated K^+ channels; this leads to the opening of voltage-dependent Ca^{2+} channels, extracellular Ca^{2+} influx, and exocytotic transmitter release (Lopez-Barneo et al., 1988; Buckler and Vaughan-Jones, 1994; Urena et al., 1994). It has also been reported that the rise in intracellular Ca^{2+} can activate Ca^2-permeant background cation channels to further potentiate Ca^{2+} entry and transmitter release (Kang et al., 2014). In addition to hypoxia, glomus cells are activated by hypercapnia, low extracellular pH, low glucose, and lactate as well as by hypoperfusion and several circulating hormones and cytokines. Although these stimuli utilize separate transduction mechanisms, they all converge on extracellular Ca^{2+} influx and the generation of a cytosolic Ca^{2+} signal that triggers transmitter release (see for a recent review Ortega-Saenz and Lopez-Barneo, 2020). The CB, classically considered to be fundamentally involved in the regulation of respiration, is now viewed as a polymodal arterial chemoreceptor needed for optimal regulation of metabolism and homeostasis of the organism (**Figure 1C**).

MITOCHONDRIA-TO-MEMBRANE SIGNALING MODEL OF ACUTE OXYGEN SENSING

Acute responsiveness to hypoxia is an intrinsic property of glomus cells that is maintained in *in vitro* preparations such as dispersed cells, CB slices, or glomus cell-petrosal neuron synapse (Lopez-Barneo et al., 1988; Peers, 1990; Buckler and Vaughan-Jones, 1994; Zhong et al., 1997; Pardal et al., 2000). The curves relating cytosolic Ca^{2+} level or single glomus cell catecholamine secretion as a function of O_2 tension (PO_2) are remarkably similar to the hyperbolic relationship existing between afferent CB sensory activity and arterial PO_2 (**Figures 1D–F**). Although the membrane events – depolarization and extracellular Ca^{2+} influx- underlying glomus cell responsiveness to hypoxia (known as the "membrane hypothesis") are broadly accepted, mitochondria have also been classically considered to be involved in CB O_2 sensing. A "metabolic hypothesis" was supported by the high sensitivity of CB to mitochondrial poisoning and the fact that mitochondrial inhibitors are powerful CB stimulants.

Indeed, the existence in the CB of a special cytochrome c oxidase with low O_2 affinity was proposed several decades ago, although it was placed in type II rather than in type I cells (Mills and Jobsis, 1972). This idea of a mitochondrial O_2 sensor was further suggested by the analysis of light-dependent interaction of CO with heme proteins in CB cells, although as the experiments were performed in whole CB preparations, the precise cellular location of the sensor was not determined precisely (Wilson et al., 1994). In addition, Duchen and Biscoe (1992a,b) showed that in dispersed CB glomus cells mitochondrial parameters (e.g., NADH level or mitochondrial membrane potential) are highly sensitive to changes in ambient PO_2, thereby strongly supporting the "metabolic hypothesis." However, these last authors proposed that Ca^{2+} release from mitochondria was the signal to trigger hypoxia-induced transmitter release, a conclusion that was in direct opposition to the well-established dependence of hypoxic glomus cell activation on extracellular Ca^{2+} influx (Lopez-Barneo et al., 1993; Buckler and Vaughan-Jones, 1994; Urena et al., 1994).

Acute O_2 Sensing Depends on Mitochondrial Complex I Signaling

The first step to resolve to conflict between the "membrane" and "metabolic" hypotheses came from experiments on PC12 cells (an O_2-sensitive catecholaminergic cell line; Taylor et al., 2000) and carotid body slices (Ortega-Saenz et al., 2003) showing that, as it occurs with hypoxia, catecholamine secretion induced by mitochondrial electron transport chain (ETC) inhibitors acting on complexes I, II, III, and IV is fully abolished by removal of extracellular Ca^{2+} or administration of 0.2 mM Cd^{2+}, a non-selective voltage-gated Ca^{2+} channel blocker (Urena et al., 1994). Separate experiments showed that ETC blockers also inhibit the O_2-sensitive background K^+ current in dispersed glomus cells (Wyatt and Buckler, 2004). These data on single cells are in good agreement by previous work on whole CBs showing that dopamine secretion during incubation with cyanide is strongly inhibited in the absence of extracellular Ca^{2+} (Obeso et al., 1989). Ortega-Saenz et al. (2003) found that rotenone, a highly selective mitochondria complex I (MCI) blocker that binds near the last Fe/S cluster (N2 site) and prevents the transfer of electrons to ubiquinone, was very effective in occluding any effect of hypoxia. In contrast, activation of glomus cells by hypoglycemia was unaffected by rotenone (Garcia-Fernandez et al., 2007). These data suggested that hypoxia and hypoglycemia are sensed by separate mechanisms and that a rotenone binding site is directly involved in acute O_2 sensing by glomus cells.

To investigate the role of MCI in acute O_2 sensing, we generated conditional knockout mice lacking the *Ndufs2* gene, which codes a 49 kDa protein that contributes to the ubiquinone/rotenone binding site and is also essential for the assembly of the catalytic core in MCI (Kashani-Poor et al., 2001; Carroll et al., 2013). Because generalized bi-allelic deletion of *Ndufs2* results in embryonic lethality, we generated conditional *Ndufs2* knockout mice with either ablation of *Ndufs2* in glomus cells and other catecholaminergic cells (TH-NDUFS2 mice) or ubiquitous tamoxifen (TMX)-induced *Ndufs2* deletion in adulthood (ESR-NDUFS2 mice). TH-NDUFS2 mice had a normal development although they had smaller size than adult wild type littermates probably due to dwarfing secondary to the loss of hypothalamic dopaminergic neurons (Diaz-Castro et al., 2012; Fernandez-Aguera et al., 2015). At 2 months of age, these mice exhibited a loss of the hypoxic ventilatory response (HVR; **Figure 2A**), although they had a normal ventilatory response to hypercapnia (Fernandez-Aguera et al., 2015). CBs from TH-NDUFS2 mice appeared slightly hypertrophied and with normal structural organization. However, Ndufs2-deficient glomus cells showed an almost complete abolition of responsiveness to hypoxia (monitored by either the catecholamine secretory response or the changes in cytosolic [Ca^{2+}]), while they responded normally to hypercapnia and hypoglycemia (**Figure 2B**). Similar results were observed in ESR-NDUFS2 mice, in which Ndufs2 deficiency was induced by TMX treatment in adulthood and exhibited an almost complete disappearance of MCI structure and function (Fernandez-Aguera et al., 2015; Arias-Mayenco et al., 2018). In contrast with the effects of Ndufs2 deficiency, ablation of the *Ndufs4* gene, which codes a non-essential MCI auxiliary subunit that reduces MCI activity by approximately 50% (Kruse et al., 2008), did not cause appreciable changes in the catecholamine release and cytosolic Ca^{2+} responses to hypoxia in glomus cells (Fernandez-Aguera et al., 2015). These data indicated that MCI function is essential for acute O_2 sensing and confirmed that hypoxia and hypoglycemia are sensed by means of separate mechanisms. Interestingly, it was found that CB cells contain high levels of succinate, suggesting a highly active Kreb's cycle, and that upregulation or downregulation of succinate dehydrogenase activity enhances or diminishes, respectively, sensitivity to hypoxia in glomus cells (Fernandez-Aguera et al., 2015; Gao et al., 2017; Arias-Mayenco et al., 2018). Although glomus cells survived several months in the absence of MCI, they rapidly died after ablation of MCII (Diaz-Castro et al., 2012; Platero-Luengo et al., 2014).

Taken together, these experimental findings suggested a model of acute O_2 sensing in which mitochondria, acting as a sensor and effector of the hypoxic response, modulate membrane excitability. We proposed that decreased cytochrome c oxidase activity under hypoxia causes a backlog of electrons along the ETC and an increase in the ratio of reduced/oxidized ubiquinone (QH_2/Q), which results in slowing down or even reversion of MCI with NADH accumulation and reactive oxygen species (ROS) production (**Figure 2C**). NADH and ROS are the signals that modulate plasmalemmal ion channels to produce depolarization and activation of glomus cells. Graded accumulation of NADH in glomus cells induced by lowering PO_2 was abolished in Ndufs2-deficient mice (Fernandez-Aguera et al., 2015; Arias-Mayenco et al., 2018; **Figure 2D**). We were also able to monitor in real time the changes in mitochondrial ROS production by means of a fluorescent genetic probe targeted to either mitochondrial intermembrane space (IMS) or matrix. Using this methodology, we demonstrated that acute hypoxia induces in glomus cells a dose-dependent increase in IMS (and cytosol) ROS, which

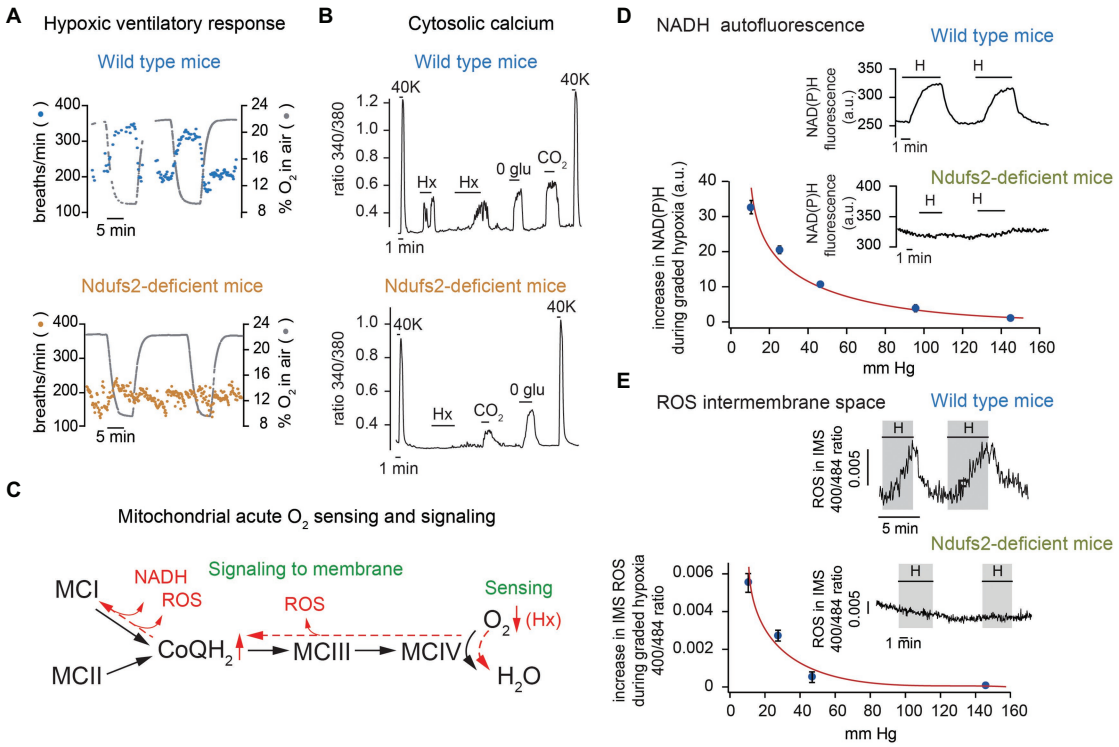

FIGURE 2 | Selective inhibition of acute oxygen sensing by arterial chemoreceptors in mitochondrial complex I (MCI)-deficient mice. **(A)** Ventilatory response to hypoxia in wild type (top) and Ndufs2-deficient (bottom) mice. **(B)** Changes in cytosolic Ca^{2+} in single wild type (top) and Ndufs2-deficient (bottom) glomus cells induced by depolarization (40 mM K^+), hypoxia (Hx, ~15 mm Hg), 0 glucose (0 glu), and hypercapnia (switching from 5 to 10% CO_2). **(C)** Scheme of the electron transport chain illustrating the mitochondria-to-membrane signaling model of acute O_2 sensing by glomus cells. Changes in chemical equilibrium induced by hypoxia (Hx) are represented in red. **(D)** Changes in NADH autofluorescence in single glomus cells from wild type and Ndufs2-deficient mice during exposure to hypoxia. Relationship between NADH levels and extracellular oxygen tension. **(E)** Measurement of reactive oxygen species (ROS) at the mitochondrial intermembrane space in single glomus cells from wild type and Ndufs2-deficient mice. Relationship between ROS levels and extracellular oxygen tension. Modified from Fernandez-Aguera et al. (2015) and Arias-Mayenco et al. (2018).

is markedly decreased by rotenone and in Ndufs2-deficient mice (**Figure 2E**). However, the possibility that IMS ROS produced in other sites along a reduced ETC (e.g., in MCIII) also contribute to the hypoxic response cannot be discarded (**Figure 2C**; Waypa et al., 2010). In support of the MMS model, we showed that intracellular dialysis of glomus cells with NADH and H_2O_2 mimic hypoxia (increase in input resistance and decrease in voltage-gated K^+ current amplitude) and prevents further modulation of K^+ channels by lowering PO_2 (Fernandez-Aguera et al., 2015). Other mitochondrial signals (e.g., decrease in cytosolic ATP level restricted to O_2-sensing microdomains; see below) could also contribute to modulation of membrane channels and the hypoxic response (Varas et al., 2007).

Signature Gene Expression Profile in O_2-Sensing Chemoreceptor Cells

In the past decades, several groups have reported gene expression data focusing on different aspects of CB glomus cell function and, recently, two such studies provided relevant clues for advancing the understanding of glomus cell acute O_2 sensing. In one case, single neonatal glomus cell RNA sequencing confirmed the constitutive high expression of Hif2α and highlighted the elevated expression of two atypical mitochondrial subunits (Ndufa4l2 and Cox4i2), and several ion channels, in particular, Task1 and the low-threshold Ca^{2+} channel α1H subunit (Zhou et al., 2016). This work also showed the high level of expression of genes coding for molecules involved in G-protein signaling, an observation compatible with the elevated number of metabotropic ligands and receptors in glomus cells. A parallel microarray study performed in our laboratory focused on the comparative expression profile of adult CB, adrenal medulla (AM), and superior cervical ganglion (SCG), which are tissues of the same neural crest embryological origin but variable O_2 sensitivity (CB>AM>SCG). Our work confirmed most of the genes reported in the single-cell sequencing study mentioned above and demonstrated a set of genes highly expressed in CB, and less markedly in the AM, in comparison with the SCG with a potential role in acute O_2 sensing (Gao et al., 2017). The most relevant genes in the CB signature gene expression profile code Hif2α, three atypical mitochondrial subunits (Ndufa4l2, Cox4i2, and Cox8b), pyruvate carboxylase (Pcx), and some types of ion channels (Task1, Task3, and the α1H Ca^{2+} channel subunit). In the context of the MMS model,

it was of special relevance the identification of Pcx and the three nuclear-encoded atypical mitochondrial subunits (Ndufa4l2, Cox4i2, and Cox8b), which could be responsible for the special O_2-sensitivity of glomus cells. In particular, the high level of *Pcx* mRNA expression is compatible with the accumulation of biotin, a cofactor necessary for the function of Pcx and other carboxylases, accumulated in large quantity in glomus cells (Ortega-Saenz et al., 2016). Pcx is an anaplerotic enzyme that catalyzes the formation of oxaloacetate, thereby replenishing the pool of Krebs's cycle intermediates required for an accelerated synthesis of substrates (NADH and $FADH_2$) for the ETC. Therefore, Pcx probably contributes to the active oxidative metabolism and high O_2 consumption characteristic of CB cells. This idea is also compatible with the high levels of succinate found in the CB and the strict dependence of CB survival and function on succinate dehydrogenase activity (Diaz-Castro et al., 2012; Platero-Luengo et al., 2014; Fernandez-Aguera et al., 2015).

Acute O_2 Sensing Through Hif2α-Dependent Expression of Atypical Mitochondrial Complex IV Subunits

Although it was known long ago that Hif2α is constitutively expressed at high levels in normoxic catecholaminergic tissues (Tian et al., 1998), the role of this factor in CB function has not been studied until the last few years. It has been shown that transgenic overexpression of *Epas1* (the gene coding Hif2α) produces CB hypertrophy (Macias et al., 2014) and embryonic ablation of *Epas1* results in CB atrophy (Macias et al., 2018), thereby suggesting that Hif2α is essential for CB development and function. Heterozygous (*Epas1*+/−) mice were reported to have an exaggerated CB responsiveness to hypoxia (Peng et al., 2011) but more recent experiments performed independently by two different groups have shown that these mice have a decrease in the HVR (Hodson et al., 2016; Moreno-Dominguez et al., 2020). Inhibition of the HVR is also seen in variable degrees in mice with homozygous partial (Hodson et al., 2016) or complete (Moreno-Dominguez et al., 2020) conditional deletion of *Epas1* in adulthood. In agreement with these observations, glomus cells from conditional *Epas1*-null mice show selective abolition of the rise in cytosolic $[Ca^{2+}]$ (**Figure 3A**, left and center) or the secretory response to hypoxia. Moreover, NADH and IMS ROS signals induced by hypoxia are strongly inhibited in *Epas1*-deficient glomus cells (**Figures 3B,C**). Interestingly, the hypoxia-induced decrease in matrix ROS (Arias-Mayenco et al., 2018) was not altered by *Epas1* deficiency (**Figure 3D**) thereby indicating that the lack of Hif2α did not change the basic mitochondria metabolism but selectively inhibited signaling in response to low PO_2. In parallel with these functional data, it has been shown that abolition of *Epas1* results in a selective downregulation of mRNAs coding Pcx and the atypical mitochondrial ETC subunits characteristic of CB cells (Moreno-Dominguez et al., 2020). These results are compatible with previous studies reporting that hypoxia induces Cox4i2 (Fukuda et al., 2007) and Ndufa4l2 (Tello et al., 2011) in a Hif-dependent manner (see also Aras et al., 2013), and that Cox8b promoter contains Hif binding sites (Gao et al., 2017). Together these findings indicate that the expression of Hif2α-dependent genes confer acute O_2 responsiveness to CB glomus cells. Indeed, the *Epas1*-null phenotype (inhibition of HVR and lack of glomus cells sensitivity to hypoxia) is also observed in mice with ablation of the *Cox4i2* gene in catecholaminergic cells (TH-COX4I2 mice; **Figure 3A**, right; Moreno-Dominguez et al., 2020).

The data reported so far provide molecular and mechanistic explanation for an MMS model of acute O_2 sensing by arterial chemoreceptor cells in which cytochrome c oxidase acts as an O_2 sensor that, depending on O_2 availability, determines the redox state of the steps upstream in the ETC. In response to hypoxia, the increase in the reduced state of MCIII and accumulation of QH_2 results in the generation of the signals (NADH and ROS) that modulate membrane ion channels (**Figures 4A,B**, see also **Figure 2C**). However, the precise role of each of the atypical MCIV subunits and how they influence acute O_2 sensing in the CB and, possibly, other acutely responding organs, remains to be studied. Ndufa4l2, which is coded by one of the most abundant mRNA species in CB glomus cells, is an isoform of the most widely expressed Ndufa4 subunit, which appears to be associated to MCIV rather than to MCI (Carroll et al., 2006; Balsa et al., 2012). Ndufa4l2 is highly expressed in lung and brain pericytes and some tumor cells (Lucarelli et al., 2018) but its function is poorly known. Expression of Ndufa4l2 attenuates oxygen consumption and decreases ROS production in mitochondria (Tello et al., 2011; Meng et al., 2019), however ablation of the *Ndufa4l2* gene did not produce any clear effect on glomus cell function or HVR (Moreno-Dominguez et al., 2020). Therefore, the precise role of Ndufa4l2 in the context of acute O_2 sensing remains to be determined. On the other hand, Cox4i2 and Cox8b are atypical isoforms of the more broadly distributed Cox4i1 and Cox8a subunits, which are part of the catalytic core of MCIV (Tsukihara et al., 1996). Besides in the CB, Cox4i2 is highly expressed in the lung and some cell types (e.g., pericytes; Huttemann et al., 2012) and Cox8b appears associated to the browning of adipose tissue (Wang et al., 2016). Interestingly, Cox4 and Cox8 subunits contain single adjacent transmembrane helices running in parallel at the periphery of MCIV (Tsukihara et al., 1996; Kadenbach and Huttemann, 2015) that, although located relatively far from the catalytic site (heme a3/CuB), could induce subtle structural changes in MCIV or in its association with supercomplexes that influence the affinity for or reaction rate with O_2. Structural studies have suggested that the Cox8 subunit contributes to the formation of mitochondrial supercomplexes (Wu et al., 2016; Rieger et al., 2017) and a recent study on tumor cells lines have reported that expression of Cox4i2 (instead Cox4i1) decreases the Km of cytochrome c oxidase for O_2 (Pajuelo Reguera et al., 2020). In this last study, the Km of cytochrome c oxidase for O_2 varied between ~0.5 mm Hg (in mitochondria expressing Cox4i1) and ~1 mm Hg (in mitochondria expressing Cox4i2). These are PO_2 values much lower than those necessary for activation of glomus cells, even assuming a steep O_2 gradient

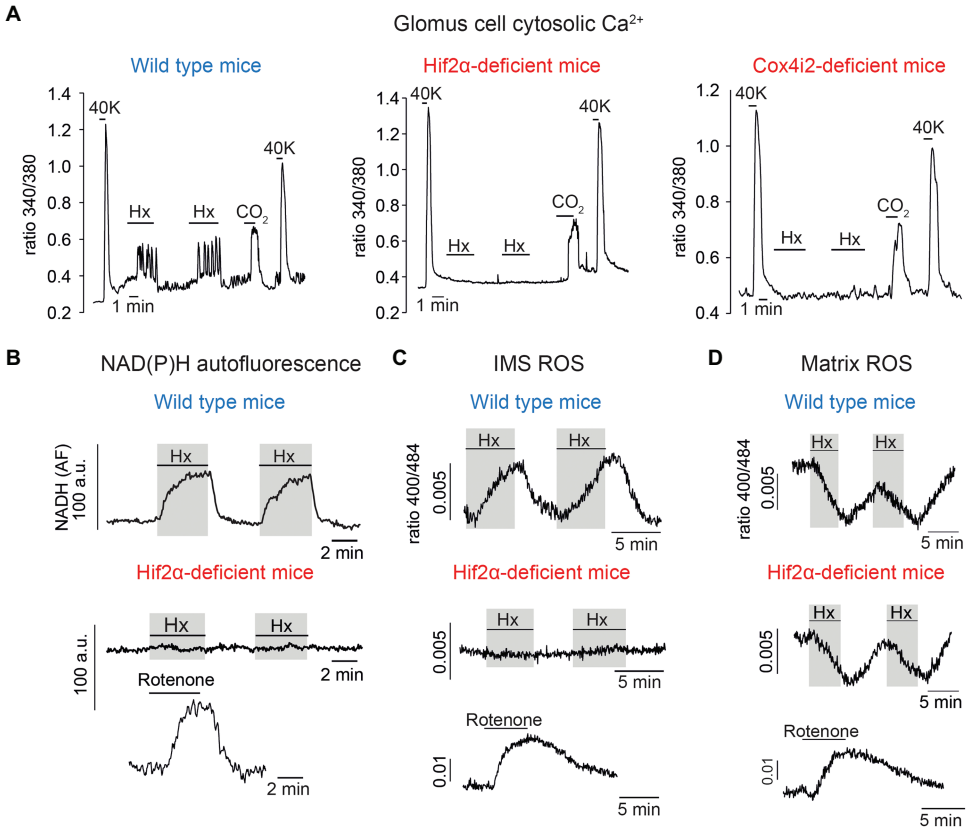

FIGURE 3 | Selective inhibition of carotid body glomus cell responsiveness to hypoxia in Hif2α- and Cox4i2-deficient mice. **(A)** Changes in cytosolic Ca^{2+} in single wild type (left), Hif2α-deficient (center), and Cox4i2-deficient (right) glomus cells induced by depolarization (40 mM K^+), hypoxia (Hx, ~15 mm Hg), and hypercapnia (switching from 5 to 10% CO_2). **(B)** Changes in NADH autofluorescence in single glomus cells from wild type and Hif2α-deficient mice during exposure to hypoxia. **(C)** Measurement of ROS at the mitochondrial intermembrane space (IMS) in single glomus cells from wild type and Hif2α-deficient mice. **(D)** Measurement of ROS at the mitochondrial matrix in single glomus cells from wild type and Hif2α-deficient mice. In B-D, response to rotenone (0.5–1 μM) was tested to show the normal function of MCI. Modified from Moreno-Dominguez et al. (2020).

between the extracellular medium and mitochondria. Therefore, it seems that in addition to the Cox4 subunit isoforms, other factors may influence the Km of cytochrome c oxidase for O_2 in glomus cells. In sum, the MMS model provides a satisfactory molecular explanation for acute O_2 sensing by arterial chemoreceptor cells, which depends on a Hif2α-dependent expression of specific genes. The special O_2 sensitivity of glomus cells seems to result from the combination of an accelerated ETC and O_2 consumption due to an active Krebs cycle and a relatively low affinity of cytochrome c oxidase for O_2. In this way, electron flux in mitochondrial ETC is modulated in a physiological range of O_2 tensions. Whether an MMS model, involving similar genes and regulatory mechanisms, also participates in acute O_2 sensing by other tissues remains to be studied. In this regard, it is important to note that Cox4i2-deficient mice exhibit strong inhibition of hypoxic pulmonary vasoconstriction (Sommer et al., 2017), an acute response to hypoxia that, similar to hypoxic glomus cell activation, depends on the production of ROS by mitochondria and the modulation of O_2-sensitive K^+ channels (Weir et al., 2005).

CLINICAL AND PHARMACOLOGICAL IMPLICATIONS

In recent years, the CB has gained renewed medical interest due to its involvement in the pathogenesis of several highly prevalent human diseases, such as neurogenic hypertension, obstructive sleep apnea, and chronic cardiac failure. In addition, CB dysfunction also contributes to the pathophysiology of respiratory depression, a frequent complication of anesthesia and drug abuse.

Carotid Body Inhibition

CB activation is the first line of defense against hypoxic challenges and, therefore, CB dysfunction may have fatal consequences. Indeed, bilateral resection of the CB, most commonly due neck tumor surgery or asthma treatment, leaves the patients unaware of hypoxemia (Timmers et al., 2003). These patients cannot adapt to hypoxic environments and although they appear to live unaffected in normoxic conditions, disturbances during sleep and unexplained cases of death have

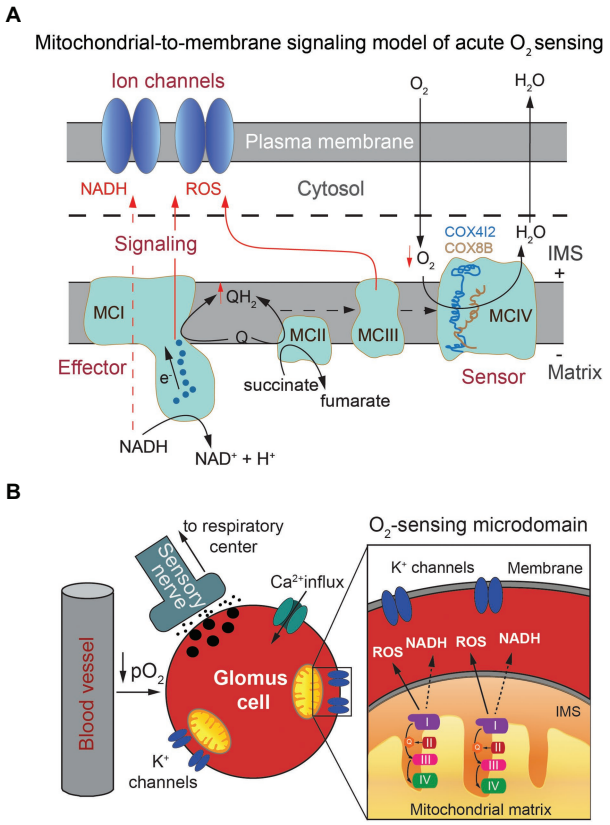

FIGURE 4 | Mitochondria-to-membrane signaling model of acute oxygen sensing by glomus cells. **(A)** Scheme illustrating the mitochondrial signals (NADH and ROS) generated upon exposure to hypoxia and their interaction with membrane ion channels. Modified from Moreno-Dominguez et al. (2020). **(B)** Model of chemosensory transduction by O_2-sensing glomus cells in the carotid body. Modified from Fernandez-Aguera et al. (2015).

been reported. Genetic/developmental CB defects, such as congenital central hypoventilation syndrome (CCHS) and sudden infant death syndrome (SIDS) are life-threatening disorders partially related to alterations in CB function that, although rare in humans, can seriously impair O_2-dependent respiratory control. CCHS is frequently associated with mutations in genes (such as *RET* or *PHOX2B*), which are relevant to development of neural crest-derived tissues (Amiel et al., 2003; Gaultier et al., 2004). Interestingly, CB glomus cells express high levels of GDNF (Villadiego et al., 2005), a neuroprotective dopaminotrophic factor that can activate RET, and genetic ablation of GDNF in adulthood results in a marked reduction in the number of TH-positive cells in the CB (Pascual et al., 2008). Decrease in size with reduction in the number of TH-positive cells and increased number of type II cells has been reported in CBs of autopsied CCHS (Cutz et al., 1997) and SIDS (Porzionato et al., 2013) patients. Prematurity and environmental factors, such as hyperoxia, retard maturation of CB chemoreceptors. Maternal smoking inhibits CB development and the excitability of AM chromaffin cells (Buttigieg et al., 2009).

The most frequent cause of CB inhibition is the use (or abuse) of anesthetics, myorelaxants, and analgesics. Volatile anesthetics (halothane and others) depress glomus cell excitability because they increase the open probability of background TASK1-like K^+ channels (Buckler et al., 2000). Most of the myorelaxant drugs used in anesthesia are cholinergic antagonists, which interfere with the activation of the CB chemosensory synapse and inhibit the hypoxic ventilatory response (Jonsson et al., 2004). Endogenous opioids (enkephalins) are produced in the CB, where they have an auto- or paracrine inhibitory effect (Kirby and McQueen, 1986). Systemic administration of opioids produces a strong respiratory depression, due in part to inhibition of peripheral chemoreceptors (Pokorski and Lahiri, 1981). However, opioid-induced respiratory depression (OIRD) in conscious rats is enhanced after bilateral CB denervation, suggesting a protective rather than causative role of the CB in OIRD (Baby et al., 2018). The design of well-tolerated drugs to activate peripheral chemoreceptors, which in turn stimulate the respiratory center, is a promising strategy to alleviate OIRD in humans; a clinical condition that has become a major health problem, particularly in the United States with a toll of over 150 deaths daily. In this regard, blockers of several types of K^+ channels are already being tested in the clinical setting as respiratory stimulants (Chokshi et al., 2015; Roozekrans et al., 2015). Within the context of this discussion, it is worth mentioning that these CB stimulants, which act downstream of the O_2-sensing mechanism, might be useful to treat "silent hypoxemia," a bewildering frequent clinical manifestation found in patients with coronavirus disease 19 (COVID-19), who exhibit severe hypoxemia without clear signs of distress (dyspnea) or significant acceleration of breathing (Tobin et al., 2020). Given that in the early stages of coronavirus infection human cells undergo profound changes in the expression of mitochondrial proteins (Gordon et al., 2020), a plausible explanation for "silent hypoxemia" is the alteration of the mitochondria-based O_2-sensor in coronavirus-infected CB glomus cells (Archer et al., 2020; Tobin et al., 2020). Another aspect of the MMS model of acute O_2 sensing with translational relevance is the identification of the mitochondrial ETC as a potential pharmacological target to stimulate respiration. In this regard, it should be tested whether MCI inhibitors, such as metformin, one of the most broadly used drugs to treat type II diabetes (Protti, 2018), can activate the CB and stimulate respiration. It could be optimal to combine metformin with novel highly membrane permeant precursors of succinate (bis-1-acetoxy-ethyl succinate or diacetoxy-methyl succinate; Ehinger et al., 2016). We have shown that increased levels of ubiquinol ($CoQH_2$) resulting from the application of membrane permeant dimethyl succinate increases responsiveness to hypoxia (Arias-Mayenco et al., 2018). A combination of both therapies (metformin plus succinate prodrugs) would potentiate CB activation and at the same time prevent lactic acidosis secondary to metformin seen in some patients (Protti, 2018).

Carotid Body Over-Activation

Chronic activation of the CB, as it occurs in patients with sleep apnea, metabolic syndrome or chronic left cardiac failure, due to intermittent hypoxia, high fat diet, or carotid

hypoperfusion, respectively, can lead to exaggerated sympathetic outflow and autonomic dysfunction (see for review Ortega-Saenz and Lopez-Barneo, 2020). Although the pathophysiology of these maladaptive processes is still poorly known (Marcus et al., 2010; Paton et al., 2013; Schultz et al., 2013; Ribeiro et al., 2018), it has been shown in animal models that CB resection or deafferentation restores the sympathetic tone and improves the associated cardiovascular and metabolic alterations (Del Rio et al., 2013, 2016; McBryde et al., 2013; Ribeiro et al., 2013). However, translation of this therapy to the clinical setting has numerous limitations because the lack of CB may be cause of cardiovascular events, particularly during episodes of hypoxia and hypercapnia. CB resection could also have severe side effects such as altered glucose regulation or a reduced ability to acclimatize to high altitudes (Johnson and Joyner, 2013; Pijacka et al., 2018). In a pilot clinical trial performed on patients with chronic heart failure, bilateral CB ablation improved the autonomic imbalance but also increased the occurrence of nocturnal hypoxia, particularly in subjects with concomitant sleep apnea (Niewinski et al., 2017). An alternative to CB resection is the development of pharmacological drugs to selectively modulate CB chemosensory activity and plasticity. In this regard, it has been shown that a purinergic P2X3 receptor blocker (AF-219) inhibits CB afferent activity and alleviates hypertension in a rat model (Pijacka et al., 2016). The translation of these findings to the clinical setting may be facilitated by the fact that purinergic P2X3 receptor blockers (i.e., AF-219; also known as MK-7264 or Gefapixant) are already used in clinical trials to treat refractory chronic cough in humans, notwithstanding the unwanted side effect that taste sensation is also affected (Smith et al., 2020). A novel potential therapeutic option is represented by Hif2 antagonists, drugs already in clinical trials for the treatment of some types of cancer (Courtney et al., 2018; Fallah and Rini, 2019). Acute O_2 sensing by glomus cells depends on Hif2α (Moreno-Dominguez et al., 2020) and systemic administration of a Hif2 inhibitor (PT2385) results in inhibition of the HVR (Cheng et al., 2020). Moreover, Hif2α is necessary for the proliferation of CB cells in hypoxia (Hodson et al., 2016) and activation of glomus cells is necessary for the proliferation and differentiation of CB progenitors and neuroblasts into mature O_2-sensitive glomus cells (Platero-Luengo et al., 2014; Sobrino et al., 2018). Hence, Hif2 inhibitors may be beneficial to selectively modulate CB responsiveness to hypoxia and sympathetic over-activation.

Carotid Body Tumorigenesis

Chemodectomas are rare and mostly benign CB tumors that have attracted special attention because they are often used as a model to investigate the pathogenesis of paragangliomas (PGL), tumors generated in tissues of the peripheral nervous system derived from neural crest precursors. The most common cause of hereditary CB PGL is germ line mutations in genes coding subunits of mitochondrial succinate dehydrogenase (most frequently mutations in Sdhd and Sdhc; Baysal, 2008; Her and Maher, 2015). Patients are heterozygous (with a normal and a mutated allele) and tumorigenesis is believed to be triggered by the loss of the normal allele (loss of heterozygosity) in CB glomus cells. However, the reasons why this allele is lost in some cell types (e.g., cells in CB and other paraganglia) and not in others as well as the mechanisms leading to tumor formation are unknown (Millan-Ucles et al., 2014). Given that the histology of CB PGL resembles that of hypertrophied CBs seen in chronically hypoxic subjects and that PGL incidence increases in populations living at high altitude (Astrom et al., 2003), a widely accepted hypothesis of tumor generation is the so called "pseudo hypoxic drive" (Selak et al., 2005; Smith et al., 2007). This hypothesis is based on the fact that succinate accumulation, secondary to succinate dehydrogenase dysfunction, causes downstream inhibition of prolyl hydroxylases involved in normal degradation of Hif as well as inhibition of histone demethylases and other enzymes, thereby causing cell proliferation. Indeed, overexpression of nondegradable Hif2α (but not Hif1α) induces CB hypertrophy (Macias et al., 2014). Moreover, deletion of the gene coding for prolyl hydroxylase 2 in mice induces Hif2α-dependent CB glomus cell proliferation with a PGL-like phenotype (Fielding et al., 2018). However, experimental evidence indicates that unlike humans, heterozygosity for mutations in succinate dehydrogenase subunits does not predispose mice to PGL. Adult knockout mice heterozygous for *Sdhd* show practically normal CB function, with only a subtle glomus cell hyperplasia and organ hypertrophy (Piruat et al., 2004). In addition, conditional (embryonic or adult) bi-allelic ablation of *Sdhd* causes a marked glomus cell loss (Diaz-Castro et al., 2012). It seems therefore that in addition to succinate dehydrogenase subunit mutations, other hits, related to animal species, age, or cell metabolism, are necessary for tumorigenesis *in vivo*. Although there is convincing *in vitro* and *in vivo* evidence that multipotent stem cells contribute to CB angiogenesis and expansion of parenchyma during exposure to sustained hypoxia (Pardal et al., 2007; Annese et al., 2017), it has also been shown that proliferation of TH-positive cells greatly contributes to the growth of the glomus cell pool during the first 2–3 days of hypoxia (Paciga et al., 1999; Chen et al., 2007; Wang et al., 2008; Fielding et al., 2018). In the rat, and probably also in other species, this initial glomus cell expansion is due to proliferation and maturation of a population of TH-positive neuroblasts, which differentiate into O_2-sensing glomus cells (Sobrino et al., 2018). Because hypoxia does not seem to induce proliferation of CB stem cells and undifferentiated progenitors *in vitro* (Platero-Luengo et al., 2014), a fundamental question that remains to be answered is whether hypoxia-induced release of transmitter and cytokines by mature glomus cells is a critical paracrine signal to trigger CB TH-positive cell proliferation and possibly the initial stages of tumor transformation. This would explain why Hif2α stabilization increases CB growth and the expansion of TH-positive cell population, and it would also support the use of Hif2 antagonists as potential therapeutic options to prevent CB PGL formation and growth.

CONCLUSIONS AND FUTURE DIRECTIONS

The knowledge of CB physiology and the sensory function of glomus cells have steadily advanced in the last years. In addition to their well-established role as arterial O_2/CO_2 sensors, with a major impact on the regulation of respiration, glomus cells are now considered polymodal receptors with a wide physiological impact and able to detect and integrate changes in numerous chemical and physical variables in the blood. Although the molecular mechanisms underlying glomus cell acute responsiveness to hypoxia have remained elusive, the MMS model summarized in this paper has provided an unprecedented integrated view of glomus cell function that robustly explains most of the data available and, in addition, can be further tested experimentally. The progress in the understanding of the molecular physiology of acute O_2 sensing by glomus cells, the prototypical O_2 sensors, will surely boost advances in the identification and characterization of other acute O_2 sensing cells in the body and in the investigation of their pathophysiological relevance. The MMS has also unraveled novel potential targets for pharmacological modulation of CB output that could be of therapeutic applicability in highly prevalent medical disorders presenting CB dysfunction. A more complete and comprehensive view of CB physiology will surely come from studies focusing on the mechanisms of CB plasticity and their impact on the pathogenesis of human diseases. In parallel, future research should also focus on the elucidation of the molecular bases of glomus cell responsiveness to stimuli, such as changes in blood glucose, lactate or flow, as well as in circulating hormones, which are still poorly known.

AUTHOR CONTRIBUTIONS

PO-S and JL-B prepared the first draft of the manuscript and figures. PO-S, JL-B, AM-D, and LG contributed to the writing of the final version of the paper. All authors contributed to the article and approved the submitted version.

FUNDING

This research was supported by the Spanish Ministries of Science and Innovation and Health (SAF2012-39343 and SAF2016-74990-R) and the European Research Council (ERC-ADGPRJ201502629).

REFERENCES

Amiel, J., Laudier, B., Attie-Bitach, T., Trang, H., de Pontual, L., Gener, B., et al. (2003). Polyalanine expansion and frameshift mutations of the paired-like homeobox gene PHOX2B in congenital central hypoventilation syndrome. *Nat. Genet.* 33, 459–461. doi: 10.1038/ng1130

Annese, V., Navarro-Guerrero, E., Rodriguez-Prieto, I., and Pardal, R. (2017). Physiological plasticity of neural-crest-derived stem cells in the adult mammalian carotid body. *Cell Rep.* 19, 471–478. doi: 10.1016/j.celrep.2017.03.065

Aras, S., Pak, O., Sommer, N., Finley, R. Jr., Huttemann, M., Weissmann, N., et al. (2013). Oxygen-dependent expression of cytochrome c oxidase subunit 4-2 gene expression is mediated by transcription factors RBPJ, CXXC5 and CHCHD2. *Nucleic Acids Res.* 41, 2255–2266. doi: 10.1093/nar/gks1454

Archer, S. L., Sharp, W. W., and Weir, E. K. (2020). Differentiating COVID-19 pneumonia from acute respiratory distress syndrome and high altitude pulmonary edema: therapeutic implications. *Circulation* 142, 101–104. doi: 10.1161/CIRCULATIONAHA.120.047915

Arias-Mayenco, I., Gonzalez-Rodriguez, P., Torres-Torrelo, H., Gao, L., Fernandez-Aguera, M. C., Bonilla-Henao, V., et al. (2018). Acute O_2 sensing: role of coenzyme QH2/Q ratio and mitochondrial ROS compartmentalization. *Cell Metab.* 28, 145–158. doi: 10.1016/j.cmet.2018.05.009

Astrom, K., Cohen, J. E., Willett-Brozick, J. E., Aston, C. E., and Baysal, B. E. (2003). Altitude is a phenotypic modifier in hereditary paraganglioma type 1: evidence for an oxygen-sensing defect. *Hum. Genet.* 113, 228–237. doi: 10.1007/s00439-003-0969-6

Baby, S. M., Gruber, R. B., Young, A. P., Macfarlane, P. M., Teppema, L. J., and Lewis, S. J. (2018). Bilateral carotid sinus nerve transection exacerbates morphine-induced respiratory depression. *Eur. J. Pharmacol.* 834, 17–29. doi: 10.1016/j.ejphar.2018.07.018

Balsa, E., Marco, R., Perales-Clemente, E., Szklarczyk, R., Calvo, E., Landazuri, M. O., et al. (2012). NDUFA4 is a subunit of complex IV of the mammalian electron transport chain. *Cell Metab.* 16, 378–386. doi: 10.1016/j.cmet.2012.07.015

Baysal, B. E. (2008). Clinical and molecular progress in hereditary paraganglioma. *J. Med. Genet.* 45, 689–694. doi: 10.1136/jmg.2008.058560

Benot, A. R., and Lopez-Barneo, J. (1990). Feedback inhibition of Ca^{2+} currents by dopamine in glomus cells of the carotid body. *Eur. J. Neurosci.* 2, 809–812. doi: 10.1111/j.1460-9568.1990.tb00473.x

Buckler, K. J., and Vaughan-Jones, R. D. (1994). Effects of hypoxia on membrane potential and intracellular calcium in rat neonatal carotid body type I cells. *J. Physiol.* 476, 423–428. doi: 10.1113/jphysiol.1994.sp020143

Buckler, K. J., Williams, B. A., and Honore, E. (2000). An oxygen-, acid- and anaesthetic-sensitive TASK-like background potassium channel in rat arterial chemoreceptor cells. *J. Physiol.* 525, 135–142. doi: 10.1111/j.1469-7793.2000.00135.x

Buttigieg, J., Brown, S., Holloway, A. C., and Nurse, C. A. (2009). Chronic nicotine blunts hypoxic sensitivity in perinatal rat adrenal chromaffin cells via upregulation of KATP channels: role of alpha7 nicotinic acetylcholine receptor and hypoxia-inducible factor-2alpha. *J. Neurosci.* 29, 7137–7147. doi: 10.1523/JNEUROSCI.0544-09.2009

Carroll, J., Ding, S., Fearnley, I. M., and Walker, J. E. (2013). Post-translational modifications near the quinone binding site of mammalian complex I. *J. Biol. Chem.* 288, 24799–24808. doi: 10.1074/jbc.M113.488106

Carroll, J., Fearnley, I. M., Skehel, J. M., Shannon, R. J., Hirst, J., and Walker, J. E. (2006). Bovine complex I is a complex of 45 different subunits. *J. Biol. Chem.* 281, 32724–32727. doi: 10.1074/jbc.M607135200

Chen, J., He, L., Liu, X., Dinger, B., Stensaas, L., and Fidone, S. (2007). Effect of the endothelin receptor antagonist bosentan on chronic hypoxia-induced morphological and physiological changes in rat carotid body. *Am. J. Phys. Lung Cell. Mol. Phys.* 292, L1257–L1262. doi: 10.1152/ajplung.00419.2006

Chen, Y., Tipoe, G. L., Liong, E., Leung, S., Lam, S. Y., Iwase, R., et al. (2002). Chronic hypoxia enhances endothelin-1-induced intracellular calcium elevation in rat carotid body chemoreceptors and up-regulates ETA receptor expression. *Pflugers Arch.* 443, 565–573. doi: 10.1007/s00424-001-0728-2

Cheng, X., Prange-Barczynska, M., Fielding, J. W., Zhang, M., Burrell, A. L., Lima, J. D., et al. (2020). Marked and rapid effects of pharmacological HIF-2α antagonism on hypoxic ventilatory control. *J. Clin. Invest.* 130, 2237–2251. doi: 10.1172/JCI133194

Chokshi, R. H., Larsen, A. T., Bhayana, B., and Cotten, J. F. (2015). Breathing stimulant compounds inhibit TASK-3 potassium channel function likely by inding at a common site in the channel pore. *Mol. Pharmacol.* 88, 926–934. doi: 10.1124/mol.115.100107

Colgan, S. P., Furuta, G. T., and Taylor, C. T. (2020). Hypoxia and innate immunity: keeping up with the HIFsters. *Annu. Rev. Immunol.* 38, 341–363. doi: 10.1146/annurev-immunol-100819-121537

Courtney, K. D., Infante, J. R., Lam, E. T., Figlin, R. A., Rini, B. I., Brugarolas, J., et al. (2018). Phase I dose-escalation trial of PT2385, a first-in-class hypoxia-

inducible factor-2α antagonist in patients with previously treated advanced clear cell renal cell carcinoma. *J. Clin. Oncol.* 36, 867–874. doi: 10.1200/JCO.2017.74.2627

Cutz, E., Ma, T. K., Perrin, D. G., Moore, A. M., and Becker, L. E. (1997). Peripheral chemoreceptors in congenital central hypoventilation syndrome. *Am. J. Respir. Crit. Care Med.* 155, 358–363. doi: 10.1164/ajrccm.155.1.9001336

Del Rio, R., Andrade, D. C., Lucero, C., Arias, P., and Iturriaga, R. (2016). Carotid body ablation abrogates hypertension and autonomic alterations induced by intermittent hypoxia in rats. *Hypertension* 68, 436–445. doi: 10.1161/HYPERTENSIONAHA.116.07255

Del Rio, R., Marcus, N. J., and Schultz, H. D. (2013). Carotid chemoreceptor ablation improves survival in heart failure: rescuing autonomic control of cardiorespiratory function. *J. Am. Coll. Cardiol.* 62, 2422–2430. doi: 10.1016/j.jacc.2013.07.079

Diaz-Castro, B., Pintado, C. O., Garcia-Flores, P., Lopez-Barneo, J., and Piruat, J. I. (2012). Differential impairment of catecholaminergic cell maturation and survival by genetic mitochondrial complex II dysfunction. *Mol. Cell. Biol.* 32, 3347–3357. doi: 10.1128/MCB.00128-12

Duchen, M. R., and Biscoe, T. J. (1992a). Mitochondrial function in type I cells isolated from rabbit arterial chemoreceptors. *J. Physiol.* 450, 13–31.

Duchen, M. R., and Biscoe, T. J. (1992b). Relative mitochondrial membrane potential and $[Ca^{2+}]i$ in type I cells isolated from the rabbit carotid body. *J. Physiol.* 450, 33–61.

Ehinger, J. K., Piel, S., Ford, R., Karlsson, M., Sjovall, F., Frostner, E. A., et al. (2016). Cell-permeable succinate prodrugs bypass mitochondrial complex I deficiency. *Nat. Commun.* 7:12317. doi: 10.1038/ncomms12317

Fallah, J., and Rini, B. I. (2019). HIF inhibitors: status of current clinical development. *Curr. Oncol. Rep.* 21:6. doi: 10.1007/s11912-019-0752-z

Fernandez-Aguera, M. C., Gao, L., Gonzalez-Rodriguez, P., Pintado, C. O., Arias-Mayenco, I., Garcia-Flores, P., et al. (2015). Oxygen sensing by arterial chemoreceptors depends on mitochondrial complex I signaling. *Cell Metab.* 22, 825–837. doi: 10.1016/j.cmet.2015.09.004

Fielding, J. W., Hodson, E. J., Cheng, X., Ferguson, D. J. P., Eckardt, L., Adam, J., et al. (2018). PHD2 inactivation in Type I cells drives HIF-2α-dependent multilineage hyperplasia and the formation of paraganglioma-like carotid bodies. *J. Physiol.* 596, 4393–4412. doi: 10.1113/JP275996

Fukuda, R., Zhang, H., Kim, J. W., Shimoda, L., Dang, C. V., and Semenza, G. L. (2007). HIF-1 regulates cytochrome oxidase subunits to optimize efficiency of respiration in hypoxic cells. *Cell* 129, 111–122. doi: 10.1016/j.cell.2007.01.047

Gao, L., Bonilla-Henao, V., Garcia-Flores, P., Arias-Mayenco, I., Ortega-Saenz, P., and Lopez-Barneo, J. (2017). Gene expression analyses reveal metabolic specifications in acute O_2-sensing chemoreceptor cells. *J. Physiol.* 595, 6091–6120. doi: 10.1113/JP274684

Garcia-Fernandez, M., Mejias, R., and Lopez-Barneo, J. (2007). Developmental changes of chromaffin cell secretory response to hypoxia studied in thin adrenal slices. *Pflugers Arch.* 454, 93–100. doi: 10.1007/s00424-006-0186-y

Gaultier, C., Amiel, J., Dauger, S., Trang, H., Lyonnet, S., Gallego, J., et al. (2004). Genetics and early disturbances of breathing control. *Pediatr. Res.* 55, 729–733. doi: 10.1203/01.PDR.0000115677.78759.C5

Gordon, D. E., Jang, G. M., Bouhaddou, M., Xu, J., Obernier, K., White, K. M., et al. (2020). A SARS-CoV-2 protein interaction map reveals targets for drug repurposing. *Nature* 583, 459–468. doi: 10.1038/s41586-020-2286-9

He, L., Chen, J., Dinger, B., Sanders, K., Sundar, K., Hoidal, J., et al. (2002). Characteristics of carotid body chemosensitivity in NADPH oxidase-deficient mice. *Am. J. Phys. Cell Phys.* 282, C27–C33. doi: 10.1152/ajpcell.2002.282.1.C27

Her, Y. F., and Maher, L. J. 3rd. (2015). Succinate dehydrogenase loss in familial paraganglioma: biochemistry, genetics, and epigenetics. *Int. J. Endocrinol.* 2015:296167. doi: 10.1155/2015/296167

Hodson, E. J., Nicholls, L. G., Turner, P. J., Llyr, R., Fielding, J. W., Douglas, G., et al. (2016). Regulation of ventilatory sensitivity and carotid body proliferation in hypoxia by the PHD2/HIF-2 pathway. *J. Physiol.* 594, 1179–1195. doi: 10.1113/JP271050

Huttemann, M., Lee, I., Gao, X., Pecina, P., Pecinova, J., Liu, A. J., et al. (2012). Cytochrome c oxidase subunit 4 isoform 2-knockout mice show reduced enzyme activity, airway hyporeactivity, and lung pathology. *FASEB J.* 26, 3916–3930. doi: 10.1096/fj.11-203273

Johnson, B. D., and Joyner, M. J. (2013). Carotid body denervation: too soon to get breathless about heart failure? *J. Am. Coll. Cardiol.* 62, 2431–2432. doi: 10.1016/j.jacc.2013.08.718

Jonsson, M., Wyon, N., Lindahl, S. G., Fredholm, B. B., and Eriksson, L. I. (2004). Neuromuscular blocking agents block carotid body neuronal nicotinic acetylcholine receptors. *Eur. J. Pharmacol.* 497, 173–180. doi: 10.1016/j.ejphar.2004.06.052

Kadenbach, B., and Huttemann, M. (2015). The subunit composition and function of mammalian cytochrome c oxidase. *Mitochondrion* 24, 64–76. doi: 10.1016/j.mito.2015.07.002

Kang, D., Wang, J., Hogan, J. O., Vennekens, R., Freichel, M., White, C., et al. (2014). Increase in cytosolic Ca^{2+} produced by hypoxia and other depolarizing stimuli activates a non-selective cation channel in chemoreceptor cells of rat carotid body. *J. Physiol.* 592, 1975–1992. doi: 10.1113/jphysiol.2013.266957

Kashani-Poor, N., Zwicker, K., Kerscher, S., and Brandt, U. (2001). A central functional role for the 49-kDa subunit within the catalytic core of mitochondrial complex I. *J. Biol. Chem.* 276, 24082–24087. doi: 10.1074/jbc.M102296200

Kirby, G. C., and McQueen, D. S. (1986). Characterization of opioid receptors in the cat carotid body involved in chemosensory depression *in vivo*. *British J. Pharmacol.* 88, 889–898. doi: 10.1111/j.1476-5381.1986.tb16263.x

Kruse, S. E., Watt, W. C., Marcinek, D. J., Kapur, R. P., Schenkman, K. A., and Palmiter, R. D. (2008). Mice with mitochondrial complex I deficiency develop a fatal encephalomyopathy. *Cell Metab.* 7, 312–320. doi: 10.1016/j.cmet.2008.02.004

Lopez-Barneo, J. (1996). O_2-sensing by ion channels and the regulation of cellular functions. *Trends Neurosci.* 19, 435–440. doi: 10.1016/S0166-2236(96)10050-3

Lopez-Barneo, J., Benot, A., and Ureña, J. (1993). Oxygen sensing and the electrophysiology of arterial chemoreceptor cells. *Physiology* 8, 191–195.

Lopez-Barneo, J., Gonzalez-Rodriguez, P., Gao, L., Fernandez-Aguera, M. C., Pardal, R., and Ortega-Saenz, P. (2016). Oxygen sensing by the carotid body: mechanisms and role in adaptation to hypoxia. *Am. J. Phys. Cell Phys.* 310, C629–C642. doi: 10.1152/ajpcell.00265.2015

Lopez-Barneo, J., Lopez-Lopez, J. R., Urena, J., and Gonzalez, C. (1988). Chemotransduction in the carotid body: K^+ current modulated by PO_2 in type I chemoreceptor cells. *Science* 241, 580–582. doi: 10.1126/science.2456613

Lopez-Barneo, J., and Simon, M. C. (2020). Cellular adaptation to oxygen deficiency beyond the Nobel award. *Nat. Commun.* 11:607. doi: 10.1038/s41467-020-14469-9

Lucarelli, G., Rutigliano, M., Sallustio, F., Ribatti, D., Giglio, A., Lepore Signorile, M., et al. (2018). Integrated multi-omics characterization reveals a distinctive metabolic signature and the role of NDUFA4L2 in promoting angiogenesis, chemoresistance, and mitochondrial dysfunction in clear cell renal cell carcinoma. *Aging* 10, 3957–3985. doi: 10.18632/aging.101685

Macias, D., Cowburn, A. S., Torres-Torrelo, H., Ortega-Saenz, P., Lopez-Barneo, J., and Johnson, R. S. (2018). HIF-2α is essential for carotid body development and function. *elife* 7:e34681. doi: 10.7554/eLife.34681

Macias, D., Fernandez-Aguera, M. C., Bonilla-Henao, V., and Lopez-Barneo, J. (2014). Deletion of the von Hippel-Lindau gene causes sympathoadrenal cell death and impairs chemoreceptor-mediated adaptation to hypoxia. *EMBO Mol. Med.* 6, 1577–1592. doi: 10.15252/emmm.201404153

Mahmoud, A. D., Lewis, S., Juricic, L., Udoh, U. A., Hartmann, S., Jansen, M. A., et al. (2016). AMP-activated protein kinase deficiency blocks the hypoxic ventilatory response and thus precipitates hypoventilation and apnea. *Am. J. Respir. Crit. Care Med.* 193, 1032–1043. doi: 10.1164/rccm.201508-1667OC

Marcus, N. J., Li, Y. L., Bird, C. E., Schultz, H. D., and Morgan, B. J. (2010). Chronic intermittent hypoxia augments chemoreflex control of sympathetic activity: role of the angiotensin II type 1 receptor. *Respir. Physiol. Neurobiol.* 171, 36–45. doi: 10.1016/j.resp.2010.02.003

McBryde, F. D., Abdala, A. P., Hendy, E. B., Pijacka, W., Marvar, P., Moraes, D. J., et al. (2013). The carotid body as a putative therapeutic target for the treatment of neurogenic hypertension. *Nat. Commun.* 4:2395. doi: 10.1038/ncomms3395

Meng, L., Yang, X., Xie, X., and Wang, M. (2019). Mitochondrial NDUFA4L2 protein promotes the vitality of lung cancer cells by repressing oxidative stress. *Thorac. Cancer* 10, 676–685. doi: 10.1111/1759-7714.12984

Millan-Ucles, A., Diaz-Castro, B., Garcia-Flores, P., Baez, A., Perez-Simon, J. A., Lopez-Barneo, J., et al. (2014). A conditional mouse mutant in the tumor suppressor SdhD gene unveils a link between p21(WAF1/Cip1) induction and mitochondrial dysfunction. *PLoS One* 9:e85528. doi: 10.1371/journal.pone.0085528

Mills, E., and Jobsis, F. F. (1972). Mitochondrial respiratory chain of carotid body and chemoreceptor response to changes in oxygen tension. *J. Neurophysiol.* 35, 405–428. doi: 10.1152/jn.1972.35.4.405

Montoro, R., Ureña, J., Fernández-Chacón, R., Alvarez de Toledo, G., and López-Barneo, J. (1996). O_2-sensing by ion channels and chemotransduction in single glomus cells. *J. Gen. Physiol.* 107, 133–143. doi: 10.1085/jgp.107.1.133

Moreno-Dominguez, A., Ortega-Saenz, P., Gao, L., Colinas, O., Garcia-Flores, P., Bonilla-Henao, V., et al. (2020). Acute O_2 sensing through HIF2α-dependent expression of atypical cytochrome oxidase subunits in arterial chemoreceptors. *Sci. Signal.* 13:eaay9452. doi: 10.1126/scisignal.aay9452

Navarro-Guerrero, E., Platero-Luengo, A., Linares-Clemente, P., Cases, I., Lopez Barneo, J., and Pardal, R. (2016). Gene expression profiling supports the neural crest origin of adult rodent carotid body stem cells and identifies CD10 as a marker for mesectoderm-committed progenitors. *Stem Cells* 34, 1637–1650. doi: 10.1002/stem.2331

Niewinski, P., Janczak, D., Rucinski, A., Tubek, S., Engelman, Z. J., Piesiak, P., et al. (2017). Carotid body resection for sympathetic modulation in systolic heart failure: results from first-in-man study. *Eur. J. Heart Fail.* 19, 391–400. doi: 10.1002/ejhf.641

Nurse, C. (2014). Synaptic and paracrine mechanisms at carotid body arterial chemoreceptors. *J. Physiol.* 592, 3419–3426. doi: 10.1113/jphysiol.2013.269829

Obeso, A., Almaraz, L., and González, C. (1989). Effects of cyanide and uncouplers on chemoreceptor activity and ATP content of the cat carotid body. *Brain Res.* 481, 250–257. doi: 10.1016/0006-8993(89)90801-9

Ortega-Saenz, P., and Lopez-Barneo, J. (2020). Physiology of the carotid body: from molecules to disease. *Annu. Rev. Physiol.* 82, 127–149. doi: 10.1146/annurev-physiol-020518-114427

Ortega-Saenz, P., Macias, D., Levitsky, K. L., Rodriguez-Gomez, J. A., Gonzalez-Rodriguez, P., Bonilla-Henao, V., et al. (2016). Selective accumulation of biotin in arterial chemoreceptors: requirement for carotid body exocytotic dopamine secretion. *J. Physiol.* 594, 7229–7248. doi: 10.1113/JP272961

Ortega-Saenz, P., Pardal, R., Garcia-Fernandez, M., and Lopez-Barneo, J. (2003). Rotenone selectively occludes sensitivity to hypoxia in rat carotid body glomus cells. *J. Physiol.* 548, 789–800. doi: 10.1113/jphysiol.2003.039693

Ortega-Saenz, P., Pascual, A., Gomez-Diaz, R., and Lopez-Barneo, J. (2006). Acute oxygen sensing in heme oxygenase-2 null mice. *J. Gen. Physiol.* 128, 405–411. doi: 10.1085/jgp.200609591

Paciga, M., Vollmer, C., and Nurse, C. (1999). Role of ET-1 in hypoxia-induced mitosis of cultured rat carotid body chemoreceptors. *Neuroreport* 10, 3739–3744. doi: 10.1097/00001756-199912160-00003

Pajuelo Reguera, D., Cunatova, K., Vrbacky, M., Pecinova, A., Houstek, J., Mracek, T., et al. (2020). Cytochrome c oxidase subunit 4 isoform exchange results in modulation of oxygen affinity. *Cells* 9:443. doi: 10.3390/cells 9020443

Pardal, R., Ludewig, U., Garcia-Hirschfeld, J., and Lopez-Barneo, J. (2000). Secretory responses of intact glomus cells in thin slices of rat carotid body to hypoxia and tetraethylammonium. *Proc. Natl. Acad. Sci. U. S. A.* 97, 2361–2366.

Pardal, R., Ortega-Saenz, P., Duran, R., and Lopez-Barneo, J. (2007). Glia-like stem cells sustain physiologic neurogenesis in the adult mammalian carotid body. *Cell* 131, 364–377. doi: 10.1016/j.cell.2007.07.043

Pascual, A., Hidalgo-Figueroa, M., Piruat, J. I., Pintado, C. O., Gomez-Diaz, R., and Lopez-Barneo, J. (2008). Absolute requirement of GDNF for adult catecholaminergic neuron survival. *Nat. Neurosci.* 11, 755–761. doi: 10.1038/nn.2136

Paton, F. R., Sobotka, A., Fudim, M., Engelman, J., Hart, C. J., McBryde, D., et al. (2013). The carotid body as a therapeutic target for the treatment of sympathetically mediated diseases. *Hypertension* 61, 5–13. doi: 10.1161/HYPERTENSIONAHA.111.00064

Peers, C. (1990). Hypoxic suppression of K^+ currents in type I carotid body cells: selective effect on the $Ca^{2(+)}$-activated K^+ current. *Neurosci. Lett.* 119, 253–256. doi: 10.1016/0304-3940(90)90846-2

Peng, Y. J., Gridina, A., Wang, B., Nanduri, J., Fox, A. P., and Prabhakar, N. R. (2020). Olfactory receptor 78 participates in carotid body response to a wide range of low O_2 levels but not to severe hypoxia. *J. Neurophysiol.* 123, 1886–1895. doi: 10.1152/jn.00075.2020

Peng, Y. J., Nanduri, J., Khan, S. A., Yuan, G., Wang, N., Kinsman, B., et al. (2011). Hypoxia-inducible factor 2α (HIF-2α) heterozygous-null mice exhibit exaggerated carotid body sensitivity to hypoxia, breathing instability, and hypertension. *Proc. Natl. Acad. Sci. U. S. A.* 108, 3065–3070. doi: 10.1073/pnas.1100064108

Pijacka, W., Katayama, P. L., Salgado, H. C., Lincevicius, G. S., Campos, R. R., McBryde, F. D., et al. (2018). Variable role of carotid bodies in cardiovascular responses to exercise, hypoxia and hypercapnia in spontaneously hypertensive rats. *J. Physiol.* 596, 3201–3216. doi: 10.1113/JP275487

Pijacka, W., Moraes, D. J., Ratcliffe, L. E., Nightingale, A. K., Hart, E. C., da Silva, M. P., et al. (2016). Purinergic receptors in the carotid body as a new drug target for controlling hypertension. *Nat. Med.* 22, 1151–1159. doi: 10.1038/nm.4173

Piruat, J. I., Pintado, C. O., Ortega-Saenz, P., Roche, M., and Lopez-Barneo, J. (2004). The mitochondrial SDHD gene is required for early embryogenesis, and its partial deficiency results in persistent carotid body glomus cell activation with full responsiveness to hypoxia. *Mol. Cell. Biol.* 24, 10933–10940. doi: 10.1128/MCB.24.24.10933-10940.2004

Platero-Luengo, A., Gonzalez-Granero, S., Duran, R., Diaz-Castro, B., Piruat, J. I., Garcia-Verdugo, J. M., et al. (2014). An O_2-sensitive glomus cell-stem cell synapse induces carotid body growth in chronic hypoxia. *Cell* 156, 291–303. doi: 10.1016/j.cell.2013.12.013

Pokorski, M., and Lahiri, S. (1981). Effects of naloxone on carotid body chemoreception and ventilation in the cat. *J. Appl. Physiol. Respir. Environ. Exerc. Physiol.* 51, 1533–1538. doi: 10.1152/jappl.1981.51.6.1533

Porzionato, A., Macchi, V., Stecco, C., and De Caro, R. (2013). The carotid body in sudden infant death syndrome. *Respir. Physiol. Neurobiol.* 185, 194–201. doi: 10.1016/j.resp.2012.05.013

Protti, A. (2018). Succinate and the shortcut to the cure of metformin-induced lactic acidosis. *Intensive Care Med. Exp.* 6:35. doi: 10.1186/s40635-018-0202-5

Rakoczy, R. J., and Wyatt, C. N. (2018). Acute oxygen sensing by the carotid body: a rattlebag of molecular mechanisms. *J. Physiol.* 596, 2969–2976. doi: 10.1113/JP274351

Ratcliffe, P. J. (2013). Oxygen sensing and hypoxia signalling pathways in animals: the implications of physiology for cancer. *J. Physiol.* 591, 2027–2042. doi: 10.1113/jphysiol.2013.251470

Ribeiro, M. J., Sacramento, J. F., Gallego-Martin, T., Olea, E., Melo, B. F., Guarino, M. P., et al. (2018). High fat diet blunts the effects of leptin on ventilation and on carotid body activity. *J. Physiol.* 596, 3187–3199. doi: 10.1113/JP275362

Ribeiro, M. J., Sacramento, J. F., González, C., Guarino, M. P., Monteiro, E. C., and Conde, S. V. (2013). Carotid body denervation prevents the development of insulin resistance and hypertension induced by hypercaloric diets. *Diabetes* 62, 2905–2291. doi: 10.2337/db12-1463

Rieger, B., Shalaeva, D. N., Sohnel, A. C., Kohl, W., Duwe, P., Mulkidjanian, A. Y., et al. (2017). Lifetime imaging of GFP at CoxVIIIa reports respiratory supercomplex assembly in live cells. *Sci. Rep.* 7:46055. doi: 10.1038/srep46055

Rong, W., Gourine, A. V., Cockayne, D. A., Xiang, Z., Ford, A. P., Spyer, K. M., et al. (2003). Pivotal role of nucleotide P2X2 receptor subunit of the ATP-gated ion channel mediating ventilatory responses to hypoxia. *J. Neurosci.* 23, 11315–11321. doi: 10.1523/JNEUROSCI.23-36-11315.2003

Roozekrans, M., Olofsen, E., Van Der Schrier, R., Van Gerven, J., Peng, S., Mcleod, J., et al. (2015). Reversal of opioid-induced respiratory depression by BK-channel blocker GAL021: a pharmacokinetic-pharmacodynamic modeling study in healthy volunteers. *Clin. Pharmacol. Ther.* 97, 641–649. doi: 10.1002/cpt.99

Schultz, H. D., Marcus, N. J., and Del Rio, R. (2013). Role of the carotid body in the pathophysiology of heart failure. *Curr. Hypertens. Rep.* 15, 356–362. doi: 10.1007/s11906-013-0368-x

Selak, M. A., Armour, S. M., Mackenzie, E. D., Boulahbel, H., Watson, D. G., Mansfield, K. D., et al. (2005). Succinate links TCA cycle dysfunction to oncogenesis by inhibiting HIF-alpha prolyl hydroxylase. *Cancer Cell* 7, 77–85. doi: 10.1016/j.ccr.2004.11.022

Semenza, G. L. (2014). Oxygen sensing, hypoxia-inducible factors, and disease pathophysiology. *Annu. Rev. Pathol.* 9, 47–71. doi: 10.1146/annurev-pathol-012513-104720

Shirahata, M., Balbir, A., Otsubo, T., and Fitzgerald, R. S. (2007). Role of acetylcholine in neurotransmission of the carotid body. *Respir. Physiol. Neurobiol.* 157, 93–105. doi: 10.1016/j.resp.2006.12.010

Smith, E. H., Janknecht, R., and Maher, L. J. 3rd. (2007). Succinate inhibition of alpha-ketoglutarate-dependent enzymes in a yeast model of paraganglioma. *Hum. Mol. Genet.* 16, 3136–3148. doi: 10.1093/hmg/ddm275

Smith, J. A., Kitt, M. M., Morice, A. H., Birring, S. S., McGarvey, L. P., Sher, M. R., et al. (2020). Gefapixant, a P2X3 receprtor antagonist, for the treatment of refractory or unexplained chornic cough: a ramdomised, double blind, controlled, parallel-group, phase 2b trial. *Lancet Respir. Med.* 8, 775–785. doi: 10.1016/S2213-2600(19)30471-0

Sobrino, V., Gonzalez-Rodriguez, P., Annese, V., Lopez-Barneo, J., and Pardal, R. (2018). Fast neurogenesis from carotid body quiescent neuroblasts accelerates adaptation to hypoxia. *EMBO Rep.* 19:e44598. doi: 10.15252/embr.201744598

Sommer, N., Huttemann, M., Pak, O., Scheibe, S., Knoepp, F., Sinkler, C., et al. (2017). Mitochondrial complex IV subunit 4 isoform 2 is essential for acute pulmonary oxygen sensing. *Circ. Res.* 121, 424–438. doi: 10.1161/CIRCRESAHA.116.310482

Taylor, S. C., Shaw, S. M., and Peers, C. (2000). Mitochondrial inhibitors evoke catecholamine release from pheochromocytoma cells. *Biochem. Biophys. Res. Commun.* 273, 17–21. doi: 10.1006/bbrc.2000.2894

Tello, D., Balsa, E., Acosta-Iborra, B., Fuertes-Yebra, E., Elorza, A., Ordonez, A., et al. (2011). Induction of the mitochondrial NDUFA4L2 protein by HIF-1alpha decreases oxygen consumption by inhibiting complex I activity. *Cell Metab.* 14, 768–779. doi: 10.1016/j.cmet.2011.10.008

Tian, H., Hammer, R. E., Matsumoto, A. M., Russell, D. W., and Mcknight, S. L. (1998). The hypoxia-responsive transcription factor EPAS1 is essential for catecholamine homeostasis and protection against heart failure during embryonic development. *Genes Dev.* 12, 3320–3324. doi: 10.1101/gad.12.21.3320

Timmers, H. J., Karemaker, J. M., Wieling, W., Marres, H. A., Folgering, H. T., and Lenders, J. W. (2003). Baroreflex and chemoreflex function after bilateral carotid body tumor resection. *J. Hypertens.* 21, 591–599. doi: 10.1097/00004872-200303000-00026

Tobin, M. J., Laghi, F., and Jubran, A. (2020). Why COVID-19 silent hypoxemia is baffling to physicians. *Am. J. Respir. Crit. Care Med.* 202, 356–360. doi: 10.1164/rccm.202006-2157CP

Torres-Torrelo, H., Ortega-Saenz, P., Macias, D., Omura, M., Zhou, T., Matsunami, H., et al. (2018). The role of Olfr78 in the breathing circuit of mice. *Nature* 561, E33–E40. doi: 10.1038/s41586-018-0545-9

Tsukihara, T., Aoyama, H., Yamashita, E., Tomizaki, T., Yamaguchi, H., Shinzawa-Itoh, K., et al. (1996). The whole structure of the 13-subunit oxidized cytochrome c oxidase at 2.8 A. *Science* 272, 1136–1144. doi: 10.1126/science.272.5265.1136

Urena, J., Fernandez-Chacon, R., Benot, A. R., Alvarez De Toledo, G. A., and Lopez-Barneo, J. (1994). Hypoxia induces voltage-dependent Ca^{2+} entry and quantal dopamine secretion in carotid body glomus cells. *Proc. Natl. Acad. Sci. U. S. A.* 91, 10208–10211.

Varas, R., Wyatt, C. N., and Buckler, K. J. (2007). Modualtion of TASK-like background potassium channels in rat arterial chemoreceptor cells by intracellular ATP and other nucelotides. *J. Physiol.* 583, 521–536. doi: 10.1113/jphysiol.2007.135657

Villadiego, J., Mendez-Ferrer, S., Valdes-Sanchez, T., Silos-Santiago, I., Farinas, I., Lopez-Barneo, J., et al. (2005). Selective glial cell line-derived neurotrophic factor production in adult dopaminergic carotid body cells in situ and after intrastriatal transplantation. *J. Neurosci.* 25, 4091–4098. doi: 10.1523/JNEUROSCI.4312-04.2005

Wang, J., Hogan, J. O., Wang, R., White, C., and Kim, D. (2017). Role of cystathionine-gamma-lyase in hypoxia-induced changes in TASK activity, intracellular $[Ca^{(2+)}]$ and ventilation in mice. *Respir. Physiol. Neurobiol.* 246, 98–106. doi: 10.1016/j.resp.2017.08.009

Wang, Y., Li, Z., Zhang, X., Xiang, X., Li, Y., Mulholland, M. W., et al. (2016). Nesfatin-1 promotes brown adipocyte phenotype. *Sci. Rep.* 6:34747. doi: 10.1038/srep34747

Wang, Z. Y., Olson, E. B. Jr., Bjorling, D. E., Mitchell, G. S., and Bisgard, G. E. (2008). Sustained hypoxia-induced proliferation of carotid body type I cells in rats. *J. Appl. Physiol.* 104, 803–808. doi: 10.1152/japplphysiol.00393.2007

Waypa, G. B., Marks, J. D., Guzy, R., Mungai, P. T., Schriewer, J., Dokic, D., et al. (2010). Hypoxia triggers subcellular compartmental redox signaling in vascular smooth muscle cells. *Circ. Res.* 106, 526–535. doi: 10.1161/CIRCRESAHA.109.206334

Weir, E. K., Lopez-Barneo, J., Buckler, K. J., and Archer, S. L. (2005). Acute oxygen-sensing mechanisms. *New Engl. J. Med.* 353, 2042–2055. doi: 10.1056/NEJMra050002

Wilson, D. F., Mokashi, A., Chugh, D., Vinogradov, S., Osanai, S., and Lahiri, S. (1994). The primary oxygen sensor of the cat carotid body is cytochrome a3 of the mitochondrial respiratory chain. *FEBS Lett.* 351, 370–374. doi: 10.1016/0014-5793(94)00887-6

Wu, M., Gu, J., Guo, R., Huang, Y., and Yang, M. (2016). Structure of mammalian respiratory supercomplex I1III2IV1. *Cell* 167, 1598–1609. doi: 10.1016/j.cell.2016.11.012

Wyatt, C. N., and Buckler, K. J. (2004). The effect of mitochondrial inhibitors on membrane currents in isolated neonatal rat carotid body type I cells. *J. Physiol.* 556, 175–191. doi: 10.1113/jphysiol.2003.058131

Xu, J., Tse, F. W., and Tse, A. (2003). ATP triggers intracellular Ca^{2+} release in type II cells of the rat carotid body. *J. Physiol.* 549, 739–747. doi: 10.1113/jphysiol.2003.039735

Zhang, M., Piskuric, N. A., Vollmer, C., and Nurse, C. A. (2012). P2Y2 receptor activation opens pannexin-1 channels in rat carotid body type II cells: potential role in amplifying the neurotransmitter ATP. *J. Physiol.* 590, 4335–4350. doi: 10.1113/jphysiol.2012.236265

Zhang, M., Vollmer, C., and Nurse, C. A. (2018). Adenosine and dopamine oppositely modulate a hyperpolarization-activated current Ih in chemosensory neurons of the rat carotid body in co-culture. *J. Physiol.* 596, 3101–3117. doi: 10.1113/JP274743

Zhang, M., Zhong, H., Vollmer, C., and Nurse, C. A. (2000). Co-release of ATP and ACh mediates hypoxic signalling at rat carotid body chemoreceptors. *J. Physiol.* 525, 143–158. doi: 10.1111/j.1469-7793.2000.t01-1-00143.x

Zhong, H., Zhang, M., and Nurse, C. A. (1997). Synapse formation and hypoxic signalling in co-cultures of rat petrosal neurones and carotid body type 1 cells. *J. Physiol.* 503, 599–612. doi: 10.1111/j.1469-7793.1997.599bg.x

Zhou, T., Chien, M. S., Kaleem, S., and Matsunami, H. (2016). Single cell transcriptome analysis of mouse carotid body glomus cells. *J. Physiol.* 594, 4225–4251. doi: 10.1113/JP271936

Conflict of Interest: The authors declare that the research was conducted in the absence of any commercial or financial relationships that could be construed as a potential conflict of interest.

frontiers in Physiology

ORIGINAL RESEARCH
published: 24 February 2021
doi: 10.3389/fphys.2021.573385

Baseline Arterial CO_2 Pressure Regulates Acute Intermittent Hypoxia-Induced Phrenic Long-Term Facilitation in Rats

Raphael R. Perim, Mohamed El-Chami, Elisa J. Gonzalez-Rothi and Gordon S. Mitchell*

Department of Physical Therapy, McKnight Brain Institute, Center for Respiratory Research and Rehabilitation, University of Florida, Gainesville, FL, United States

Moderate acute intermittent hypoxia (mAIH) elicits a progressive increase in phrenic motor output lasting hours post-mAIH, a form of respiratory motor plasticity known as phrenic long-term facilitation (pLTF). mAIH-induced pLTF is initiated by activation of spinally-projecting raphe serotonergic neurons during hypoxia and subsequent serotonin release near phrenic motor neurons. Since raphe serotonergic neurons are also sensitive to pH and CO_2, the prevailing arterial CO_2 pressure ($PaCO_2$) may modulate their activity (and serotonin release) during hypoxic episodes. Thus, we hypothesized that changes in background $PaCO_2$ directly influence the magnitude of mAIH-induced pLTF. mAIH-induced pLTF was evaluated in anesthetized, vagotomized, paralyzed and ventilated rats, with end-tidal CO_2 (i.e., a $PaCO_2$ surrogate) maintained at: (1) ≤39 mmHg (hypocapnia); (2) ∼41 mmHg (normocapnia); or (3) ≥48 mmHg (hypercapnia) throughout experimental protocols. Although baseline phrenic nerve activity tended to be lower in hypocapnia, short-term hypoxic phrenic response, i.e., burst amplitude ($\Delta = 5.1 \pm 1.1$ μV) and frequency responses ($\Delta = 21 \pm 4$ bpm), was greater than in normocapnic ($\Delta = 3.6 \pm 0.6$ μV and 8 ± 4, respectively) or hypercapnic rats ($\Delta = 2.0 \pm 0.6$ μV and -2 ± 2, respectively), followed by a progressive increase in phrenic burst amplitude (i.e., pLTF) for at least 60 min post mAIH. pLTF in the hypocapnic group ($\Delta = 4.9 \pm 0.6$ μV) was significantly greater than in normocapnic ($\Delta = 2.8 \pm 0.7$ μV) or hypercapnic rats ($\Delta = 1.7 \pm 0.4$ μV). In contrast, although hypercapnic rats also exhibited significant pLTF, it was attenuated versus hypocapnic rats. When pLTF was expressed as percent change from maximal chemoreflex stimulation, all pairwise comparisons were found to be statistically significant ($p < 0.05$). We conclude that elevated $PaCO_2$ undermines mAIH-induced pLTF in anesthetized rats. These findings contrast with well-documented effects of $PaCO_2$ on ventilatory LTF in awake humans.

Keywords: acute intermittent hypoxia, phrenic long-term facilitation, respiratory plasticity, $PaCO_2$, phrenic activity

OPEN ACCESS

Edited by:
Richard James Wilson, University of Calgary, Canada

Reviewed by:
Vincent Joseph, Laval University, Canada
Julian Paton, University of Bristol, United Kingdom

****Correspondence:***
Raphael R. Perim
r.perimr@gmail.com;
rperim@phhp.ufl.edu

Specialty section:
This article was submitted to Respiratory Physiology, a section of the journal Frontiers in Physiology

Received: *16 June 2020*
Accepted: *02 February 2021*
Published: *24 February 2021*

Citation:
Perim RR, El-Chami M, Gonzalez-Rothi EJ and Mitchell GS (2021) Baseline Arterial CO_2 Pressure Regulates Acute Intermittent Hypoxia-Induced Phrenic Long-Term Facilitation in Rats. Front. Physiol. 12:573385. doi: 10.3389/fphys.2021.573385

INTRODUCTION

One of the most well-studied forms of respiratory motor plasticity is phrenic long-term facilitation (pLTF), characterized by a progressive increase in phrenic burst amplitude following moderate acute intermittent hypoxia (mAIH; Hayashi et al., 1993; Baker-Herman and Mitchell, 2002; Baker-Herman et al., 2004). During hypoxic episodes, carotid body neural network are activated, including brainstem neurons of the caudal, spinally-projecting raphe nuclei (Holtman et al., 1986; Pilowsky et al., 1990; Erickson and Millhorn, 1991, 1994; Morris et al., 1996). These raphe neurons release serotonin in the ventral spinal cord, including the phrenic motor nucleus (Kinkead et al., 2001), thereby activating spinal serotonin type 2 receptors that initiate an intracellular signaling cascade giving rise to pLTF (MacFarlane and Mitchell, 2009; Tadjalli and Mitchell, 2019).

Raphe serotonergic neurons are also activated directly by increased CO_2 and/or decreased pH (Hodges and Richerson, 2010; Teran et al., 2014). On the other hand, hypercapnia amplifies carotid body hypoxic chemo-sensitivity (Lahiri and DeLaney, 1975; Kumar and Prabhakar, 2012), increasing synaptic inputs to raphe neurons. Thus, one might predict greater activation and serotonin-release from raphe neurons during hypoxia with a background of hypercapnia versus hypocapnia. Since both hypoxia (indirect) and CO_2 (direct and indirect) modulate raphe serotonergic neuron activity, mAIH-induced pLTF expression may depend, at least in part, on the prevailing arterial CO_2 pressure ($PaCO_2$). The impact of background $PaCO_2$ on pLTF has never been systematically investigated in anesthetized rats, although it's impact on ventilatory LTF has been investigated extensively in humans (Harris et al., 2006; Syed et al., 2013; Tester et al., 2014).

mAIH-induced pLTF was first demonstrated in anesthetized, vagotomized, paralyzed and ventilated rats (Hayashi et al., 1993). Although not formally tested, the authors acknowledged that pLTF magnitude was greater when background $PaCO_2$ was closer to the CO_2 recruitment threshold, defined as the lowest end-tidal CO_2 causing resumption of inspiratory phrenic bursts after hypocapnia-induced apnea. Since then, the existence of pLTF has been verified in many studies, typically with end-tidal CO_2 regulated 2–3 mmHg above the recruitment threshold (Fuller et al., 2000; Baker-Herman and Mitchell, 2008). However, in several studies, anesthetized and spontaneously breathing rats failed to elicit diaphragm LTF (Janssen and Fregosi, 2000; Cao and Ling, 2010). These authors attributed the lack of diaphragm LTF either to: (1) hypercapnia inherent in spontaneously breathing, anesthetized rats (Janssen and Fregosi, 2000), and/or (2) the specific anesthetic or paralytic drugs used (Cao and Ling, 2010). Conversely, unanesthetized, spontaneously breathing rats exhibit robust ventilatory and/or diaphragm long-term facilitation (Olson et al., 2001; McGuire et al., 2008; Nakamura et al., 2010; Terada and Mitchell, 2011; Navarrete-Opazo and Mitchell, 2014a), demonstrating that normocapnic (versus hypercapnic) spontaneous breathing is compatible with LTF expression.

The main objective of the present study was to evaluate the effect of background $PaCO_2$ on pLTF in the "standard" anesthetized and ventilated rat preparation. Contrary to expectations, we report that mAIH-induced pLTF is inversely correlated with baseline $PaCO_2$ in rats, unlike humans (Harris et al., 2006; Syed et al., 2013; Tester et al., 2014). Possible factors contributing to CO_2 interactions with pLTF, and differences between humans and rats are discussed. Our findings increase understanding of the diverse factors regulating pLTF expression. An understanding of these factors is essential to properly design future experiments, and for the translation of AIH-induced motor plasticity as a therapeutic modality to treat neuromuscular disorders that compromise respiratory and non-respiratory movements (Dale et al., 2014; Gonzalez-Rothi et al., 2015).

MATERIALS AND METHODS

Animals

All experiments were approved by the University of Florida Institutional Animal Care and Use Committee (protocol #201408657). Adult male Sprague Dawley rats (329–415 g; 208A Colony, Envigo; IN, United States) were housed in pairs under standard conditions with 12:12-h light/dark cycle and free access to food and water. Sample sizes were estimated based on our extensive experience with this experimental preparation and knowledge of expected variance.

Surgical Procedures

All surgical procedures have been previously described (Perim et al., 2018, 2019, 2020a,b). Rats were anesthetized in an acrylic chamber with 3% isoflurane in 3 L/min O_2. They were weighed and transferred to a heated surgical table to regulate body temperature at 37.5 ± 1°C throughout experiments. Anesthesia was maintained with 3% isoflurane in 60% inspired O_2 delivered through a nose cone. Additional inspired CO_2 was added to keep end-tidal CO_2 constant at target levels depending on the experimental group (see below).

Rats were tracheotomized with a 1 cm polyethylene catheter (I.D., 1.67 mm) for mechanical ventilation [0.007 × mass (g), ∼2.5 mL tidal volume; ∼70 breaths/min; VentElite small animal ventilator; Harvard Apparatus, Holliston, MA, United States]. Urethane (2.1 g/kg, 6 mL/hour) was administered through a tail vein catheter (24 Gauge; Surflash, Somerset, NJ, United States) while slowly reducing isoflurane until conversion was complete. Both vagus nerves were isolated and cut ∼1 cm caudal to thyroid cartilage. The right femoral artery was exposed and cannulated with a polyethylene catheter (I.D., 0.58 mm) to monitor blood pressure (Argon Pressure Transducer, DTXPlus, Plano, TX, United States) and sample arterial blood for blood gas analysis using heparinized capillary tubes (60 μL per blood sample; ABL 90 Flex, Radiometer, OH, United States).

Approximately 1 cm of the phrenic nerve was isolated near the brachial plexus, cut distally and partially de-sheathed to record electrical activity using suction electrodes. Signal was acquired at 25 kHz sampling frequency, amplified (1,000x), band-pass filtered (0.3–5 kHz) and digitalized using a differential amplifier (Model 1700, A-M Systems; Sequim, WA, United States) and an analog/digital converter (CED 1401; Cambridge Electronic

Design, Cambridge, United Kingdom). Data were stored on a computer, rectified and smoothed with 50 ms time constant using Spike2 software (version 8.18; Cambridge Electronic Design; Cambridge, United Kingdom). Rats received the neuromuscular paralytic, pancuronium bromide (3 mg/kg, i.v., Sigma-Aldrich; Saint Louis, MO, United States), to eliminate spontaneous breathing efforts. Adequate anesthetic depth was confirmed by absence of withdrawal reflex or blood pressure response (i.e., after paralysis) to toe pinch. Fluids were administered intravenously (0.5–2.5 mL/h; 1:4 solution of 8.4% sodium bicarbonate mixed in standard lactated Ringer's solution) to maintain acid-base balance.

Experimental Design

Rats were randomly assigned to one of three groups: (1) Hypocapnia: end-tidal CO_2 was maintained $\leq$ 39 mmHg during surgical procedures, and adjusted to ensure minimal rhythmic respiratory activity during baseline conditions as indicated by an unstable bursting pattern typically observed before a hypocapnia-induced apnea (**Figure 3**). End-tidal CO_2 adjustments were made based on visual inspection of phrenic neurogram by an experienced investigator; (2) Normocapnia: end-tidal CO_2 was maintained ∼41 mmHg throughout experiments. This level, based on previous studies, is ∼2 mmHg above the CO_2 recruitment threshold (Perim et al., 2019, 2020a); (3) Hypercapnia: end-tidal CO_2 was maintained ≥48 mmHg throughout experiments, corresponding to an average $PaCO_2$ of ∼50 mmHg.

The mAIH protocol consisted of 3, 5-min hypoxic episodes (0.14 inspired O_2 fraction) with 5-minute intervals (0.60 inspired O_2 fraction). Targeted PaO_2 during the last minute of hypoxic episodes was 35 to 55 mmHg; inspired O_2 fraction was adjusted as necessary to remain within this range. Phrenic nerve activity was monitored for at least 60 min post-mAIH, while maintaining $PaCO_2$, standard base excess and temperature at baseline values. At the end of experiments, all rat groups were exposed to maximal chemoreflex stimulation, consisting of hypoxia (0.10 inspired O_2 fraction) combined with hypercapnia (0.07 inspired CO_2 fraction) to assess maximal phrenic nerve activity.

Data Analyses

Phrenic nerve activity was rectified and smoothed (0.05 s time constant) for off-line analyses. Peak phrenic burst amplitude and frequency were averaged over 1 min immediately before blood samples were taken at baseline, during the first hypoxic episode, and at 30 and 60 min post-mAIH. Data were analyzed using absolute values. We published a meta-analysis comparing absolute values of integrated phrenic nerve activity across groups and conclude that it is highly repeatable when adequate precautions are taken (Nichols and Mitchell, 2016), including adequate experimenter experience/skill, consistent electrode properties and recording setup. Experiments were only considered in the analysis if: (1) $PaCO_2$ ± 1.5 mmHg and mean arterial pressure ± 30 mmHg relative to baseline; (2) PaO_2 was > 150 mmHg during baseline and post-mAIH, and within the predefined range during hypoxia; and (3) the phrenic response to maximal chemoreceptor stimulation was greater than during hypoxic episodes. In total, 1 rat from normocapnic and 1 rat from the hypercapnic group were not considered for analysis based on the latter exclusion criteria. Normal distribution of residual errors was confirmed by visual inspection of histograms and normal probability plots. A one-way ANOVA was used to compare mean response among groups. Pairwise comparisons were carried out when appropriate using Fisher's Least Significant Difference *post hoc* test. Values are expressed as mean ± 1 standard error of the mean. An alpha-level of 0.05 was used to assess statistical significance for all comparisons. All analyses were carried out using R Version 3.4.2 (R Core Team, Vienna, Austria).

RESULTS

Figure 1A shows average phrenic burst amplitude and frequency throughout the mAIH protocol. This form of data presentation provides a thorough examination of the outcome, which often leads to identification of group-specific trends not considered in *a priori* defined analyses. For example: (1) all groups reached similar absolute phrenic burst amplitudes 60 min post-mAIH, despite different background respiratory drive (i.e., as indicated by $PaCO_2$); (2) the hypercapnic group had a blunted burst frequency response during hypoxia, which remained below baseline levels following mAIH. This burst frequency response pattern during mAIH was not expected based on previous studies from our laboratory (Fuller et al., 2000; Baker-Herman and Mitchell, 2008) and was clearly not observed in hypocapnic or normocapnic groups. A correlation between frequency LTF and baseline burst frequency has been noted before (Baker-Herman and Mitchell, 2008). **Figure 1B** shows group-representative phrenic neurograms, and **Table 1** describes blood gases and mean arterial pressure throughout the protocol.

Group average end-tidal CO_2 during baseline is presented in **Figure 2A**. After baseline, the end-tidal CO_2 trace is omitted since it was used only as a guide to help maintain isocapnia. Typically, end-tidal CO_2 was ∼2 mmHg below baseline $PaCO_2$. During and post mAIH, isocapnia was determined by $PaCO_2$ analysis (**Figure 2B**). There was a significant group effect of $PaCO_2$ ($p < 0.001$), but no effect of time ($p = 0.43$) or time × group interaction ($p = 0.35$) detected by mixed two-way ANOVA. Pairwise comparisons of group main effect showed that $PaCO_2$ in the hypocapnic group was lower versus normocapnic ($p = 0.0218$) or hypercapnic groups ($p < 0.001$); and lower in the normocapnic versus hypercapnic group ($p < 0.001$). Because $PaCO_2$ is a major determinant of respiratory depth and rate, phrenic burst amplitude and frequency progressively increase with $PaCO_2$ as expected (**Figures 2C,D**). Although one-way ANOVA did not reach statistical significance for baseline phrenic burst amplitude among groups ($p = 0.08$), this result was affected by an outlier in the hypocapnic group, confirmed by a two-tailed Grubb's test ($p = 0.0014$). When this outlier was no longer considered in the analysis, the ANOVA was highly significant ($p = 0.0078$). Then, pairwise comparisons showed that phrenic burst amplitude in the hypocapnic group was lower than in normocapnic ($p = 0.0066$) and hypercapnic groups ($p = 0.0046$).

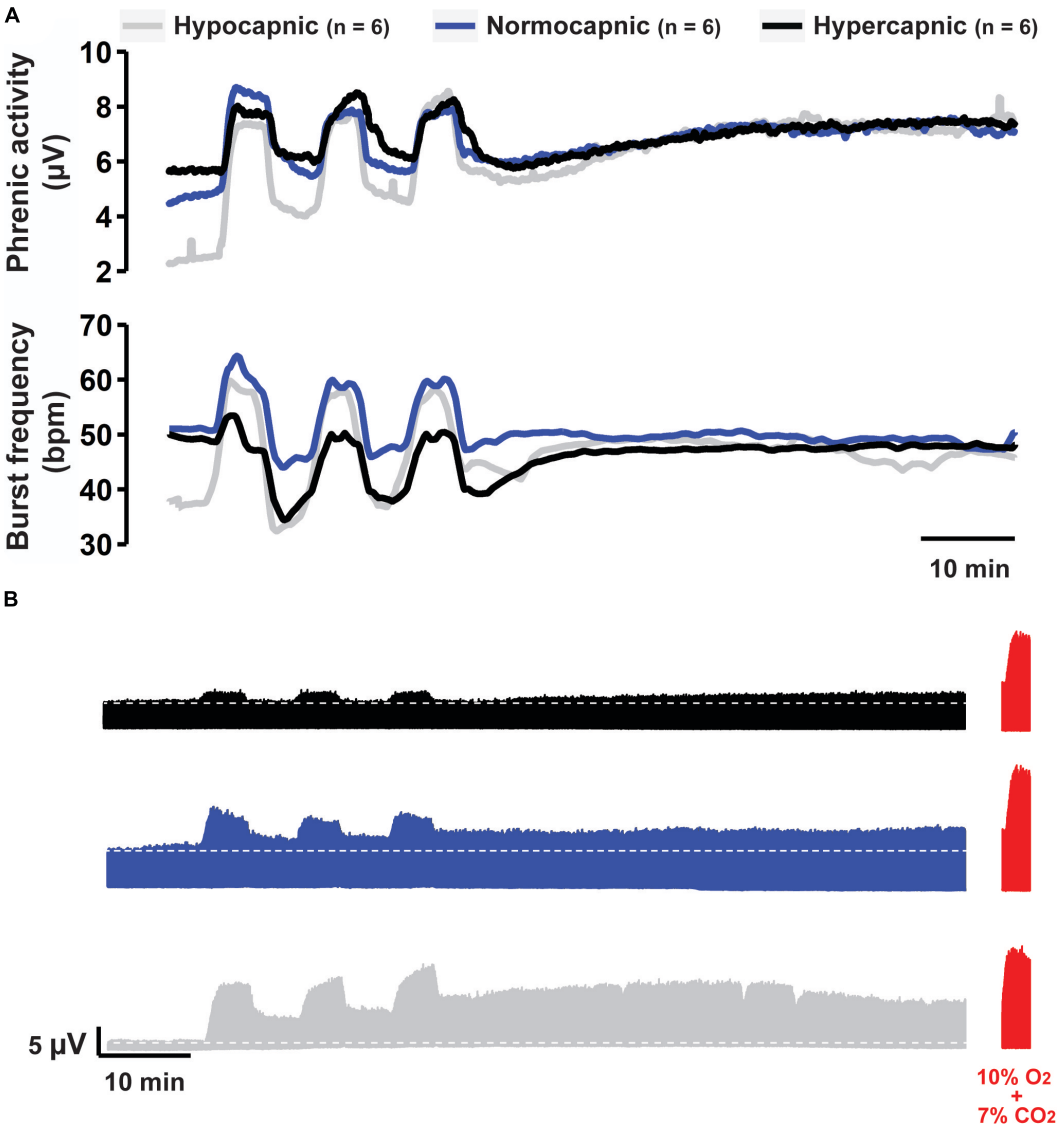

FIGURE 1 | Overall summary of our findings. **(A)** Average traces of phrenic activity (top) and burst frequency (bottom) throughout the mAIH protocol from rat groups kept under constant hypocapnia (gray line), normocapnia (blue line) or hypercapnia (black line). **(B)** Group-representative phrenic neurograms during mAIH protocol. At the end of each experiment (shown in red), maximal phrenic output was assessed with 10% oxygen plus 7% CO_2 (i.e., maximal chemoreflex stimulation, MCS).

Similarly, baseline frequency was significantly reduced in the hypocapnic versus normocapnic (p = 0.0048) and hypercapnic groups (p = 0.0019).

Poincaré plots indicate that there is considerable variability between consecutive phrenic burst intervals (i.e., BBn versus BBn + 1) in the hypocapnic group (**Figure 3A**). On the other hand, normocapnic and hypercapnic groups presented more symmetrical phrenic burst intervals during baseline (**Figures 3B,C**). Visual inspection of group-representative baseline phrenic activity also indicates unstable pattern with low $PaCO_2$ (**Figure 3D**). The oscillation between consecutive phrenic burst intervals was quantified by SD1 measure of short-term variability (Poincaré cloud width). Group average SD1 tended to be higher in hypocapnic rats (**Figure 3E**), but did not reach statistical significance in one-way ANOVA (p = 0.052). Increased variability in consecutive burst intervals during hypocapnia provide evidence of unstable breathing at low respiratory drive. $PaCO_2$ was just sufficient to maintain rhythmic bursting in the hypocapnic group.

The short-term hypoxic phrenic response, expressed as absolute phrenic burst amplitude (μV) was similar among groups (**Figure 4A**), despite different baseline values (**Figures 1A**, **2D**). A better approach under this condition is to assess hypoxic phrenic response as a change in phrenic activity from baseline (Δ from baseline), since it accounts for differences in background activity. The hypoxic phrenic response expressed this way

TABLE 1 | Stability of blood samples and mean arterial pressure (MAP) among experimental groups throughout the moderate acute intermittent hypoxia protocol (mAIH).

	Experimental groups		
	Hypocapnic	**Normocapnic**	**Hypercapnic**
PaO_2, mmHg	(*n* = 6)	(*n* = 6)	(*n* = 6)
Baseline	313 ± 10	287 ± 16	269 ± 15
Hx	43.9 ± 2*	41.2 ± 1*	42.6 ± 2*
30	256 ± 18	280 ± 12	236 ± 16
60	282 ± 14	276 ± 12	263 ± 12
$PaCO_2$, mmHg			
Baseline	41.9 ± 1.1	43.9 ± 0.7	54.1 ± 0.5
Hx	41.0 ± 1.4	44.3 ± 0.7	52.8 ± 0.8
30	42.1 ± 1.5	45.4 ± 0.9	51.9 ± 1.5
60	42.4 ± 1.2	44.6 ± 0.9	54.6 ± 0.9
sBE, mmol/L			
Baseline	2.2 ± 1.1	2.4 ± 0.7	2.2 ± 0.4
Hx	−0.2 ± 0.6	0.7 ± 0.9	0.3 ± 0.7
30	−0.3 ± 1.1	0.6 ± 1.3	1.0 ± 0.8
60	0.8 ± 1.2	0.3 ± 0.8	2.5 ± 0.6
Ph			
Baseline	7.41 ± 0.01	7.40 ± 0.01	7.33 ± 0.00
Hx	7.39 ± 0.01	7.38 ± 0.01	7.31 ± 0.00
30	7.37 ± 0.01	7.36 ± 0.02	7.33 ± 0.01
60	7.39 ± 0.01	7.37 ± 0.01	7.33 ± 0.01
ctHb, g/dL			
Baseline	16.4 ± 0.2	16.6 ± 0.2	16.0 ± 0.1
Hx	15.8 ± 0.2	16.3 ± 0.0	15.8 ± 0.2
30	15.6 ± 0.4	16.3 ± 0.2	15.1 ± 0.4
60	15.6 ± 0.3	15.7 ± 0.2	15.4 ± 0.3
MAP, mmHg			
Baseline	120 ± 7	144 ± 3	133 ± 5
Hx	83 ± 9*	104 ± 6*	111 ± 13*
30	110 ± 6	122 ± 4	126 ± 5
60	117 ± 7	124 ± 4	136 ± 6

Asterisks indicate significant differences in PaO_2 and MAP relative to baseline values ($p < 0.05$). ANOVA indicated that only group main effect was significant ($p < 0.001$); pairwise comparisons of group main effect show that $PaCO_2$ is lowest in the hypocapnic followed by normocapnic and then the hypercapnic rats.

was higher in hypocapnic versus hypercapnic rats ($p = 0.03$; **Figure 4B**). Burst frequency during hypoxic episodes showed a similar pattern. The hypocapnic and normocapnic groups tended to present higher hypoxic frequency responses to hypoxia versus hypercapnia when expressed in absolute values ($p = 0.075$ and $p = 0.01$, respectively), although only normocapnic versus hypercapnic comparison was significant (**Figure 4C**). Analyzed as a change from baseline, the frequency response was higher in hypocapnia versus normocapnia ($p = 0.045$) and hypercapnia ($p = 0.001$, **Figure 4D**).

Mixed two-way ANOVA with phrenic burst amplitude as dependent variable shows significant interaction between group and time ($p = 0.0025$). Pairwise comparisons within groups indicate that phrenic burst amplitude was elevated at 60 min post-mAIH in all groups relative to baseline, demonstrating development of pLTF ($p < 0.05$; **Figures 1A**, **5A**). However, pLTF magnitude varied substantially among groups. In hypocapnia, the change in phrenic burst amplitude versus baseline at 60 min post-mAIH was significantly higher than in normocapnia ($p = 0.039$) or hypercapnia ($p = 0.001$; **Figure 5B**). Linear regression analysis showed a significant negative correlation between baseline $PaCO_2$ and pLTF ($R^2 = 0.28$, $p = 0.014$; **Figure 5C**). The correlation between the hypoxic phrenic response and pLTF 60 min post-mAIH did not reach statistical significance ($R^2 = 0.17$, $p = 0.052$; **Figure 5D**). The association between hypoxic phrenic response and pLTF magnitude has been assessed in two meta-analysis from our laboratory and a positive correlation was found in both studies. Thus, we used Bayesian inference (rjags package) to account for relevant prior information when interpreting p-values (Fuller et al., 2000; Baker-Herman and Mitchell, 2008), in accordance with recent statistical guidelines (Kennedy-Shaffer, 2019; Wasserstein et al., 2019). The 95% confidence intervals (0.4 and 0.5) of the Bayesian regression line slope indicated a positive correlation between hypoxic phrenic response and pLTF magnitude.

Although pLTF is often reported as percent change from baseline, we intentionally omitted data normalized in this way since baseline phrenic burst amplitude was different among groups; thus, results based on normalized data would be misleading, reflecting baseline versus pLTF changes. Average frequency change at 60 min post-mAIH tended to be higher in hypocapnia, but this small difference was not statistically significant ($p = 0.22$; **Figure 5E**).

Phrenic response to maximal chemoreflex stimulation showed a consistent pattern across analytical approaches. There were no significant differences in phrenic burst amplitude (absolute values) between groups (one-way ANOVA, $p = 0.53$; **Figure 6A**). Although significant differences were not found when phrenic response to maximal chemoreflex stimulation was expressed as a change from 60 min post-mAIH (one-way ANOVA, $p = 0.110$; **Figure 6B**), trends became significant when expressed as percent change in phrenic activity versus pre-stimulation values (one-way ANOVA, $p = 0.006$; data not shown), with lowest values found in the hypercapnic group. Interestingly, pLTF magnitude quantified as percent change from maximal chemoreflex stimulation was lower in hypocapnic rats, followed by normocapnic and then hypercapnic group ($p < 0.05$; **Figure 6C**), demonstrating that our results are not an artifact of phrenic neurogram saturation or changes in baseline due to the different background $PaCO_2$ levels. There was a significant correlation between phrenic activity during maximal chemoreflex activation and pLTF ($R^2 = 0.45$, $p = 0.001$; **Figure 6D**).

DISCUSSION

Contrary to expectations, mAIH-induced pLTF is greater with background $PaCO_2$ levels near the CO_2 apneic threshold; pLTF decreases as background $PaCO_2$ is increased in anesthetized rats. Short-term hypoxic phrenic response (both burst amplitude and frequency) was also greater in hypocapnia, which confirms previously published meta-analyses of large data sets, suggesting

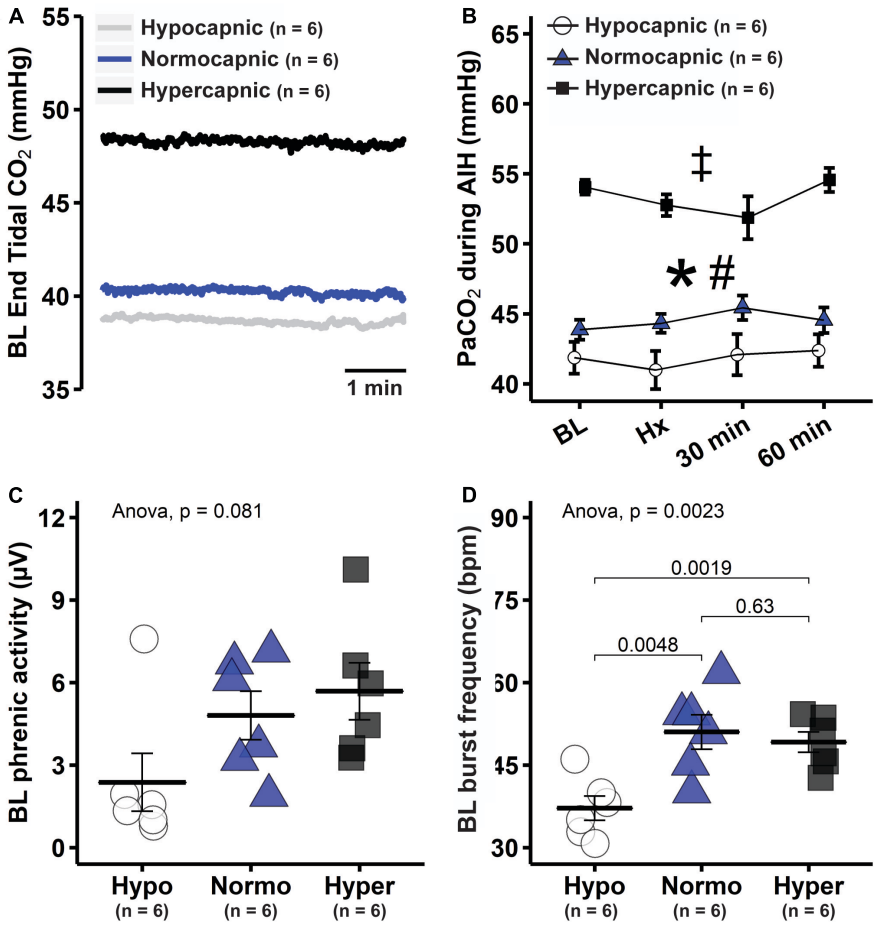

FIGURE 2 | Reduced background $PaCO_2$ in hypocapnic rats led to lower baseline respiratory activity. **(A)** Group average end-tidal CO_2 traces during baseline. **(B)** Average $PaCO_2$ at specific time points during mAIH protocol in hypocapnic, normocapnic and hypercapnic groups. ANOVA indicated that only group main effect was significant ($p < 0.001$); pairwise comparisons of group main effect show that $PaCO_2$ is lowest in the hypocapnic followed by normocapnic and then the hypercapnic rats. *, significant differences between hypocapnic and normocapnic group; #, significant differences between normocapnic and hypercapnic group; ‡, significant differences between hypocapnic and hypercapnic group. **(C)** Group average baseline phrenic burst amplitude. **(D)** Group average phrenic burst frequency. Data are presented as mean ± standard error of the mean.

that short-term hypoxic phrenic response is a strong predictor of pLTF magnitude (Fuller et al., 2000; Baker-Herman and Mitchell, 2008). Since this response was enhanced with lower background $PaCO_2$ in the present study, it may help explain increased pLTF magnitude during hypocapnia.

Raphe serotonergic neuron activation during mAIH triggers serotonin release into the phrenic motor nucleus (Kinkead et al., 2001), initiating a serotonin receptor type 2-dependent signaling cascade to pLTF (Tadjalli and Mitchell, 2019). Thus, one key determinant of pLTF is the extent of AIH-induced raphe serotonergic neuron activation. Since conditions that mitigate serotonergic neuron activity during hypoxia are expected to undermine pLTF, the present results were unexpected.

Raphe serotonergic neurons are CO_2 sensitive, responding rapidly to increased CO_2 or decreased pH (Hodges and Richerson, 2010; Teran et al., 2014). Since raphe neurons decrease their activity with hypocapnia (Nuding et al., 2015), they may have a greater relative increase in (but lower level of) activity in response to hypoxia at low background $PaCO_2$ levels. Further, hypoxia and CO_2 are synergistic in their actions on carotid body chemoreceptors (Lahiri and DeLaney, 1975), predicting greater absolute raphe neuron activity and serotonin release in relative hypercapnia, although the physiological impact of serotonin release during hypoxia may be greatest at low background $PaCO_2$ levels. Several lines of evidence suggest that episodic (not continuous) serotonin release is a more relevant stimulus to synaptic plasticity (Carew et al., 1972; Clark and Kandel, 1993; Emptage and Carew, 1993; Baker et al., 2001; MacFarlane and Mitchell, 2009), and that low-dose serotonin is a more potent stimulus to phrenic motor plasticity (MacFarlane and Mitchell, 2009). Thus, episodic raphe serotonergic neuron activation in a low (hypocapnic) versus high (hypercapnic) range may elicit greater mAIH-induced pLTF based on the dose-response relationship between phrenic motor facilitation and serotonin release. However, it is unknown whether serotonergic raphe neuron responses to mAIH vary with the prevailing

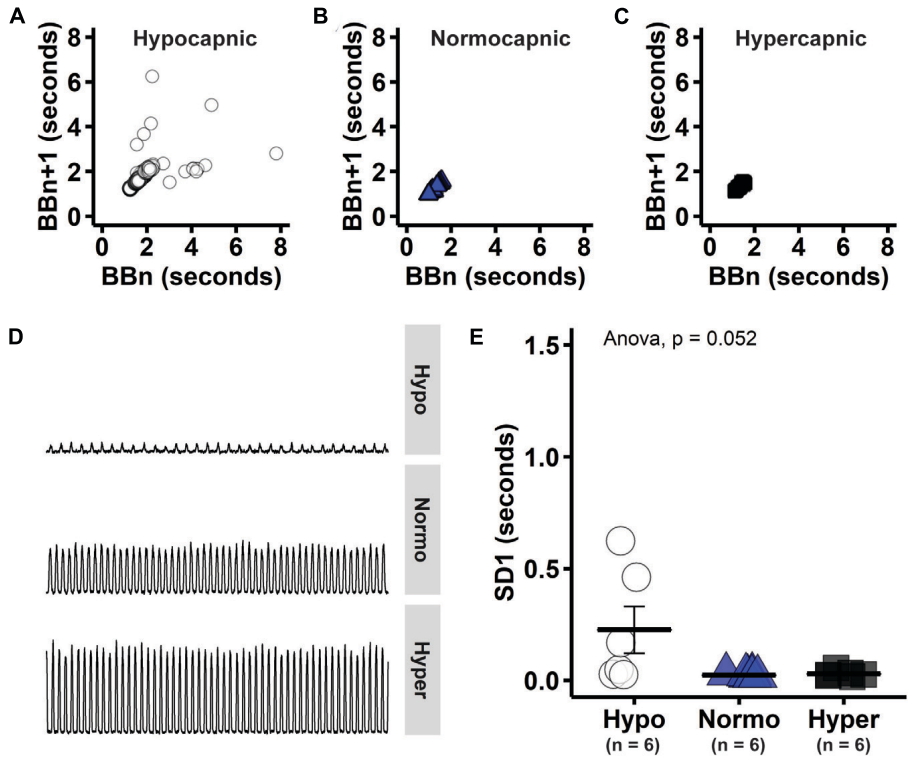

FIGURE 3 | Consecutive phrenic burst intervals tended to be more variable in hypocapnic group, consistent with unstable breathing that is expected near CO_2 apneic threshold. **(A–C)** Consecutive phrenic burst intervals (i.e., BBn versus BBn + 1) in hypocapnic, normocapnic and hypercapnic group, respectively. **(D)** Group-representative baseline phrenic activity. **(E)** Measure of Poincaré length that indicates long-term variability (SD1).

brain tissue CO_2 level. From a very different perspective, the impact of background $PaCO_2$ on mAIH-induced pLTF may arise from the integrative properties of phrenic motor neurons. Accumulating evidence suggests that mAIH elicits plasticity within phrenic motor neurons *per se* (Devinney et al., 2015; Dale et al., 2017). Whether the hypocapnia increases mAIH-induced pLTF magnitude *via* differential regulation of raphe serotonergic neurons was not tested in the present study. This possibility deserves further investigation.

In some experimental preparations, a negative interaction between central (hypercapnia) and peripheral chemoreceptors (hypoxia) has been reported (Day and Wilson, 2008, 2009). For example, phrenic responses to isolated carotid body hypoxia are enhanced when the brainstem is independently perfused with 25 versus 50 mmHg $PaCO_2$ (Day and Wilson, 2007). If this finding mirrors increased short-term hypoxic phrenic response and raphe neuron activation in hypocapnic rats, it is consistent with augmented short-term hypoxic phrenic response and pLTF in hypocapnic rats, as found here. An augmented hypoxic response of brainstem respiratory neurons in hypocapnia might produce greater serotonergic neuron activation and pLTF *via* indirect projections from brainstem ventral respiratory group neurons to midline raphe (Morris et al., 1996).

In a previous report, baseline $PaCO_2$ was suggested (not demonstrated) to impact pLTF expression (Hayashi et al., 1993). Interestingly, diaphragm LTF was not observed when mAIH was applied in anesthetized, spontaneously breathing rats (Janssen and Fregosi, 2000). These authors suggested that this absence of diaphragm LTF was likely due to the presence of hypercapnia characteristic of anesthetized, spontaneously breathing rats. Accordingly, subsequent studies demonstrating robust AIH-induced ventilatory and/or diaphragm LTF in unanesthetized, spontaneously breathing and normocapnic rats (Olson et al., 2001; McGuire et al., 2008; Nakamura et al., 2010; Terada and Mitchell, 2011; Navarrete-Opazo and Mitchell, 2014a) are consistent with the idea that baseline $PaCO_2$, and not spontaneous breathing *per se* suppressed diaphragm LTF. We acknowledge that other factors may have been involved, such as the specific anesthetic used. For example, Cao and Ling (2010) reported genioglossus LTF in spontaneously breathing rats anesthetized with a chloralose/urethane mixture, but not urethane alone.

Although mAIH-induced phrenic motor plasticity is primarily expressed as an increase in phrenic burst amplitude in rats (Hayashi et al., 1993; Baker-Herman et al., 2004; Baker-Herman and Mitchell, 2008; Nakamura et al., 2010; Terada and Mitchell, 2011; Perim and Mitchell, 2019), small increases in post-mAIH burst frequency have been reported (Baker-Herman and Mitchell, 2008). In a meta-analysis, baseline phrenic burst frequency was inversely correlated with the magnitude (and sign) of frequency LTF; frequency changes within hypoxic episodes, and pLTF magnitude are also positively correlated with frequency LTF.

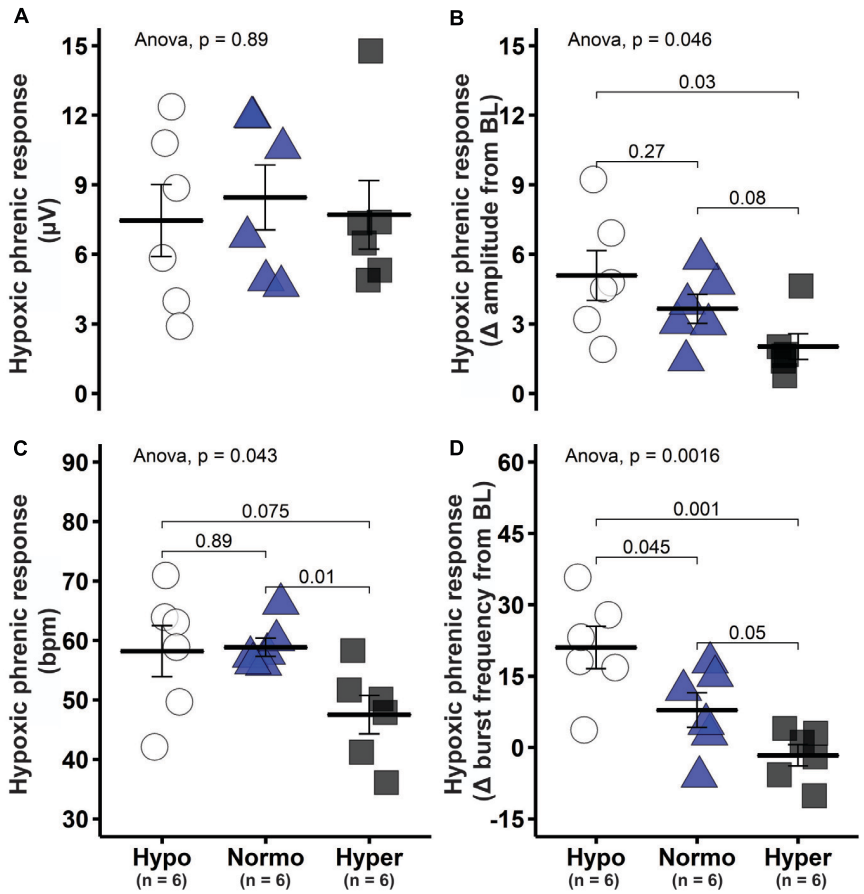

FIGURE 4 | Short-term hypoxic phrenic response was enhanced in the hypocapnic group. **(A)** Group average short-term hypoxic phrenic response in absolute burst amplitude values. **(B)** Group average short-term hypoxic phrenic response as delta burst amplitude from baseline. **(C)** Group average short-term hypoxic phrenic response in absolute burst frequency values. **(D)** Group average short-term hypoxic phrenic response as delta burst frequency from baseline. Data are presented as mean ± standard error of the mean.

Nevertheless, since frequency LTF is less than 20% of pLTF amplitude in anesthetized rats (Baker-Herman and Mitchell, 2008), it is not surprising that only a non-significant trend toward frequency LTF occurs in hypocapnic rats.

Unlike most prior studies from our group using this same experimental preparation, the CO_2 apneic/recruitment threshold was not determined in the present study. The CO_2 recruitment threshold is an important reference condition adopted in most studies from our laboratory to normalize respiratory activity among rats within and across studies. We intentionally omitted this procedure here since our main goal was to investigate background CO_2 effects on pLTF and, therefore, we hoped to minimize influences from other variables. For example, prolonged or repetitive central neural apnea is sufficient to trigger a distinct, interacting form of respiratory motor plasticity known as inactivity-induced phrenic motor facilitation which, although phenotypically similar to pLTF, occurs *via* distinct mechanisms (Strey et al., 2012; Baertsch and Baker-Herman, 2015; Baertsch and Baker, 2017). Brief repetitive apneas, leading to inactivity-induced phrenic motor facilitation, constrain mAIH-induced pLTF in rats (Fields et al., 2019). Although the apnea protocols most often used to elicit inactivity-induced phrenic motor facilitation are different in pattern and duration from our apnea/recruitment threshold determination (Strey et al., 2012; Baertsch and Baker-Herman, 2015; Baertsch and Baker, 2017), the impact of apneic/recruitment threshold determination on pLTF magnitude is simply not known.

Multiple brain regions have chemoreceptor neurons, including the retrotrapezoid nucleus (Mulkey et al., 2004), nucleus tractus solitaries (Dean et al., 1990), locus coeruleus (Pineda and Aghajanian, 1997) and hypothalamus (Dillon and Waldrop, 1992). Phox2b-expressing retrotrapezoid neurons and raphe serotonergic neurons project throughout the respiratory network and contribute to maximal chemoreflex stimulated phrenic responses (Severson et al., 2003; Mulkey et al., 2004; Corcoran et al., 2013). Although retrotrapezoid neurons have intrinsic CO_2/pH sensitivity, part of their chemosensitivity appears to result from serotonergic neuronal inputs (Wu et al., 2019). Thus, enhanced phrenic responses to maximal chemoreflex activation in hypocapnia may be explained by reduced pre-stimulus raphe neuron activity (i.e., low $PaCO_2$), leading to greater relative activity changes during maximal chemoreflex activation.

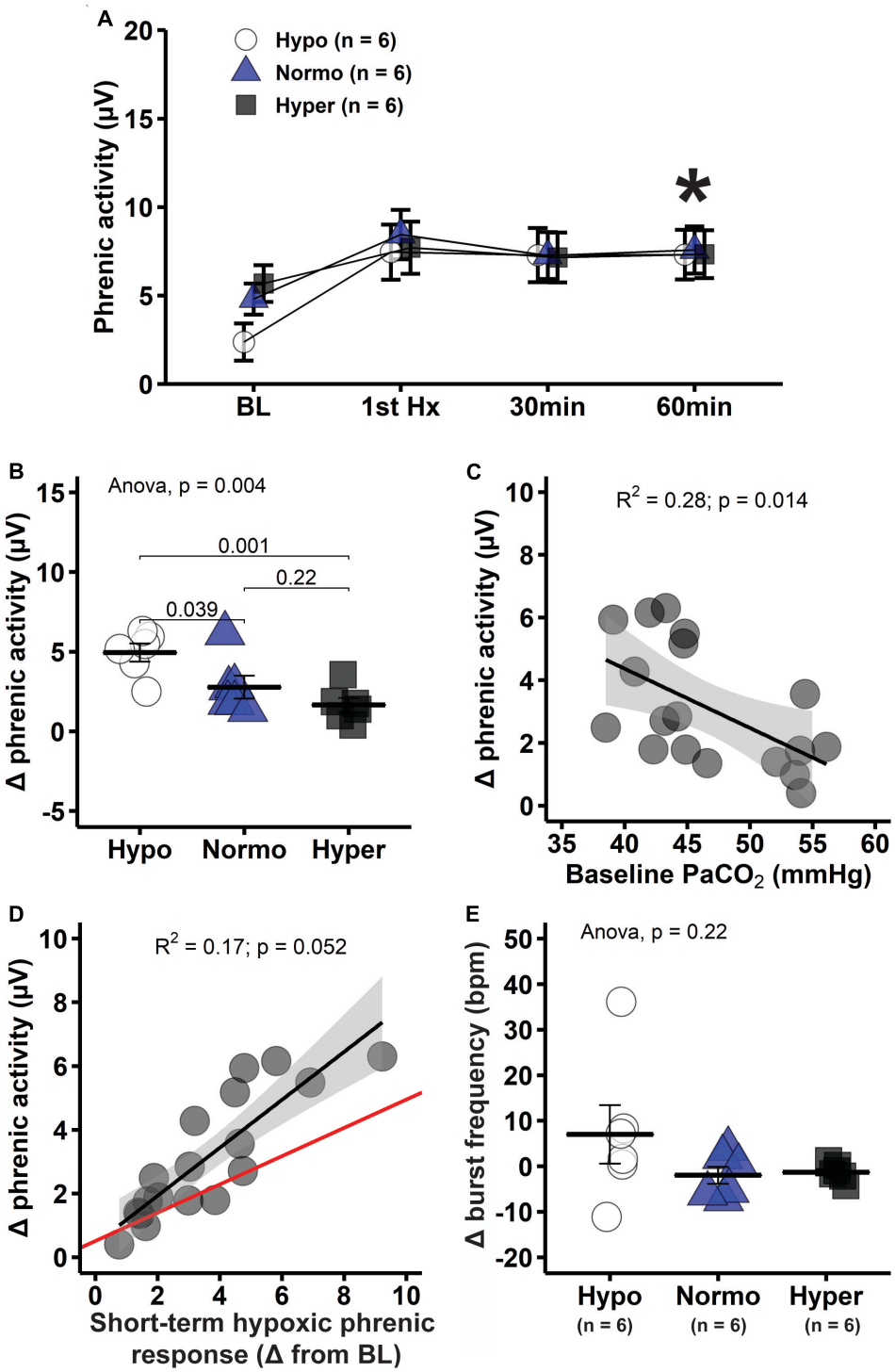

FIGURE 5 | Hypocapnic rats presented the greatest pLTF, which decreases progressively with increasing $PaCO_2$. **(A)** Average phrenic burst amplitude at specific times during mAIH protocol. Asterisk indicates significant differences at 60 min post-mAIH compared to baseline within hypocapnic, normocapnic and hypercapnic group (mixed ANOVA; $p = 0.002514$ for group × time interaction). **(B)** Average change in phrenic burst amplitude from baseline to 60 min post-mAIH. **(C)** Linear regression between baseline $PaCO_2$ and change in phrenic burst amplitude from baseline to 60 min post-mAIH. **(D)** Linear regression between short-term hypoxic phrenic response and change in phrenic burst amplitude from baseline to 60 min post-mAIH. Bayesian regression line (red) describes the association between short-term hypoxic phrenic response and pLTF magnitude, taking into account prior data from our laboratory (Fuller et al., 2000; Baker-Herman and Mitchell, 2008). The 95% confidence interval of the regression slope was 0.4 and 0.5. **(E)** Average change in phrenic burst frequency from baseline to 60 min post-mAIH. Data are presented as mean ± standard error of the mean.

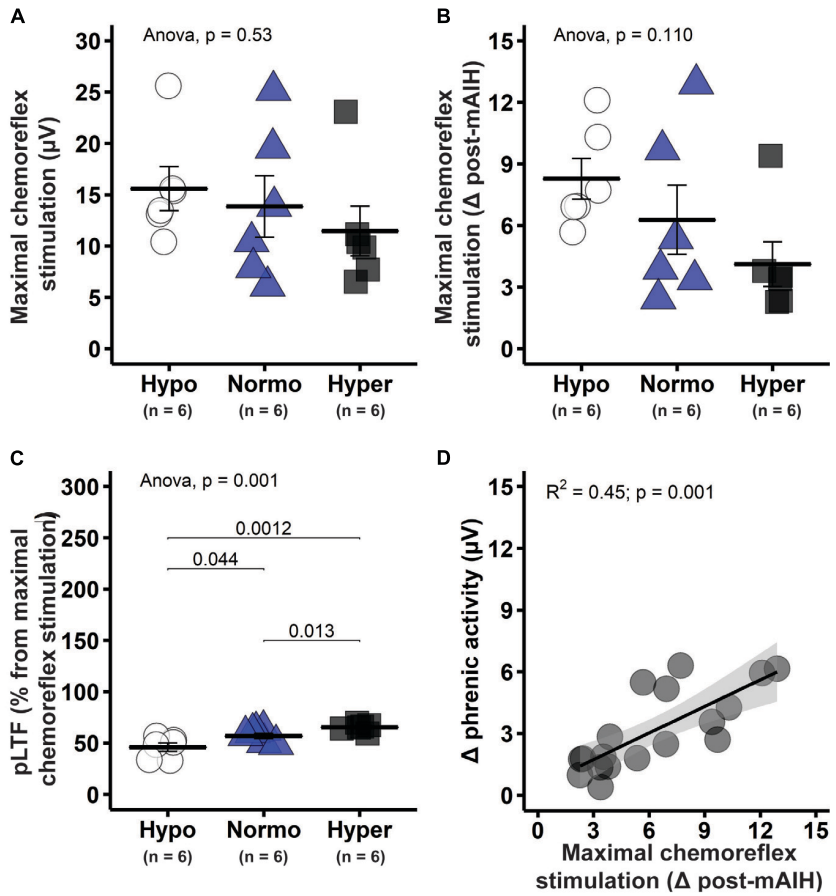

FIGURE 6 | Maximal chemoreflex stimulation (MCS) tended to be greater in hypocapnic rats, suggesting enhanced capacity following mAIH. **(A)** Group average phrenic response to maximal chemoreflex stimulation in absolute burst amplitude values. **(B)** Average phrenic response to maximal chemoreflex stimulation as delta burst amplitude from 60 min post-mAIH (pre-stimulus level). **(C)** Average magnitude of phrenic long-term facilitation (pLTF) as percent from maximal chemoreflex stimulation. **(D)** Linear regression between phrenic response to maximal chemoreflex stimulation [data from panel **(B)**] and delta phrenic burst amplitude from baseline to 60 min post-mAIH. Data are presented as mean ± standard error of the mean.

In awake humans, AIH-induced ventilatory LTF occurs in healthy individuals and in people with obstructive sleep apnea or spinal cord injury, but only if baseline $PaCO_2$ is elevated by ∼2 mmHg (Harris et al., 2006; Lee et al., 2009; Gerst et al., 2011; Tester et al., 2014). The need for supplemental CO_2 in humans is in direct contrast with our results in anesthetized paralyzed and ventilated rats. It is not known if this discrepancy is due to species or technical issues. However, a negative correlation between baseline ventilation and ventilatory long-term facilitation has been reported (Gerst et al., 2011), suggesting a negative CO_2 influence at more extreme levels. Ventilatory LTF is often expressed in humans without supplemental CO_2 during sleep, where $PaCO_2$ is elevated by loss of the "wakefulness drive" (Babcock and Badr, 1998; Shkoukani et al., 2002; Babcock et al., 2003; Mateika and Sandhu, 2011).

Here, we demonstrate that background $PaCO_2$ level is a key factor that can influence the capacity to elicit mAIH-induced pLTF expression. At $PaCO_2$ levels barely sufficient to maintain rhythmic phrenic activity, both the short-term hypoxic phrenic response and pLTF are enhanced. These findings increase our understanding of factors regulating pLTF. Greater understanding of respiratory motor plasticity is relevant in at least 2 translationally relevant contexts: (1) it increases our understanding about non-respiratory motor systems and their response to AIH (Lovett-Barr et al., 2012; Prosser-Loose et al., 2015), and (2) it guides/refines our ability to harness repetitive mAIH as a therapeutic modality to treat breathing and other movement disorders during devastating traumatic, ischemic, infectious and/or neurodegenerative disorders that compromise movements, including breathing (Mitchell, 2007; Dale et al., 2014; Navarrete-Opazo and Mitchell, 2014b; Gonzalez-Rothi et al., 2015).

DATA AVAILABILITY STATEMENT

The original contributions presented in the study are included in the article/supplementary material, further inquiries can be directed to the corresponding author/s.

ETHICS STATEMENT

The animal study was reviewed and approved by University of Florida Institutional Animal Care and Use Committee.

AUTHOR CONTRIBUTIONS

RP and ME-C performed the experiments and analyzed the data. Statistical analyses were performed by RP. RP and GM interpreted the results of the experiments. RP prepared the figures and drafted the manuscript. ME-C, EG-R, and GM revised the manuscript for intellectual content. RP, ME-C, EG-R, and GM approved the final version of the manuscript. All authors contributed to the article and approved the submitted version.

FUNDING

Sources of Funding: Support provided by NIH HL148030, Craig H. Neilsen Foundation SCIRTS Pilot Research Grant #476951 and the University of Florida McKnight Brain Institute.

REFERENCES

Babcock, M. A., and Badr, M. S. (1998). Long-term facilitation of ventilation in humans during NREM sleep. *Sleep* 21, 709–716.

Babcock, M., Shkoukani, M., Aboubakr, S. E., and Badr, M. S. (2003). Determinants of long-term facilitation in humans during NREM sleep. *J. Appl. Physiol.* 94, 53–59. doi: 10.1152/japplphysiol.00476.2002

Baertsch, N. A., and Baker, T. L. (2017). Intermittent apnea elicits inactivity-induced phrenic motor facilitation via a retinoic acid- and protein synthesis-dependent pathway. *J. Neurophysiol.* 118, 2702–2710. doi: 10.1152/jn.00212.2017

Baertsch, N. A., and Baker-Herman, T. L. (2015). Intermittent reductions in respiratory neural activity elicit spinal TNF-alpha-independent, atypical PKC-dependent inactivity-induced phrenic motor facilitation. *Am. J. Physiol. Regul. Integr. Comp. Physiol.* 308, R700–R707. doi: 10.1152/ajpregu.00359.2014

Baker, T. L., Fuller, D. D., Zabka, A. G., and Mitchell, G. S. (2001). Respiratory plasticity: differential actions of continuous and episodic hypoxia and hypercapnia. *Respir. Physiol.* 129, 25–35. doi: 10.1016/S0034-5687(01)00280-8

Baker-Herman, T. L., and Mitchell, G. S. (2002). Phrenic long-term facilitation requires spinal serotonin receptor activation and protein synthesis. *J. Neurosci.* 22, 6239–6246. doi: 10.1523/JNEUROSCI.22-14-06239.2002

Baker-Herman, T. L., and Mitchell, G. S. (2008). Determinants of frequency long-term facilitation following acute intermittent hypoxia in vagotomized rats. *Respir. Physiol. Neurobiol.* 162, 8–17. doi: 10.1016/j.resp.2008.03.005

Baker-Herman, T. L., Fuller, D. D., Bavis, R. W., Zabka, A. G., Golder, F. J., Doperalski, N. J., et al. (2004). BDNF is necessary and sufficient for spinal respiratory plasticity following intermittent hypoxia. *Nat. Neurosci.* 7, 48–55. doi: 10.1038/nn1166

Cao, Y., and Ling, L. (2010). Urethane inhibits genioglossal long-term facilitation in un-paralyzed anesthetized rats. *Neurosci. Lett.* 477, 124–128. doi: 10.1016/j.neulet.2010.04.047

Carew, T. J., Pinsker, H. M., and Kandel, E. R. (1972). Long-term habituation of a defensive withdrawal reflex in aplysia. *Science* 175, 451–454. doi: 10.1126/science.175.4020.451

Clark, G. A., and Kandel, E. R. (1993). Induction of long-term facilitation in *Aplysia* sensory neurons by local application of serotonin to remote synapses. *Proc. Natl. Acad. Sci. U.S.A.* 90, 11411–11415. doi: 10.1073/pnas.90.23.11411

Corcoran, A. E., Richerson, G. B., and Harris, M. B. (2013). Serotonergic mechanisms are necessary for central respiratory chemoresponsiveness in situ. *Respir. Physiol. Neurobiol.* 186, 214–220. doi: 10.1016/j.resp.2013.02.015

Dale, E. A., Ben Mabrouk, F., and Mitchell, G. S. (2014). Unexpected benefits of intermittent hypoxia: enhanced respiratory and nonrespiratory motor function. *Physiology* 29, 39–48. doi: 10.1152/physiol.00012.2013

Dale, E. A., Fields, D. P., Devinney, M. J., and Mitchell, G. S. (2017). Phrenic motor neuron TrkB expression is necessary for acute intermittent hypoxia-induced phrenic long-term facilitation. *Exp. Neurol.* 287, 130–136. doi: 10.1016/j.expneurol.2016.05.012

Day, T. A., and Wilson, R. J. (2007). Brainstem PCO_2 modulates phrenic responses to specific carotid body hypoxia in an in situ dual perfused rat preparation. *J. Physiol.* 578, 843–857. doi: 10.1113/jphysiol.2006.119594

Day, T. A., and Wilson, R. J. (2008). A negative interaction between central and peripheral respiratory chemoreceptors may underlie sleep-induced respiratory instability: a novel hypothesis. *Adv. Exp. Med. Biol.* 605, 447–451. doi: 10.1007/978-0-387-73693-8_78

Day, T. A., and Wilson, R. J. (2009). A negative interaction between brainstem and peripheral respiratory chemoreceptors modulates peripheral chemoreflex magnitude. *J. Physiol.* 587, 883–896. doi: 10.1113/jphysiol.2008.160689

Dean, J. B., Bayliss, D. A., Erickson, J. T., Lawing, W. L., and Millhorn, D. E. (1990). Depolarization and stimulation of neurons in nucleus tractus solitarii by carbon dioxide does not require chemical synaptic input. *Neuroscience* 36, 207–216. doi: 10.1016/0306-4522(90)90363-9

Devinney, M. J., Fields, D. P., Huxtable, A. G., Peterson, T. J., Dale, E. A., and Mitchell, G. S. (2015). Phrenic long-term facilitation requires PKCtheta activity within phrenic motor neurons. *J. Neurosci.* 35, 8107–8117. doi: 10.1523/JNEUROSCI.5086-14.2015

Dillon, G. H., and Waldrop, T. G. (1992). In vitro responses of caudal hypothalamic neurons to hypoxia and hypercapnia. *Neuroscience* 51, 941–950. doi: 10.1016/0306-4522(92)90531-6

Emptage, N. J., and Carew, T. J. (1993). Long-term synaptic facilitation in the absence of short-term facilitation in Aplysia neurons. *Science* 262, 253–256. doi: 10.1126/science.8211146

Erickson, J. T., and Millhorn, D. E. (1991). Fos-like protein is induced in neurons of the medulla oblongata after stimulation of the carotid sinus nerve in awake and anesthetized rats. *Brain Res.* 567, 11–24. doi: 10.1016/0006-8993(91)91430-9

Erickson, J. T., and Millhorn, D. E. (1994). Hypoxia and electrical stimulation of the carotid sinus nerve induce Fos-like immunoreactivity within catecholaminergic and serotoninergic neurons of the rat brainstem. *J. Comp. Neurol.* 348, 161–182. doi: 10.1002/cne.903480202

Fields, D. P., Braegelmann, K. M., Meza, A. L., Mickelson, C. R., Gumnit, M. G., and Baker, T. L. (2019). Competing mechanisms of plasticity impair compensatory responses to repetitive apnoea. *J. Physiol.* 597, 3951–3967. doi: 10.1113/JP277676

Fuller, D. D., Bach, K. B., Baker, T. L., Kinkead, R., and Mitchell, G. S. (2000). Long term facilitation of phrenic motor output. *Respir. Physiol.* 121, 135–146. doi: 10.1016/S0034-5687(00)00124-9

Gerst, D. G. III, Yokhana, S. S., Carney, L. M., Lee, D. S., Badr, M. S., Qureshi, T., et al. (2011). The hypoxic ventilatory response and ventilatory long-term facilitation are altered by time of day and repeated daily exposure to intermittent hypoxia. *J. Appl. Physiol.* 110, 15–28. doi: 10.1152/japplphysiol.00524.2010

Gonzalez-Rothi, E. J., Lee, K. Z., Dale, E. A., Reier, P. J., Mitchell, G. S., and Fuller, D. D. (2015). Intermittent hypoxia and neurorehabilitation. *J. Appl. Physiol.* 119, 1455–1465. doi: 10.1152/japplphysiol.00235.2015

Harris, D. P., Balasubramaniam, A., Badr, M. S., and Mateika, J. H. (2006). Long-term facilitation of ventilation and genioglossus muscle activity is evident in the presence of elevated levels of carbon dioxide in awake humans. *Am. J. Physiol. Regul. Integr. Comp. Physiol.* 291, R1111–R1119. doi: 10.1152/ajpregu.00896.2005

Hayashi, F., Coles, S. K., Bach, K. B., Mitchell, G. S., and McCrimmon, D. R. (1993). Time-dependent phrenic nerve responses to carotid afferent activation: intact vs. decerebellate rats. *Am. J. Physiol.* 265, R811–R819. doi: 10.1152/ajpregu.1993.265.4.R811

Hodges, M. R., and Richerson, G. B. (2010). Medullary serotonin neurons and their roles in central respiratory chemoreception. *Respir. Physiol. Neurobiol.* 173, 256–263. doi: 10.1016/j.resp.2010.03.006

Holtman, J. R. Jr., Dick, T. E., and Berger, A. J. (1986). Involvement of serotonin in the excitation of phrenic motoneurons evoked by stimulation of the raphe obscurus. *J. Neurosci.* 6, 1185–1193. doi: 10.1523/JNEUROSCI.06-04-01185.1986

Janssen, P. L., and Fregosi, R. F. (2000). No evidence for long-term facilitation after episodic hypoxia in spontaneously breathing, anesthetized rats. *J. Appl. Physiol.* 89, 1345–1351. doi: 10.1152/jappl.2000.89.4.1345

Kennedy-Shaffer, L. (2019). Before $p < 0.05$ to beyond $p < 0.05$: using history to contextualize p-values and significance testing. *Am. Stat.* 73, 82–90. doi: 10.1080/00031305.2018.1537891

Kinkead, R., Bach, K. B., Johnson, S. M., Hodgeman, B. A., and Mitchell, G. S. (2001). Plasticity in respiratory motor control: intermittent hypoxia and hypercapnia activate opposing serotonergic and noradrenergic modulatory systems. *Comp. Biochem. Physiol. A Mol. Integr. Physiol.* 130, 207–218. doi: 10.1016/S1095-6433(01)00393-2

Kumar, P., and Prabhakar, N. R. (2012). Peripheral chemoreceptors: function and plasticity of the carotid body. *Compr. Physiol.* 2, 141–219. doi: 10.1002/cphy.c100069

Lahiri, S., and DeLaney, R. G. (1975). Stimulus interaction in the responses of carotid body chemoreceptor single afferent fibers. *Respir. Physiol.* 24, 249–266. doi: 10.1016/0034-5687(75)90017-1

Lee, D. S., Badr, M. S., and Mateika, J. H. (2009). Progressive augmentation and ventilatory long-term facilitation are enhanced in sleep apnoea patients and are mitigated by antioxidant administration. *J. Physiol.* 587, 5451–5467. doi: 10.1113/jphysiol.2009.178053

Lovett-Barr, M. R., Satriotomo, I., Muir, G. D., Wilkerson, J. E., Hoffman, M. S., Vinit, S., et al. (2012). Repetitive intermittent hypoxia induces respiratory and somatic motor recovery after chronic cervical spinal injury. *J. Neurosci.* 32, 3591–3600. doi: 10.1523/JNEUROSCI.2908-11.2012

MacFarlane, P. M., and Mitchell, G. S. (2009). Episodic spinal serotonin receptor activation elicits long-lasting phrenic motor facilitation by an NADPH oxidase-dependent mechanism. *J. Physiol.* 587, 5469–5481. doi: 10.1113/jphysiol.2009.176982

Mateika, J. H., and Sandhu, K. S. (2011). Experimental protocols and preparations to study respiratory long term facilitation. *Respir. Physiol. Neurobiol.* 176, 1–11. doi: 10.1016/j.resp.2011.01.007

McGuire, M., Liu, C., Cao, Y., and Ling, L. (2008). Formation and maintenance of ventilatory long-term facilitation require NMDA but not non-NMDA receptors in awake rats. *J. Appl. Physiol.* 105, 942–950. doi: 10.1152/japplphysiol.01274.2006

Mitchell, G. S. (2007). "Respiratory plasticity following intermittent hypoxia: a guide for novel therapeutic approaches to ventilatory control disorders?," in *Genetic Basis for Respiratory Control Disorders*, ed. C. Gaultier (Berlin: Springer), 291–311. doi: 10.1007/978-0-387-70765-5_17

Morris, K. F., Arata, A., Shannon, R., and Lindsey, B. G. (1996). Long-term facilitation of phrenic nerve activity in cats: responses and short time scale correlations of medullary neurones. *J. Physiol.* 490(Pt 2), 463–480. doi: 10.1113/jphysiol.1996.sp021158

Mulkey, D. K., Stornetta, R. L., Weston, M. C., Simmons, J. R., Parker, A., Bayliss, D. A., et al. (2004). Respiratory control by ventral surface chemoreceptor neurons in rats. *Nat. Neurosci.* 7, 1360–1369. doi: 10.1038/nn1357

Nakamura, A., Olson, E. B. Jr., Terada, J., Wenninger, J. M., Bisgard, G. E., and Mitchell, G. S. (2010). Sleep state dependence of ventilatory long-term facilitation following acute intermittent hypoxia in Lewis rats. *J. Appl. Physiol.* 109, 323–331. doi: 10.1152/japplphysiol.90778.2008

Navarrete-Opazo, A., and Mitchell, G. S. (2014a). Recruitment and plasticity in diaphragm, intercostal, and abdominal muscles in unanesthetized rats. *J. Appl. Physiol.* 117, 180–188. doi: 10.1152/japplphysiol.00130.2014

Navarrete-Opazo, A., and Mitchell, G. S. (2014b). Therapeutic potential of intermittent hypoxia: a matter of dose. *Am. J. Physiol. Regul. Integr. Comp. Physiol.* 307, R1181–R1197. doi: 10.1152/ajpregu.00208.2014

Nichols, N. L., and Mitchell, G. S. (2016). Quantitative assessment of integrated phrenic nerve activity. *Respir. Physiol. Neurobiol.* 226, 81–86. doi: 10.1016/j.resp.2015.12.005

Nuding, S. C., Segers, L. S., Iceman, K. E., O'Connor, R., Dean, J. B., Bolser, D. C., et al. (2015). Functional connectivity in raphe-pontomedullary circuits supports active suppression of breathing during hypocapnic apnea. *J. Neurophysiol.* 114, 2162–2186. doi: 10.1152/jn.00608.2015

Olson, E. B. Jr., Bohne, C. J., Dwinell, M. R., Podolsky, A., Vidruk, E. H., Fuller, D. D., et al. (2001). Ventilatory long-term facilitation in unanesthetized rats. *J. Appl. Physiol.* 91, 709–716. doi: 10.1152/jappl.2001.91.2.709

Perim, R. R., and Mitchell, G. S. (2019). Circulatory control of phrenic motor plasticity. *Respir. Physiol. Neurobiol.* 265, 19–23. doi: 10.1016/j.resp.2019.01.004

Perim, R. R., Fields, D. P., and Mitchell, G. S. (2018). Cross-talk inhibition between 5-HT2B and 5-HT7 receptors in phrenic motor facilitation via NADPH oxidase and PKA. *Am. J. Physiol. Regul. Integr. Comp. Physiol.* 314, R709–R715. doi: 10.1152/ajpregu.00393.2017

Perim, R. R., Fields, D. P., and Mitchell, G. S. (2019). Protein kinase Cdelta constrains the S-pathway to phrenic motor facilitation elicited by spinal 5-HT7 receptors or severe acute intermittent hypoxia. *J. Physiol.* 597, 481–498. doi: 10.1113/JP276731

Perim, R. R., Fields, D. P., and Mitchell, G. S. (2020a). Spinal AMP kinase activity differentially regulates phrenic motor plasticity. *J. Appl. Physiol.* 128, 523–533. doi: 10.1152/japplphysiol.00546.2019

Perim, R. R., Kubilis, P. S., Seven, Y. B., and Mitchell, G. S. (2020b). Hypoxia-induced hypotension elicits adenosine-dependent phrenic long-term facilitation after carotid denervation. *Exp. Neurol.* 333:113429. doi: 10.1016/j.expneurol.2020.113429

Pilowsky, P. M., de Castro, D., Llewellyn-Smith, I., Lipski, J., and Voss, M. D. (1990). Serotonin immunoreactive boutons make synapses with feline phrenic motoneurons. *J. Neurosci.* 10, 1091–1098. doi: 10.1523/JNEUROSCI.10-04-01091.1990

Pineda, J., and Aghajanian, G. K. (1997). Carbon dioxide regulates the tonic activity of locus coeruleus neurons by modulating a proton- and polyamine-sensitive inward rectifier potassium current. *Neuroscience* 77, 723–743. doi: 10.1016/S0306-4522(96)00485-X

Prosser-Loose, E. J., Hassan, A., Mitchell, G. S., and Muir, G. D. (2015). Delayed intervention with intermittent hypoxia and task training improves forelimb function in a rat model of cervical spinal injury. *J. Neurotrauma* 32, 1403–1412. doi: 10.1089/neu.2014.3789

Severson, C. A., Wang, W., Pieribone, V. A., Dohle, C. I., and Richerson, G. B. (2003). Midbrain serotonergic neurons are central pH chemoreceptors. *Nat. Neurosci.* 6, 1139–1140. doi: 10.1038/nn1130

Shkoukani, M., Babcock, M. A., and Badr, M. S. (2002). Effect of episodic hypoxia on upper airway mechanics in humans during NREM sleep. *J. Appl. Physiol.* 92, 2565–2570. doi: 10.1152/japplphysiol.00938.2001

Strey, K. A., Nichols, N. L., Baertsch, N. A., Broytman, O., and Baker-Herman, T. L. (2012). Spinal atypical protein kinase C activity is necessary to stabilize inactivity-induced phrenic motor facilitation. *J. Neurosci.* 32, 16510–16520. doi: 10.1523/JNEUROSCI.2631-12.2012

Syed, Z., Lin, H. S., and Mateika, J. H. (2013). The impact of arousal state, sex, and sleep apnea on the magnitude of progressive augmentation and ventilatory long-term facilitation. *J. Appl. Physiol.* 114, 52–65. doi: 10.1152/japplphysiol.00985.2012

Tadjalli, A., and Mitchell, G. S. (2019). Cervical spinal 5-HT2A and 5-HT2B receptors are both necessary for moderate acute intermittent hypoxia-induced phrenic long-term facilitation. *J. Appl. Physiol.* 127, 432–443. doi: 10.1152/japplphysiol.01113.2018

Terada, J., and Mitchell, G. S. (2011). Diaphragm long-term facilitation following acute intermittent hypoxia during wakefulness and sleep. *J. Appl. Physiol.* 110, 1299–1310. doi: 10.1152/japplphysiol.00055.2011

Teran, F. A., Massey, C. A., and Richerson, G. B. (2014). Serotonin neurons and central respiratory chemoreception: where are we now? *Prog. Brain Res.* 209, 207–233. doi: 10.1016/B978-0-444-63274-6.00011-4

Tester, N. J., Fuller, D. D., Fromm, J. S., Spiess, M. R., Behrman, A. L., and Mateika, J. H. (2014). Long-term facilitation of ventilation in humans with chronic spinal cord injury. *Am. J. Respir. Crit. Care Med.* 189, 57–65. doi: 10.1164/rccm.201401-0089LE

Wasserstein, R. L., Schirm, A. L., and Lazar, N. A. (2019). Moving to a world beyond "$p < 0.05$". *Am. Stat.* 73, 1–19. doi: 10.1080/00031305.2019.1583913

Wu, Y., Proch, K. L., Teran, F. A., Lechtenberg, R. J., Kothari, H., and Richerson, G. B. (2019). Chemosensitivity of Phox2b-expressing retrotrapezoid neurons is mediated in part by input from 5-HT neurons. *J. Physiol.* 597, 2741–2766. doi: 10.1113/JP277052

Conflict of Interest: The authors declare that the research was conducted in the absence of any commercial or financial relationships that could be construed as a potential conflict of interest.

frontiers in Physiology

BRIEF RESEARCH REPORT
published: 05 March 2021
doi: 10.3389/fphys.2021.645392

Pentobarbital Anesthesia Suppresses the Glucose Response to Acute Intermittent Hypoxia in Rat

*Polina E. Nedoboy[1,2], Callum B. Houlahan[1,2] and Melissa M. J. Farnham[1,2]**

[1] Cardiovascular Neuroscience Unit, Heart Research Institute, Newtown, NSW, Australia, [2] Department of Physiology, School of Medical Sciences, Faculty of Medicine and Health, The University of Sydney, Camperdown, NSW, Australia

A key feature of sleep disordered breathing syndromes, such as obstructive sleep apnea is intermittent hypoxia. Intermittent hypoxia is well accepted to drive the sympathoexcitation that is frequently associated with hypertension and diabetes, with measurable effects after just 1 h. The aim of this study was to directly measure the glucose response to 1 h of acute intermittent hypoxia in pentobarbital anesthetized rats, compared to conscious rats. However, we found that while a glucose response is measurable in conscious rats exposed to intermittent hypoxia, it is suppressed in anesthetized rats. Intermittent hypoxia for 1, 2, or 8 h increased blood glucose by 0.7 ± 0.1 mmol/L in conscious rats but had no effect in anesthetized rats (−0.1 ± 0.2 mmol/L). These results were independent of the frequency of the hypoxia challenges, fasting state, vagotomy, or paralytic agents. A supraphysiological challenge of 3 min of hypoxia was able to induce a glycemic response indicating that the reflex response is not abolished under pentobarbital anesthesia. We conclude that pentobarbital anesthesia is unsuitable for investigations into glycemic response pathways in response to intermittent hypoxia in rats.

Keywords: anesthesia-general, acute intermittent hypoxia, Sprague Dawley rat, blood glucose, glucoregulatory circuit, pentobarbital

OPEN ACCESS

Edited by:
Mieczyslaw Pokorski, Opole University, Poland

Reviewed by:
Silvia Pagliardini, University of Alberta, Canada
Irene C. Solomon, Stony Brook University, United States

***Correspondence:**
Melissa M. J. Farnham
melissa.farnham@hri.org.au

Specialty section:
This article was submitted to Respiratory Physiology, a section of the journal Frontiers in Physiology

Received: *23 December 2020*
Accepted: *17 February 2021*
Published: *05 March 2021*

Citation:
Nedoboy PE, Houlahan CB and Farnham MMJ (2021) Pentobarbital Anesthesia Suppresses the Glucose Response to Acute Intermittent Hypoxia in Rat. Front. Physiol. 12:645392. doi: 10.3389/fphys.2021.645392

INTRODUCTION

Obstructive Sleep Apnea (OSA) (Heinzer et al., 2015; Yacoub et al., 2017) is a highly prevalent, but underdiagnosed condition characterized by repetitive airway collapse during sleep. OSA affects up to 30% of the population (Peppard et al., 2013) and is present in ∼70% of diabetics (Pamidi and Tasali, 2012; Rajan and Greenberg, 2015). Intermittent hypoxia (IHx), caused by repetitive collapse of the airways during OSA, is considered a key driver of insulin resistance and hence the development of type 2 diabetes. Current therapies prevent the physical collapse of the airways but are hindered by poor compliance and conflicting reports of improved cardio-metabolic health (da Silva Paulitsch and Zhang, 2019). Although OSA is commonly linked to obesity, of growing concern is the prevalence (25–30%) of OSA in healthy, non-overweight people (Pamidi et al., 2012; Gray et al., 2017), who, without any other risk factors, show signs of pre-diabetes. The natural history of cardio-metabolic impairment in the context of OSA and obesity is unclear, therefore causal directions remain elusive. Activation of the sympathetic nervous system (Leung et al., 2012) is widely recognized as an important mediator of OSA-induced pathophysiology, although mechanisms remain unproven.

IHx models developed in cell culture (Hunyor and Cook, 2018) and rodents (Polak et al., 2013; Rafacho et al., 2013; Farnham et al., 2019) are therefore used to simplify the disease process and isolate the hypoxia driven effects. The cardio-metabolic effects of IHx are rapid with elevated sympathetic activity (Farnham et al., 2019) and glucose after 1–2 h (Rafacho et al., 2013) in rats, and elevated glucose after 3 h (Newhouse et al., 2017) in humans. The sympathetic effects of OSA are well accepted, with patients presenting with increased daytime muscle sympathetic activity (Narkiewicz and Somers, 1997). IHx in *anesthetized* rodent models (Dick et al., 2007; Xing and Pilowsky, 2010; Blackburn et al., 2018; Kakall et al., 2018b; Kim et al., 2018; Roy et al., 2018; Farnham et al., 2019) and *conscious* humans (Louis and Punjabi, 2009; Gilmartin et al., 2010; Tamisier et al., 2011) also both demonstrate persistent increases in sympathetic nerve activity. In the case of chronic IHx, *conscious* rodent models develop increases in blood pressure (Sharpe et al., 2013) and glucose dysregulation (Polak et al., 2013; Fu et al., 2015). Rafacho et al. (2013) was the first to demonstrate that just 1 h of acute IHx elevated blood glucose in *conscious* rats which was attributed to sympathoactivation since administration of a β-blocker prevented this response (Rafacho et al., 2013). However in mice, β-adrenoceptor blockade had no effect, but α-adrenoceptor blockade and adrenomedullectomy blocked the response (Jun et al., 2014). While the mechanism remains contentious, these findings are both supportive of sympathoactivation driving the glucose response to acute IHx. However, no one has directly measured sympathetic activity and blood glucose in response to acute IHx. The purpose of this study was to measure the blood glucose response to 1 h of acute IHx in anesthetized rats and compare with conscious rats.

Here we report that pentobarbital anesthesia suppresses the increase in blood glucose seen in conscious rats. We report that increases in blood glucose are measurable after 1 and 2 h of IHx in conscious rats but are absent in anesthetized rats subjected to either 10 or 16 episodes of IHx within 1 h. We modified multiple experimental parameters including fasting, vagotomy, use of paralytic agents and "priming" with 1 h of conscious IHx before anesthesia. There was a significant but biologically irrelevant effect of "priming" leading to the conclusion that pentobarbital anesthesia is incompatible with investigations of IHx-induced changes in blood glucose.

MATERIALS AND METHODS

Animals

Procedures and protocols were approved by the Sydney Local Area Health District Animal Care and Ethics Committee and conducted in accordance with the Australian codes of practice for the care and use of animals for scientific purposes. Rats are used as the experiments described involve an integrative approach and no artificial models of these systems currently exist.

Experiments were conducted on $n = 78$ adult male Sprague-Dawley (SD) rats (300–500 g; Animal Resource Centre, Perth, Australia).

Animals were housed in 12 h light cycle with lights "on" from 7 a.m. to 7 p.m. This constitutes the rat's "night" when they spent most their time sleeping. We conducted all our experiments during the "night" cycle to align with the human condition of OSA.

Measurement of Blood Glucose

Great care was taken to ensure minimal stress during the blood glucose measurement procedure in conscious untrained animals. Rats (either unfasted or 3 h fasted) were either allowed to walk freely into a dark cloth "sock" or in most cases remained in their home cage without any form of restraint. A scalpel was used to make a small nick at the tip of the tail. The first drop of blood was discarded, and the second drop was drawn up into a glucose test strip attached to a glucometer (AccuCheck or LifeSmart).

Immediately after the conclusion of the IHx or Sham protocol, the tail nick was reopened with gentle abrasion, while the rat remained unrestrained. The first drop of blood was discarded and the second used in the glucometer.

In the anesthetized animals, the tail nick and blood collection were conducted in the same manner.

Intermittent Hypoxia

Conscious

Following blood glucose measurement, a single rat was placed in a small plastic container for 10 min before the IHx protocol was commenced. Rats that underwent the 8 h protocol were housed in groups of 3 and the experiment conducted in their home cage. Oxygen levels within the hypoxia chamber were continuously monitored with an OxyStar (CWE). A customized GSM-3 (CWE) programmable gas mixer was used to deliver 4 different gas mixes at 4 different flow rates to rapidly cycle between 21% O_2 and 6/10% O_2. In the conscious cohort of animals, 4 different IHx protocols were used, with 3 corresponding Sham protocols which consisted of normal room air (21% O_2) being delivered to the animal at the same flow rates and timing as the IHx protocol:

1. 1 h (10 episodes) of 1 min of 10 ± 1% O_2 in N_2, each separated by a 5 min recovery period of 21% O_2 ($n = 9$); Sham ($n = 8$).
2. 1 h (16 episodes) of 1 min of 6 ± 0.5% O_2 in N_2 each separated by a 2.5 min recovery period of 21% O_2 ($n = 7$). The animals in this group were then anesthetized and surgically prepared for the anesthetized protocol and referred to as the "primed" group.
3. 2 h (16 episodes/h) of 1 min of 6 ± 0.5% O_2 in N_2 each separated by a 2.5 min recovery period of 21% O_2 (n = 8); Sham ($n = 6$).
4. 8 h (16 episodes/h) of 1 min of 6 ± 0.5% O_2 in N_2 each separated by a 2.5 min recovery period of 21% O_2 ($n = 9$); Sham ($n = 9$).

Immediately after the conclusion of the IHx or Sham protocol, blood glucose was measured again.

Anesthetized

Following baseline blood glucose measurements and blood gas analysis to ensure the animals were in good metabolic health, the IHx protocol ($n = 26$) was commenced and consisted of either:

5. 10 episodes of 45 s of 10% O_2 in N_2, each separated by a 5 min recovery period (Farnham et al., 2019) ($n = 18$).
6. 1 h (∼16 episodes) of 45 s of 10% O_2 in N_2 each separated by 3min recovery period ($n = 8$).

The Sham protocol ($n = 7$) consisted of the same time frames, but without any alteration of oxygen content of the inspired air.

Single 3 min Hypoxia Challenge

In a subset of 2 anesthetized animals, 2 separate 3 min challenge of 10% O_2 were conducted 30 min apart and 60 min following the conclusion of IHx. Blood glucose was measured just prior to the 3 min challenge and immediately after.

Surgical Preparation

$N = 33$ rats were initially anesthetized with an intraperitoneal injection of pentobarbital sodium (65 mg/kg; Lethobarb). All animals were placed on a homeothermic heat mat to maintain core body temperature at 37 ± 0.5°C. The right carotid artery was cannulated for the measurement of arterial blood pressure and the right jugular vein was cannulated for the administration of fluids and drugs. A continuous infusion of pentobarbital in saline was commenced to deliver 65 mg/kg at a rate of 2 ml/h. Anesthetic depth was monitored continuously and anesthetic delivery was adjusted as necessary. A tracheostomy was performed to permit mechanical ventilation with room air supplemented with 100% O_2. $N = 4$ did not have supplemental O_2. Most animals ($n = 21$) were bilaterally vagotomized before being mechanically ventilated and paralyzed with pancuronium bromide (0.8 mg/kg i.v., followed by an infusion of 0.8 mg/kg/h of pancuronium in 0.9% saline at a rate of 2 ml/h; Astra Zeneca, Australia), while n = 4 were not vagotomized but mechanically ventilated and paralyzed with pancuronium bromide. In other instances ($n = 9$ the vagii were left intact and the animals entrained to the ventilator. The IHx or Sham protocol started within 1–1.5 h from the induction of anesthesia. Prior to the commencement of the IHx or Sham protocol, 0.2 ml of arterial blood was withdrawn for respiratory and electrolyte blood gas analysis (VetStat; IDEXX Laboratories, United States). Ventilation was adjusted, if necessary, to keep blood gases within physiologically normal ranges. After the final blood glucose measurement, a final blood gas analysis was conducted to ensure readings were still within physiological range.

Data Analysis

Recordings of arterial blood pressure, expired CO_2, heart rate and core temperature in the anesthetized rats were acquired using a CED 1401 ADC system and Spike 2 acquisition and analysis software (v. 8.11b; Cambridge, United Kingdom). Recordings of the O_2 levels within the conscious hypoxia chambers was also acquired with a CED 1401 ADC system. Blood glucose measurements from the glucometer were entered into an excel spreadsheet which was used to calculate the change in blood glucose following the IHx or Sham protocol. Statistical analysis was conducted in Graph Pad Prism software (v9). Non-parametric *t*-tests (Mann-Whitney) or one-way ANOVA (Kruskal-Wallis with *post hoc* Dunn's multiple comparisons tests) were performed due to small sample sizes. Data are presented as mean ± SEM and $P < 0.05$ was deemed significant.

RESULTS

1, 2, and 8 h of Acute Intermittent Hypoxia Elevates Blood Glucose in Conscious Rats

1 h of 10% IHx and 1 h of 6% IHx raised blood glucose by 0.7 ± 0.4 vs. 0.6 ± 0.6 mmol/L, respectively (**Figure 1A**) and so the data were grouped together. In agreement with the findings of Rafacho et al. (2013), 1 h of IHx elevated blood glucose (0.7 ± 0.4 vs. 0.0 ± 0.3 mmol/L; $P = 0.0023$; **Figure 1A**), regardless of fasted state or severity/frequency of hypoxia challenges.

Sham for 1 h (0.0 ± 0.3 mmol/L), 2 h (−0.2 ± 0.5 mmol/L), or 8 h (0.1 ± 0.4 mmol/L) had no effect on blood glucose ($P = 0.6696$; Kruskal-Wallis; **Figure 1A**) indicating that the experimental conditions were not inducing a confounding stress response.

IHx for 2 h (0.9 ± 0.9 mmol/L) and 8 h (0.5 ± 0.6 mmol/L) both increased blood glucose to the same degree as 1 h IHx 0.7 ± 0.4 mmol/L; $P = 0.3266$; Kruskal-Wallis; **Figure 1A**), however only 1 and 2 h increases were significantly elevated compared with the equivalent Sham group. **Figure 1B** shows all data points grouped into either Sham or IHx groups. Raw blood glucose readings are presented in **Table 1** for each of the groups.

1 h of Acute Intermittent Hypoxia Fails to Elevate Blood Glucose in Anesthetized Rats

Under pentobarbital anesthesia, blood glucose did not rise but appeared to decrease following 1 h of Sham (−0.5 ± 0.3 mmol/L; **Figure 2A**). 1 h of IHx produced the expected effects on cardiovascular parameters as described before **Table 2** (Farnham et al., 2019) but failed to raise blood glucose (−0.1 ± 0.6 mmol/L; **Figure 2A**) and was no different to the change in blood glucose of the Sham group ($P = 0.8787$; Kruskal-Wallis). None of the protocol adjustments (O_2 supplementation, vagotomy, paralytic agents or length of hypoxia challenge (45 vs. 60 s) had any effect so data are presented as a single group.

However, a priming stimulus of 1 h IHx in conscious animals prior to the anesthetized IHx resulted in a significant rise in blood glucose compared with Sham anesthetized animals (0.3 ± 0.4 vs. −0.5 ± 0.3 mmol/L; $P = 0.0094$; Kruskal-Wallis; **Figure 2A**). While promising for conducting these experiments under anesthesia, this result is unlikely to be biologically relevant as the change in blood glucose was no different to that seen after 1 h of Sham treatment in conscious rats ($P > 0.9999$; Kruskal-Wallis).

A single 3min hypoxia challenge was able to evoke a significant elevation of blood glucose (2.4 ± 1.2 mmol/L;

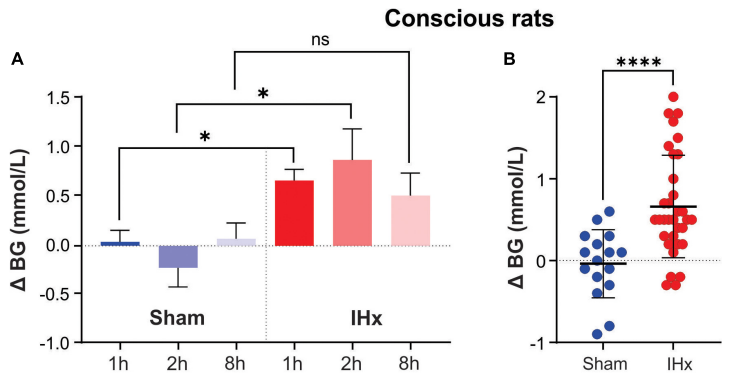

FIGURE 1 | Intermittent hypoxia (IHx) elevates blood glucose in conscious rats. **(A)** The Sham condition of intermittent room air delivered at the same flow rate and volume as that of intermittent hypoxia (IHx) for 1, 2, or 8 h, does not elevate blood glucose in conscious rats. 1 and 2 h of IHx significantly elevated blood glucose compared to the respective Sham conditions. **(B)** Individual data points for Sham and IHx treatment groups. In both cases 1, 2, and 8 h are grouped together. $^{*}P < 0.05$; $^{****}P < 0.001$. BG, blood glucose; Sham, intermittent room air; IHx, intermittent hypoxia.

Figure 2B) compared to both Sham ($P = 0.0038$; Kruskal-Wallis) and IHx ($P = 0.0171$; Kruskal-Wallis) indicating that the glucoregulatory system is capable of raising blood glucose in response to a hypoxic challenge, under anesthesia.

TABLE 1 | Baseline and final blood glucose readings.

Treatment group	*n*	Baseline BG mmol/L (mean ± SD)	Final BG mmol/L (mean ± SD)
Conscious			
Sham 1 h (all)	8	5.7 ± 0.8	5.7 ± 0.8
Sham 1 h (fasted)	2	4.5 ± 0.1	4.6 ± 0.1
Sham 1 h (non-fasted)	6	6.1 ± 0.4	6.1 ± 0.6
Sham 2 h (all fasted)	6	5.2 ± 0.6	5.0 ± 0.6
Sham 8 h (all fasted)	6	5.9 ± 0.6	6.0 ± 0.3
IHx 1 h 10% (all)	9	5.7 ± 1.2	6.4 ± 1.2
IHx 1 h 10% (fasted)	5	5.8 ± 1.1	6.6 ± 0.7
IHx 1 h 10% (non-fasted)	4	5.6 ± 1.5	6.1 ± 1.5
IHx 2 h 6% (all fasted)	8	6.2 ± 0.7	7.1 ± 1.3
IHx 8 h 6% (all fasted)	9	5.4 ± 0.4	5.9 ± 0.7
Anesthetized			
Sham (all)	7	5.3 ± 0.7	4.8 ± 0.6
Sham (vagotomized + paralyzed)	4	5.0 ± 0.8	4.5 ± 0.6
Sham (paralyzed)	3	5.6 ± 0.2	5.2 ± 0.5
IHx 1 h 10% (all)	15	4.9 ± 0.6	4.8 ± 0.8
IHx 1 h 10% (vagotomized + paralyzed)	11	5.0 ± 0.7	4.7 ± 0.9
IHx 1 h 10% (paralyzed)	4	4.7 ± 0.5	5.1 ± 0.7
Single 3 min Hx 10% (all vagotomized + paralyzed)	2	4.4 ± 0.9	6.6 ± 1.4
Priming			
Conscious IHx 1 h 6%	7	5.3 ± 0.4	5.9 ± 0.4
Anesthetized IHx 10% primed (all)	11	4.9 ± 0.4	5.2 ± 0.5
Anesthetized IHx 10% primed (vagotomized + paralyzed)	2	4.7 ± 0.2	4.6 ± 0.7
Anesthetized IHx 10% primed (non-vagotomized + non-paralyzed)	9	4.9 ± 0.4	5.3 ± 0.4

DISCUSSION

The primary finding of this study was that 1 h of acute IHx is insufficient to raise blood glucose levels under pentobarbital anesthesia. In conscious animals, however, our findings agree with that of Rafacho et al. (2013), showing that 1 h of IHx raises blood glucose levels in both fasted and unfasted rats. Our findings extend those of Rafacho et al. (2013) and show that the response is not dependent on the number of hypoxic challenges in a 1 h period, the severity of the hypoxia, nor the duration of the IHx. Additionally, we also show that this response is maintained for longer periods of IHx, up to 8 h. This is important when using animal models of a human condition. IHx models are often employed to investigate mechanisms involved in the physiological or pathological processes observed in human sleep disordered breathing syndromes, such as obstructive sleep apnea (OSA). Human OSA is extraordinarily variable both between patients and within patients from night to night, but alterations in sympathetic and glucoregulatory control, associated with hypertension and diabetes are common. Animals models that mimic this variability in hypoxic challenges while producing the same outcomes are sound models.

It is well established that acute IHx in rodents under anesthesia produces long lasting sympathoexcitation (Dick et al., 2007; Xing and Pilowsky, 2010; Roy et al., 2018; Farnham et al., 2019), which can be blocked at the level of carotid bodies, the spinal cord, and brainstem (Kakall et al., 2018b; Kim et al., 2018; Farnham et al., 2019). The involvement of the sympathetic system in glucose regulation is similarly well established and involves regions within the hypothalamus (Frohman and Bernardis, 1971; Grayson et al., 2013) including the ventromedial hypothalamus (Meek et al., 2016; Shimazu and Minokoshi, 2017) and paraventricular nucleus (Sharpe et al., 2013; Menuet et al., 2014; Zhao et al., 2017), the brainstem (Verberne and Sartor, 2010; Kakall et al., 2019), the adrenal gland (Jun et al., 2014), and carotid bodies (López-Barneo, 2003). Increases in blood glucose following acute, conscious IHx can be blocked by adrenergic blockade or

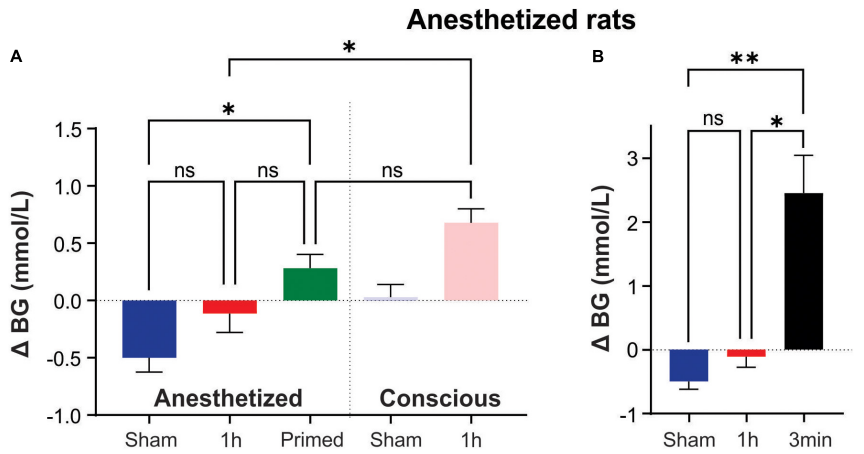

FIGURE 2 | Intermittent hypoxia (IHx) does not elevate blood glucose in anesthetized rats. **(A)** Neither Sham, nor 1 h of IHx elevated blood glucose in pentobarbital anesthetized rats. Primed rats which received 1 h of conscious IHx prior to being anesthetized did have a significantly elevated blood glucose response to IHx under anesthesia when compared with Sham. This response was no different to the conscious Sham response and unlikely to be biologically meaningful. **(B)** A single 3 min hypoxia did evoke a large and significant increase in blood glucose compared to both Sham and 1 h IHx. *$P < 0.05$; **P, 0.001. BG, blood glucose; Sham, intermittent room air; Primed, 1 h conscious IHx prior to anesthetized IHx; 1 h, 1 h of IHx; 3 min, a single 3 min challenge of 10% oxygen.

TABLE 2 | Baseline and final blood pressure (BP), heart rate (HR) and end-tidal CO_2 ($ETCO_2$).

Treatment group	*n*	Baseline BP mmHg (mean ± SD)	Final BP mmHg (mean ± SD)	Baseline HR bpm (mean ± SD)	Final HR bpm (mean ± SD)	Baseline $ETCO_2$ % (mean ± SD)	Final $ETCO_2$ % (mean ± SD)
Anesthetized							
Sham	7	124.5 ± 17.8	116.6 ± 25.5	379.7 ± 48.9	349.4 ± 47.5	1.6 ± 0.6	1.6 ± 0.6
IHx 1 h 10%	15	110.7 ± 18.3	109 ± 21.3	370.6 ± 44.0	348.8 ± 48.0	2.0 ± 0.6	2.2 ± 0.8
Single 3 min Hx 10%	4	81.8 ± 15.9	86.5 ± 5.2	312.1 ± 22.9	302.2 ± 17.5	3.1 ± 0.1	3.2 ± 0.1
Priming							
Anesthetized IHx 10% primed	10	119.6 ± 13.4	115.7 ± 17.3	357.8 ± 34.2	325.7 ± 26.3	2.3 ± 1.1	2.3 ± 1.1

adrenal medullectomy (Rafacho et al., 2013; Jun et al., 2014) indicating sympathetic involvement via catecholamine release. Sympathetic involvement in glucose metabolism dysfunction was also demonstrated in humans subjected to acute IHx (Louis and Punjabi, 2009). Therefore, it seemed reasonable to assume that the sympathetically driven elevation in blood glucose would be measurable under anesthesia.

As anesthesia has varying effects on blood glucose, the choice of anesthetic was critical for the current study. Long lasting urethane anesthesia causes marked hyperglycemia (Sánchez-Pozo et al., 1988) as does the short-acting anesthetics ketamine/xylazine and isoflurane (Sano et al., 2016; Windelov et al., 2016), most likely due to sympathoadrenal stimulation and subsequent release of catecholamines from the adrenal gland (Oyama, 1973). Pentobarbital exerts its anesthetic effects by acting on inhibitory GABA receptors and hence can cause quite severe cardiorespiratory depression (Field et al., 1993), an effect described in dogs over 40 years ago (Cox and Bagshaw, 1979). Pentobarbital suppresses both sympathetic and parasympathetic arms of cardiovascular reflexes; however, is still used in studies investigating autonomic cardiovascular control (Solomon et al., 1999; Nedoboy et al., 2016; Kakall et al., 2018a) since these effects appear to be minimal if anesthetic depth is tightly controlled (Eikermann et al., 2009). Unlike the other anesthetics mentioned, pentobarbital does not raise blood glucose levels (Sano et al., 2016; Windelov et al., 2016) and is used in anesthetized studies investigating the glucoregulatory system (Korim et al., 2016), so it was chosen for this study.

Our findings following IHx combined with the previous studies indicate that pentobarbital anesthesia suppresses the autonomic reflex responses to physiological challenges, but does not abolish it, as responses can still be elicited from suprathreshold challenges. Indeed, the supraphysiological nature of the challenge is a notable feature of previously reported anesthetized experiments. To stimulate a measurable sympathoadrenal reflex, large doses of 2-DG are administered (Kakall et al., 2018a). To stimulate a similar level of catecholamine release in pentobarbital anesthetized dogs, compared with conscious dogs, a 3× greater dose of 2-DG was needed (Taborsky et al., 1984), which was also the same dose used in anesthetized rats (Kakall et al., 2018a). Our current results support this as the physiological hypoxic challenges were insufficient to raise blood glucose under pentobarbital, but a single 3 min hypoxia challenge did produce a robust response (**Figure 2B**). Pentobarbital was shown to prevent the elevation in glucose in response to transport in goats (Sanhouri et al., 1991), to impair

the hypoglycemic effect of insulin in rats (Bailey et al., 1975) and to markedly blunt sympathoadrenal release of noradrenaline in response to hemorrhage in rats (Hamberger et al., 1984). The sympathoadrenal reflex is dependent on catecholamines and in addition to suppressing stimulated release levels, pentobarbital also suppresses resting levels (Hamberger et al., 1984; Taborsky et al., 1984). This current study did not measure catecholamines, so it is plausible that other mechanisms may contribute. Nevertheless the glucose results in the anesthetized animals are indicative of decreasing resting catecholamine levels as blood glucose levels appeared to fall in the anesthetized Sham condition but not in the conscious Sham condition, although this did not reach statistical significance.

The brain circuitry involved in driving the glucose response to acute IHx remains unknown, as does the implication of the mild increase. It is most likely that the glucose response is a sympathetically mediated stress response that serves as an important mechanism to protect the brain during acute stress by maintaining fuel supply during periods of low oxygen. There are multiple sites along the sympathetic stress axis where pentobarbital can exert its effects. Decreased levels of arterial oxygen is first sensed by the carotid bodies, located at the carotid bifurcation and are the primary oxygen sensory organs of the body. The carotid body also has a critical role in stimulating the glucose counter-regulatory response to increase blood glucose (Gao et al., 2014), but how this occurs, and whether it is direct (Gao et al., 2014) or indirect (Conde et al., 2007; O'Halloran, 2016; Thompson et al., 2016) is a matter of debate. The afferent information from the carotid bodies is conveyed to the nucleus of the solitary tract (NTS); studies showed the depressant effects of GABA or GABA agonists on ventilation when applied at the level NTS (Tabata et al., 2001), making it a potential site where pentobarbital can affect GABAergic transmission.

Hypoxia-activated NTS neurons project to multiple hypothalamic and brainstem autonomic nuclei, such as the hypothalamic paraventricular nucleus (PVN) and ventrolateral medulla (VLM). In the face of severe stress, the PVN and VLM are critical areas for mediating the hyperglycemic response (Zhao et al., 2017). Another important area of the hypothalamus for glucose homeostasis is the ventromedial hypothalamus (VMH) which projects to a wide range of sympathetic targets, including the PVN, the VLM and the NTS (Lindberg et al., 2013), which are all involved in the responses to intermittent hypoxia as described above (Mifflin et al., 2015; Shell et al., 2016; Blackburn et al., 2018; Maruyama et al., 2019). While there is no clear evidence of the neurocircuitry involved in the glycemic response to acute IHx, there is substantial knowledge of the effects of GABA on the glucoregulatory neurons in the VMH and the sympathoadrenal glucoregulatory reflex. The VMH contains glucose excited (GE) neurons that are primarily responsible for glucose utilization and regulating insulin sensitivity, as well as glucose-inhibited (GI) neurons that activate the counterregulatory reflex to raise glucose in response to falling glucose levels (Shimazu and Minokoshi, 2017). Female mice lacking glutamate receptors in the VMH have impaired insulin sensitivity and glucose regulation but without any deficit in responding to a hypoglycemia challenge (Fagan et al., 2020) suggesting that glutamate input is not the primary driver of GI neuron activation within the VMH. Inhibition of synaptic glutamate release (Tong et al., 2007) or optogenetic inhibition of neuronal firing (Meek et al., 2016) in the VMH does impair the counterregulatory reflex to hypoglycemia suggesting that the GI neurons are glutamatergic and tonically inhibited. The GI neurons that are responsible for this sympathoadrenal reflex are tonically inhibited by GABA since glucose prevents the decrease in GABA normally seen in response to hypoglycemia (Zhu et al., 2010) and antagonism of GABA (A) receptors results in a an exaggerated sympathoadrenal response to hypoglycemia (Chan et al., 2006). Elevated levels of GABA in the VMH are associated with an impaired/suppressed counterregulatory reflex (Chan et al., 2008, 2011) further highlighting the importance of GABA signaling in the brains ability to raise systemic glucose levels.

Given the abundance of GABA receptors in the central glucose- and hypoxia-sensitive areas, it is highly feasible that the GABAergic effects of pentobarbital are suppressing the glucoregulatory neurons within the central nervous system responsible for stimulating a glycemic response to acute IHx, as well as diminishing the sympathoadrenal reflex. We conclude that pentobarbital anesthesia is unsuitable for measuring the glycemic response to physiological challenges such as IHx.

DATA AVAILABILITY STATEMENT

The raw data supporting the conclusions of this article will be made available by the authors, without undue reservation.

ETHICS STATEMENT

The animal study was reviewed and approved by the Sydney Local Area Health District Animal Care and Ethics Committee.

AUTHOR CONTRIBUTIONS

MF was the guarantor of this work and, as such, had full access to all the data in the study and takes responsibility for the integrity of the data, and the accuracy of the data analysis, designed the project, analyzed, and interpreted data. PN, CH, and MF conducted the experiments. MF and PN prepared the figures, wrote, revised, and edited the manuscript. All authors reviewed the manuscript.

FUNDING

The work was supported by funding from the Rebecca L. Cooper Foundation, the Heart Research Institute, and The University of Sydney.

ACKNOWLEDGMENTS

We acknowledge Dr. Zohra Kakall for assisting with some data acquisition.

REFERENCES

Bailey, C. J., Atkins, T. W., and Matty, A. J. (1975). Blood glucose and plasma insulin levels during prolonged pentobarbitone anaesthesia in the rat. *Endocrinol. Exp.* 9, 177–185.

Blackburn, M. B., Andrade, M. A., and Toney, G. M. (2018). Hypothalamic PVN contributes to acute intermittent hypoxia-induced sympathetic but not phrenic long-term facilitation. *J. Appl. Physiol.* 124, 1233–1243. doi: 10.1152/japplphysiol.00743.2017

Chan, O., Cheng, H., Herzog, R., Czyzyk, D., Zhu, W., Wang, A., et al. (2008). Increased GABAergic tone in the ventromedial hypothalamus contributes to suppression of counterregulatory responses after antecedent hypoglycemia. *Diabetes* 57, 1363–1370. doi: 10.2337/db07-1559

Chan, O., Paranjape, S., Czyzyk, D., Horblitt, A., Zhu, W., Ding, Y., et al. (2011). Increased GABAergic output in the ventromedial hypothalamus contributes to impaired hypoglycemic counterregulation in diabetic rats. *Diabetes* 60, 1582–1589. doi: 10.2337/db10-1579

Chan, O., Zhu, W., Ding, Y., Mccrimmon, R. J., and Sherwin, R. S. (2006). Blockade of GABA(A) receptors in the ventromedial hypothalamus further stimulates glucagon and sympathoadrenal but not the hypothalamo-pituitary-adrenal response to hypoglycemia. *Diabetes* 55, 1080–1087. doi: 10.2337/diabetes.55.04.06.db05-0958

Conde, S. V., Obeso, A., and Gonzalez, C. (2007). Low glucose effects on rat carotid body chemoreceptor cells' secretory responses and action potential frequency in the carotid sinus nerve. *J. Physiol.* 585, 721–730. doi: 10.1113/jphysiol.2007.144261

Cox, R. H., and Bagshaw, R. J. (1979). Influence of anesthesia on the response to carotid hypotension in dogs. *Am. J. Physiol.* 237, H424–H432. doi: 10.1152/ajpheart.1979.237.4.H424

da Silva Paulitsch, F., and Zhang, L. (2019). Continuous positive airway pressure for adults with obstructive sleep apnea and cardiovascular disease: a meta-analysis of randomized trials. *Sleep Med.* 54, 28–34. doi: 10.1016/j.sleep.2018.09.030

Dick, T. E., Hsieh, Y. H., Wang, N., and Prabhakar, N. (2007). Acute intermittent hypoxia increases both phrenic and sympathetic nerve activities in the rat. *Exp. Physiol.* 92, 87–97. doi: 10.1113/expphysiol.2006.035758

Eikermann, M., Fassbender, P., Zaremba, S., Jordan, A. S., Rosow, C., Malhotra, A., et al. (2009). Pentobarbital dose-dependently increases respiratory genioglossus muscle activity while impairing diaphragmatic function in anesthetized rats. *Anesthesiology* 110, 1327–1334. doi: 10.1097/ALN.0b013e3181a16337

Fagan, M. P., Ameroso, D., Meng, A., Rock, A., Maguire, J., and Rios, M. (2020). Essential and sex-specific effects of mGluR5 in ventromedial hypothalamus regulating estrogen signaling and glucose balance. *Proc. Natl. Acad. Sci.U.S.A.* 117, 19566–19577. doi: 10.1073/pnas.2011228117

Farnham, M. M. J., Tallapragada, V. J., O'connor, E. T., Nedoboy, P. E., Dempsey, B., Mohammed, S., et al. (2019). PACAP-PAC1 receptor activation is necessary for the sympathetic response to acute intermittent hypoxia. *Front. Neurosci.* 13:881. doi: 10.3389/fnins.2019.00881

Field, K. J., White, W. J., and Lang, C. M. (1993). Anaesthetic effects of chloral hydrate, pentobarbitone and urethane in adult male rats. *Lab. Anim.* 27, 258–269. doi: 10.1258/002367793780745471

Frohman, L. A., and Bernardis, L. L. (1971). Effect of hypothalamic stimulation on plasma glucose, insulin, and glucagon levels. *Am. J. Physiol.* 221, 1596–1603. doi: 10.1152/ajplegacy.1971.221.6.1596

Fu, C., Jiang, L., Zhu, F., Liu, Z., Li, W., Jiang, H., et al. (2015). Chronic intermittent hypoxia leads to insulin resistance and impaired glucose tolerance through dysregulation of adipokines in non-obese rats. *Sleep Breath.* 19, 1467–1473. doi: 10.1007/s11325-015-1144-8

Gao, L., Ortega-Saenz, P., Garcia-Fernandez, M., Gonzalez-Rodriguez, P., Caballero-Eraso, C., and Lopez-Barneo, J. (2014). Glucose sensing by carotid body glomus cells: potential implications in disease. *Front. Physiol.* 5:398. doi: 10.3389/fphys.2014.00398

Gilmartin, G. S., Lynch, M., Tamisier, R., and Weiss, J. W. (2010). Chronic intermittent hypoxia in humans during 28 nights results in blood pressure elevation and increased muscle sympathetic nerve activity. *Am. J. Physiol.* 299, H925–H931. doi: 10.1152/ajpheart.00253.2009

Gray, E. L., Mckenzie, D. K., and Eckert, D. J. (2017). Obstructive sleep apnea without obesity is common and difficult to treat: evidence for a distinct pathophysiological phenotype. *J. Clin. Sleep Med.* 13, 81–88. doi: 10.5664/jcsm.6394

Grayson, B. E., Seeley, R. J., and Sandoval, D. A. (2013). Wired on sugar: the role of the CNS in the regulation of glucose homeostasis. *Nat. Rev. Neurosci.* 14, 24–37. doi: 10.1038/nrn3409

Hamberger, B., Bengtsson, L., Jarnberg, P. O., and Farnebo, L. O. (1984). Anesthetic agents and sympatho-adrenal response to hemorrhage in the rat. *Acta Chir. Scand. Suppl.* 520, 109–113.

Heinzer, R., Vat, S., Marques-Vidal, P., Marti-Soler, H., Andries, D., Tobback, N., et al. (2015). Prevalence of sleep-disordered breathing in the general population: the hypnoLaus study. *Lancet Respir. Med.* 3, 310–318. doi: 10.1016/S2213-2600(15)00043-0

Hunyor, I., and Cook, K. M. (2018). Models of intermittent hypoxia and obstructive sleep apnea: molecular pathways and their contribution to cancer. *Am. J. Physiol.* 315, R669–R687. doi: 10.1152/ajpregu.00036.2018

Jun, J. C., Shin, M. K., Devera, R., Yao, Q., Mesarwi, O., Bevans-Fonti, S., et al. (2014). Intermittent hypoxia-induced glucose intolerance is abolished by alpha-adrenergic blockade or adrenal medullectomy. *Am. J. Physiol.* 307, E1073–E1083. doi: 10.1152/ajpendo.00373.2014

Kakall, Z. M., Kavurma, M. M., Cohen, E. M., Howe, P. R., Nedoboy, P. E., and Pilowsky, P. M. (2019). Repetitive hypoglycemia reduces activation of glucose-responsive neurons in C1 and C3 medullary brain regions to subsequent hypoglycemia. *Am. J. Physiol.* 317, E388–E398. doi: 10.1152/ajpendo.00051.2019

Kakall, Z. M., Nedoboy, P. E., Farnham, M. M. J., and Pilowsky, P. M. (2018a). Activation of micro-opioid receptors in the rostral ventrolateral medulla blocks the sympathetic counterregulatory response to glucoprivation. *Am. J. Physiol.* 315, R1115–R1122. doi: 10.1152/ajpregu.00248.2018

Kakall, Z. M., Pilowsky, P. M., and Farnham, M. M. J. (2018b). PACAP-(6-38) or kynurenate microinjections in the RVLM prevent the development of sympathetic long-term facilitation after acute intermittent hypoxia. *Am. J. Physiol.* 314, H563–H572. doi: 10.1152/ajpheart.00596.2017

Kim, S. J., Fong, A. Y., Pilowsky, P. M., and Abbott, S. B. G. (2018). Sympathoexcitation following intermittent hypoxia in rat is mediated by circulating angiotensin II acting at the carotid body and subfornical organ. *J. Physiol.* 596, 3217–3232. doi: 10.1113/JP275804

Korim, W. S., Llewellyn-Smith, I. J., and Verberne, A. J. (2016). Activation of medulla-projecting perifornical neurons modulates the adrenal sympathetic response to hypoglycemia: involvement of orexin type 2 (OX2-R) receptors. *Endocrinology* 157, 810–819. doi: 10.1210/en.2015-1712

Leung, R. S., Comondore, V. R., Ryan, C. M., and Stevens, D. (2012). Mechanisms of sleep-disordered breathing: causes and consequences. *Pflugers Arch.* 463, 213–230. doi: 10.1007/s00424-011-1055-x

Lindberg, D., Chen, P., and Li, C. (2013). Conditional viral tracing reveals that steroidogenic factor 1-positive neurons of the dorsomedial subdivision of the ventromedial hypothalamus project to autonomic centers of the hypothalamus and hindbrain. *J. Comp. Neurol.* 521, 3167–3190. doi: 10.1002/cne.23338

López-Barneo, J. (2003). Oxygen and glucose sensing by carotid body glomus cells. *Curr. Opin. Neurobiol.* 13, 493–499. doi: 10.1016/S0959-4388(03)00093-X

Louis, M., and Punjabi, N. M. (2009). Effects of acute intermittent hypoxia on glucose metabolism in awake healthy volunteers. *J. Appl. Physiol.* 106, 1538–1544. doi: 10.1152/japplphysiol.91523.2008

Maruyama, N. O., Mitchell, N. C., Truong, T. T., and Toney, G. M. (2019). Activation of the hypothalamic paraventricular nucleus by acute intermittent hypoxia: implications for sympathetic long-term facilitation neuroplasticity. *Exp. Neurol.* 314, 1–8. doi: 10.1016/j.expneurol.2018.12.011

Meek, T. H., Nelson, J. T., Matsen, M. E., Dorfman, M. D., Guyenet, S. J., Damian, V., et al. (2016). Functional identification of a neurocircuit regulating blood glucose. *Proc. Natl. Acad. Sci. U.S.A.* 113, E2073–E2082. doi: 10.1073/pnas.1521160113

Menuet, C., Sevigny, C. P., Connelly, A. A., Bassi, J. K., Jancovski, N., Williams, D. A., et al. (2014). Catecholaminergic C3 neurons are sympathoexcitatory and involved in glucose homeostasis. *J. Neurosci.* 34, 15110–15122. doi: 10.1523/JNEUROSCI.3179-14.2014

Mifflin, S., Cunningham, J. T., and Toney, G. M. (2015). Neurogenic mechanisms underlying the rapid onset of sympathetic responses to intermittent hypoxia. *J. Appl. Physiol.* 119, 1441–1448. doi: 10.1152/japplphysiol.00198.2015

Narkiewicz, K., and Somers, V. K. (1997). The sympathetic nervous system and obstructive sleep apnea: implications for hypertension. *J. Hypertens.* 15, 1613–1619. doi: 10.1097/00004872-199715120-00062

Nedoboy, P. E., Mohammed, S., Kapoor, K., Bhandare, A. M., Farnham, M. M., and Pilowsky, P. M. (2016). pSer40 tyrosine hydroxylase immunohistochemistry identifies the anatomical location of C1 neurons in rat RVLM that are activated by hypotension. *Neuroscience* 317, 162–172. doi: 10.1016/j.neuroscience.2016.01.012

Newhouse, L. P., Joyner, M. J., Curry, T. B., Laurenti, M. C., Man, C. D., Cobelli, C., et al. (2017). Three hours of intermittent hypoxia increases circulating glucose levels in healthy adults. *Physiol. Rep.* 5:e13106. doi: 10.14814/phy2.13106

O'Halloran, K. D. (2016). Counter-regulatory control of homeostasis during hypoglycaemia: adrenaline hits the sweet spot in the controversy concerning carotid body glucose sensing. *J. Physiol.* 594, 4091–4092. doi: 10.1113/JP272506

Oyama, T. (1973). Endocrine responses to anaesthetic agents. *Br. J. Anaesth.* 45, 276–281. doi: 10.1093/bja/45.3.276

Pamidi, S., Wroblewski, K., Broussard, J., Day, A., Hanlon, E. C., Abraham, V., et al. (2012). Obstructive sleep apnea in young lean men: impact on insulin sensitivity and secretion. *Diabetes Care* 35, 2384–2389. doi: 10.2337/dc12-0841

Pamidi, S., and Tasali, E. (2012). Obstructive sleep apnea and type 2 diabetes: is there a link? *Front. Neurol.* 3:126. doi: 10.3389/fneur.2012.00126

Peppard, P. E., Young, T., Barnet, J. H., Palta, M., Hagen, E. W., and Hla, K. M. (2013). Increased prevalence of sleep-disordered breathing in adults. *Am. J. Epidemiol.* 177, 1006–1014. doi: 10.1093/aje/kws342

Polak, J., Shimoda, L. A., Drager, L. F., Undem, C., Mchugh, H., Polotsky, V. Y., et al. (2013). Intermittent hypoxia impairs glucose homeostasis in C57BL6/J mice: partial improvement with cessation of the exposure. *Sleep* 36, 1483–1490, 1490A–1490B. doi: 10.5665/sleep.3040

Rafacho, A., Goncalves-Neto, L. M., Ferreira, F. B., Protzek, A. O., Boschero, A. C., Nunes, E. A., et al. (2013). Glucose homoeostasis in rats exposed to acute intermittent hypoxia. *Acta Physiol.* 209, 77–89. doi: 10.1111/apha.12118

Rajan, P., and Greenberg, H. (2015). Obstructive sleep apnea as a risk factor for type 2 diabetes mellitus. *Nat. Sci. Sleep* 7, 113–125. doi: 10.2147/NSS.S90835

Roy, A., Farnham, M. M. J., Derakhshan, F., Pilowsky, P. M., and Wilson, R. J. A. (2018). Acute intermittent hypoxia with concurrent hypercapnia evokes P2X and TRPV1 receptor-dependent sensory long-term facilitation in naive carotid bodies. *J. Physiol.* 596, 3149–3169. doi: 10.1113/JP275001

Sánchez-Pozo, A., Alados, J. C., and Sánchez-Medina, F. (1988). Metabolic changes induced by urethane-anesthesia in rats. *Gen. Pharmacol.* 19, 281–284. doi: 10.1016/0306-3623(88)90077-8

Sanhouri, A. A., Jones, R. S., and Dobson, H. (1991). Pentobarbitone inhibits the stress response to transport in male goats. *Br. Vet. J.* 147, 42–48. doi: 10.1016/0007-1935(91)90065-U

Sano, Y., Ito, S., Yoneda, M., Nagasawa, K., Matsuura, N., Yamada, Y., et al. (2016). Effects of various types of anesthesia on hemodynamics, cardiac function, and glucose and lipid metabolism in rats. *Am. J. Physiol.* 311, H1360–H1366. doi: 10.1152/ajpheart.00181.2016

Sharpe, A. L., Calderon, A. S., Andrade, M. A., Cunningham, J. T., Mifflin, S. W., and Toney, G. M. (2013). Chronic intermittent hypoxia increases sympathetic control of blood pressure: role of neuronal activity in the hypothalamic paraventricular nucleus. *Am. J. Physiol.* 305, H1772–H1780. doi: 10.1152/ajpheart.00592.2013

Shell, B., Faulk, K., and Cunningham, J. T. (2016). Neural control of blood pressure in chronic intermittent hypoxia. *Curr. Hypertens. Rep.* 18:19. doi: 10.1007/s11906-016-0627-8

Shimazu, T., and Minokoshi, Y. (2017). Systemic glucoregulation by glucose-sensing neurons in the ventromedial hypothalamic nucleus (VMH). *J. Endocr. Soc.* 1, 449–459. doi: 10.1210/js.2016-1104

Solomon, S. G., Llewellyn-Smith, I. J., Minson, J. B., Arnolda, L. F., Chalmers, J. P., and Pilowsky, P. M. (1999). Neurokinin-1 receptors and spinal cord control of blood pressure in spontaneously hypertensive rats. *Brain Res.* 815, 116–120. doi: 10.1016/S0006-8993(98)01107-X

Tabata, M., Kurosawa, H., Kikuchi, Y., Hida, W., Ogawa, H., Okabe, S., et al. (2001). Role of GABA within the nucleus tractus solitarii in the hypoxic ventilatory decline of awake rats. *Am. J. Physiol.* 281, R1411–R1419. doi: 10.1152/ajpregu.2001.281.5.R1411

Taborsky, G. J. Jr., Halter, J. B., Baum, D., Best, J. D., and Porte, D. Jr. (1984). Pentobarbital anesthesia suppresses basal and 2-deoxy-D-glucose-stimulated plasma catecholamines. *Am. J. Physiol.* 247, R905–R910. doi: 10.1152/ajpregu.1984.247.5.R905

Tamisier, R., Pepin, J. L., Remy, J., Baguet, J. P., Taylor, J. A., Weiss, J. W., et al. (2011). 14 nights of intermittent hypoxia elevate daytime blood pressure and sympathetic activity in healthy humans. *Eur. Respir. J.* 37, 119–128. doi: 10.1183/09031936.00204209

Thompson, E. L., Ray, C. J., Holmes, A. P., Pye, R. L., Wyatt, C. N., Coney, A. M., et al. (2016). Adrenaline release evokes hyperpnoea and an increase in ventilatory CO2 sensitivity during hypoglycaemia: a role for the carotid body. *J. Physiol.* 594, 4439–4452. doi: 10.1113/JP272191

Tong, Q., Ye, C., Mccrimmon, R. J., Dhillon, H., Choi, B., Kramer, M. D., et al. (2007). Synaptic glutamate release by ventromedial hypothalamic neurons is part of the neurocircuitry that prevents hypoglycemia. *Cell Metab.* 5, 383–393. doi: 10.1016/j.cmet.2007.04.001

Verberne, A. J., and Sartor, D. M. (2010). Rostroventrolateral medullary neurons modulate glucose homeostasis in the rat. *Am. J. Physiol.* 299, E802–E807. doi: 10.1152/ajpendo.00466.2010

Windelov, J. A., Pedersen, J., and Holst, J. J. (2016). Use of anesthesia dramatically alters the oral glucose tolerance and insulin secretion in C57Bl/6 mice. *Physiol. Rep.* 4:e12824. doi: 10.14814/phy2.12824

Xing, T., and Pilowsky, P. M. (2010). Acute intermittent hypoxia in rat in vivo elicits a robust increase in tonic sympathetic nerve activity that is independent of respiratory drive. *J. Physiol.* 588, 3075–3088. doi: 10.1113/jphysiol.2010.190454

Yacoub, M., Youssef, I., Salifu, M. O., and Mcfarlane, S. I. (2017). Cardiovascular disease risk in obstructive sleep apnea: an update. *J. Sleep Disord. Ther.* 7:283. doi: 10.4172/2167-0277.1000283

Zhao, Z., Wang, L., Gao, W., Hu, F., Zhang, J., Ren, Y., et al. (2017). A central catecholaminergic circuit controls blood glucose levels during stress. *Neuron* 95, 138–152.e5. doi: 10.1016/j.neuron.2017.05.031

Zhu, W., Czyzyk, D., Paranjape, S. A., Zhou, L., Horblitt, A., Szabo, G., et al. (2010). Glucose prevents the fall in ventromedial hypothalamic GABA that is required for full activation of glucose counterregulatory responses during hypoglycemia. *Am. J. Physiol.* 298, E971–E977. doi: 10.1152/ajpendo.00749.2009

Conflict of Interest: The authors declare that the research was conducted in the absence of any commercial or financial relationships that could be construed as a potential conflict of interest.

frontiers in Physiology

ORIGINAL RESEARCH
published: 25 March 2021
doi: 10.3389/fphys.2021.645904

Calcium Imaging Analysis of Cellular Responses to Hypercapnia and Hypoxia in the NTS of Newborn Rat Brainstem Preparation

Hiroshi Onimaru[1], Itaru Yazawa[2], Kotaro Takeda[3], Isato Fukushi[4,5] and Yasumasa Okada[5]*

[1] Department of Physiology, Showa University School of Medicine, Tokyo, Japan, [2] Global Research Center for Innovative Life Science, Hoshi University School of Pharmacy and Pharmaceutical Sciences, Tokyo, Japan, [3] Faculty of Rehabilitation, School of Healthcare, Fujita Health University, Toyoake, Japan, [4] Faculty of Health Sciences, Uekusa Gakuen University, Chiba, Japan, [5] Clinical Research Center, Murayama Medical Center, Musashimurayama, Japan

It is supposed that the nucleus of the solitary tract (NTS) in the dorsal medulla includes gas sensor cells responsive to hypercapnia or hypoxia in the central nervous system. In the present study, we analyzed cellular responses to hypercapnia and hypoxia in the NTS region of newborn rat *in vitro* preparation. The brainstem and spinal cord were isolated from newborn rat (P0-P4) and were transversely cut at the level of the rostral area postrema. To detect cellular responses, calcium indicator Oregon Green was pressure-injected into the NTS just beneath the cut surface of either the caudal or rostral block of the medulla, and the preparation was superfused with artificial cerebrospinal fluid (25–26°C). We examined cellular responses initially to hypercapnic stimulation (to 8% CO_2 from 2% CO_2) and then to hypoxic stimulation (to 0% O_2 from 95% O_2 at 5% CO_2). We tested these responses in standard solution and in two different synapse blockade solutions: (1) cocktail blockers solution including bicuculline, strychnine, NBQX and MK-801 or (2) TTX solution. At the end of the experiments, the superfusate potassium concentration was lowered to 0.2 from 3 mM to classify recorded cells into neurons and astrocytes. Excitation of cells was detected as changes of fluorescence intensity with a confocal calcium imaging system. In the synaptic blockade solutions (cocktail or TTX solution), 7.6 and 8% of the NTS cells responded to hypercapnic and hypoxic stimulation, respectively, and approximately 2% of them responded to both stimulations. Some of these cells responded to low K^+, and they were classified into astrocytes comprising 43% hypercapnia-sensitive cells, 56% hypoxia-sensitive cells and 54% of both stimulation-sensitive cells. Of note, 49% of the putative astrocytes identified by low K^+ stimulation were sensitive to hypercapnia, hypoxia or both. In the presence of a glia preferential blocker, 5 mM fluoroacetate (plus 0.5 μM TTX), the percentage of hypoxia-sensitive cells was significantly reduced compared to those of all other conditions. This is the first study to reveal that the NTS includes hypercapnia and hypoxia dual-sensitive cells. These results suggest that astrocytes in the NTS region could act as a central gas sensor.

Keywords: NTS, astrocyte, hypoxia, hypercapnia, calcium imaging, rat, isolated brainstem-spinal cord preparation

OPEN ACCESS

Edited by:
Gregory D. Funk, University of Alberta, Canada

Reviewed by:
Daniel K. Mulkey, University of Connecticut, United States
Stephen B. G. Abbott, University of Virginia, United States

****Correspondence:***
Hiroshi Onimaru
oni@med.showa-u.ac.jp

Specialty section:
This article was submitted to Respiratory Physiology, a section of the journal Frontiers in Physiology

Received: *24 December 2020*
Accepted: *08 March 2021*
Published: *25 March 2021*

Citation:
Onimaru H, Yazawa I, Takeda K, Fukushi I and Okada Y (2021) Calcium Imaging Analysis of Cellular Responses to Hypercapnia and Hypoxia in the NTS of Newborn Rat Brainstem Preparation. Front. Physiol. 12:645904. doi: 10.3389/fphys.2021.645904

INTRODUCTION

The nucleus of the solitary tract (NTS) located in the dorsal medulla is the first relay station of sensory inputs involving autonomic functions and works as an integrative system that processes these inputs. Indeed, there are many reports that the NTS plays a role in controlling sympathetic activity and eupneic breathing (Andresen and Kunze, 1994; Braga et al., 2007; Subramanian et al., 2007; Braccialli et al., 2008; Abdala et al., 2009; Accorsi-Mendonca et al., 2011; Costa et al., 2013). Moreover, it is supposed that the NTS includes gas sensor cells responsive to hypercapnia and/or hypoxia in the central nervous system. It is known that the NTS region contributes to the regulation of the hypercapnic ventilatory response (Nattie and Li, 2002, 2008, 2009). Indeed, CO_2/H^+ chemosensitive neurons were found in various subnuclei of the NTS (Dean et al., 2001; Nichols et al., 2008; Dean and Putnam, 2010; Huda et al., 2012). Recent studies showed that a subgroup of Phox2b-expressing neurons in the NTS exhibited intrinsic chemosensitivity to hypercapnic stimulation (Fu et al., 2017) and was presumed to participate in the hypercapnic ventilatory response (Fu et al., 2019).

There is significant evidence that astrocytes in the ventral medulla are involved in central chemosensory mechanisms that maintain cardiorespiratory homeostasis (Gourine et al., 2010; Marina et al., 2016; Turovsky et al., 2016). Systemic hypercapnia, which leads to decreases in blood and brain pH, is associated with a rapid release of ATP within the ventral chemosensory areas of the brainstem (Gourine et al., 2005a). It was also suggested that astrocytes in the NTS contribute to the CO_2/H^+ response by affecting synaptic transmission (Huda et al., 2013). In the ventral medulla, ATP-dependent mechanism to regulate respiratory activity is also involved in hypoxic response (Gourine et al., 2005b; Rajani et al., 2017). In the dorsal medulla, Tadmouri et al. (2014) suggested that astrocytes in the NTS contributed to the neuronal response during the first hour of hypoxia. Enhanced firing in the NTS neurons induced by short-term sustained hypoxia was modulated by glia-neuron interaction (Accorsi-Mendonca et al., 2015). Astrocytic modulation of glutamatergic synaptic transmission was reduced in the NTS of rats submitted to short-term sustained hypoxia (Accorsi-Mendonca et al., 2019). In contrast, acute inhibition of glial cells by bilateral microinjections of fluorocitrate in the NTS did not affect respiratory or sympathetic activities in rats exposed to chronic intermittent hypoxia (Costa et al., 2013).

Thus, cells in the NTS are presumed to be involved directly or indirectly in responses to hypercapnia or hypoxia. However, no study has investigated detailed structures of cell components in the responses, i.e., hypercapnia sensitive, hypoxia sensitive or both types. To answer this question, we analyzed cellular responses to hypercapnia and hypoxia in the NTS region of newborn rat *in vitro* preparation by multi-cell recordings using calcium imaging.

MATERIALS AND METHODS

The experimental protocols were approved by the Ethics Committee for Animal Experiments of Murayama Medical Center. The brainstem and spinal cord were isolated together from newborn rat (Wistar, P0–P4) under deep isoflurane anesthesia and were transversely cut at the level of the rostral area postrema with a custom-made vibratome. From a single brainstem-spinal cord, two preparations were obtained, a rostral block of the medulla and a caudal block of the medulla-spinal cord, and used for recordings. The preparation was set on silicon rubber with the cut surface facing up (**Figure 1A**). To record cellular activities, a calcium indicator, Oregon Green 488 BAPTA-1 AM (200 μM; Invitrogen, Carlsbad, CA), was pressure-injected into the NTS just beneath the cut surface of either the rostral or caudal block preparation (**Figure 1B**), and the preparation was superfused with artificial cerebrospinal fluid (ACSF) composed of the following (in mM): 118 NaCl, 3 KCl, 1 $CaCl_2$, 1 $MgCl_2$, 26 $NaHCO_3$, 1.2 NaH_2PO_4 and 30 glucose equilibrated with 95% O_2 and 5% CO_2, pH 7.4, at 25–26°C (Okada et al., 2012). We examined cellular responses initially to hypercapnic stimulation (to 8% CO_2 from 2% CO_2) and then to hypoxic stimulation (to 0% O_2 from 95% O_2 at 5% CO_2) (**Figure 1C**). We then tested these responses in standard ACSF and two different synapse blockade solutions including (1) 5 μM (-)-bicuculline methiodide (Sigma-Aldrich, Tokyo, Japan), 5 μM strychnine sulfate (FUJIFILM Wako Pure Chemical, Osaka, Japan), 2 μM NBQX (Sigma-Aldrich) and 10 μM (+)-MK-801 maleate (Tocris, Funakoshi Co., Tokyo, Japan) and (2) 0.5 μM TTX (Latoxan Laboratory, Portes-lès-Valence, France). In some experiments, responses to hypercapnia and hypoxia were examined in the presence of glia preferential blocker fluoroacetate (FA; Hülsmann et al., 2000) (FUJIFILM Wako Pure Chemical). At the end of the experiments, the superfusate potassium concentration was lowered from 3 to 0.2 mM to classify recorded cells into neurons and astrocytes because lowered potassium induces vigorous rises in intracellular calcium in astrocytes but not in neurons (Dallwig et al., 2000; Dallwig and Deitmer, 2002; Hartel et al., 2007). Preparations were pre-incubated for 15 min in the pre-stimulus solution (2% CO_2 or 2% CO_2 + blockers) before application of the first test solution (**Figure 1C**). Each measurement was separated by an interval of least 10–15 min to allow wash-out. The Oregon Green dye is pH insensitive in the physiological range (Invitrogen Technical Information Sheet). Therefore, changes in the fluorescence intensity during hypercapnic stimulation (2–8% CO_2 corresponding to pH 7.8–7.2) would not be disturbed by the pH-dependent property of the dye itself.

Superfusing ACSF was supplied via two routes: (1) a main route perfusing the entire recording chamber (blue arrows in **Figure 1A**) and (2) a sub-route (red arrows) through a glass tube (inside diameter, 2 mm) that was placed close to the preparation. Under the control condition, the control solution was perfused through both routes. The test solution was applied to the preparation via the sub-route by replacing the control solution with the test solution. The rate of superfusion was set at 2–3 mL/min in each route. This system allowed rapid application (within 30 s) of the test solution to the preparation.

The cell-bound calcium indicator dye in the NTS was excited by a 488-nm laser beam using a laser diode (Cobolt 06-MLD, HÜBNER Photonics, Kassel, Germany), and cellular activities were visualized through a 520-nm long-pass emission filter.

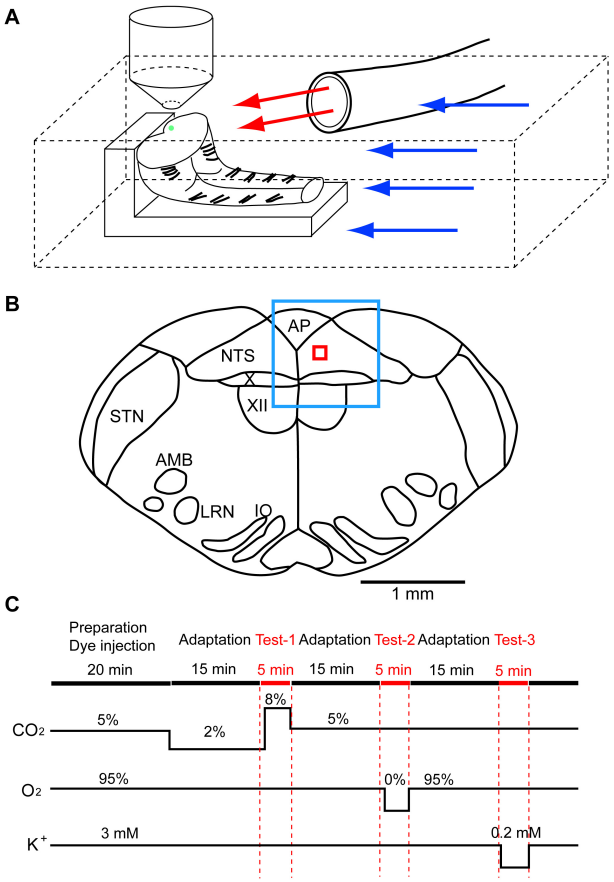

FIGURE 1 | Setup of preparation and rapid exchange system of superfusate and an approximate region of fluorescence recording. **(A)** The preparation (in this case, caudal block) was set on silicon rubber with the cut surface facing up. Artificial cerebrospinal fluid was superfused through two lines, (1) a main route perfusing the experimental chamber (blue arrows) and (2) a sub-route (red arrows) through a glass tube (inside diameter, 2 mm) that was placed close to the preparation. Under the control condition, the control solution was perfused through both routes. The test solution was applied to the preparation via the sub-route by replacing the control solution with the test solution. This system allowed rapid exchange (within 30 s) of the test solution. The green dot on the cut surface denotes an approximate injection area of the calcium indicator Oregon Green. **(B)** A typical cut surface of the medulla and an approximate region of the recording. The blue square denotes the focused area at low magnification (4×), and the red square denotes the recording area of fluorescence intensity at high magnification (40×). AMB, nucleus ambiguus; AP, area postrema; IO, inferior olivary nucleus; LRN, lateral reticular nucleus; NTS, nucleus of the tractus solitarius; STN, spinal trigeminal nucleus; X, dorsal motor nucleus of the vagus; XII, hypoglossal nucleus. **(C)** Protocol of experiments. Red marks denote periods of calcium imagings: Test-1, hypercapnic stimulation; Test-2, hypoxic stimulation; Test-3, low K^+ stimulation.

Images were captured every 0.3 s for 5 min in each measurement using a Nipkow-disk confocal scanner unit (CSU21; Yokogawa Electric, Tokyo, Japan), an electron-multiplying CCD camera (Luca S 658M; Andor Technology, Belfast, United Kingdom), an upright fluorescent microscope (Eclipse E600FN; Nikon, Tokyo, Japan) and a water-immersion objective lens (40×, 0.8 NA, Fluor, Nikon). **Figure 1B** shows an approximate region of the recording: the blue square denotes a focused area at low magnification (4×), and the red square denotes a recording area of fluorescence intensity at high magnification (40×). Test solutions (hypercapnia or hypoxia) were applied at 1 min after the start of data acquisition in each measurement. Low K^+ solution was applied at 30 s after the start of data acquisition. Mean fluorescence intensity at 3.5 × 3.5 μm^2 of the region of interest (ROI) was calculated by the software Andor SOLIS for Imaging (Oxford Instruments plc, Abingdon, United Kingdom). Cells responding to stimulation were detected by rapid change (typically more than 5% within less than 5 s) of the brightness in a cell within the ROI. We calculated $\Delta F/F$ of the peak value, which is the ratio of difference of the fluorescence intensity against that of the baseline (average of 10 frames) immediately before the peak. The time taken for fluorescence intensity to increase compared with the baseline (duration of excitation) was also calculated. The first 50 frames (15 s) were removed because of a light-intensity settling artifact. We made an effort to minimize laser illumination time throughout the experiments to avoid a photobleaching effect.

We counted the number of cells that responded to stimulation. Statistical examination of the percentage of responding cells was evaluated by chi-square test (Microsoft Excel) at a confidence level of $P < 0.05$. Data such as peak values are presented as means ± SD, and the significance of the values was analyzed by one-way ANOVA, followed by a Tukey–Kramer multiple comparisons test at a confidence level of $P < 0.05$ using the GraphPad InStat software program (GraphPad Software, La Jolla, CA, United States).

RESULTS

Responses in the Standard Solution or Synapse Blockers

First, we examined cellular responses in the standard ACSF (**Figure 2**). In this example, 12 cells (Nos. 1–12) responded to hypercapnic stimulation and 10 cells (Nos. 1, 2, 13–20) responded to hypoxic stimulation. Two of these cells (Nos. 1 and 2) responded to both stimulations, and 14 of these cells responded to low K^+ stimulation (**Supplementary Video 1**). The activity pattern was rather complex, and the duration of excitation was variable (4–160 s); some cells showed a relatively short transient increase with one or several peaks (e.g., trace 1 or 2 in **Figure 2C** Hypercapnia) and others showed a long-lasting plateau-like increase (e.g., trace 8 or 10 in **Figure 2C** Hypercapnia). We counted the number of cells that responded to stimulation regardless of the activity pattern. Results from 5 preparations are shown in **Table 1A**. Next, we examined cellular responses in the synaptic blockade ACSF (cocktail blockers solution, **Figure 3**). In this example, 8 cells (Nos. 1–8) responded to hypercapnic stimulation, and 14 cells (Nos. 1–4, 9–18) responded to hypoxic stimulation. Four of these cells (Nos. 1–4) responded to both stimulations, and 8 cells responded to low K^+ stimulation. Results from 5 preparations are shown in **Table 1B**. Then, we examined cellular responses in the presence of TTX (0.5 μM TTX solution, **Figure 4**). In this example, 10 cells (Nos. 1–10)

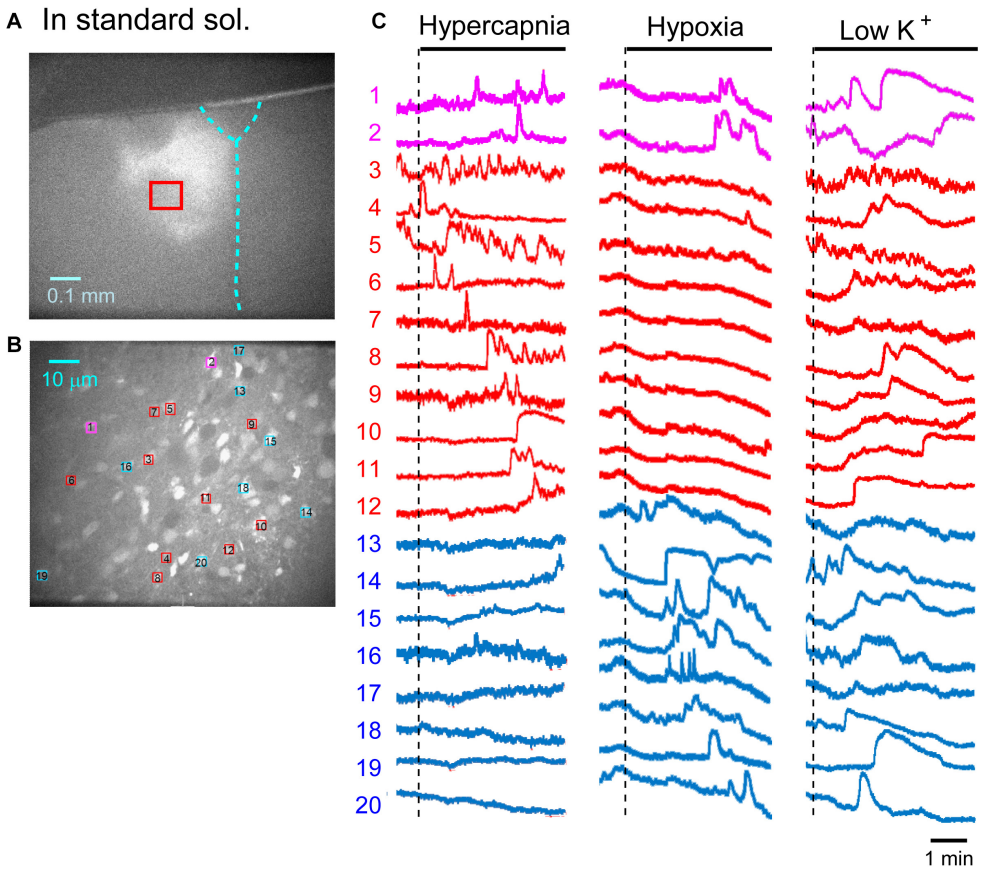

FIGURE 2 | Calcium imaging in the NTS in standard solution (sol.). **(A)** Low-magnification image of the cut surface where Oregon Green was injected and calcium imaging was performed. **(B)** Optical image of the cut surface stained with Oregon Green. The red square in **(A)** corresponds to the measured area shown in **(B)**. **(C)** Calcium signals plotted as fluorescence intensity in identified NTS cells numbered in the image in **(B)** in response to hypercapnia (left), hypoxia (middle) and low K^+ (right) stimulation. Magenta traces denote calcium signal intensity of cells (Nos. 1 and 2) responding to stimulation of both hypercapnia and hypoxia. Red traces denote calcium signal intensity of cells (Nos. 3–12) responding only to hypercapnia. Blue traces denote calcium signal intensity of cells (Nos. 13–20) responding only to hypoxia.

responded to hypercapnic stimulation, and 7 cells (Nos. 1, 2, 11–15) responded to hypoxic stimulation. Two of these cells (Nos. 1 and 2) responded to both stimulations, and 8 cells responded to low K^+ stimulation. Results from 5 preparations are shown in **Table 1C**.

Based on the total cell number from 5 preparations of each condition (**Table 1**), the percentages of responding cells were calculated. In the standard ACSF (control solution), 10.5% of the NTS cells responded to hypercapnic stimulation, 8.4% responded to hypoxic stimulation, and 2.4% responded to both stimulations. In the synaptic blockade solutions (cocktail or 0.5 μM TTX solutions), the number of NTS cells responding to hypercapnic stimulation tended to decrease, but not significantly so. Thus, similar percentages of hypercapnia- and/or hypoxia-responding cells were observed regardless of whether the synaptic transmission was intact or blocked. Some of these cells responded to low K^+, and thus they were classified into astrocytes: 43% of the hypercapnia-sensitive cells, 56% of the hypoxia-sensitive cells and 54% of both stimulation-sensitive cells under a synaptic blockade condition (i.e., cocktail and TTX solution). Of note, 49% of the putative astrocytes identified by low K^+ stimulation were sensitive to hypercapnia, hypoxia or both.

Responses in the Presence of a Glia Preferential Blocker

In the next step, we examined cellular responses in the presence of a glia preferential blocker, FA. A typical example is shown in **Figure 5**. In the presence of 5 mM FA (plus 0.5 μM TTX), the percentage of hypercapnia-sensitive cells was significantly lower compared to that in the standard solution ($P < 0.01$). The percentage of hypoxia-sensitive cells was significantly reduced compared to those of all other conditions (**Figure 6** and **Table 1**), and that of low K^+-responding cells in FA (+ TTX) solution was also significantly lower than that in TTX solution without FA ($P < 0.01$).

When we analyzed the duration of excitation (**Supplementary Table 1**), it tended to be longest during low K^+ stimulation and shortest during hypercapnic stimulation. There was no significant difference in the averaged peak amplitude (ΔF/F)

TABLE 1 | Summary of number of responding cells and total cell number.

	N	% (1)	Low K^+	% (2)
A. In Standard sol (5 preparations)				
Hypercapnia	49	10.5	27	55.1
Hypoxia	39	8.4	25	64.1
Both	11	2.4	9	81.8
Sum	77	16.5	42	54.5
Total cell number	467		89	19.1
B. In cocktail (5 preparations)				
Hypercapnia	38	7.9	17	44.7
Hypoxia	40	8.4	22	55.0
Both	12	2.7	6	50.0
Sum	66	13.8	33	50.0
Total cell number	479		67	14.0
C. In TTX (5 preparations)				
Hypercapnia	34	7.3	14	41.2
Hypoxia	35	7.5	20	57.1
Both	7	1.5	4	57.1
Sum	62	13.3	30	48.4
Total cell number	466		95	20.4
D. In fluoroacetate (5 preparations)				
Hypercapnia	24	5.2	6	25.0
Hypoxia	18	3.9	7	38.9
Both	6	1.3	2	33.3
Sum	36	7.9	11	30.6
Total cell number	458		57	12.4

Hypercapnia, cells that responded to hypercapnic stimulation (2% CO_2→8% CO_2); Hypoxia, cells that responded to hypoxic stimulation (95% O_2→0% O_2); Both, cells that responded to both hypercapnic and hypoxic stimulations; Total cell number, sum of cell number from 5 preparations in the visual field of fluorescence measurement; N, number of cells;% (1), percentage of responding cells to total cell number; Low K^+, number of cells responding to low K^+ stimulation of the cells that responded to each stimulation; Total cell number of Low K^+, total cell number of low K^+-responding cells that includes cells that did not respond to the gas stimulation;% (2), percentage of low K^+-responding cells of the cells that responded to gas stimulation;% (2) of Total cell number, percentage of low K^+-responding cells to total cell number; A, in standard solution; B, in cocktail blockers solution; C, in 0.5 μM TTX solution and D, in 5 mM fluoroacetate + 0.5 μM TTX solution. The red color indicates values whose statistical significance was evaluated (see text).

within each experimental condition (standard, cocktail, TTX and FA in **Supplementary Table 1**). However, ΔF/F tended to be lower in the TTX and FA solutions when values in the same stimulus condition (i.e., hypercapnia, hypoxia and low K^+) were compared.

Our experimental protocol was performed sequentially: first hypercapnia, next hypoxia and finally low K^+ test. Therefore, responses to hypoxia and low K^+ might be affected by the preceding test and elapsed time. To evaluate these effects, we conducted subsequent additional tests: initially hypoxia and then the low K^+ test in the absence (n = 7) and presence (n = 5) of TTX. The percentage of cells responding to hypoxia was comparable to the case in which hypercapnia tests were performed first. However, the percentage of low K^+-responding cells tended to decrease in the case in which hypercapnia was followed by hypoxia prior to low K^+ testing (**Table 2**), suggesting that some astrocytes might not be responding to low K^+.

DISCUSSION

We investigated cellular responses in the NTS during the first 4 min after hypercapnic or hypoxic stimulation by calcium imaging. We found that the NTS included cells that were sensitive to hypercapnia or hypoxia and some that were sensitive to both stimulations. Furthermore, some of the cells were identified as astrocytes by low K^+ stimulation (Dallwig et al., 2000; Dallwig and Deitmer, 2002; Hartel et al., 2007). The activity pattern of the responding cells varied. The duration of excitation tended to differ between the types of stimulation: hypercapnia < hypoxia < low K^+. The peak fluorescence intensity (ΔF/F) also tended to differ between the experimental solutions and was lower in the TTX and FA solutions. In the presence of a glia preferential blocker (FA), the percentage of cells that responded to hypoxic stimulation was significantly reduced compared with those in standard solution, cocktail blocker solution and TTX solution. In contrast, the percentage of cells that responded to hypercapnic stimulation was significantly reduced compared with that only in the standard solution. Moreover, FA treatment significantly reduced the percentage of cells that responded to low K^+ stimulation. Thus, our findings suggest that the contribution of astrocytes as gas sensors may be larger in hypoxia than in hypercapnia, whereas time dependent effects of FA treatment should be considered.

FA and its toxic metabolite fluorocitrate cause inhibition of aconitase. In brain tissue, both substances are preferentially taken up by glial cells and lead to reversible dysfunction of astrocytes with unimpaired neuronal function in the usage of appropriate doses (Clarke, 1991; Swanson and Graham, 1994; Fonnum et al., 1997; Lian and Stringer, 2004; Erlichman and Leiter, 2010). We applied FA totally for 60 min, i.e., for 20 min until the end of hypercapnic stimulation, 40 min until the end of hypoxic stimulation and 60 min until the end of low K^+ stimulation. Hülsmann et al. (2000) reported that in experiments using the medullary slice preparation, respiratory rhythm could be restored by application of isocitrate or glutamine even after 60 min incubation with 5 mM FA. Therefore, the depression of cell activity induced by FA was probably not due to irreversible cell damage.

Although lowering the extracellular K^+ concentration hyperpolarizes neurons and astrocytes, it is suggested that Ca^{2+} would enter into astrocytes via Kir4.1 channels during low K^+ stimulation (Hartel et al., 2007). Therefore, cells that responded to low K^+ were classified into astrocytes (Dallwig et al., 2000; Dallwig and Deitmer, 2002; Hartel et al., 2007). However, the number of putative astrocytes identified in the present study might have been underestimated because some astrocytes might not have responded to low K^+ due to the possibly exhausting effects of the preceding tests and elapsed time. Thus, although we could not conclude that cells that did not respond to low K^+ were neurons, we could conclude that cells that responded to low K^+ were astrocytes and not neurons because neurons should not be excited by low K^+ stimulation (Okada et al., 2005).

There are CO_2/H^+ chemosensitive neurons in the NTS (Dean et al., 2001; Nichols et al., 2008; Dean and Putnam, 2010; Huda et al., 2012). The transcription factor Phox2b is one of the genetic

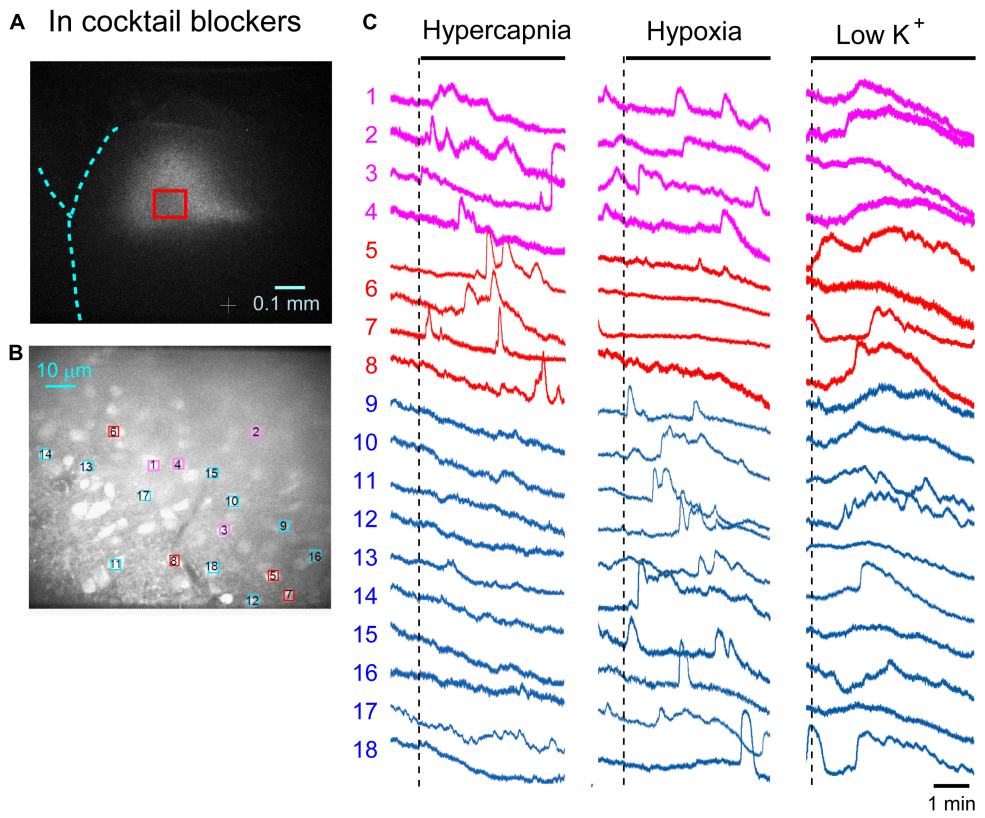

FIGURE 3 | Calcium imaging in the NTS in cocktail blockers solution. **(A)** Low-magnification image of the cut surface where Oregon Green was injected and calcium imaging was performed. **(B)** Optical image of the cut surface stained with Oregon Green. The red square in **(A)** corresponds to the measured area shown in **(B)**. **(C)** Calcium signals plotted as fluorescence intensity in identified NTS cells numbered in the image in **(B)** in response to hypercapnia (left), hypoxia (middle) and low K^+ (right) stimulation. Magenta traces denote calcium signal intensity of cells (Nos. 1–4) responding to stimulation of both hypercapnia and hypoxia. Red traces denote calcium signal intensity of cells (Nos. 5–8) responding only to hypercapnia. Blue traces denote calcium signal intensity of cells (Nos. 9–18) responding only to hypoxia.

markers of CO_2-sensitive neurons in the rostral ventrolateral medulla (Stornetta et al., 2006; Dubreuil et al., 2008; Guyenet et al., 2008; Onimaru et al., 2008). Some chemosensitive neurons in the NTS also express Phox2b (Fu et al., 2017). In the present study, therefore, hypercapnia-sensitive cells in the NTS might include Phox2b-positive neurons. A calcium imaging study of EYFP-expressing Phox2b-positive neurons was performed in the parafacial region (Onimaru et al., 2018), and this method would be applicable to Phox2b-positive cells in the NTS.

We found that some of the cells (including putative astrocytes) responded to stimulation of both hypercapnia and hypoxia, although the intracellular mechanisms were unknown. It is known that hypercapnic stimulation induced the closing of potassium channels and then depolarized neurons in the ventral medulla (Guyenet et al., 2008; Onimaru et al., 2008, 2012; Kumar et al., 2015) and in the NTS (Huda et al., 2012; Fu et al., 2017). It is also reported that in medullary astrocytes, lowering of pH-activated Na^+/HCO_3^- cotransport raised intracellular Na^+. Elevation of intracellular Na^+ activated the Na^+/Ca^{2+} exchanger, thus inducing Ca^{2+} entry (Turovsky et al., 2016). In contrast, the ionic mechanism in hypoxia response is not well understood. The TRPA1 channel at least partly contributes to cellular responses to moderate hypoxia (Mori et al., 2017; Uchiyama et al., 2020). However, further study is needed to clarify the contribution of the TRPA1 channel mechanism to the hypoxia response of NTS cells.

Functional Consideration

Several previous studies suggested that astrocytes in the NTS play a role in hypoxic responses (Tadmouri et al., 2014; Accorsi-Mendonca et al., 2015, 2019). In contrast, Costa et al. (2013) showed that acute inhibition of glial cells by bilateral microinjections of fluorocitrate into the NTS did not affect respiratory or sympathetic activities in rats exposed to chronic intermittent hypoxia. However, this finding does not mean that glia cells in the NTS do not contribute to the acute hypoxic response. Huda et al. (2013) reported that acidification-dependent regulation of glial function affects synaptic transmission within the NTS. They suggest that glia play a modulatory role in the NTS by integrating local tissue signals (such as pH) with synaptic inputs from peripheral afferents. The present results suggest that astrocytes in the NTS region could play a role as a central gas sensor, although the physiological function remains to be elucidated.

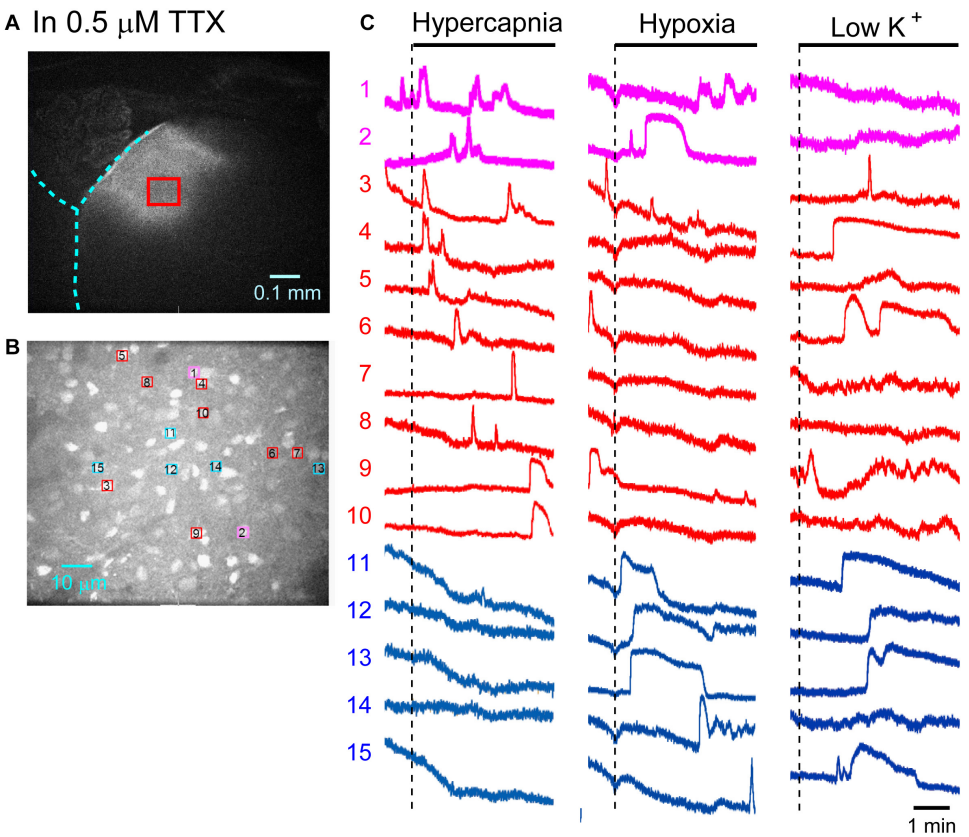

FIGURE 4 | Calcium imaging in the NTS in TTX solution. **(A)** Low-magnification image of the cut surface where Oregon Green was injected and calcium imaging was performed. **(B)** Optical image of the cut surface stained with Oregon Green. The red square in **(A)** corresponds to the measured area in **(B)**. **(C)** Calcium signals plotted as fluorescence intensity in identified NTS cells numbered in the image in **(B)** in response to hypercapnia (left), hypoxia (middle) and low K + (right) stimulation. Magenta traces denote calcium signal intensity of cells (Nos. 1 and 2) responding to stimulation of both hypercapnia and hypoxia. Red traces denote calcium signal intensity of cells (Nos. 3–10) responding only to hypercapnia. Blue traces denote calcium signal intensity of cells (Nos. 11–15) responding only to hypoxia.

Previous studies have proposed a presence of central hypoxic sensors that are involved in respiratory response to hypoxia (Gourine and Funk, 2017; Funk and Gourine, 2018). In the ventral medulla, preBötzinger Complex astrocytes contribute to hypoxia sensing and biphasic hypoxic ventilator response, independent of activation of peripheral chemoreceptors (Gourine et al., 2005b; Angelova et al., 2015; Rajani et al., 2017). The physiological relevance of the biphasic hypoxic response in different types of preparations is debatable due to difference of experimental conditions (Funk and Gourine, 2018; Teppema, 2018). In the en bloc preparation, the change of respiratory rhythm during hypoxic stimulation is typically biphasic, with initial augmentation followed by a decline (Okada et al., 1998; see also **Supplementary Figure 1**). Although the biphasic respiratory response patterns in unanesthetized peripheral-chemodenervated *in vivo* animals and the en bloc preparation look similar, it must be noted that the tissue oxygen environments in these preparations are significantly different (Okada et al., 1993; Funk and Gourine, 2018) (see below). Therefore, caution is necessary when evaluating the functional significance of the biphasic respiratory responses in these preparations. The time window of the calcium imaging in the present study corresponds to initial (∼4 min) excitatory responses to changes in external gas concentration.

It has been reported that ATP release from astrocytes in the ventral medulla is important in central chemosensory mechanisms (Gourine et al., 2005a,b, 2010; Marina et al., 2016; Rajani et al., 2017). This mechanism should work after the blockade of conventional neurotransmission by TTX or cocktail blockers and should enable glia-glia and glia-neuron interactions. This type of signaling could be present in the NTS. Therefore, it is possible that the response of cells in the present study may be secondly induced by TTX- or cocktail blockers-independent mechanisms. Future study using other blockers is required to clarify these suppositions.

Our study is the first report, to our knowledge, that the NTS includes cells that may be dually sensitive to hypercapnia and hypoxia. Such dually sensitive cells may be important in the detection of hypoventilation frequently seen in patients with hypoventilation syndrome (Chebbo et al., 2011), chronic obstructive pulmonary disease (Jacono, 2013) and sleep-disordered breathing (Sowho et al., 2014), who suffer from hypercapnic hypoxemia. This report could be the basis for a better understanding of the cardiorespiratory

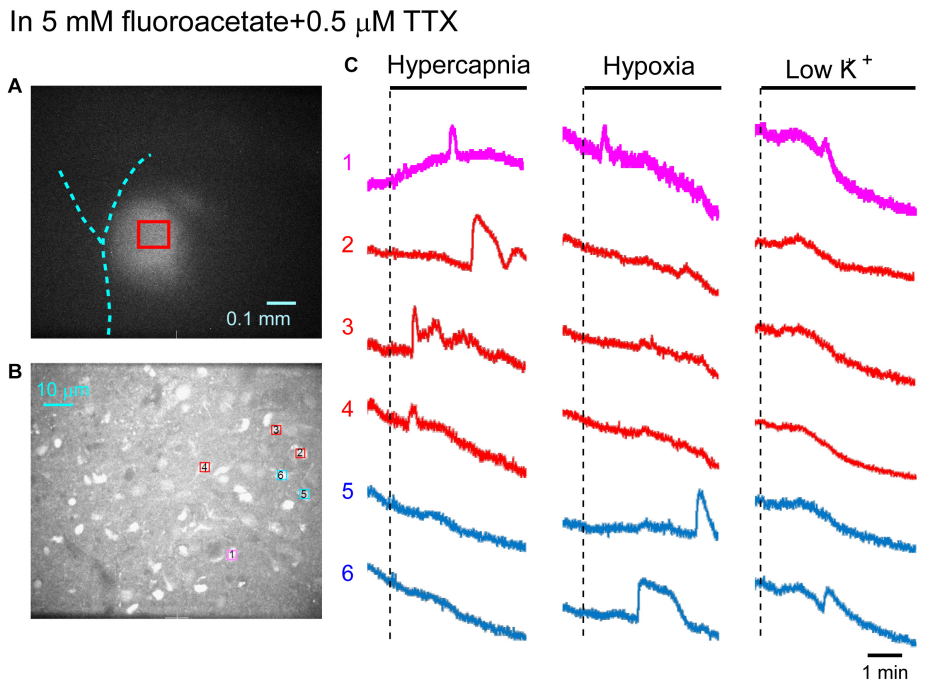

FIGURE 5 | Calcium imaging in the NTS in fluoroacetate plus TTX solution. **(A)** Low-magnification image of the cut surface where Oregon Green was injected and calcium imaging was performed. **(B)** Optical image of the cut surface stained with Oregon Green. The red square in **(A)** corresponds to measured area in **(B)**. **(C)** Calcium signals plotted as fluorescence intensity in identified NTS cells numbered in the image in **(B)** in response to hypercapnia (left), hypoxia (middle) and low K^+ (right) stimulation. Magenta trace denotes calcium signal intensity of cells (No. 1) responding to stimulation of both hypercapnia and hypoxia. Red traces denote calcium signal intensity of cells (Nos. 2–4) responding only to hypercapnia. Blue traces denote calcium signal intensity of cells (Nos. 5 and 6) responding only to hypoxia.

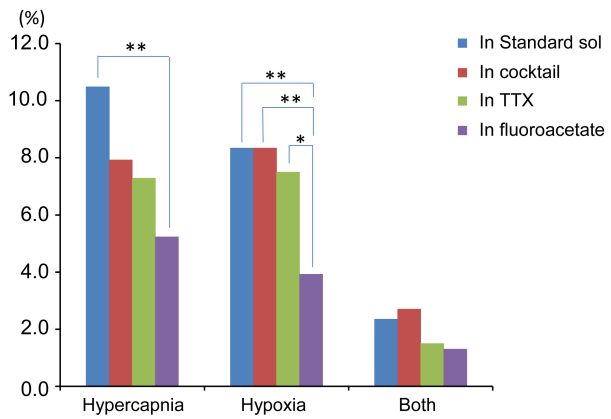

FIGURE 6 | Summary of percentage of responding cells to total cell number based on **Table 1**. Hypercapnia, cells that responded to hypercapnic stimulation (2% CO_2→8% CO_2). Hypoxia, cells that responded to hypoxic stimulation (95% O_2→0% O_2). Both, cells that responded to both hypercapnic and hypoxic stimulations. Each bar indicates different extracellular conditions: standard solution (sol), cocktail blockers solution, 0.5 μM TTX solution and 5 mM fluoroacetate + 0.5 μM TTX solution. *$P < 0.05$, **$P < 0.01$.

TABLE 2 | Effects of preceding treatments on responses to hypoxic stimulation and low K^+ stimulation.

	Hypoxia → Low K^+		Hypercapnia → Hypoxia → Low K^+		
	Standard	TTX	Standard	Cocktail	TTX
Hypoxia (%)	9.9	9.5	8.4	9.8	7.9
Low K^+ (%) to responding cells	66.2	56.8	54.5	38.3	54.1
Low K^+ (%) to total	23.7	23.8	19.1	13.6	20.4

Hypoxia→Low K^+, initially hypoxic stimulation (95% O_2→0% O_2) was tested and then low K^+ was tested; Hypercapnia→Hypoxia→Low K^+, initially hypercapnic stimulation (2% CO_2→8% CO_2) was tested and then hypoxia and low K^+ were tested; Standard, in standard solution; TTX, in 0.5 μM TTX solution; Cocktail, in cocktail blockers solution; Hypoxia (%), percentage of cells that responded to hypoxic stimulation; Low K^+ (%) to responding cells, percentage of low K^+-responding cells of the cells that responded to hypoxic stimulation; Low K^+ (%) to total, percentage of low K^+-responding cells to total cell number.

regulatory mechanisms of hypercapnia and hypoxia and could contribute to the elucidation of the pathophysiology of diseases with disturbed cardiorespiratory responses to hypercapnia and hypoxia.

Technical Limitations

The calcium responses tended to gradually decrease with time mainly due to photobleaching by laser illumination. Thus, the response should be highest in the initial test. Although this tendency was observed in the effects of the first hypercapnic test

on the following hypoxia test (**Table 2**), it was statistically not significant. We treated as responses those that indicated a rapid change (typically more than 5% within less than 5 s, see also **Supplementary Table 1**). However, it was also possible that a single short response could be induced by chance (but not by the stimulation).

In the standard solution and cocktail blockers solution, it was expected that an increase in fluorescence would be detected in neurons in association with the increased firing rate during CO_2 exposure. However, this was not clear in the present study. We think that our sampling rate (3.3 Hz) might have been too low for the detection and/or a calcium transient associated with a single action potential in each neuron would be less than the detection level of our measurement system. However, this sampling rate was enough to detect astrocyte activity (Dallwig and Deitmer, 2002; Hartel et al., 2007; Okada et al., 2012; Stobart et al., 2018) as well as respiratory related neuronal burst activity in the ventral medulla (Ruangkittisakul et al., 2008; Onimaru et al., 2018). Considering recording time (5 min/test) and data size, we thought that 3.3 Hz was enough and appropriate to record astrocyte activity.

We used low K^+ stimulation to identify astrocytes, although some astrocytes would not respond to this stimulation as discussed above. As another method of identification, sulforhodamine 101, which can be taken up specifically into astrocytes in the hippocampus and cortex (Schnell et al., 2012) might be applicable. However, this method has several drawbacks and could not be applicable to the identification of astrocytes in the medullary regions (Schnell et al., 2012; Hülsmann et al., 2017). For identification of cell types, it would be useful to compare soma size (Huxtable et al., 2010; Okada et al., 2012), although this remains for future study.

We used only newborn rats (P0–P4). As the number of astrocytes in the brain increases with development (Voigt, 1989; Botchkina and Morin, 1995), the functional importance would change with development. Thus, we should carefully compare the results in preparations from rats of different ages.

In the en bloc preparation, oxygen is supplied from the superfusate to the tissue via diffusion through the surface of the preparation, and there is a gradient in PO_2 which is high on the surface and lower in the deeper region (Brockhaus et al., 1993; Okada et al., 1993; Funk and Greer, 2013). In the present study, we recorded cellular activities by calcium imaging using a confocal microscope. This method enabled us to visualize cells in the NTS region up to approximately 100 μm deep from the cut surface of the preparation (Onimaru et al., 2018). Indeed, the focal plane in our imaging was limited in this superficial region, where the tissue might be under hyperoxic condition (Brockhaus et al., 1993; Okada et al., 1993). Thus, NTS cells in the region analyzed can respond to a hypoxic stimulus, but the physiological significance of this sensitivity remains to be established.

CONCLUSION

Calcium imaging in the NTS revealed that this region included cells that could respond to hypercapnic, hypoxic and both types of stimulation, and some of the cells were suggested to be astrocytes. These cells may possess a basic ability to act as a central gas sensor.

DATA AVAILABILITY STATEMENT

The raw data supporting the conclusions of this article will be made available by the authors, without undue reservation.

ETHICS STATEMENT

The animal study was reviewed and approved by Ethics Committee for Animal Experiments of Murayama Medical Center.

AUTHOR CONTRIBUTIONS

HO and IY designed and performed the experiments, analyzed the data, and wrote the manuscript. IF and KT contributed to data acquisition and analysis. YO contributed to design of the experimentation and helped to draft the manuscript. All authors read and approved the final manuscript.

FUNDING

This work was supported by JSPS KAKENHI (Grant Nos. 19K06946, 17K08559, 18K17783, 19K17386, 19K17620, 20K19368, and 20K19474) and by the Japanese Physical Therapy Association (Grant Nos. JPTA2019 and JPTA2020).

SUPPLEMENTARY MATERIAL

The Supplementary Material for this article can be found online at: https://www.frontiersin.org/articles/10.3389/fphys.2021.645904/full#supplementary-material

Supplementary Video 1 | Calcium imaging by Oregon Green of cell activity in the NTS in response to low K^+ stimulation, corresponding to **Figure 2**.

REFERENCES

Abdala, A. P., Rybak, I. A., Smith, J. C., Zoccal, D. B., Machado, B. H., St-John, W. M., et al. (2009). Multiple pontomedullary mechanisms of respiratory rhythmogenesis. *Respir. Physiol. Neurobiol.* 168, 19–25. doi: 10.1016/j.resp.2009.06.011

Accorsi-Mendonca, D., Almado, C. E., Bonagamba, L. G., Castania, J. A., Moraes, D. J., and Machado, B. H. (2015). Enhanced firing in NTS induced by short-term

sustained hypoxia is modulated by glia-neuron interaction. *J. Neurosci.* 35, 6903–6917. doi: 10.1523/JNEUROSCI.4598-14.2015

Accorsi-Mendonca, D., Bonagamba, L. G. H., and Machado, B. H. (2019). Astrocytic modulation of glutamatergic synaptic transmission is reduced in NTS of rats submitted to short-term sustained hypoxia. *J. Neurophysiol.* 121, 1822–1830. doi: 10.1152/jn.00279.2018

Accorsi-Mendonca, D., Castania, J. A., Bonagamba, L. G., Machado, B. H., and Leao, R. M. (2011). Synaptic profile of nucleus tractus solitarius neurons involved with the peripheral chemoreflex pathways. *Neuroscience* 197, 107–120. doi: 10.1016/j.neuroscience.2011.08.054

Andresen, M. C., and Kunze, D. L. (1994). Nucleus tractus solitarius–gateway to neural circulatory control. *Annu. Rev. Physiol.* 56, 93–116. doi: 10.1146/annurev.ph.56.030194.000521

Angelova, P. R., Kasymov, V., Christie, I., Sheikhbahaei, S., Turovsky, E., Marina, N., et al. (2015). Functional oxygen sensitivity of astrocytes. *J. Neurosci.* 35, 10460–10473. doi: 10.1523/JNEUROSCI.0045-15.2015

Botchkina, G. I., and Morin, L. P. (1995). Ontogeny of radial glia, astrocytes and vasoactive intestinal peptide immunoreactive neurons in hamster suprachiasmatic nucleus. *Brain Res. Dev. Brain Res.* 86, 48–56. doi: 10.1016/0165-3806(95)00017-8

Braccialli, A. L., Bonagamba, L. G., and Machado, B. H. (2008). Glutamatergic and purinergic mechanisms on respiratory modulation in the caudal NTS of awake rats. *Respir. Physiol. Neurobiol.* 161, 246–252. doi: 10.1016/j.resp.2008.02.011

Braga, V. A., Soriano, R. N., Braccialli, A. L., de Paula, P. M., Bonagamba, L. G., Paton, J. F., et al. (2007). Involvement of L-glutamate and ATP in the neurotransmission of the sympathoexcitatory component of the chemoreflex in the commissural nucleus tractus solitarii of awake rats and in the working heart-brainstem preparation. *J. Physiol.* 581(Pt 3), 1129–1145. doi: 10.1113/jphysiol.2007.129031

Brockhaus, J., Ballanyi, K., Smith, J. C., and Richter, D. W. (1993). Microenvironment of respiratory neurons in the *in vitro* brainstem-spinal cord of neonatal rats. *J. Physiol.* 462, 421–445. doi: 10.1113/jphysiol.1993.sp019562

Chebbo, A., Tfaili, A., and Jones, S. F. (2011). Hypoventilation syndromes. *Med. Clin. North Am.* 95, 1189–1202. doi: 10.1016/j.mcna.2011.09.002

Clarke, D. D. (1991). Fluoroacetate and fluorocitrate: mechanism of action. *Neurochem. Res.* 16, 1055–1058. doi: 10.1007/BF00965850

Costa, K. M., Moraes, D. J., and Machado, B. H. (2013). Acute inhibition of glial cells in the NTS does not affect respiratory and sympathetic activities in rats exposed to chronic intermittent hypoxia. *Brain Res.* 1496, 36–48. doi: 10.1016/j.brainres.2012.12.003

Dallwig, R., and Deitmer, J. W. (2002). Cell-type specific calcium responses in acute rat hippocampal slices. *J. Neurosci. Methods* 116, 77–87. doi: 10.1016/s0165-0270(02)00030-4

Dallwig, R., Vitten, H., and Deitmer, J. W. (2000). A novel barium-sensitive calcium influx into rat astrocytes at low external potassium. *Cell Calcium* 28, 247–259. doi: 10.1054/ceca.2000.0153

Dean, J. B., Kinkade, E. A., and Putnam, R. W. (2001). Cell-cell coupling in CO(2)/H(+)-excited neurons in brainstem slices. *Respir. Physiol.* 129, 83–100. doi: 10.1016/s0034-5687(01)00284-5

Dean, J. B., and Putnam, R. W. (2010). The caudal solitary complex is a site of central CO(2) chemoreception and integration of multiple systems that regulate expired CO(2). *Respir. Physiol. Neurobiol.* 173, 274–287. doi: 10.1016/j.resp.2010.07.002

Dubreuil, V., Ramanantsoa, N., Trochet, D., Vaubourg, V., Amiel, J., Gallego, J., et al. (2008). A human mutation in Phox2b causes lack of CO2 chemosensitivity, fatal central apnea, and specific loss of parafacial neurons. *Proc. Natl. Acad. Sci. U.S.A.* 105, 1067–1072. doi: 10.1073/pnas.0709115105

Erlichman, J. S., and Leiter, J. C. (2010). Glia modulation of the extracellular milieu as a factor in central CO2 chemosensitivity and respiratory control. *J. Appl. Physiol.* 108, 1803–1811. doi: 10.1152/japplphysiol.01321.2009

Fonnum, F., Johnsen, A., and Hassel, B. (1997). Use of fluorocitrate and fluoroacetate in the study of brain metabolism. *Glia* 21, 106–113. doi: 10.1002/(sici)1098-1136(199709)21:1<106::aid-glia12>3.0.co;2-w

Fu, C., Shi, L., Wei, Z., Yu, H., Hao, Y., Tian, Y., et al. (2019). Activation of Phox2b-expressing neurons in the nucleus Tractus solitarii drives breathing in mice. *J. Neurosci.* 39, 2837–2846. doi: 10.1523/JNEUROSCI.2048-18.2018

Fu, C., Xue, J., Wang, R., Chen, J., Ma, L., Liu, Y., et al. (2017). Chemosensitive Phox2b-expressing neurons are crucial for hypercapnic ventilatory response in the nucleus tractus solitarius. *J. Physiol.* 595, 4973–4989. doi: 10.1113/JP274437

Funk, G. D., and Gourine, A. V. (2018). CrossTalk proposal: a central hypoxia sensor contributes to the excitatory hypoxic ventilatory response. *J. Physiol.* 596, 2935–2938. doi: 10.1113/JP275707

Funk, G. D., and Greer, J. J. (2013). The rhythmic, transverse medullary slice preparation in respiratory neurobiology: contributions and caveats. *Respir. Physiol. Neurobiol.* 186, 236–253. doi: 10.1016/j.resp.2013.01.011

Gourine, A. V., and Funk, G. D. (2017). On the existence of a central respiratory oxygen sensor. *J. Appl. Physiol.* 123, 1344–1349. doi: 10.1152/japplphysiol.00194.2017

Gourine, A. V., Kasymov, V., Marina, N., Tang, F., Figueiredo, M. F., Lane, S., et al. (2010). Astrocytes control breathing through pH-dependent release of ATP. *Science* 329, 571–575. doi: 10.1126/science.1190721

Gourine, A. V., Llaudet, E., Dale, N., and Spyer, K. M. (2005a). ATP is a mediator of chemosensory transduction in the central nervous system. *Nature* 436, 108–111. doi: 10.1038/nature03690

Gourine, A. V., Llaudet, E., Dale, N., and Spyer, K. M. (2005b). Release of ATP in the ventral medulla during hypoxia in rats: role in hypoxic ventilatory response. *J. Neurosci.* 25, 1211–1218. doi: 10.1523/JNEUROSCI.3763-04.2005

Guyenet, P. G., Stornetta, R. L., and Bayliss, D. A. (2008). Retrotrapezoid nucleus and central chemoreception. *J. Physiol.* 586, 2043–2048. doi: 10.1113/jphysiol.2008.150870

Hartel, K., Singaravelu, K., Kaiser, M., Neusch, C., Hulsmann, S., and Deitmer, J. W. (2007). Calcium influx mediated by the inwardly rectifying K+ channel Kir4.1 (KCNJ10) at low external K+ concentration. *Cell Calcium* 42, 271–280. doi: 10.1016/j.ceca.2006.12.004

Huda, R., McCrimmon, D. R., and Martina, M. (2013). pH modulation of glial glutamate transporters regulates synaptic transmission in the nucleus of the solitary tract. *J. Neurophysiol.* 110, 368–377. doi: 10.1152/jn.01074.2012

Huda, R., Pollema-Mays, S. L., Chang, Z., Alheid, G. F., McCrimmon, D. R., and Martina, M. (2012). Acid-sensing ion channels contribute to chemosensitivity of breathing-related neurons of the nucleus of the solitary tract. *J. Physiol.* 590, 4761–4775. doi: 10.1113/jphysiol.2012.232470

Hülsmann, S., Hagos, L., Heuer, H., and Schnell, C. (2017). Limitations of sulforhodamine 101 for brain imaging. *Front. Cell. Neurosci.* 11:44. doi: 10.3389/fncel.2017.00044

Hülsmann, S., Oku, Y., Zhang, W., and Richter, D. W. (2000). Metabolic coupling between glia and neurons is necessary for maintaining respiratory activity in transverse medullary slices of neonatal mouse. *Eur. J. Neurosci.* 12, 856–862. doi: 10.1046/j.1460-9568.2000.00973.x

Huxtable, A. G., Zwicker, J. D., Alvares, T. S., Ruangkittisakul, A., Fang, X., Hahn, L. B., et al. (2010). Glia contribute to the purinergic modulation of inspiratory rhythm-generating networks. *J. Neurosci.* 30, 3947–3958. doi: 10.1523/JNEUROSCI.6027-09.2010

Jacono, F. J. (2013). Control of ventilation in COPD and lung injury. *Respir. Physiol. Neurobiol.* 189, 371–376. doi: 10.1016/j.resp.2013.07.010

Kumar, N. N., Velic, A., Soliz, J., Shi, Y., Li, K., Wang, S., et al. (2015). PHYSIOLOGY. Regulation of breathing by CO(2) requires the proton-activated receptor GPR4 in retrotrapezoid nucleus neurons. *Science* 348, 1255–1260. doi: 10.1126/science.aaa0922

Lian, X. Y., and Stringer, J. L. (2004). Astrocytes contribute to regulation of extracellular calcium and potassium in the rat cerebral cortex during spreading depression. *Brain Res.* 1012, 177–184. doi: 10.1016/j.brainres.2004.04.011

Marina, N., Teschemacher, A. G., Kasparov, S., and Gourine, A. V. (2016). Glia, sympathetic activity and cardiovascular disease. *Exp. Physiol.* 101, 565–576. doi: 10.1113/EP085713

Mori, Y., Takahashi, N., Kurokawa, T., and Kiyonaka, S. (2017). TRP channels in oxygen physiology: distinctive functional properties and roles of TRPA1 in O2 sensing. *Proc. Jpn. Acad. Ser. B Phys. Biol. Sci.* 93, 464–482. doi: 10.2183/pjab.93.028

Nattie, E., and Li, A. (2008). Muscimol dialysis into the caudal aspect of the Nucleus tractus solitarii of conscious rats inhibits chemoreception. *Respir. Physiol. Neurobiol.* 164, 394–400. doi: 10.1016/j.resp.2008.09.004

Nattie, E. E., and Li, A. (2002). CO2 dialysis in nucleus tractus solitarius region of rat increases ventilation in sleep and wakefulness. *J. Appl. Physiol.* 92, 2119–2130. doi: 10.1152/japplphysiol.01128.2001

Nattie, E. E., and Li, A. (2009). Central chemoreception is a complex system function that involves multiple brainstem sites. *J. Appl. Physiol.* 106, 1464–1466. doi: 10.1152/japplphysiol.00112.2008

Nichols, N. L., Hartzler, L. K., Conrad, S. C., Dean, J. B., and Putnam, R. W. (2008). Intrinsic chemosensitivity of individual nucleus tractus solitarius (NTS) and locus coeruleus (LC) neurons from neonatal rats. *Adv. Exp. Med. Biol.* 605, 348–352. doi: 10.1007/978-0-387-73693-8_61

Okada, Y., Kawai, A., Muckenhoff, K., and Scheid, P. (1998). Role of the pons in hypoxic respiratory depression in the neonatal rat. *Respir. Physiol.* 111, 55–63. doi: 10.1016/s0034-5687(97)00105-9

Okada, Y., Kuwana, S., Kawai, A., Muckenhoff, K., and Scheid, P. (2005). Significance of extracellular potassium in central respiratory control studied in the isolated brainstem-spinal cord preparation of the neonatal rat. *Respir. Physiol. Neurobiol.* 146, 21–32. doi: 10.1016/j.resp.2004.10.009

Okada, Y., Muckenhoff, K., Holtermann, G., Acker, H., and Scheid, P. (1993). Depth profiles of pH and PO2 in the isolated brain stem-spinal cord of the neonatal rat. *Respir. Physiol.* 93, 315–326. doi: 10.1016/0034-5687(93)90077-n

Okada, Y., Sasaki, T., Oku, Y., Takahashi, N., Seki, M., Ujita, S., et al. (2012). Preinspiratory calcium rise in putative pre-Bötzinger complex astrocytes. *J. Physiol.* 590, 4933–4944. doi: 10.1113/jphysiol.2012.231464

Onimaru, H., Ikeda, K., and Kawakami, K. (2008). CO2-sensitive preinspiratory neurons of the parafacial respiratory group express Phox2b in the neonatal rat. *J. Neurosci.* 28, 12845–12850. doi: 10.1523/jneurosci.3625-08.2008

Onimaru, H., Ikeda, K., and Kawakami, K. (2012). Postsynaptic mechanisms of CO2 responses in parafacial respiratory neurons of newborn rats. *J. Physiol.* 590, 1615–1624. doi: 10.1113/jphysiol.2011.222687

Onimaru, H., Nakamura, S., Ikeda, K., Kawakami, K., and Inoue, T. (2018). Confocal calcium imaging analysis of respiratory-related burst activity in the parafacial region. *Brain Res. Bull.* 139, 16–20. doi: 10.1016/j.brainresbull.2018.01.013

Rajani, V., Zhang, Y., Jalubula, V., Rancic, V., SheikhBahaei, S., Zwicker, J. D., et al. (2017). Release of ATP by pre-Botzinger complex astrocytes contributes to the hypoxic ventilatory response via a Ca(2+) -dependent P2Y1 receptor mechanism. *J. Physiol.* 596, 3245–3269. doi: 10.1113/JP274727

Ruangkittisakul, A., Schwarzacher, S. W., Secchia, L., Ma, Y., Bobocea, N., Poon, B. Y., et al. (2008). Generation of eupnea and sighs by a spatiochemically organized inspiratory network. *J. Neurosci.* 28, 2447–2458. doi: 10.1523/JNEUROSCI.1926-07.2008

Schnell, C., Hagos, Y., and Hulsmann, S. (2012). Active sulforhodamine 101 uptake into hippocampal astrocytes. *PLoS One* 7:e49398. doi: 10.1371/journal.pone.0049398

Sowho, M., Amatoury, J., Kirkness, J. P., and Patil, S. P. (2014). Sleep and respiratory physiology in adults. *Clin. Chest Med.* 35, 469–481. doi: 10.1016/j.ccm.2014.06.002

Stobart, J. L., Ferrari, K. D., Barrett, M. J. P., Stobart, M. J., Looser, Z. J., Saab, A. S., et al. (2018). Long-term *in vivo* calcium imaging of astrocytes reveals distinct cellular compartment responses to sensory stimulation. *Cereb. Cortex* 28, 184–198. doi: 10.1093/cercor/bhw366

Stornetta, R. L., Moreira, T. S., Takakura, A. C., Kang, B. J., Chang, D. A., West, G. H., et al. (2006). Expression of Phox2b by brainstem neurons involved in chemosensory integration in the adult rat. *J. Neurosci.* 26, 10305–10314. doi: 10.1523/JNEUROSCI.2917-06.2006

Subramanian, H. H., Chow, C. M., and Balnave, R. J. (2007). Identification of different types of respiratory neurones in the dorsal brainstem nucleus tractus solitarius of the rat. *Brain Res.* 1141, 119–132. doi: 10.1016/j.brainres.2007.01.013

Swanson, R. A., and Graham, S. H. (1994). Fluorocitrate and fluoroacetate effects on astrocyte metabolism *in vitro*. *Brain Res.* 664, 94–100. doi: 10.1016/0006-8993(94)91958-5

Tadmouri, A., Champagnat, J., and Morin-Surun, M. P. (2014). Activation of microglia and astrocytes in the nucleus tractus solitarius during ventilatory acclimatization to 10% hypoxia in unanesthetized mice. *J. Neurosci. Res.* 92, 627–633. doi: 10.1002/jnr.23336

Teppema, L. J. (2018). CrossTalk opposing view: the hypoxic ventilatory response does not include a central, excitatory hypoxia sensing component. *J. Physiol.* 596, 2939–2941. doi: 10.1113/JP275708

Turovsky, E., Theparambil, S. M., Kasymov, V., Deitmer, J. W., Del Arroyo, A. G., Ackland, G. L., et al. (2016). Mechanisms of CO2/H+ sensitivity of astrocytes. *J. Neurosci.* 36, 10750–10758. doi: 10.1523/JNEUROSCI.1281-16.2016

Uchiyama, M., Nakao, A., Kurita, Y., Fukushi, I., Takeda, K., Numata, T., et al. (2020). O2-dependent protein internalization underlies astrocytic sensing of acute hypoxia by restricting multimodal TRPA1 Channel Responses. *Curr. Biol.* 30, 3378–3396.e7. doi: 10.1016/j.cub.2020.06.047

Voigt, T. (1989). Development of glial cells in the cerebral wall of ferrets: direct tracing of their transformation from radial glia into astrocytes. *J. Comp. Neurol.* 289, 74–88. doi: 10.1002/cne.902890106

Conflict of Interest: The authors declare that the research was conducted in the absence of any commercial or financial relationships that could be construed as a potential conflict of interest.

frontiers in Physiology

ORIGINAL RESEARCH
published: 25 May 2021
doi: 10.3389/fphys.2021.623599

Augmented Respiratory–Sympathetic Coupling and Hemodynamic Response to Acute Mild Hypoxia in Female Rodents With Chronic Kidney Disease

*Manash Saha[1,2,3], Qi-Jian Sun[1], Cara M. Hildreth[1], Peter G. R. Burke[1,4] and Jacqueline K. Phillips[1]**

[1] Department of Biomedical Sciences, Macquarie University, Sydney, NSW, Australia, [2] Department of Nephrology, National Institute of Kidney Disease and Urology, Dhaka, Bangladesh, [3] Graduate School of Medicine, Wollongong University, Wollongong, NSW, Australia, [4] Neuroscience Research Australia, Sydney, NSW, Australia

OPEN ACCESS

Edited by:
Yasumasa Okada,
Murayama Medical Center (NHO), Japan

Reviewed by:
Thiago S. Moreira,
University of São Paulo, Brazil
Satoshi Koba,
Tottori University, Japan

***Correspondence:**
Jacqueline K. Phillips
jacqueline.phillips@mq.edu.au

Specialty section:
This article was submitted to Respiratory Physiology, a section of the journal Frontiers in Physiology

Received: 30 October 2020
Accepted: 15 April 2021
Published: 25 May 2021

Citation:
Saha M, Sun QJ, Hildreth CM, Burke PGR and Phillips JK (2021) Augmented Respiratory–Sympathetic Coupling and Hemodynamic Response to Acute Mild Hypoxia in Female Rodents With Chronic Kidney Disease. Front. Physiol. 12:623599. doi: 10.3389/fphys.2021.623599

Carotid body feedback and hypoxia may serve to enhance respiratory–sympathetic nerve coupling (respSNA) and act as a driver of increased blood pressure. Using the Lewis polycystic kidney (LPK) rat model of chronic kidney disease, we examined respSNA in adult female rodents with CKD and their response to acute hypoxia or hypercapnia compared to Lewis control animals. Under urethane anesthesia, phrenic nerve activity, splanchnic sympathetic nerve activity (sSNA), and renal sympathetic nerve activity (rSNA) were recorded under baseline conditions and during mild hypoxic or hypercapnic challenges. At baseline, tonic SNA and blood pressure were greater in female LPK rats versus Lewis rats (all $P < 0.05$) and respSNA was at least two-fold larger [area under the curve (AUC), sSNA: 7.8 ± 1.1 vs. 3.4 ± 0.7 μV s, rSNA: 11.5 ± 3 vs. 4.8 ± 0.7 μV s, LPK vs. Lewis, both $P < 0.05$]. Mild hypoxia produced a larger pressure response in LPK [Δ mean arterial pressure (MAP) 30 ± 6 vs. 12 ± 6 mmHg] and augmented respSNA (ΔAUC, sSNA: 8.9 ± 3.4 vs. 2 ± 0.7 μV s, rSNA: 6.1 ± 1.2 vs. 3.1 ± 0.7 μV s, LPK vs. Lewis, all $P \leq 0.05$). In contrast, central chemoreceptor stimulation produced comparable changes in blood pressure and respSNA (ΔMAP 13 ± 3 vs. 9 ± 5 mmHg; respSNA ΔAUC, sSNA: 2.5 ± 1 vs. 1.3 ± 0.7 μV s, rSNA: 4.2 ± 0.9 vs. 3.5 ± 1.4 μV s, LPK vs. Lewis, all $P > 0.05$). These results demonstrate that female rats with CKD exhibit heightened respSNA coupling at baseline that is further augmented by mild hypoxia, and not by hypercapnia. This mechanism may be a contributing driver of hypertension in this animal model of CKD.

Keywords: female, respiratory sympathetic modulation, chronic kidney disease, hypertension, chemoreflex, hypoxia, hypercapnia

INTRODUCTION

Sympathetic nerve activity (SNA) varies across different phases of the respiratory cycle. This harmonious relationship is termed respiratory sympathetic modulation or coupling (respSNA) (Haselton and Guyenet, 1989; Czyzyk-Krzeska and Trzebski, 1990; Dick et al., 2004) and is an important homeostatic mechanism that allows synchronization between the cardiovascular and respiratory systems. Respiratory sympathetic coupling can change in response to metabolic challenges such as hypoxia, with peripheral chemoreceptor activation inducing reflex respiratory and autonomic adjustments (Dick et al., 2004; Mandel and Schreihofer, 2009). For instance, hypoxia can generate an active expiratory motor pattern that is coupled to increased sympathetic activity (Moraes et al., 2014). Augmentation of respSNA has been linked explicitly to sympathetic hyperactivity and hypertension in animal models of both primary and secondary hypertension (Simms et al., 2009; Toney et al., 2010; Zoccal and Machado, 2010).

In patients with chronic kidney disease (CKD), high blood pressure is a common comorbidity, and sympathetic hyperactivity is believed to contribute to their hypertensive state and increased risk of cardiovascular morbidity (Tonelli et al., 2006; Hering et al., 2007; Rubinger et al., 2012; Salman et al., 2014; Santoro and Mandreoli, 2014). Studies utilizing chemoreflex deactivation with 100% oxygen in CKD patients support the hypothesis that tonic activation of peripheral chemoreceptors contributes to this elevated sympathetic activity (Hering et al., 2007). The concept of tonic activation of peripheral chemoreceptors in CKD aligns with chronic systemic hypoxia in CKD patients, which has been proposed to be mediated by a combination of vascular changes and anemia (Prommer et al., 2018). Increased tonicity and sensitivity of carotid body afferents are documented in human and mammalian models of hypertension (Tan et al., 2010; Abdala et al., 2012; Sinski et al., 2012; Paton et al., 2013; Moraes et al., 2018), heart failure (Marcus et al., 2014, 2018), human sleep apnea (Narkiewicz et al., 1998, 1999), and other cardiovascular diseases and are a causal mechanism for the observed increase in SNA.

We have previously shown an association between respSNA and sympathetic hyperactivity in adult male Lewis polycystic kidney (LPK) rats, a genetic CKD rat model of secondary hypertension (Saha et al., 2019). We demonstrated in these animals that peripheral chemoreceptor activation evoked a larger increase in respSNA compared to control animals (Saha et al., 2019), consistent with rats who have been exposed to conditions of chronic hypoxia, which present an enhanced pattern of central sympathetic–respiratory coupling (Zoccal et al., 2008).

Population-based studies suggest that female CKD patients may have a reduced risk of cardiovascular morbidity and mortality compared to male patients (Franczyk-Skora et al., 2012; Nitsch et al., 2013). Noting that sex differences exist in autonomic, cardiovascular, and ventilatory responses to cardiorespiratory reflex activation in healthy individuals (Crofton et al., 1988; Chen and DiCarlo, 1996; Tank et al., 2005; Kim et al., 2011; Joshi and Edgell, 2019), this sexual dimorphism may be a contributing pathophysiological mechanism to the apparent protective impact of female sex on cardiovascular disease risk. For example, we have previously demonstrated that female LPK show a lesser degree of hypertension compared to male animals (Phillips et al., 2007) and that the mechanism underpinning sympathetic nerve and heart rate (HR) baroreflex dysfunction operates differently between males and females (Salman et al., 2014, 2015b), with male animals demonstrating reduced baroreflex control due to disturbances in both afferent and central baroreflex processing, whereas female animals demonstrate altered processing within the central component of the baroreflex only. Further, sex differences exist within rodents in the profile of respSNA after exposure to chronic intermittent hypoxia, with both sexes showing increased SNA modulation, but female rats exhibiting a change during inspiration, whereas for male rats, it is during expiration (Souza et al., 2016, 2017). To our knowledge, it is unknown whether sex differences exist in either the pattern of respSNA or the response to respiratory challenge in CKD. This is important to study in order to provide completeness of representation of sex in biomedical research studies (Beery and Zucker, 2011) as different therapeutic approaches may need to be considered if there is an underlying mechanistic difference in the disease state.

The present study therefore was designed to characterize the pattern of respiratory-related SNA in female rodents with CKD and assess changes in respSNA and hemodynamic responses induced by chemoreceptor stimulation, comparing responses to peripheral or central CO_2 chemoreception, thereby allowing determination of the key components of the integrated chemoreflex response to be considered. Our primary hypothesis was that the CKD-related hypertensive female rats would exhibit both heightened sympathetic–respiratory coupling and responsiveness to hypoxic chemoreceptor stimulation when compared to normotensive controls. Based on our previous demonstration of a milder hypertensive phenotype and that afferent baroreceptor function is unaffected in the female LPK, we further hypothesized that the cardiorespiratory reactivity to hypoxic chemoreceptor stimulation would be milder in females with CKD relative to male CKD animals examined under the same experimental conditions.

MATERIALS AND METHODS

All procedures were approved by the Animal Ethics Committee of Macquarie University, Sydney, New South Wales, Australia, and adhered to the Australian Code of Practice for the Care and Use of Animals for Scientific Purposes. Adult female LPK rats aged 12 to 13 weeks (n = 8) and age-matched control female Lewis rats (n = 9) were used. Stage of estrus cycle was not determined in the female animals. Animals were obtained from the Animal Resources Center, Perth, Western Australia. Animals arrived 2 weeks prior to experiments. During this period, animals underwent the process of acclimatization to a new housing environment and experimental procedures, including training for metabolic cage placement for 24-h urine collection. During this period, animals were monitored for normal weight and growth for their age. The male data to which

the female results are compared (**Supplementary Tables 1–5**) have been published prior (Saha et al., 2019). The male and female experiments were undertaken in parallel under the same experimental conditions, with animals acquired from the same source, held in the same facility and physiological data acquired using the same equipment. The data from the female animals have not been previously published.

Renal Function

Urine samples over a 24-h period were collected from all animals 48 h before experimentation. Urine volume, urinary creatinine, and protein levels were determined using an IDEXX Vetlab analyzer (IDEXX Laboratories Pty Ltd., Sydney, New South Wales, Australia). An arterial blood sample was collected on the day of the experiment to determine plasma urea and creatinine. An estimate of creatinine clearance was also calculated (Yao et al., 2015).

Surgical Procedures

Anesthesia was induced with 10% (wt/vol) ethyl carbamate (Urethane; Sigma–Aldrich, St. Louis, MO, United States) dissolved in 0.9% NaCl solution at a dose of 1.3 g/kg delivered intraperitoneally (i.p.). Anesthetic depth was assessed by periodic hind-paw pinch and supplemental doses of urethane given [65 mg/kg i.p. before catheterization and then intravenous (i.v.)] as required. Body temperature was maintained at 37°C ± 0.5°C using a homeothermic heating blanket (Harvard Apparatus, Holliston, MA, United States) and infrared heating lamp. The right femoral artery was cannulated for measurement of arterial pressure (AP) and for measurements of arterial blood chemistry. The femoral vein cannulated for administration of Ringer's lactate, 5 mL/kg per hour. The arterial cannula was connected to pressure transducer. The AP signal was passed through a bioamplifier, digitized, and sampled at 200 Hz using a CED 1401 with Spike 2 software (Cambridge Electronic Designs Ltd., Cambridge, United Kingdom). A tracheostomy was performed, and an endotracheal tube secured in place to permit mechanical ventilation. A bilateral vagotomy was performed to eliminate lung stretch receptor afferents entraining central inspiratory activity. Animals were ventilated with O_2-enriched room air (7025 Rodent Ventilator; Ugo Basile, Gemonio, Italy) and paralyzed with pancuronium bromide (induction: 2 mg/kg i.v.; maintenance; 1 mg/kg) (AstraZeneca, Australia). The left phrenic nerve was approached dorsally, isolated, tied with silk thread, and cut distal to the tie (Burke et al., 2010). The left splanchnic sympathetic and renal sympathetic nerves were dissected using a retroperitoneal approach as previously described (Burke et al., 2011; Saha et al., 2019). All nerves were bathed in a liquid paraffin pool, and the central end recorded using bipolar silver wire recording electrodes, amplified, and bandpass-filtered (100–3,000 Hz) with a bioamplifier (CWE Inc., Ardmore, PA, United States) and sampled at 5 kHz using a CED 1401 plus and Spike 2 software. All recordings were calibrated to a presetting 50 μV using the same bioamplifier for all experiments.

The preparation was then stabilized for 30 min and arterial blood collected and analyzed for Sa_{O_2}, pH, P_{CO_2}, and HCO_3 (VetStat Electrolyte and arterial blood gas analyzer; IDEXX Laboratories Pty Ltd.). Sa_{O_2} was used to measure the oxygenation of blood instead of Pa_{O_2} as Sa_{O_2} and is directly relatable to human studies (Hering et al., 2007). If required, arterial blood chemistry status was adjusted to maintain parameters within the following range: pH 7.4 ± 0.05, P_{CO_2} = 40 ± 5 mmHg, HCO_3^- = 24 ± 2 mmol/L, Sa_{O_2} = 100%, and end-tidal CO_2 = 4.5% ± 0.5%. This was achieved by adjusting the rate and depth of the mechanical ventilator and/or slow bolus of 5% sodium bicarbonate. A second arterial blood gas analysis was undertaken as required.

Experimental Protocol

The experimental protocol followed was as we have published previously (Saha et al., 2019). Briefly, following stabilization, the integrity of recordings of the splanchnic and renal nerve activity (sSNA and rSNA, respectively) was confirmed by SNA pulse modulation and demonstration of a baroreflex response to a bolus injection of phenylephrine (50 μg/kg i.v.; Sigma–Aldrich). Baseline recordings were then established under control conditions for 30 min. As documented in male animals (Saha et al., 2019), mild hypoxia was induced by switching animals to room air, without oxygen supplementation, for 3 min without any change in ventilator rate or volume, as confirmed by arterial blood gas analysis (range of 82–84% Sa_{O_2}). After hypoxic exposure, the preparation recovered for 30 min before a hypercapnic challenge of 5% carbogen (5% CO_2 in 95% O_2) for 3 min without any change in the ventilator rate or volume, as confirmed by arterial blood gas analyses (range of 65 ± 8 mmHg P_{CO_2}).

At completion of the study, animals were euthanized with 3 M potassium chloride delivered i.v. The electrical noise levels for phrenic nerve activity (PNA), sSNA, and rSNA were recorded and later subtracted in the data analysis.

Data Analysis

Acquired data were analyzed offline in Spike 2. Mean arterial pressure (MAP), systolic blood pressure (SBP), diastolic blood pressure (DBP), pulse pressure (PP), and HR were determined. The splanchnic and renal sympathetic recordings were rectified and smoothed 0.1 s. PNA was rectified and smoothed 0.05 s. Baseline data for the analysis were defined as the 30-s period at the end of the control ventilation period immediately prior to the hypoxic and hypercapnic exposures. Response to each chemo challenge was analyzed over a 30-s period once PNA had stabilized for 1 to 2 min. Responses are expressed as a change (Δ) relative to the 30-s period immediately before each stimulus. The PNA amplitude, frequency (number cycle.min^{-1}), and inspiratory duration (in seconds) were determined. Ensemble averages of rectified and smoothed rSNA and sSNA triggered to PNA were then generated from the last 30 s of the hypoxic or hypercapnia epoch. The respiratory cycle was divided into three phases: inspiratory (I), postinspiratory (PI) and late expiratory (E) based on well-established features of the respiratory motor pattern (Bautista et al., 2010; Burke et al., 2010, 2015). For the renal and splanchnic SNA, the mean level was measured from the period 200 ms before the onset of the phrenic burst corresponding to the late-expiratory E phase, and this was

considered the baseline for all other measurements. From the ensemble averages, the following parameters were calculated: peak SNA activity (PA [μV]) being the maximal SNA burst coincident with inspiratory/PI phase, the duration [from onset of excitatory activity to return to baseline (in seconds)], and area under the curve (AUC) of respSNA excitatory peak (μV s) determined as the integral of the waveform. AUCs of respSNA for I, PI, and E phase of the phrenic cycle were also calculated from the integral of the waveform.

Statistical Analysis

Data are presented as mean ± SEM. Unpaired two-tailed Student *t* test was used to examine strain differences in renal function, cardiorespiratory function, and SNA. Two-way analysis of variance with repeated measures and Bonferroni corrections was used to examine strain differences in respiratory modulation of SNA under control conditions and in response to hypoxia or hypercapnia, with strain and ventilatory condition (i.e., normoxia, hypoxia, or hypercapnia) as variables. An unpaired two-tailed Student *t*-test was used to determine strain differences in delta changes from control to hypoxia or hypercapnia in cardiorespiratory function. Statistical analyses were performed with GraphPad Prism (GraphPad Software Inc., United States), and significance is indicated where $P \leq 0.05$.

RESULTS

Female LPK animals exhibited elevated blood urea (LPK 23.7 ± 2.7 vs. Lewis 6.7 ± 0.5 mmol/L) and plasma creatinine (44.7 ± 7.9 vs. 13.1 ± 2.6 μmol/L) and reduced creatinine clearance (1.5 ± 0.3 vs. 7.4 ± 1.2 mL/min) (LPK n = 8 vs. Lewis n = 9; $P < 0.001$). This degree of renal dysfunction was not significantly different from that of male LPK animals of the same age [(Saha et al., 2019); **Supplementary Table 1**].

Baseline Cardiorespiratory Parameters

Figure 1 illustrates individual recordings of SNA, PNA, and AP from a Lewis and LPK rat under baseline conditions. SBP, MAP, DBP, PP, HR, and SNA (both rSNA and sSNA) were elevated in the adult female LPK compared with age-matched Lewis controls (**Table 1**). In the adult female LPK, phrenic burst frequency was higher, and the duration of the phrenic burst shorter than the age- and arterial blood gas–matched Lewis controls (**Table 1**; $P < 0.05$). There was no significant difference in PNA amplitude ($P = 0.23$).

To identify if respSNA was altered in female LPK, we first examined the temporal relationship between SNA and the respiratory cycle. Both sympathetic nerves exhibited respiratory sympathetic harmony, with a clear burst in SNA in the PI period observed in both Lewis and LPK rats (**Figures 1**, **2A,B,E,F**, **4A,B,E,F**). In Lewis rats, both sympathetic nerves showed weak PI coupling. In contrast, respSNA in the LPK exhibited inhibition during early I that was most obvious in rSNA (rSNA, I AUC, LPK vs. Lewis: −0.3 ± 0.1 vs. 0.2 ± 0.1 μV; $P < 0.05$; sSNA, I AUC, LPK vs. Lewis: 0.02 ± 0.05 vs. 0.2 ± 0.07 μV; $P > 0.05$) with a persistence of excitation in both rSNA and sSNA during the E period that was not different between strains (rSNA, E AUC, LPK vs. Lewis: 0.1 ± 0.04 vs. −0.03 ± 0.08 μV; $P > 0.05$; sSNA, E AUC, LPK vs. Lewis: 0.09 ± 0.06 vs. 0.03 ± 0.07 μV; $P > 0.05$).

TABLE 1 | Baseline cardiorespiratory function in female Lewis and LPK rats.

	Lewis	LPK
MAP (mmHg)	93 ± 4	126 ± 10*
SBP (mmHg)	125 ± 8	184 ± 18*
DBP (mmHg)	77 ± 4	99 ± 9*
PP (mmHg)	47 ± 8	84 ± 15*
HR (bpm)	427 ± 7	456 ± 37*
PNA amplitude (μV)	13.1 ± 3.5	20.9 ± 5.4
PNA frequency (cycles/min)	32 ± 1	42 ± 1*
PNA duration (s)	1.01 ± 0.05	0.69 ± 0.02*
rSNA (μV)	4.4 ± 0.8	7.5 ± 1.05*
sSNA (μV)	3.02 ± 0.5	6.4 ± 1.1*

*Measures of cardiorespiratory parameters in Lewis and LPK rats. LPK, Lewis polycystic kidney; MAP, mean arterial pressure; SBP, systolic blood pressure; DBP, diastolic blood pressure; PP, pulse pressure; HR, heart rate; bpm, beats per minute; PNA, phrenic nerve amplitude; rSNA, renal sympathetic nerve activity; sSNA, splanchnic sympathetic nerve activity. Results are expressed as mean ± SEM. *P < 0.05 between Lewis rats and LPK rats as determined by Student t-test. n = 9 Lewis and n = 8 LPK except rSNA where n = 6 Lewis and n = 5 LPK.*

Under control conditions, baseline respSNA in both nerves was significantly greater in the female LPK as reflected by a larger AUC (**Table 2**). This amplified respSNA was associated with both a higher magnitude of PA and longer duration of respSNA in LPK compared to Lewis control rats (**Table 2**).

Responses to Chemoreceptor Challenge

In the female LPK rats, peripheral chemoreceptor stimulation using a mild hypoxic challenge evoked a heightened pressor response compared to Lewis rats (**Table 3**). There was no significant difference in the increase in HR seen in both strains (**Table 3**). Hypoxia in the female LPK resulted in an increase in phrenic nerve amplitude, shortened burst duration, and slowed phrenic nerve frequency. The Lewis rats also responded to mild hypoxia with a comparable increase in phrenic nerve amplitude, a reduction of phrenic duration that was of a greater magnitude than that seen in the LPK, and a slight increase in frequency.

When comparing respSNA parameters after exposure to hypoxic conditions, the PA and AUC of respSNA of both rSNA and sSNA significantly increased in LPK rats, whereas in Lewis rats, the PA and AUC of respSNA of rSNA increased (**Figures 2**, **3**). The increase in AUC in both rSNA and sSNA was greater in the LPK than that seen in Lewis rats Δ AUC, rSNA: LPK vs. Lewis: 6.07 ± 1.1 vs. 3.1 ± 0.7μV s, sSNA: LPK vs. Lewis: 8.9 ± 3.4 vs. 2 ± 0.7, both $P \leq 0.05$). Of note was that under hypoxic conditions, in LPK rats, sympathoinhibition during inspiration increased significantly in rSNA (I AUC, rSNA, control vs. hypoxia: −0.25 ± 0.1 vs. −1.08 ± 0.2 μV, $P \leq 0.05$; **Figure 2**). A comparable directional response was seen in sSNA in the LPK but did not reach significance (I AUC, sSNA, control vs. hypoxia: 0.02 ± 0.05 vs. −0.5 ± 0.1 μV, $P = 0.08$) (**Figure 2**). The AUC during E in the LPK was greater during hypoxia (E

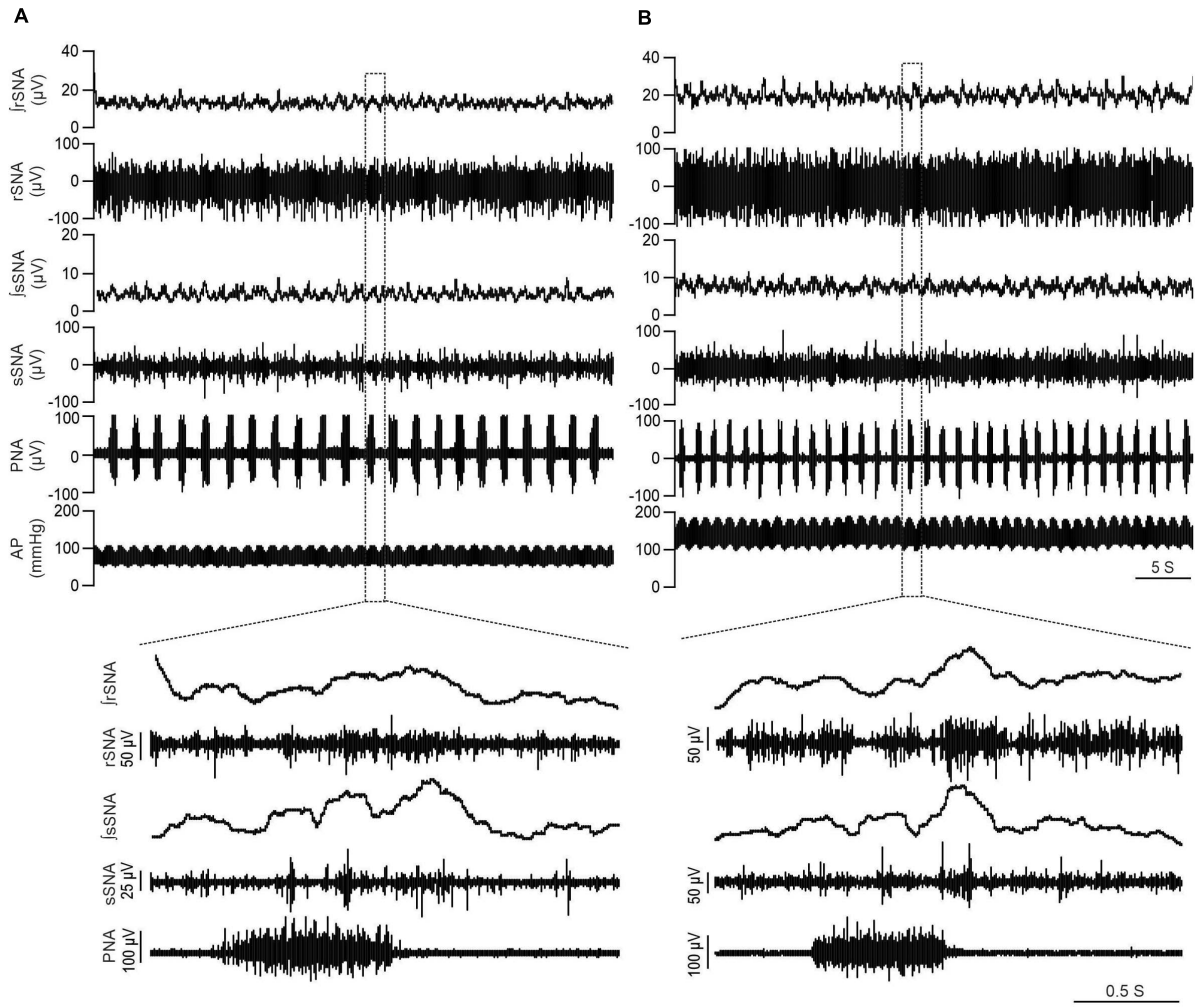

FIGURE 1 | LPK rats exhibit higher SNA and BP in baseline recordings. Physiological recordings under urethane anesthesia representing raw and integrated renal sympathetic nerve activity (rSNA and ∫rSNA), splanchnic sympathetic nerve activity (sSNA and ∫sSNA), phrenic nerve activity (PNA) and arterial pressure (AP) in a 12-week-old Lewis rat **(A)** and 12-week-old LPK rat **(B)**. Note the higher rSNA, sSNA, and arterial pressure in the LPK in comparison to Lewis rats. Bottom panels illustrate Enlarged traces of one respiratory cycle with corresponding splanchnic and renal SNA.

AUC, sSNA, control vs. hypoxia: 0.09 ± 0.06 vs. 0.75 ± 0.3 μV, $P < 0.05$), but there was no change in E AUC in the rSNA ($P > 0.05$). There was no change in I AUC or E AUC for either the renal or splanchnic nerves in the Lewis female rats ($P > 0.05$).

Mild hypercapnic stimuli produced a comparable increase in blood pressure between the strains (**Table 3**). Hypercapnia in the female LPK resulted in an increase in phrenic nerve amplitude, shortened burst duration, and slowed phrenic nerve frequency. The Lewis rats also responded to hypercapnia with an increase in phrenic nerve amplitude and reduced phrenic nerve frequency, which was not significantly different from that seen in the LPK. There was, however, an increased in phrenic duration as compared to the reduction seen in the LPK.

When comparing respSNA parameters after exposure to hypercapnic conditions, in Lewis rats, both the renal and splanchnic nerves demonstrated an increase in PA, and in the renal nerve, there was also an increase in the measured AUC (**Figures 4**, **5**). In the LPK, hypercapnia increased the AUC in both nerves, and there was also an increase in PA in the splanchnic nerve. Hypercapnia did not alter the duration of the curves in either strain, although it was greater in the LPK rats compared to Lewis rats under treatment conditions. The magnitude of observed changes in respSNA was comparable between the strains (Δ AUC, rSNA: LPK vs. Lewis: 4.2 ± 0.9 vs. 3.5 ± 1.4 sSNA: LPK vs. Lewis: 2.5 ± 1 vs. 1.3 ± 0.7μV s, both $P > 0.05$).

Sympathoinhibition during inspiration in the LPK did not significantly change in either rSNA or sSNA (I AUC, rSNA, control vs. hypercapnia: −0.21 ± 0.1 vs. −0.34 ± 0.1 sSNA: 0.04 ± 0.07 vs. 0.08 ± 0.09 μV s, both $P > 0.05$), and AUC

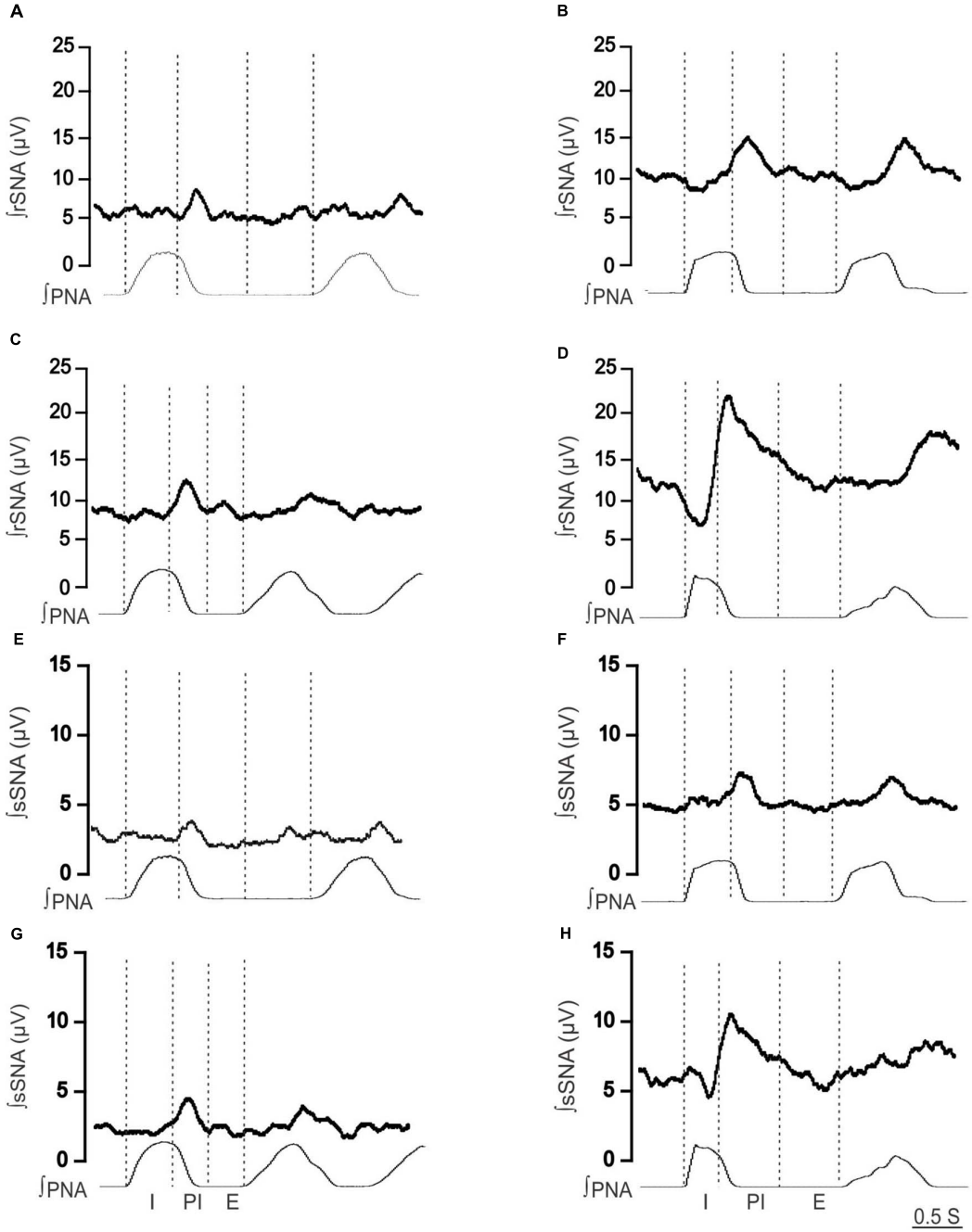

FIGURE 2 | Effect of hypoxia on respiratory-related sympathetic nerve activity in adult female Lewis and LPK rats. Phrenic-triggered ensemble averages of renal sympathetic (∫rSNA) and splanchnic sympathetic nerve activity (∫sSNA) during different phases of the phrenic cycle (I, inspiration; PI, postinspiration; E, expiration) under control **(A,B,E,F)** and hypoxic conditions **(C,D,G,H)** in a Lewis rat **(A,C,E,G)** and LPK rat **(B,D,F,H)**.

in the E phase of respSNA for both nerves was comparable in response to hypercapnia in LPK rats (E AUC, rSNA, control vs. hypercapnia: 0.06 ± 0.03 vs. 0.04 ± 0.05 sSNA: 0.04 ± 0.03 vs. 0.04 ± 0.04 μV s, both $P > 0.05$). In Lewis rats, both nerves also showed no significant differences in inspiratory and expiratory period during hypercapnia (both $P > 0.05$).

Female and Male LPK Rats Both Exhibit Augmented Respiratory–Sympathetic Coupling and Pressor Responses to Acute Mild Hypoxia and Hypercapnia

We have previously shown that when compared to normotensive control Lewis, male LPK rats are hypertensive and exhibit

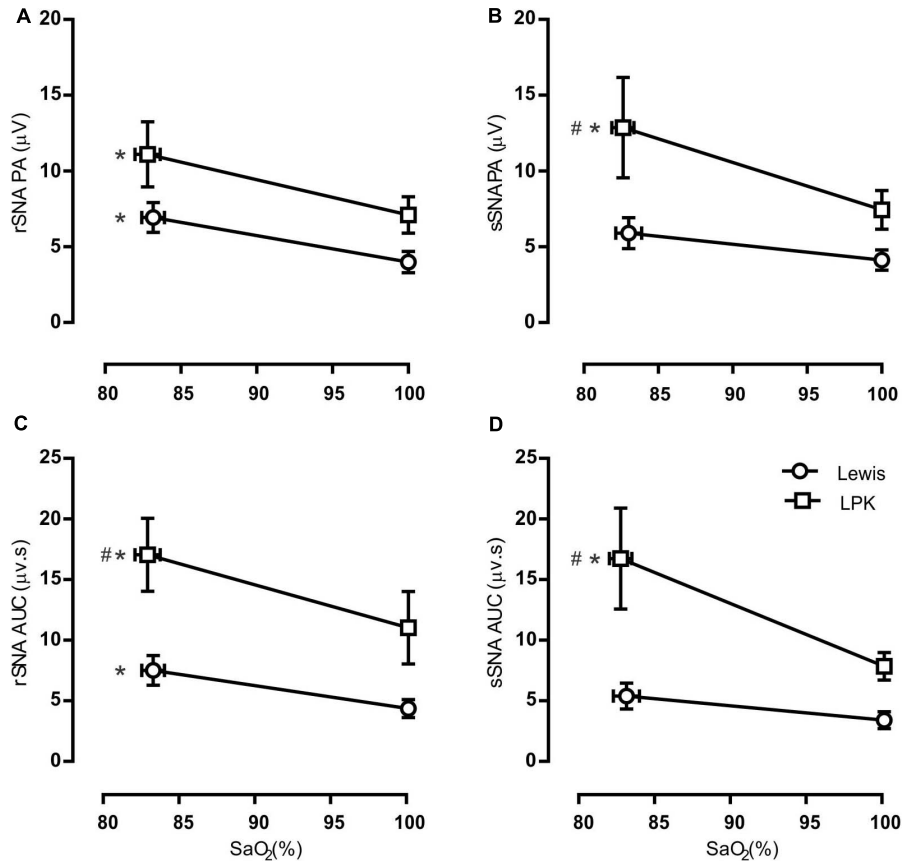

FIGURE 3 | Group data of the effect of mild hypoxia on respiratory-related sympathetic nerve activity in adult female Lewis and LPK rats. Respiratory-related sympathetic nerve activity was measured as peak amplitude **(A,B)**, or area under the curve (AUC; **C,D**) of the phrenic triggered ∫rSNA **(A,C)** and ∫sSNA **(B,D)** during normoxia (control) and hypoxic conditions. Data are expressed as mean ± SEM $n \geq 5$ per group. *$P < 0.05$ hypoxia versus baseline (normoxia) within each strain; #$P < 0.05$ LPK versus treatment-matched Lewis.

heightened respiratory-related sympathetic bursts at baseline, and mild hypoxia evokes larger increase in respSNA (Saha et al., 2019). The female rats in this study also exhibited a heightened pressor response and respSNA to both hypoxia and hypercapnia. Comparing our previous male data with the female data presented in this study, we observed no sex differences in the LPK or Lewis control rat in their pressor response or respSNA during hypoxia or hypercapnia. Comparison of renal functional data indicated that at the age studied, the degree of renal decline was also not significantly different (**Supplementary Tables 1–5**).

DISCUSSION

Summary

The major findings of this study are that female rodents with CKD demonstrate increased sympathetic tone and amplified respSNA under baseline conditions and further demonstrate enhanced respSNA and hemodynamic responses to a hypoxic chemoreflex challenge when compared to female Lewis control rats. Moreover, female LPK rats exhibit the same distinctive temporal pattern of respSNA seen in male LPK rats, featuring the peak of respSNA in the PI period and increased inhibition of rSNA during the inspiratory period, with the magnitude of augmentation of respSNA during hypoxia likewise similar (Saha et al., 2019). These results support our hypothesis that CKD-related hypertensive female rats would exhibit heightened sympathetic–respiratory coupling when compared to normotensive controls but do not support our hypothesis that their cardiorespiratory reactivity to chemoreceptor stimulation would be milder when compared to male CKD animals examined under similar experimental conditions.

Increased SNA

It has been suggested that sympathetic hyperactivity contributes to hypertension in both hypertensive female rat models and women (Hart and Charkoudian, 2014; Maranon et al., 2014). Our demonstration of increased SNA in adult female LPK rats under control conditions corresponds with the marked elevation in blood pressure we observe in these female LPK rats from an early age (Kandukuri et al., 2012; Salman et al., 2015b) and evidence that sympathetic overactivity is a crucial pathological feature in this model, being evident before renal function becomes significantly compromised

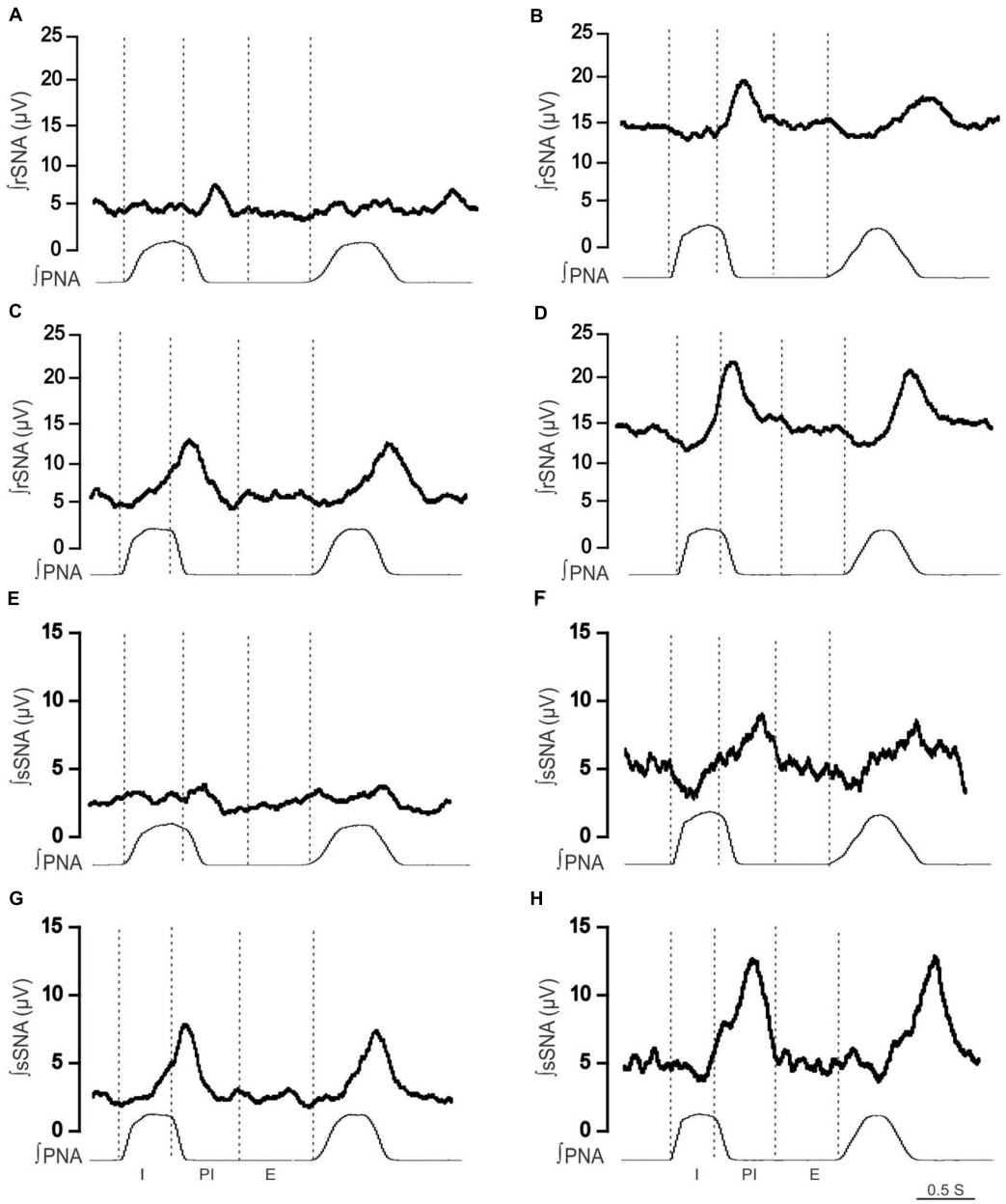

FIGURE 4 | Effect of hypercapnia on respiratory-related sympathetic nerve activity in adult female Lewis and LPK rats. Phrenic-triggered ensemble averages of renal sympathetic (∫rSNA) and splanchnic sympathetic nerve activity (∫sSNA) during different phases of the phrenic cycle (I, inspiration; PI, postinspiration; E, expiration) under control **(A,B,E,F)** and hypercapnic conditions **(C,D,G,H)** in a Lewis rat **(A,C,E,G)** and LPK rat **(B,D,F,H)**.

(Salman et al., 2015b). Current knowledge on the underlying pathogenesis of sympathetic overactivity in female patients with kidney disease, however, is limited.

Heightened respSNA and Characteristic Temporal Pattern

Our present study demonstrates heightened respSNA in adult female LPK rats in association with hypertension and echoes our data from male juvenile and adult LPK, studied *in situ* and *in vivo*, respectively (Saha et al., 2019). It is also in alignment with studies examining exposure to chronic intermittent hypoxia, where female rats similarly exhibit an augmented respSNA and hypertension (Souza et al., 2016). As demonstrated in male animals (Saha et al., 2019; Toor et al., 2019), in both the female LPK and normotensive control Lewis animals, the peak of respSNA from the onset of the phrenic burst was observed persistently in the PI period under all conditions tested. This is distinct from the findings in male SHR rats, where the peak of respSNA was in the inspiratory

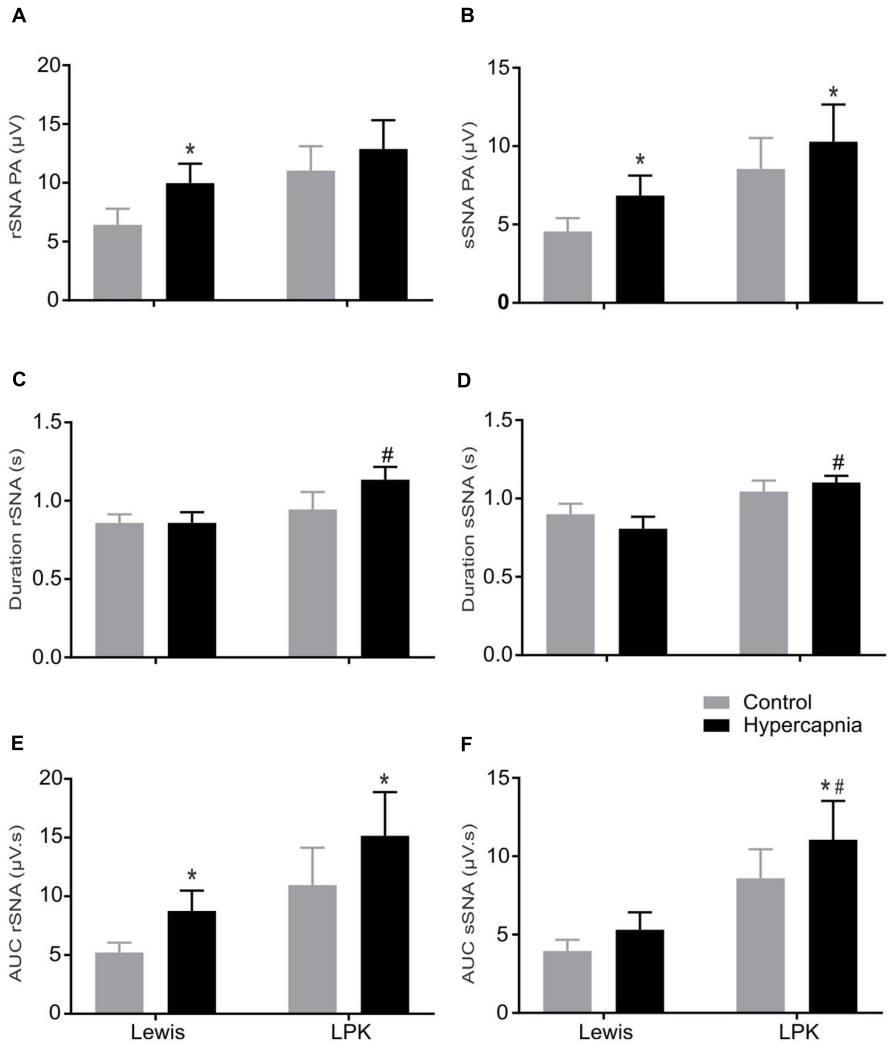

FIGURE 5 | The effect of hypercapnia on respiratory-related sympathetic nerve activity in adult female Lewis and LPK rats: group data. Respiratory-related sympathetic nerve activity measured as peak amplitude **(A,B)**, duration **(C,D)**, or area under the curve (AUC; **E,F**) of the phrenic triggered ∫rSNA **(A,C,E)** and ∫sSNA **(B,D,F)** during normoxia (control) and hypercapnic conditions. Data are expressed as mean ± SEM $n \geq 5$ per group. *$P < 0.05$ hypercapnia versus control within each strain; #$P < 0.05$ LPK versus treatment-matched Lewis.

phase (Czyzyk-Krzeska and Trzebski, 1990; Simms et al., 2009).

Notably, the temporal pattern of respSNA in female LPK exhibited inspiratory inhibition during control conditions, most apparent in the renal nerve, and this was exaggerated under hypoxic conditions, as we also describe for male animals (Saha et al., 2019). The pattern of respSNA in female LPK rats is therefore not overtly distinguishable to that of male LPK rats, suggesting that sex differences do not exist in the augmented respSNA features of this model of CKD.

Respiratory Pattern

Exploring the respiratory pattern in the context of augmented respSNA further, we did find in the anesthetized animal that respiratory rate was higher in female LPK rats compared to Lewis controls, as also demonstrated in male LPK rats under control conditions (Saha et al., 2019). Moreover, the duration of PNA was significantly reduced in female LPK rats. This is in contrast to what we saw in male LPK rats, where the duration of the PNA was the same between LPK and Lewis rats. Similarly, in response to chronic intermittent hypoxia, juvenile Wistar female rats exhibited a reduction in inspiratory period compared with control animals (Souza et al., 2016). In contrast, however, juvenile Wistar male rats exposed to chronic intermittent hypoxia showed similar phrenic frequency and duration compared to controls (Zoccal et al., 2008). These findings suggest that sex variations do exist in different phases of the respiratory cycle in disease models, including CKD. Such variation in the respiratory phases between male and female animals is proposed to depend on multiple interrelated inputs at the level of rhythm-generating inspiratory neurons at the brainstem (Garcia et al., 2013, 2016). Therefore, although not examined in this study, it is conceivable

TABLE 2 | RespSNA parameters in splanchnic and renal nerves in adult female Lewis and LPK rats under baseline conditions.

		Lewis	LPK
PA (μV)	Splanchnic	4.0 ± 0.7	7.4 ± 1.3*
	Renal	5.9 ± 0.9	9.8 ± 1.5*
AUC	Splanchnic	3.4 ± 0.7	7.8 ± 1.1*
	Renal	4.8 ± 0.7	11.5 ± 3.0*
Duration (s)	Splanchnic	0.8 ± 0.08	1.1 ± 0.06*
	Renal	0.8 ± 0.06	1.1 ± 0.12*

*Measures of respiratory–sympathetic coupling parameters for ∫sSNA and ∫rSNA in Lewis and LPK rats. LPK, Lewis polycystic kidney; PA, peak SNA activity (PA [μV]); AUC, area under the curve (s × μV), duration (of peak), and position (time from the onset of inspiration to PA). Results are expressed as mean ± SEM. *P ≤ 0.05 between Lewis rats and LPK rats as determined by Student t-test. n = 9 Lewis and n = 8 LPK for sSNA and n = 6 Lewis and n = 5 LPK for rSNA.*

TABLE 3 | Effects of peripheral or central chemoreceptor stimulation on cardiorespiratory pattern in adult female Lewis and LPK rats.

		Lewis (*n* = 9)	LPK (*n* = 8)
Hypoxia	Δ MAP (mmHg)	12 ± 6	30 ± 6*
	Δ SBP (mmHg)	15 ± 6	41 ± 8*
	Δ DBP (mmHg)	9 ± 5	27 ± 6*
	Δ PP (mmHg)	5 ± 1	15 ± 5*
	Δ HR (bpm)	25 ± 6	23 ± 3
	Δ PNA amplitude (μV)	7.3 ± 1.7	11.01 ± 1.9
	Δ PNA duration (s)	−0.2 ± 0.03	−0.07 ± 0.03*
	Δ PNA frequency (cycles/min)	5 ± 2	−10 ± 3*
Hypercapnia	Δ MAP (mmHg)	9 ± 5	13 ± 3
	Δ SBP (mmHg)	12 ± 6	20 ± 5
	Δ DBP (mmHg)	8 ± 4	10 ± 2
	Δ PP (mmHg)	3 ± 2	10 ± 3
	Δ HR (bpm)	−0.3 ± 1	2 ± 4
	Δ PNA amplitude (μV)	9.4 ± 2.8	9 ± 2.3
	Δ PNA duration (s)	0.8 ± 0.03	−0.06 ± 0.02*
	Δ PNA frequency (cycles/min)	−0.2 ± 1	−2 ± 1

*Delta change (Δ) in phrenic triggered integrated phrenic nerve activity (PNA) and blood pressure (mmHg) in hypoxia (ventilated with only room air) or hypercapnia (ventilated with 5% CO_2 with 95% O_2) when switched from control condition (ventilated with room air enriched with 100% O_2) in adult Lewis and LPK rats under urethane anesthesia. LPK, Lewis polycystic kidney; MAP, mean arterial pressure; SBP, systolic blood pressure; DBP, diastolic blood pressure; PP, pulse pressure. Results are expressed as mean ± SEM. *P ≤ 0.05 between Lewis rats and LPK rats as determined by Student t-test. n = number of animals per group.*

that in female LPK rats, the input to respiratory neurons causing variation in the phases of the respiratory cycle may be different from that of male LPK rats.

Intriguingly, our present study also shows that in response to peripheral chemoreceptor stimulation, phrenic frequency was reduced in female LPK rats compared to control rats. This was also reduced in male LPK rats compared to male Lewis rats. These findings are in contrast to the findings of other studies of adult female animals, which demonstrate that respiratory frequency was not changed during acute hypoxia (Garcia et al., 2013) and after chronic intermittent hypoxia (Souza et al., 2015). Given that the study by Garcia et al. (2013) was performed in neonate animals and the work of Souza et al. (2015) in prepubertal animals, the age and stage of development could be one of the reasons for this contrasting result. Different forms of respiratory input to various subclasses of presympathetic motor neurons may therefore trigger this variation in the pattern of respSNA observed during hypoxia in the female LPK rats. Future work is required to explore this possibility.

Cardiorespiratory Responses to Chemoreceptor Stimulation

In the present study, stimulation of peripheral chemoreceptors using a mild hypoxic stimulus induced an increase in blood pressure and respSNA in both strains, the magnitude of which was significantly greater in LPK rats compared to Lewis. This is consistent with studies that indicate increased sensitivity of peripheral chemoreceptors is a driver of increased sympathetic activity in hypertension and CKD (Hering et al., 2007; Abdala et al., 2012; Paton et al., 2013).

In contrast, hypercapnia produced changes of a similar magnitude between the strains. Thus, in this disease model of CKD, the increase in respiratory sympathetic coupling is not a uniform phenomenon responding to increased chemosensitive drive or increased central respiratory drive (or by corollary, increased breathing effort), but is specific to hypoxic drive and carotid body feedback. Further, although not examined in this study, the augmented response to hypoxia is unlikely to be relayed via central respiratory chemoreceptors such as the retrotrapezoid nucleus neurons, which are an important site of integration between central and peripheral chemoreception (Takakura et al., 2006; Basting et al., 2015; Guyenet et al., 2016). Notably, our findings are comparable to studies in humans that demonstrated specific potentiation of autonomic and ventilatory responses to peripheral chemoreceptor activation in obstructive sleep apnea (OSA) patients using similar isocapnic hypoxia and hyperoxic hypercapnia stimulation paradigms, making the conclusion that tonic chemoreflex activation may contribute to increased sympathetic activity and blood pressure in patients with OSA (Narkiewicz et al., 1998, 1999).

Changes in Expiratory Phase Activity

There are several classes of presympathetic rostral ventrolateral medulla (RVLM) neurons based on their respiratory modulation, including I activated, PI activated, I inhibited, and non-modulated neurons (Moraes et al., 2013). Interactions between these RVLM presympathetic neurons and respiratory neurons contribute to the phasic respiratory modulation of sympathetic outflow studied in this article (Haselton and Guyenet, 1989; Guyenet, 2006). From studies using male rats, it has been suggested that a hypoxic stimulus with subsequent peripheral chemoreceptor activation drives respiratory neurons and premotor sympathetic neurons to contribute to amplified respSNA during expiration, leading to increased sympathetic drive and hypertension (Zoccal et al., 2008; Zoccal and Machado, 2010; Wong-Riley et al., 2013). In contrast, in studies using female rats, peripheral chemoreceptor stimulation has been shown to drive inspiratory and premotor sympathetic neurons to contribute to amplified respSNA during inspiration, again, however, leading to increased sympathetic drive and

hypertension (Souza et al., 2016, 2017). In our present study in female LPK rats, respSNA in the splanchnic nerve under hypoxic conditions showed persistence of excitation in expiration, although renal SNA did not show this expiratory change. This finding contrasts with the finding of male LPK rats, which did not show any excitation of respSNA during expiration.

Study Limitations

A number of caveats should be considered in the review of the data presented in this article. First, these experiments were performed under urethane anesthetic, which has known impact on central neural control of cardiovascular reflexes (Accorsi-Mendonca et al., 2007), and this is a caveat for all studies performed under these conditions; however, our results are comparable to our studies using the working heart brainstem preparation (Saha et al., 2019), where experiments are performed in the absence of anesthetic, and support translatability of these findings to more physiological conditions. Another consideration is that our sympathetic nerve recording data analysis is reported as absolute value microvolt recordings from multifiber sympathetic nerve preparations. While differences in the contact between the nerve and electrode can result in differences in the microvolt signal amplitude, our work, in this study and previously under both conscious (Salman et al., 2015a) and anesthetized conditions (Yao et al., 2015; Saha et al., 2019), demonstrated SNA at baseline was heightened in the LPK model with a low level of variance within each group of animals. This is consistent with the work of others who similarly report SNA data when comparing baseline activity between different groups of animals (Guild et al., 2010; Stocker and Muntzel, 2013; Burke et al., 2016; Ong et al., 2019) and, importantly, as presented in the seminal study in this field by Simms et al. (2009), who used microvolt data to measure respiratory and sympathetic responses to changes in chemoreceptor stimuli in the SHR rat. Notably, foundational studies that served to establish the high level of SNA in the SHR strain were also analyzed using microvolt data to compare animals across a range of different ages (Judy et al., 1976, 1979). Confidence in our data is further supported by our prior work demonstrating that LPK rats have significantly elevated circulating levels of both norepinephrine and epinephrine (Wyse et al., 2011) and the alignment of our AUC analysis with our μV data in the current study.

CONCLUSION

Our present study demonstrates that amplified respSNA is associated with sympathetic overactivity and hypertension in female LPK rats and that peripheral chemoreceptor stimulation provokes a significantly greater increase in respSNA compared to normotensive control animals. Importantly, this fundamental response did not differentiate from our findings in male animals who were studied under similar conditions with a comparable degree of renal dysfunction.

Although hypertension in CKD is a complex and multifactorial disease, in terms of increasing our understanding of the pathophysiology, our results indicate that amplified respSNA is an inherent character of CKD likely driving autonomic dysfunction regardless of sex and highlight that controlling hypertension through reduction of sympathetic activity should be a key focus in the management of this disease. And although we did not delineate the central neural pathways underlying these changes, our findings might be explained in part by tonic activation and increased sensitivity of excitatory chemoreflex afferents. In terms of translational outcomes, this means that future therapeutics directed at reducing SNA, and in turn hypertension, in CKD that target this pathway are applicable to both males and females.

DATA AVAILABILITY STATEMENT

The original contributions presented in the study are included in the article/**Supplementary Material**, further inquiries can be directed to the corresponding author/s.

ETHICS STATEMENT

The animal study was reviewed and approved by the Animal Ethics Committee of Macquarie University, NSW Australia.

AUTHOR CONTRIBUTIONS

MS was the major contributor to the initial drafting of the manuscript and contributed to experimental design, performed all experiments, analyzed the data, and interpreted results. Q-JS contributed to the experimental work, interpretation of results, and final approval of manuscript. JP and CH contributed to experimental design, analysis, and interpretation of results, drafting of manuscript and final approval. PB contributed to experimental design, interpretation of results, manuscript revision, and final approval. All authors contributed to the article and approved the submitted version.

FUNDING

MS was a recipient of a Macquarie University International Research Scholarship.

SUPPLEMENTARY MATERIAL

The Supplementary Material for this article can be found online at: https://www.frontiersin.org/articles/10.3389/fphys.2021.623599/full#supplementary-material

Data for male animals contained within the Supplementary Material are republished with permission of Elsevier from Saha et al. (2019); permission conveyed through Copyright Clearance Center, Inc.

REFERENCES

Abdala, A. P., McBryde, F. D., Marina, N., Hendy, E. B., Engelman, Z. J., Fudim, M., et al. (2012). Hypertension is critically dependent on the carotid body input in the spontaneously hypertensive rat. *J. Physiol.* 590, 4269–4277. doi: 10.1113/jphysiol.2012.237800

Accorsi-Mendonca, D., Leao, R. M., Aguiar, J. F., Varanda, W. A., and Machado, B. H. (2007). Urethane inhibits the GABAergic neurotransmission in the nucleus of the solitary tract of rat brain stem slices. *Am. J. Physiol. Regul. Integr. Comp. Physiol.* 292, R396–R402.

Basting, T. M., Burke, P. G., Kanbar, R., Viar, K. E., Stornetta, D. S., Stornetta, R. L., et al. (2015). Hypoxia silences retrotrapezoid nucleus respiratory chemoreceptors via alkalosis. *J. Neurosci.* 35, 527–543. doi: 10.1523/jneurosci.2923-14.2015

Bautista, T. G., Burke, P. G., Sun, Q. J., Berkowitz, R. G., and Pilowsky, P. M. (2010). The generation of post-inspiratory activity in laryngeal motoneurons: a review. *Adv. Exp. Med. Biol.* 669, 143–149. doi: 10.1007/978-1-4419-5692-7_29

Beery, A. K., and Zucker, I. (2011). Sex bias in neuroscience and biomedical research. *Neurosci. Biobehav. Rev.* 35, 565–572. doi: 10.1016/j.neubiorev.2010.07.002

Burke, P. G., Abbott, S. B., McMullan, S., Goodchild, A. K., and Pilowsky, P. M. (2010). Somatostatin selectively ablates post-inspiratory activity after injection into the Botzinger complex. *Neuroscience* 167, 528–539. doi: 10.1016/j.neuroscience.2010.01.065

Burke, P. G., Kanbar, R., Basting, T. M., Hodges, W. M., Viar, K. E., Stornetta, R. L., et al. (2015). State-dependent control of breathing by the retrotrapezoid nucleus. *J. Physiol.* 593, 2909–2926. doi: 10.1113/jp270053

Burke, P. G., Neale, J., Korim, W. S., McMullan, S., and Goodchild, A. K. (2011). Patterning of somatosympathetic reflexes reveals nonuniform organization of presympathetic drive from C1 and non-C1 RVLM neurons. *Am. J. Physiol. Regul. Integr. Comp. Physiol.* 301, R1112–R1122.

Burke, S. L., Lim, K., Moretti, J. L., and Head, G. A. (2016). Comparison of sympathetic nerve activity normalization procedures in conscious rabbits. *Am. J. Physiol. Heart Circ. Physiol.* 310, H1222–H1232.

Chen, C. Y., and DiCarlo, S. E. (1996). Daily exercise and gender influence arterial baroreflex regulation of heart rate and nerve activity. *Am. J. Physiol.* 271, H1840–H1848.

Crofton, J. T., Share, L., and Brooks, D. P. (1988). Pressor responsiveness to and secretion of vasopressin during the estrous cycle. *Am. J. Physiol.* 255, R1041–R1048.

Czyzyk-Krzeska, M. F., and Trzebski, A. (1990). Respiratory-related discharge pattern of sympathetic nerve activity in the spontaneously hypertensive rat. *J. Physiol.* 426, 355–368. doi: 10.1113/jphysiol.1990.sp018142

Dick, T. E., Hsieh, Y. H., Morrison, S., Coles, S. K., and Prabhakar, N. (2004). Entrainment pattern between sympathetic and phrenic nerve activities in the Sprague-Dawley rat: hypoxia-evoked sympathetic activity during expiration. *Am. J. Physiol. Regul. Integr. Comp. Physiol.* 286:4.

Franczyk-Skora, B., Gluba, A., Banach, M., Kozlowski, D., Malyszko, J., and Rysz, J. (2012). Prevention of sudden cardiac death in patients with chronic kidney disease. *BMC Nephrol.* 13:162.

Garcia, A. J. III, Rotem-Kohavi, N., Doi, A., and Ramirez, J. M. (2013). Post-hypoxic recovery of respiratory rhythm generation is gender dependent. *PLoS One* 8:e60695. doi: 10.1371/journal.pone.0060695

Garcia, A. J. III, Zanella, S., Dashevskiy, T., Khan, S. A., Khuu, M. A., Prabhakar, N. R., et al. (2016). Chronic intermittent hypoxia alters local respiratory circuit function at the level of the preBotzinger complex. *Front. Neurosci.* 10:4.

Guild, S. J., Barrett, C. J., McBryde, F. D., Van Vliet, B. N., Head, G. A., Burke, S. L., et al. (2010). Quantifying sympathetic nerve activity: problems, pitfalls and the need for standardization. *Exp. Physiol.* 95, 41–50. doi: 10.1113/expphysiol.2008.046300

Guyenet, P. G. (2006). The sympathetic control of blood pressure. *Nat. Rev. Neurosci.* 7, 335–346.

Guyenet, P. G., Bayliss, D. A., Stornetta, R. L., Ludwig, M. G., Kumar, N. N., Shi, Y., et al. (2016). Proton detection and breathing regulation by the retrotrapezoid nucleus. *J. Physiol.* 594, 1529–1551. doi: 10.1113/jp271480

Hart, E. C., and Charkoudian, N. (2014). Sympathetic neural regulation of blood pressure: influences of sex and aging. *Physiology* 29, 8–15. doi: 10.1152/physiol.00031.2013

Haselton, J. R., and Guyenet, P. G. (1989). Central respiratory modulation of medullary sympathoexcitatory neurons in rat. *Am. J. Physiol.* 256, R739–R750.

Hering, D., Zdrojewski, Z., Krol, E., Kara, T., Kucharska, W., Somers, V. K., et al. (2007). Tonic chemoreflex activation contributes to the elevated muscle sympathetic nerve activity in patients with chronic renal failure. *J. Hypertens.* 25, 157–161. doi: 10.1097/hjh.0b013e3280102d92

Joshi, H., and Edgell, H. (2019). Sex differences in the ventilatory and cardiovascular response to supine and tilted metaboreflex activation. *Physiol. Rep.* 7:e14041. doi: 10.14814/phy2.14041

Judy, W. V., Watanabe, A. M., Henry, D. P., Besch, H. R. Jr., Murphy, W. R., and Hockel, G. M. (1976). Sympathetic nerve activity: role in regulation of blood pressure in the spontaenously hypertensive rat. *Circ. Res.* 38, 21–29. doi: 10.1161/01.res.38.6.21

Judy, W. V., Watanabe, A. M., Murphy, W. R., Aprison, B. S., and Yu, P. L. (1979). Sympathetic nerve activity and blood pressure in normotensive backcross rats genetically related to the spontaneously hypertensive rat. *Hypertension* 1, 598–604. doi: 10.1161/01.hyp.1.6.598

Kandukuri, D. S., Hildreth, C. M., and Phillips, J. K. (2012). Cardiac autonomic dysfunction in chronic kidney disease. *J. Hypertens.* 30:e82. doi: 10.1097/01.hjh.0000420163.91204.b3

Kim, A., Deo, S. H., Vianna, L. C., Balanos, G. M., Hartwich, D., Fisher, J. P., et al. (2011). Sex differences in carotid baroreflex control of arterial blood pressure in humans: relative contribution of cardiac output and total vascular conductance. *Am. J. Physiol. Heart Circ. Physiol.* 301, H2454–H2465.

Mandel, D. A., and Schreihofer, A. M. (2009). Modulation of the sympathetic response to acute hypoxia by the caudal ventrolateral medulla in rats. *J. Physiol.* 587, 461–475. doi: 10.1113/jphysiol.2008.161760

Maranon, R. O., Lima, R., Mathbout, M., do Carmo, J. M., Hall, J. E., Roman, R. J., et al. (2014). Postmenopausal hypertension: role of the sympathetic nervous system in an animal model. *Am. J. Physiol. Regul. Integr. Comp. Physiol.* 306, R248–R256.

Marcus, N. J., Del Rio, R., Ding, Y., and Schultz, H. D. (2018). KLF2 mediates enhanced chemoreflex sensitivity, disordered breathing and autonomic dysregulation in heart failure. *J. Physiol.* 596, 3171–3185. doi: 10.1113/jp273805

Marcus, N. J., Del Rio, R., Schultz, E. P., Xia, X. H., and Schultz, H. D. (2014). Carotid body denervation improves autonomic and cardiac function and attenuates disordered breathing in congestive heart failure. *J. Physiol.* 592, 391–408. doi: 10.1113/jphysiol.2013.266221

Moraes, D. J. A., da Silva, M. P., Bonagamba, L. G. H., Mecawi, A. S., Zoccal, D. B., Antunes-Rodrigues, J., et al. (2013). Electrophysiological properties of rostral ventrolateral medulla presympathetic neurons modulated by the respiratory network in rats. *J. Neurosci.* 33:19223. doi: 10.1523/jneurosci.3041-13.2013

Moraes, D. J. A., da Silva, M. P., Spiller, P. F., Machado, B. H., and Paton, J. F. R. (2018). Purinergic plasticity within petrosal neurons in hypertension. *Am. J. Physiol. Regul. Integr. Comp. Physiol.* 315, R963–R971.

Moraes, D. J., Bonagamba, L. G., Costa, K. M., Costa-Silva, J. H., Zoccal, D. B., and Machado, B. H. (2014). Short-term sustained hypoxia induces changes in the coupling of sympathetic and respiratory activities in rats. *J. Physiol.* 592, 2013–2033. doi: 10.1113/jphysiol.2013.262212

Narkiewicz, K., van de Borne, P. J., Montano, N., Dyken, M. E., Phillips, B. G., and Somers, V. K. (1998). Contribution of tonic chemoreflex activation to sympathetic activity and blood pressure in patients with obstructive sleep apnea. *Circulation* 97, 943–945. doi: 10.1161/01.cir.97.10.943

Narkiewicz, K., van de Borne, P. J., Pesek, C. A., Dyken, M. E., Montano, N., and Somers, V. K. (1999). Selective potentiation of peripheral chemoreflex sensitivity in obstructive sleep apnea. *Circulation* 99, 1183–1189. doi: 10.1161/01.cir.99.9.1183

Nitsch, D., Grams, M., Sang, Y., Black, C., Cirillo, M., Djurdjev, O., et al. (2013). Associations of estimated glomerular filtration rate and albuminuria with mortality and renal failure by sex: a meta-analysis. *BMJ* 346:f324. doi: 10.1136/bmj.f324

Ong, J., Kinsman, B. J., Sved, A. F., Rush, B. M., Tan, R. J., Carattino, M. D., et al. (2019). Renal sensory nerves increase sympathetic nerve activity and blood pressure in 2-kidney 1-clip hypertensive mice. *J. Neurophysiol.* 122, 358–367. doi: 10.1152/jn.00173.2019

Paton, J. F., Sobotka, P. A., Fudim, M., Engelman, Z. J., Hart, E. C., McBryde, F. D., et al. (2013). The carotid body as a therapeutic target for the treatment

of sympathetically mediated diseases. *Hypertension* 61, 5–13. doi: 10.1161/hypertensionaha.111.00064

Phillips, J. K., Hopwood, D., Loxley, R. A., Ghatora, K., Coombes, J. D., Tan, Y. S., et al. (2007). Temporal relationship between renal cyst development, hypertension and cardiac hypertrophy in a new rat model of autosomal recessive polycystic kidney disease. *Kidney Blood Press. Res.* 30, 129–144. doi: 10.1159/000101828

Prommer, H. U., Maurer, J., von Websky, K., Freise, C., Sommer, K., Nasser, H., et al. (2018). Chronic kidney disease induces a systemic microangiopathy, tissue hypoxia and dysfunctional angiogenesis. *Sci. Rep.* 8:5317.

Rubinger, D., Backenroth, R., and Sapoznikov, D. (2012). Sympathetic activation and baroreflex function during intradialytic hypertensive episodes. *PLoS One* 7:e36943. doi: 10.1371/journal.pone.0036943

Saha, M., Menuet, C., Sun, Q.-J., Burke, P. G. R., Hildreth, C. M., Allen, A. M., et al. (2019). Respiratory sympathetic modulation is augmented in chronic kidney disease. *Respir. Physiol. Neurobiol.* 262, 57–66. doi: 10.1016/j.resp.2019.02.001

Salman, I. M., Hildreth, C. M., Ameer, O. Z., and Phillips, J. K. (2014). Differential contribution of afferent and central pathways to the development of baroreflex dysfunction in chronic kidney disease. *Hypertension* 63, 804–810. doi: 10.1161/hypertensionaha.113.02110

Salman, I. M., Kandukuri, D. S., Harrison, J. L., Hildreth, C. M., and Phillips, J. K. (2015a). Direct conscious telemetry recordings demonstrate increased renal sympathetic nerve activity in rats with chronic kidney disease. *Front. Physiol.* 6:218. doi: 10.3389/fphys.2015.00218

Salman, I. M., Phillips, J. K., Ameer, O. Z., and Hildreth, C. M. (2015b). Abnormal central control underlies impaired baroreflex control of heart rate and sympathetic nerve activity in female Lewis Polycystic Kidney rats. *J. Hypertens.* 33, 1418–1428. doi: 10.1097/hjh.0000000000000572

Santoro, A., and Mandreoli, M. (2014). Chronic renal disease and risk of cardiovascular morbidity-mortality. *Kidney Blood Press. Res.* 39, 142–146. doi: 10.1159/000355789

Simms, A. E., Paton, J. F., Pickering, A. E., and Allen, A. M. (2009). Amplified respiratory-sympathetic coupling in the spontaneously hypertensive rat: does it contribute to hypertension? *J. Physiol.* 587, 597–610. doi: 10.1113/jphysiol.2008.165902

Sinski, M., Lewandowski, J., Przybylski, J., Bidiuk, J., Abramczyk, P., Ciarka, A., et al. (2012). Tonic activity of carotid body chemoreceptors contributes to the increased sympathetic drive in essential hypertension. *Hypertens. Res.* 35, 487–491. doi: 10.1038/hr.2011.209

Souza, G. M. P. R., Bonagamba, L. G. H., Amorim, M. R., Moraes, D. J. A., and Machado, B. H. (2015). Cardiovascular and respiratory responses to chronic intermittent hypoxia in adult female rats. *Exp. Physiol.* 100, 249–258. doi: 10.1113/expphysiol.2014.082990

Souza, G. M. P. R., Bonagamba, L. G. H., Amorim, M. R., Moraes, D. J. A., and Machado, B. H. (2016). Inspiratory modulation of sympathetic activity is increased in female rats exposed to chronic intermittent hypoxia. *Exp. Physiol.* 101, 1345–1358. doi: 10.1113/ep085850

Souza, G., Amorim, M. R., Moraes, D. J. A., and Machado, B. H. (2017). Sex differences in the respiratory-sympathetic coupling in rats exposed to chronic intermittent hypoxia. *Respir. Physiol. Neurobiol.* 256, 109–118. doi: 10.1016/j.resp.2017.09.003

Stocker, S. D., and Muntzel, M. S. (2013). Recording sympathetic nerve activity chronically in rats: surgery techniques, assessment of nerve activity, and quantification. *Am. J. Physiol. Heart Circulat. Physiol.* 305, H1407–H1416.

Takakura, A. C., Moreira, T. S., Colombari, E., West, G. H., Stornetta, R. L., and Guyenet, P. G. (2006). Peripheral chemoreceptor inputs to retrotrapezoid nucleus (RTN) CO2-sensitive neurons in rats. *J. Physiol.* 572, 503–523. doi: 10.1113/jphysiol.2005.103788

Tan, Z. Y., Lu, Y., Whiteis, C. A., Simms, A. E., Paton, J. F., Chapleau, M. W., et al. (2010). Chemoreceptor hypersensitivity, sympathetic excitation, and overexpression of ASIC and TASK channels before the onset of hypertension in SHR. *Circ. Res.* 106, 536–545. doi: 10.1161/circresaha.109.206946

Tank, J., Diedrich, A., Szczech, E., Luft, F. C., and Jordan, J. (2005). Baroreflex regulation of heart rate and sympathetic vasomotor tone in women and men. *Hypertension* 45, 1159–1164. doi: 10.1161/01.hyp.0000165695.98915.9a

Tonelli, M., Wiebe, N., Culleton, B., House, A., Rabbat, C., Fok, M., et al. (2006). Chronic kidney disease and mortality risk: a systematic review. *J. Am. Soc. Nephrol.* 17, 2034–2047.

Toney, G. M., Pedrino, G. R., Fink, G. D., and Osborn, J. W. (2010). Does enhanced respiratory-sympathetic coupling contribute to peripheral neural mechanisms of angiotensin II-salt hypertension? *Exp. Physiol.* 95, 587–594. doi: 10.1113/expphysiol.2009.047399

Toor, R. U. A. S., Sun, Q. J., Kumar, N. N., Le, S., Hildreth, C. M., Phillips, J. K., et al. (2019). Neurons in the intermediate reticular nucleus coordinate postinspiratory activity, swallowing, and respiratory-sympathetic coupling in the rat. *J. Neurosci.* 39, 9757–9766. doi: 10.1523/jneurosci.0502-19.2019

Wong-Riley, M. T. T., Liu, Q., and Gao, X.-p. (2013). Peripheral-central chemoreceptor interaction and the significance of a critical period in the development of respiratory control. *Respir. Physiol. Neurobiol.* 185, 156–169. doi: 10.1016/j.resp.2012.05.026

Wyse, B. F., Harrison, J., and Phillips, J. K. (2011). Neurohumoral and renal mechanisms in the pathogenesis of hypertension in polycystic kidney disease. *J. Am. Soc. Nephrol.* 22:844A.

Yao, Y., Hildreth, C. M., Farnham, M. M., Saha, M., Sun, Q. J., Pilowsky, P. M., et al. (2015). The effect of losartan on differential reflex control of sympathetic nerve activity in chronic kidney disease. *J. Hypertens.* 33, 1249–1260. doi: 10.1097/hjh.0000000000000535

Zoccal, D. B., and Machado, B. H. (2010). Sympathetic overactivity coupled with active expiration in rats submitted to chronic intermittent hypoxia. *Respir. Physiol. Neurobiol.* 174, 98–101. doi: 10.1016/j.resp.2010.08.011

Zoccal, D. B., Simms, A. E., Bonagamba, L. G., Braga, V. A., Pickering, A. E., Paton, J. F., et al. (2008). Increased sympathetic outflow in juvenile rats submitted to chronic intermittent hypoxia correlates with enhanced expiratory activity. *J. Physiol.* 586, 3253–3265. doi: 10.1113/jphysiol.2008.154187

Conflict of Interest: The authors declare that the research was conducted in the absence of any commercial or financial relationships that could be construed as a potential conflict of interest.

frontiers in Physiology

ORIGINAL RESEARCH
published: 08 October 2021
doi: 10.3389/fphys.2021.757731

Activation of Astrocytes in the Persistence of Post-hypoxic Respiratory Augmentation

Isato Fukushi[1,2], Kotaro Takeda[2,3], Mieczyslaw Pokorski[4,5], Yosuke Kono[2,6], Masashi Yoshizawa[2,6], Yohei Hasebe[2,6], Akito Nakao[7], Yasuo Mori[7], Hiroshi Onimaru[8] and Yasumasa Okada[2]*

[1]Faculty of Health Sciences, Uekusa Gakuen University, Chiba, Japan, [2]Clinical Research Center, Murayama Medical Center, Musashimurayama, Japan, [3]Faculty of Rehabilitation, School of Healthcare, Fujita Health University, Toyoake, Japan, [4]Institute of Health Sciences, University of Opole, Opole, Poland, [5]Faculty of Health Sciences, The Jan Dlugosz University in Czestochowa, Czestochowa, Poland, [6]Department of Pediatrics, Faculty of Medicine, University of Yamanashi, Yamanashi, Japan, [7]Laboratory of Molecular Biology, Department of Synthetic Chemistry and Biological Chemistry, Graduate School of Engineering, Kyoto University, Kyoto, Japan, [8]Department of Physiology, Showa University School of Medicine, Tokyo, Japan

OPEN ACCESS

Edited by:
Yu Ru Kou, National Yang-Ming University, Taiwan

Reviewed by:
Kun-Ze Lee, National Sun Yat-sen University, Taiwan
Ching Jung Lai, Tzu Chi University, Taiwan
Raphael Rodrigues Perim, The University of Texas Health Science Center at San Antonio, United States

***Correspondence:**
Isato Fukushi
fukushi@1998.jukuin.keio.ac.jp

Specialty section:
This article was submitted to Respiratory Physiology, a section of the journal Frontiers in Physiology

Received: *12 August 2021*
Accepted: *15 September 2021*
Published: *08 October 2021*

Citation:
Fukushi I, Takeda K, Pokorski M, Kono Y, Yoshizawa M, Hasebe Y, Nakao A, Mori Y, Onimaru H and Okada Y (2021) Activation of Astrocytes in the Persistence of Post-hypoxic Respiratory Augmentation. Front. Physiol. 12:757731. doi: 10.3389/fphys.2021.757731

Acute hypoxia increases ventilation. After cessation of hypoxia loading, ventilation decreases but remains above the pre-exposure baseline level for a time. However, the mechanism of this post-hypoxic persistent respiratory augmentation (PHRA), which is a short-term potentiation of breathing, has not been elucidated. We aimed to test the hypothesis that astrocytes are involved in PHRA. To this end, we investigated hypoxic ventilatory responses by whole-body plethysmography in unanesthetized adult mice. The animals breathed room air, hypoxic gas mixture (7% O_2, 93% N_2) for 2 min, and again room air for 10 min before and after i.p. administration of low (100 mg/kg) and high (300 mg/kg) doses of arundic acid (AA), an astrocyte inhibitor. AA suppressed PHRA, with the high dose decreasing ventilation below the pre-hypoxic level. Further, we investigated the role of the astrocytic TRPA1 channel, a putative ventilatory hypoxia sensor, in PHRA using astrocyte-specific *Trpa1* knockout (as*Trpa1*$^{-/-}$) and floxed *Trpa1* (*Trpa1*$^{f/f}$) mice. In both *Trpa1*$^{f/f}$ and as*Trpa1*$^{-/-}$ mice, PHRA was noticeable, indicating that the astrocyte TRPA1 channel was not directly involved in PHRA. Taken together, these results indicate that astrocytes mediate the PHRA by mechanisms other than TRPA1 channels that are engaged in hypoxia sensing.

Keywords: astrocyte, hypoxia, post-hypoxic respiratory augmentation, plasticity, short-term potentiation, respiratory control, arundic acid, TRPA1

INTRODUCTION

Acute hypoxia increases ventilation. After brief hypoxic exposure, a switchback to room air is accompanied by a ventilatory fall-off in the recovery phase, but ventilation remains above the pre-hypoxic baseline for a time. Post-hypoxic persistent respiratory augmentation (PHRA) is a form of neural plasticity, which is defined as a change in the neural control system based

on the memory-like experience (Mitchell and Johnson, 2003). The poststimulus overshoot in ventilatory activity may even go above the stimulus level as is evident in the acute hypoxic ventilatory response (HVR) to static exercise, with the mechanism ascribed to the interaction with the cardiovascular brain control or rapid release of the volitional hypothalamic control over sustained muscle tension (Pokorski et al., 1990). Neural plasticity is essential for stabilizing respiratory control, but the underlying mechanisms are not yet well known (Eldridge and Millhorn, 1986; Dahan et al., 1995; Eldridge, 1996; Powell et al., 1998).

There are plastic interactions in relay circuits of hypoxic stimulus between peripheral chemoreceptors, among which carotid body chemoreceptors are most engaged in creating the HVR, and brain respiratory control pathways (Pamenter and Powell, 2016). The multipronged complexity of PHRA is highlighted by increased carotid chemoreceptor sensitivity due to the withdrawal of the central efferent activity component running down the sinus nerve to the carotid body (Lahiri et al., 1983). That feature has been unraveled in adaptive plasticity to chronic hypoxia but is plausibly also present in repeat acute hypoxic episodes characteristic of sleep apnea syndrome, the disease that distinctly affects brain function and increases chemoreflex sensitivity (Prabhakar, 2016).

Limited understanding of peripheral and central underliers of respiratory plasticity spurred novel lines of research, one of which is the role of transient receptor potential ankyrin 1 (TRPA1) channel. These channels participate in shaping the acute HVR (Pokorski et al., 2014). However, the channels have never been verified in carotid chemoreceptor cells and their effects on the HVR are mediated by mechanisms other than the carotid body (Pokorski et al., 2014). It has been shown that TRPA1 is localized in the chemosensitive parafacial respiratory group (pFRG/RTN) astrocytes in which hypoxia-induced TRPA1 activation facilitates exocytosis of ATP-containing vesicles (Uchiyama et al., 2020). On the basis of these findings, TRPA1 channels in astrocytes have been proposed as an oxygen sensor for respiratory control (Uchiyama et al., 2020). The proposition is in line with studies that show the role of astrocytes in brain synaptic plasticity (De Pittà et al., 2016; Schiera et al., 2020). Astrocytes are also influential for various aspects of respiratory control, including rhythm generation (Okada et al., 2012; Sheikhbahaei et al., 2018) and hypoxic and hypercapnic ventilatory responses (Gourine et al., 2010; Funk et al., 2015; Pokorski et al., 2016; Beltrán-Castillo et al., 2017; Gourine and Funk, 2017; Funk and Gourine, 2018; Sheikhbahaei et al., 2018; Guyenet et al., 2019). It has been reported that astrocytes can detect hypoxia (Tadmouri et al., 2014; Angelova et al., 2015; Fukushi et al., 2016; Onimaru et al., 2021). Therefore, we aimed to test the hypothesis that astrocytes are involved in PHRA and define the role of astrocytes, notably through TRPA1 channels, in the PHRA phenomenon. We used arundic acid (AA) as a pharmacological tool to inhibit astrocytic function in wild-type mice. We also used astrocyte *Trpa1* knockout mice to investigate the role of astrocytic TRPA1 channels in PHRA. We found that the presence of active astrocytes is indispensable for the expression of PHRA, but their action is mediated by mechanisms other than TRPA1 channels.

MATERIALS AND METHODS

Animal Welfare

All animal experiments were performed with the approval of the Ethics Committee for Animal Experiments of the Murayama Medical Center in Tokyo and complied with the Guidelines for Care and Use of Laboratory Animals released by the National Research Council of the National Academies (8th edition, revised 2011) and with the Guiding Principles for Care and Use of Animals of the Physiological Society of Japan. A total of 34 mice (including the mice in experiments for **Supplementary Figures 1**, **2**) were used in the experiments. All efforts were made to minimize the number of animals used.

Experiments With Arundic Acid

We used unanesthetized adult male C57BL/6 mice aged 24.0 ± 3.0 weeks (mean ± SE). It should be the same weeks, weighing 29.6 ± 0.7 g ($n = 9$). The respiratory flow was measured noninvasively using an "open flow" whole-body plethysmograph (PLY 310, EMMS, Bordon, United Kingdom) consisting of recording (volume of 530 ml) and reference chambers as previously described (Oyamada et al., 2008; Pokorski et al., 2014; Fukushi et al., 2016, 2020). Briefly, the chambers were placed inside a transparent acrylic box (size 20 × 20 × 20 cm). Each mouse was placed in the pre-calibrated recording chamber. The chamber temperature was maintained at 25°C throughout. The air in the recording chamber was suctioned with a constant flow generator (MV-6005VP, E.M.P-Japan, Tokyo, Japan), with a flow rate of 250 ml/min. To calculate the airflow, the pressure difference between the recording and reference chambers was measured with a differential pressure transducer (TPF100, EMMS) connected to an amplifier (AIU060, Information & Display Systems, Bordon, United Kingdom) and was bandpass filtered at 0.1–20 Hz. We calculated tidal volume (V_T; μl/g b.w.) for each breath by integrating the airflow whose changes are proportional to those in the chamber pressure (Lundblad et al., 2002). We counted the number of breaths and obtained respiratory rate (RR; breaths/min). Minute ventilation (V_E; ml/g/min) was calculated as $V_T \times RR$ for each minute. The V_E during hypoxia was calculated as a 2-min average and during the recovery phase as an average of the first 5 min (Recovery 1) and second 5 min (Recovery 2). The O_2 concentration in the chamber was monitored with an O_2 analyzer incorporating a polarographic sensor (Respina IH 26, San-ei, Tokyo, Japan) and was adjusted by controlling the mixing of N_2 and air blown into the acrylic box. The pressure and O_2 concentration data were simultaneously digitized at a 400 Hz sampling rate with an A/D converter (PowerLab4/26) and stored in a PC with LabChart7 software. The signal processing was performed using MATLAB 2020a (MathWorks, Natick, MA).

To evaluate the HVR, mice breathed room air, then a hypoxic gas mixture (7% O_2, 93% N_2 for 2 min), and room air again before and after i.p. administration of AA. The experimental protocol consisted of three repeats of hypoxic challenges. First, dimethyl sulfoxide (DMSO), a vehicle for AA diluted in saline, was injected and the mouse was placed into the chamber to acclimatize in room air for 60 min. Then, after recording

normoxic baseline data for 1 min, N_2 gas was blown into the acrylic box. The chamber O_2 concentration rapidly declined to 7%, which was maintained for 2 min and followed by a switchback to room air. The measurement for the recovery continued for 10 min. This protocol was repeated after injections of two doses of AA solubilized in a mixture of DMSO and saline (1:4:5 *v*/*v*) at 30-min intervals. Thus, injections were made in the following sequence (1) vehicle – 0.45 ml/kg DMSO, (2) AA – 100 mg/kg, and (3) AA – 200 mg/kg (cumulative AA dose of 300 mg/kg). Although DMSO alone can affect the brain function when the dose is high, a total dose of DMSO used in the present experiment did not exceed 2.0 g/kg, which is much below the 3.5 g/kg, a dose that starts affecting respiration (Takeda et al., 2016). The total volume of saline used in the experiment was 2.24 ml/kg, which is much below the 10 ml/kg reported to affect respiration in mice (Receno et al., 2018). The dosing of AA was chosen according to previous studies using this agent in *in-vivo* rodents (Higashino et al., 2009; Fukushi et al., 2016, 2020). Any apparent movement and sniffing artifacts interfering with breathing patterns were discarded off-line from the recording traces during the final data elaboration. The mean values of V_E were submitted to a two-factor within-subject analysis of variance (ANOVA), with three pharmacological conditions: DMSO vehicle and the two doses of AA, and four air phases (Baseline room air, Hypoxia, Recovery 1, and Recovery 2). The same statistical tests were performed for RR and V_T as for V_E. A Greenhouse–Geisser adjustment was used to correct for violations of sphericity whenever necessary. Then, to quantitatively evaluate the magnitude of PHRA, we calculated the difference in V_E between the post-hypoxic recovery and pre-hypoxic baseline levels. This difference was divided by the difference in V_E between the hypoxic loading and pre-hypoxic levels to normalize for the degree of hypoxic ventilatory augmentation. The calculation provided the parameter $\Delta V_{ERecovery}/\Delta V_{EHypoxia}$ to compare the PHRA magnitude among three drug conditions (without AA and with low and high doses of AA) in the post-hypoxic Recovery 1 and Recovery 2 phases. Statistical differences were assessed with a paired t-test. Bonferroni correction was performed for the multiple comparisons.

Experiments Using Astrocyte-Specific *Trpa1* Knockout Mice

We examined the role of astrocyte TRPA1 channels in HVR and PHRA using astrocyte-specific *Trpa1* knockout mice (as*Trpa1*$^{-/-}$). To generate the as*Trpa1*$^{-/-}$, two lines of mice were crossed: a transgenic mouse GFAP-Cre (mGFAP-Cre) and a recombinant *Trpa1* floxed (*Trpa1*$^{f/f}$) mouse (Gregorian et al., 2009; Zappia et al., 2017; Uchiyama et al., 2020). We conducted 7% hypoxia loading experiments in as*Trpa1*$^{-/-}$ mice (seven males and five females, aged 21.8 ± 0.4 weeks, weighing 25.8 ± 1.1 g) and *Trpa1*$^{f/f}$ mice (two males and four females, aged 22.7 ± 1.3 weeks, weighing 24.2 ± 0.9 g) according to the same protocol and measurement methods as outlined above for the AA experiments. The mean values of V_E, V_T, and RR were submitted to two-way ANOVA with two TRPA1 conditions (as*Trpa1*$^{-/-}$ and *Trpa1*$^{f/f}$) as between-factor and with four air phases (Baseline room air, Hypoxia, Recovery 1, and Recovery 2) as within-factor. A Greenhouse–Geisser adjustment was used to correct for violations of sphericity. We calculated the $\Delta V_{ERecovery}/\Delta V_{EHypoxia}$ to compare the PHRA magnitude between the two TRPA1 conditions (as*Trpa1*$^{-/-}$ and *Trpa1*$^{f/f}$) in the post-hypoxic Recovery 1 and Recovery 2 phases using the Welch test. The Bonferroni correction was used for multiple comparisons in *post hoc* tests. A $p < 0.05$ defined statistically significant differences. The analysis was performed using SPSS 24.0 (IBM, Armonk, NY).

RESULTS

Effects of Arundic Acid on HVRs

The exemplary recordings of V_E profiles in the two AA conditions vs. the control condition with no AA across the baseline room air, hypoxia, and Recovery 1 and 2 phases are shown in **Figure 1**. There was a significant interaction between pharmacological conditions × ventilatory phases [$F(6, 42) = 8.08$, $p < 0.001$]. On average, AA failed to affect V_E, despite some increases in RR after the higher dose of AA in room air. While V_E increased during hypoxia on the background of AA, there were differences in the post-hypoxia recovery course. In the control condition, V_E decreased from the hypoxic hyperventilation level but remained higher than the pre-hypoxic baseline level in both recovery phases. In the low-dose AA condition, V_E immediately returned to the pre-hypoxic baseline level during Recovery 1 but increased again above it during Recovery 2. In the high-dose AA condition, V_E decreased significantly below the pre-hypoxic baseline level during Recovery 1 and then tended to revert to the baseline level in Recovery 2 failing to reach it. The time courses of V_E, V_T, and RR as outlined in the example shown above are summarized in **Figure 2**. **Figure 3A** shows that the $\Delta V_{ERecovery}/\Delta V_{EHypoxia}$, assessing the PHRA magnitude, was significantly smaller in Recovery 1 between control (no AA) and 100 mg/kg AA ($p < 0.01$) or 300 mg/kg AA ($p < 0.001$), and between 100 and 300 mg/kg AA ($p < 0.05$). The differences between control (no AA) and 300 mg/kg AA and between 100 and 300 mg/kg AA distinctly persisted in Recovery 2 (**Figure 3B**). Thus, blockade of astrocyte activation significantly attenuated PHRA; the effect was greatly potentiated at the higher AA dose.

HVRs in as*Trpa1*$^{-/-}$ Mice

V_E profiles in as*Trpa1*$^{-/-}$ and *Trpa1*$^{f/f}$ mice are shown in **Figures 4A,B**. There was a significant main effect of the ventilatory response phases [$F(3, 48) = 85.011$, $p < 0.001$] but not between the TRPA1 conditions [$F(1, 16) = 1.843$, $p = 0.193$]. In both as*Trpa1*$^{-/-}$ and *Trpa1*$^{f/f}$ mice, V_E increased during hypoxia when compared to the pre-hypoxic baseline level ($p < 0.001$) and then decreased in Recovery 1. However, V_E stayed above the baseline level throughout the recovery phases in both as*Trpa1*$^{-/-}$ and *Trpa1*$^{f/f}$ mice. Both V_T and RR components drove ventilatory changes throughout the hypoxic course in both as*Trpa1*$^{-/-}$ and *Trpa1*$^{f/f}$ mice (**Figures 4C,D**).

Although there was no significant interaction of TRPA1 conditions × ventilatory phases [$F(3, 48) = 2.352$, $p = 0.084$], we performed a between-TRPA1 comparison in each phase.

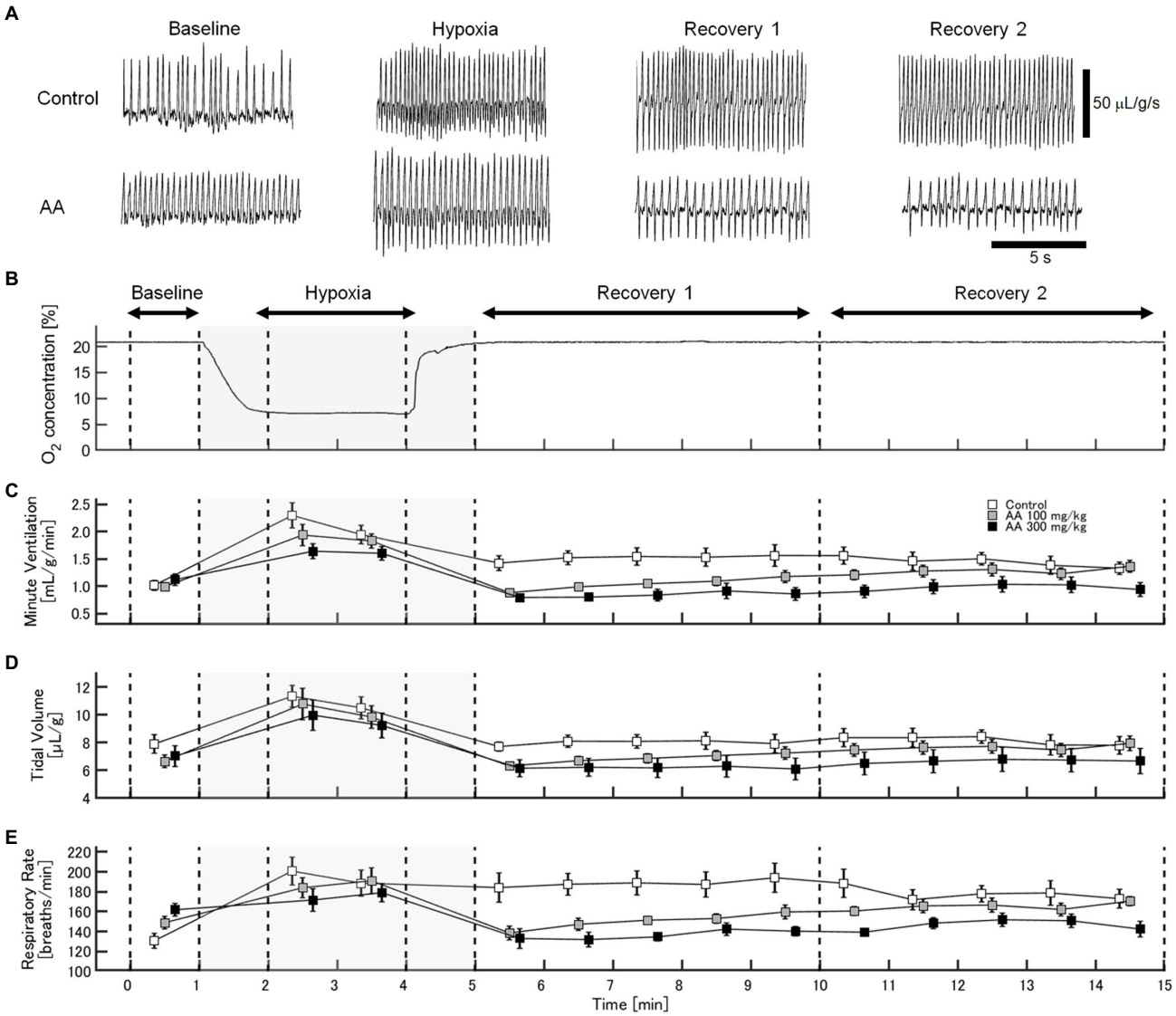

FIGURE 1 | Effects of arundic acid (AA) on hypoxic ventilatory responses (HVRs) in mice by whole-body plethysmography. **(A)** Representative recordings of respiratory flow (inspiration upward) in mice without and with the higher dose of AA in room air (baseline), 7% hypoxia, Recovery 1 (first 5 min), and Recovery 2 (second 5 min). AA did not affect minute ventilation (V_E) at pre-hypoxic baseline but tended to suppress the acute hypoxic hyperventilation. After the lower AA dose, V_E immediately returned to the pre-hypoxic baseline in Recovery 1 but rebounded in Recovery 2. After the higher AA dose, V_E decreased below the pre-hypoxic baseline in Recovery 1 and tended to revert to the baseline level in Recovery 2 failing to reach it. **(B)** Time-profile of chamber oxygen changes. **(C–E)** Time-series data for minute ventilation, tidal volume, and respiratory rate (RR), respectively, in the control (no AA) and low- and high-AA dose conditions.

V_E tended to be smaller in *Trpa1*$^{f/f}$ than as*Trpa1*$^{-/-}$ mice during hypoxia, but the difference was not significant ($p = 0.158$). V_E became significantly smaller in as*Trpa1*$^{-/-}$ mice during Recovery 1 ($p = 0.034$), but the PHRA phenomenon remained noticeable in both as*Trpa1*$^{-/-}$ and *Trpa1*$^{f/f}$ mice (**Figure 4B**). On average, $\Delta V_{ERecovery}/\Delta V_{EHypoxia}$ percentage values denoting PHRA magnitude were little different between as*Trpa1*$^{-/-}$ and *Trpa1*$^{f/f}$ in post-hypoxic Recovery 1 and 2 phases (**Figures 5A,B**, respectively). Although we did not conduct statistical analysis because the number of *Trpa1*$^{f/f}$ mice was small, there seems to be a gender difference; $\Delta V_{ERecovery1}/\Delta V_{EHypoxia}$ values in male and female *Trpa1*$^{f/f}$, and male and female as*Trpa1*$^{-/-}$ mice were 52, 61, 67, and 16%, respectively. $\Delta V_{ERecovery2}/\Delta V_{EHypoxia}$ values in these mice were 38, 36, 51, and 40%, respectively.

DISCUSSION

This study investigated the role of astrocytes in the PHRA, representing short-term potentiation of respiration. The findings show that astrocytes mediate PHRA. Pharmacological blockade of astrocyte activation by AA inhibited PHRA. The knockout as*Trpa1*$^{-/-}$ mice showed less increase in ventilation in response to hypoxia than *Trpa1*$^{f/f}$ mice. However, the magnitude of PHRA

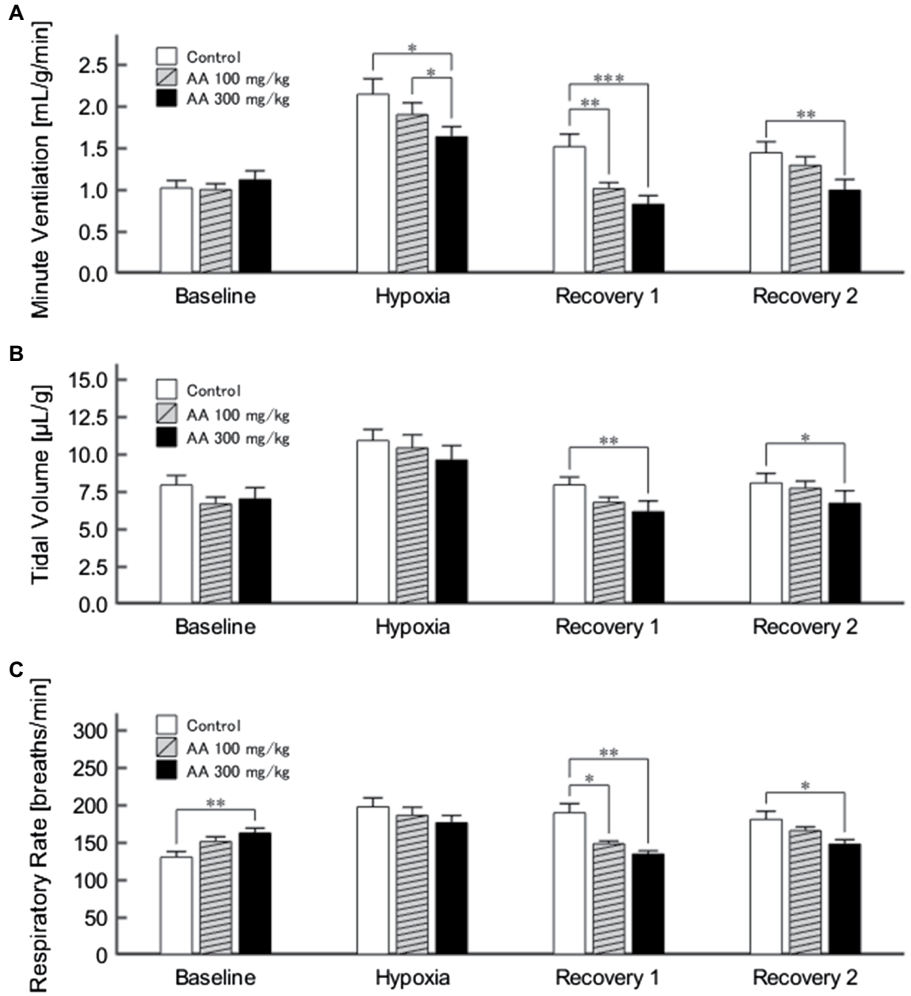

FIGURE 2 | (A) Minute ventilation (V_E) profiles ($n = 9$) in the control (no AA) and low- and high-AA dose conditions across the successive ventilatory phases. V_E differed significantly in the following pairwise comparisons: Control vs. AA 100 and AA 100 vs. AA 300 in hypoxia (both $p < 0.05$); Control vs. AA 100 ($p < 0.01$) and Control vs. AA 300 ($p < 0.001$) in Recovery 1; and Control vs. AA 300 ($p < 0.01$) in Recovery 2. **(B)** The time-course of tidal volume (V_T). There were main effects on V_T of the AA condition ($F_{2,16} = 6.596$, $p < 0.01$) and oxygen concentration ($F_{3,24} = 89.579$, $\varepsilon_{GG} = 0.424$, $p < 0.001$), but no interaction between the two ($F_{6,48} = 1.205$, $\varepsilon_{GG} = 0.522$, $p = 0.329$). V_T differed significantly in the following comparisons: Control vs. AA 300 in Recovery 1 and Control vs. AA 300 in Recovery 2 (both $p < 0.01$). **(C)** Time-course of RR. There was a significant interaction between control (no AA) and two AA conditions × HVR phases ($F_{6,42} = 12.208$, $p < 0.001$). RR differed significantly in the following comparisons: Control vs. AA 300 at baseline ($p < 0.01$); Control vs. AA 100 ($p < 0.05$) and Control vs. AA 300 ($p < 0.01$) in Recovery 1; and Control vs. AA 300 ($p < 0.05$) in Recovery 2. $^{*}p < 0.05$, $^{**}p < 0.01$, and $^{***}p < 0.001$, Bonferroni corrected.

was not attenuated in as*Trpa1*$^{-/-}$ when compared to *Trpa1*$^{f/f}$ mice. Our findings demonstrate the putative role of the astrocyte TRPA1 channels in hypoxia sensing, which confirms the recent findings by Uchiyama et al. (2020). We expanded the role of astrocytes to the mediation of PHRA as well. However, TRPA1 detects mild hypoxia (13%) more closely than severe hypoxia (7%; Takahashi et al., 2011; Pokorski et al., 2014). This suggests that PHRA is more likely to occur under conditions of severe hypoxia. Astrocyte-related action on the short-term PHRA occurs through yet unsettled mechanisms other than TRPA1 channels. The involvement of astrocyte TRPA1 channels has been reported in the hippocampal long-term potentiation in mice (Shigetomi et al., 2013). The contribution of these channels may vary depending on the type of brain plasticity.

In the present study, we used AA, as an inhibitory modulator of astrocyte function. AA inhibits the inflammatory response of astrocytes by reducing GFAP and S100 protein synthesis, increasing the expression of the astroglial glutamate transporter GLAST and releases the glutamate receptor antagonist kynurenic acid from astrocytes (Tateishi et al., 2002; Mori et al., 2004; Asano et al., 2005; Wajima et al., 2013; Yamamura et al., 2013; Yanagisawa et al., 2015). We have previously reported that AA delays the occurrence of seizures and prevents respiratory arrest in severe hypoxia (Fukushi et al., 2020).

The present finding of counteracting the PHRA by AA indicates that astrocytes are influential in shaping respiratory neural plasticity. Hypoxia activates the carotid body, and the information is relayed *via* the carotid sinus nerve to the

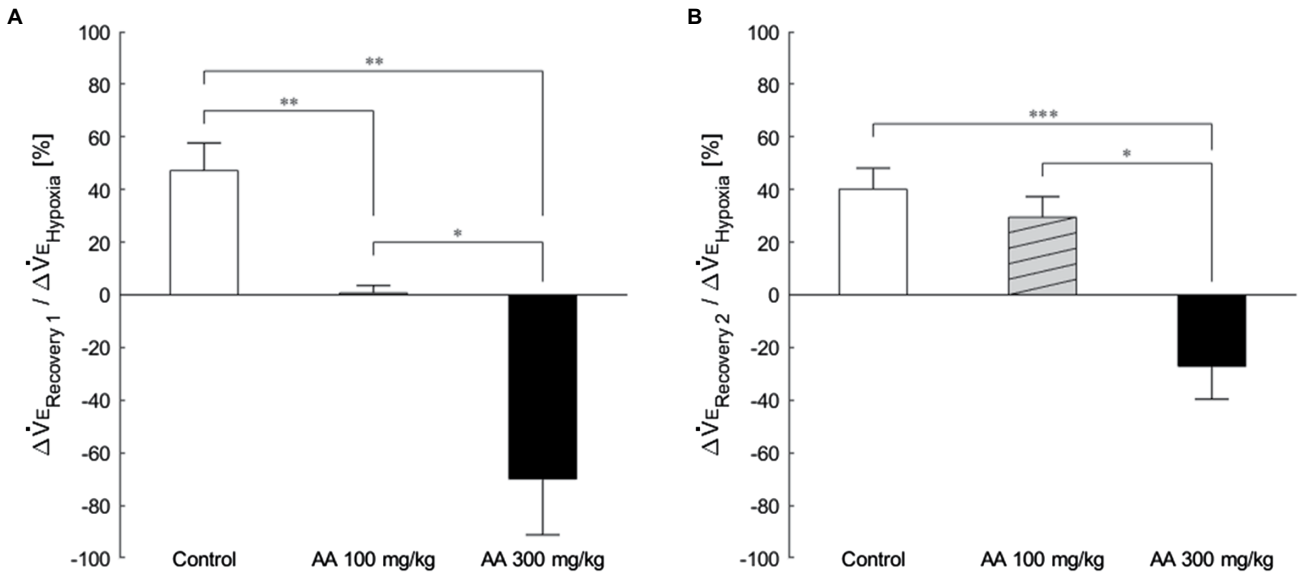

FIGURE 3 | The magnitude of effects of AA on post-hypoxic persistent respiratory augmentation (PHRA) evaluated according to the formula $\Delta V_{ERecovery}/\Delta V_{EHypoxia}$ (see Materials and Methods for details). **(A)** Recovery 1 – PHRA differed between control (no AA) vs. AA 100, control vs. AA 300, and AA 100 vs. AA 300 conditions. **(B)** Recovery 2 – PHRA differed between control (no AA) vs. AA 300. Data are means ± SE. $^{*}p < 0.05$, $^{**}p < 0.01$, and $^{***}p < 0.001$, Bonferroni corrected.

medullary solitary tract nucleus, emanating to other respiratory regions in the brainstem and spinal cord (Guyenet, 2014). Astrocytes around the excited neurons are activated *via* neurotransmitters spilled from neurons. Once activated, they release gliotransmitters that in turn activate respiratory neurons responsible for the sustenance of respiratory potentiation. Of note, the hitherto mechanistic studies on respiratory neural plasticity have been explicitly focused on neurons but not on glial cells. The present study is the first to demonstrate that astrocytes mediate the neural plasticity of respiration.

The short-term potentiation of brain excitability, leading to the continuation of respiratory augmentation after the stimulus cessation, referred to as neural plasticity, has been previously reported (Eldridge, 1973, 1976; Tawadrous and Eldridge, 1974; Eldridge and Gill-Kumar, 1980; Wagner and Eldridge, 1991). The mechanisms of respiratory plasticity are also present in the spinal cord (Feldman et al., 2003; Mitchell and Johnson, 2003; Fuller and Mitchell, 2017). One of the most extensively investigated phenomena in this context is the phrenic long-term facilitation following acute intermittent hypoxia. Regarding the cellular mechanism of facilitation, the Q and S signaling cascades in the phrenic motor nucleus have been proposed, induced by activation of metabotropic receptors coupled to Gq and Gs proteins, respectively, interacting *via* crosstalk inhibition. The serotonin-dependent Q pathway dominates in the phrenic facilitation during mild-to-moderate hypoxia. In contrast, the S pathway is serotonin-independent and dominates during severe hypoxia (Devinney et al., 2013; Fuller and Mitchell, 2017).

Recent studies have revealed an active role of astrocytes in brain plasticity related to other than respiratory functions, with a notable reference to hippocampal memory (Magistretti, 2006; Ota et al., 2013; Croft et al., 2015; Sims et al., 2015; De Pittà et al., 2016). Astrocytes secrete synapse-modulating gliotransmitters such as glutamate, ATP, D-serine, and GABA (Jourdain et al., 2007; Henneberger et al., 2010; Takata et al., 2011; Kang et al., 2013; Shigetomi et al., 2013; Verkhratsky et al., 2016; Zorec et al., 2018; Santello et al., 2019). The regulation of postsynaptic glutamate receptors, particularly α-amino-3-hydroxy-5-methyl-4-isoxazolepropionic acid (AMPA) receptors, is dependent on ATP released from astrocytes. The elevation in astrocytic Ca^{2+}, occurring slowly in the order of seconds, stimulates glutamate release which activates astrocytic metabotropic glutamate receptors (Agulhon et al., 2012; Navarrete et al., 2012). The classical form of neural plasticity also depends on *N*-methyl-D-aspartate (NMDA) receptors and Ca^{2+}-dependent slow release of D-serine from astrocytes (Henneberger et al., 2010). Further, astrocytes express a variety of receptors such as acetylcholine, ATP, GABA, and endocannabinoids (Porter and McCarthy, 1997; Haydon, 2001; Charles et al., 2003).

There are an increasing number of studies referring to the functional role of astrocytes in respiratory control other than respiratory plasticity. Astrocytes in the brainstem are sensitive to hypoxia and involved in HVR (Tadmouri et al., 2014; Angelova et al., 2015; Marina et al., 2015; Fukushi et al., 2016; Pokorski et al., 2016; Rajani et al., 2018; Uchiyama et al., 2020). Astrocytes in the ventral respiratory network, including the pre-Bötzinger complex, release ATP, which increases respiratory activity during hypoxia, putatively counteracting the depressive effects of hypoxia (Gourine et al., 2005; Marina et al., 2016a; Gourine and Funk, 2017; Funk and Gourine, 2018; Rajani et al., 2018). ATP acts *via* $P2Y_1$ receptors in the pre-Bötzinger complex to increase the respiratory burst rate with increases in intracellular Ca^{2+} and glutamate release (Lorier et al., 2007; Huxtable et al., 2010). Astrocytes also are strongly

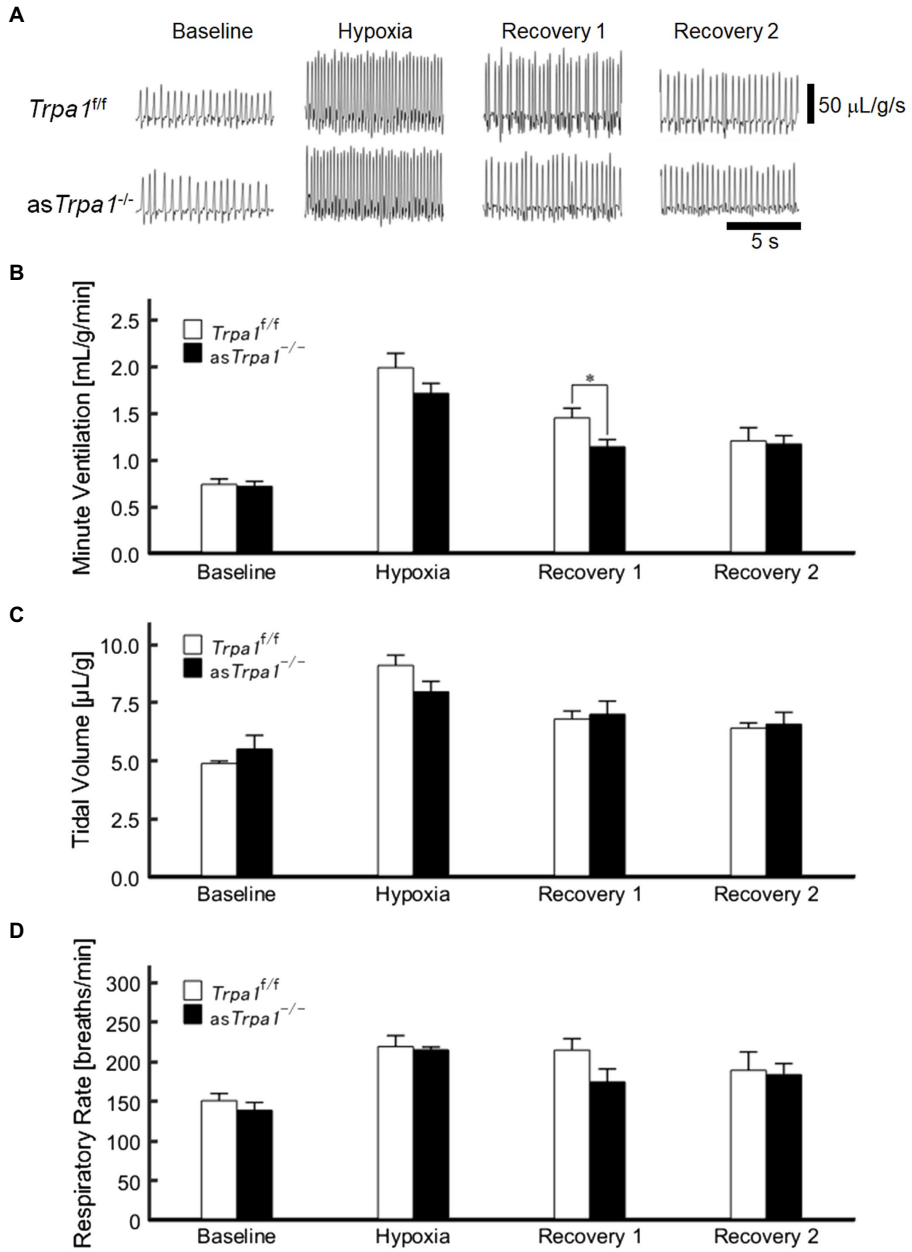

FIGURE 4 | Hypoxic ventilatory responses in as*Trpa1*$^{-/-}$ and *Trpa1*$^{f/f}$ mice. **(A)** Representative recordings of respiratory flow (inspiration upward) in room air (baseline), 7% hypoxia, Recovery 1 (first 5 min), and Recovery 2 (second 5 min). In both as*Trpa1*$^{-/-}$ and *Trpa1*$^{f/f}$ mice, minute ventilation (V_E) increased during hypoxia and then decreased in Recovery 1, remaining significantly elevated over the baseline level throughout both recovery phases. In Recovery 1, V_E was smaller in as*Trpa1*$^{-/-}$ than *Trpa1*$^{f/f}$ mice **(B)** Minute ventilation (V_E) in *Trpa1*$^{f/f}$ ($n = 12$) and as*Trpa1*$^{-/-}$ ($n = 6$) mice in successive ventilatory phases. Of note, V_E was significantly smaller in as*Trpa1*$^{-/-}$ than *Trpa1*$^{f/f}$ in Recovery 1 ($p = 0.034$). **(C)** Tidal volume (V_T) in successive ventilatory phases. There was a significant interaction between transient receptor potential ankyrin 1 (TRPA1) conditions (as*Trpa1*$^{-/-}$ and *Trpa1*$^{f/f}$) × ventilatory response phases ($F_{3,48}$ in as*Trpa1*$^{-/-}$ and *Trpa1*$^{f/f}$ mice = 3.318, $\varepsilon_{GG} = 0.658$, $p < 0.05$) but not between TRPA1 condition and V_T in any of the ventilatory phases. Pairwise comparisons in as*Trpa1*$^{-/-}$: Baseline vs. Hypoxia ($p < 0.001$), Baseline vs. Recovery 1 and Baseline vs. Recovery 2 (both $p < 0.01$), and Hypoxia vs. Recovery 2 ($p < 0.05$) and in *Trpa1*$^{f/f}$ Baseline vs. Hypoxia ($p < 0.001$), Baseline vs. Recovery 1, Baseline vs. Recovery 2, Hypoxia vs. Recovery 1, and Hypoxia vs. Recovery 2 (all $p < 0.01$). **(D)** RR in successive ventilatory phases. There was a significant main effect on RR of the ventilatory response phases ($F_{3,48} = 17.967$, $p < 0.001$) but no significant interaction between RR and TRPA1 conditions ($F_{3,48} = 1.396$, $p = 0.08$). There were no significant pairwise differences between ventilatory response phases in either as*Trpa1*$^{-/-}$ or *Trpa1*$^{f/f}$. Data are means ± SE. *$p < 0.05$; Bonferroni corrected.

involved in the central control of sympathetic activity and cardiovascular function, including systemic hypertension (Marina et al., 2016b), which are enhanced by acute and particularly repeat hypoxia episodes sensed by carotid chemoreceptors (Prabhakar et al., 2015). There is a biological plausibility that medullary astrocytes, respiratory neurons, and peripheral

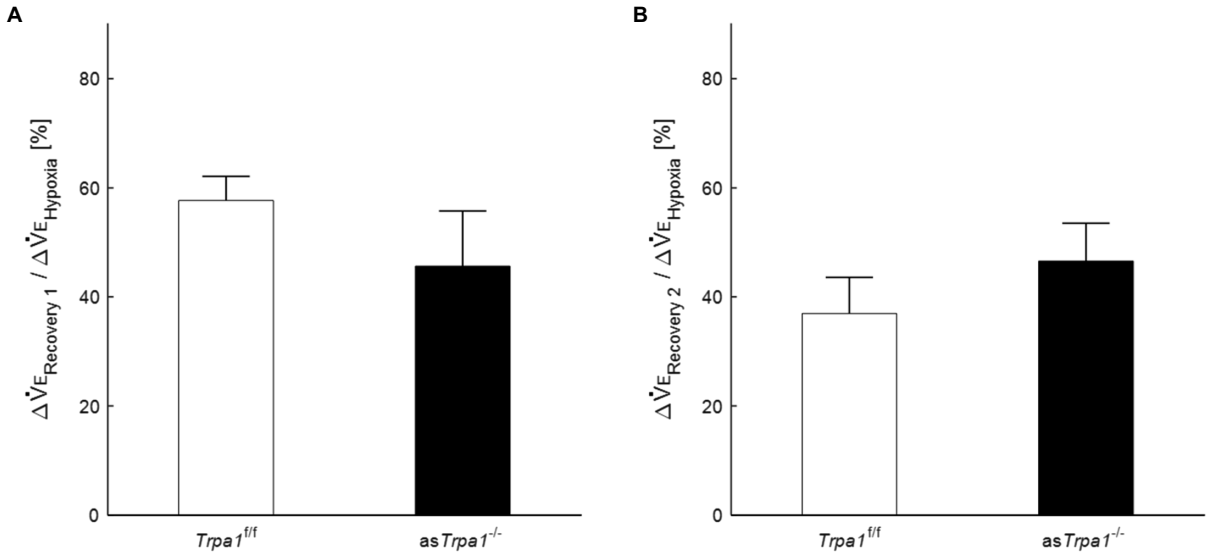

FIGURE 5 | Post-hypoxic persistent respiratory augmentation in astrocyte-specific *Trpa1* knockout mice. The $\Delta V_{ERecovery}/\Delta V_{EHypoxia}$, denoting PHRA, were not significantly different between as*Trpa1*$^{-/-}$ and *Trpa1*$^{f/f}$ in either Recovery 1 **(A)** or Recovery 2 **(B)**. Data are means ± SE.

chemosensing intertwine with each other in shaping PHRA. Alternative study designs are needed to further explore this issue.

In the present study, AA failed to affect V_E, although RR was increased in mice receiving a high dose of AA in room air. This phenomenon suggests that AA can affect breathing, i.e., inhibition of astrocyte activation may alter breathing patterns. In line with this notion, we showed that HVR was attenuated by a high dose of AA. However, AA blunted PHRA much more, suggesting that PHRA is activity-dependent plasticity.

There may be a concern over the time-dependent stability of minute ventilation on the background of a high dose of AA. Our additional investigation revealed that minute ventilation was stable over 240 min in this condition (**Supplementary Figure 1**). Likewise, another set of control investigations showed that hypoxia loadings repeated three times provide close reproducibility (**Supplementary Figure 2**).

One potential limitation of this study could be a lack of the animal's temperature control. In the classical "closed chamber" whole-body plethysmography, tidal volume is calculated by measuring the chamber pressure based on the combined gas law stating that the ratio of the product of gas pressure and volume to the absolute gas temperature is equal to a constant (Drorbaugh and Fenn, 1955). The chamber pressure is recorded while the chamber is sealed, and the body temperature weighs in on the result (Mayer et al., 2014; Rourke et al., 2016; Baby et al., 2018). In practice, however, the body temperature changes are so small during the hypoxic challenges of a couple of minutes that they are usually neglected for the sake of simplicity (Onodera et al., 1997). In the present study, we adopted the "open flow" plethysmography in which the chamber gas is continuously suctioned at a constant flow rate during the continuous recording. We calculated the tidal volume by integrating the airflow whose changes are proportional to those in the chamber pressure (Lundblad et al., 2002). In this case, tidal volume is expressed at ambient temperature (25°C), which obviates the need for taking the animal's body temperature. Another limitation of this study was that we failed to examine metabolic rate in knock-out mice or its potential alterations by AA, which could influence respiration. Metabolic aspects require further exploration using alternative study designs.

The ultimate purpose of this research was to refer to the mechanism of post-hypoxic short-term respiratory plasticity in unanesthetized humans, which is essential to get insights into the pathophysiology of and preventive measures for periodic breathing, e.g., sleep apnea. This purpose stemmed from the studies showing that PHRA is involved in the mitigation of periodic breathing in sleep apnea (Georgopoulus et al., 1992; Mahamed and Mitchell, 2007; Mateika and Syed, 2013; Mateika and Komnenov, 2017) and heart failure (Ahmed et al., 1994); the notion supported in a computer simulation study (Eldridge, 1996). Our results showed that astrocytes, but not the astrocytic TRPA1 channel, were involved in the development of PHRA, suggesting that the TRPA1 is engaged in shaping HVR but not PHRA. The TRPA1 channel likely plays a (patho)physiological role in acute hypoxic conditions such as an attack of bronchial asthma (Shen et al., 2012). In diseases with periodic breathing such as sleep apnea, astrocytes may contribute to its prevention by exerting PHRA. Additionally, the observation that $\Delta V_{ERecovery1}/\Delta V_{EHypoxia}$ tended to be smaller in the female as*Trpa1*$^{-/-}$ mice raises the implication of a greater role of astrocytic TRPA1 in the female gender, which requires further exploration.

In conclusion, we have provided novel aspects of PHRA's role linking it to astrocyte activation and suggesting that this tandem arrangement contributes to respiratory stability and potentially might be influential in the prevention of periodic breathing. However, caution should be exercised in the translation of animal findings to human settings before further exploratory research. We conclude that astrocytes mediate the post-hypoxic

persisting respiratory augmentation by mechanisms other than the hitherto recognized role of TRPA1 channels in hypoxia sensing.

DATA AVAILABILITY STATEMENT

The original contributions presented in the study are included in the article/**Supplementary Material**, further inquiries can be directed to the corresponding author.

ETHICS STATEMENT

The animal study was reviewed and approved by Ethics Committee for Animal Experiments of the Murayama Medical Center.

AUTHOR CONTRIBUTIONS

IF conceived and designed the study, performed the animal experiments, analyzed the data, and drafted the manuscript. KT performed the statistical analysis and drafted the manuscript. MP edited and revised the manuscript. YK, MY, and YH participated in the design of the study. AN and YM provided the animals and revised the manuscript. HO supervised the experiments and revised the manuscript. YO conceived and designed the study, analyzed the data, and revised the manuscript. All authors contributed to the article and approved the submitted version.

FUNDING

This work was supported by JSPS KAKENHI (17K08559, 18K17783, 19K17386, 19K17620, 20K19368, and 20K19474) and the Japanese Physical Therapy Association (JPTA2019 and JPTA2020).

SUPPLEMENTARY MATERIAL

The Supplementary Material for this article can be found online at: https://www.frontiersin.org/articles/10.3389/fphys.2021.757731/full#supplementary-material

REFERENCES

Agulhon, C., Sun, M. Y., Murphy, T., Myers, T., Lauderdale, K., and Fiacco, T. A. (2012). Calcium signaling and gliotransmission in normal vs. reactive astrocytes. *Front. Pharmacol.* 3:139. doi: 10.3389/fphar.2012.00139

Ahmed, M., Serrette, C., Kryger, M. H., and Anthonisen, N. R. (1994). Ventilatory instability in patients with congestive heart failure and nocturnal Cheyne-stokes breathing. *Sleep* 17, 527–534. doi: 10.1093/sleep/17.6.527

Angelova, P. R., Kasymov, V., Christie, I., Sheikhbahaei, S., Turovsky, E., Marina, N., et al. (2015). Functional oxygen sensitivity of astrocytes. *J. Neurosci.* 35, 10460–10473. doi: 10.1523/JNEUROSCI.0045-15.2015

Asano, T., Mori, T., Shimoda, T., Shinagawa, R., Satoh, S., Yada, N., et al. (2005). Arundic acid (ONO-2506) ameliorates delayed ischemic brain damage by preventing astrocytic overproduction of S100B. *Curr. Drug Targets CNS Neurol. Disord.* 4, 127–142. doi: 10.2174/1568007053544084

Baby, S. M., Gruber, R. B., Young, A. P., MacFarlane, P. M., Teppema, L. J., and Lewis, S. J. (2018). Bilateral carotid sinus nerve transection exacerbates morphine-induced respiratory depression. *Eur. J. Pharmacol.* 834, 17–29. doi: 10.1016/j.ejphar.2018.07.018

Beltrán-Castillo, S., Olivares, M. J., Contreras, R. A., Zúñiga, G., Llona, I., von Bernhardi, R., et al. (2017). D-serine released by astrocytes in brainstem regulates breathing response to CO_2 levels. *Nat. Commun.* 8:838. doi: 10.1038/s41467-017-00960-3

Charles, K. J., Deuchars, J., Davies, C. H., and Pangalos, M. N. (2003). GABAB receptor subunit expression in glia. *Mol. Cell. Neurosci.* 24, 214–223. doi: 10.1016/S1044-7431(03)00162-3

Croft, W., Dobson, K. L., and Bellamy, T. C. (2015). Plasticity of neuron-glial transmission: equipping glia for long-term integration of network activity. *Neural Plast.* 2015:765792. doi: 10.1155/2015/765792

Dahan, A., Berkenbosch, A., DeGoede, J., van den Elsen, M., Olievier, I., and van Kleef, J. (1995). Influence of hypoxic duration and post-hypoxic inspired O_2 concentration on short term potentiation of breathing in humans. *J. Physiol.* 488, 803–813. doi: 10.1113/jphysiol.1995.sp021012

De Pittà, M., Brunel, N., and Volterra, A. (2016). Astrocytes: orchestrating synaptic plasticity? *Neuroscience* 323, 43–61. doi: 10.1016/j.neuroscience.2015.04.001

Devinney, M. J., Huxtable, A. G., Nichols, N. L., and Mitchell, G. S. (2013). Hypoxia-induced phrenic long-term facilitation: emergent properties. *Ann. N. Y. Acad. Sci.* 1279, 143–153. doi: 10.1111/nyas.12085

Drorbaugh, J. E., and Fenn, W. O. (1955). A barometric method for measuring ventilation in newborn infants. *Pediatrics* 16, 81–87.

Eldridge, F. L. (1973). Posthyperventilation breathing: different effects of active and passive hyperventilation. *J. Appl. Physiol.* 34, 422–430. doi: 10.1152/jappl.1973.34.4.422

Eldridge, F. L. (1976). Central neural stimulation of respiration in unanesthetized decerebrate cats. *J. Appl. Physiol.* 40, 23–28. doi: 10.1152/jappl.1976.40.1.23

Eldridge, F. L. (1996). "The North Carolina respiratory model," in *Bioengineering Approaches to Pulmonary Physiology and Medicine*. ed. M. C. K. Khoo (Boston, MA: Springer).

Eldridge, F. L., and Gill-Kumar, P. (1980). Central neural respiratory drive and afterdischarge. *Respir. Physiol.* 40, 49–63. doi: 10.1016/0034-5687(80)90004-3

Eldridge, F. L., and Millhorn, D. E. (1986). "Oscillation, gating, and memory in the respiratory control system," in *Handbook of Physiology, Section 3: The Respiratory System: Control of Breathing, Part 1. Vol. 2*. eds. N. S. Cherniack and J. G. Widdicombe (Washington, DC: American Physiological Society), 93–114.

Feldman, J. L., Mitchell, G. S., and Nattie, E. E. (2003). Breathing: rhythmicity, plasticity, chemosensitivity. *Annu. Rev. Neurosci.* 26, 239–266. doi: 10.1146/annurev.neuro.26.041002.131103

Fukushi, I., Takeda, K., Uchiyama, M., Kurita, Y., Pokorski, M., Yokota, S., et al. (2020). Blockade of astrocytic activation delays the occurrence of severe hypoxia-induced seizure and respiratory arrest in mice. *J. Comp. Neurol.* 528, 1257–1264. doi: 10.1002/cne.24828

Fukushi, I., Takeda, K., Yokota, S., Hasebe, Y., Sato, Y., Pokorski, M., et al. (2016). Effects of arundic acid, an astrocytic modulator, on the cerebral and respiratory functions in severe hypoxia. *Respir. Physiol. Neurobiol.* 226, 24–29. doi: 10.1016/j.resp.2015.11.011

Fuller, D. D., and Mitchell, G. S. (2017). Respiratory neuroplasticity – overview, significance and future directions. *Exp. Neurol.* 287, 144–152. doi: 10.1016/j.expneurol.2016.05.022

Funk, G. D., and Gourine, A. V. (2018). CrossTalk proposal: a central hypoxia sensor contributes to the excitatory hypoxic ventilatory response. *J. Physiol.* 596, 2935–2938. doi: 10.1113/JP275707

Funk, G. D., Rajani, V., Alvares, T. S., Revill, A. L., Zhang, Y., Chu, N. Y., et al. (2015). Neuroglia and their roles in central respiratory control; an overview. *Comp. Biochem. Physiol. A Mol. Integr. Physiol.* 186, 83–95. doi: 10.1016/j.cbpa.2015.01.010

Georgopoulus, D., Giannouli, E., Tsara, V., Argiropoulou, P., Patakas, D., and Anthonisen, N. R. (1992). Respiratory short-term poststimulus potentiation (after-discharge) in patients with obstructive sleep apnea. *Am. Rev. Respir. Dis.* 146, 1250–1255. doi: 10.1164/ajrccm/146.5_Pt_1.1250

Gourine, A. V., and Funk, G. D. (2017). On the existence of a central respiratory oxygen sensor. *J. Appl. Physiol. (1985)* 123, 1344–1349. doi: 10.1152/japplphysiol.00194.2017

Gourine, A. V., Kasymov, V., Marina, N., Tang, F., Figueiredo, M. F., Lane, S., et al. (2010). Astrocytes control breathing through pH-dependent release of ATP. *Science* 329, 571–575. doi: 10.1126/science.1190721

Gourine, A. V., Llaudet, E., Dale, N., and Spyer, K. M. (2005). Release of ATP in the ventral medulla during hypoxia in rats: role in hypoxic ventilatory response. *J. Neurosci.* 25, 1211–1218. doi: 10.1523/JNEUROSCI.3763-04.2005

Gregorian, C., Nakashima, J., Le Belle, J., Ohab, J., Kim, R., Liu, A., et al. (2009). Pten deletion in adult neural stem/progenitor cells enhances constitutive neurogenesis. *J. Neurosci.* 29, 1874–1886. doi: 10.1523/JNEUROSCI.3095-08.2009

Guyenet, P. G. (2014). Regulation of breathing and autonomic outflows by chemoreceptors. *Comp. Physiol.* 4, 1511–1562. doi: 10.1002/cphy.c140004

Guyenet, P. G., Stornetta, R. L., Souza, G. M. P. R., Abbott, S. B. G., Shi, Y., and Bayliss, D. A. (2019). The retrotrapezoid nucleus: central chemoreceptor and regulator of breathing automaticity. *Trends Neurosci.* 42, 807–824. doi: 10.1016/j.tins.2019.09.002

Haydon, P. G. (2001). GLIA: listening and talking to the synapse. *Nat. Rev. Neurosci.* 2, 185–193. doi: 10.1038/35058528

Henneberger, C., Papouin, T., Oliet, S. H., and Rusakov, D. A. (2010). Long-term potentiation depends on release of D-serine from astrocytes. *Nature* 463, 232–236. doi: 10.1038/nature08673

Higashino, H., Niwa, A., Satou, T., Ohta, Y., Hashimoto, S., Tabuchi, M., et al. (2009). Immunohistochemical analysis of brain lesions using S100B and glial fibrillary acidic protein antibodies in arundic acid- (ONO-2506) treated stroke-prone spontaneously hypertensive rats. *J. Neural Transm.* 116, 1209–1219. doi: 10.1007/s00702-009-0278-x

Huxtable, A. G., Zwicker, J. D., Alvares, T. S., Ruangkittisakul, A., Fang, X., Hahn, L. B., et al. (2010). Glia contribute to the purinergic modulation of inspiratory rhythm-generating networks. *J. Neurosci.* 30, 3947–3958. doi: 10.1523/JNEUROSCI.6027-09.2010

Jourdain, P., Bergersen, L. H., Bhaukaurally, K., Bezzi, P., Santello, M., Domercq, M., et al. (2007). Glutamate exocytosis from astrocytes controls synaptic strength. *Nat. Neurosci.* 10, 331–339. doi: 10.1038/nn1849

Kang, N., Peng, H., Yu, Y., Stanton, P. K., Guilarte, T. R., and Kang, J. (2013). Astrocytes release D-serine by a large vesicle. *Neuroscience* 240, 243–257. doi: 10.1016/j.neuroscience.2013.02.029

Lahiri, S., Smatresk, N., Pokorski, M., Barnard, P., and Mokashi, A. (1983). Efferent inhibition of carotid body chemoreception in chronically hypoxic cats. *Am. J. Phys.* 245, R678–R683. doi: 10.1152/ajpregu.1983.245.5.R678

Lorier, A. R., Huxtable, A. G., Robinson, D. M., Lipski, J., Housley, G. D., and Funk, G. D. (2007). P2Y1 receptor modulation of the pre-Bötzinger complex inspiratory rhythm generating network *in vitro*. *J. Neurosci.* 27, 993–1005. doi: 10.1523/JNEUROSCI.3948-06.2007

Lundblad, L. K., Irvin, C. G., Adler, A., and Bates, J. H. (2002). A reevaluation of the validity of unrestrained plethysmography in mice. *J. Appl. Physiol.* 93, 1198–1207. doi: 10.1152/japplphysiol.00080.2002

Magistretti, P. J. (2006). Neuron-glia metabolic coupling and plasticity. *J. Exp. Biol.* 209, 2304–2311. doi: 10.1242/jeb.02208

Mahamed, S., and Mitchell, G. S. (2007). Is there a link between intermittent hypoxia-induced respiratory plasticity and obstructive sleep apnoea? *Exp. Physiol.* 92, 27–37. doi: 10.1113/expphysiol.2006.033720

Marina, N., Ang, R., Machhada, A., Kasymov, V., Karagiannis, A., Hosford, P. S., et al. (2015). Brainstem hypoxia contributes to the development of hypertension in the spontaneously hypertensive rat. *Hypertension* 65, 775–783. doi: 10.1161/HYPERTENSIONAHA.114.04683

Marina, N., Kasymov, V., Ackland, G. L., Kasparov, S., and Gourine, A. V. (2016a). Astrocytes and brain hypoxia. *Adv. Exp. Med. Biol.* 903, 201–207. doi: 10.1007/978-1-4899-7678-9_14

Marina, N., Teschemacher, A. G., Kasparov, S., and Gourine, A. V. (2016b). Glia, sympathetic activity and cardiovascular disease. *Exp. Physiol.* 101, 565–576. doi: 10.1113/EP085713

Mateika, J. H., and Komnenov, D. (2017). Intermittent hypoxia initiated plasticity in humans: a multipronged therapeutic approach to treat sleep apnea and overlapping co-morbidities. *Exp. Neurol.* 287, 113–129. doi: 10.1016/j.expneurol.2016.05.011

Mateika, J. H., and Syed, Z. (2013). Intermittent hypoxia, respiratory plasticity and sleep apnea in humans: present knowledge and future investigations. *Respir. Physiol. Neurobiol.* 188, 289–300. doi: 10.1016/j.resp.2013.04.010

Mayer, C. A., Di Fiore, J. M., Martin, R. J., and Macfarlane, P. M. (2014). Vulnerability of neonatal respiratory neural control to sustained hypoxia during a uniquely sensitive window of development. *J. Appl. Physiol.* 116, 514–521. doi: 10.1152/japplphysiol.00976.2013

Mitchell, G. S., and Johnson, S. M. (2003). Neuroplasticity in respiratory motor control. *J. Appl. Physiol.* 94, 358–374. doi: 10.1152/japplphysiol.00523.2002

Mori, T., Tateishi, N., Kagamiishi, Y., Shimoda, T., Satoh, S., Ono, S., et al. (2004). Attenuation of a delayed increase in the extracellular glutamate level in the peri-infarct area following focal cerebral ischemia by a novel agent ONO-2506. *Neurochem. Int.* 45, 381–387. doi: 10.1016/j.neuint.2003.06.001

Navarrete, M., Perea, G., Fernandez de Sevilla, D., Gómez-Gonzalo, M., Núñez, A., Martín, E. D., et al. (2012). Astrocytes mediate *in vivo* cholinergic-induced synaptic plasticity. *PLoS Biol.* 10:e1001259. doi: 10.1371/journal.pbio.1001259

Okada, Y., Sasaki, T., Oku, Y., Takahashi, N., Seki, M., Ujita, S., et al. (2012). Preinspiratory calcium rise in putative pre-Bötzinger complex astrocytes. *J. Physiol.* 590, 4933–4944. doi: 10.1113/jphysiol.2012.231464

Onimaru, H., Yazawa, I., Takeda, K., Fukushi, I., and Okada, Y. (2021). Calcium imaging analysis of cellular responses to hypercapnia and hypoxia in the NTS of newborn rat brainstem preparation. *Front. Physiol.* 12:645904. doi: 10.3389/fphys.2021.645904

Onodera, M., Kuwaki, T., Kumada, M., and Masuda, Y. (1997). Determination of ventilatory volume in mice by whole body plethysmography. *Jpn. J. Physiol.* 47, 317–326. doi: 10.2170/jjphysiol.47.317

Ota, Y., Zanetti, A. T., and Hallock, R. M. (2013). The role of astrocytes in the regulation of synaptic plasticity and memory formation. *Neural Plast.* 2013:185463. doi: 10.1155/2013/185463

Oyamada, Y., Murai, M., Harada, N., Ishizaka, A., and Okada, Y. (2008). Age-dependent involvement of ATP-sensitive potassium channel Kir6.2 in hypoxic ventilatory depression of mouse. *Respir. Physiol. Neurobiol.* 162, 80–84. doi: 10.1016/j.resp.2008.04.003

Pamenter, M. E., and Powell, F. L. (2016). Time domains of the hypoxic ventilatory response and their molecular basis. *Compr. Physiol.* 6, 1345–1385. doi: 10.1002/cphy.c150026

Pokorski, M., Masuda, A., Paulev, P. E., Sakakibara, Y., Ahn, B., Takaishi, S., et al. (1990). Ventilatory and cardiovascular responses to hypoxic and hyperoxic static handgrip exercise in man. *Respir. Physiol.* 81, 189–202. doi: 10.1016/0034-5687(90)90045-Z

Pokorski, M., Takeda, K., and Okada, Y. (2016). Oxygen sensing mechanisms: a physiological penumbra. *Adv. Exp. Med. Biol.* 952, 1–8. doi: 10.1007/5584_2016_67

Pokorski, M., Takeda, K., Sato, Y., and Okada, Y. (2014). The hypoxic ventilatory response and TRPA1 antagonism in conscious mice. *Acta Physiol.* 210, 928–938. doi: 10.1111/apha.12202

Porter, J. T., and McCarthy, K. D. (1997). Astrocytic neurotransmitter receptors in situ and *in vivo*. *Prog. Neurobiol.* 51, 439–455. doi: 10.1016/S0301-0082(96)00068-8

Powell, F. L., Milsom, W. K., and Mitchell, G. S. (1998). Time domains of the hypoxic ventilatory response. *Respir. Physiol.* 112, 123–134. doi: 10.1016/S0034-5687(98)00026-7

Prabhakar, N. R. (2016). Carotid body chemoreflex: a driver of autonomic abnormalities in sleep apnoea. *Exp. Physiol.* 101, 975–985. doi: 10.1113/EP085624

Prabhakar, N. R., Peng, Y. J., Kumar, G. K., and Nanduri, J. (2015). Peripheral chemoreception and arterial pressure responses to intermittent hypoxia. *Comp. Physiol.* 5, 561–577. doi: 10.1002/cphy.c140039

Rajani, V., Zhang, Y., Jalubula, V., Rancic, V., SheikhBahaei, S., Zwicker, J. D., et al. (2018). Release of ATP by pre-Bötzinger complex astrocytes contributes to the hypoxic ventilatory response via a Ca^{2+} −dependent P2Y1 receptor mechanism. *J. Physiol.* 596, 3245–3269. doi: 10.1113/JP274727

Receno, C. N., Glausen, T. G., and DeRuisseau, L. R. (2018). Saline as a vehicle control does not alter ventilation in male CD-1 mice. *Physiol. Rep.* 6:e13702. doi: 10.14814/phy2.13702

Rourke, K. S., Mayer, C. A., and MacFarlane, P. M. (2016). A critical postnatal period of heightened vulnerability to lipopolysaccharide. *Respir. Physiol. Neurobiol.* 232, 26–34. doi: 10.1016/j.resp.2016.06.003

Santello, M., Toni, N., and Volterra, A. (2019). Astrocyte function from information processing to cognition and cognitive impairment. *Nat. Neurosci.* 22, 154–166. doi: 10.1038/s41593-018-0325-8

Schiera, G., Di Liegro, C. M., and Di Liegro, I. (2020). Cell-to-cell communication in learning and memory: from neuro- and glio-transmission to information exchange mediated by extracellular vesicles. *Int. J. Mol. Sci.* 21:266. doi: 10.3390/ijms21010266

Sheikhbahaei, S., Turovsky, E. A., Hosford, P. S., Hadjihambi, A., Theparambil, S. M., Liu, B., et al. (2018). Astrocytes modulate brainstem respiratory rhythm-generating circuits and determine exercise capacity. *Nat. Commun.* 9:370. doi: 10.1038/s41467-017-02723-6

Shen, M. Y., Luo, Y. L., Yang, C. H., Ruan, T., and Lai, C. J. (2012). Hypersensitivity of lung vagal C fibers induced by acute intermittent hypoxia in rats: role of reactive oxygen species and TRPA1. *Am. J. Phys. Regul. Integr. Comp. Phys.* 303, R1175–R1185. doi: 10.1152/ajpregu.00227.2012

Shigetomi, E., Jackson-Weaver, O., Huckstepp, R. T., O'Dell, T. J., and Khakh, B. S. (2013). TRPA1 channels are regulators of astrocyte basal calcium levels and long-term potentiation via constitutive D-serine release. *J. Neurosci.* 33, 10143–10153. doi: 10.1523/JNEUROSCI.5779-12.2013

Sims, R. E., Butcher, J. B., Parri, H. R., and Glazewski, S. (2015). Astrocyte and neuronal plasticity in the somatosensory system. *Neural Plast.* 2015:732014. doi: 10.1155/2015/732014

Tadmouri, A., Champagnat, J., and Morin-Surun, M. P. (2014). Activation of microglia and astrocytes in the nucleus tractus solitarius during ventilatory acclimatization to 10% hypoxia in unanesthetized mice. *J. Neurosci. Res.* 92, 627–633. doi: 10.1002/jnr.23336

Takahashi, N., Kuwaki, T., Kiyonaka, S., Numata, T., Kozai, D., Mizuno, Y., et al. (2011). TRPA1 underlies a sensing mechanism for O_2. *Nat. Chem. Biol.* 7, 701–711. doi: 10.1038/nchembio.640

Takata, N., Mishima, T., Hisatsune, C., Nagai, T., Ebisui, E., Mikoshiba, K., et al. (2011). Astrocyte calcium signaling transforms cholinergic modulation to cortical plasticity *in vivo*. *J. Neurosci.* 31, 18155–18165. doi: 10.1523/JNEUROSCI.5289-11.2011

Takeda, K., Pokorski, M., Sato, Y., Oyamada, Y., and Okada, Y. (2016). Respiratory toxicity of dimethyl sulfoxide. *Adv. Exp. Med. Biol.* 885, 89–96. doi: 10.1007/5584_2015_187

Tateishi, N., Mori, T., Kagamiishi, Y., Satoh, S., Katsube, N., Morikawa, E., et al. (2002). Astrocytic activation and delayed infarct expansion after permanent focal ischemia in rats. Part II: suppression of astrocytic activation by a novel agent (R)-(−)-2-propyloctanoic acid (ONO-2506) leads to mitigation of delayed infarct expansion and early improvement of neurologic deficits. *J. Cereb. Blood Flow Metab.* 22, 723–734. doi: 10.1097/00004647-200206000-00011

Tawadrous, F. D., and Eldridge, F. L. (1974). Posthyperventilation breathing patterns after active hyperventilation in man. *J. Appl. Physiol.* 37, 353–356. doi: 10.1152/jappl.1974.37.3.353

Uchiyama, M., Nakao, A., Kurita, Y., Fukushi, I., Takeda, K., Numata, T., et al. (2020). O_2-dependent protein internalization underlies astrocytic sensing of acute hypoxia by restricting multimodal TRPA1 channel responses. *Curr. Biol.* 30, 3378.e7–3396.e7. doi: 10.1016/j.cub.2020.06.047

Verkhratsky, A., Matteoli, M., Parpura, V., Mothet, J. P., and Zorec, R. (2016). Astrocytes as secretory cells of the central nervous system: idiosyncrasies of vesicular secretion. *EMBO J.* 35, 239–257. doi: 10.15252/embj.201592705

Wagner, P. G., and Eldridge, F. L. (1991). Development of short-term potentiation of respiration. *Respir. Physiol.* 83, 129–139. doi: 10.1016/0034-5687(91)90098-4

Wajima, D., Nakagawa, I., Nakase, H., and Yonezawa, T. (2013). Neuroprotective effect of suppression of astrocytic activation by arundic acid on brain injuries in rats with acute subdural hematomas. *Brain Res.* 1519, 127–135. doi: 10.1016/j.brainres.2013.05.002

Yamamura, S., Hoshikawa, M., Dai, K., Saito, H., Suzuki, N., Niwa, O., et al. (2013). ONO-2506 inhibits spike-wave discharges in a genetic animal model without affecting traditional convulsive tests via gliotransmission regulation. *Br. J. Pharmacol.* 168, 1088–1100. doi: 10.1111/j.1476-5381.2012.02132.x

Yanagisawa, M., Aida, T., Takeda, T., Namekata, K., Harada, T., Shinagawa, R., et al. (2015). Arundic acid attenuates retinal ganglion cell death by increasing glutamate/aspartate transporter expression in a model of normal tension glaucoma. *Cell Death Dis.* 6:e1693. doi: 10.1038/cddis.2015.45

Zappia, K. J., O'Hara, C. L., Moehring, F., Kwan, K. Y., and Stucky, C. L. (2017). Sensory neuron-specific deletion of TRPA1 results in mechanical cutaneous sensory deficits. *eNeuro* 4:ENEURO.0069-16.2017. doi: 10.1523/ENEURO.0069-16.2017

Zorec, R., Parpura, V., and Verkhratsky, A. (2018). Astroglial vesicular network: evolutionary trends, physiology and pathophysiology. *Acta Physiol.* 222:e12915. doi: 10.1111/apha.12915

Conflict of Interest: The authors declare that the research was conducted in the absence of any commercial or financial relationships that could be construed as a potential conflict of interest.

Publisher's Note: All claims expressed in this article are solely those of the authors and do not necessarily represent those of their affiliated organizations, or those of the publisher, the editors and the reviewers. Any product that may be evaluated in this article, or claim that may be made by its manufacturer, is not guaranteed or endorsed by the publisher.

Advantages of publishing in Frontiers

OPEN ACCESS
Articles are free to read for greatest visibility and readership

FAST PUBLICATION
Around 90 days from submission to decision

HIGH QUALITY PEER-REVIEW
Rigorous, collaborative, and constructive peer-review

TRANSPARENT PEER-REVIEW
Editors and reviewers acknowledged by name on published articles

Frontiers
Avenue du Tribunal-Fédéral 34
1005 Lausanne | Switzerland

Visit us: www.frontiersin.org
Contact us: frontiersin.org/about/contact

REPRODUCIBILITY OF RESEARCH
Support open data and methods to enhance research reproducibility

DIGITAL PUBLISHING
Articles designed for optimal readership across devices

FOLLOW US
@frontiersin

IMPACT METRICS
Advanced article metrics track visibility across digital media

EXTENSIVE PROMOTION
Marketing and promotion of impactful research

LOOP RESEARCH NETWORK
Our network increases your article's readership